NOSC

NOSC TD 352 Vol 1

NOSC TD 352 Vol 1

Technical Document 352

STRATEGIC LASER COMMUNICATIONS PROGRAM

Volume 1 — Proceedings of the Navy/DARPA Fourth Technical Interchange Meeting, 25-27 March 1980

31 July 1980

Prepared for
PME 117
NAVELEX 310
ONR 220
DARPA DEO

Approved for public release; distribution unlimited

NAVAL OCEAN SYSTEMS CENTER
SAN DIEGO, CALIFORNIA 92152

NAVAL OCEAN SYSTEMS CENTER, SAN DIEGO, CA 92152

AN ACTIVITY OF THE NAVAL MATERIAL COMMAND

SL GUILLE, CAPT, USN
Commander

HL BLOOD
Technical Director

ADMINISTRATIVE INFORMATION

The 25-27 March 1980 Navy/DARPA Technical Interchange Meeting on the Strategic Laser Communications Program was arranged under NOSC Work Unit CM06 by members of the Strategic Laser Communications Program Office (Code 8105) for PME 117, NAVELEX 310, ONR 220, and DARPA DEO. This document is a compilation of the unclassified papers presented at the meeting and was approved for publication 31 July 1980.

Released by
CA Nelson, Head
Long Range Plans and
Policy Office

Under authority of
HD Smith, Head
Communications Systems and
Technology Department

UNCLASSIFIED

SECURITY CLASSIFICATION OF THIS PAGE (When Data Entered)

(14) NOSC/TD-352-Vol 1

REPORT DOCUMENTATION PAGE

READ INSTRUCTIONS BEFORE COMPLETING FORM

1. REPORT NUMBER: NOSC Technical Document 352 Vol 1	2. GOVT ACCESSION NO.: AD A091619
3. RECIPIENT'S CATALOG NUMBER: (4)	
4. TITLE (and Subtitle): (6) STRATEGIC LASER COMMUNICATIONS PROGRAM. Volume 1, Proceedings of the Navy/DARPA Fourth Technical Interchange Meeting, 25-27 March 1980	5. TYPE OF REPORT & PERIOD COVERED: Technical document
	6. PERFORMING ORG. REPORT NUMBER:
7. AUTHOR(s):	8. CONTRACT OR GRANT NUMBER(s):
9. PERFORMING ORGANIZATION NAME AND ADDRESS: Naval Ocean Systems Center, San Diego, CA 92152	10. PROGRAM ELEMENT, PROJECT, TASK AREA & WORK UNIT NUMBERS: NOSC CM06
11. CONTROLLING OFFICE NAME AND ADDRESS: Naval Electronic Systems Command (NAVELEX 310), Washington, DC 20360	12. REPORT DATE: (11) 31 July 1980 13. NUMBER OF PAGES: 646
14. MONITORING AGENCY NAME & ADDRESS (if different from Controlling Office): (12) 631	15. SECURITY CLASS. (of this report): Unclassified 15a. DECLASSIFICATION/DOWNGRADING SCHEDULE:

16. DISTRIBUTION STATEMENT (of this Report)

Approved for public release; distribution unlimited

Volume 2 is available to qualified requestors.

17. DISTRIBUTION STATEMENT (of the abstract entered in Block 20, if different from Report)

18. SUPPLEMENTARY NOTES

19. KEY WORDS (Continue on reverse side if necessary and identify by block number)

Strategic communications
Optical communications
Laser communications
Submarines

20. ABSTRACT (Continue on reverse side if necessary and identify by block number)

Compilation of papers presented at TIM IV of the Strategic Laser Communications Program, held at NOSC. Objective of the program is to determine the practicality and suitability of an optical solution to strategic communications to submerged submarines.

DD FORM 1 JAN 73 1473 EDITION OF 1 NOV 65 IS OBSOLETE
S/N 0102-LF-014-6601

UNCLASSIFIED

SECURITY CLASSIFICATION OF THIS PAGE (When Data Entered)

AD L59

FOREWORD

This document is a compilation of material presented at the Fourth Technical Interchange Meeting (TIM IV) of the Strategic Laser Communications (SLC) Program held at NOSC 25-27 March 1980. The meeting was sponsored by the Naval Electronic Systems Command, the Defense Advanced Research Projects Agency, Directed Energy Office, and the Office of Naval Research. The SLC Program addresses the practicality and suitability of an optical solution for transmitting strategic information to submerged submarines. The purpose of the meeting was to assemble present and potential program contributors to exchange information on recent progress in each of the following areas:

- System engineering
  - Space-based laser concept
  - Earth-based laser concept
    - Single-bounce approach
    - Double-bounce approach
- Threat definition/System vulnerability
- Channel characterization
  - Propagation characteristics
  - Climatology and oceanic property statistics
- Subsystem technology
  - Lasers (eg XeCl, HgBr)
  - Downconversion techniques
  - Filters

Many of the illustrations are inferior copies of Vugraphs and photographs, but they were the only copies available at the time of printing.

The NOSC point of contact for the Strategic Laser Communications Program is LB Stotts, Code 8105, telephone (714) 225-7245 (commercial) or 933-7245 (Autovon).

CONTENTS
(In order of conference presentation)

CONTENTS (Continued)

INTRODUCTION

PROGRAM OVERVIEW

by

LB Stotts
NOSC

NOSC

NAVY/DARPA

STRATEGIC BLUE-GREEN OPTICAL COMMUNICATIONS PROGRAM

TECHNICAL INTERCHANGE MEETING

08262

NOSC

STRATEGIC BLUE/GREEN OPTICAL COMMUNICATIONS PROGRAM

- Sponsors: PME 117, NAVELEX 310, ONR 220, DARPA STO
- Technical Advisor: NOSC
- Objective: Determine practicality and suitability of an optical solution to strategic communications to submerged submarines
- Approach:
  - Resolve uncertainties in the transmission channel
  - Determine and/or develop realistic component capabilities
  - Define strategic submarine operational requirements
  - Define various communication system concepts to be pursued
  - Assess their projected performance levels relative to operational requirements
- Major program task areas to reduce uncertainty:
  - Operational requirements and threat definition analysis
  - Communications systems engineering
  - Channel characterization
  - Subsystem technology
  - Systems demonstrations and experiments

08261

NOSC

SUMMARY OF CRITICAL ISSUES

Components

1. Laser TX
   (a) Energy per pulse
   (b) Efficiency
   (c) Lifetime
   (d) Color
2. Receiver
   (a) Filter narrow bandwidth, wide field of view
   (b) Optics-transmission efficiency, area
   (c) Detector-sensitivity, gain, area, quantum efficiency, noise factor
3. HEL Space mirror and adaptive optics

Modeling

1. Cloud
   (a) Bulk loss
   (b) Spatial spreading
   (c) Time dispersion
2. Water loss off zenith
3. Optimum detection of photons in an angular/ temporal dispersive channel in the presence of background

Propagation Availability

1. Water loss worldwide
2. Cloud losses/ occurrences
3. Noise variations
   (a) Bioluminescence
   (b) Short term loss variation
4. Turbulence statistics worldwide

08256

NOSC

NAVY/DARPA BLUE-GREEN LASER PROGRAM

SPACE-BASED LASER

- Objective

  Demonstrate laser performance by 1985
  - Power—200-1000 watts (100-300 pps)
  - System efficiency > 1%
  - Run time—10^{10} shots

- Approach

  Three-phase main program thrust
  - Phases I & II—200 watt breadboard for two candidates—FY82
  - Phase III—200-1000 watt brassboard—FY85

  Technology program

08268

NOSC

XeCl FREQUENCY SHIFTED LASER

- Status

  Wavelength—308 nm raman shifted to
  459—Pb vapor
  499—H_2
  Single pulse energy—5 j (x-ray pre-ionized)--UCSD
  Efficiency (capacitor store) XeCl--1.4%—UCSD
  Converter—50% Pb at 25 mJ—NRL
  Bandwidth—XeCl:Pb < 0.05A—NRL
  Repped pulse—55 W at 600 pps—LLL

- Current programs

  XeCl kinetics—NRL
  Molecular conversion—NRTC
  X-ray pre-ionization—UCSD
  Pb conversion at 1-2J—NRL/UCSD
  Repped pulse—100 pps/.1J—NRL

NOSC

HgBr LASER

- Status

  Wavelength—439-502 nm
  Single pulse energy—100 mJ (UV preionized)—NOSC
  Efficiency (capacitor store)—1% (at 60 mJ)—NOSC
  Bandwidth—1A (low efficiency)—NOSC
  Repped pulse—1 pps, 10's of seconds—NOSC

- Current programs

  E-beam sustained discharges—UTRC
  Pre-ionization techniques—MSNW, Westinghouse
  Rep-rate testing—NOSC
  Modeling—NRL, UTRC, Kansas State

C8267

NOSC

GROUND-BASED BLUE-GREEN LASER CANDIDATES

Molecular freq. shifted XeCl or XeF via H_2/D_2 — 450-500 nm

XeF—20% at 20 mj

Resonantly pumped Tm:YLF (XeF)—453 nm

Photolytically pumped Xe_2Cl— tunable 470-520 nm

Photolytically pumped XeF(C-A)—tunable 460-500 nm

Atomic freq. shifted XeCl via Pb—459 nm

20% at 1j

08260

NOSC

STRATEGIC BLUE-GREEN OPTICAL COMMUNICATIONS DOWNLINK EXPERIMENT

OBJECTIVE: DEVELOP AND CONDUCT AN AIRCRAFT-(MEDIUM ALTITUDE)-TO-SUBSURFACE COMMUNICATIONS EXPERIMENT DESIGNED TO SIMULATE STRATEGIC SUBMARINE COMMUNICATIONS IN AN OPERATIONAL ENVIRONMENT.

KEY ISSUES TO BE ADDRESSED:

- PERFORMANCE OF ASYNCHRONOUS PIM IN A HIGH BACKGROUND, DISPERSIVE TRANSMISSION CHANNEL
- ASSESSMENT OF CRITICAL SIGNAL DEGRADATION EFFECTS BY THE CHANNEL
- PERFORMANCE OF CLOUD SENSING DEVICES IN SIMULATED ADAPTIVE SCAN MODE.

NOSC

BIREFRINGENT (LYOT) FILTER (LOCKHEED)

Objective

- Develop large aperture, narrowband, wide FOV, blue-green filter for SLC
- Program goal: 30 cm diameter, 0.1 nm, ± 30°

Background

- Lyot filter technology well developed
  - Flown on Spacelab 1
  - Given material characteristics, performance predictable with high accuracy
- Crystal birefringent materials not suitable for large aperture, 0.1 nm filters
- Must develop large plastic birefringent components
  - Small tunable all-plastic filter already produced

Status

- Foster-Grant PVA identified as 10" filter material
  - Large area, 100-sheet lamination techniques developed
- Extend technology to Mylar in FY80
  - Highly birefringent
  - Sub-angstrom bandwidths possible

08255

NOSC

NARROWBAND FILTER/RECEIVER DEVELOPMENT (MDAC)

Objective

- Develop wide FOV, sub-angstrom bandwidth blue-green filter technology

Approaches

- Atomic resonance absorption and fluorescence filter
  - Bandwidth .01-.001 nm
  - Potentially scalable to large aperture
- Spectral hole burning filter
  - Transmission wavelength and bandwidth controliable
  - Basic physical process not fully understood

Status

- Preliminary atomic resonance filter design completed
  - Materials, coatings, reasonable configuration identified
  - Cs device → 31% effective transmission, 32 μsec pulse stretching @ 455 nm
- Hole burning filter cryogenics requirements roughly defined
  - 7 kw, 1300 kg refrigerator/container required for liquid helium temp.

08257

NOSC

LIGHT PROPAGATION THROUGH CLOUDS (SYLVANIA)

Objective

- Experimentally characterize optical attentuation and pulse stretching produced by thick clouds

Approach

- Project diverging pulsed laser beam from aircraft at 40,000 ft.
  Spot diameter = 6km
  Cloud altitude = 3km — Simulates satellite transmitter
  Detect and analyze using 6-inch-diameter pm on ground
- Determine cloud optical thickness via
  Knollenberg on second aircraft
  530 nm irradiance measurements on ground

Status

- Experiment completed
  18 flights, 325 passes, 30 data points/pass
- 22 μsec pulse stretching observed
- Double exponential decay observed; not understood
- Finite area cloud model needed

08265

NOSC

LOW LIGHT LEVEL TELERADIOMETER (HSS)

Objective

- Provide simple means for measuring cloud optical thickness
- Relate measured optical thickness to observed laser pulse stretching

Approach

- Design, fabricate, deliver two channel low light level teleradiometer
- Measure moonlight, through cloud, at wavelengths in and outside O_2 absorption band
- Determine optical path length from relative attenuation, known path absorption characteristics

Status

- Successfully participated in Kauai experiment
  117 simultaneous teleradiometer/laser runs
- Data reduction underway
  Good qualitative agreement with laser measurements
  Moon-light and laser-light received through different clouds
- Model refinement and deployable instrument design in FY80

08264

NOSC

BLUE-GREEN PULSE PROPAGATION THROUGH FOGS/CLOUDS (NOSC)

Objective

- Experimentally determine effect of medium-dense clouds on pulsed optical propagation
- Compare results to theory
- Analyze impact upon satellite-to-sub optical communication

Approach

- Measure laser beam attenuation through coastal fog over 1-2.4 km paths
  - Characterize fog through Knollenberg measurements
- Perform low-medium density cloud measurements on Kauai

Status

- Measurements made for fog paths of medium optical density
  - Losses 20 dB smaller than predicted by diffusion theory
  - Scattering predominately less than 2°
  - Pulse stretching less than few hundred nsec
  - Knollenberg data taken; reduction underway
- Analysis of Kauai data underway

08263

NOSC

OPTICAL CHANNEL MODELING (PSR)

Objective

- Develop analytic model for optical propagation from satellite through clouds, to sea surface

  Ray directions at cloud bottom
  Attenuation
  Pulse stretching

- Compare model predictions with experimental results

Status

- Model completed
- Comparison with cloud propagation experimental results in FY80

08266

NOSC

OPTICAL CLIMATOLOGY (MDAC)

Objective

- Provide global data base of cloud optical thickness occurrence statistics
- Allow accurate optical link availability estimates for strategically important locations

Approach

- Obtain cloud statistics from 3D NEPH tapes
- Use existing model/code to estimate statistics of optical/physical thickness

Progress

- Data generated for 50 locations uniformly spaced over op area
- Data accurately represented by polynomial curves
- Variations with latitude, longitude, and season established

Plans

- Refine temporal and spacial resolution
- Establish spacial correlation statistics
- Expand model to treat clouds of finite lateral extent

08252

NOSC

OCEAN OPTICAL PROPERTIES (SIO)

Objective

- Develop data base and model for optical properties of large ocean areas

Approach

- Develop Technique for determining surface K from NIMBUS G CZCS data
- Develop model to calculate depth dependence of K from surface value
- Develop required instrumentation and perform ground-truth measurements
- Establish worldwide ocean optical property data bank

Status

- Surface K algorithm developed; to depth extrapolation initiated
- Four ground-truth cruises completed
- Comparison of algorithm predictions with ground-truth underway
  - 20% accuracy anticipated
  - 20 entry comparison table due end of February
- Data storage/retrieval system development initiated

08253

NOSC

NEW FY80 STARTS

Diffuse optical propagation

Objective: Determine angle/depth dependence of signal beam diffusion

Background: Degree diff. → receiver FOV, Eff. water range

Approach: Measure solar radiance Vrs. depth using digital camera

XeCl laser/Cs filter system

Objective: Establish compatibility Pb-XeCl laser/Cs filter

Background: Pb-XeCl laser leading space-based candidate
Cs filter → 31% Eff. Trans., Sub-Ang. bandwidth

Approach: Tune/frequency-narrow laser to match filter
Pressurize filter Gas to broaden pass band, reduce pulse stretching

08255

NOSC

BACKGROUND BIOLUMINESCENCE

Objective:	Characterize SLC background bioluminescence noise
Background:	Biolum, can dominate at night; stimulated by sub. motion Temporal char., occurrence statistics unknown
Approach	Literature survey, laboratory exps., ?? Workshop Feb 25-29

RECEIVER STUDY

Objective:	Address system aspects of sub. receiver
Background:	PMT's for blue-green detection available Filter technology dev. underway
Approach:	Study transmitter system concepts and SSBN environment Design receiver system; state-of-the-art technology Exper. verify untested concepts/subsystem designs

08270

NOSC

Cloud propagation data analysis

Objective:	Obtain max. info. from Kauai cloud prop. experiment
Background:	Five simultaneous experiments; three organizations
	Careful data correlation necessary
Approach:	Collect/analyze all data
	Compare with navy model predictions
	Expand model if necessary

Nonclassical noise

Objective:	Characterize underwater optical fluctuation noise
Background:	Shot-noise on D.C. optical background considered so far
	Variable cloud cover, surface waves, etc → fluctuations
Approach:	Measure background fluctuation spectrum with fast irradiance receiver

NOSC

SUBMARINE BACKGROUND MEASUREMENT

Objective: Characterize optical noise under sub. operational conditions

Approach: Irradiance detector on submarine
Scope problems
Design detection system
Fabricate and test sensor

NOSC

APPROACH TO AN AIR-TO-SUBSURFACE COMMUNICATION EXPERIMENT

- OBTAIN A 0.5-1.0 JOULE/PULSE, 100 PPS AIRBORNE TRANSMITTER
  - — OPTIONS: (a) USC ODACS LASER/AIRPLANE
    (b) DEVELOP A DOWN-CONVERTED XeCl HgBr LASER/AIRBORNE PLATFORM
    (c) TBD
- DEVELOP AN UNDERWATER NARROWBAND, ASYNCHRONOUS PIM RECEIVER AND INTEGRATE INTO A TACTICAL/RESEARCH SUBMARINE
- DEVELOP TEST PLAN AROUND ABOVE TO MEET EXPERIMENTAL OBJECTIVE
- FIELD WITH NECESSARY SUPPORT AND CHANNEL CHARACTERIZATION EQUIPMENT

02251

NOSC

GEOMETRY OF A STRATEGIC BLUE-GREEN OPTICAL COMMUNICATIONS DOWNLINE EXPERIMENT

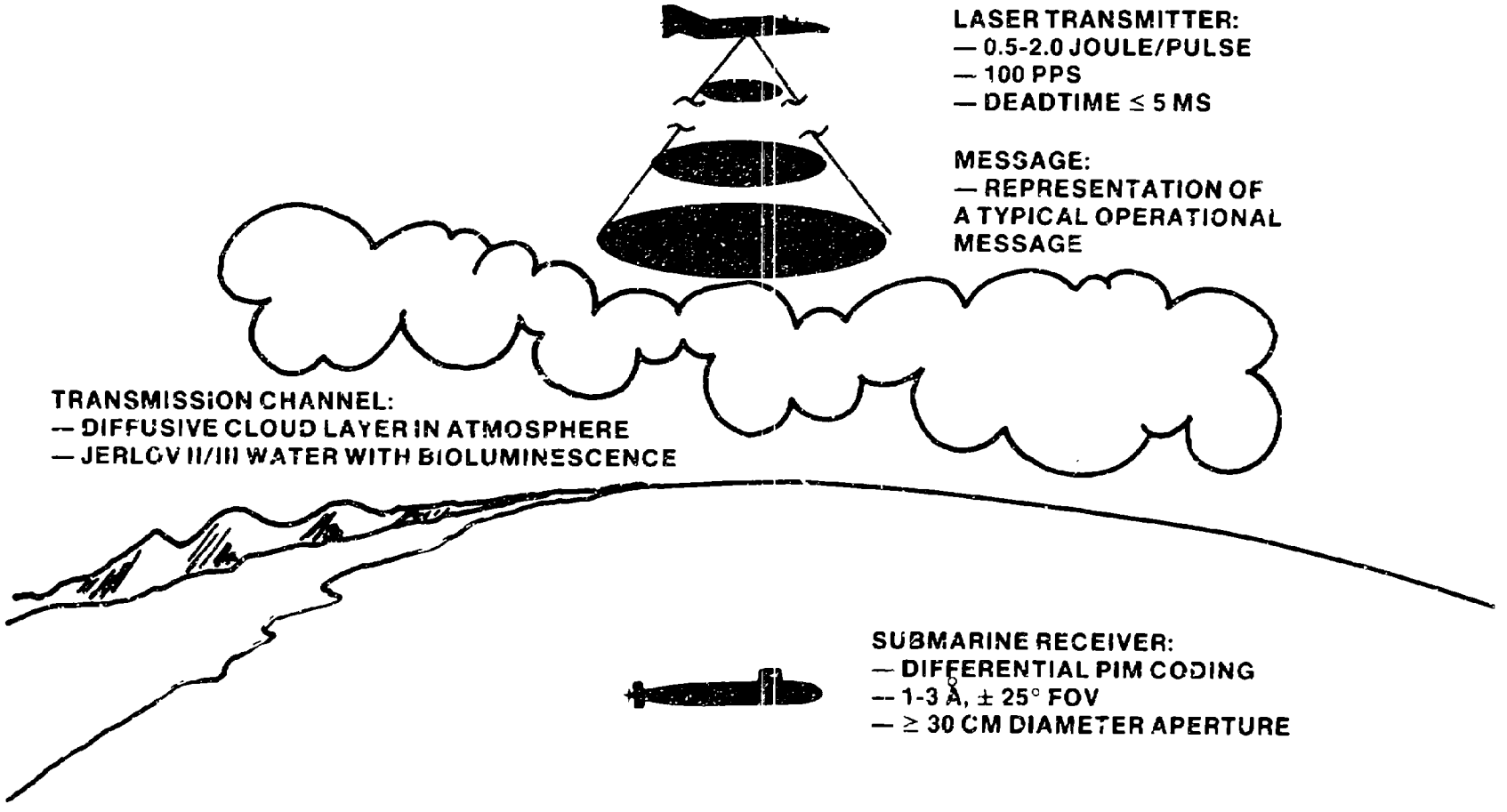

LASER TRANSMITTER:
— 0.5-2.0 JOULE/PULSE
— 100 PPS
— DEADTIME ≤ 5 MS

MESSAGE:
— REPRESENTATION OF A TYPICAL OPERATIONAL MESSAGE

TRANSMISSION CHANNEL:
— DIFFUSIVE CLOUD LAYER IN ATMOSPHERE
— JERLOV II/III WATER WITH BIOLUMINESCENCE

SUBMARINE RECEIVER:
— DIFFERENTIAL PIM CODING
— 1-3 Å, ± 25° FOV
— ≥ 30 CM DIAMETER APERTURE

08248

SYSTEM ENGINEERING SESSION

Papers 3 and 4 are contained in volume 2.

OSCAR SPACEBORNE SYSTEM: PHASE IB

T. E. FLOM AND P. J. TITTERTON

GTE SYLVANIA

Phase IB of the Optical Submarine Communications by Aerospace Relay (OSCAR) has initially concentrated on two main tasks: test case evaluation and experiment definition.

16 environmental test cases provided by NOSC were used as inputs to the propagation and system models developed in Phase IA, and a system design which met the full system requirements for these 16 cases was developed. The driving factors and sensitivity of the results for these test cases has also been explored.

All critical sub-system, sub-system interfaces, sets, set interfaces and units were identified; and critical experiments were identified and defined.

GTE Sylvania
PO Box 188
Mountain View CA 94042

UNCLASSIFIED

Optical Submarine Communications by Aerospace Relay
Sponsor- Naval Electronics System Command (U)

UNCLASSIFIED

TEST CASE EVALUATION

GTE Systems

BASELINE RESULTS:

SYSTEM REQUIREMENTS MET FOR:

(1) SATELLITE/MOLNIYA COMMUNICATION

(2) $\text{TEST}_{\text{FOM}} = 1600 \text{ BITS} \left(\frac{\text{DATA}}{\text{SECOND}}\right) \left(\frac{\text{TIME POWER}}{\text{AVAILABLE}}\right) \times \left[\frac{\text{RECEIVER OPTICAL JITTER BANDPASS}}{\text{TRANSMISSION}}\right]^{-2}$

(3) TEST CASES AND MODELS EITHER AVAILABLE OR INTERPRETED

TEST CASE EVALUATION
CHANGES FROM PHASE IA TO IB TEST CASES

GTE Systems

MODELS

CHANGE IN BACKGROUND MODELS:

(1) INCREASE SOLAR AND LUNAR RADIANCE AT DEPTH BY X π

(2) INCREASE BLUE SKY RADIANCE AT DEPTH BY X 2.5

DATA BASES

CLOUDS:

MORE, AND MUCH THICKER CLOUDS PRESENT

WATER:

THERMOCLINE AT 50m

DIFFUSE ATTENUATION COEFFICIENT BELOW 50m IS SET TO 2/3 OF ITS VALUE ABOVE 50m

BIOLUMINESCENCE:

ALWAYS PRESENT

Sylvania Systems Group
Western Division

SUN AND MOON LOCATIONS AND CLOUD PROPERTIES FOR 16 TEST CASES (U)

GTE Systems

		SUN		MOON	
		LONGITUDE	LATITUDE	LONGITUDE	LATITUDE
1	A-1	[illegible]	[illegible]	[illegible]	[illegible]
2	A-2	90	[illegible]	[illegible]	5.1
3	A-3	[illegible]	0	0	5.1
4	A-4	270	0	90	5.1
5	A-5	0	23.5	180	28.6
6	A-6	90	23.5	270	28.6
7	A-7	180	23.5	0	28.6
8	A-8	270	23.5	90	28.6
9	A-A	0	0	180	5.1
10	A-7	90	0	270	5.1
11	A-6	[illegible]	0	0	[illegible]
12	A-5	[illegible]	[illegible]	[illegible]	5.1
13	A-4	0	[illegible]	[illegible]	[illegible]
14	A-3	[illegible]	[illegible]	[illegible]	[illegible]
15	A-2	[illegible]	[illegible]	[illegible]	[illegible]
16	A-1	[illegible]	[illegible]	[illegible]	[illegible]

UNCLASSIFIED

Sylvania Systems Group
Western Division

DOWNLINK AVAILABILITY OF OSCAR SYSTEM IN TEST SCENARIOS

GTE Systems

CASE	CLOUD PROPERTIES	SUN LONGITUDE	SUN LATITUDE	SATELLITE POSITION*	AVAILABILITY PACIFIC	AVAILABILITY ATLANTIC	AVAILABILITY OVERALL
1	A-1	[illegible]	[illegible]	0	.996	.617	.93
2	A-2	90	0	6	.684	.635	.663
3	A-3	180	0	12	1.0	1.0	1.0
4	A-4	270	0	18	1.0	.9868	.995
5	A-5	0	23.5	6	.978	.958	.9706
6	A-6	90	23.5	12	.979	1.0	.9867
7	A-7	180	23.5	18	.935	.964	.97
8	A-8	270	23.5	0	.997	.964	985
9	A-9	0	0	12	.969	1.0	.98
10	A-10	90	0	18	.991	.966	.9765
11	A-11	180	0	0	1.0	1.0	1.0
12	A-12	270	0	6	.989	1.0	.9935
13	A-13	0	-23.5	18	1.0	.9864	.995
14	A-14	90	-23.5	0	1.0	1.0	1.0
15	A-15	180	-23.5	6	.967	.928	.956
16	A-16	270	-23.5	12	.949	.956	.951

UNCLASSIFIED

SATELLITE POSITION*	ATLANTIC	PACIFIC
0	1	2
6	1	1
12	2	1
18	1	1

Sylvania Systems Group
Western Division

SYSTEM EFFECTIVENESS

GTE Systems

GROUND STATION:		0.999
UPLINK	:	0.9999
SATELLITE	:	0.987
DOWNLINK	:	0.9229
SUBMARINE	:	0.99
SYSTEM		0.901

DISCUSSION OF DOWNLINK RESULTS

GTE Systems

ENVIRONMENTAL EFFECTS

TIME-OF-DAY DEPENDENCE AND DOMINANT BACKGROUNDS

TEMPORAL ASPECTS

BEAM DIVERGENCE

ALTERNATIVE WIDE PULSE/NARROW SLOT COMPENSATION TECHNIQUE

MASTER CHART

TEST CASES: ORDERING

GTE Systems

CASE NO.	CLOUD PROPERTY NO.	AVAILABILITY
15	A-2	.656
2	A-2	.669
16	A-1	.851
7	A-7	.87
10	A-7	.9165
1	A-1	.93
12	A-5	.9515
5	A-5	.9706
9	A-8	.98
8	A-8	.985
6	A-6	.9867
4	A-4	.995
13	A-4	.995
11	A-6	1.0
14	A-3	1.0
3	A-3	1.0

DAYTIME DOMINANT BACKGROUND NOISE SOURCES

GTE Systems

WATER TYPE	CLOUD OPTICAL THICKNESS		
	0	10	100
IB	SUN FOR $\phi_{SU} \leq 64°$ SKY FOR $\phi_{SU} \geq 64°$	SUN FOR $\phi_{SU} \leq 63°$ SKY FOR $\phi_{SU} \geq 63°$	SUN FOR $\phi_{SU} \leq 75°$ SKY FOR $\phi_{SU} \geq 75°$
II	SUN FOR $\phi_{SU} \leq 56°$ SKY FOR $\phi_{SU} \geq 56°$	SUN FOR $\phi_{SU} \leq 57°$ SKY FOR $\phi_{SU} \geq 57°$	SUN FOR $\phi_{SU} \leq 75°$ SKY FOR $\phi_{SU} \geq 75°$
III	SUN FOR $\phi_{SU} \leq 46°$ SKY FOR $\phi_{SU} \geq 46°$	SUN FOR $\phi_{SU} \leq 49°$ BIO FOR $\phi_{SU} \geq 48°$	SUN FOR $\phi_{SU} \leq 58°$ BIO FOR $\phi_{SU} \geq 58°$

ϕ_{SU} = SOLAR ZENITH ANGLE

JOINT TEST CASE RESULTS

NIGHT TIME:	100% BIOLUMINESCENCE LIMITED
DAWN/DUSK:	61.4% BIOLUMINESCENCE LIMITED
DAY TIME:	14% BIOLUMINESCENCE LIMITED

TEMPORAL EFFECTS

GTE Systems

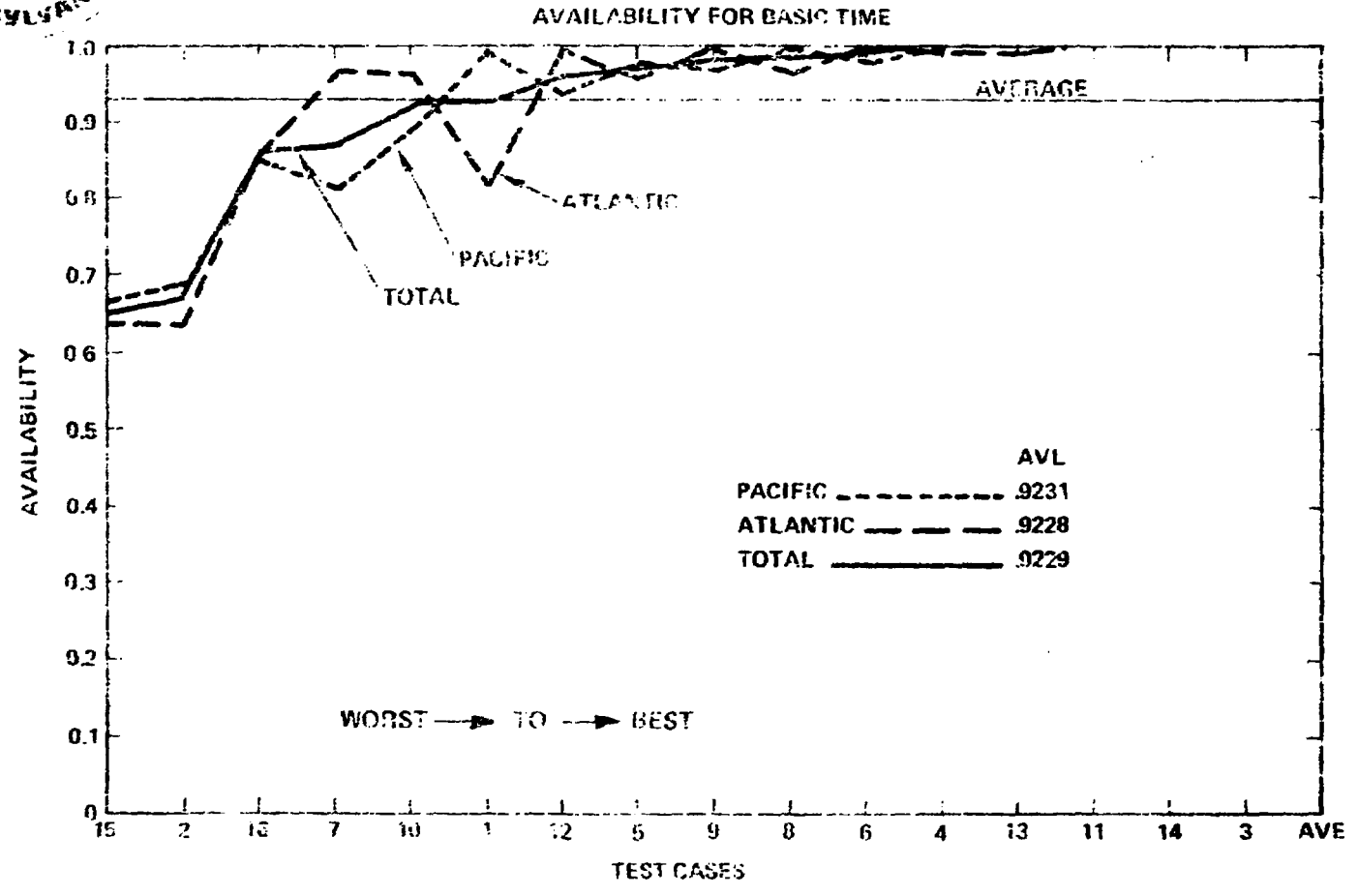

NEGLECT NO. 15 AND NO. 2 ⇨ AVL_{DL} = 0.9601

THE VALIDITY OF THE DATA BASES FOR THE WORST CLOUD CASES ARE OF PRIMARY IMPORTANCE.

GTE Systems

TEMPORAL EFFECTS CONTINUED

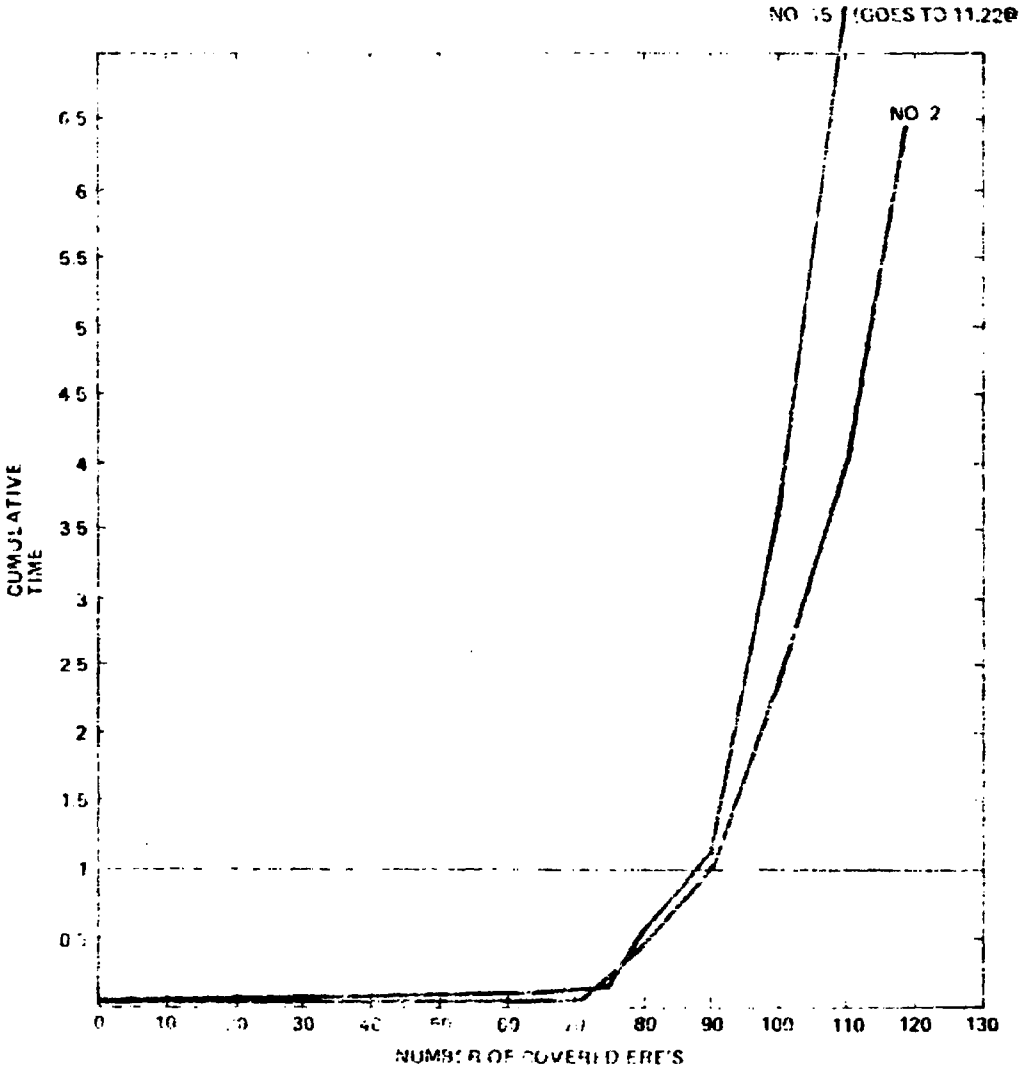

CUMULATIVE TIME TO COVER ERE's PACIFIC CASES 15, 2

Sylvania Systems Group
Western Division

TEMPORAL EFFECTS CONTINUED

GTE Systems

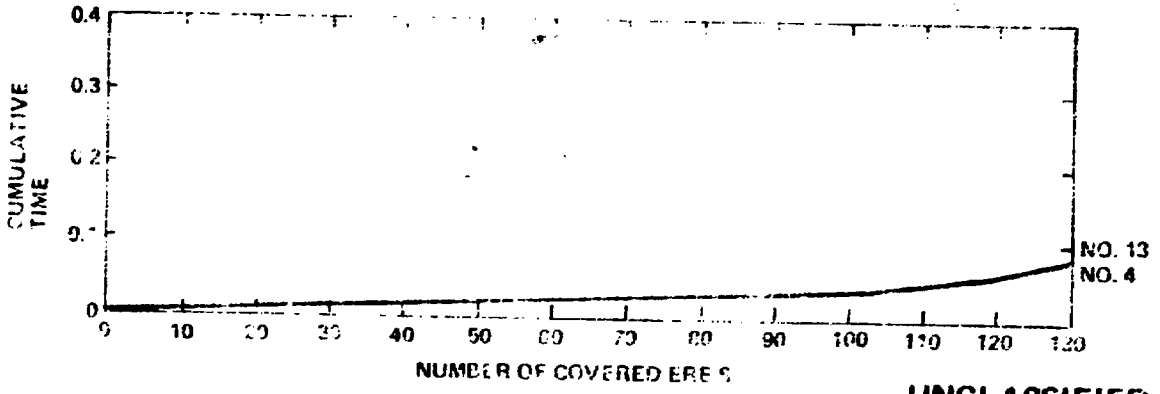

CUMULATIVE TIME TO COVER EREs PACIFIC PASSES 13, 4.

TEMPORAL CONCLUSIONS

GTE Systems

	TOTAL ERE'S COVERED IN REQUIRED TIME	% COVERED IN 1/3 OF REQUIRED TIME, OR LESS
ATLANTIC		
# 2/15	48/48	77%/77% (37)
# 7/10	73/73	82%/82% (60)
# 4/13	76/76	87%/86% (66, 65)
PACIFIC		
# 2/15	90/87	87%/89% (77)
# 7/10	106/116	77%/89% (82, 103)
# 4/13	130/130	100% IN 10% OF REQUIRED TIME

BEAM DIVERGENCE

GTE Systems

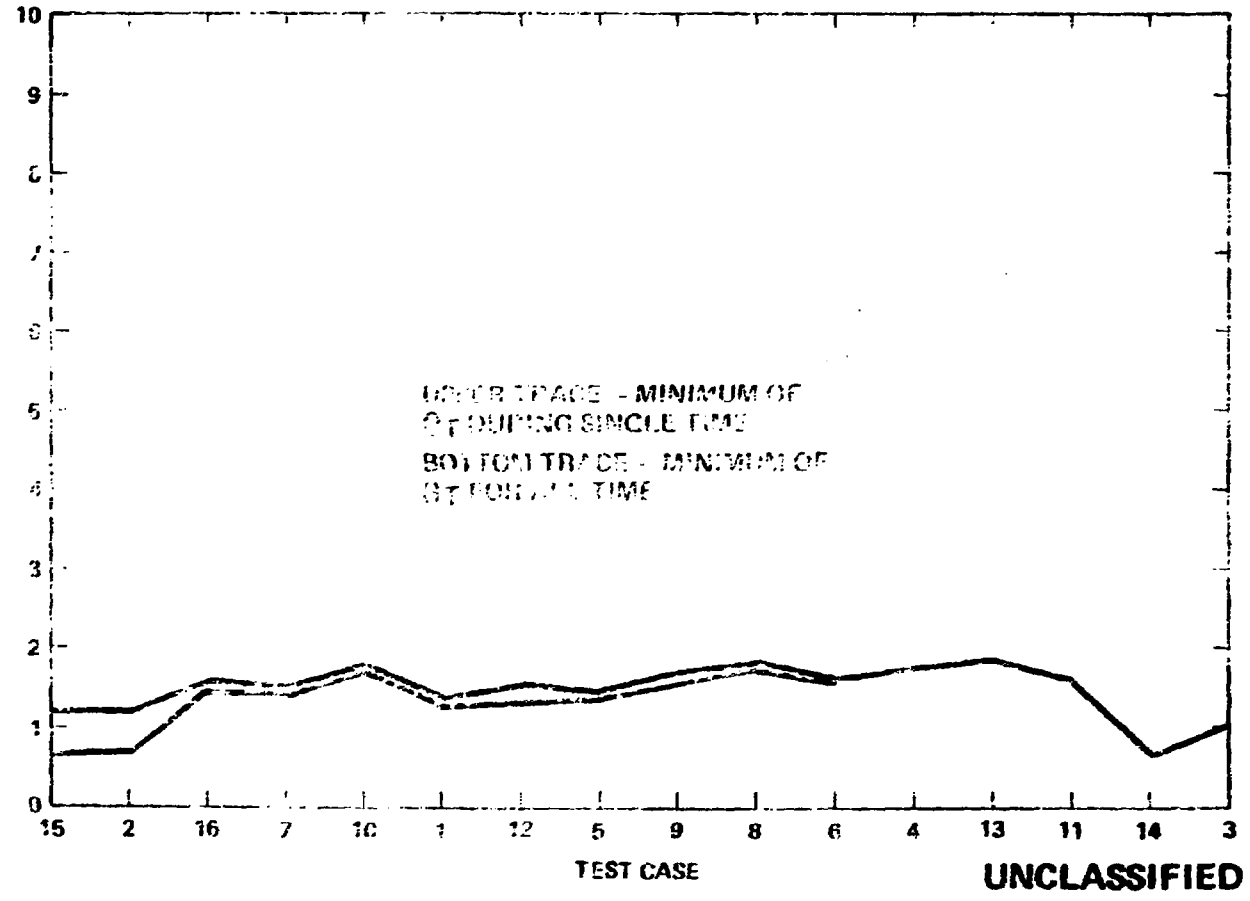

SYSTEM ONLY NEEDS A BEAM DIVERGENCE
CAPABILITY >1 MILLIRADIANS FROM MOLNYA ORBIT

MINIMUM BEAM DIVERGENCE FOR THE TEST CASES

Sylvania Systems Group
Western Division

MAJOR CONCLUSIONS DRAWN FROM 16 TEST CASE EVALUATIONS

GTE Systems

- 3 SATELLITES FOR FULL COVERAGE
- MOST OF BROADCAST AREA CAN BE COVERED IN A FRACTION OF THE REQUIRED DELIVERY TIME
- CLOUD DISTRIBUTION IS THE DOMINANT AVAILABILITY DRIVER
- RELATIVE DAY VERSUS NIGHT PERFORMANCE COMPARISONS CANNOT BE MADE FROM THESE CASES
- SINCE BIOLUMINESCENCE IS THE DOMINANT BACKGROUND SOURCE, A CHANGE IN IT WOULD HAVE THE LARGEST IMPACT OF ANY MODEL CHANGES
- SINCE THE SYSTEM DESIGN IS DRIVEN BY THE WORST CLOUD CASES, THE VALIDITY OF THE WORST CASE CLOUD DISTRIBUTIONS IS OF PRIME IMPORTANCE
- THESE RESULTS CANNOT BE EXTRAPOLATED TO OTHER TEST CASES
- PROPAGATION MODELS AND DATA BASES

FIGURE 23 EACH OF 16 TEST CASE RESULTS

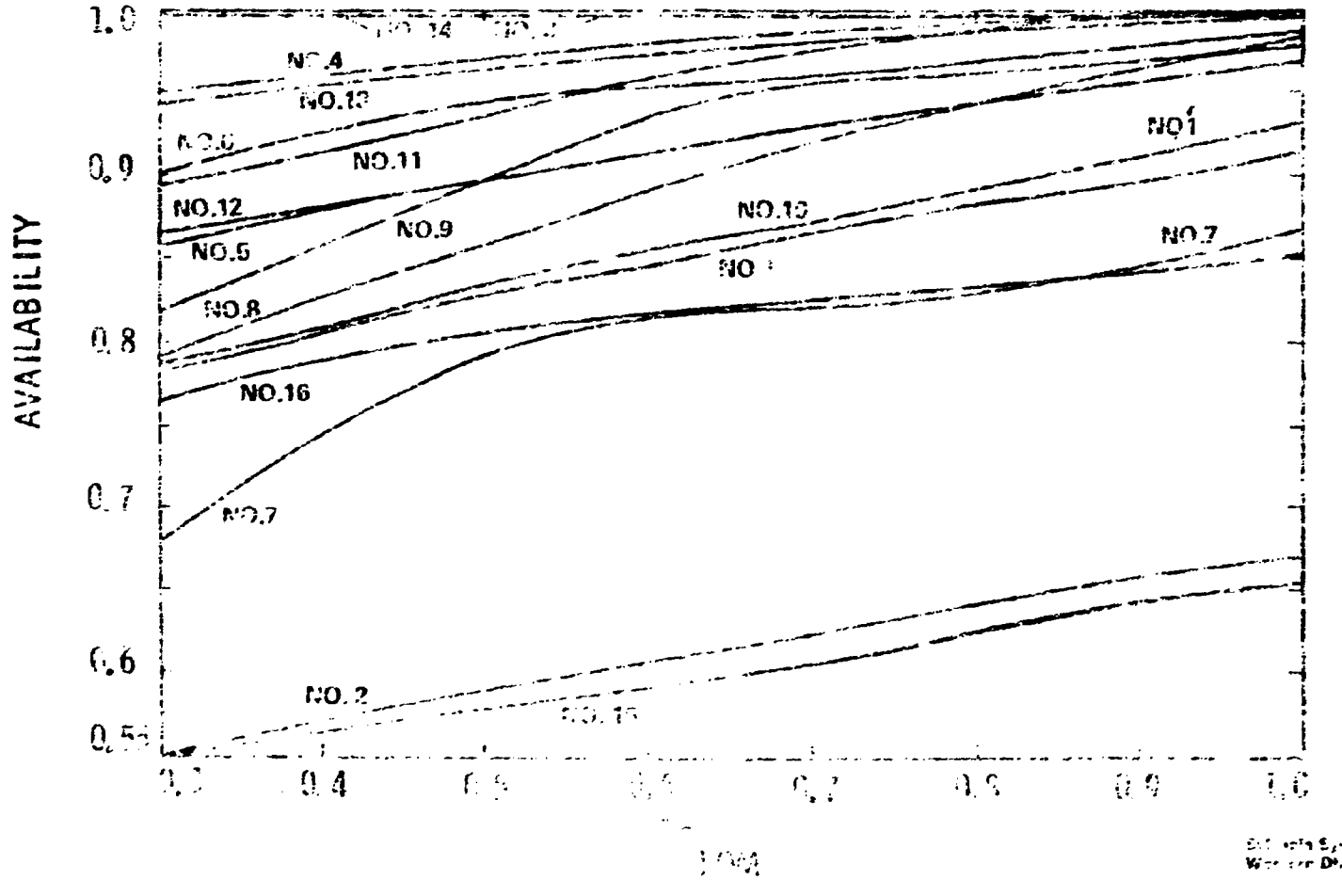

TECHNOLOGY SCALING OF AVERAGED TEST CASE RESULTS

GTE Systems

FIGURE 2b AVERAGE OF 16 TEST CASE RESULTS

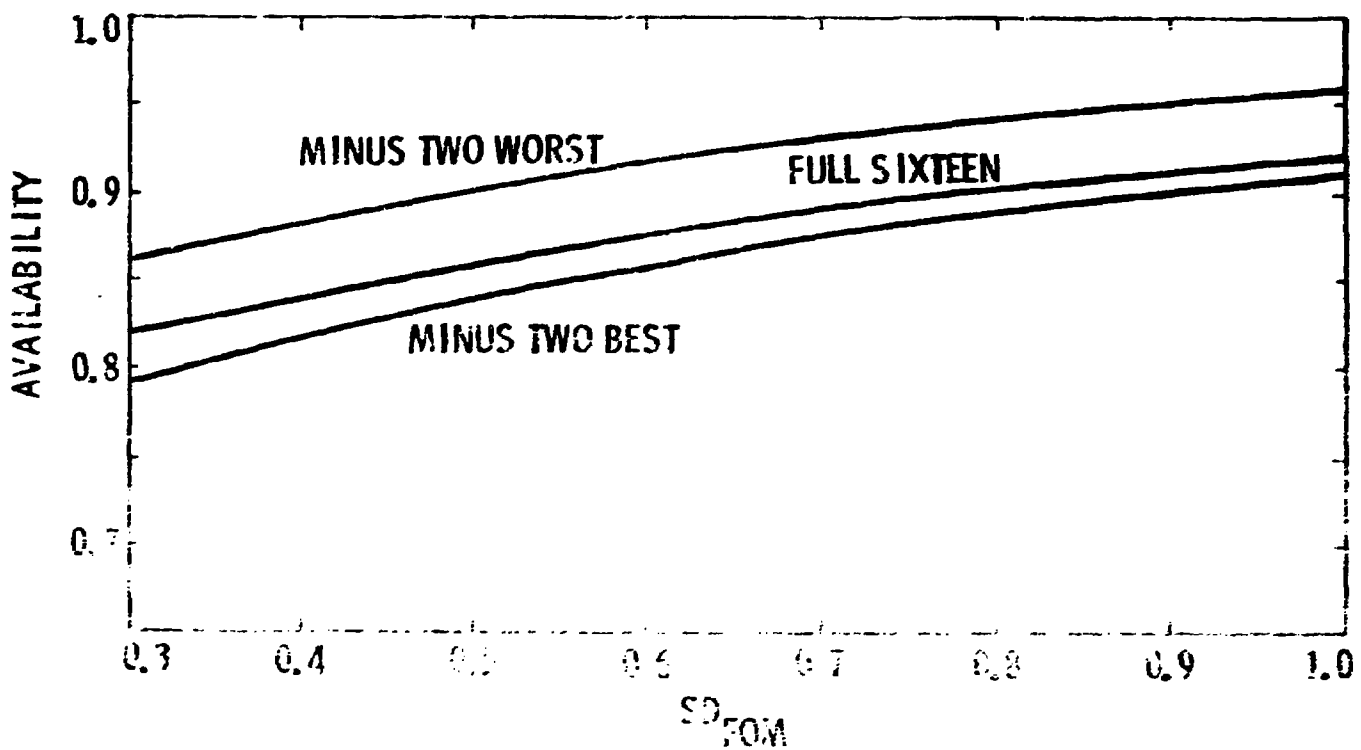

Sylvania Systems Group
Western Division

EXPERIMENT DEFINITION

GTE Systems

- IDENTIFY THOSE AREAS WITH ISSUES REQUIRING EXPERIMENTAL RESOLUTION

- METHOD - EXAMINE OSCAR DESIGN AT SYSTEM, SUB-SYSTEM, SET, SET INTERFACE AND UNIT LEVEL, FOR HIGH RISK/ UNCERTAINTY AREAS. (ALSO CONSIDER CHANNEL CHARACTERIZATION.)

DEFINITION OF RISK CATAGORIES

GTE Systems

CATEGORY	DESCRIPTION
1.	OFF THE SHELF (PRODUCTION COMPONENTS).
2.	STRAIGHTFORWARD DESIGN USING EXISTING TECHNOLOGY.
3.	IS FEASIBLE, BUT REQUIRES ADVANCES NOT YET ACHIEVED.
4.	IS POSSIBLE, BUT REQUIRES SOME FEASIBILITY DEVELOPMENT.
5.	IS POSSIBLE IN PRINCIPLE, ALTHOUGH THERE ARE MANY FEASIBILITY ISSUES.
6.	MAY BE POSSIBLE.

OSCAR EXPERIMENTS

GTE Systems

1. POWER, THERMAL, LASER
2. POINTING, SCANNING, AND BEAM SHAPING
3. MODULATION, DEMODULATION, AND SYNCHRONIZATION
4. OPTICAL RECEIVER
5. DOWNLINK COMMUNICATIONS
6. SATELLITE REMOTE SENSOR
7. SUBMARINE REMOTE SENSOR
8. CHANNEL CHARACTERIZATION

EXPERIMENT DEFINITION METHODOLOGY

GTE Systems

FOR EACH AREA

- OBJECTIVE OF EXPERIMENT
- REQUIREMENTS AND SPECIFICATIONS
- IDENTIFICATION OF KEY ISSUES
- APPROACHES TO MEETING REQUIREMENTS
- TRADE-OFFS AND APPROACH SELECTION
- RECOMMENDED WORK

50

SPACEBORNE LASER EXPERIMENT

GTE Systems

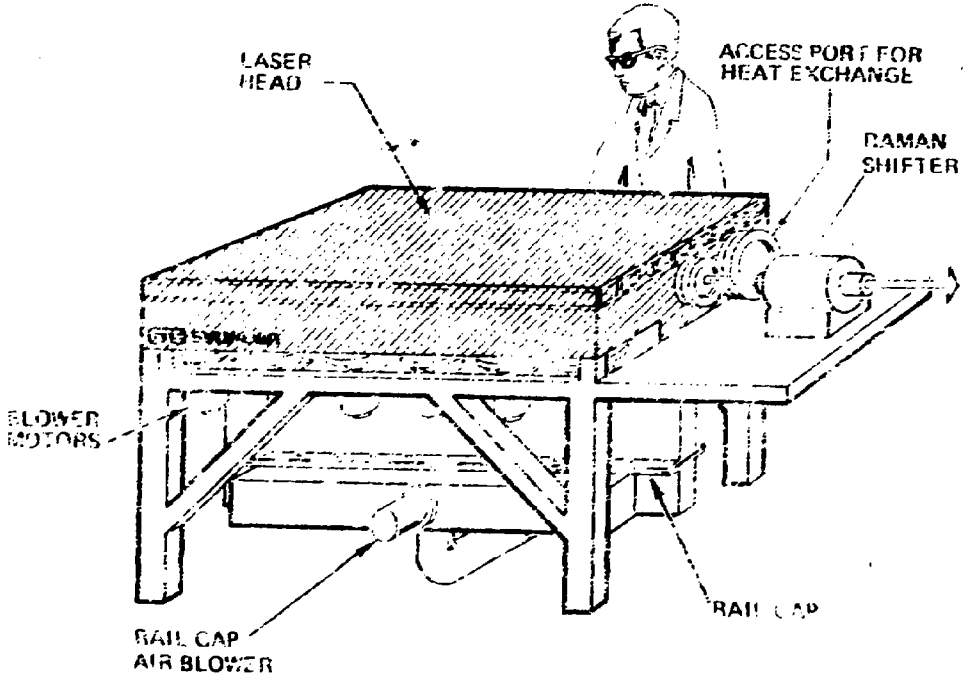

- λ = 440-510 NANOMETERS (BLUE-GREEN)
- $\geq$ 1% EFFICIENCY
- 1-15 JOULES/PULSE
- 50-100 PULSE PER SECOND
- < 1 ANGSTROM LINEWIDTH
- 5 YEAR LIFE
  - GAS CLEAN-UP
  - ELECTRODES AND PREIONIZER
  - POWER AND SWITCHING

UNCLASSIFIED

POINTING, SCANNING AND BEAM SHAPING EXPERIMENT

GTE Systems

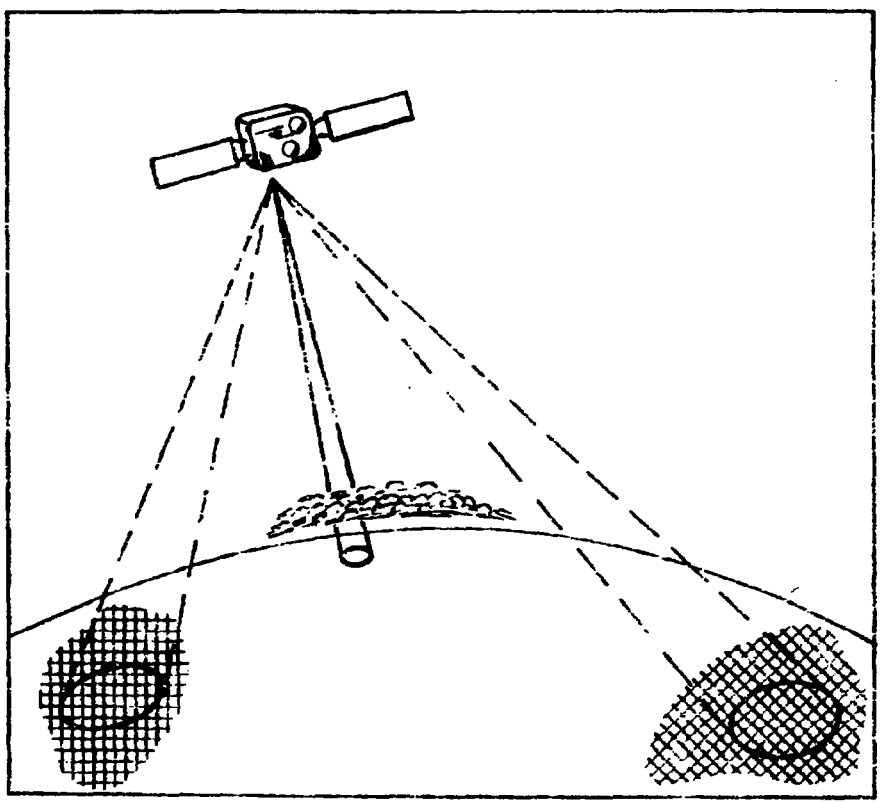

- RANDOM SCAN
- SCAN SPEED
- ADAPT TO PATH LOSSES

MODULATION, DEMODULATION AND SYNCHRONIZATION

GTE Systems

PPM

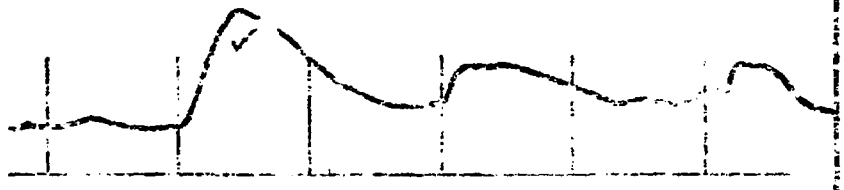

SINGLE PULSE DETECTION--ONE OF 1024 SLOTS
(= 10)

MESSAGE -- YX FRAMES

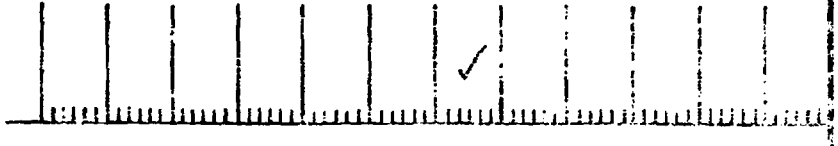

MESSAGE IDENTIFICATION--ONE OF ≈ 2,000
MESSAGE WINDOWS

SINGLE PULSE DETECTION

- PULSE WIDTH/SLOT WIDTH RATIO
- INTEGRATION OR MATCHED FILTER
- MISREGISTRATION SENSITIVITY

MESSAGE ID

- SIGNATURE PULSES ADDED, OR PEAK VALUE SCORING

OPTICAL RECEIVER EXPERIMENT

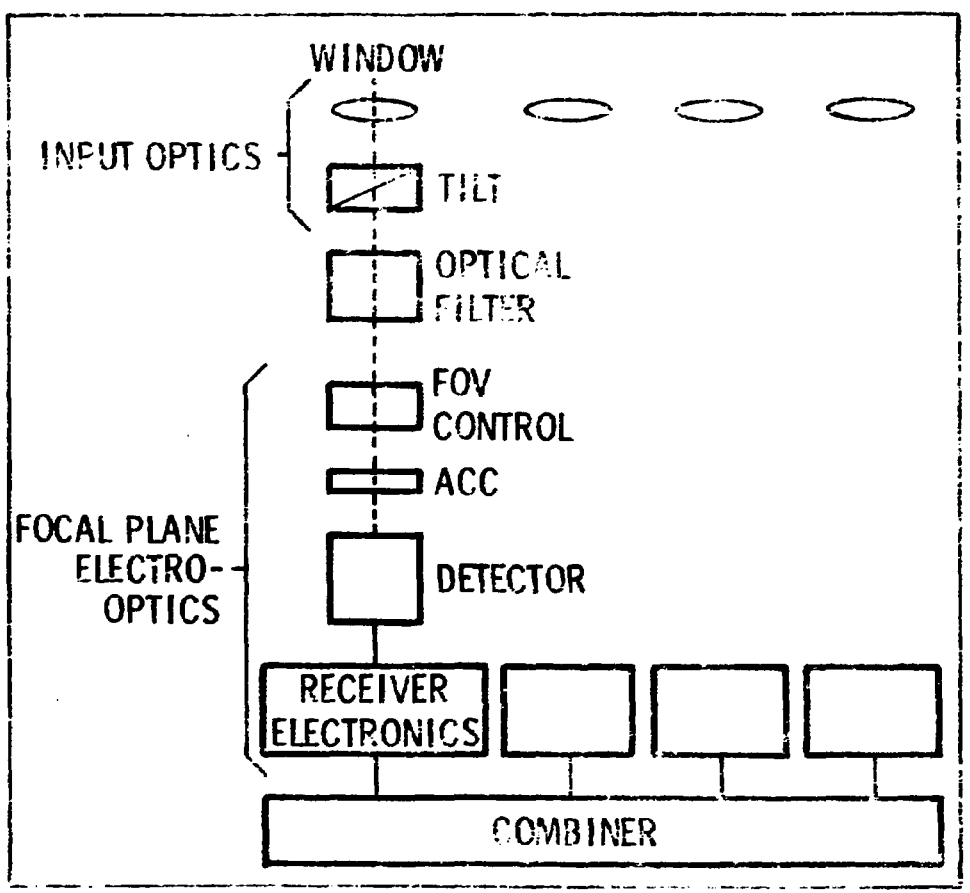

- 0.1 ANGSTROM FILTER BANDWIDTH
- ± 30° FIELD-OF-VIEW
- 1 METER EFFECTIVE APERTURE (SIZE AND LOCATION OF MODULES)
- POINTING
- DETECTOR ACCEPTANCE ANGLE AND PACKING DENSITY

DOWNLINK COMMUNICATION EXPERIMENT

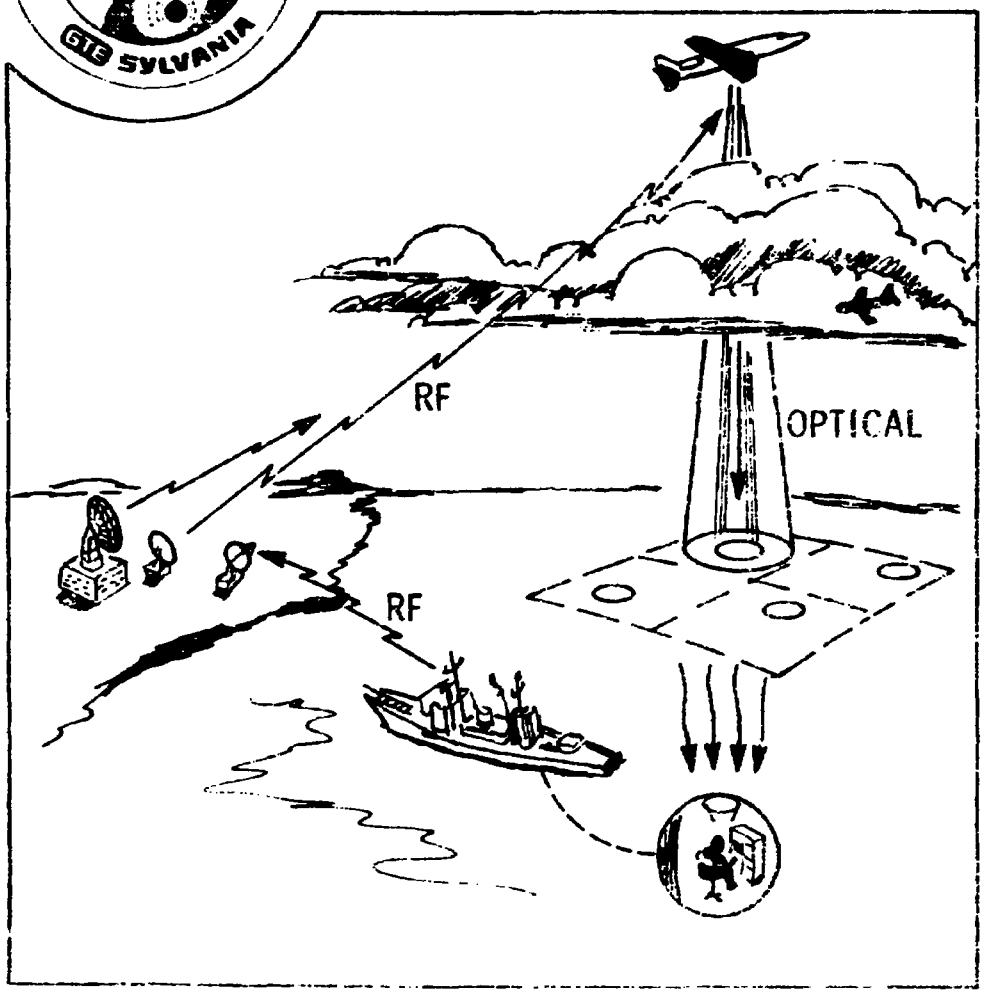

- DETERMINE AND EVALUATE PERFORMANCE OF LASER COMMUNICATION DOWN-LINK IN REALISTIC ENVIRONMENT
  - CLOUDS
  - WATER
  - SUN
  - MOON
  - BLUE SKY
  - BIOLUMINESCENCE

SATELLITE REMOTE SENSOR EXPERIMENT

GTE Systems

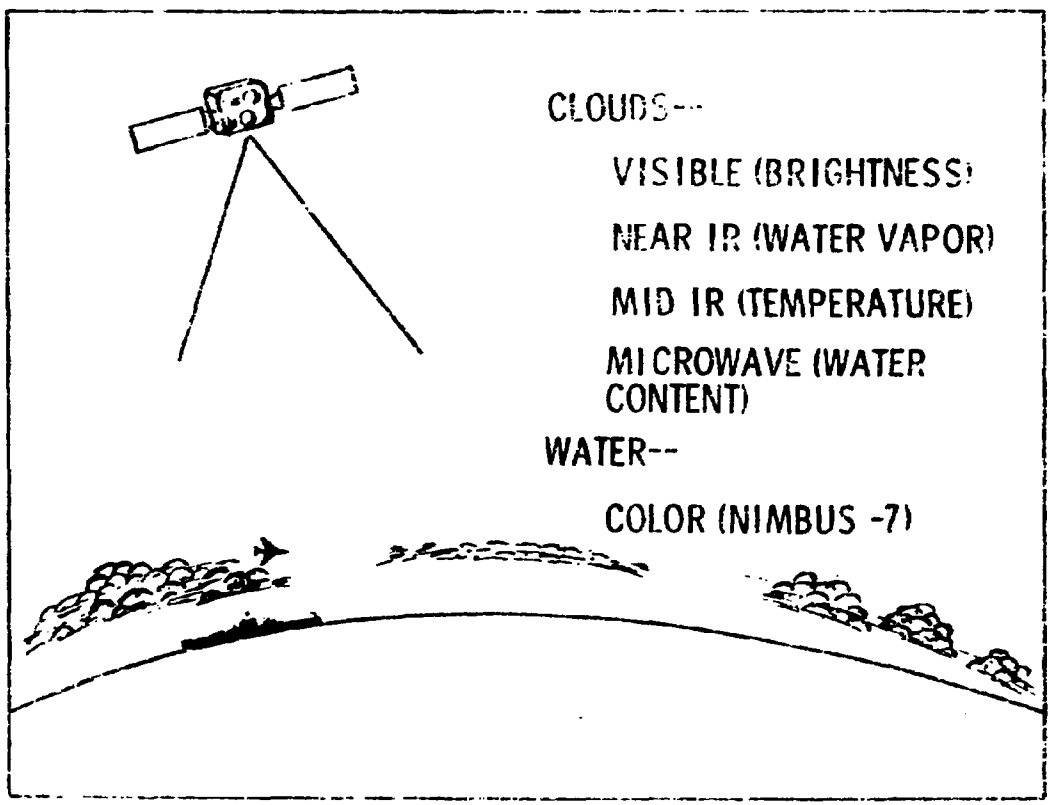

AIRBORNE AND SHIPBORNE MEASUREMENTS

- CLOUDS
  - THICKNESS ~10-30%
  - EXTINCTION COEFF ~20-80%
- WATER
  - ATTENUATION COEFF ~5-20%
  - LAYER THICKNESS ~5-20%
  - BIOLUMINESCENCE ~50-200%

SUBMARINE REMOTE SENSOR EXPERIMENT

GTE Systems

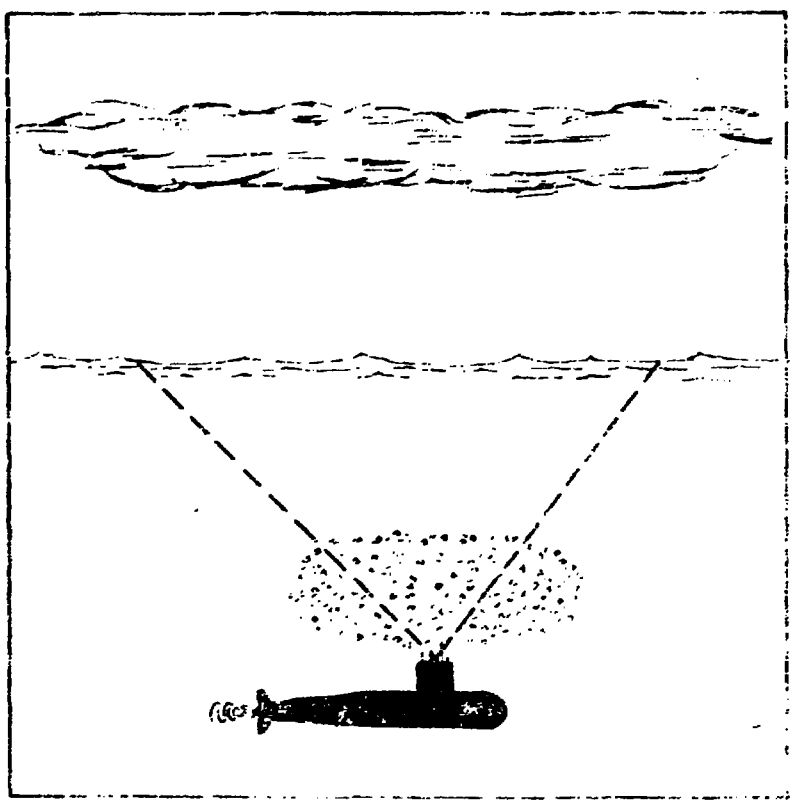

- BIOLUMINESCENCE OBSCURES CLOUD AND WATER MEASUREMENTS

WHAT CAN BE LEARNED FROM PREVIOUS DOWNLINK MESSAGES?

- SHAPE OF PREVIOUS PULSES
- CONTENT--SATELLITE PREDICTS FUTURE CONDITIONS

WHAT IS THE PENALTY FOR NO REMOTE SENSING?

CHANNEL CHARACTERIZATION EXPERIMENTS

GTE Systems

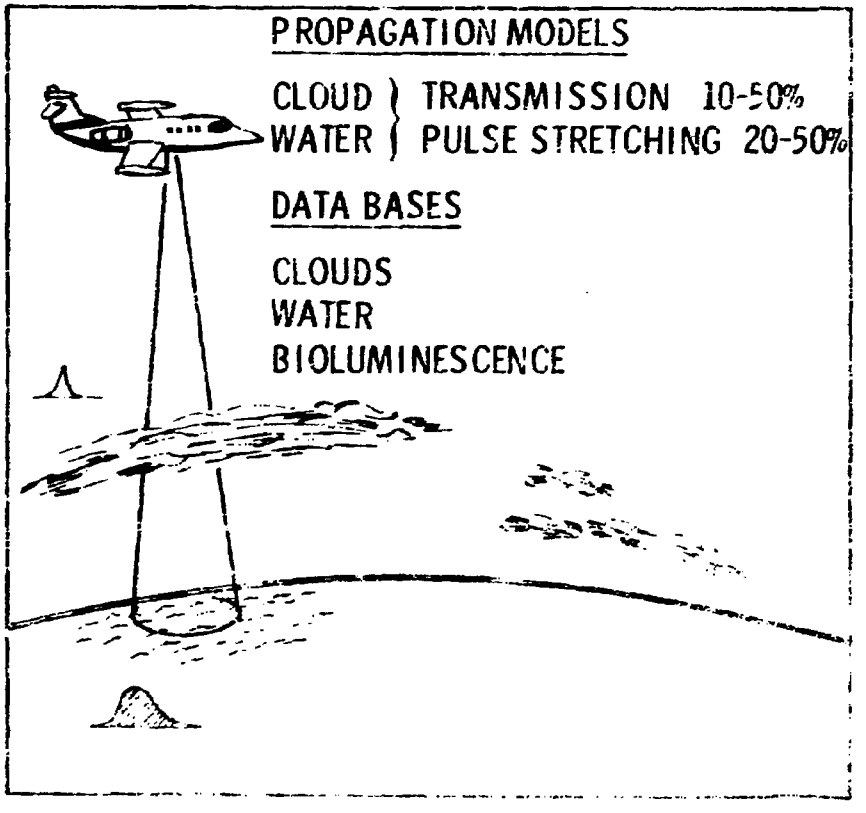

- PROPAGATION MODELS--
  - CLOUDS-- SIG PULSE SHAPE & TRANSMISSION
  - WATER-- SIG PULSE SHAPE & TRANSMISSION FOV AND POINTING
  - COMPLETE PATH-- SUPERPOSTITON OF CLOUD AND WATER EFFECTS
- DATA BASES--
  - CLOUDS-- USE OF RAW 3-D NEPH DATA, AND GROUND TRUTH MEASUREMENTS
  - WATER-- NIMBUS-7 ?
  - BIOLUMINESCENCE--FIELD MEASUREMENTS

SUBSYSTEM TECHNOLOGY SESSION

CESIUM ATOMIC RESONANCE FILTER STUDIES

R. Burnham and B. Wexler
Naval Research Laboratory
Washington, D. C. 20375

SUMMARY

Several aspects of the atomic cesium resonance filter are being studied experimentally to determine its usefulness for strategic blue-green communications. First, the temporal response of the filter is being investigated as a function of pressure broadening on the 459 and 894 nm resonance lines. Calculations indicate that the resonance trapping time on the 894 nm line can be reduced to ~ 1 μsec at reasonable buffer gas pressures. Second, the effect of broadening on the actual filter linewidth is also being measured. Finally, the tunability of the XeCl laser downshifted in Pb vapor is being studied to determine if efficient extraction from this laser can be obtained at the frequency of the 459 nm Cs filter.

NRL – Cs Atomic Resonance Filter Studies

- Filter Wavelength @ 459.3nm
- $0.01 \leq \Delta\lambda \leq 0.1$ Å
- FOV $\simeq 180°$

Issues:

- Matching Filter to XeCl-Pb Laser
- Filter Response Time Vs. Linewidth

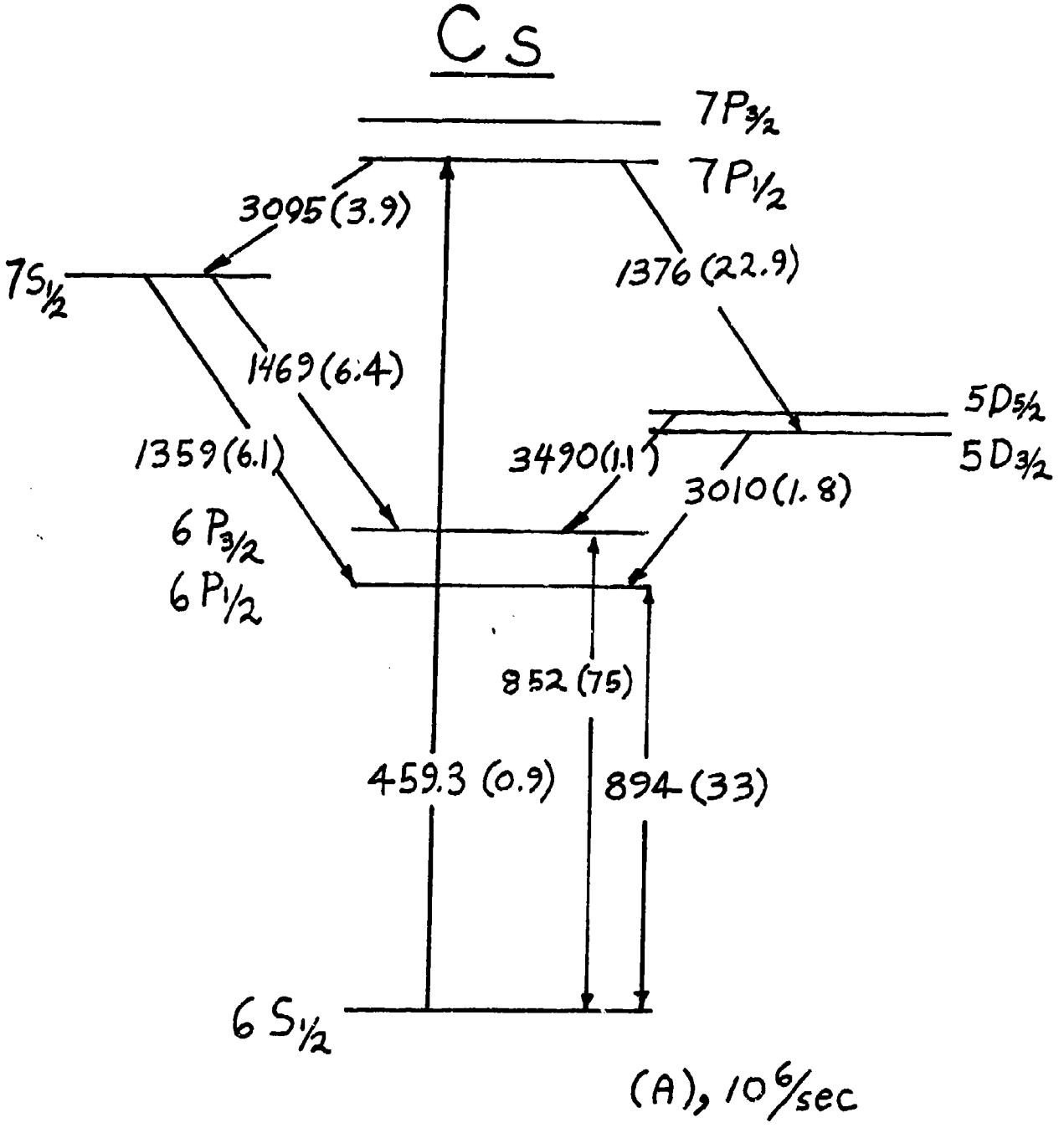
Cs
7P3/2
7P1/2
3095 (3.9)
7S1/2
1376 (22.9)
1469 (6.4)
5D5/2
5D3/2
1359 (6.1)
3490 (1.1)
3010 (1.8)
6P3/2
6P1/2
852 (75)
459.3 (0.9)
894 (33)
6S1/2
(A), 10^6/sec

Schematic of Cs Filter

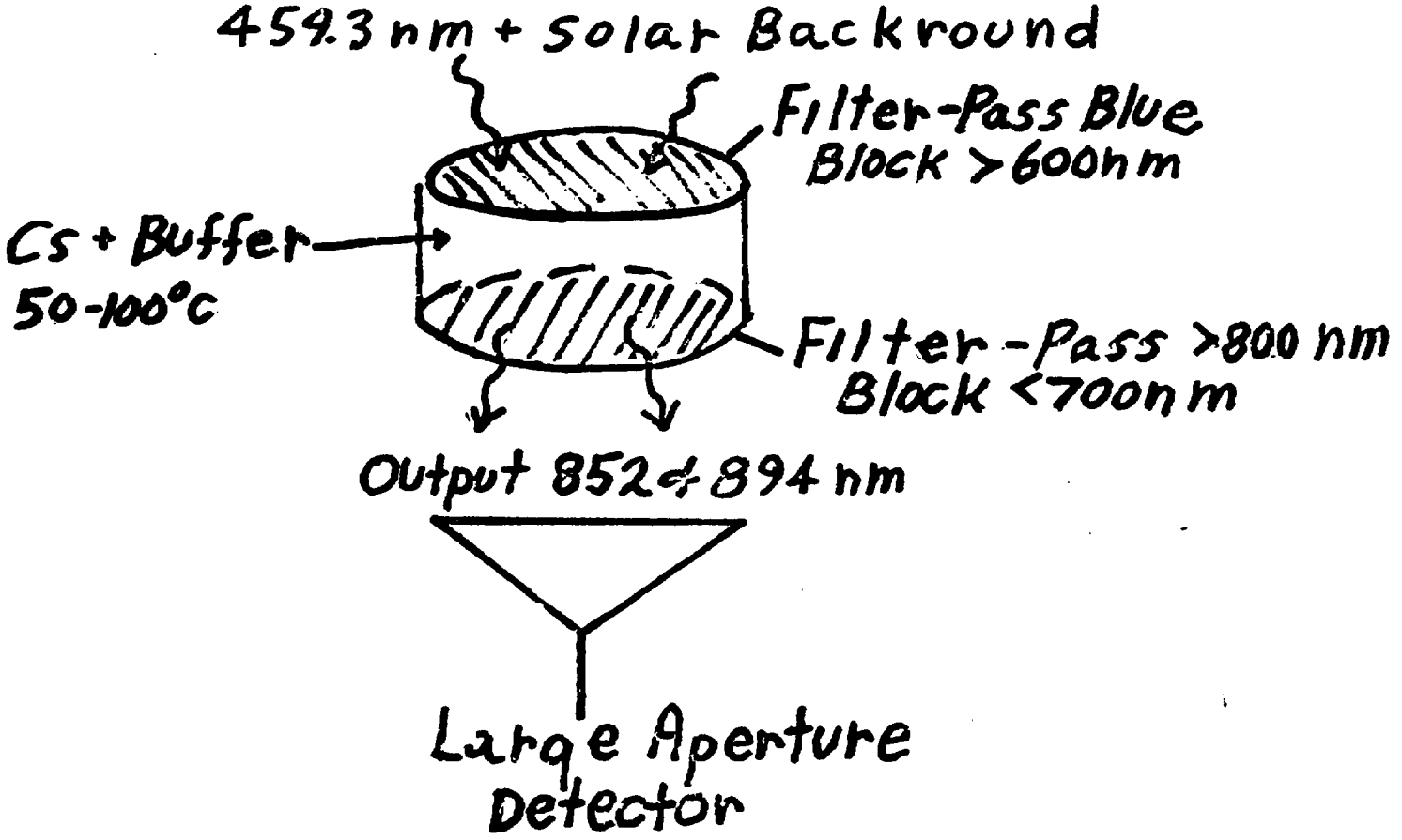

Radiation Trapping on Cs 894 nm line

Assume: $k_0 l = 3$ on 459 nm line

then $k'_0 l = 800$ at 894 nm

$\tau' = \frac{1}{GA}$ where $G = \frac{1.9}{k_0 l \sqrt{\pi k'_0 l/2}} = 5 \times 10^{-4}$

$\tau' = 56 \mu sec$ (DOPPLER ONLY)

For VOIGT PROFILE:

$$a = \frac{\Delta\nu_n}{\Delta\nu_D}\sqrt{2} = \begin{cases} 1.4 \times 10^{-4} & (459) \\ 0.01 & (894) \end{cases}$$

From SISUN CALCULATION:

$\tau' = 13.5 \mu sec$ (VOIGT)

IF $a' > 0.1$ USE LORENTZIAN LINESHAPE

$\tau' = \frac{1}{GA}$ WHERE $G = \frac{1.1}{\sqrt{\pi k'_0 l}}$

FOR BROADENING OF 1.5×10^9/sec @ 100T

$\tau' = 1 \mu sec$ (PRESSURE BROADENED)

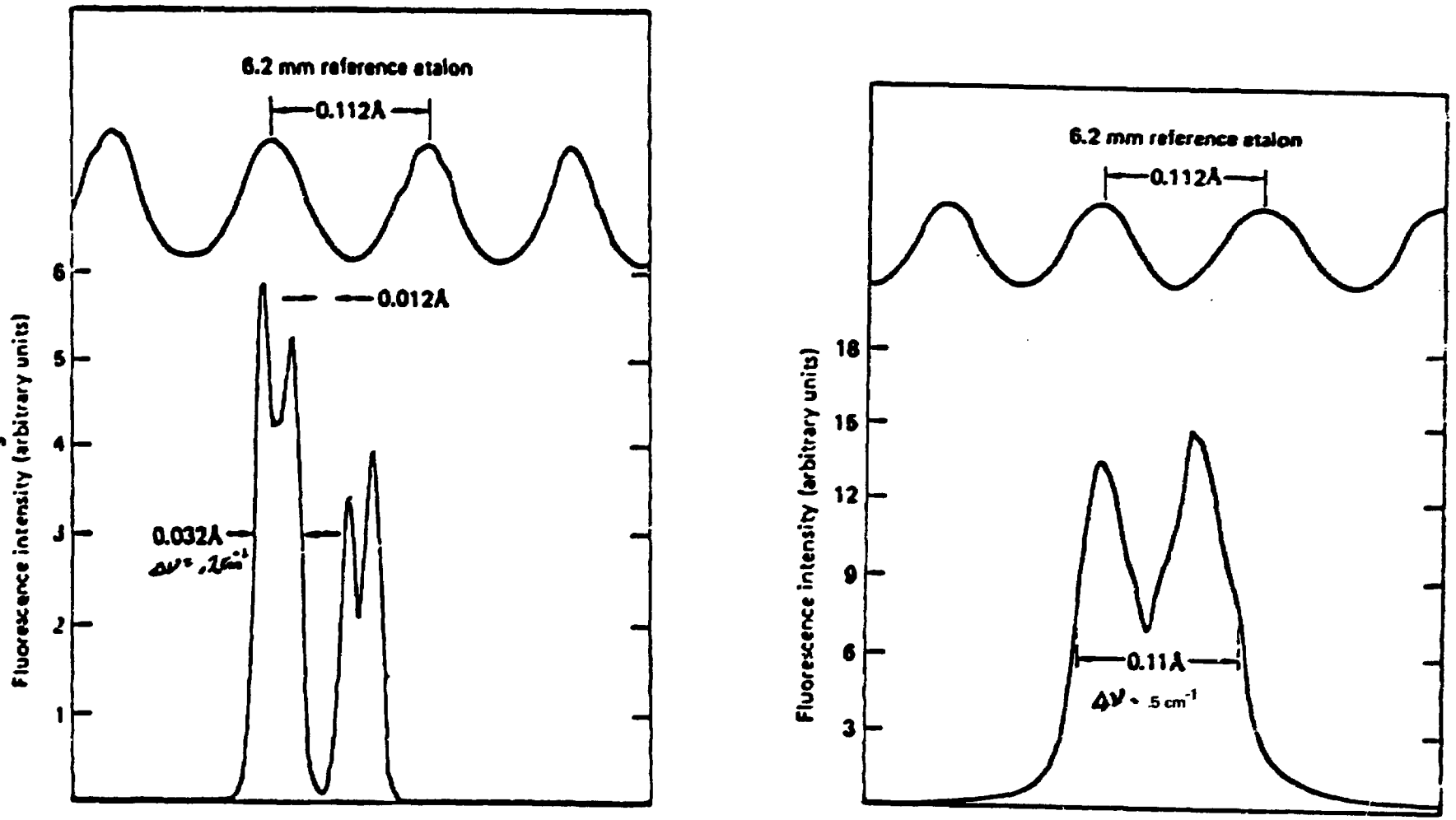

FIGURE 3 - Hyperfine structure of the 459 nm line of cesium. a) at low temperature (45°C) and b) at 140°C. (From Ref. 1).

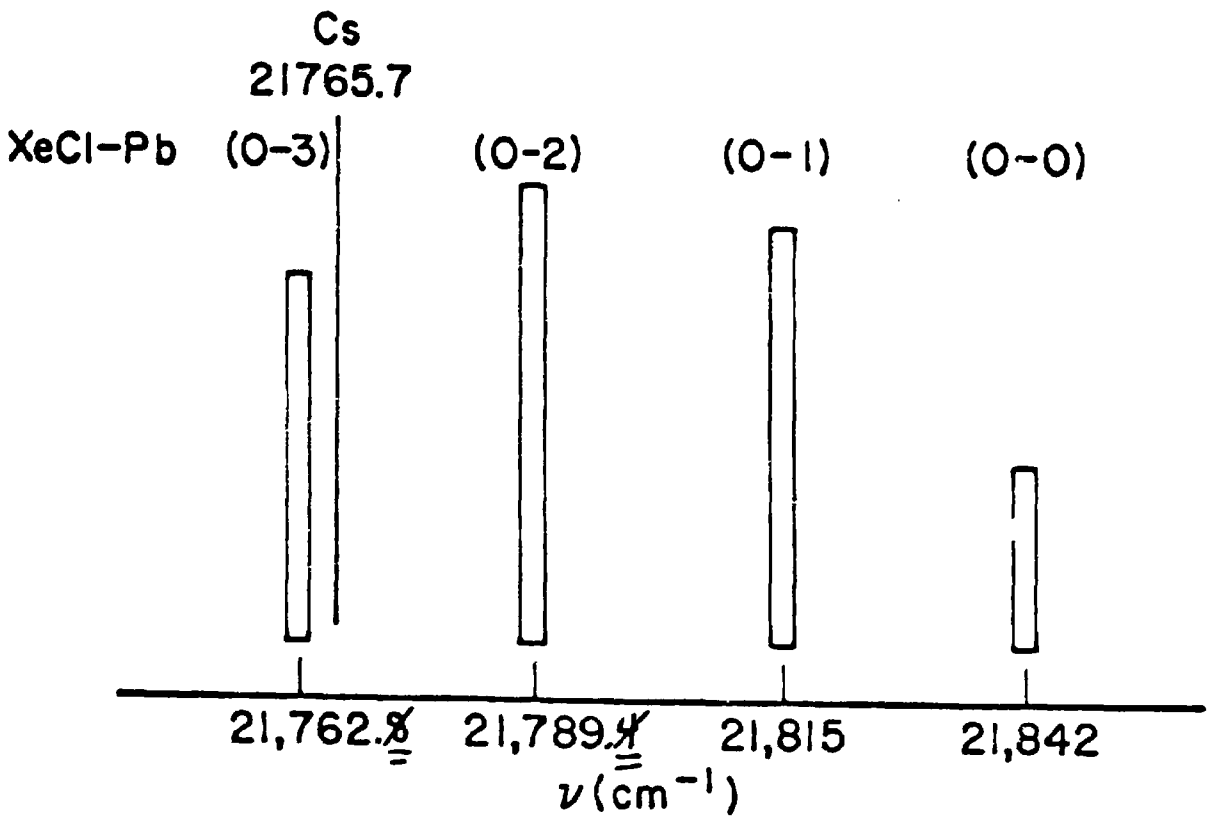

FIGURE 1 - Spectrum of the XeCl laser downshifted in lead vapor. The height of each laser line is proportional to the Franck-Condon factor for the particular vibrational transition. The position of the Cs

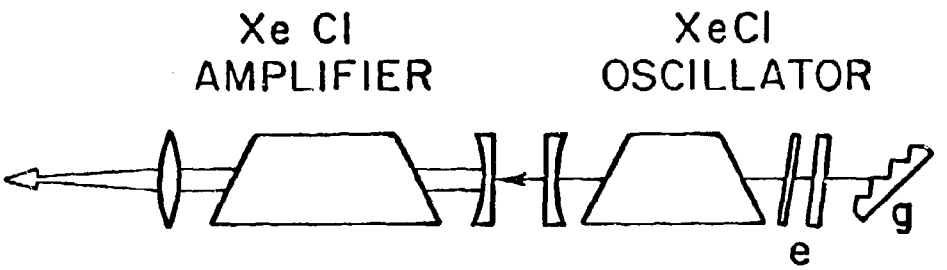

e–INTRACAVITY ETALONS
g–ETCHELLE GRATING

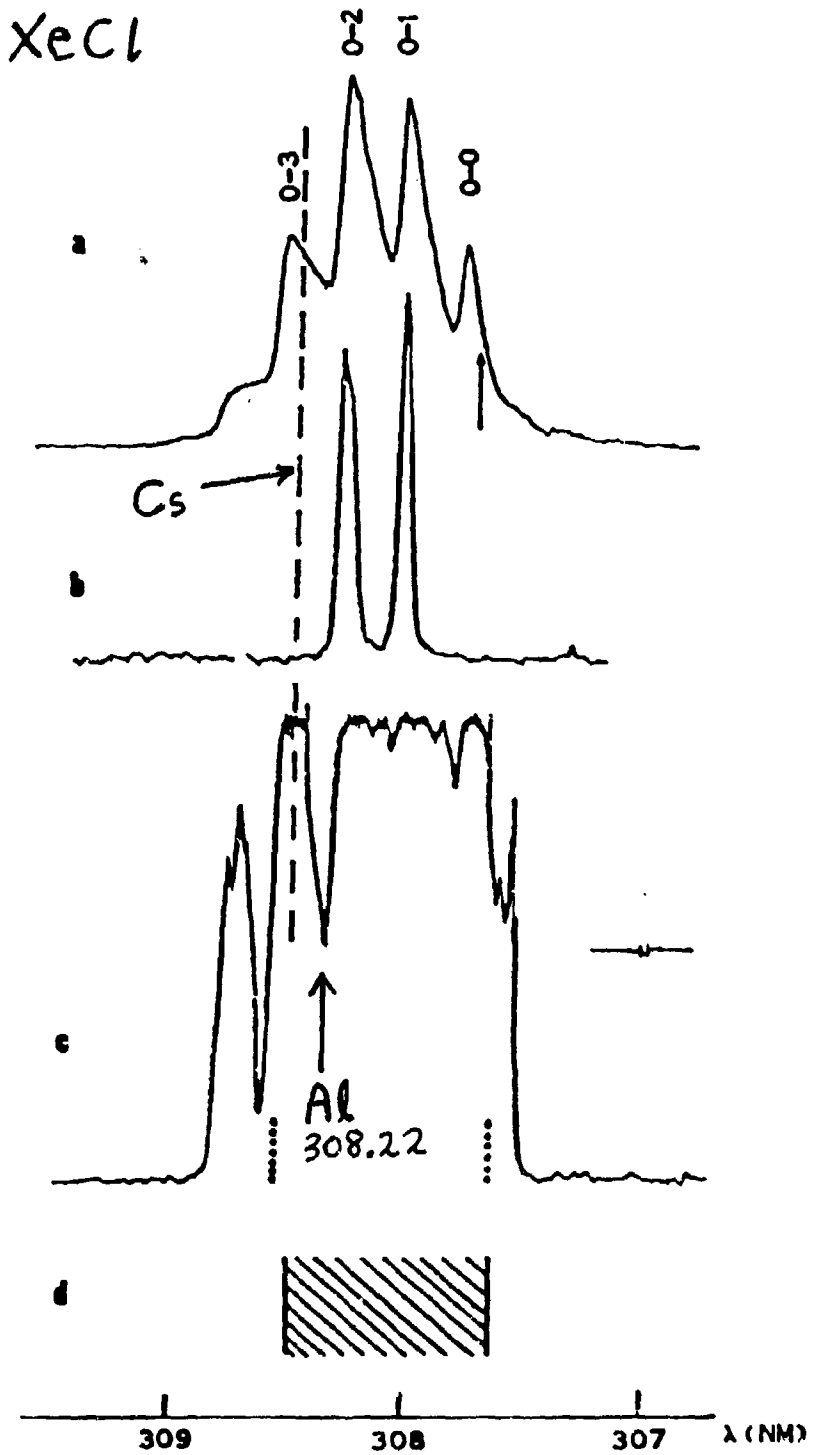
XeCl
N
I
I
0-3
a
Cs
b
c
Al
308.22
d
309
308
307
λ (NM)

BIREFRINGENT BLUE-GREEN FILTERS

March 25, 1980

Alan M. Title
William J. Rosenberg

ABSTRACT

The status of plastic film elements is reviewed. Poly vinyl alcohol can be laminated to make 30 cm elements or waveplates while polyesters still have too many non-uniformities. For elements smaller than 30 cm, quartz mosaic filters and Michelson interferometer elements are attractive. An actual Michelson analog birefringent element is discussed with a candidate configuration for a narrow band (<1Å) filter of such elements.

A new, highly efficient Solc filter design is presented. This design, using only 16 elements and 3 polarizers, results in a finesse of 240 with an integrated out-of-band transmission below $<10^{-3}$. In band transmission of 80-90% in polarized light should be possible.

At the present time it is practical to build a quartz filter with a 30 cm x 30 cm aperture, 2Å FWHM, and a 19° half angle field of view. It is suggested that construction of such a filter be started for near term experimentation.

Lockheed Palo Alto Research Laboratory
3251 Hanover St
Palo Alto CA 94304

BIREFRINGENT BLUE-GREEN FILTERS

LOCKHEED

PROGRAM REVIEW

MARCH 25, 1980

ALAN M. TITLE
WILLIAM J. ROSENBERG
LOCKHEED RESEARCH LABS.
3251 HANOVER STREET
PALO ALTO, CA 94304
(415) 493-4411

BIREFRINGENT BLUE-GREEN FILTERS

LOCKHEED

* PLASTIC FILM TECHNOLOGY
* OTHER MATERIAL/TECHNOLOGY
* FILTER DESIGNS
* FUTURE DIRECTION

PLASTIC FILM TECHNOLOGY

LOCKHEED

PVA LAMINATION

* CAN PRODUCE LARGE ELEMENTS
* ESSENTIAL FOR LARGE APERTURE WAVEPLATES
* WELL ESTABLISHED

POLYESTER NONUNIFORMITIES

* INHERENT IN THE ORIENTATION PROCESS
* MAY BE ABLE TO POLISH OR COMPENSATE
* STILL QUESTIONABLE

OTHER MATERIALS/TECHNOLOGY

LOCKHEED

* QUARTZ MOSAIC
* QUARTZ - KDP TYPE II ELEMENTS
* WIDE FIELD MICHELSON ANALOG ELEMENTS
* HIGH TRANSMISSION POLARIZERS

WIDE FIELD MICHELSON

LOCKHEED

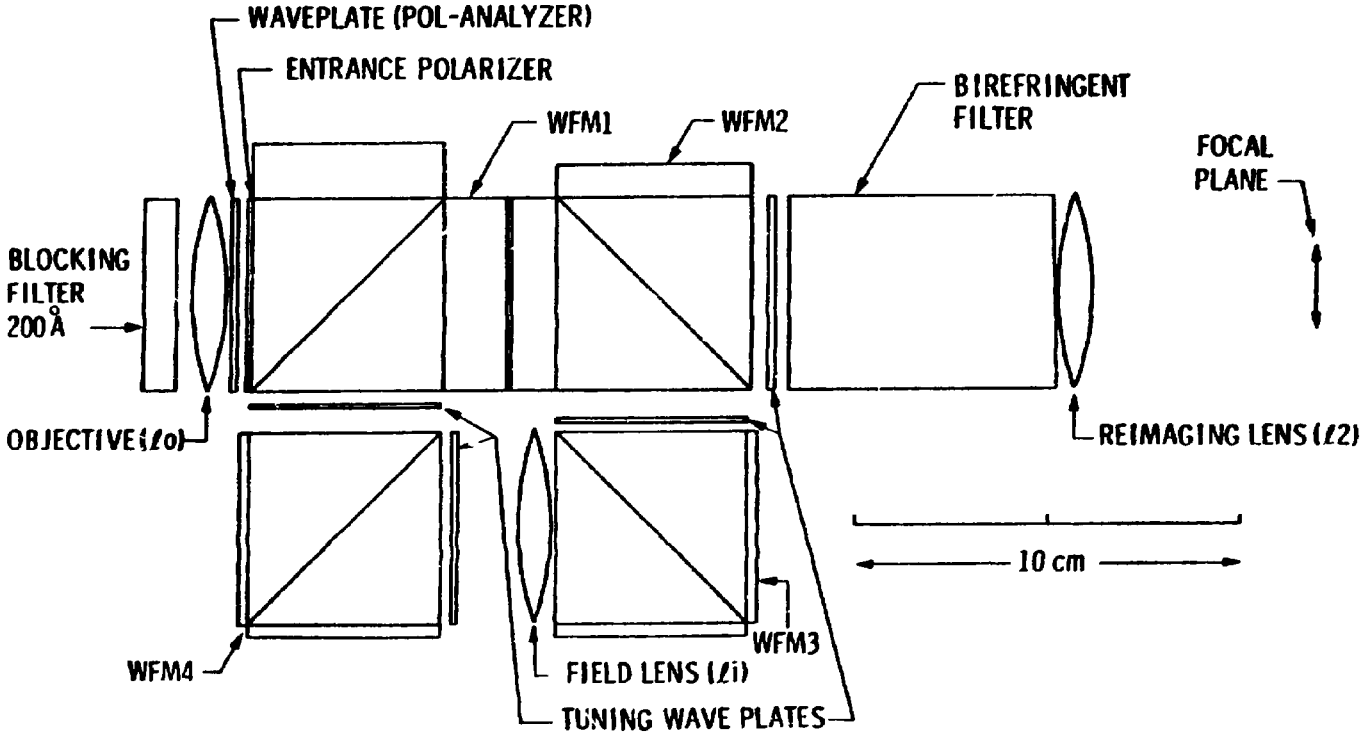

WIDE FIELD MICHELSON

LOCKHEED

SOLC FILTER DESIGNS

LOCKHEED

* COLLAPSABLE (DEGENERATE) SOLUTIONS
* WAVEPLATE ROTATORS
* ANALYSIS-SYNTHESIS CALIBRATION
* HYBRID DESIGNS HAVE HIGH FINESSE/PLATE
* TRANSMISSION 85-90% (POLARIZED)
* WIDEFIELD ANALYSIS APPLICABLE

LYOT FILTER

FWHM: 1.25 FINESSE: 288.0 SIDELOBE: 0.47E-01

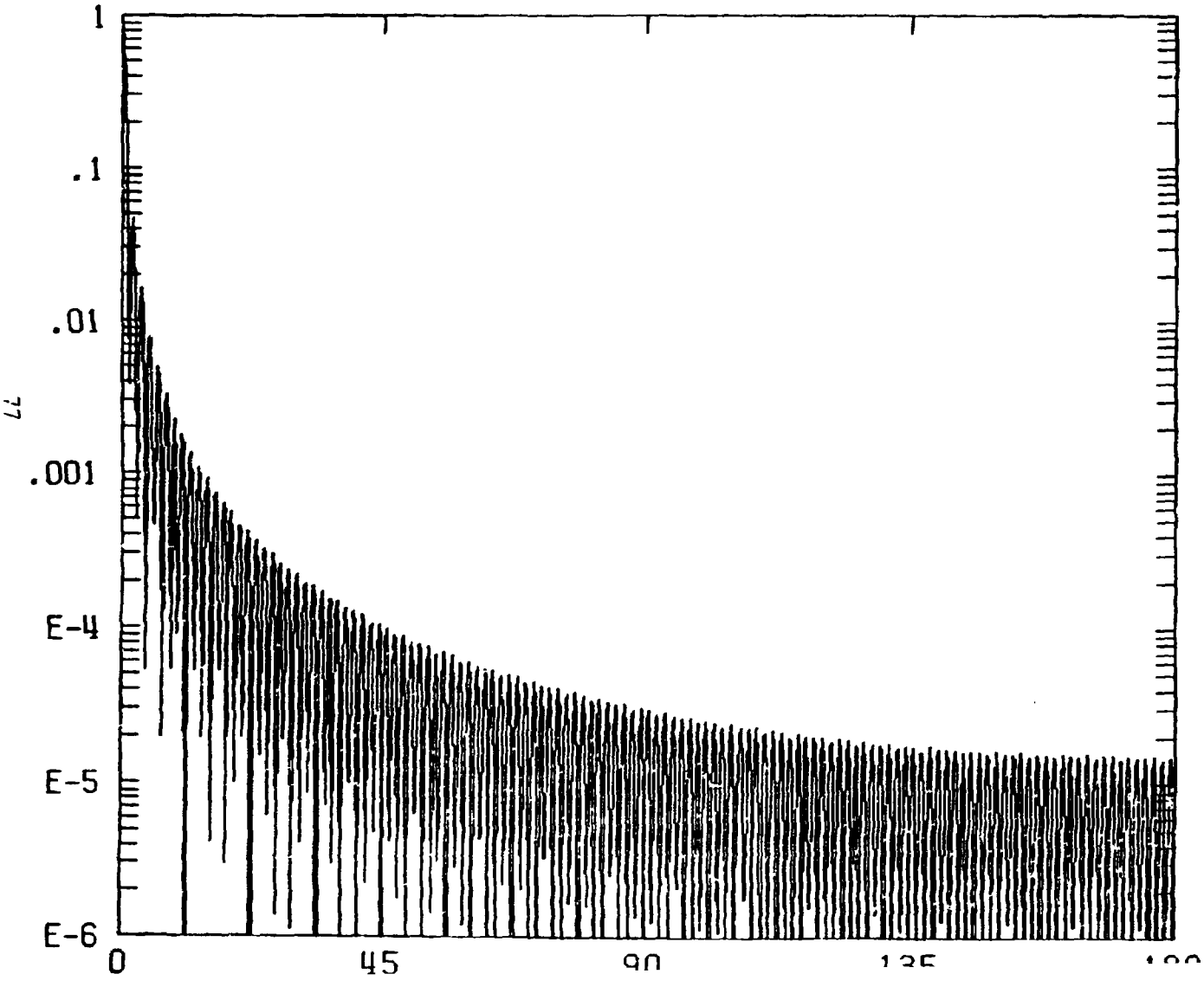

PLATES

	RET	ANG
1	1.00	45.00
2	2.00	45.00
3	4.00	45.00
4	8.00	45.00
5	16.00	45.00
6	32.00	45.00
7	64.00	45.00
8	64.00	45.00
9	64.00	45.00

POLARIZERS

	RHO	ANG
1	0.00	0.00
2	0.00	0.00
3	0.00	0.00
4	0.00	0.00
5	0.00	0.00
6	0.00	0.00
7	0.00	0.00

COLLAPSED SOLC

LOCKHEED

FWHM: 22.40 FINESSE: 16.1 SIDELOBE: 0.29E-02

PLATES

	RET	ANG
1	6.00	78.50
2	1.00	6.50
3	1.00	20.25
4	1.00	36.38
5	1.00	53.63
6	1.00	69.75
7	1.00	83.50
8	6.00	11.50

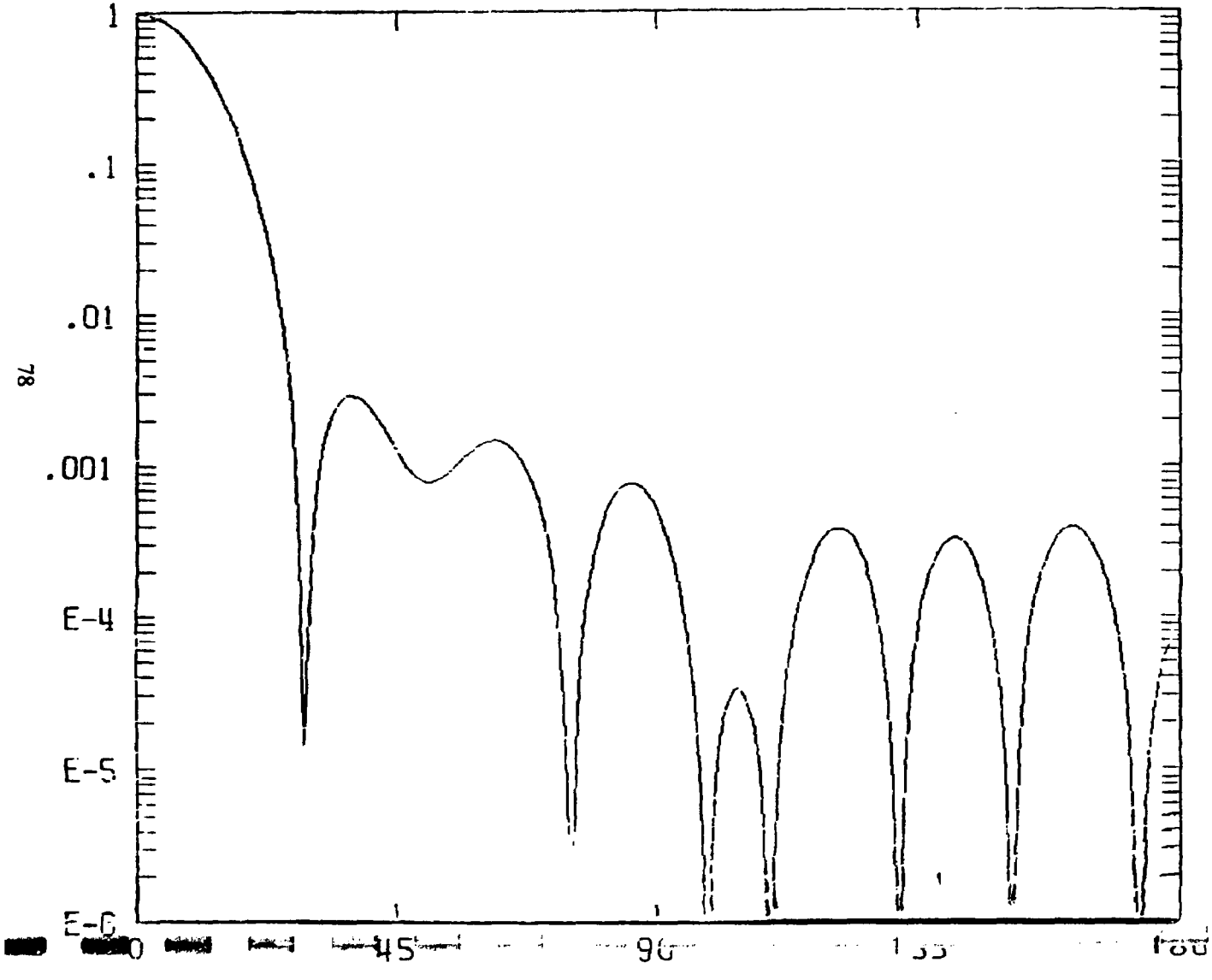

HYBRID SOLC

LOCKHEED

FWHM: 1.60 FINESSE: 224.8 SIDELOBE: 0.75E-02

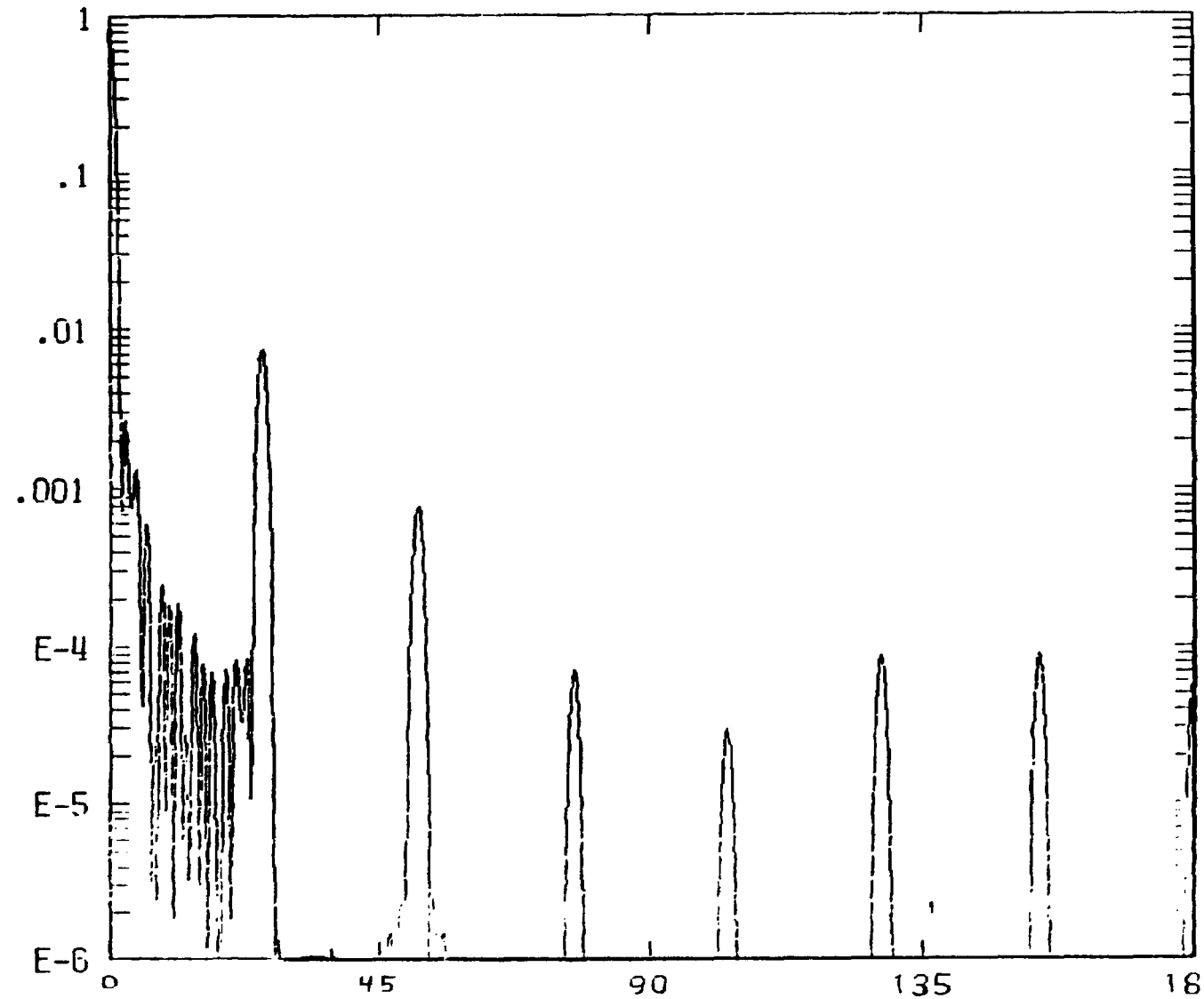

PLATES	RET	ANG
1	6.00	78.50
2	1.00	6.50
3	1.00	20.25
4	1.00	36.38
5	1.00	53.63
6	1.00	69.75
7	1.00	83.50
8	6.00	11.50
984.00	78.50	
1014.00	6.50	
1114.00	20.25	
1214.00	36.38	
1314.00	53.63	
1414.00	69.75	
1514.00	83.50	
1684.00	11.50	

POLARIZERS	RHO	ANG
8	0.00	0.00

BIREFRINGENT FILTERS

LOCKHEED

MATERIAL	BANDWIDTH	HALF ANGLE	APERTURE
QUARTZ	1.Ø	19.	1Ø-15 CM OR MOSAIC
	3.Ø	25.	
KDP	Ø.5	8.	15-3Ø CM
	1.Ø	12.	
	3.Ø	2Ø.	
QUARTZ -KDP	1.Ø	13.	SAME AS QUARTZ
	3.Ø	25.	
MYLAR	Ø.5	6.	15-3Ø CM
	1.Ø	9.	

MICHELSON FILTERS

LOCKHEED

TYPE	BANDWIDTH	HALF ANGLE	APERTURE
WIDE FIELD	Ø.2 Ø.5 1.Ø	12. 15. 19.	1Ø CM SQUARE
DYSON	Ø.2 Ø.5 1.Ø	26.-35.	1Ø CM SQUARE

NEXT PHASE

LOCKHEED

OPERATIONAL FILTER

HYBRID SOLC FILTER	QUARTZ	2.0 A	10 CM DIAM
HYBRID SOLC MOSAIC	QUARTZ	2.0 A	22 X 30 CM

DEVELOPMENT PROGRAM

WIDE FIELD MICHELSON	10 CM SQUARE	- PRACTICAL TODAY
DYSON MICHELSON	10 CM SQUARE	- NO MAJOR PROBLEMS
MYLAR ELEMENTS	30 CM DIAM.	- UNIFORMITY

ISO-INDEX ELECTRO-OPTIC FILTER: RECENT EXPERIMENTAL RESULTS

J. F. Lotspeich
D. M. Henderson

Hughes Research Laboratories
3011 Malibu Canyon Road
Malibu, CA 90265

ABSTRACT

Recent high-resolution measurements of $AgGaS_2$ iso-index filter samples have confirmed earlier theoretical predictions first presented in 1979. We have observed a filter passband of less than 1.0Å at 4970Å in a sample 3mm thick and have achieved electro-optic control of transmission efficiency up to a maximum of 60% for polarized light with about 1000V. These results translate to filter passbands of less than 0.3Å in a 1-cm sample with comparable voltage requirements and with negligible electric power dissipation. The filter response for off-normal light beams indicates a field-of-view capability in excess of 45° half angle (f/0.5) with less than 20% increase in passband over the narrow field condition. Temperature tuning of the pass wavelength has also been observed, with a tuning rate of 0.25Å/°C. A larger tuning range, for matching

a particular laser transmitter wavelength, is possible by variation of chemical composition.

The presence of optical activity in $AgGaS_2$ was confirmed. Its effect on transmittance at zero voltage and on passband characteristics for various crystal orientations is currently being addressed.

A theoretical model for characterizing iso-index materials has been developed, based on the classical dispersion theory of doubly-resonant damped harmonic oscillators (band edge splitting). The analysis indicated that the best candidate materials should exhibit (a) a large non-resonant birefringence, (b) a short wavelength band edge, and (c) a small band splitting.

HUGHES

HUGHES AIRCRAFT COMPANY
RESEARCH LABORATORIES

8691-3

ISO–INDEX ELECTRO–OPTIC FILTER
RECENT EXPERIMENTAL RESULTS
BY

JAMES F. LOTSPEICH

ISO–INDEX COUPLED–WAVE FILTER

HUGHES
HUGHES AIRCRAFT COMPANY
RESEARCH LABORATORIES

OPERATING CHARACTERISTICS

8691–4

- REQUIRES A BIREFRINGENT MATERIAL
- OPERATES BY POLARIZATION COUPLING
- OPERATES BETWEEN CROSSED POLARIZERS
- RESONANCE OCCURS AT ZERO CROSSING OF BIREFRINGENCE
- COUPLING MAY BE INDUCED BY
  - (1) ELECTRIC FIELD
  - (2) STRESS/STRAIN FIELD
  - (3) MAGNETIC FIELD
- FILTER CAN BE TUNED BY
  - (1) TEMPERATURE VARIATION
  - (2) COMPOSITION VARIATION
  - (3) PERIODIC PERTURBATION

ISO-INDEX ELECTRO-OPTIC FILTER

HUGHES
HUGHES AIRCRAFT COMPANY
RESEARCH LABORATORIES

7991 -9

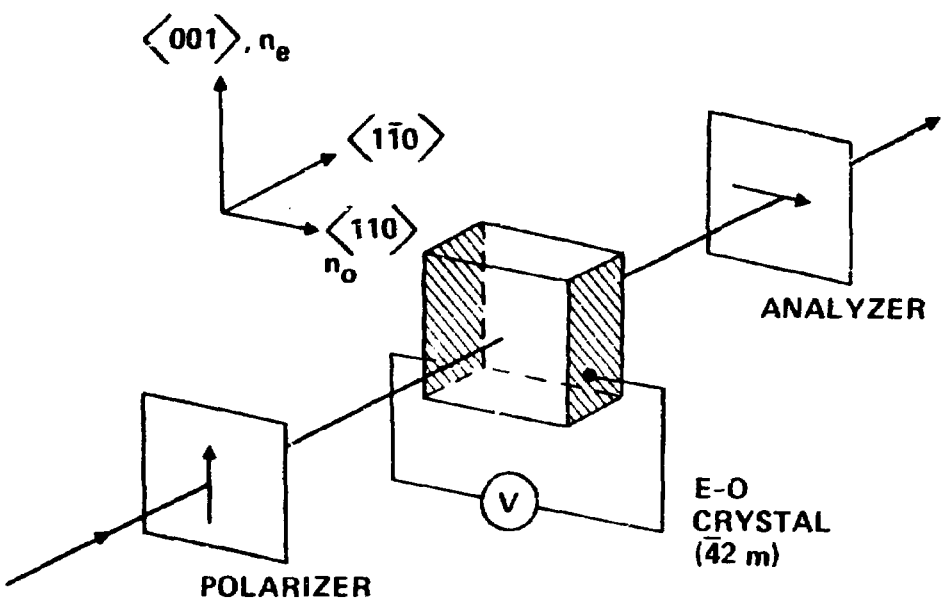

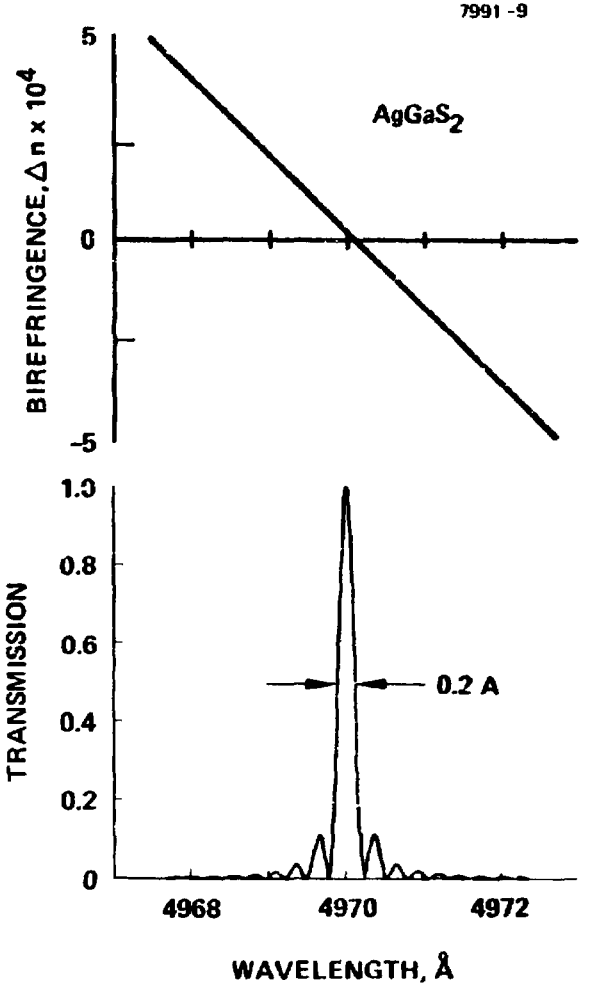

COUPLED-WAVE FILTER

HUGHES
HUGHES AIRCRAFT COMPANY
RESEARCH LABORATORIES

7701-3

PRINCIPAL DIRECTIONS OF INDEX EIGENVECTORS

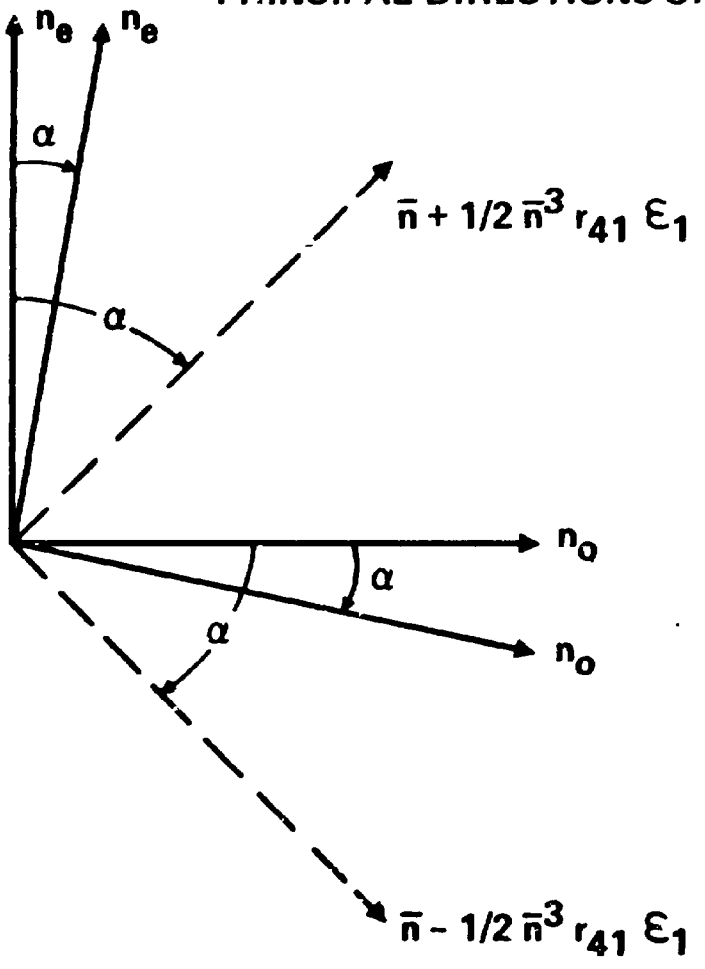

$$\tan 2\alpha = \frac{2 n_o^2 n_e^2 r_{41} \varepsilon_1}{n_o^2 - n_e^2}$$

JUL 1978

ISO-INDEX E-O FILTER EXPERIMENTAL SET-UP

HUGHES
HUGHES AIRCRAFT COMPANY
RESEARCH LABORATORIES

8691-5

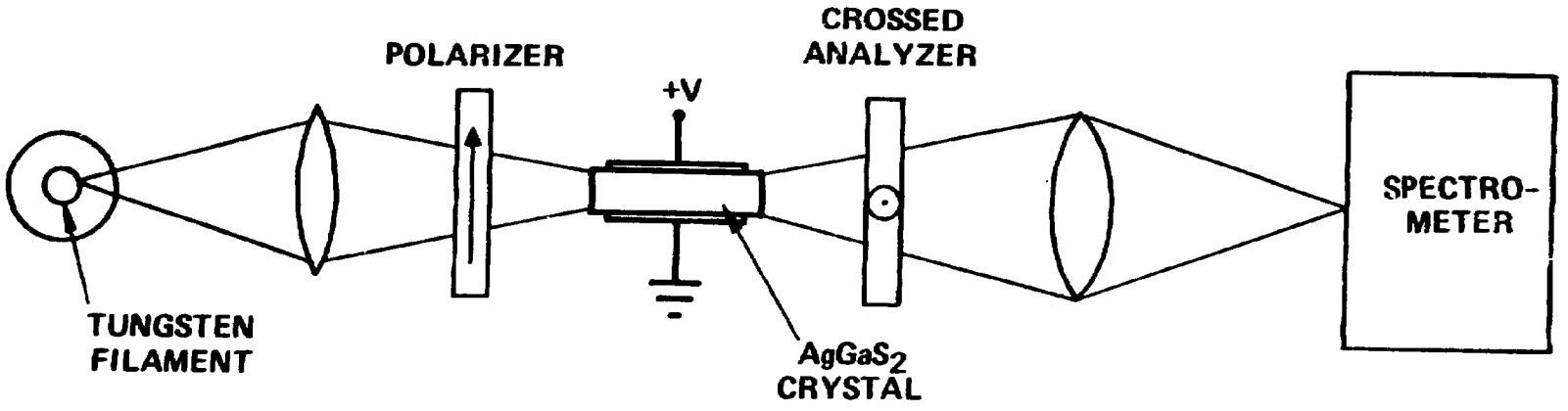

MAY 1979

ISO–INDEX E–O FILTER VOLTAGE SENSITIVITY

HUGHES
HUGHES AIRCRAFT COMPANY
RESEARCH LABORATORIES

9470–2

d = 0.84 mm
ℓ = 3.2 mm

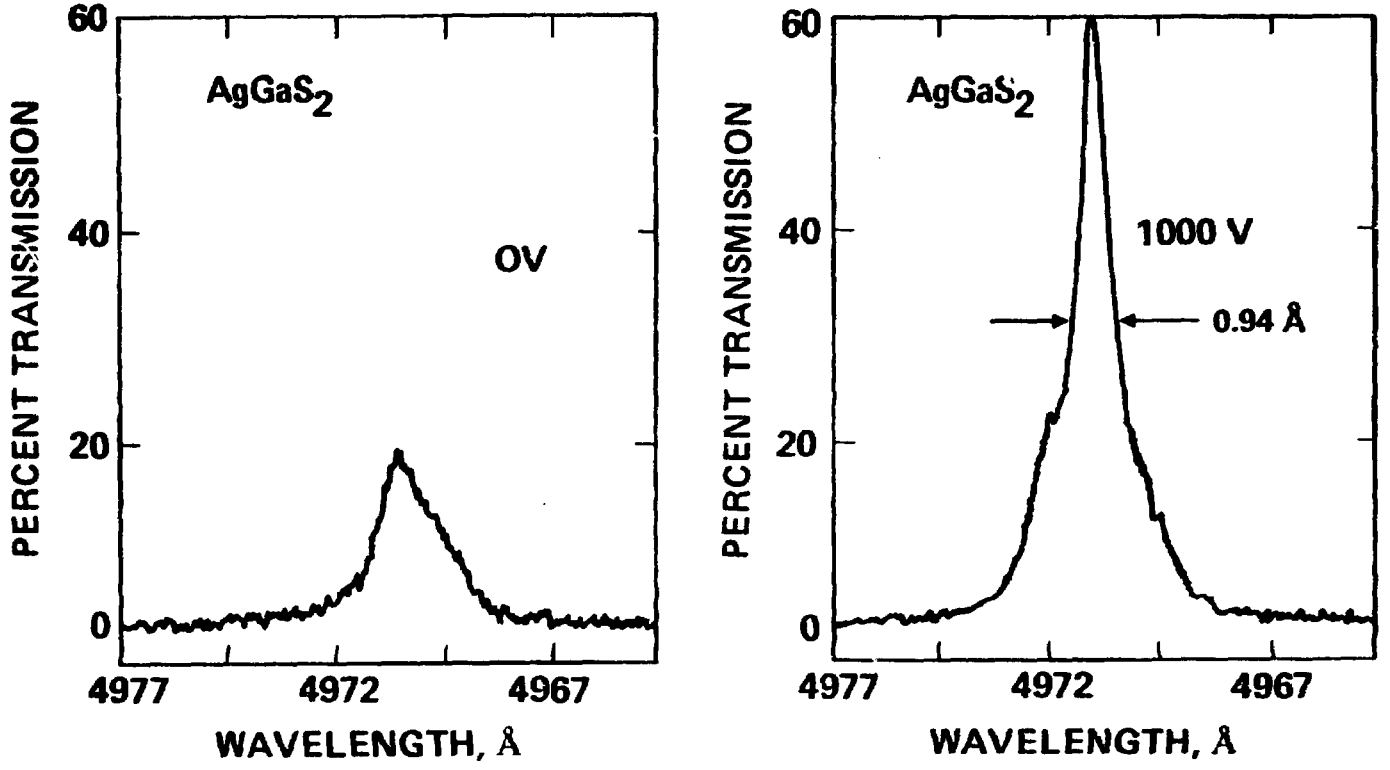

ISO–INDEX E–O FILTER VOLTAGE RESPONSE

HUGHES
HUGHES AIRCRAFT COMPANY
RESEARCH LABORATORIES

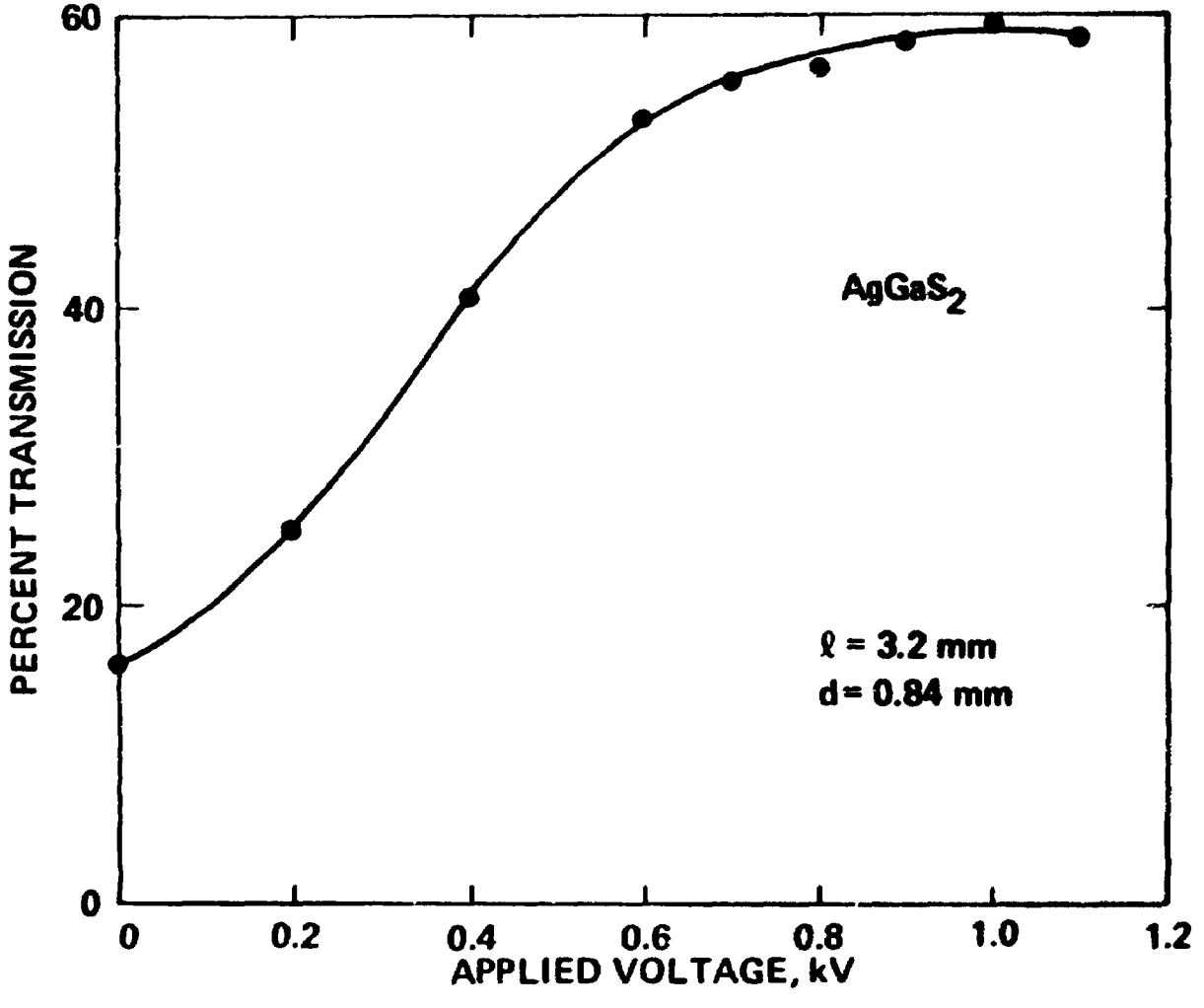

ISO–INDEX E–O FILTER FOV CHARACTERISTICS

HUGHES
HUGHES AIRCRAFT COMPANY
RESEARCH LABORATORIES

9470–1

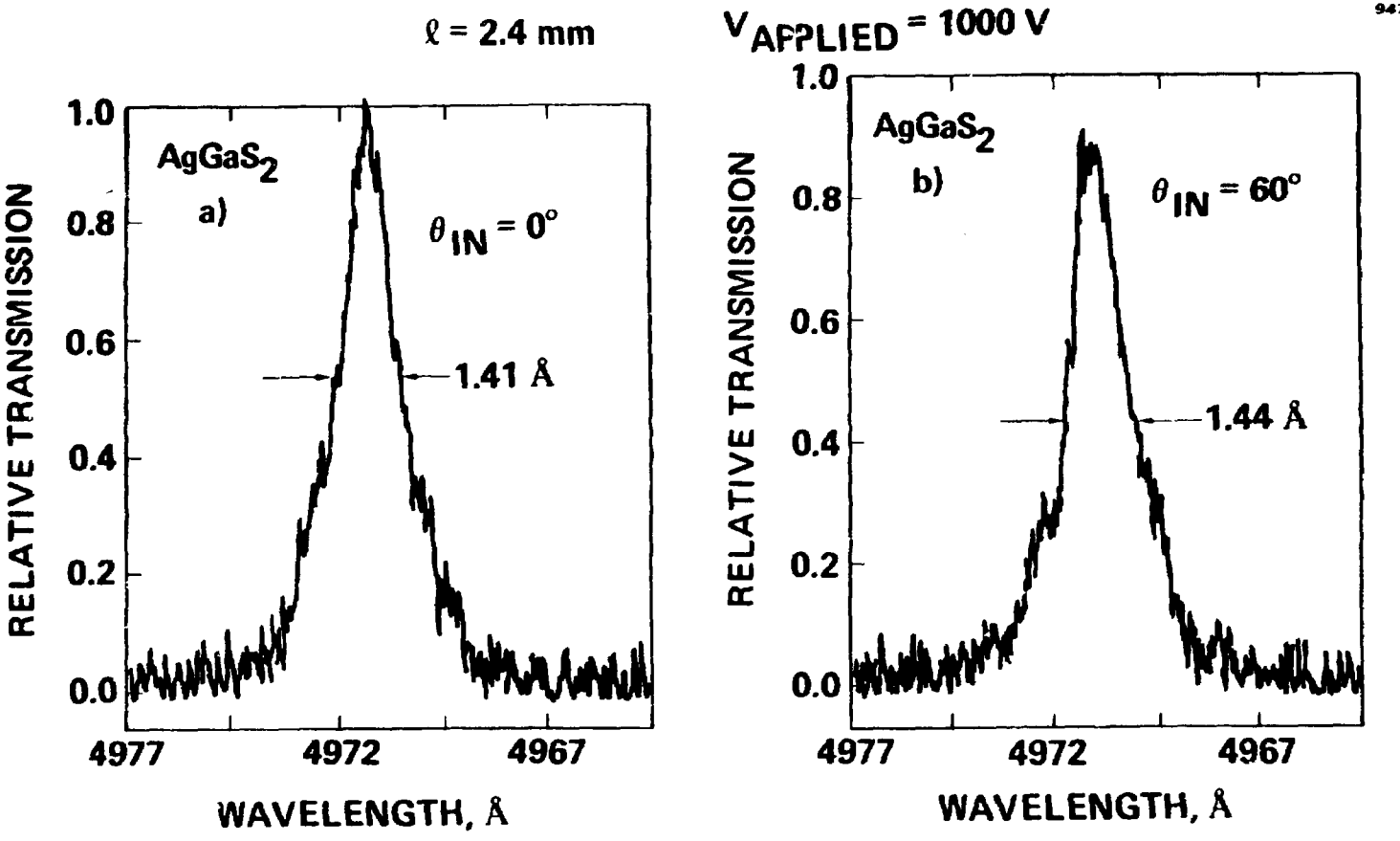

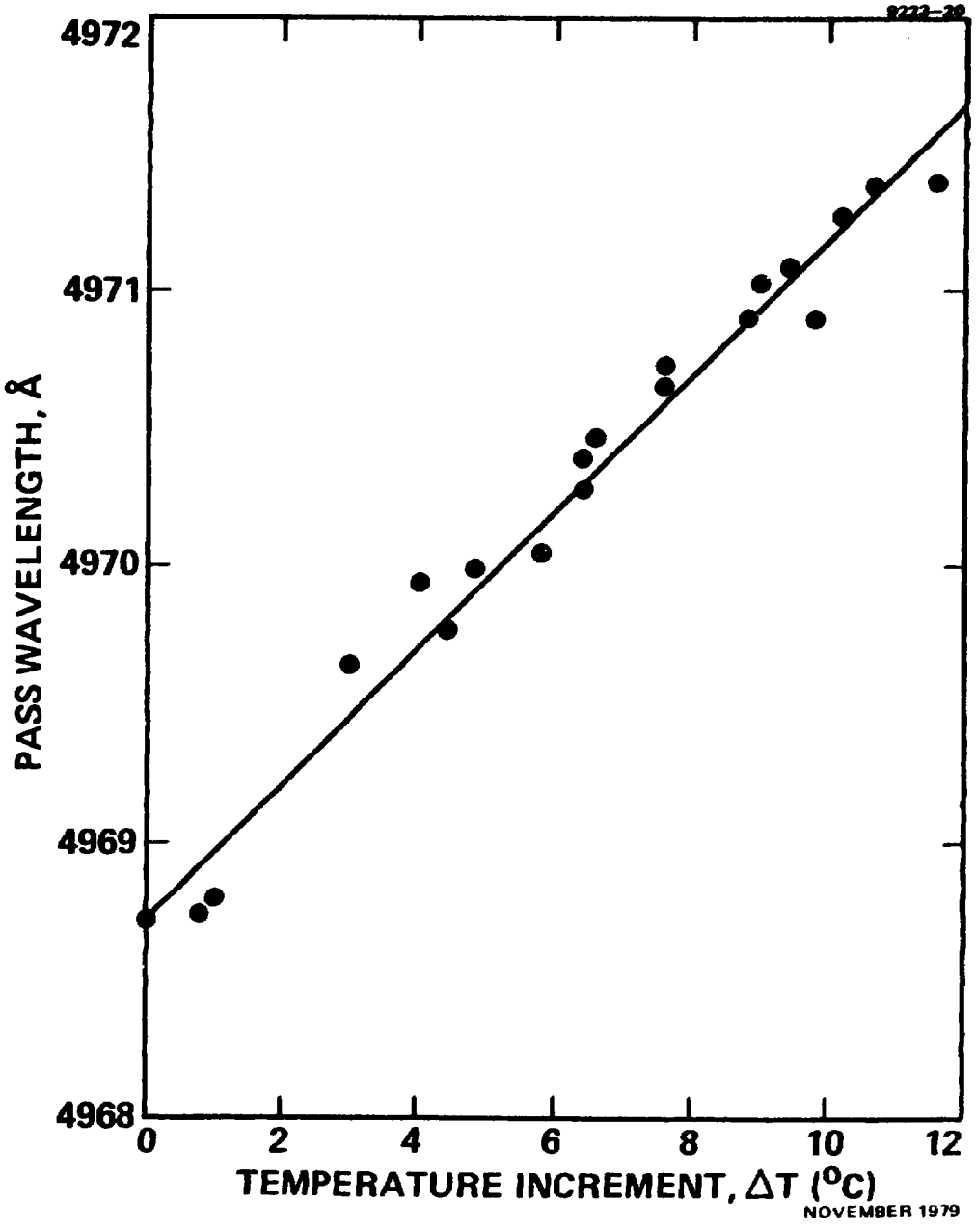

HUGHES
HUGHES AIRCRAFT COMPANY
RESEARCH LABORATORIES

$AgGaS_2$ BLUE/GREEN FILTER TEMPERATURE DEPENDENCE OF PASS WAVELENGTH

ISO–INDEX ELECTRO–OPTICAL FILTER THEORETICAL MODEL

HUGHES
HUGHES AIRCRAFT COMPANY
RESEARCH LABORATORIES

9629-2

RESULTS OF ANALYSIS

- GOOD AGREEMENT BETWEEN MEASUREMENTS AND CALCULATION OF ISO–INDEX POINT AND SLOPE OF BIREFRINGENCE FOR KNOWN ISO–INDEX CRYSTALS.

- BEST CANDIDATE CRYSTALS HAVE:
  - LARGE BIREFRINGENCE
  - SHORT WAVELENGTH BANDGAP
  - SMALL BANDGAP SPLITTING

MEASURED OFFSET OF ISO-INDEX POINT FROM BAND EDGE AS FUNCTION OF MATERIAL PARAMETERS

HUGHES
HUGHES AIRCRAFT COMPANY
RESEARCH LABORATORIES

9223–26

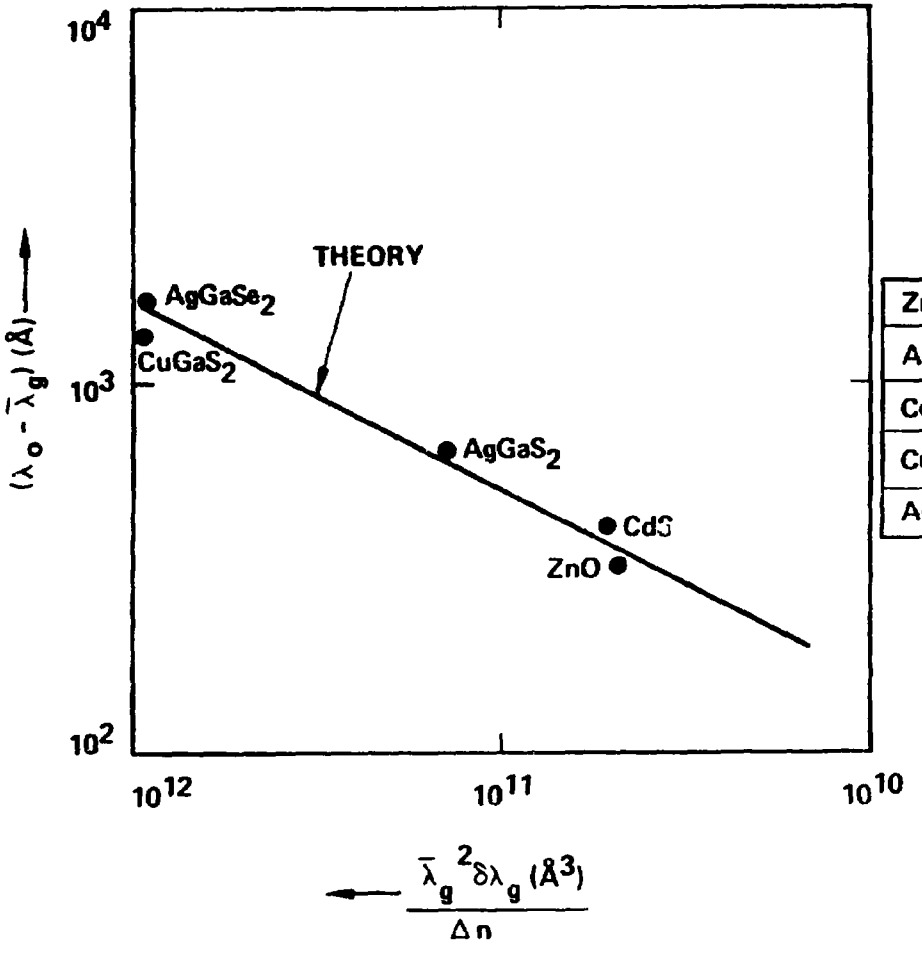

	$\bar{\lambda}_g$ (Å)	$\delta\lambda_g$ (Å)	Δn	$(\lambda_o - \lambda_g$ Å)
ZnO	3637	48	0.013	323
AgGaS$_2$	4322	422	0.055	648
CdS	4834	38	0.017	411
CuGaS$_2$	4973	240	0.006	1341
AgGaSe$_2$	6429	686	0.03	1607

MEASURED SLOPE AT ISO-INDEX POINT AS FUNCTION OF MATERIAL PARAMETERS

HUGHES
HUGHES AIRCRAFT COMPANY
RESEARCH LABORATORIES

9223-25

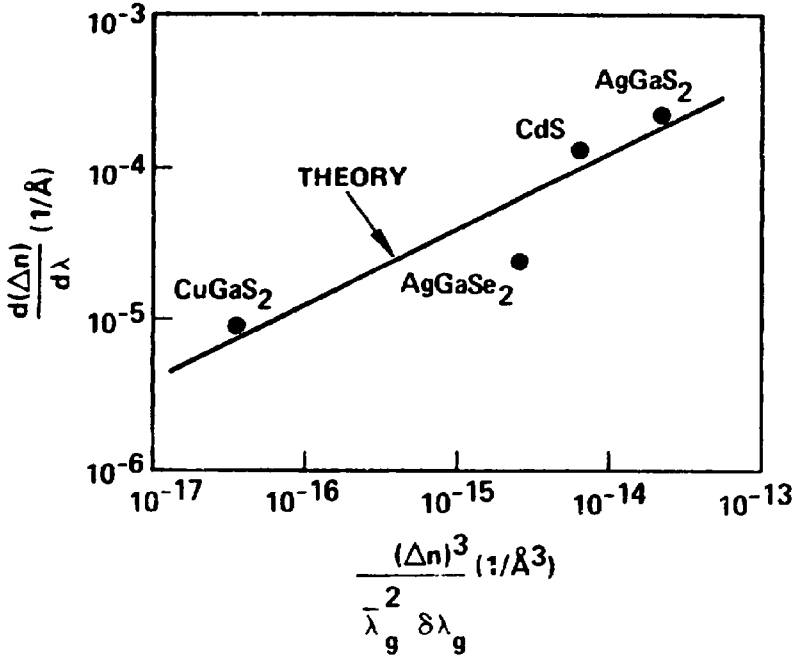

	$\bar{\lambda}_g$ (Å)	$\delta\lambda_g$ (Å)	Δn	$d(\Delta n)/d\lambda$	α
AgGaS$_2$	4322	422	0.055	1.9×10^{-4}	0.26
CdS	4834	38	0.017	1.2×10^{-4}	0.44
CuGaS$_2$	4973	240	0.006	8.0×10^{-6}	7.9
AgGaSe$_2$	6429	686	0.030	1.9×10^{-5}	4.2

BLUE/GREEN CANDIDATE MATERIALS

HUGHES
HUGHES AIRCRAFT COMPANY
RESEARCH LABORATORIES

9593-5

II - VI

CdS - ZnO

CdS - ZnS

I - III - VI

$CuAlS_2$ - $AgGaS_2$

$CuAlS_2$ - $CuAlSe_2$

$CuAlS_2$ - $CuGaS_2$

MARCH 1980

ISO–INDEX ELECTRO–OPTIC FILTER:

HUGHES
HUGHES AIRCRAFT COMPANY
RESEARCH LABORATORIES

8691-6R1

CONCLUSION

- RESULTS
  - NARROW BANDWIDTH:~ 0.3Å IN 1-CM SAMPLE
  - WIDE FIELD OF VIEW: ~ f/0.3 (± 60°)
  - TUNABLE (TEMPERATURE, COMPOSITION)
  - THROUGHPUT IS CONTROLLABLE ELECTRICALLY
  - WORKABLE THEORETICAL MODEL
- AREAS OF FURTHER INVESTIGATION
  - PASSBAND SELECTIVITY
  - OPTICAL ACTIVITY
  - MATERIALS STUDIES
  - MATERIALS PRODUCTION (SCALE UP)

CHRISTIANSEN-BRAGG FILTERS

P Yeh and J Tracy

Summary

A new type of narrowband wide field-of-view filter is proposed and analyzed. This filter is made of a periodic layered structure which consists of alternating layers of two dielectric materials such that the dispersion curves of these two media intersect at a desired wavelength λ_c. This layered structure is optically homogeneous only to the radiation of wavelength λ_c. Other radiation will be reflected provided the thicknesses of the layers are properly chosen. In particular, if the layered structure is made of a chirped quarter-wave stack, this forms a broadband reflector for all wavelengths except those near λ_c. A broadband Bragg reflector generally has a wide angular rejection cone. In addition, the transmission of light at λ_c is a material property of the layered structure which is independent of the angle of incidence. Therefore a chirped Christiansen-Bragg filter can be a narrowband transmission filter with a large field-of-view. The field-of-view can, in principle, be as large as 2π steradians.

Rockwell International
1049 Camino Dos Rios, PO Box 1085, MS A20
Thousand Oaks CA 91360

CHRISTIANSEN-BRAGG FILTERS

1. INTRODUCTION

2. CHRISTIANSEN FILTERS

3. BROADBAND BRAGG REFLECTORS

4. CHRISTIANSEN-BRAGG FILTERS

5. MATERIALS AND DISCUSSIONS

Rockwell International
Science Center

CHRISTIANSEN EFFECT

SC79-5501

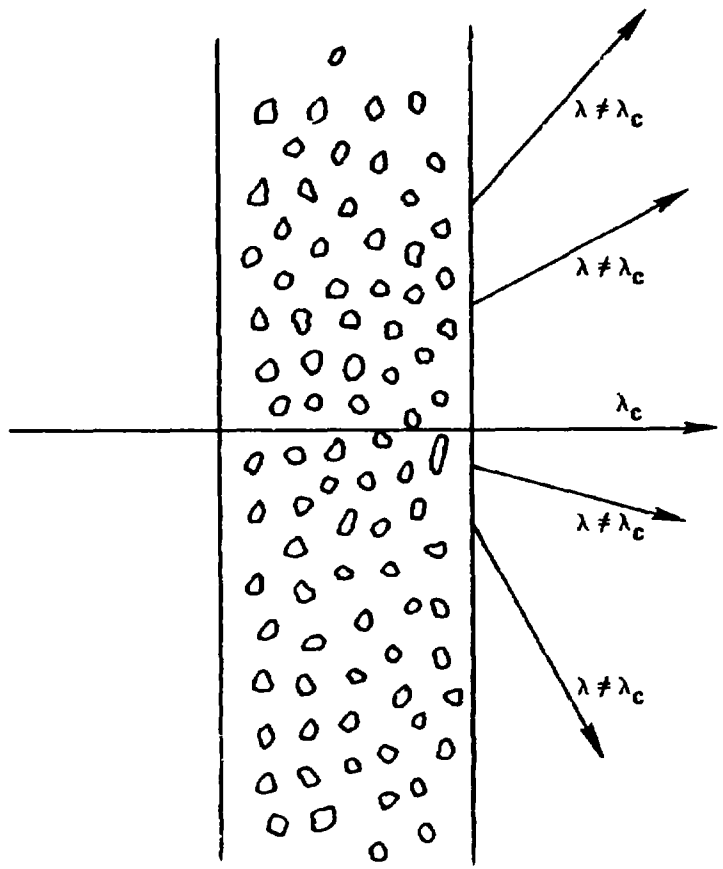

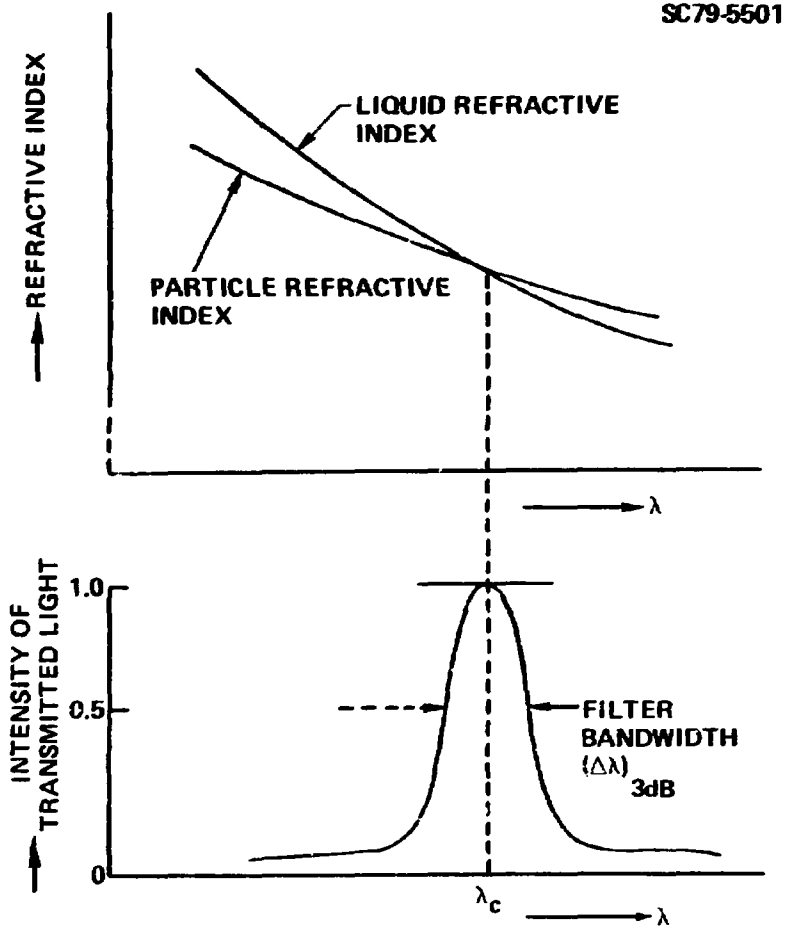

Rockwell International
Science Center

BANDWIDTH OF A CHRISTIANSEN FILTER

$\Delta\lambda_{0.5}/\lambda_c$ OF A CHRISTIANSEN FILTER:

$$T = \exp\left[-KcLa(\Delta n')^2\left(\frac{\Delta\lambda}{\lambda_c}\right)^2\right]$$

$$\frac{\Delta\lambda_{0.5}}{\lambda_c} = \left(\frac{2.77}{K}\right)^{1/2} \frac{1}{(cLa)^{1/2}\,\Delta n'}$$

WHERE c = PARTICLE VOLUME PER UNIT VOLUME

n_0 = REFRACTIVE INDEX OF LIQUID

n_p = REFRACTIVE INDEXES OF PARTICLES

L = LENGTH OF CELL

a = AVERAGE PARTICLE SIZE

$$\Delta n' = \frac{d}{d\lambda}\,(n_0 - n_p)$$

λ_c = WAVELENGTH AT WHICH $n_0 = n_p$

$\Delta\lambda$ = SHIFT IN WAVELENGTH AWAY FROM λ_c

THE CONSTANT K MAY ASSUME A VALUE BETWEEN 8 AND 49, DEPENDING ON THE PARTICULAR MECHANISM FOR SCATTERING ASSUMED.

TRANSMISSION CHARACTERISTICS AND SPECTRAL TUNING OF CHRISTIANSEN FILTER

SC79-5504

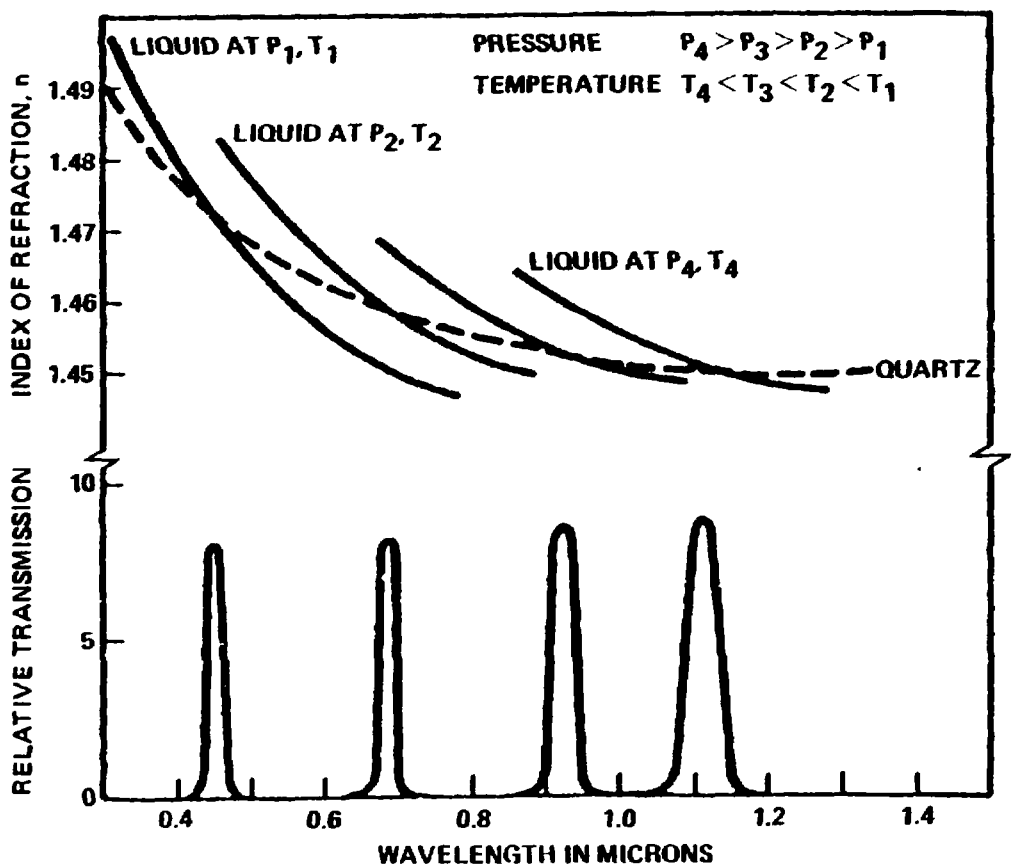

Rockwell International
Science Center

TYPICAL CHRISTIANSEN FILTER OPTICAL SYSTEM

SC79-5502

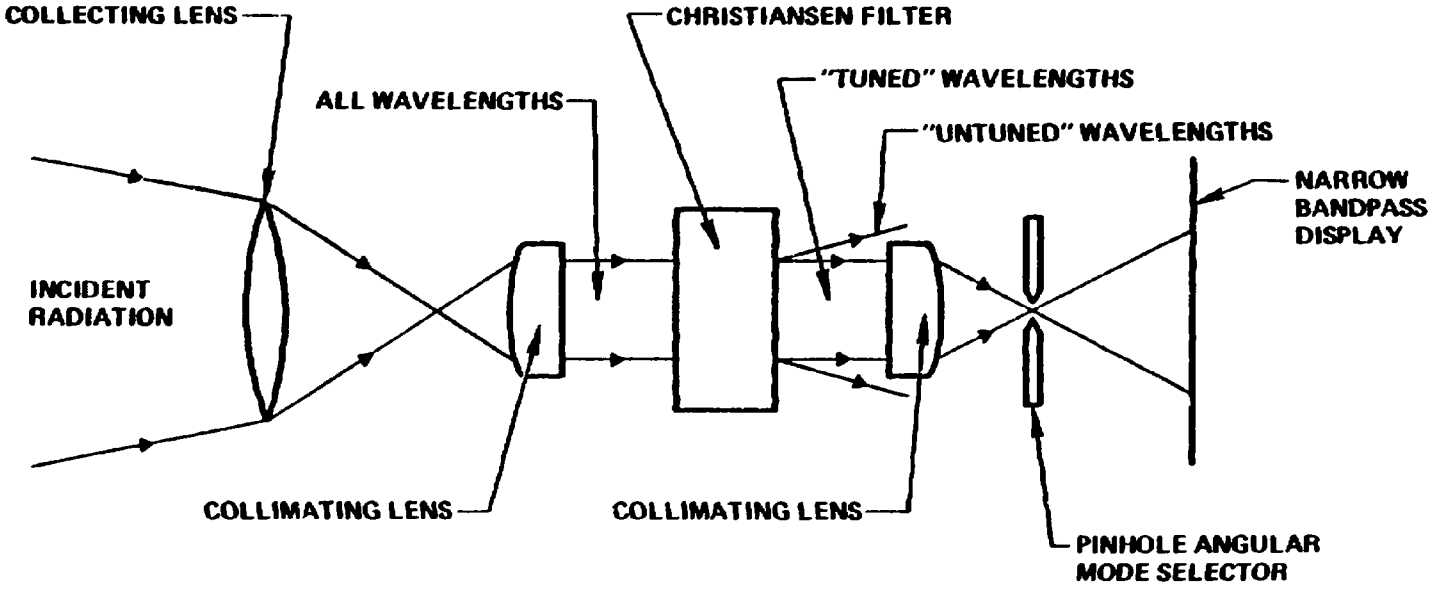

Rockwell International
Science Center

A BROADBAND BRAGG REFLECTOR

SC78-2000A

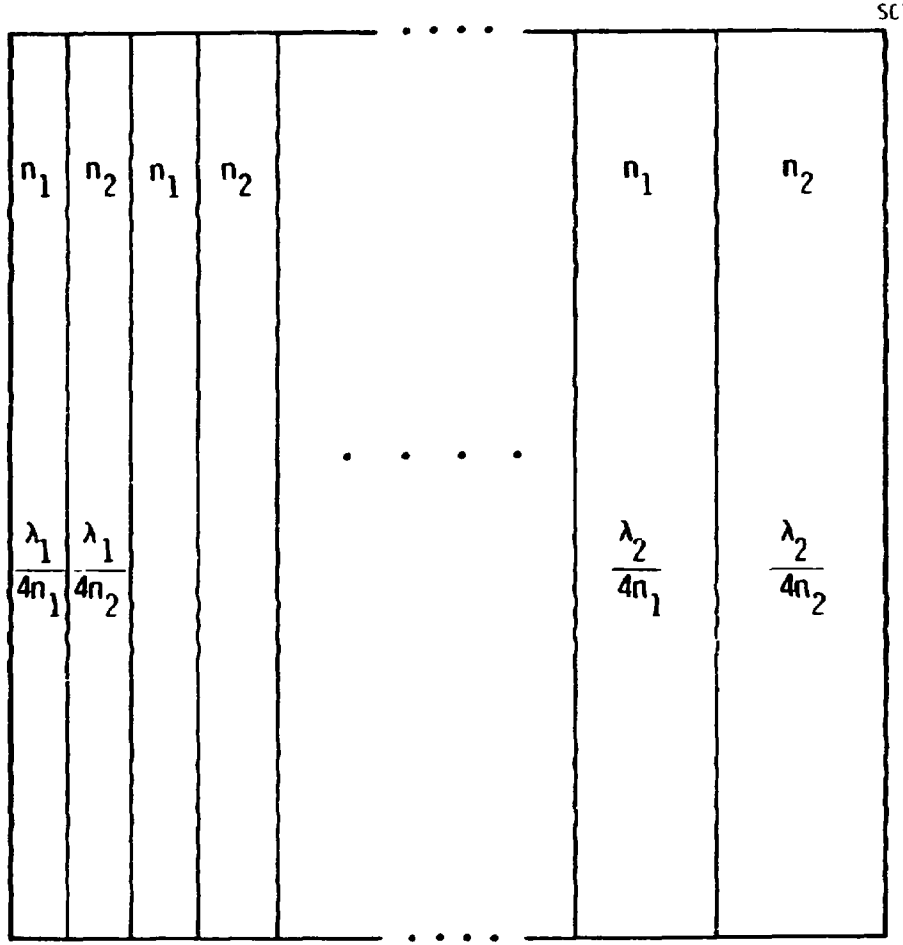

Rockwell International
Science Center

REFLECTIVITY OF A BROADBAND BRAGG REFLECTOR

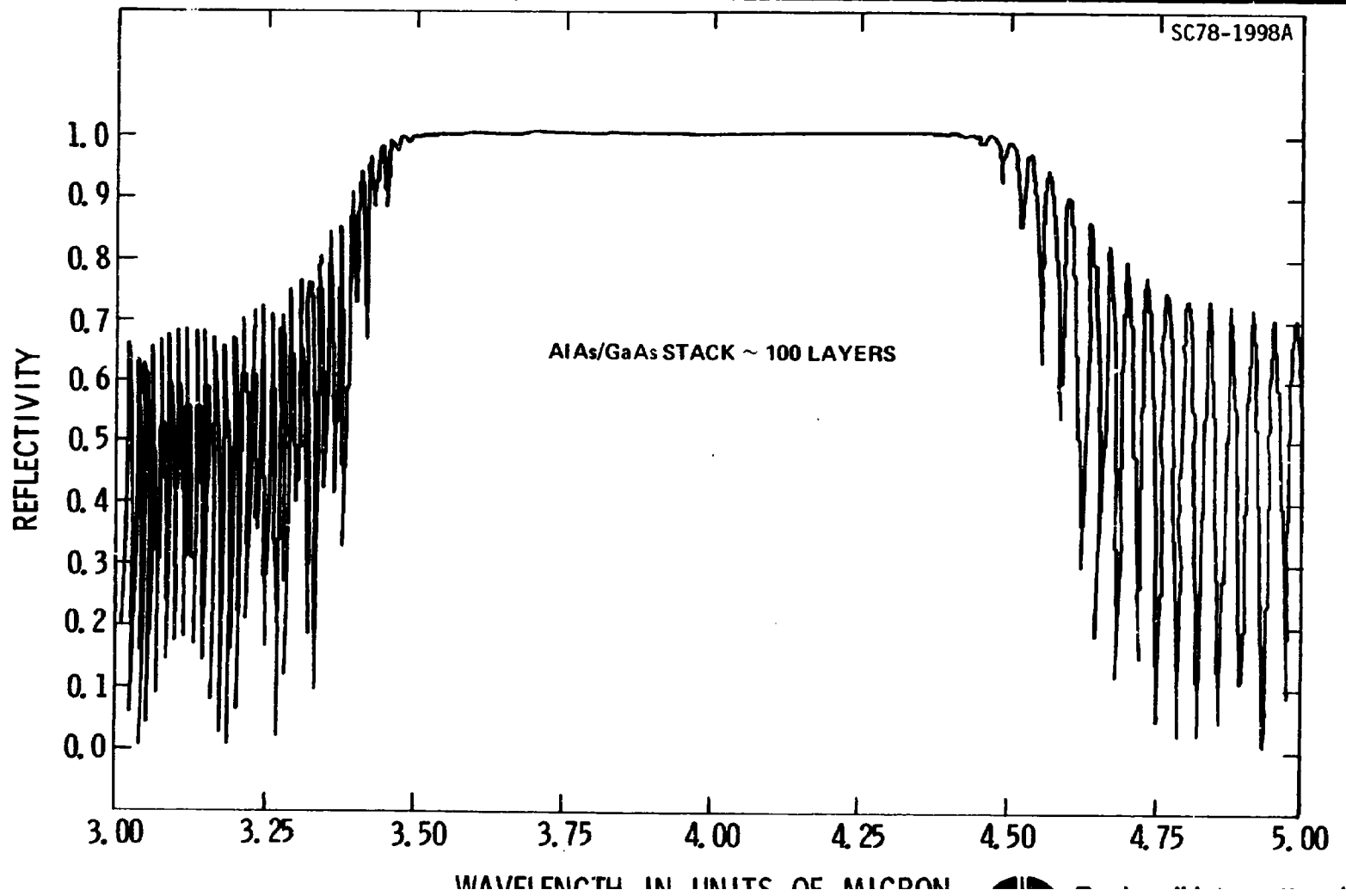

CHRISTIANSEN-BRAGG FILTER STRUCTURE

SC79-5242

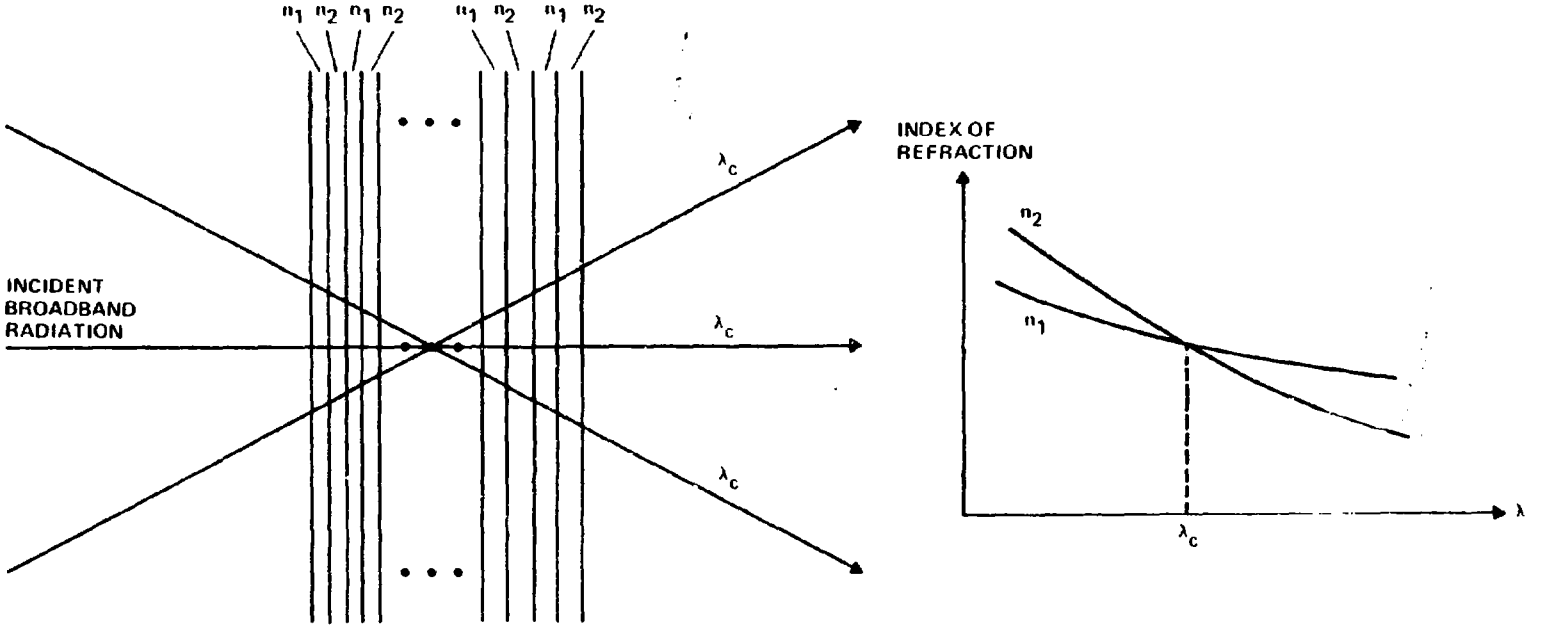

Rockwell International
Science Center

CHRISTIANSEN-BRAGG FILTER TRANSMISSION SPECTRA AT DIFFERENT ANGLES

SC79-5505

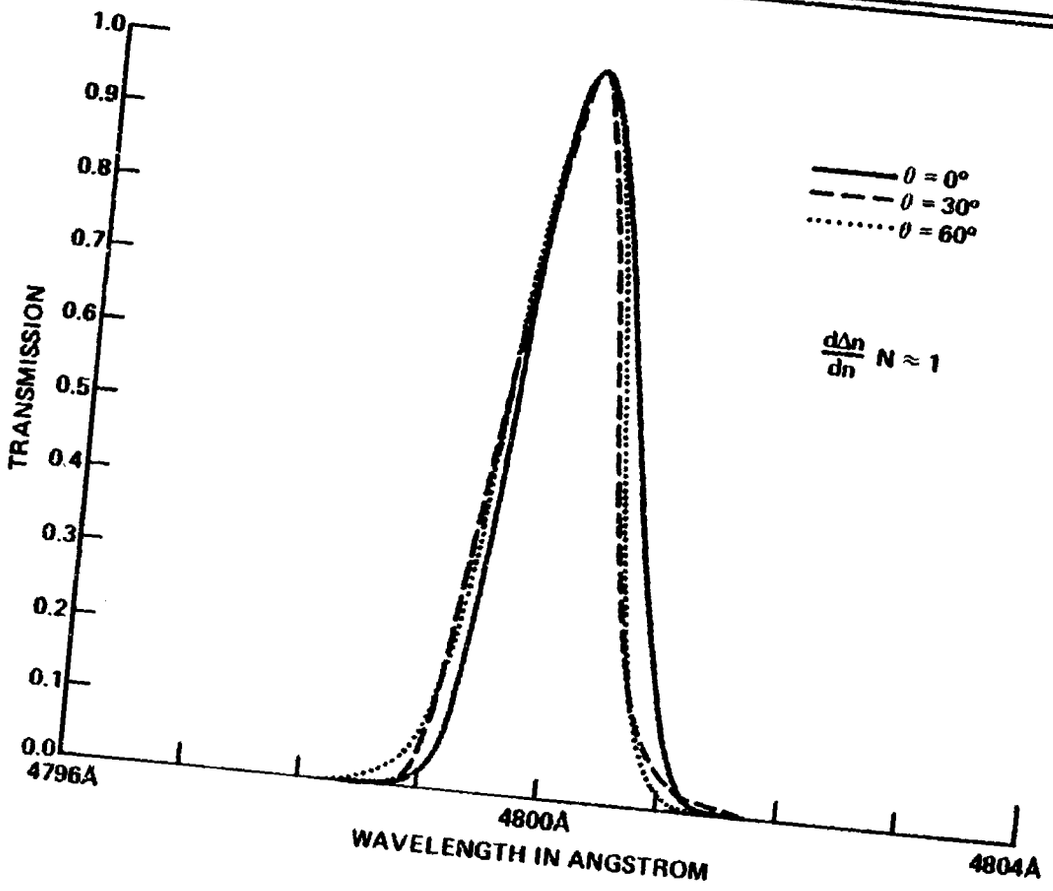

Rockwell International
Science Center

BANDWIDTH OF CHRISTIANSEN-BRAGG FILTER

SC79-5324

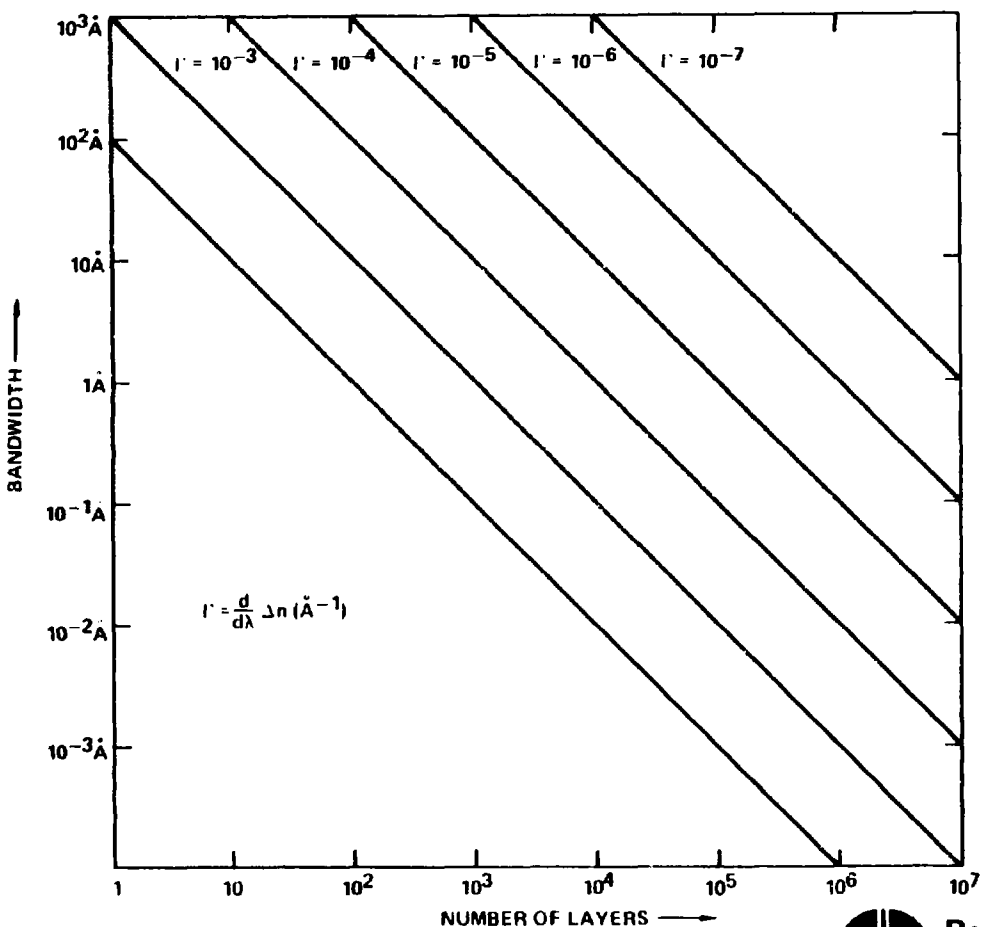

Rockwell International
Science Center

MATERIAL DISPERSION

SC79-5503

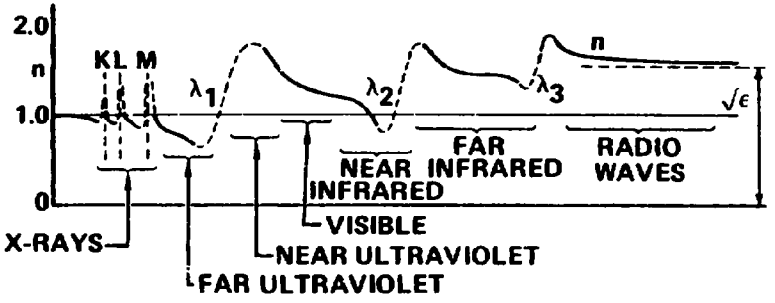

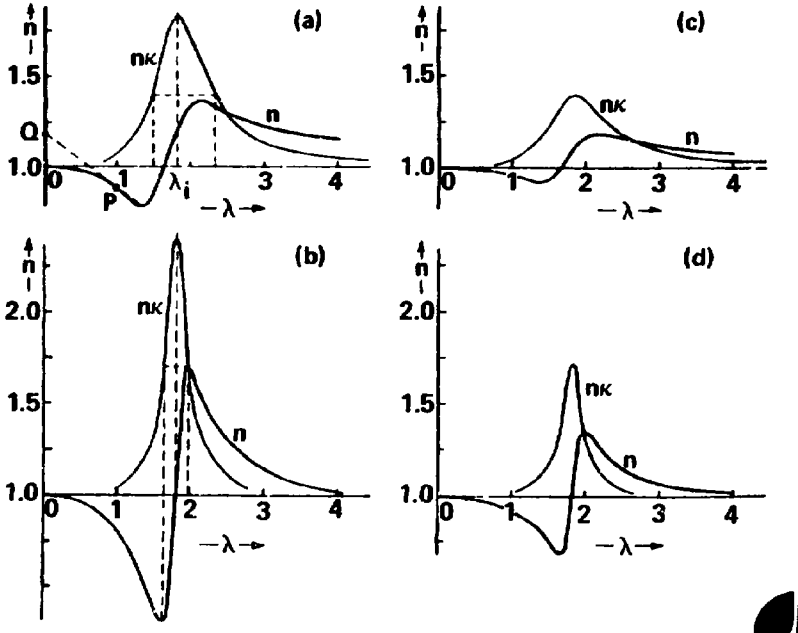

Rockwell International
Science Center

MEASURED DISPERSION

SC79-5323

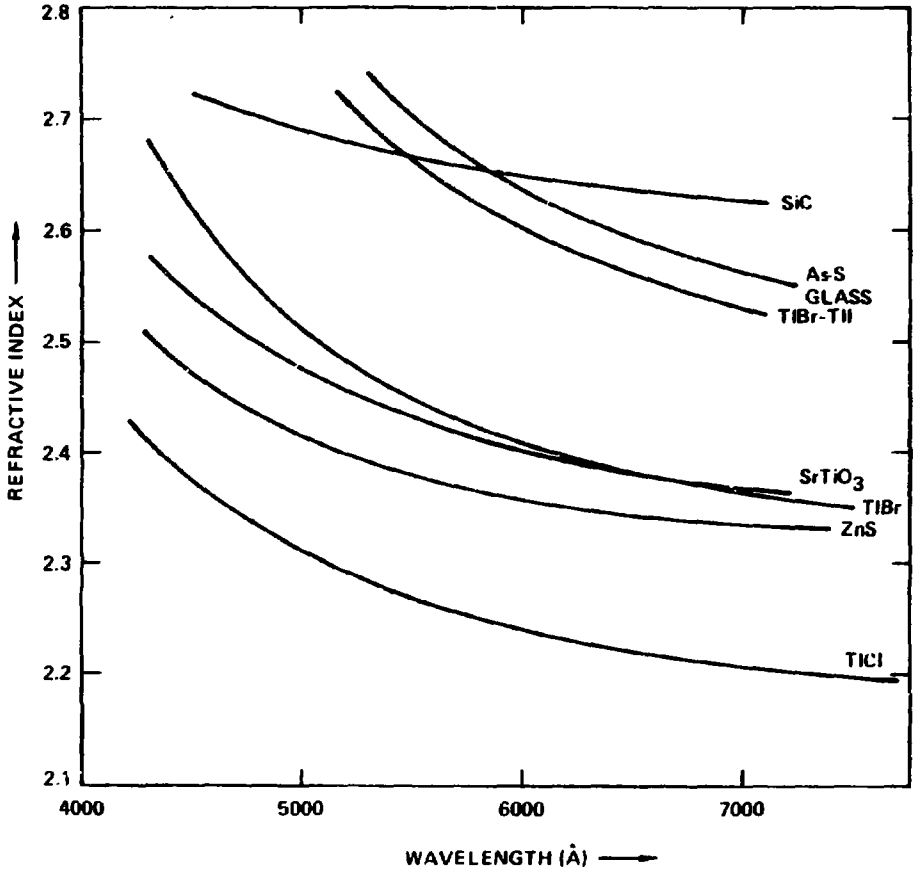

MEASURED DISPERSION

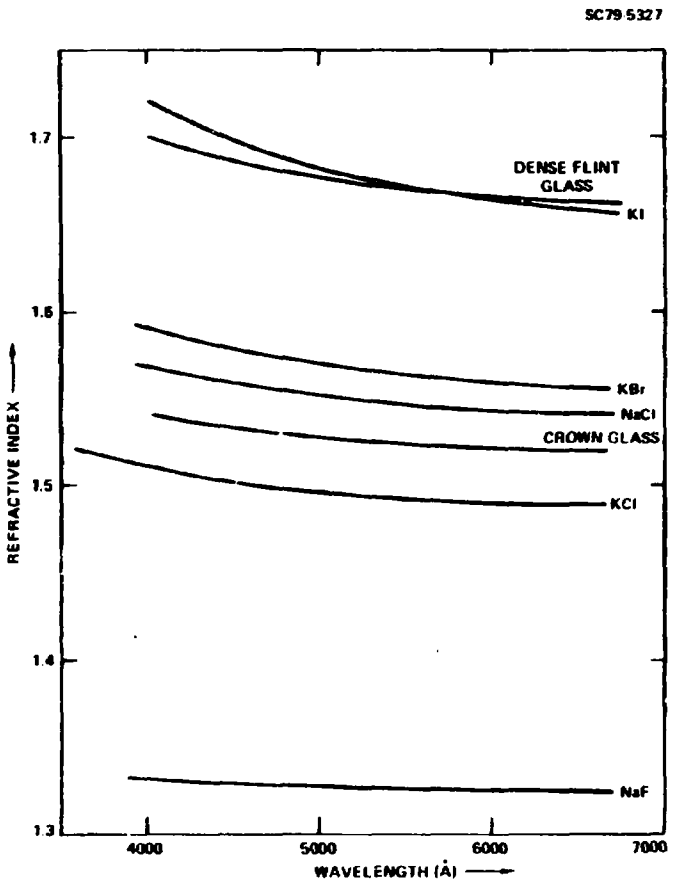

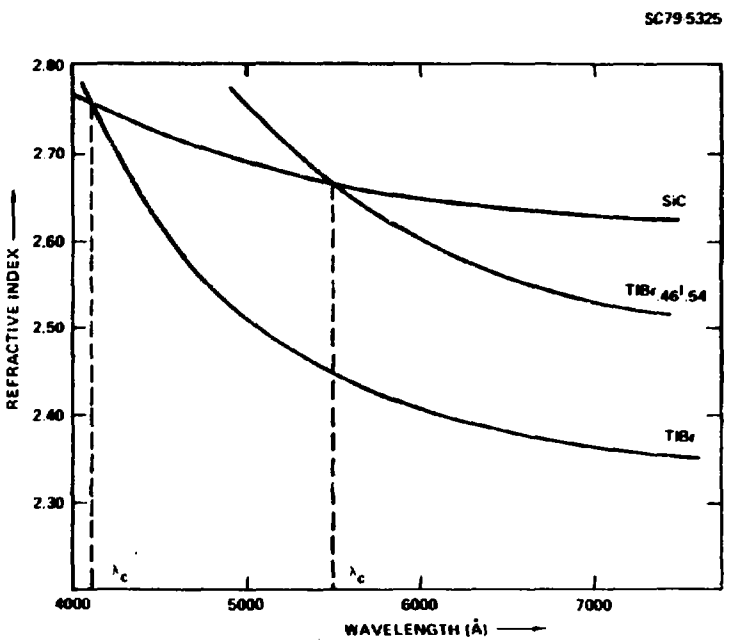

Rockwell International
Science Center

MEASURED DISPERSION

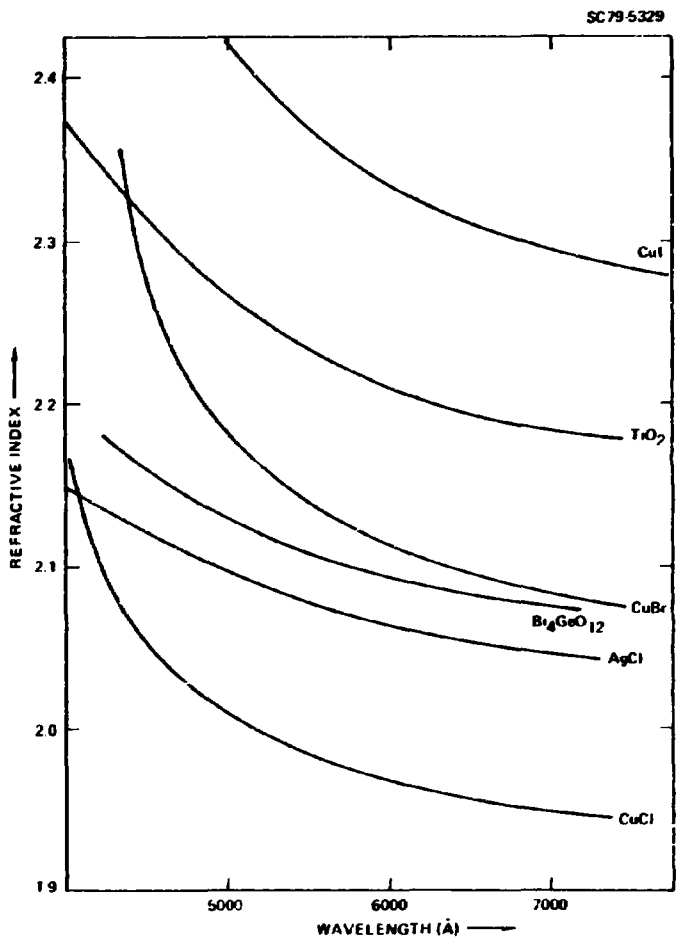

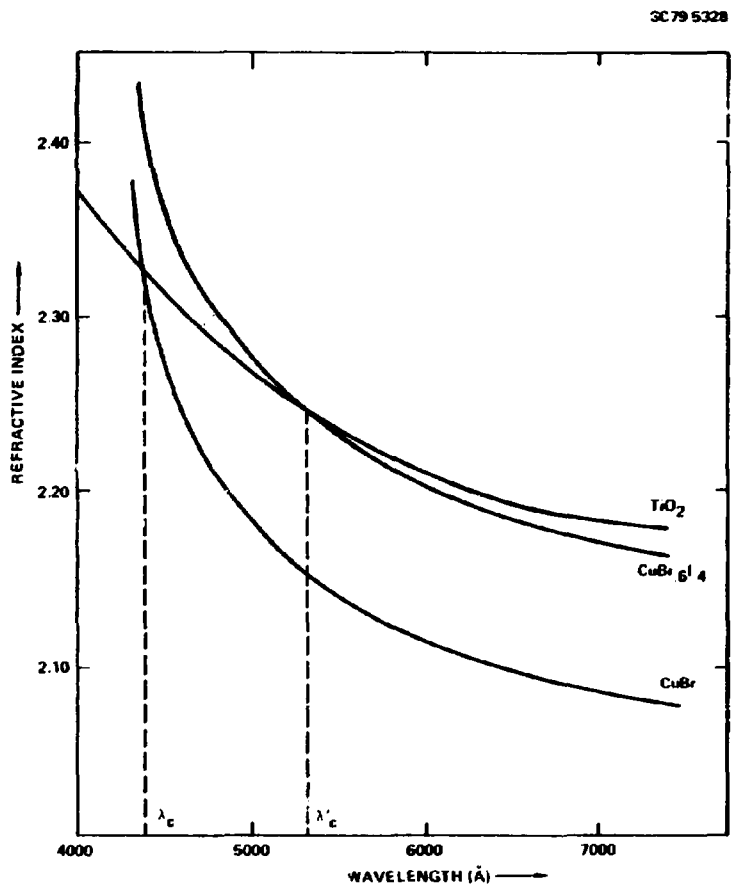

Rockwell International
Science Center

COMPARISON OF OUT-OF-BAND PROPERTIES

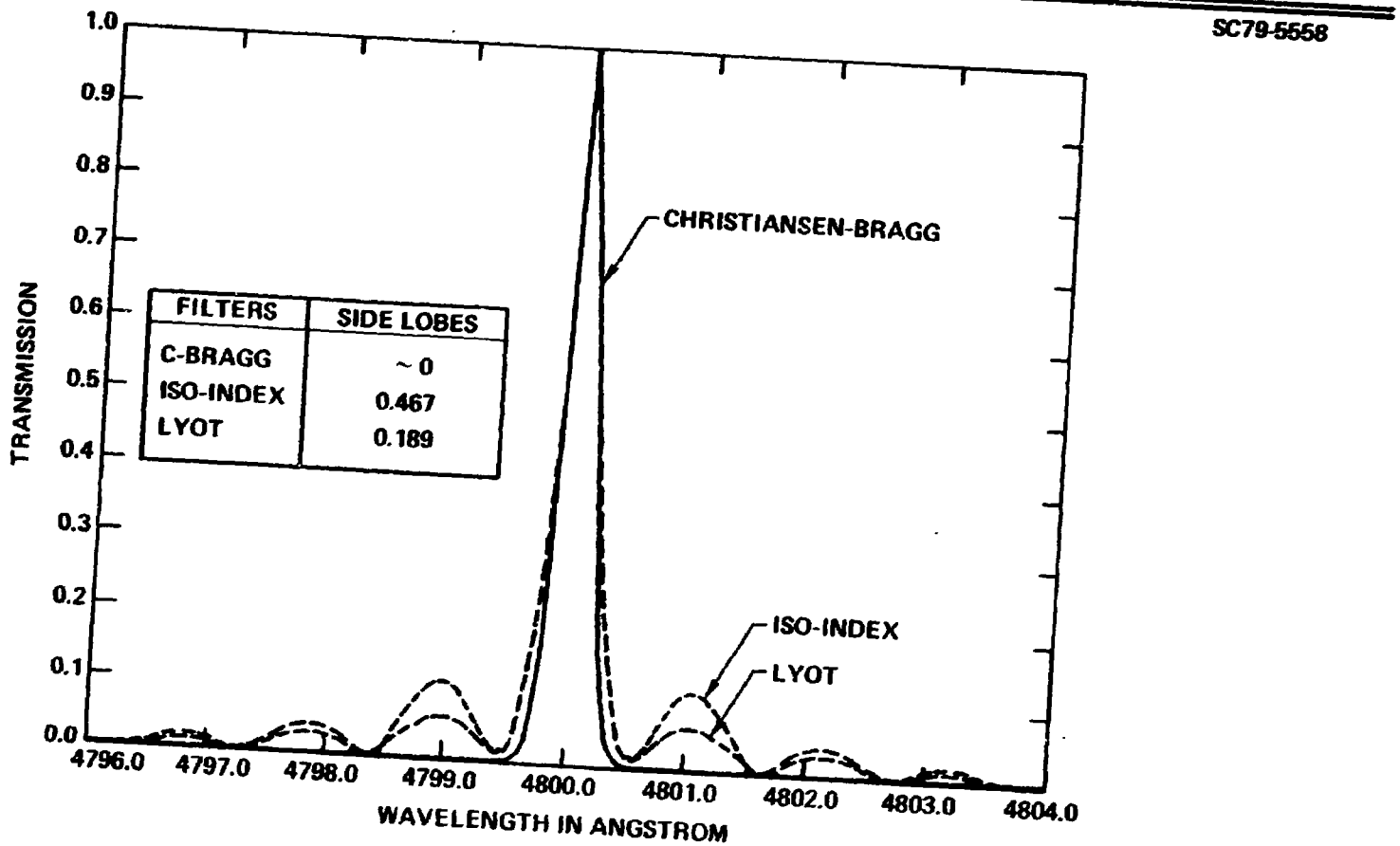

Rockwell International
Science Center

Summary: Thermal Control For Hole-Burning Filter

by R. Rochat and J. E. Jackson

This paper describes the hole-burning filter concept. At this point in time, it is only a concept since no research has been directed to develop material systems exhibiting the required filtering characteristics for the blue-green laser receiver. Conceptually the hole burning-filter possesses most of the characteristics sought for in this application: very narrow bandwidth, hemispherical field of view, unlimited aperture size, potentially high transmission, selectable center bandpass, and high out of band rejection. Conceptually a receiver employing the hole-burning filter would require about 10 dB less laser power than a receiver employing any of the other filter concepts. The research in hole-burning has been directed to memory devices and studies of fundamental material properties at cryogenic temperatures. There are two types of hole-burning: photochemical hole-burning (PHB) and nonphotochemical hole-burning (NPHB). Most all glasses and polymers exhibit NPHB but only about twenty glasses and crystallines have been observed to date that exhibit PHB. PHB is the preferred since a more stable and higher transmission filter could be fabricated. Examples of both NPHB and PHB material systems are given.

A small study has been done to determine the size, weight, and power of the cryogenic system required for the hole-burning filter. The results of this study are included.

McDonnell Douglas Astronautics Corp
PO Box 516
St Louis MO 63166

HOLE BURNING FILTER
CRYOGENIC COOLING FEASIBILITY STUDY

R.D. ROCHAT

MCDONNELL DOUGLAS

DESIGN CONDITIONS/CONSTRAINTS

ENVIRONMENTAL	PERFORMANCE
TEMPERATURE = 20°C PRESSURE = 1 ATM LOADS = 5g 3 AXES	SIZE = 1 METER DIA. TRANSMISSION = 50% AT 0.5 μm HEAT LOAD = 0 W. (ONLY HEAT LEAK) INPUT POWER = DESIGN FOR MINIMUM

REFRIGERATION SYSTEM CONCEPT

- 3 STAGE CLAUDE CYCLE
- HELIUM WORKING FLUID

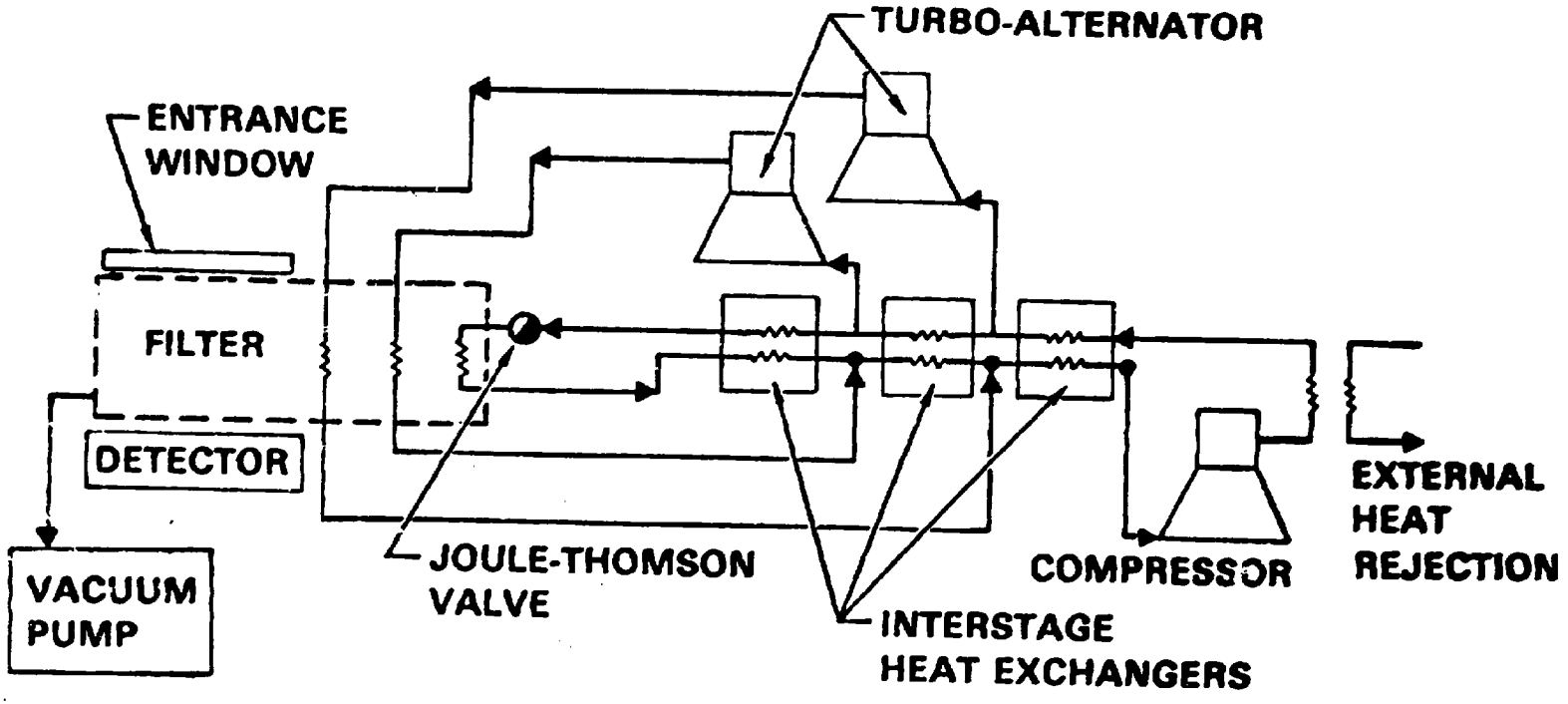

CARNOT COEFFICIENT OF PERFORMANCE

10-3482

$$COP = \frac{TC}{(-TC+TH)}$$

TC = COLD SIDE
TH = HOT SIDE = 20°C

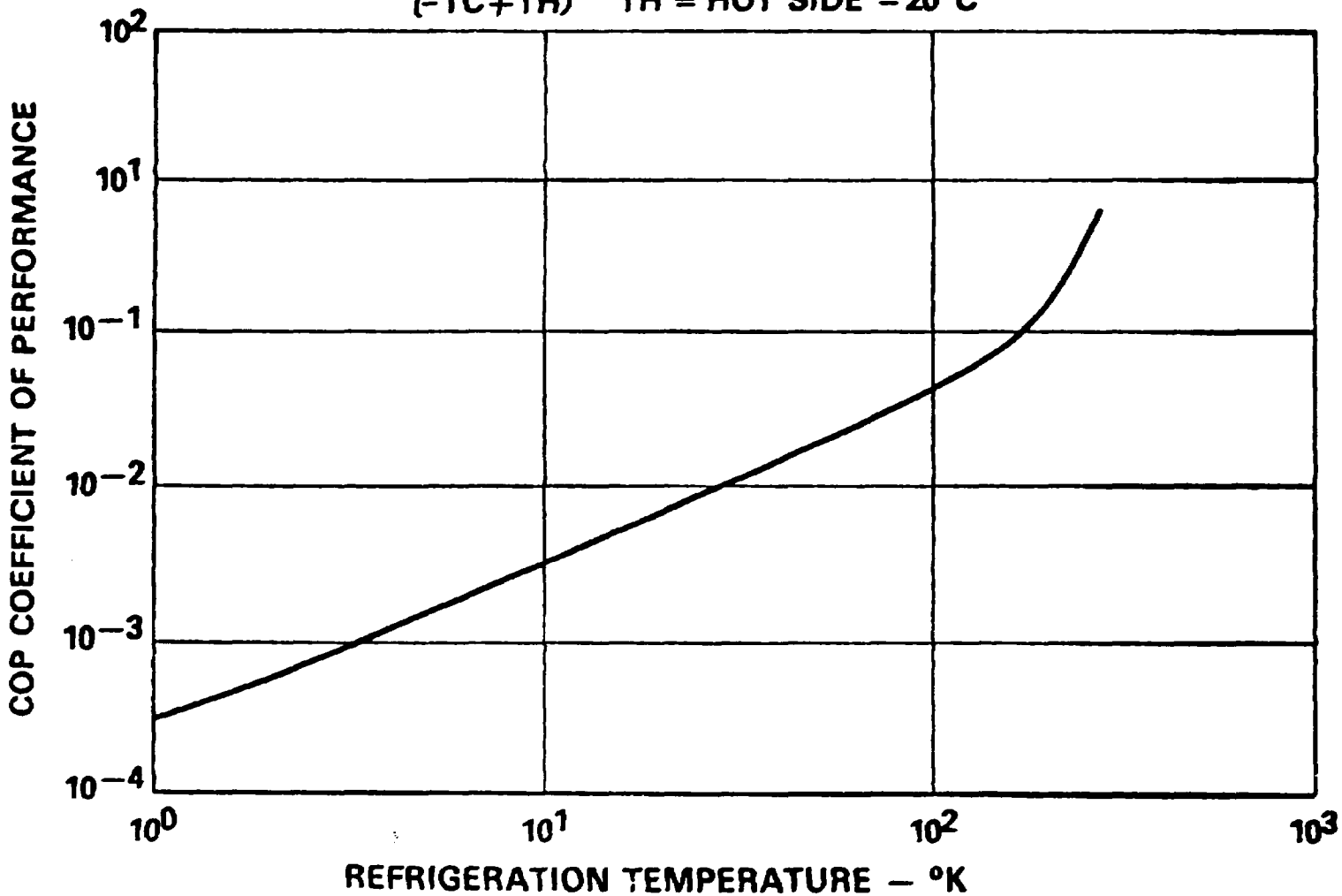

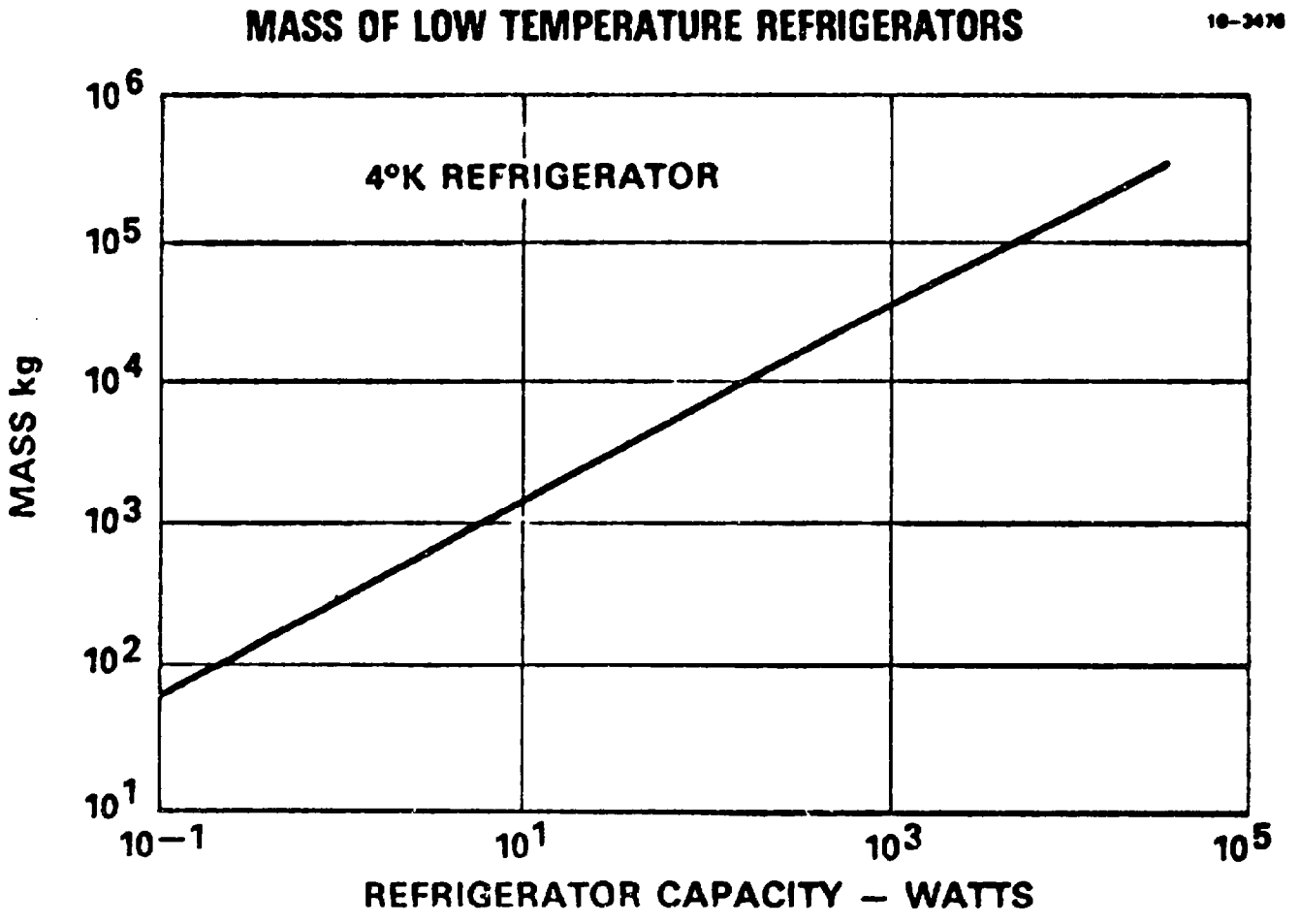
MASS OF LOW TEMPERATURE REFRIGERATORS
10-3478
4°K REFRIGERATOR
MASS kg
10^6
10^5
10^4
10^3
10^2
10^1
10^{-1}
10^1
10^3
10^5
REFRIGERATOR CAPACITY – WATTS

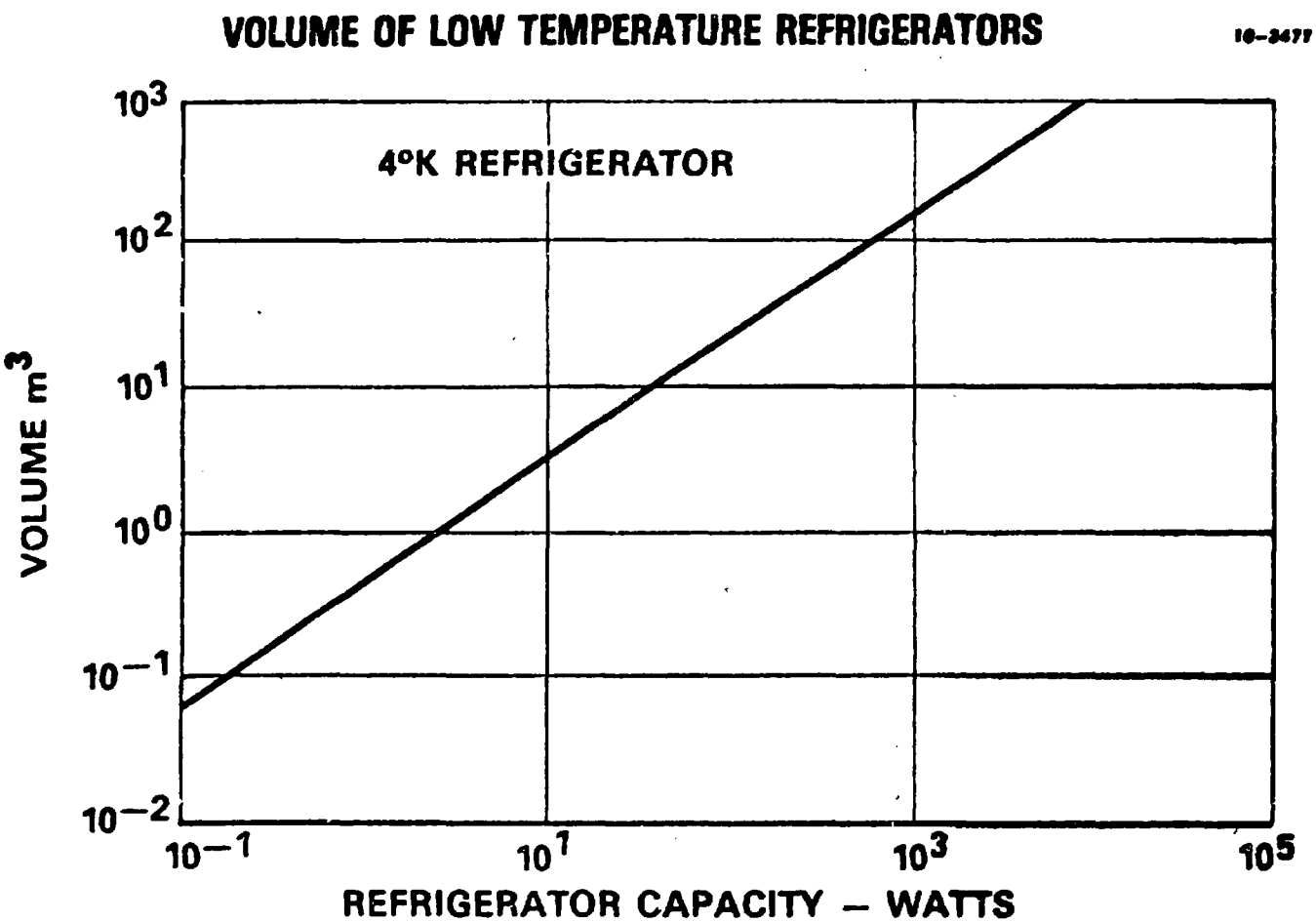
VOLUME OF LOW TEMPERATURE REFRIGERATORS
10-3477
4°K REFRIGERATOR
VOLUME m3
10^3
10^2
10^1
10^0
10^-1
10^-2
10^-1
10^1
10^3
10^5
REFRIGERATOR CAPACITY – WATTS

EFFICIENCY OF LOW TEMPERATURE REFRIGERATORS

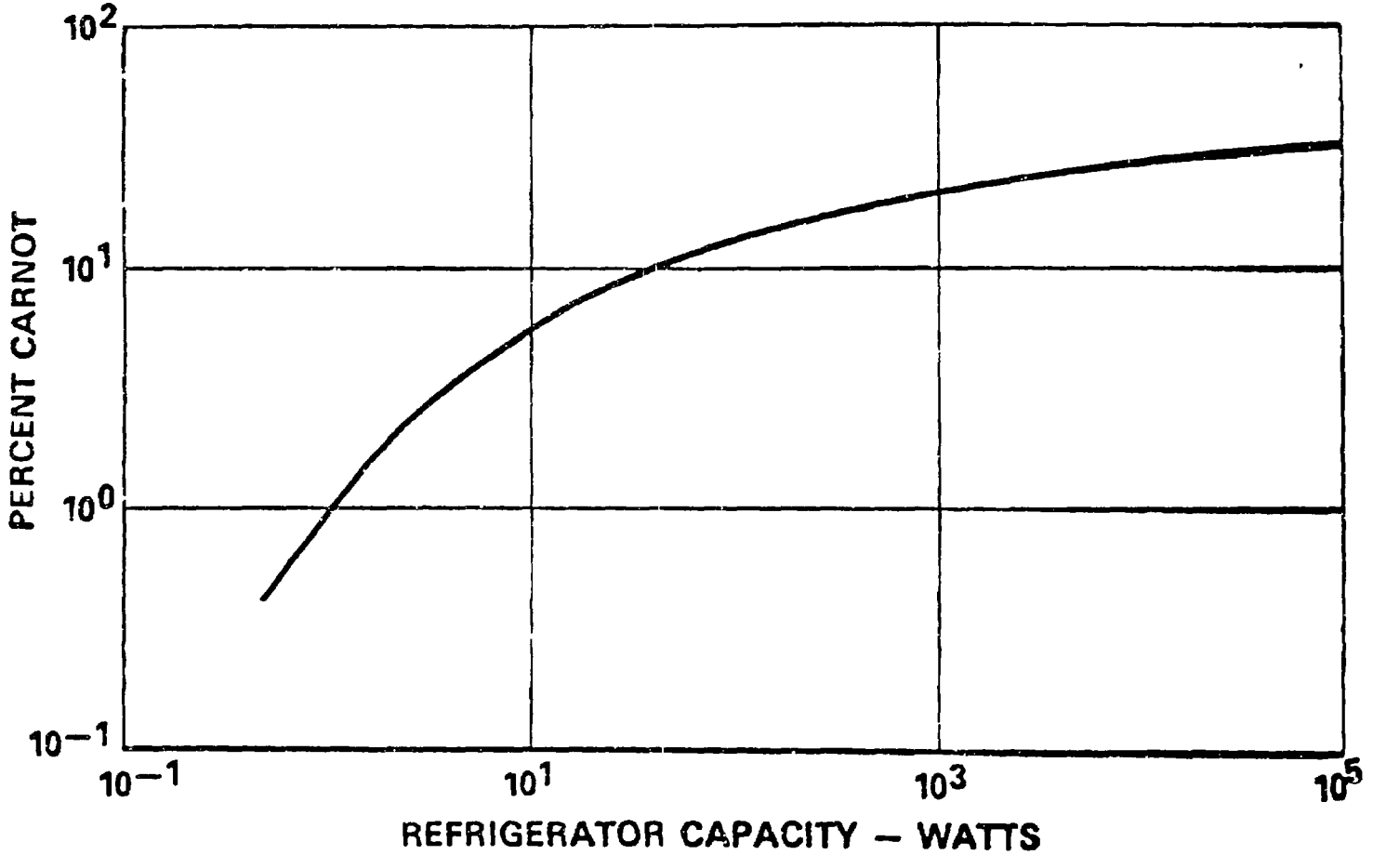

THERMAL CONDUCTIVITY STAINLESS STEEL 303

10-3478

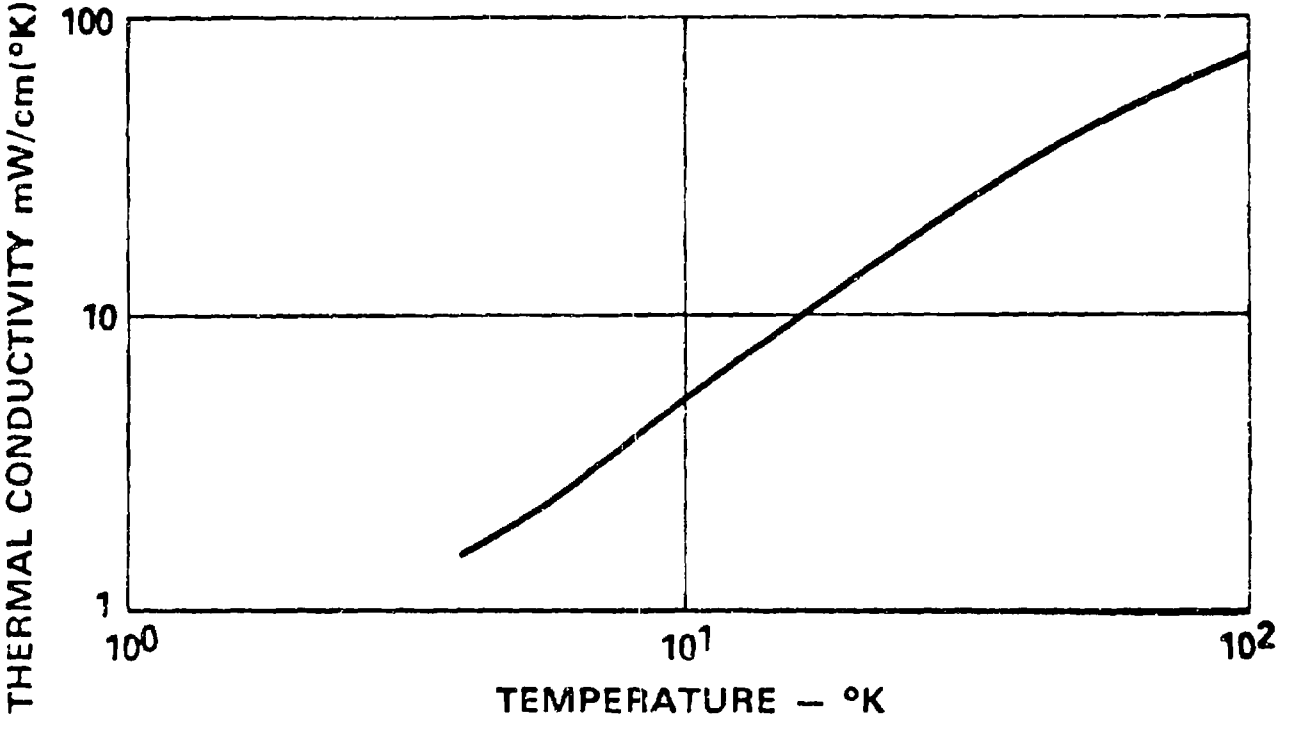

OPTICAL PROPERTIES OF INDUCED TRANSMISSION FILTER

10--3478

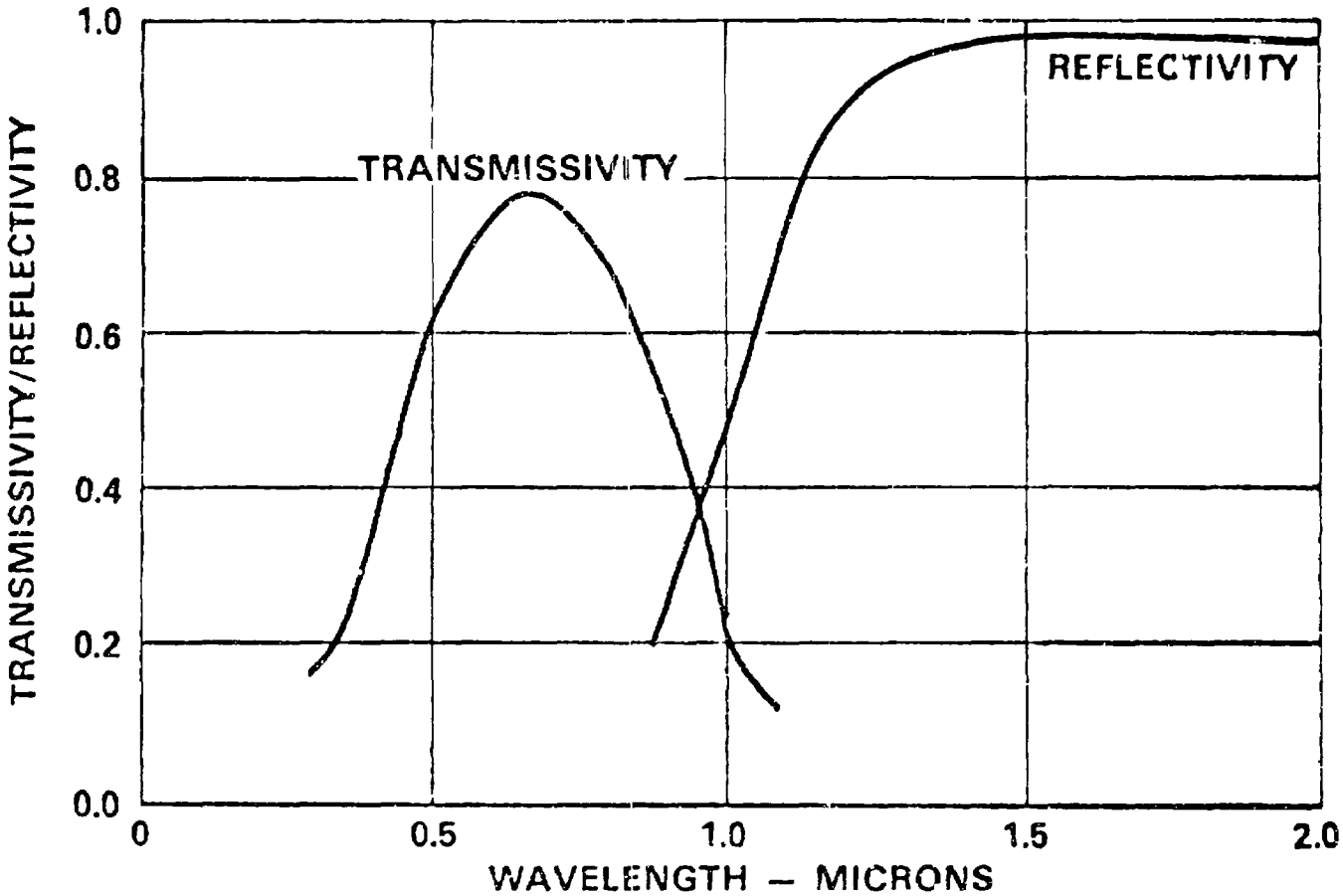

EFFECT OF NUMBER OF WINDOWS ON HEAT LEAK AND OPTICAL TRANSMISSION

10-3479

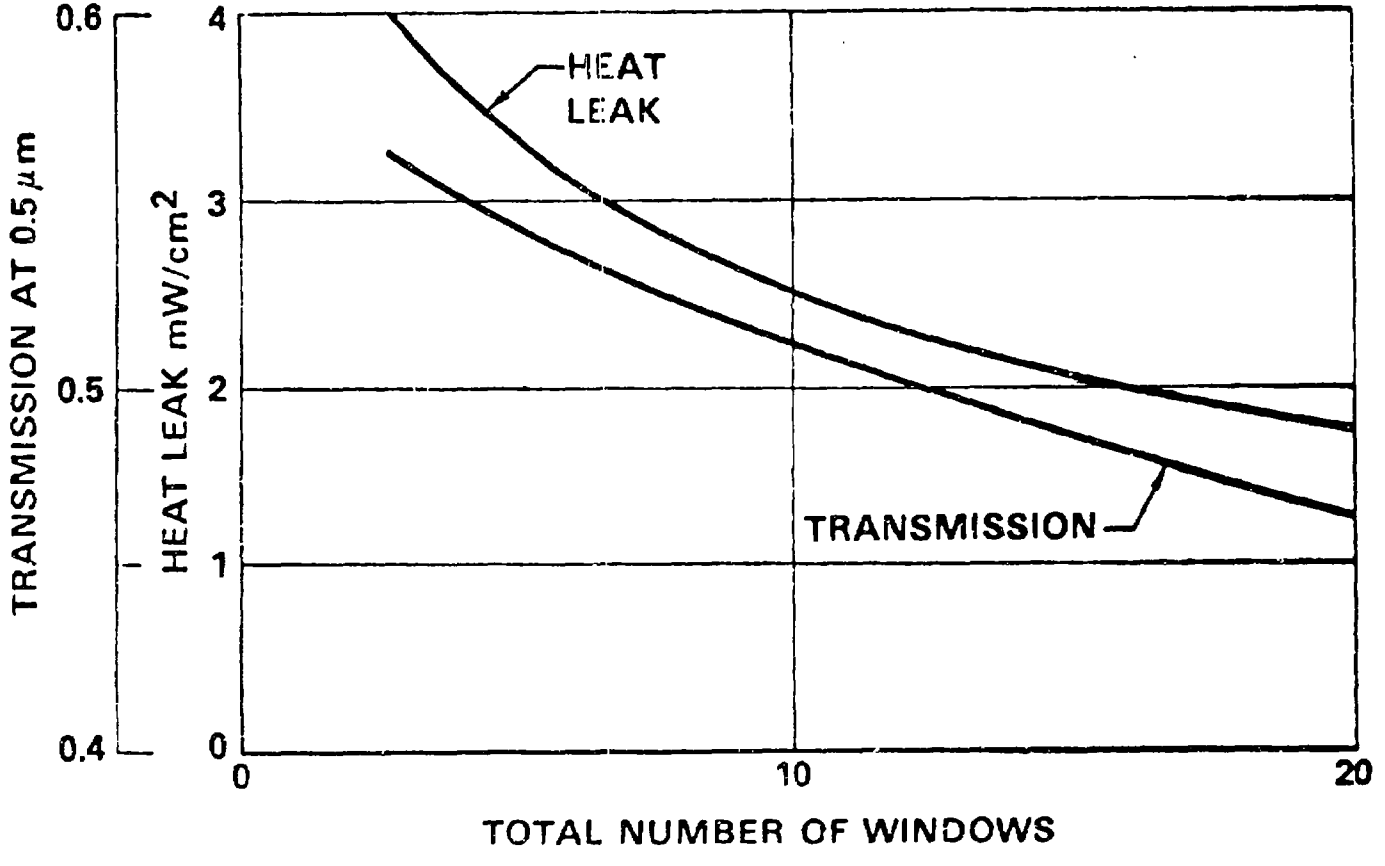

FILTER CONTAINMENT

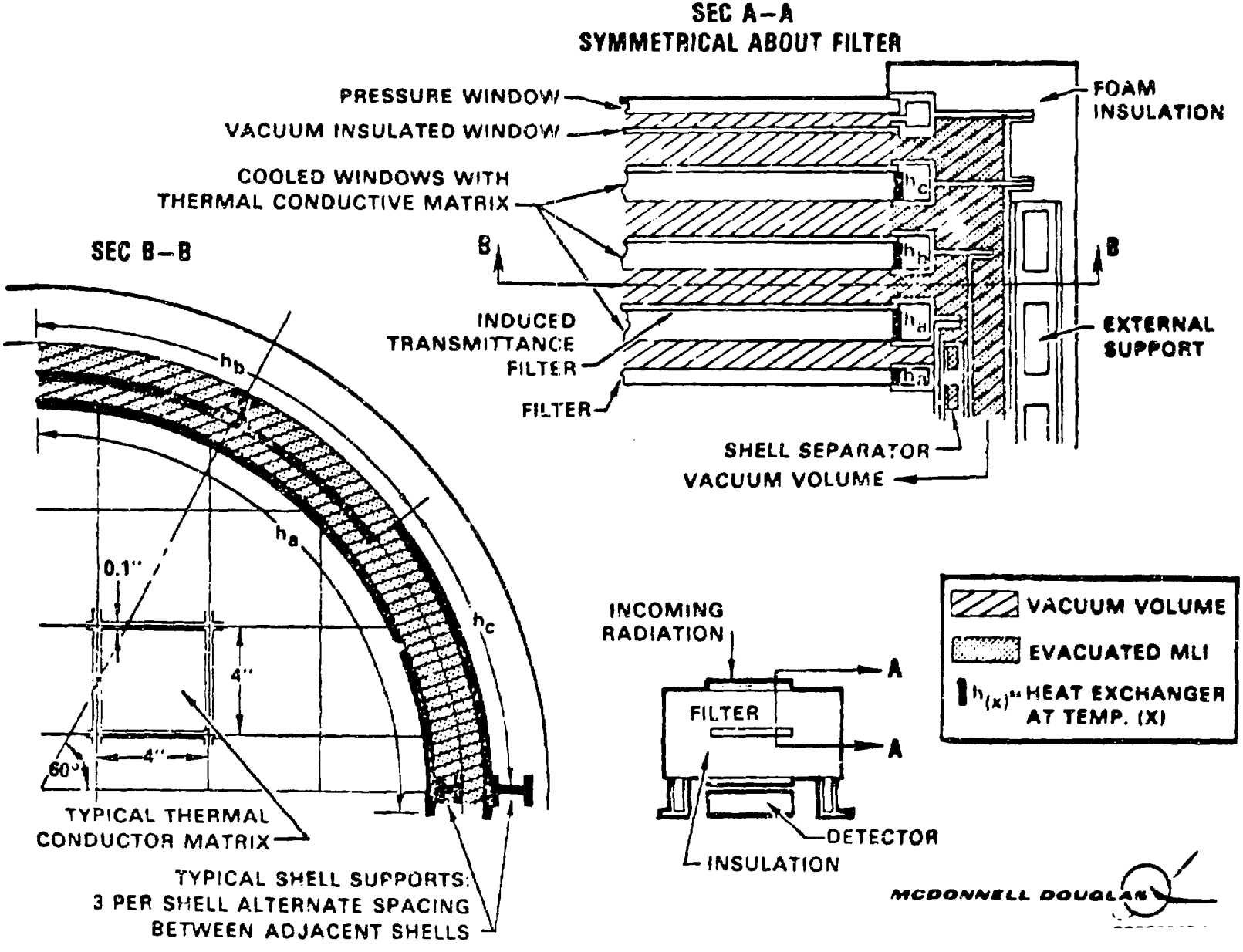

MCDONNELL DOUGLAS

FILTER CONTAINMENT THERMAL MODEL

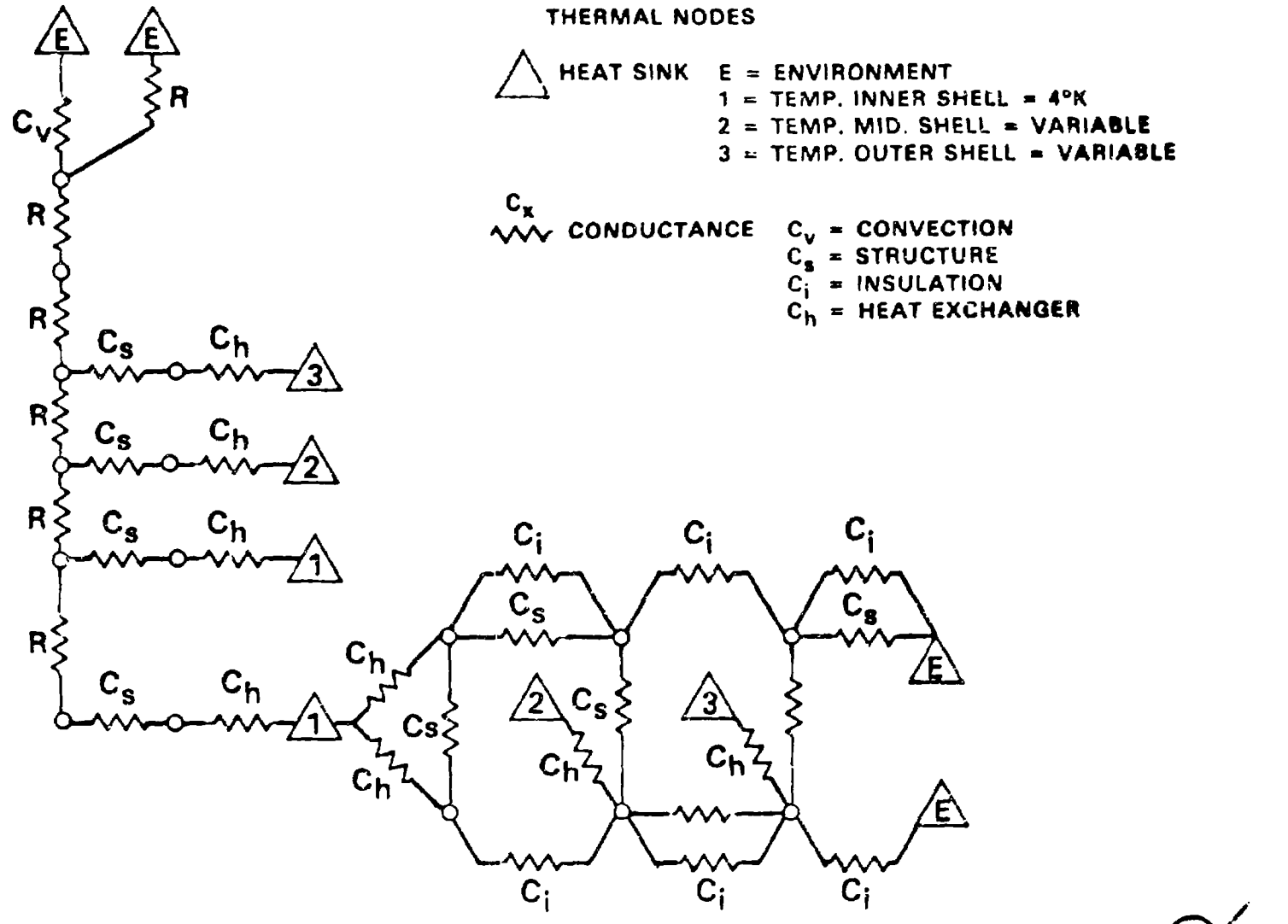

SENSITIVITY OF REFRIGERATOR POWER TO COOLER STAGE TEMPERATURES

10-3484

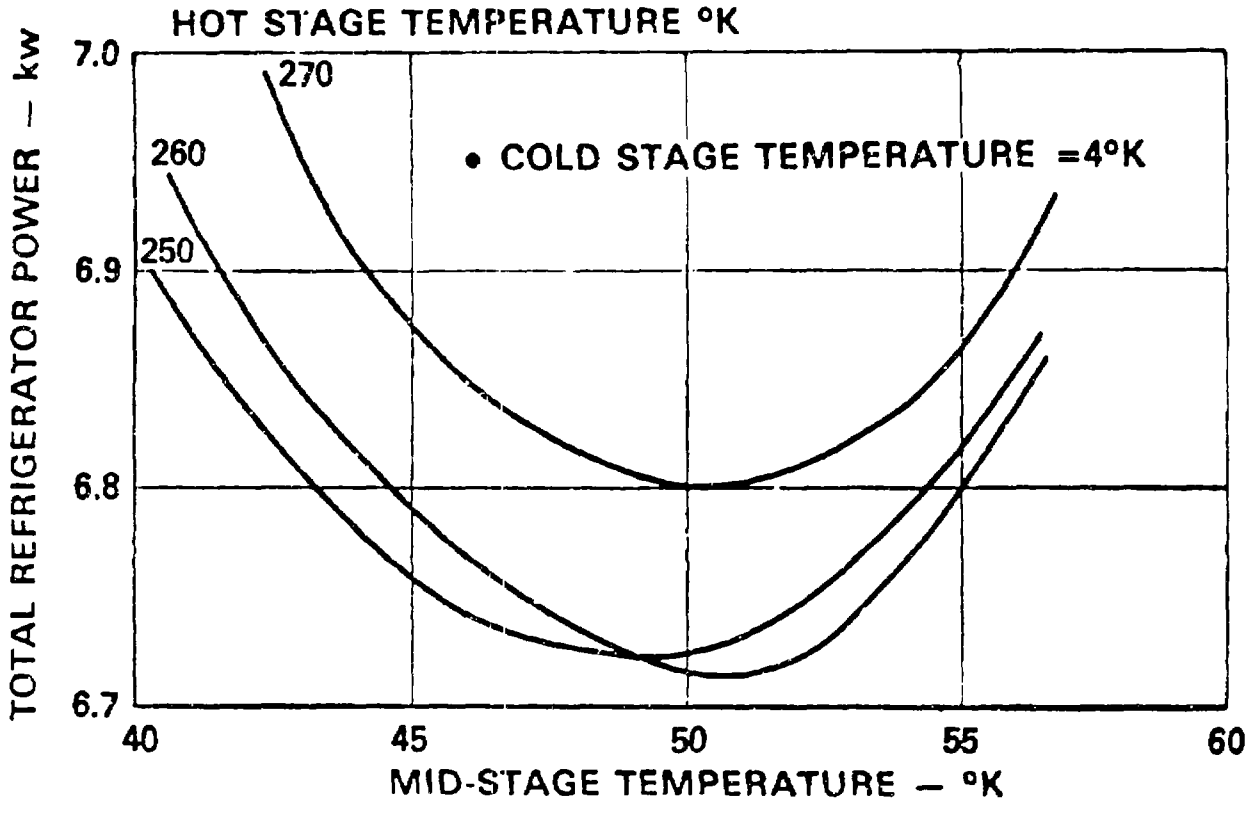

FILTER CONTAINMENT SUMMARY

HEAT LEAK/POWER SUMMARY

HEAT SINK	HEAT LEAK WATTS	REFRIGERATOR POWER WATTS
Containment Shells		
Cold Stage, 4°K	0.7	950
Mid Stage, 51°K	22.0	2090
Hot Stage, 260°K	74.0	155
Optical Windows		
Cold Stage, 4°K	2.2	3010
Mid Stage, 51°K	5.2	490
Hot Stage, 260°K	2.0	5
TOTAL	106.1	6700

CONFIGURATION SUMMARY

	REFRIGERATOR	CONTAINMENT
Power	6.7 kW	--
Size	1.4 m^3	0.8 m^3
Weight	860 kg	450 kg

	WEIGHT	% TRIDENT WEIGHT	% TRIDENT SAIL WEIGHT
Hole Burning Filter Refrigerator and Containment	1310	<.01	5.2
Birefringement Filter Receiver System	320	<.003	1.3

HOLE BURNING FILTER RECEIVER CONCEPT

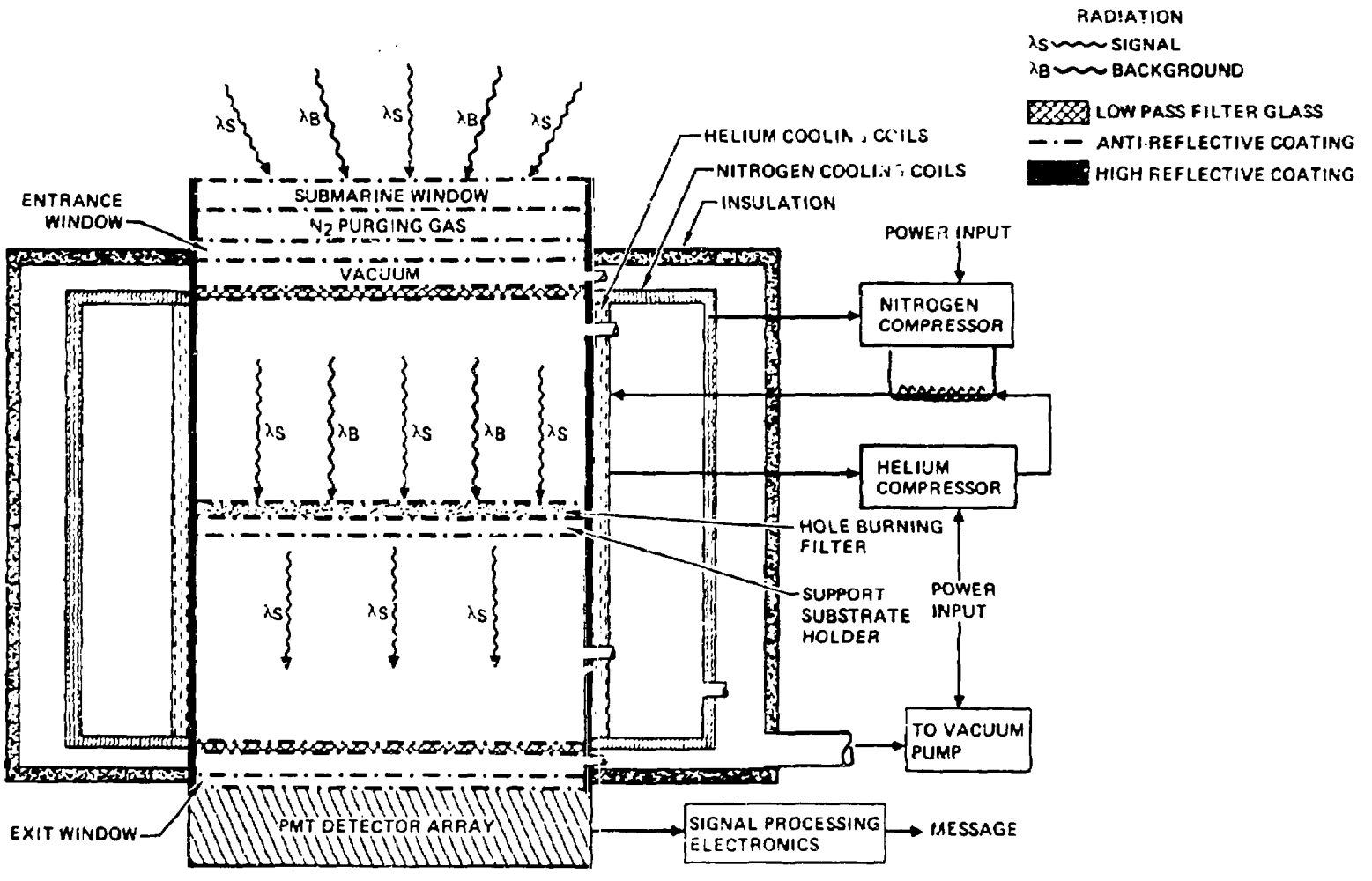

10-4364

HOLE BURNING FILTER CHARACTERISTICS

- VERY NARROW BANDWIDTH (CUSTOMIZING) $< 10^{-3}$ Å POSSIBLE
- ANGLE OF INCIDENCE INDEPENDENCE
- NOT APERTURE SIZE LIMITED
- TRANSMISSION
  - SHOULD IN PRINCIPLE BE VERY HIGH
  - HAVE OBSERVED UP TO 50% IN SOME SAMPLES
- CENTER BANDPASS IS SELECTABLE
- NO TIME DISPERSION
- HIGH OUT-OF-BAND REJECTION
- LIFETIME
  - MAY REUIRE IN SITU RENEWING DUE TO BLEACHING
- NOISE MECHANISMS
  - FLUORESCENCE
  - OTHERS

FILTER-RECEIVER CONCEPT COMPARISONS

10–3519

PERFORMANCE	ARAF CESIUM		BIREFRINGENT FILTER		HOLE BURNING FILTER	
WAVELENGTH (Å)	4255	dB	5183.6	dB	5183.6	dB
TRANSMISSION WINDOW-WATER INTERFACE TO PMT ARRAY (%)	31.8	−2.49	25.2*	−2.99	35	−2.28
FIELD OF VIEW IN WATER (DEGREES)	±49	0	±1.64*	−12.96	*49	0
TIME SPREAD (μSEC)	32.1	−0.66	0	0	0	0
PMT QUANTUM EFFICIENCY (%)	7.8	−5.54	15.7	−4.02	15.7	−4.02
RELATIVE TYPE 111 WATER TRANSMISSION (%/m)	87.83	−2.70	89	0	89	0
RELATIVE SOURCE IRRADIANCE (WATTS $.m^{-2}.\mu^{-1}$)	1046.7	−5.43	(.07)*1200 (FRAUNHOFER)	0	(.07)*1200 (FRAUNHOFER)	0
BACKGROUND BANDPASS (Å)	0.06	0.11	0.1*	5.00	0.1	5
SIGNAL BANDPASS (Å)	0.006	0	0.1*	0	0.01	0
OUT OF BAND REJECTION RADIO	10^{-6}	0	10^{-6}*	0	10^{-6}	0
FILTER RELATED NOISE	10^{-4}	0	–	0	–	0
RELATIVE TOTAL SIGNAL POWER DIFFERENCES (dB)		−9.41		−13.67		0

* DR. A TITLE OF LOCKHEED (PRIVATE COMMUNICATIONS) ESTIMATE OF EXPECTED PERFORMANCE.

HISTORY: HOLE BURNING FILTER

- FIRST PROPOSED BY RUSSIANS — OPT. SPECTROSC. VOL 39 PAGE 140, AUGUST 1975

- U. S. BEGAN HOLE BURNING RESEARCH ~ 1976
  - IBM
  - EASTMAN
  - AMES LABORATORY, IOWA STATE UNIVERSITY

UNCLASSIFIED

10–4361

HOLE BURNING FILTER TYPES

- PHOTOCHEMICAL
  - IBM
  - EASTMAN KODAK

  } MEMORY DEVICE RESEARCH

- NONPHOTOCHEMICAL (PHOTO PHYSICAL)
  - AMES LABORATORY: STUDIES OF MATERIAL PROPERTIES AT CRYOGENIC TEMPERATURES

10–4362

MATERIAL SYSTEMS UNDERGOING NPHB AND PHB

NPHB

- INORGANIC GLASSES
- ORGANIC GLASSES
- POLYMERS

PHB

- LESS THAN 20 HAVE BEEN INVESTIGATED
  - GLASSES
  - CRYSTALLINES

MOLECULAR ENERGY LEVELS AND ABSORPTION SPECTRA

10-4379

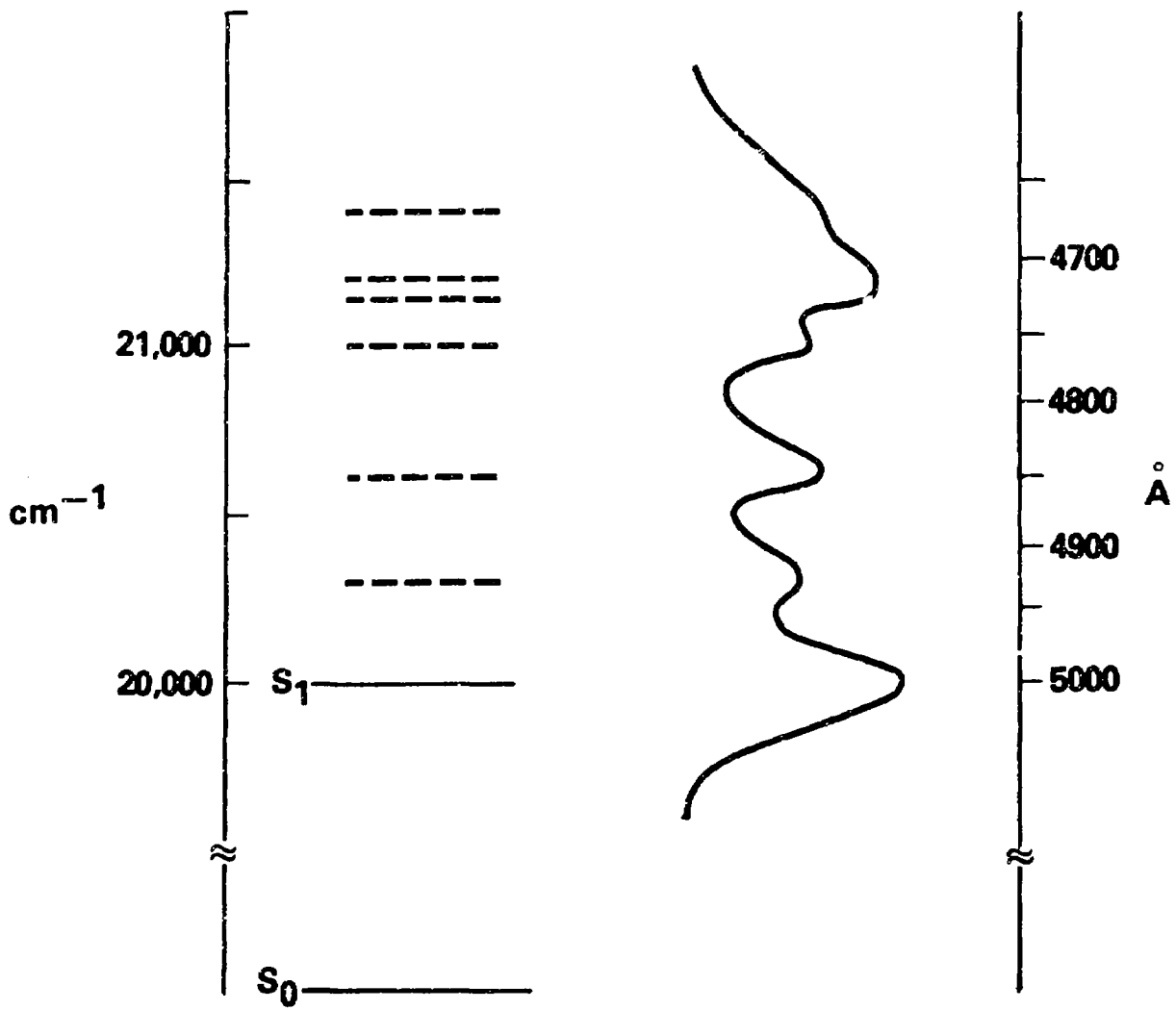

LINE BROADENING IN GLASSES

10-4376

a) HOMOGENEOUS: LIFETIME $< 10^{-1}$ cm^{-1}

b) INHOMOGENEOUS: AMORPHOUS STRUCTURE YIELDS STATISTICAL DISTRIBUTION OF IMPURITY SITES WITH VERY LARGE ($\sim$ 200 cm^{-1}) DISTRIBUTION OF SITE EXCITATION ENERGIES

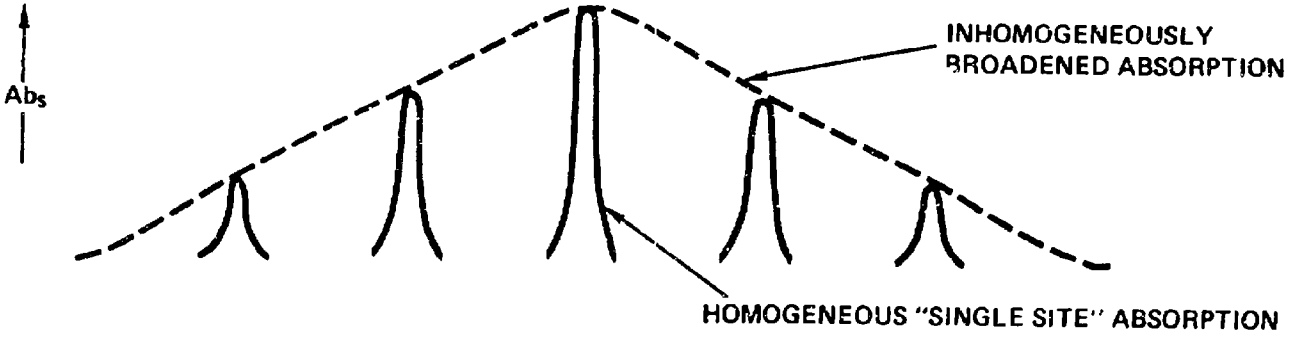

AT LOW TEMPERATURES (<10K) WHERE SITE INTERCHANGE IS SLOW, NARROWBAND SOURCES (LASERS) CAN PROBE "SINGLE SITE" PROCESSES

$A_\nu + h_\nu \longrightarrow A^*_\nu$ "SINGLE SITE" ABSORPTION

$A^*_\nu \longrightarrow A_\nu + h_\nu$ "SINGLE SITE" FLUORESCENCE

IF, DURING THE LIFETIME OF THE STATE A^*_ν, THERE IS SOME PROCESS WHICH PREVENTS RETURN OF A^*_ν TO THE STATE A_ν, THEN A GAP WILL APPEAR IN THE INHOMOGENEOUSLY BROADENED ABSORPTION AT THE FREQUENCY, ν., I.E., A HOLE WILL BE BURNT AT ν.

PHOTOCHEMICAL HOLE BURNING

10-4374

$A_\nu + h\nu \rightarrow A^*_\nu$ SINGLE SITE ABSORPTION

$A^*_\nu \longrightarrow B^*_{\nu'}$ PHOTO REARRANGEMENT

OR

$A^*_\nu + S \longrightarrow B^*_{\nu'}$ SOLVENT ADDITION

$B^*_\nu \longrightarrow B_{\nu'}$ PRODUCT FLUORESCENCE

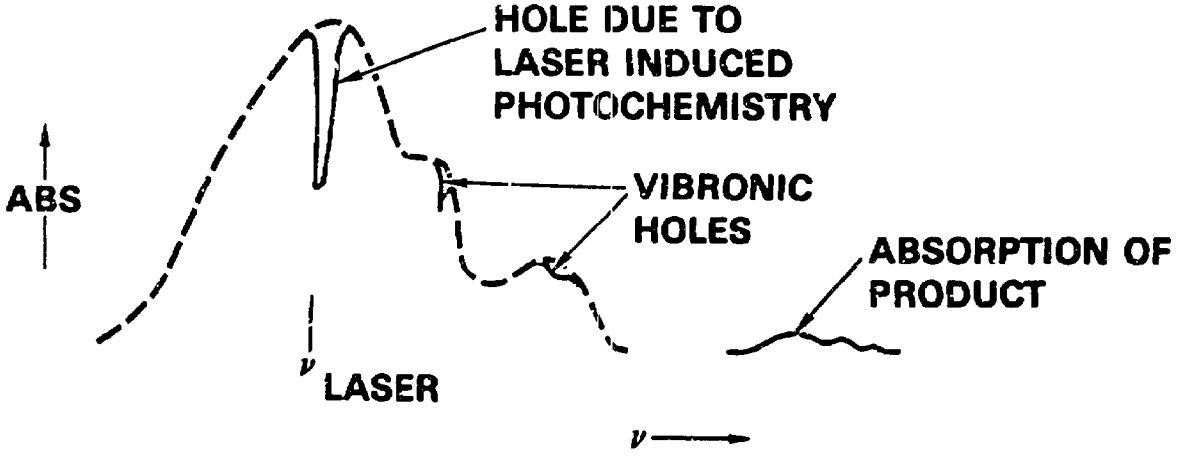

NON-PHOTOCHEMICAL HOLE BURNING

10-4372

$A_\nu + h\nu \longrightarrow A_\nu^*$ SINGLE SITE ABSORPTION

$A_\nu^* \longrightarrow A_{\nu'}^*$ SITE REARRANGEMENT

$A_{\nu'}^* \longrightarrow A_{\nu'} + h_{\nu'}$ NEW SITE FLUORESCENCE

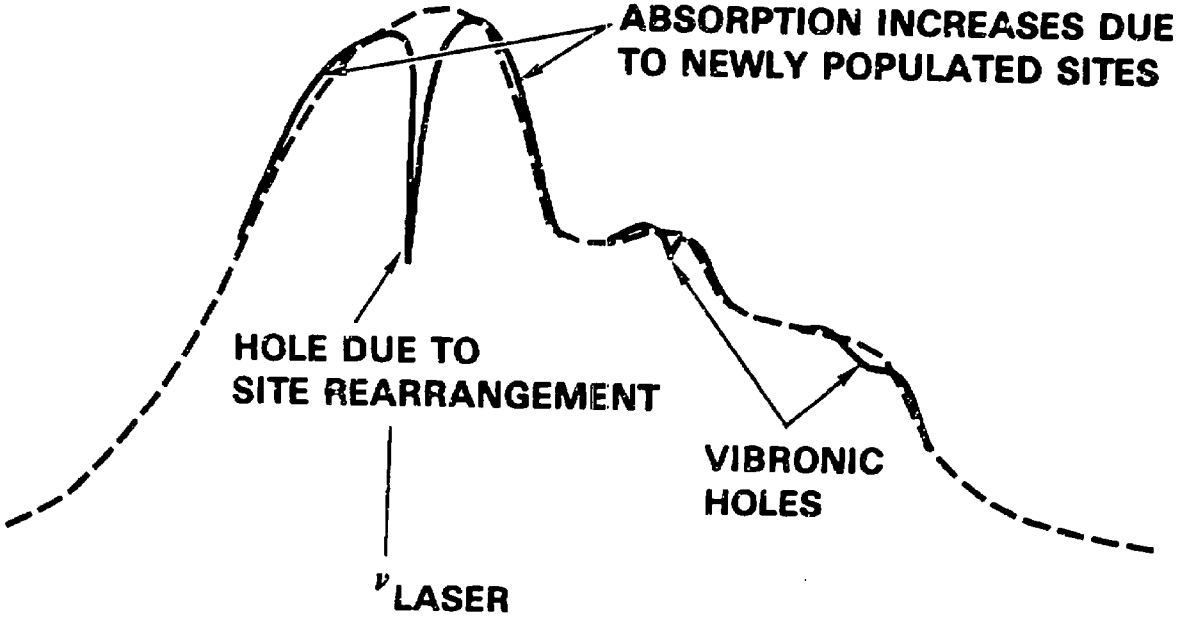

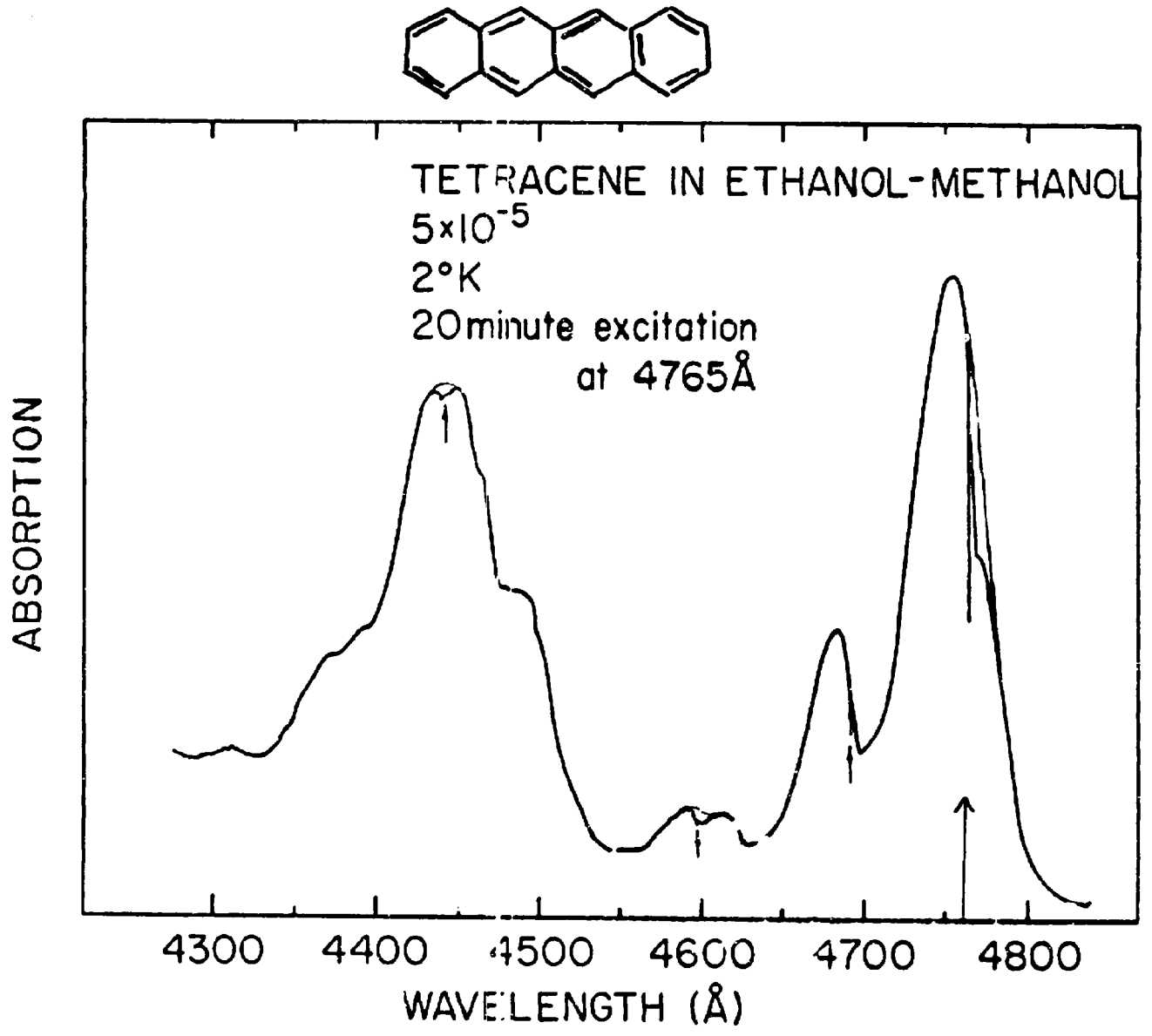
TETRACENE IN ETHANOL-METHANOL
5x10-5
2°K
20minute excitation
at 4765Å
ABSORPTION
4300
4400
4500
4600
4700
4800
WAVELENGTH (Å)

10-4375

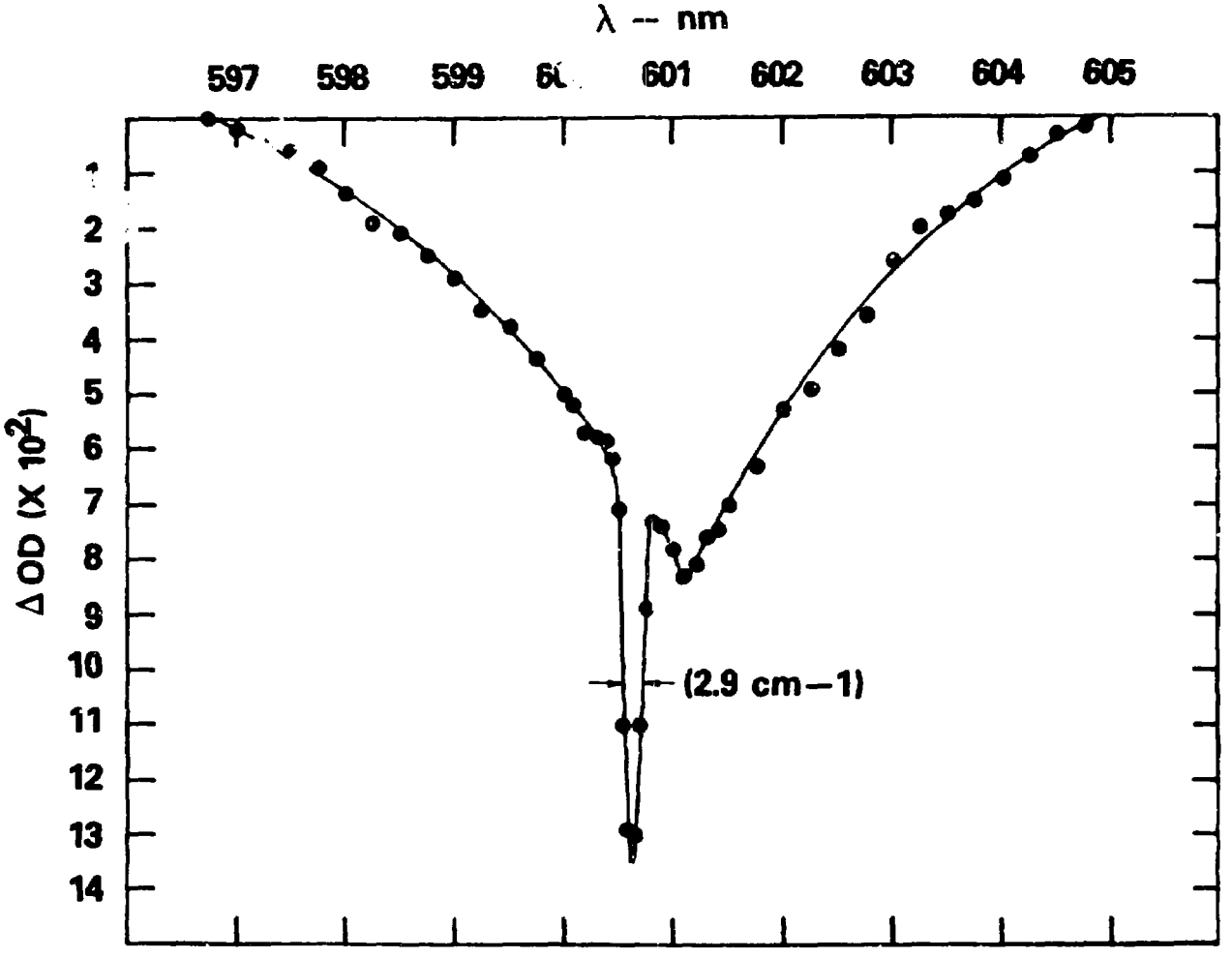

NPHB BURNING OF RHODAMINE 640 IN PMMA, T_B = 4.2K. IRRADIATION WAS INTO 0–0 BAND OF R640'S ABSORPTION SPECTRUM. THE SHARP DIP (2 9 cm^{-1} WIDE) IS COINCIDENT WITH ν_B. ΔOD DENOTES THE CHANGE IN OPTICAL DENSITY PRODUCED BY BURNING.

UNCLASSIFIED

10—4351

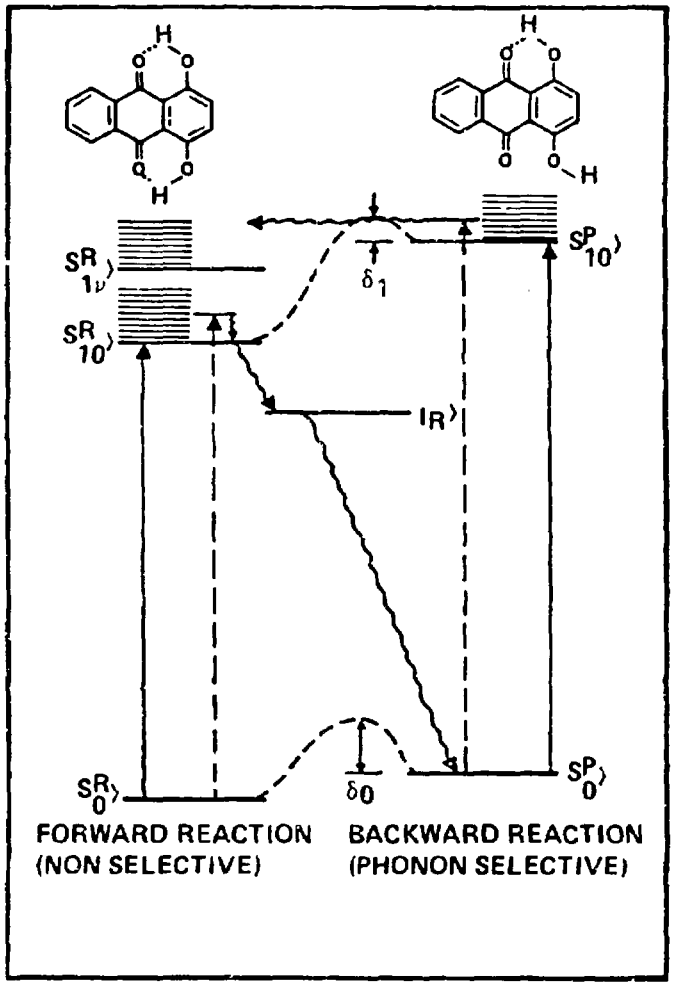

THE ENERGY LEVEL SCHEME FOR QUINIZARIN (R) AND ITS PHOTOPRODUCT (P). SUPERIMPOSED ON THE ELECTRONIC AND VIBRATIONAL STATES (ν) ARE THE PHONON STATES OF THE GLASS. $|R\rangle$ REPRESENTS AN INTERMEDIATE STATE IN THE PHOTOCHEMICAL REACTION SCHEME. δ_0 AND δ_1 ARE REACTION BARRIERS IN THE GROUND AND EXCITED STATE ENERGY SURFACE.

UNCLASSIFIED

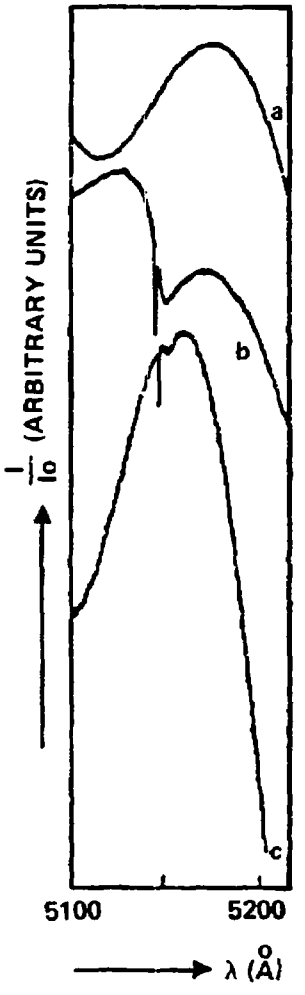

A) FIRST SINGLET ABSORPTION BAND OF QUINIZARIN IN AN EtOH-MeOH GLASS (3:1).
B) AFTER 20 MINUTE EXPOSURE TO THE RADIATION OF AN Ar ION LASER
C) AFTER 5 MINUTE EXPOSURE TO THE RADIATION OF A Xe-HIGH PRESSURE LAMP (75W, TRACE c IS ON A DIFFERENT SCALE).

UNCLASSIFIED

10-4350

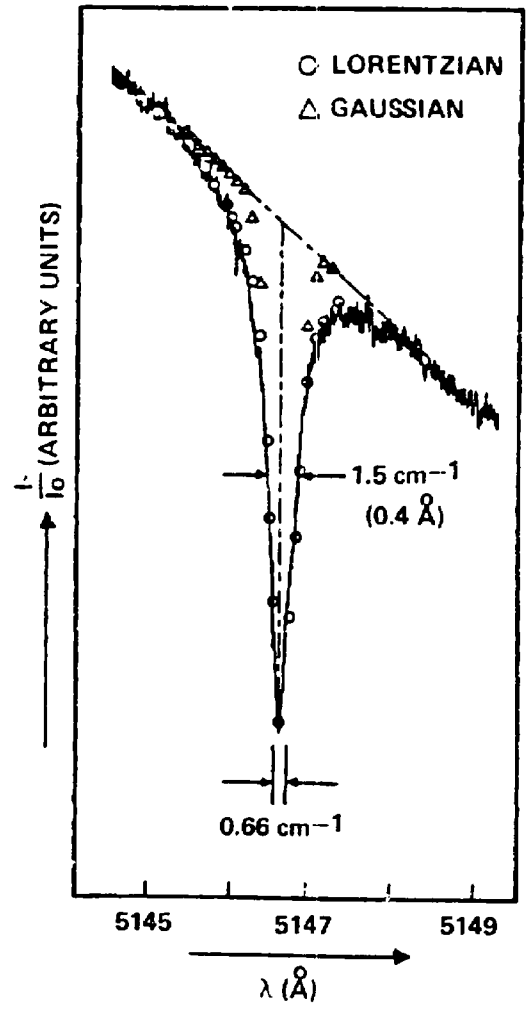

PHOTOCHEMICAL HOLE IN THE FIRST SINGLET ABSORPTION OF QUINIZARIN IN A 3:1 MIXTURE OF EtOH AND MeOH (2°K), PRODUCED BY 15 MINUTE IRRADIATION, WITH AN Ar ION LASER (3mW). THE BANDPASS OF THE SPECTROMETER WAS 0.66 cm^{-1}.

HUGHES
HUGHES AIRCRAFT COMPANY

PRESENTATION _____

REQUESTER ORIGINATOR _____ DATE _____

HUGHES
HUGHES AIRCRAFT COMPANY
RESEARCH LABORATORIES

NON LINEAR OPTICAL PHASE CONJUGATION FOR SLC UPLINK

C R GIULIANO

Hughes Research Laboratory
3011 Malibu Canyon Road
Malibu CA 90265

ELEMENTS OF PRESENTATION

HUGHES
HUGHES AIRCRAFT COMPANY
RESEARCH LABORATORIES

8703-1

- WHAT IS PHASE CONJUGATION?
- HOW CAN IT BE USED?
- HOW DO WE MAKE CONJUGATORS?
- WHERE DO WE STAND?
- WHAT'S LEFT TO BE DONE

BACKGROUND

EARLY SOVIET WORK (ZELDOVICH, et al; STEPANOV, et al.)	(1972)
DEVELOPMENT OF CONCEPT FOR LASER APPLICATIONS AT HRL	(1974)
CONCEPT FOR REAL-TIME HOLOGRAPHIC CONJUGATION AT HRL	(1974)
EXPERIMENTAL DEMONSTRATION AT HRL	(1976)
DARPA/ONR SUPPORT	(1977)
DOE/LASL SUPPORT	(1978)
AFOSR SUPPORT	(1979)

RAPIDLY EXPANDING ACTIVITY
OVER 100 PUBLICATIONS SINCE 1972

AREAS OF ACTIVITY

USSR	USA
LEBEDEV INSTITUTE	HUGHES
MOSCOW UNIVERSITY	CAL TECH
UKRANIAN SSR	USC
INSTITUTE FOR RADIOPHYSICS	BELL LABS
USSR ACADEMY OF SCIENCES	LASL
	AFWL/U. ARIZONA

HUGHES
HUGHES AIRCRAFT COMPANY

PRESENTATION

REQUESTER ORIGINATOR

DATE

UNCLASSIFIED

B703-5

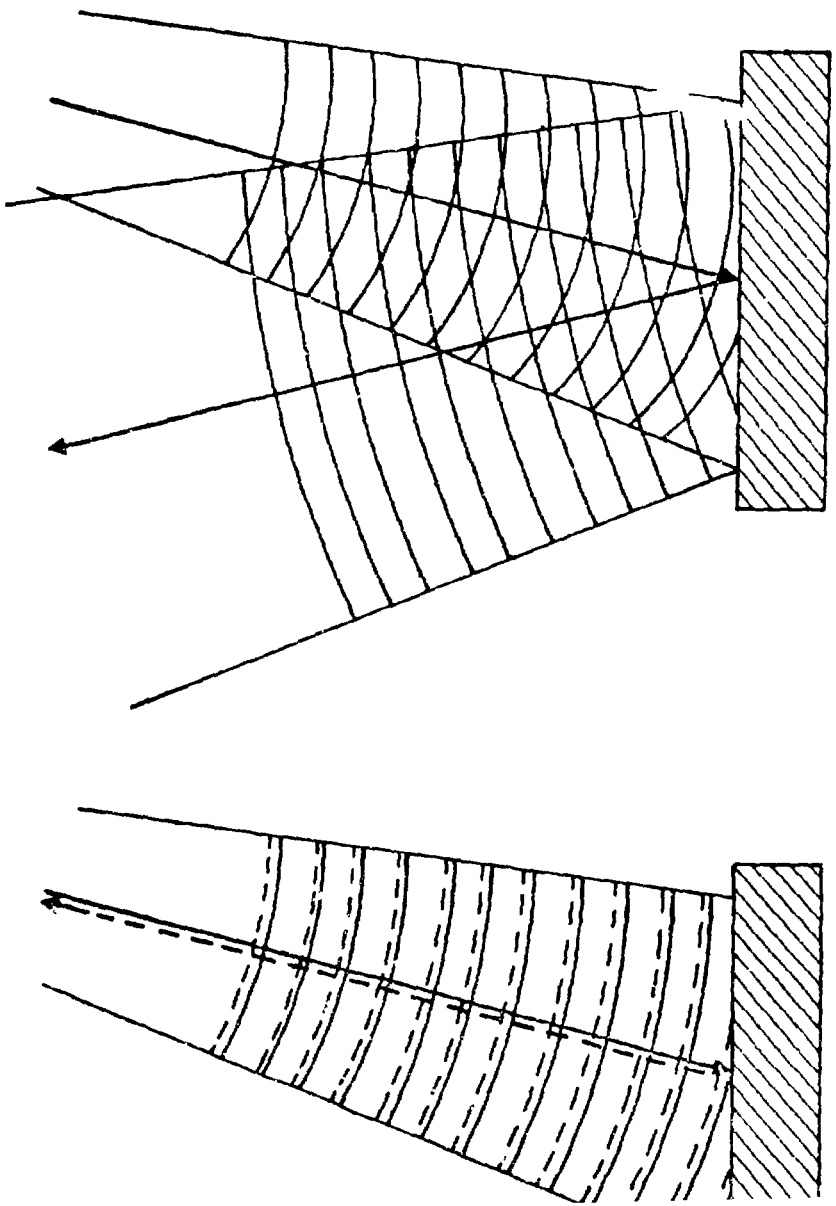

HUGHES
HUGHES AIRCRAFT COMPANY
RESEARCH LABORATORIES

ORDINARY MIRROR AND CONJUGATE MIRROR

HUGHES
HUGHES AIRCRAFT COMPANY

RESERVATION

REQUESTER ORIGINATOR _____ DATE _____

HUGHES
HUGHES AIRCRAFT COMPANY
RESEARCH LABORATORIES

CONJUGATOR, CONJUGATOR, ON THE WALL.....

HUGHES
HUGHES AIRCRAFT COMPANY

PRESENTATION _____

REQUESTER ORIGINATOR _____ DATE _____

UNCLASSIFIED

WHAT DO YOU SEE IN A CONJUGATE MIRROR?

HUGHES
HUGHES AIRCRAFT COMPANY
RESEARCH LABORATORIES

8686-23

A. YOUR IMAGE

B. YOUR IMAGE, INVERTED

C. YOUR IMAGE, TIME-REVERSED (i.e., YOUNGER)

D. YOUR IMAGE, ABERRATION-FREE

E. THE BACK OF YOUR HEAD

F. YOUR INNER SELF

G. TOTAL BLACKNESS

H. NONE OF THE ABOVE

7991-6

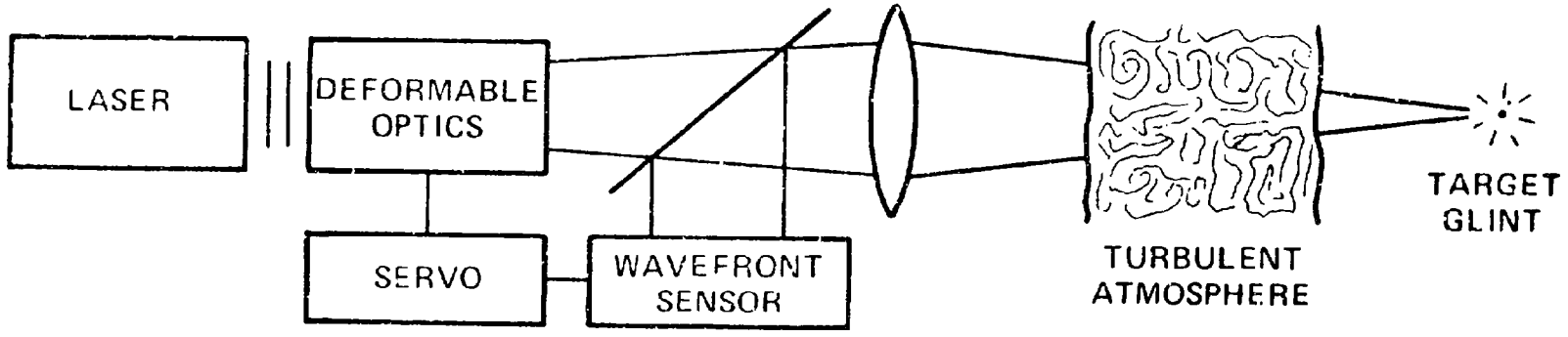

"CONVENTIONAL"

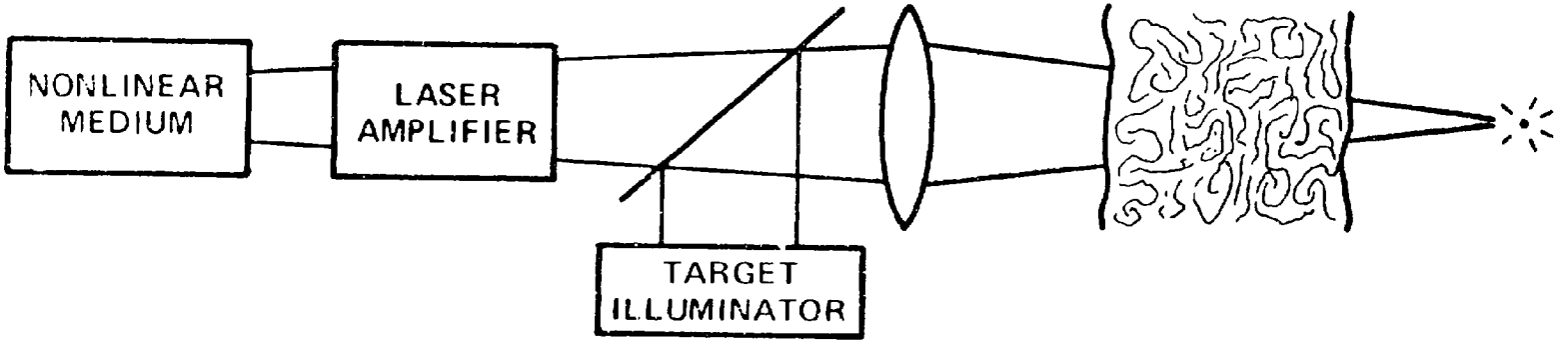

"NONLINEAR"

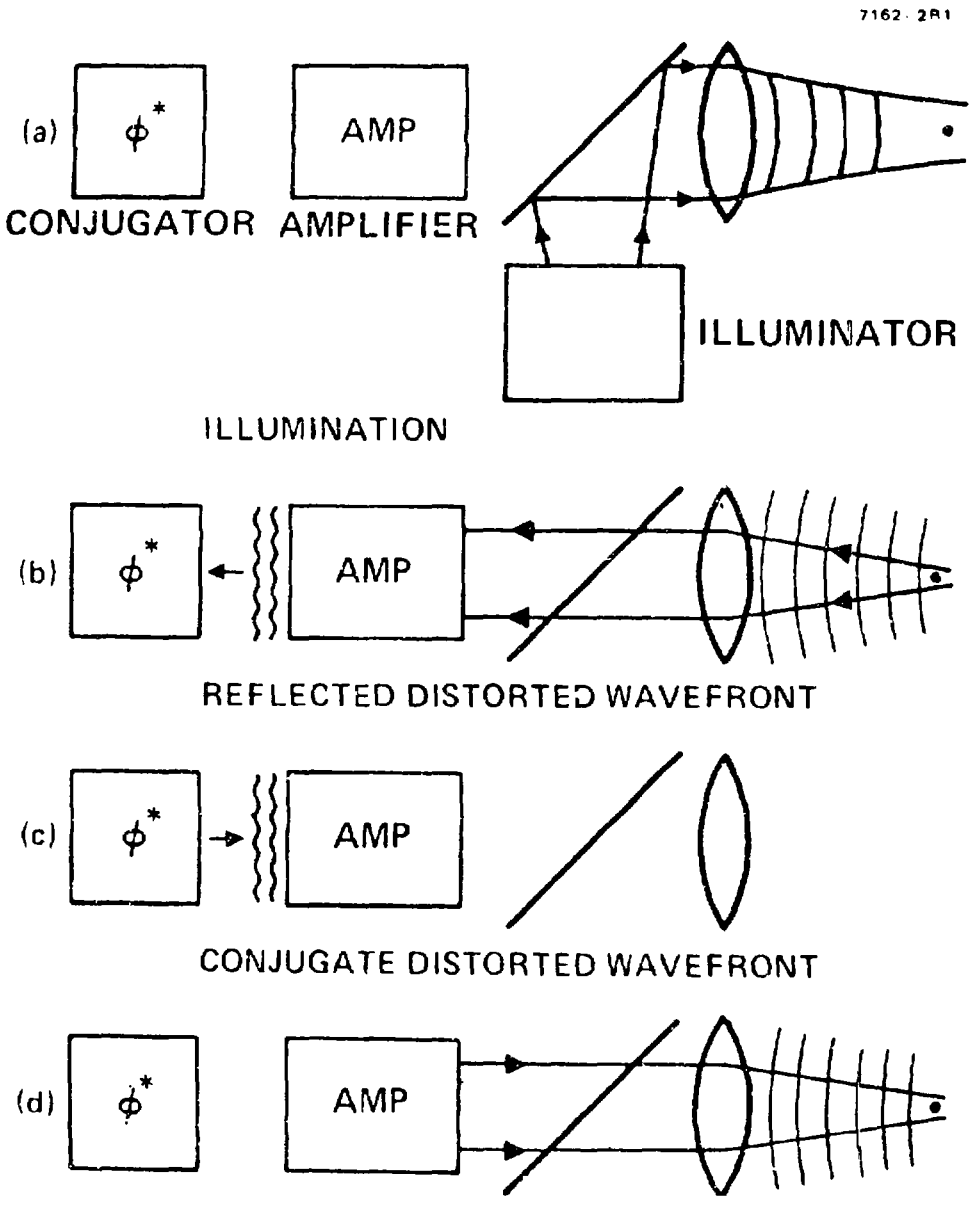

HUGHES
HUGHES AIRCRAFT COMPANY
RESEARCH LABORATORIES

BASIC NONLINEAR PHASE CONJUGATION SCHEME

HUGHES
HUGHES AIRCRAFT COMPANY

PRESENTATION

REQUESTER ORIGINATOR DATE

LASER UPLINK USING PHASE CONJUGATION

HUGHES
HUGHES AIRCRAFT COMPANY
RESEARCH LABORATORIES

9630-1

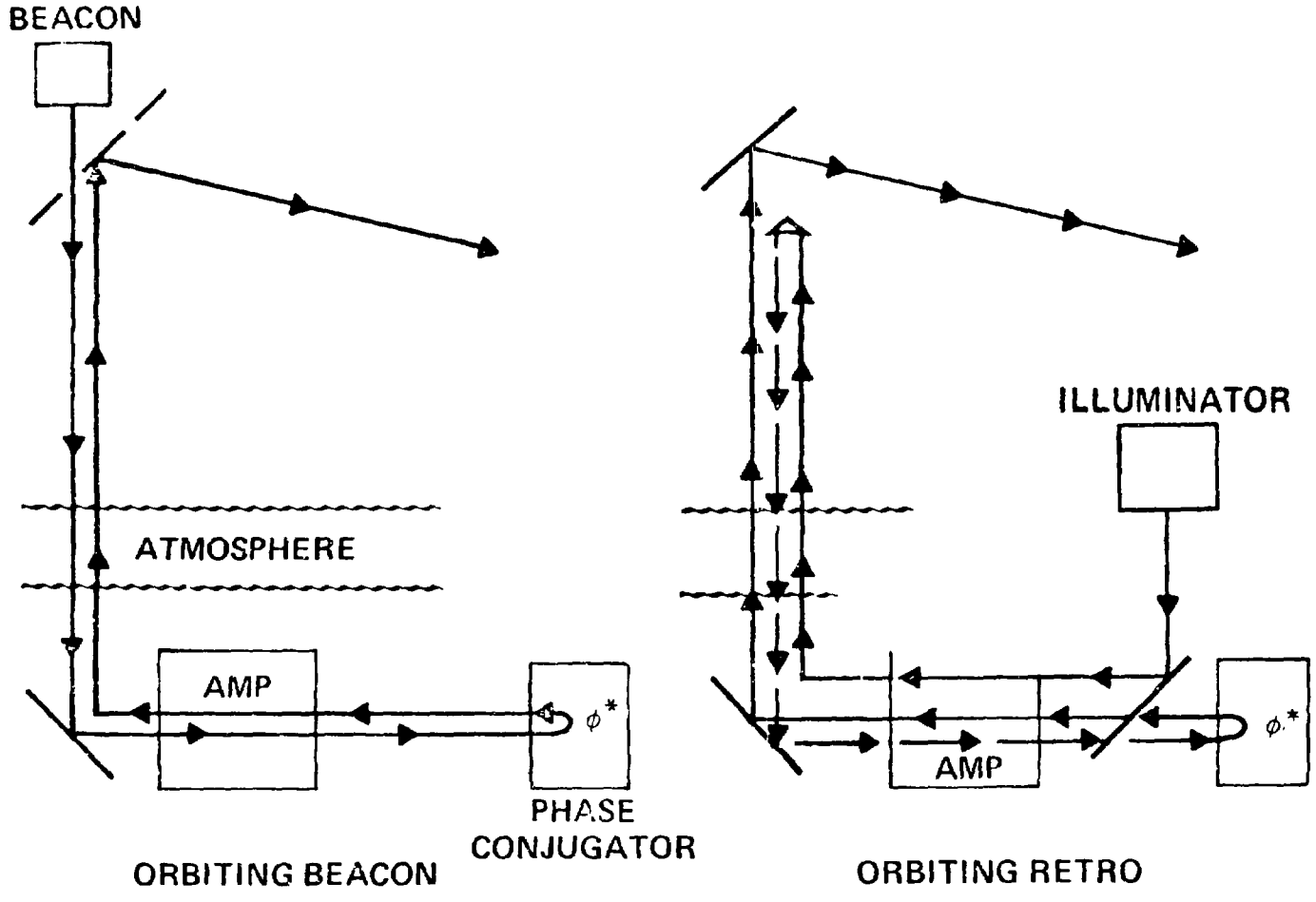

CANDIDATE UPLINK SYSTEM CONCEPT

HUGHES
HUGHES AIRCRAFT COMPANY
RESEARCH LABORATORIES

9473-1

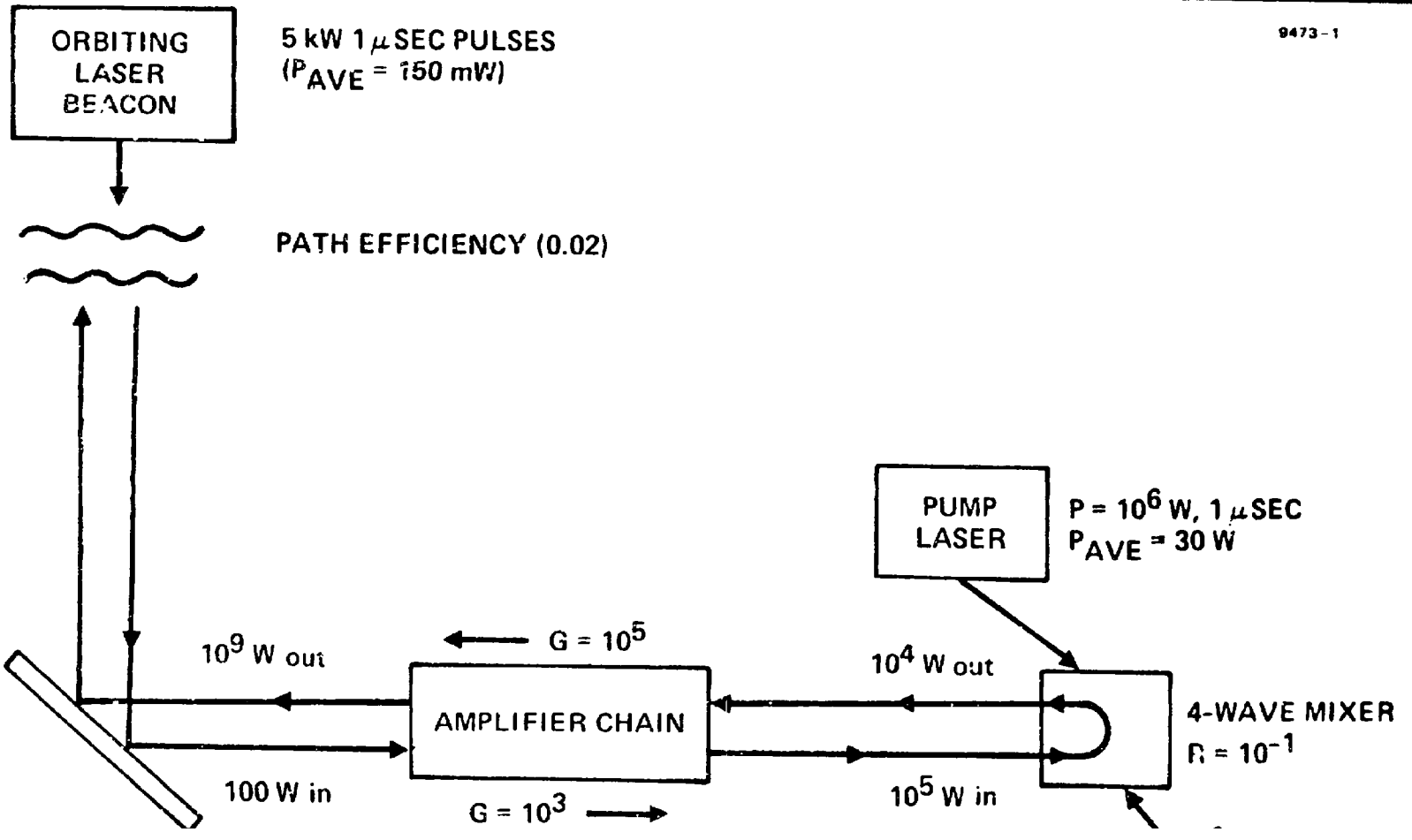

NONLINEAR vs CONVENTIONAL ADAPTIVE OPTICS

9392-110

ADVANTAGES

- SIMPLICITY (NO MOVING PARTS, NO ACTUATORS, NO WAVEFRONT SENSORS, NO SERVOS)
- SUPERIOR CORRECTION OF HIGH SPATIAL FREQUENCIES (SUBAPERTURE ORDER OF WAVELENGTH)
- HIGH SPEED OF RESPONSE
- MULTIPLE WAVELENGTH OPERATION

CONSTRAINTS

- NEED BRIGHT REFERENCE AND/OR HIGH GAIN AMPLIFIERS
- NEED TO OVERRIDE CONJUGATOR IF POINTING (OR FOCUS) ADJUSTMENT IS REQUIRED
- MAY NEED TO PROVIDE SEPARATE LASER PUMPS
- MAY NEED TO COMPENSATE FOR DOPPLER SHIFTS
- NOT YET DEMONSTRATED AT HIGH AVERAGE POWER

CANDIDATE NONLINEAR PHENOMENA

HUGHES
HUGHES AIRCRAFT COMPANY
RESEARCH LABORATORIES

9472-4

- STIMULATED BRILLOUIN SCATTERING, SBS
- DEGENERATE FOUR-WAVE MIXING, DFWM

STIMULATED BRILLOUIN SCATTERING-SBS

HUGHES
HUGHES AIRCRAFT COMPANY
RESEARCH LABORATORIES

9392-66

INCIDENT WAVE BACKSCATTERS INTO STOKES WAVE

- PROCESS

INPUT WAVE ω_1, k_1 (PHOTON) $\rightarrow$

ω_2, k_2 (PHOTON)

OUTPUT WAVE $\leftarrow$ ω_s, k_s (PHONON) $\rightsquigarrow$ ACOUSTIC WAVE

$\vec{k}_2 + \vec{k}_s = \vec{k}_1$

$\omega_2 + \omega_s = \omega_1$

FOR COLLINEAR GEOMETRY

$$|k_1| = |k_2| = 1/2\ |k_s|$$

$$\frac{\omega_s}{\omega_1} = \frac{\omega_1 - \omega_2}{\omega_1} = \frac{V_s}{C} \sim 10^{-5} \text{ (TYPICALLY)}$$

- SBS MEDIUM AUTOMATICALLY ACTS AS A PHASE CONJUGATE REFLECTOR WHEN SBS THRESHOLD IS EXCEEDED (THRESHOLD ~ 10 - 500 Mw/cm^2 IN BULK MATERIALS, CAN BE MUCH LESS IN WAVEGUIDE CONFIGURATIONS)
- OVER 90% OF BACKSCATTERED WAVE IS THE CONJUGATE OF THE INPUT WAVE

6282-4 R1

HUGHES

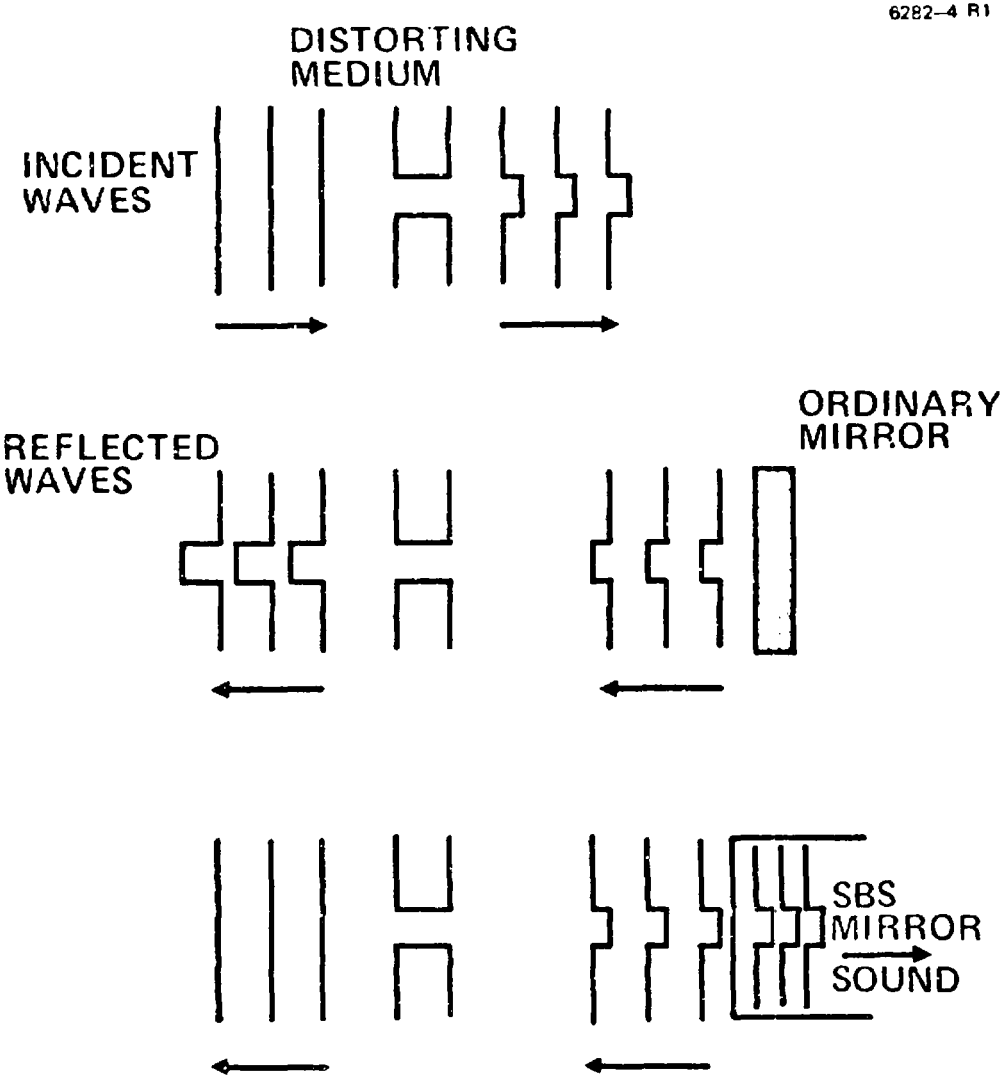

PHASE CONJUGATION VIA SBS

9392-116

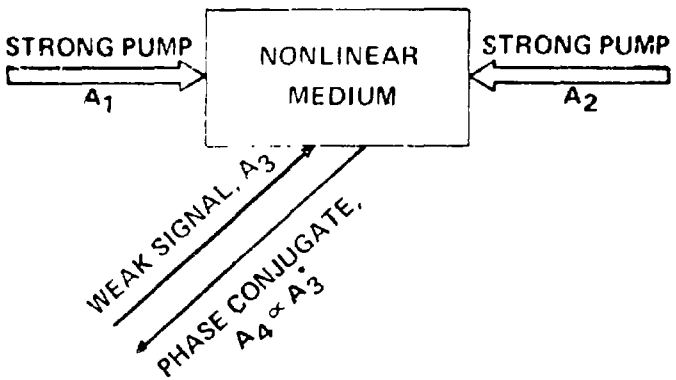

FORMATION

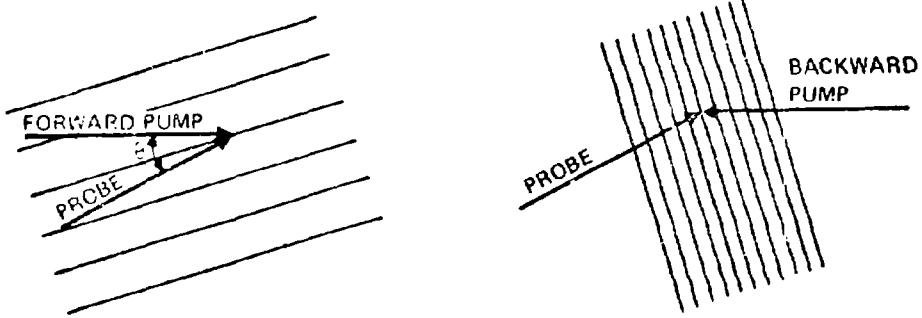

READOUT

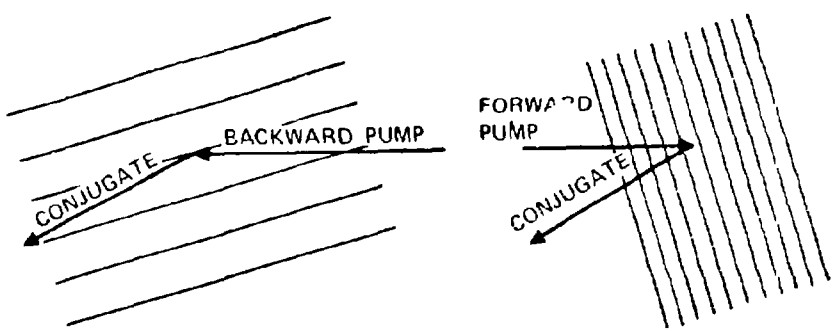

GRATING SPACING $D = \lambda / 2 \sin \theta/2$

FEBRUARY 1980

HUGHES
HUGHES AIRCRAFT COMPANY
RESEARCH LABORATORIES

FOUR-WAVE MIXING/ DUAL GRATING PICTURE

INDUCED POLARIZATION FOR 4 WAVE MIXING

HUGHES
HUGHES AIRCRAFT COMPANY
RESEARCH LABORATORIES

8703-6

$$\vec{P} = A(\theta)[\vec{E}_f \cdot \vec{E}_p^*]\vec{E}_b + A(\pi - \theta)[\vec{E}_b \cdot \vec{E}_p^*] \cdot \vec{E}_f + B[\vec{E}_f \cdot \vec{E}_b]\vec{E}_p^*$$

θ = ANGLE BETWEEN PUMP AND PROBE

$\vec{E}_f$ = FORWARD PUMP FIELD

$\vec{E}_b$ = BACKWARD PUMP FIELD

$\vec{E}_p$ = PROBE FIELD

COMPARISON OF NONLINEAR EFFECTS FOR PHASE CONJUGATION

HUGHES
HUGHES AIRCRAFT COMPANY
RESEARCH LABORATORIES

8703-2

SBS AND SRS	FOUR-WAVE MIXING
HIGH EFFICIENCY POSSIBLE (UP TO 99%)	GREATER THAN UNITY EFFICIENCY WITH RESONANT ENHANCEMENT
THRESHOLD REQUIREMENT	NO THRESHOLD
NO SEPARATE PUMPS REQUIRED	REQUIRES SEPARATE PUMPS
OCCURS WITH FREQUENCY SHIFT	NO FREQUENCY SHIFT WITH DEGENERATE OPERATION
GENERATES RETRO BEAM ONLY	BEAM ANGLE MAY BE VARIED ABOUT RETRO DIRECTION
INPUT AND OUTPUT POLARIZATIONS ARE THE SAME	OUTPUT POLARIZATION CAN BE VARIED RELATIVE TO INPUT BY PROPER CHOICE OF PARAMETERS

HUGHES

PRESENTATION

HUGHES AIRCRAFT COMPANY REQUESTER/ORIGINATOR DATE

ONGOING HRL ACTIVITIES

HUGHES
HUGHES AIRCRAFT COMPANY
RESEARCH LABORATORIES

9473-2

DARPA/ONR

- SBS AND FOUR-WAVE MIXING IN THE VISIBLE (BLUE-GREEN, RUBY)
- MULTIFREQUENCY PHASE CONJUGATION
- EXPERIMENT, THEORY, SYSTEMS APPLICATIONS

DOE/LASL

- FOUR-WAVE MIXING AT 10.6 μm
- RESONANT ENHANCEMENT, MULTI-LINE CONJUGATION

IR&D

- HIGH EFFICIENCY CONJUGATORS (VISIBLE, 1.06 μm, 10.6 μm)
- THEORY OF RESONATORS WITH CONJUGATE "MIRRORS"
- PICOSECOND PHASE CONJUGATION
- NEW APPLICATIONS CONCEPTS

AFOSR

- PHASE CONJUGATE OPTICAL RESONATORS
- EXPERIMENTAL DEMO OF LOW POWER PULSED PHASE CONJUGATE RESONATOR
- FOUR-WAVE MIXING IN SODIUM VAPOR
- DYE AMPLIFIER

ISSUES ADDRESSED ON THIS PROGRAM

- WHAT SORT OF CONJUGATE EFFICIENCIES CAN WE GET?

  NEW MATERIALS, RESONANT ENHANCEMENT, FURTHER THEORETICAL DEVELOPMENT, EXPERIMENTAL OPTIMIZATION

- HOW GOOD IS THE CONJUGATION CORRECTION?

  DETAILED FAR-FIELD MEASUREMENTS

- WHAT ARE THE CONSTRAINTS ON THE PROCESS?

  ANGULAR MISALIGNMENT, FREQUENCY SHIFTS, PUMP ABERRATIONS, COHERENCE EFFECTS

- HOW CAN WE EXPLOIT THE CONSTRAINTS?

  POINT AHEAD, DOPPLER COMPENSATION, FOCUS OVERRIDE, POLARIZATION ROTATION

- HOW DOES IT APPLY TO DARPA NEEDS?

  UPLINK SYSTEM CONCEPTS, BEACON VS RETRO REFERENCE, GAIN AND EFFICIENCY REQUIREMENTS

HUGHES
HUGHES AIRCRAFT COMPANY

PRESENTATION _____

REQUESTER ORIGINATOR _____ DATE _____

DFWM PHASE CONJUGATION-FAR FIELD PHOTOGRAPHS

HUGHES
HUGHES AIRCRAFT COMPANY
RESEARCH LABORATORIES

9392-12

INPUT LASER SIGNAL

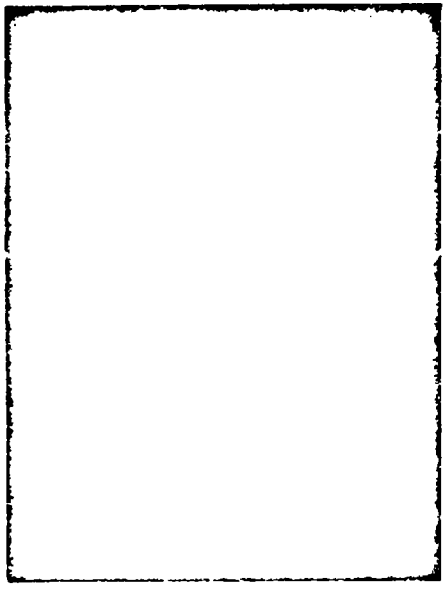

ABERRATED INPUT SIGNAL

CORRECTED SIGNAL

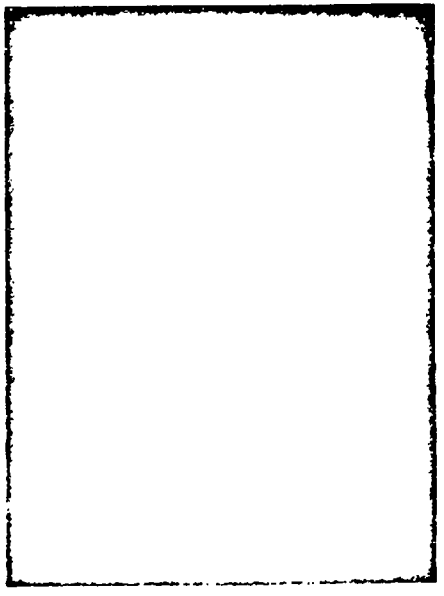

HUGHES

PRESENTATION

REQUESTER/ORIGINATOR DATE

INTENSITY PROFILES

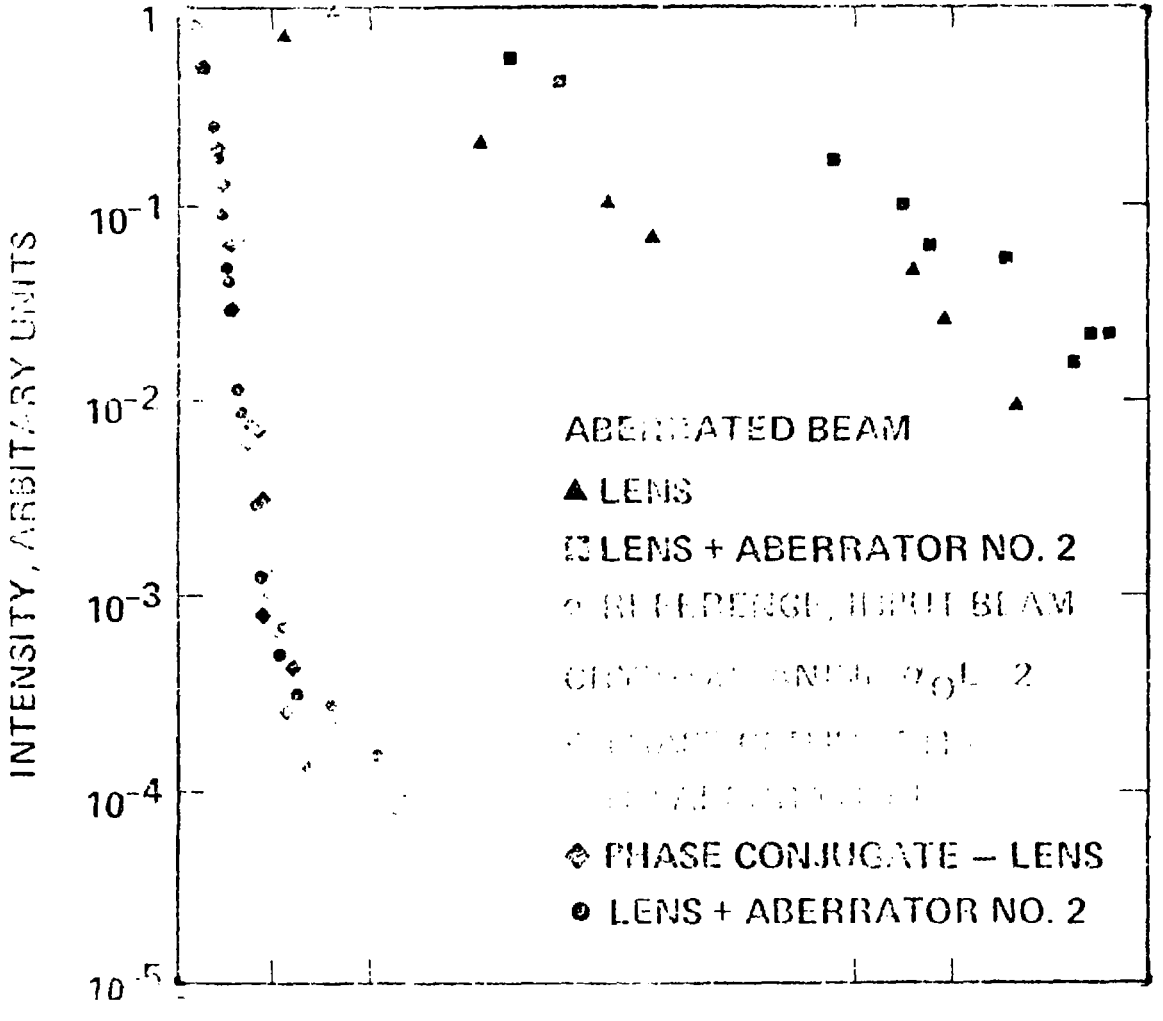

POINT AHEAD CAPABILITY WITH DFWM

HUGHES
HUGHES AIRCRAFT COMPANY
RESEARCH LABORATORIES

9392-114

NONCOLLINEAR PUMP GEOMETRY CAN PROVIDE MODERATE POINT AHEAD

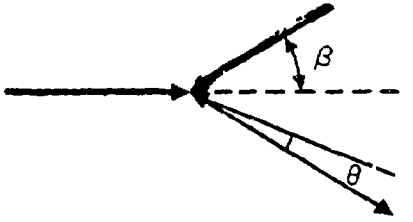

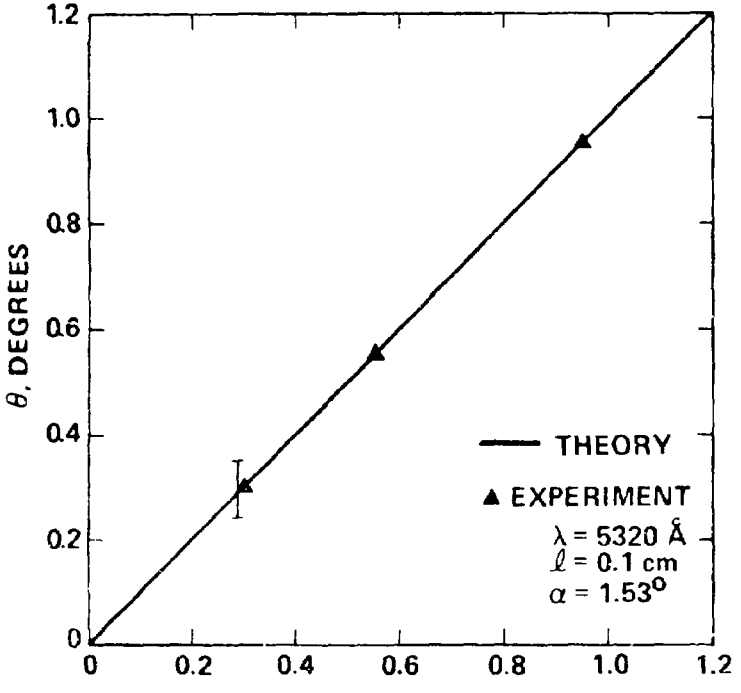

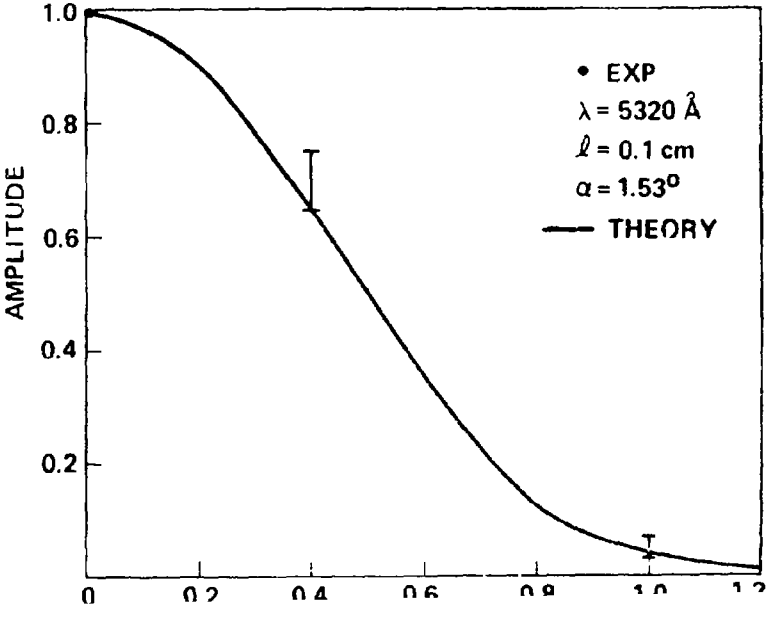

THE USE OF POLARIZATION IN D4WM FOR SEPARATE CONTROL OF THE CONJUGATE WAVE

HUGHES
HUGHES AIRCRAFT COMPANY
RESEARCH LABORATORIES

8686-21

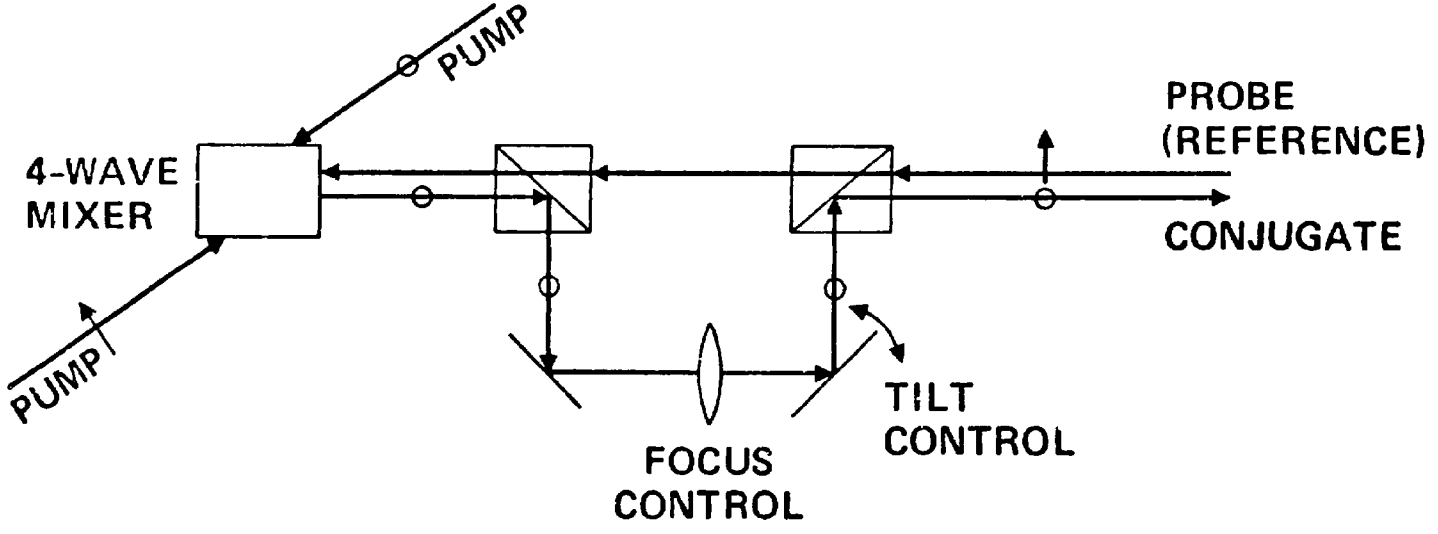

WHAT'S BEEN DONE

HUGHES
HUGHES AIRCRAFT COMPANY
RESEARCH LABORATORIES

9392-71

WAVELENGTH	LASER	PULSED OR CW	NONLINEAR INTERACTION	NONLINEAR MEDIUM	COMMENTS
10μm	CO_2	PULSED	DFWM	SF_6*	37%, 200 kW/cm^2, 2 cm
			DFWM	HgCdTe*	10%, 100 kW/cm^2, 0.5 mm
			DFWM	CO_2 (INVERTED)	0.5%
			DFWM	Ge	25%, 10 MW/cm^2, 15 cm
			DFWM	NH_3*	~1% (PRELIM)
			DFWM	KCl:R_eO_4	
3.8μm	DF	PULSED	DFWM	G_e	
1.06μm	Nd:YAG	PULSED	DFWM	Si*	180%, 1 mm, 6 MW/cm^2
			SBS	CS_2, CH_4*	10 - 90%
			DFWM	Nd: YAG	~0.5%
			3 WM	Li FORMATE	POOR CORRECTION
0.69μm	RUBY	PULSED	SBS	CS_2*	10 - 90%
			SBS	CH_4	
			DFWM	CRYPTOCYANINE*	30% (PRELIM)
			DFWM	CdS CdSe GLASS*	~5%
			DFWM	CS_2	>100%, 40 cm
5890Å	DYE	CW	DFWM	Na*	17%, NARROW BAND
		PULSED	DFWM	Na	10^4%, NARROW BAND
5320Å	DOUBLED Nd: YAG	PULSED	DFWM	CdS, CdSe GLASSES*	~30%
			DFWM	IODINE VAPOR*	~0.1% (PRELIM)
			DFWM	RHODAMINE 6G*	>100%, 1 mm
			DFWM	RHODAMINE B*	~10% (PRELIM) (ALSO 5650Å)
5100Å	DYE	PULSED	DFWM	CdS, CdSe GLASS*	~1% (PRELIM)
4880Å, 5145Å	Ar^+	CW	DFWM	RUBY	~0.2%
			DFWM	BSO	~1% SLOW
			DFWM	$BaTiO_3$	~25% SLOW
			DFWM	LIQUID CRYSTALS*	~0.1% SLOW

PERFORMANCE OF PHASE CONJUGATE RESONATOR MODEL FOR DIFFERENT FRESNEL NUMBERS

HUGHES
HUGHES AIRCRAFT COMPANY
RESEARCH LABORATORIES

9392-55 R1

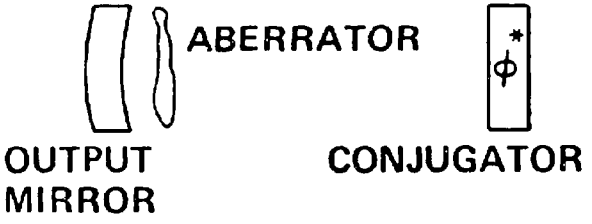

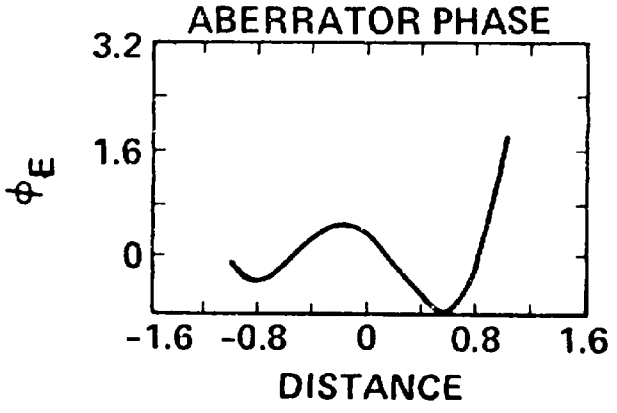

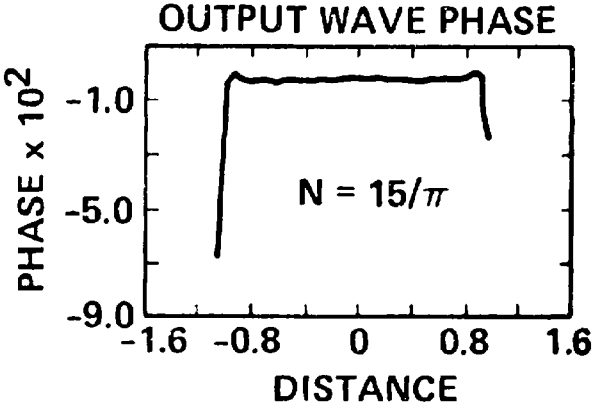

KEY RESULT: PHASE OF OUTPUT WAVE DEPENDS ONLY ON OUTPUT MIRROR QUALITY – NOT ON INTRACAVITY DISTORTIONS

REMAINING ISSUES

HUGHES
HUGHES AIRCRAFT COMPANY
RESEARCH LABORATORIES

9473-5

TECHNOLOGICAL

CHOICE OF MATERIAL FOR SPECIFIC APPLICATION

- SPECIFIC WAVELENGTH(S) OF OPERATION
- TEMPORAL AND SPECTRAL BANDWIDTH
- EFFICIENCY (CONJUGATE WAVE REFLECTIVITY)
- POWER HANDLING CAPABILITIES/PHYSICAL SIZE
- COMPETING NONLINEAR EFFECTS AT HIGH AVERAGE/PEAK POWER

SYSTEMS

- MOPA OR INTRACAVITY
- BEACON OR RETRO-REFERENCE
- AMPLIFIER GAIN REQUIREMENTS
- POINT AHEAD
- DOPPLER

SPACE-BASED LASER SESSION

Paper 23 is contained in volume 2.

STATUS OF BLUE-GREEN DISCHARGE LASER WORK AT NRL

R. Burnham
Naval Research Laboratory
Washington, D. C. 20375

SUMMARY

Experiments designed to demonstrate the feasibility of a 1 J/pulse 100 pps blue-green laser using XeCl, Raman shifted to 459 nm in lead vapor are being carried out. In initial experments we have obtained ~ 30% energy conversion from 308 nm to 459 nm using an x-ray preionized discharge laser with an output of > 1.0 J in a 100 nsec pulse. The principal limitation to conversion efficiency appears to be the quality of the pump laser beam which contained considerable superfluorescence. Injection locking experiments are being carried out to correct this limitation. We have also investigated problems concerning high-repetition-rate downconversion using a 100 Hz XeCl laser. Preliminary results indicate that there is no fundamental problem with inter-pulse relaxation at repetition rates up to 100 Hz.

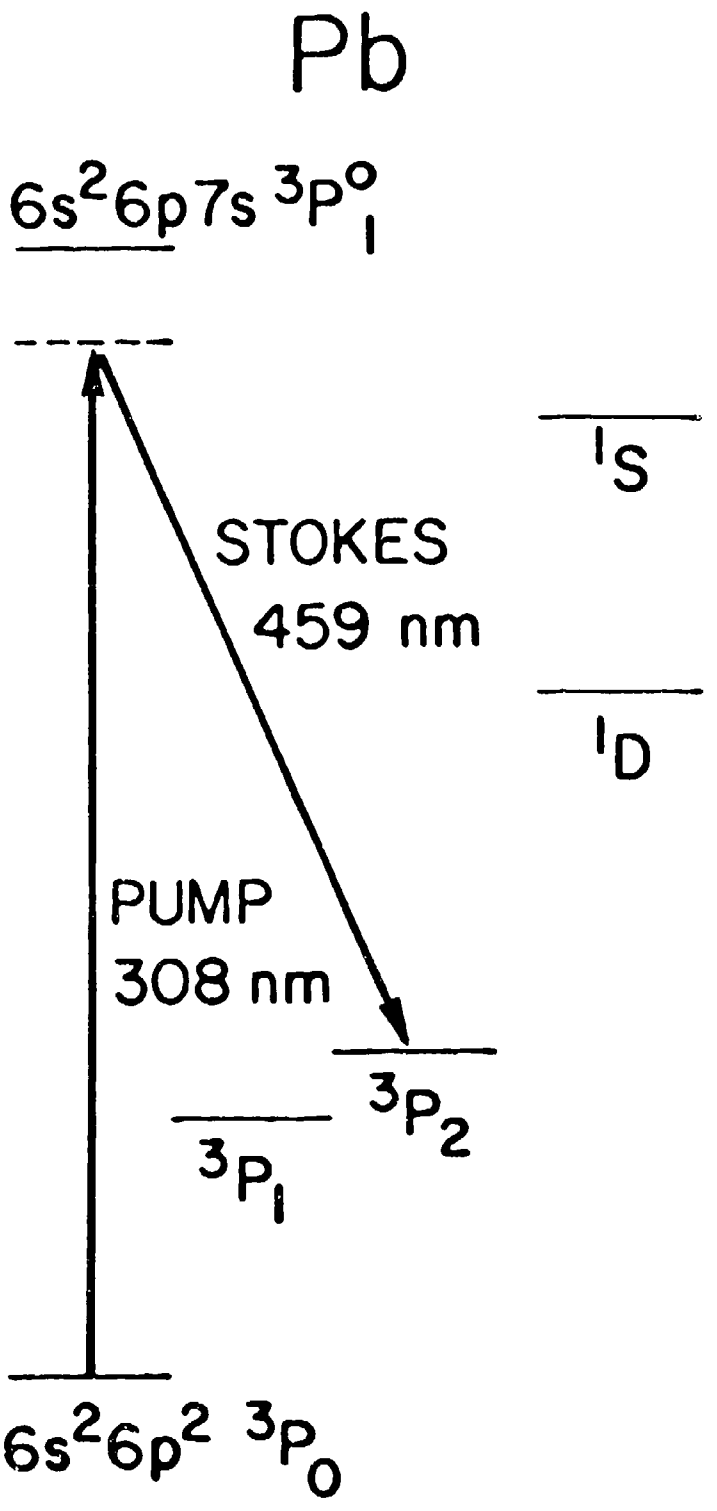
Pb
6s²6p7s ³P°₁
¹S
STOKES
459 nm
¹D
PUMP
308 nm
³P₂
³P₁
6s²6p² ³P₀

RAMAN CONVERSION OF XeCl LASER TO BLUEGREEN

MATERIAL	P_B	B_A
WAVELENGTH (NM)	458.4, 458.8	474.5, 475.0
ENERGY CONVERSION EFFICIENCY	45%	20%
PHOTON CONVERSION EFFICIENCY	67%	31%
LIMITATIONS	$\leq$10% SCATTERING IN PRESENT EXPERIMENTS	SCATTERING IN MEDIUM RESONANCE ABSORPTION

FORWARD SRS WITH PUMP DEPLETION

$$\frac{dI_s}{dz} = g_0 I_p I_s N \quad ; \quad I_p = \left(I_{p0} - h\nu_p/h\nu_s\, I_s\right)$$

$$\frac{dI_s}{dz} = g_0 N\left(I_s I_{p0} - h\nu_s/h\nu_p\, I_s^2\right)$$

Solution:

$$I_s(z) = \frac{I_{p0}}{\left(I_{p0}/I_{s0} - h\nu_p/h\nu_s\right)\exp\left(-g_0 N I_{p0} z\right) + h\nu_p/h\nu_s}$$

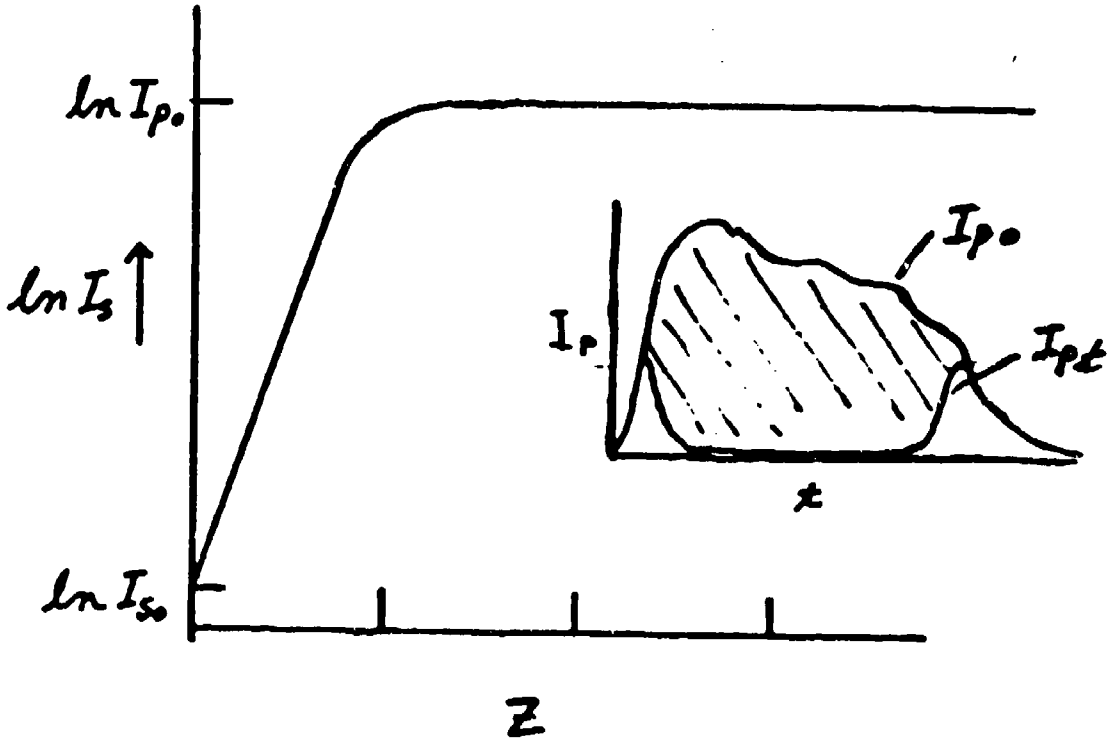

RAMAN LASER SCALING

FOR COLLIMATED PUMP BEAM

1. $g_o N I_{po} \ell = \alpha G_t$ (GAIN REQUIREMENT)

2. $NA\ell = \beta E_{po}/h\nu_p$ (NO MEDIUM SATURATIO

3. $I_{po} = E_{po}/\Delta t\, A$

SOLVING FOR ℓ GIVES:

$$\ell = \left(\frac{\alpha \beta G \Delta t}{N^2 g_o h \nu_p} \right)^{1/2}$$

FOR $N = 2\times10^{17}\,cm^{-3}$; $g_o = 2\times10^{-25}\,cm^4/W\cdot$
$\alpha = \beta = 2$ and $G = 30$

$$\ell = 1.4 \times 10^2 \,(\Delta t(\mu sec))^{1/2} \text{ cm}$$

$$E_p/A = 6.4\times10^{-2}\,\ell \ J/cm^2$$

Δt	0.01	0.1	1.0 μsec
ℓ cm	14	44	140
A cm^2	1.1	.35	0.1
E_p/A J/cm^2	1	2.9	10

1 J XeCl-Pb Downconversion

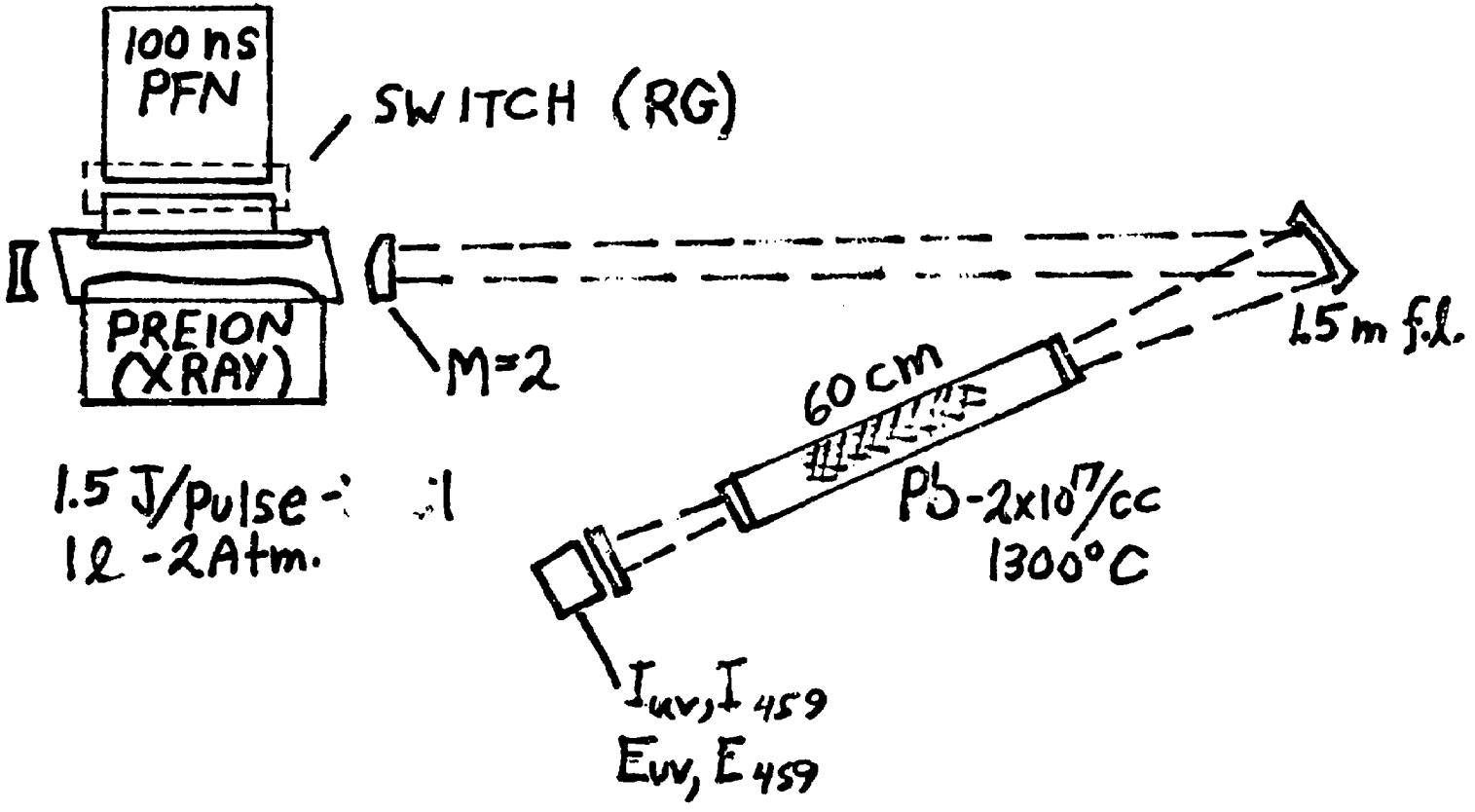

1 JOULE XeCl-Pb DOWN-CONVERSION

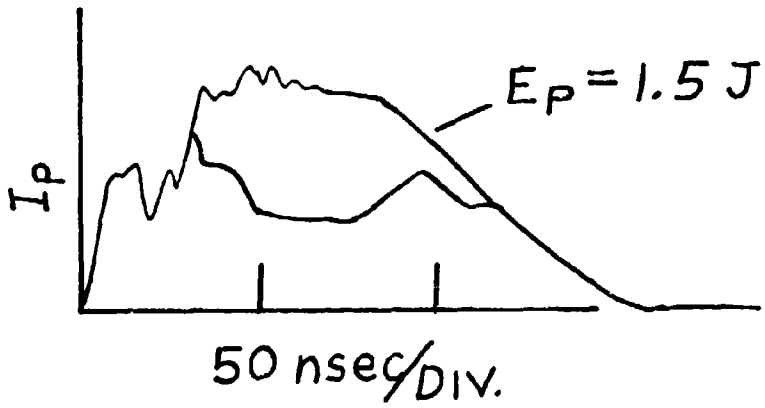

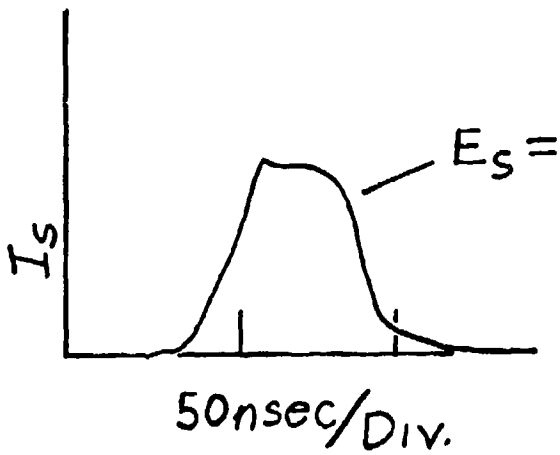

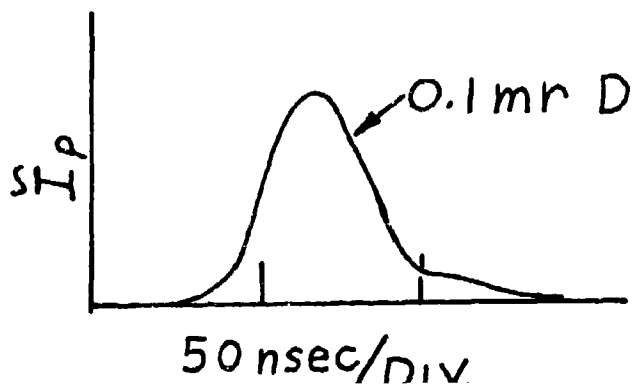

XeCl-Pb Raman Down-Conversion

I. 1 J Conversion Experiments

II. 100 Hz Down-Conversion

CAVITY BUILDUP TIME WITH UNSTABLE RES.

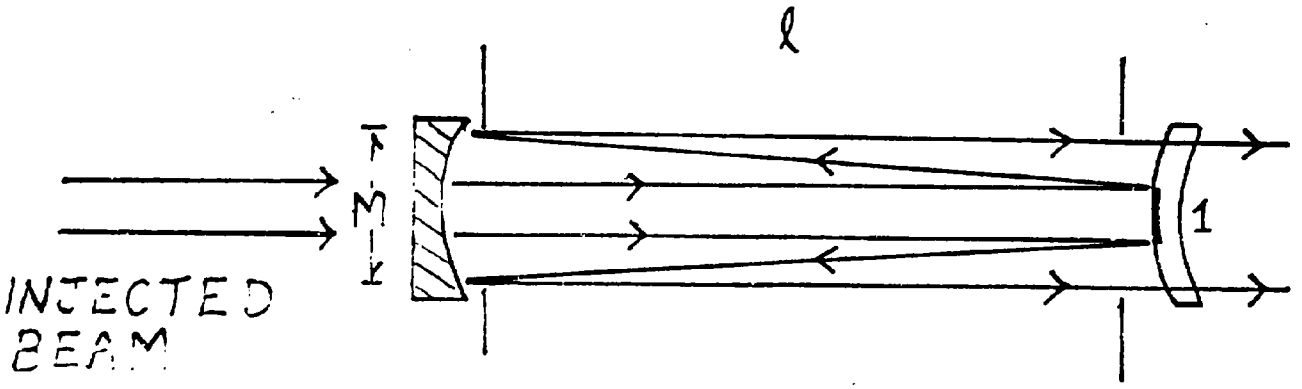

$$\tau_B \simeq \frac{\ln n}{\ln M}\, \ell/c$$

for $n = 400$, $M = 2$, $\ell/c = 3$ nsec

$\tau_B \simeq 30$ nsec

WITH INJECTED BEAM WITH DIAM. 1:

$$\tau_B' = 2\text{-}3\,\frac{\ell}{c} \leq 10 \text{ nsec.}$$

100 Hz XeCl-Pb Downconversion

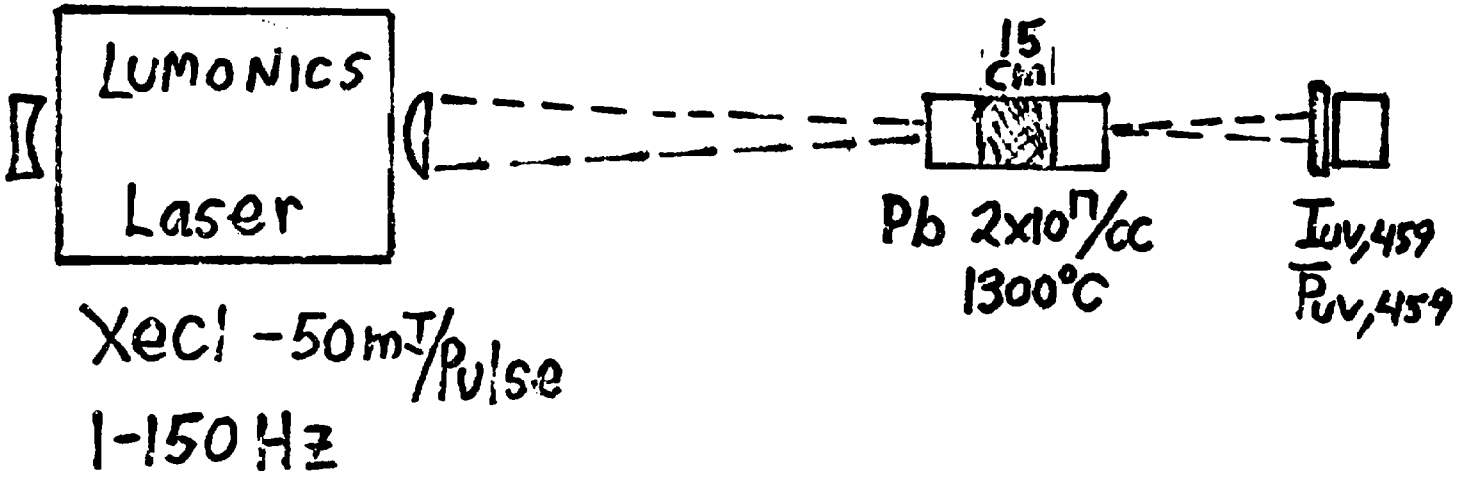

100 Hz XeCl - Pb Down-Conversion

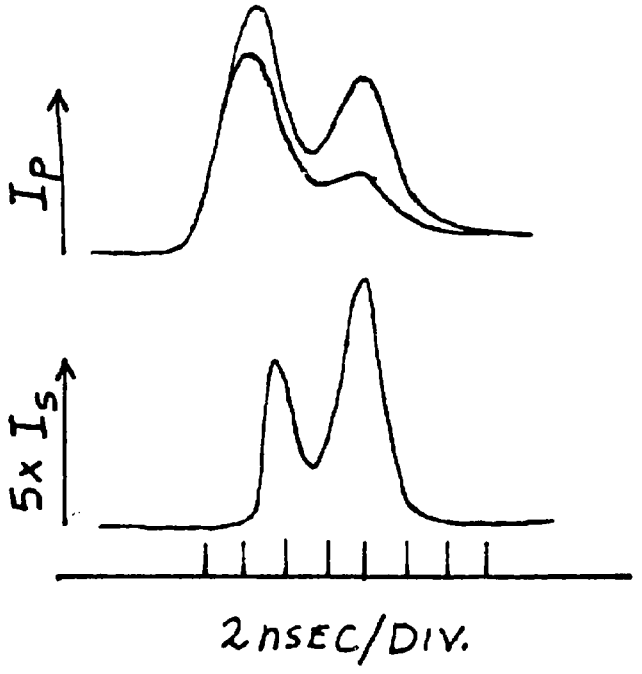

- No Change in η_{LR} - 10 - 100 Hz PRF

INTER-PULSE RELAXATION IN METAL VAPORS

Pb VAPOR (10^{17}/cc - 1250°C) + 10^{17}-10^{19}/cc BUFFER

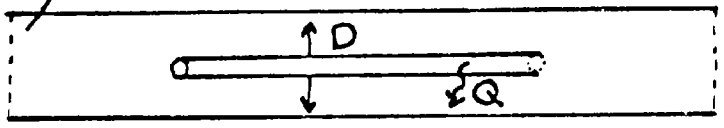

USING THALLIUM DATA: $\sigma_D^2 \simeq 100\ \text{Å}^2$

$\sigma_Q^2 \simeq 5\ \text{Å}^2$

$\tau_Q \cong 10^{-7}$ sec.

$\tau_D \simeq 10^{-2}$ sec. (1cm.)

- MEASURE SELF-QUENCHING & DIFFUSION IN Pb VAPOR
- INVESTIGATE PROPAGATION OF ACOUSTIC DISTURBANCES W/ INTERFEROMETER

EFFICIENT RAMAN CONVERSION OF XeCl LASER INTO THE BLUE-GREEN REGION

H. Komine, E. A. Stappaerts, W. H. Long, Jr.
Northrop Corporation
Northrop Research and Technology Center
One Research Park
Palos Verdes Peninsula, California 90274

March 1980

ABSTRACT

An efficient, blue-green laser source is urgently needed for the Navy submarine communication system. The rare-gas halide excimer lasers developed over the last few years appear to meet the requirements on efficiency and scalability, but the wavelength of their near-uv emission is too short for direct use. Recently, Raman shifting of the excimer laser wavelengths has been investigated using atomic metal vapor and molecular gases as conversion media. During the past year, under a Navy-sponsored program, Northrop Research and Technology Center (NRTC) has demonstrated the feasibility of a novel conversion scheme, based on higher order Raman scattering, for efficiently shifting the uv wavelengths of these excimer lasers to the blue-green region.

The technique uses an oscillator-amplifier combination, and the Raman medium is typically a gas such as hydrogen or deuterium at a pressure of a few atmospheres. In preliminary experiments with a frequency-tripled Nd:YAG laser (355 nm), energy conversion efficiencies as high as 35 percent was obtained for the second Stokes order, in good agreement with computer simulations. The laser pulse length in these initial experiments was very short (6 ns), which limits the amplifier efficiency because of reduced Raman gain at the leading and trailing edges of the pulse. For longer, nearly-rectangular pulses, and flat-topped beam profiles as obtained with large Fresnel number unstable resonators, conversion efficiencies approaching the quantum limit should be possible for second and third order converters.

During the experimental investigation of the new scheme, the pump laser bandwidth was found to have a major effect on the amplifier gain. A comprehensive analytical model has been developed which explains these observations in terms of the interference between the various longitudinal modes of the pump and Stokes waves. In addition, a gain enhancement technique, which increases broadband gains to the value observed for monochromatic pumping, has been proposed and demonstrated. This new technique eliminates the necessity for injection-locking the pump laser in those cases where a narrow bandwidth is not necessary for other reasons. For the Navy application, injection-locking will probably be necessary in order to maximize the signal-to-noise ratio of the receiver. Experiments with an injection-locked, spectrally narrowed XeCl laser are in progress.

EFFICIENT RAMAN CONVERSION OF XeCl LASER

INTO THE BLUE-GREEN REGION

March 1980

H. Komine
E. A. Stappaerts
W. H. Long, Jr.

Northrop Corporation
Northrop Research and Technology Center
One Research Park
Palos Verdes Peninsula, California 90274

OUTLINE

- RAMAN OSCILLATOR-AMPLIFIER SCHEME
- SUMMARY OF Nd:YAG THIRD HARMONIC PUMPING EXPERIMENTS
- BROADBAND PUMPING ANALYSIS
- GAIN ENHANCEMENT TECHNIQUE
- XeCl LASER INJECTION-LOCKING

XeCl/ RAMAN CONVERSION MEDIA

ATOMIC METAL VAPOR:

- Pb(459 nm)

MOLECULAR GAS:

- H_2 (500 nm)
- H_2/D_2 (472 nm)

HIGHER-ORDER RAMAN SHIFTING OSCILLATOR/AMPLIFIER SCHEME

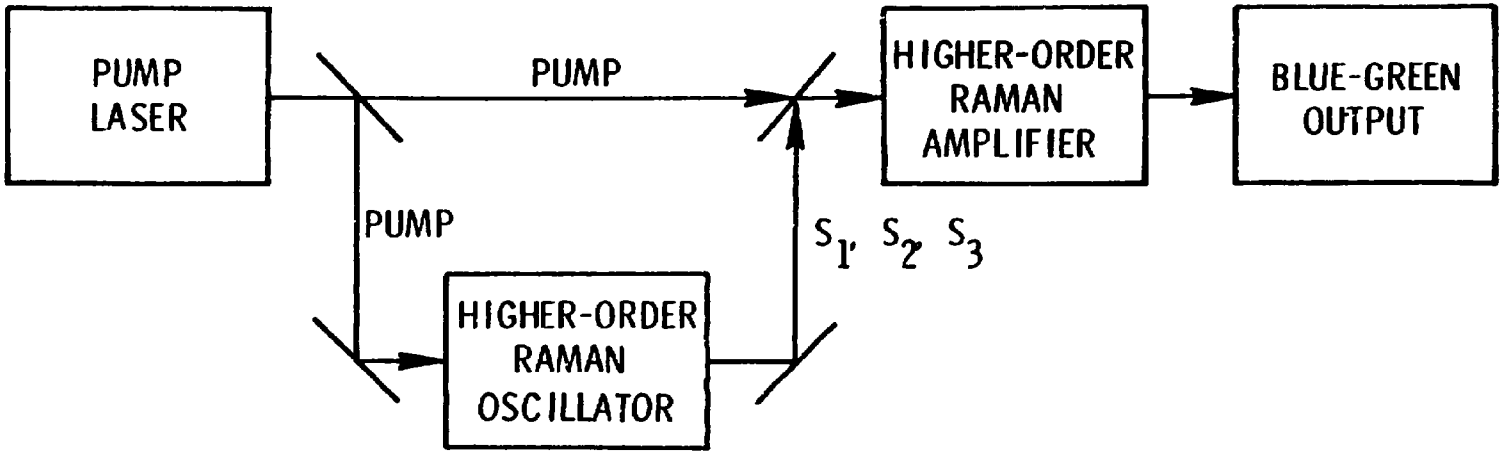

NORTHROP

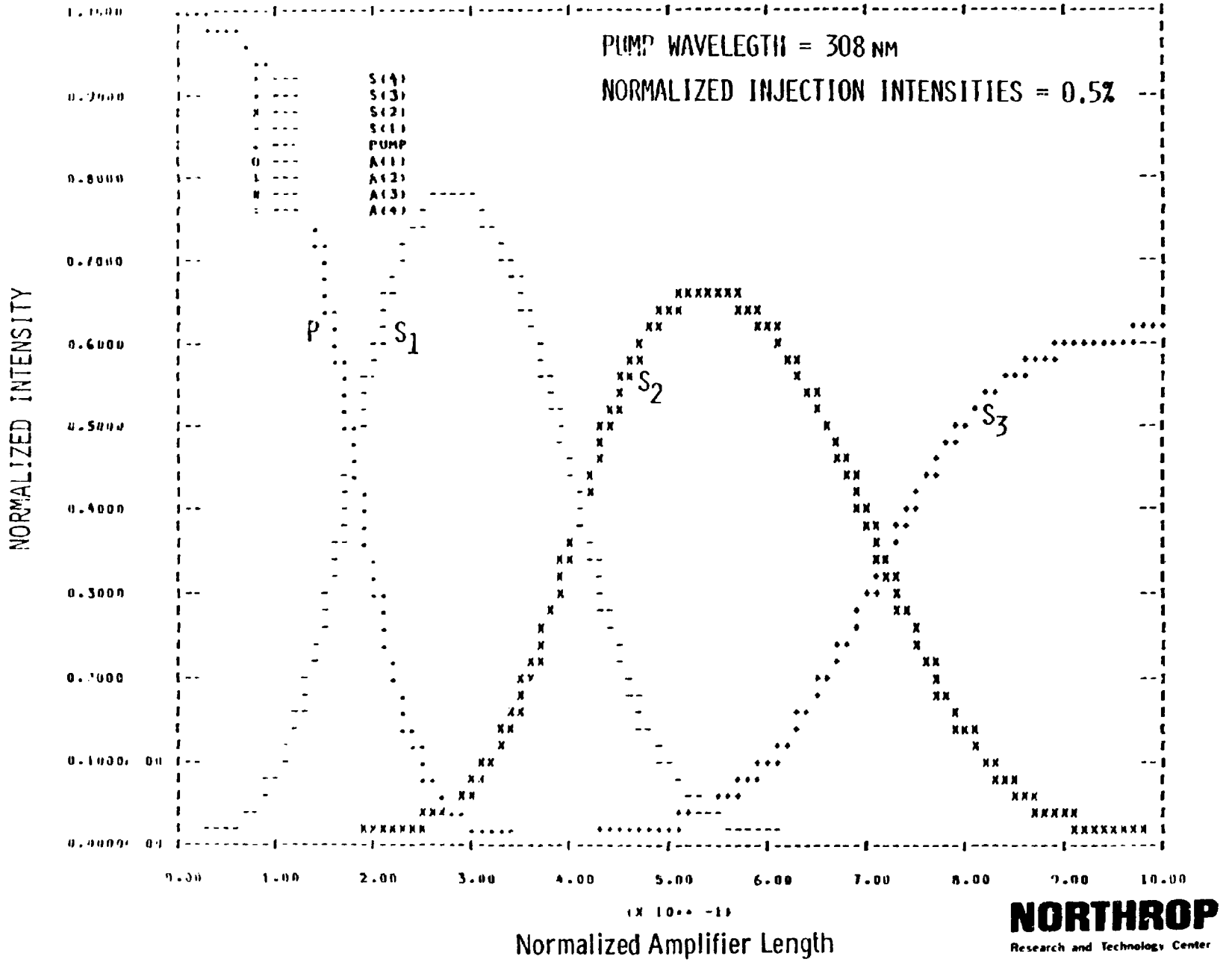

NORTHROP
Research and Technology Center

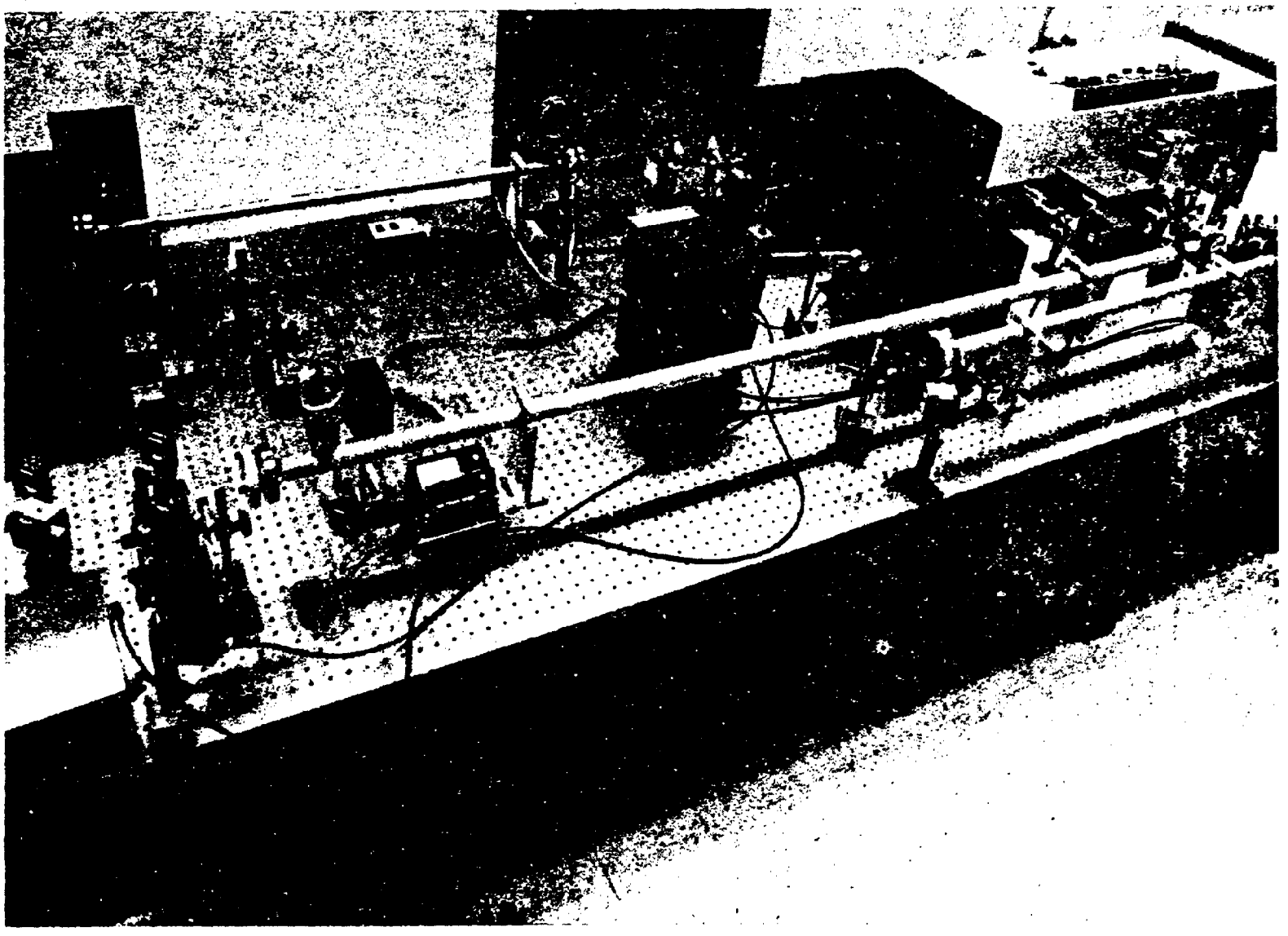

Nd:YAG THIRD HARMONIC (355 nm) PUMPING EXPERIMENT

SUMMARY

RAMAN OSCILLATOR:

- MULTIPLE-STOKES-ORDER OUTPUT (S_1, S_2, S_3, etc.)
- NEAR DIFFRACTION-LIMITED BEAM
- ~90% PUMP DEPLETION

RAMAN AMPLIFIER:

- ~35% ENERGY CONVERSION (~50% PHOTON EFFICIENCY) INTO 503 nm (S_2)
- SUPPRESSION OF FOUR-WAVE MIXING
- NON-EXPONENTIAL RAMAN AMPLIFICATION (PUMP LASER BANDWIDTH EFFECT)

RAMAN GAINS VS PUMP ENERGY FOR A BROADBAND PUMP LASER

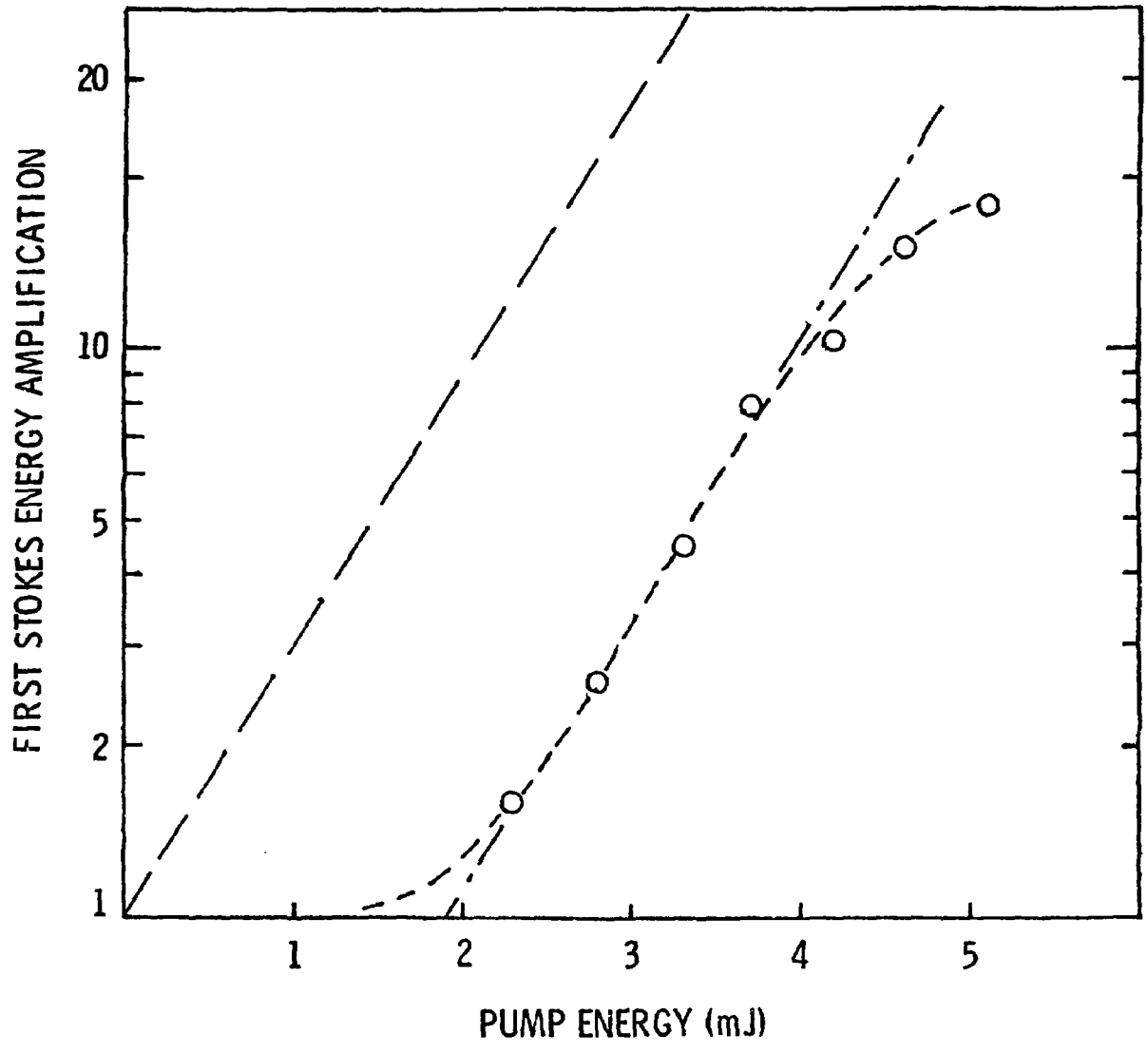

NORTHROP

STIMULATED RAMAN SCATTERING OF A NONMONOCHROMATIC PUMP

$$\frac{\partial v_j}{\partial z} = \frac{g}{2} \sum_n \sum_k \frac{v_k u^*_{k-n} u_{j-n}}{1 + i \frac{2n\gamma}{\Gamma}} \exp\left[i(k - j)\gamma\upsilon z\right]$$

$$\frac{\partial u_j}{\partial z} = -\frac{g}{2} \frac{\omega_L}{\omega_S} \sum_n \sum_k \frac{u_k v^*_{k-n} v_{j-n}}{1 + i \frac{2n\gamma}{\Gamma}} \exp\left[i(j - k)\gamma\upsilon z\right]$$

u_j, v_j	AMPLITUDES OF PUMP AND STOKES COMPONENTS
g	MONOCHROMATIC GAIN COEFFICIENT
Γ	HOMOGENEOUSLY BROADENED MOLECULAR LINEWIDTH
γ	MODE SPACING
υ	DISPERSION PARAMETER

NORTHROP
Research and Technology Center

INCREMENTAL FORWARD GAIN

$$G_f = \frac{g}{\sum_j |v_j|^2} \sum_n \frac{\left|\sum_j u^*_{j-n} v_j\right|^2}{1 + i\frac{2n\gamma}{\Gamma}}$$

INCREMENTAL BACKWARD GAIN

$$G_b = \frac{g}{\sum_j |v_j|^2} \sum_n \frac{\sum_j |u_{j-n}|^2 |v_j|^2}{1 + i\frac{2n\gamma}{\Gamma}}$$

MONOCHROMATIC GAIN

$$G = g\bar{I}_{LO}$$

WHERE $\bar{I}_{LO} = \sum_j |u_j|^2$

IS THE AVERAGE INCIDENT PUMP INTENSITY

NORTHROP
Research and Technology Center

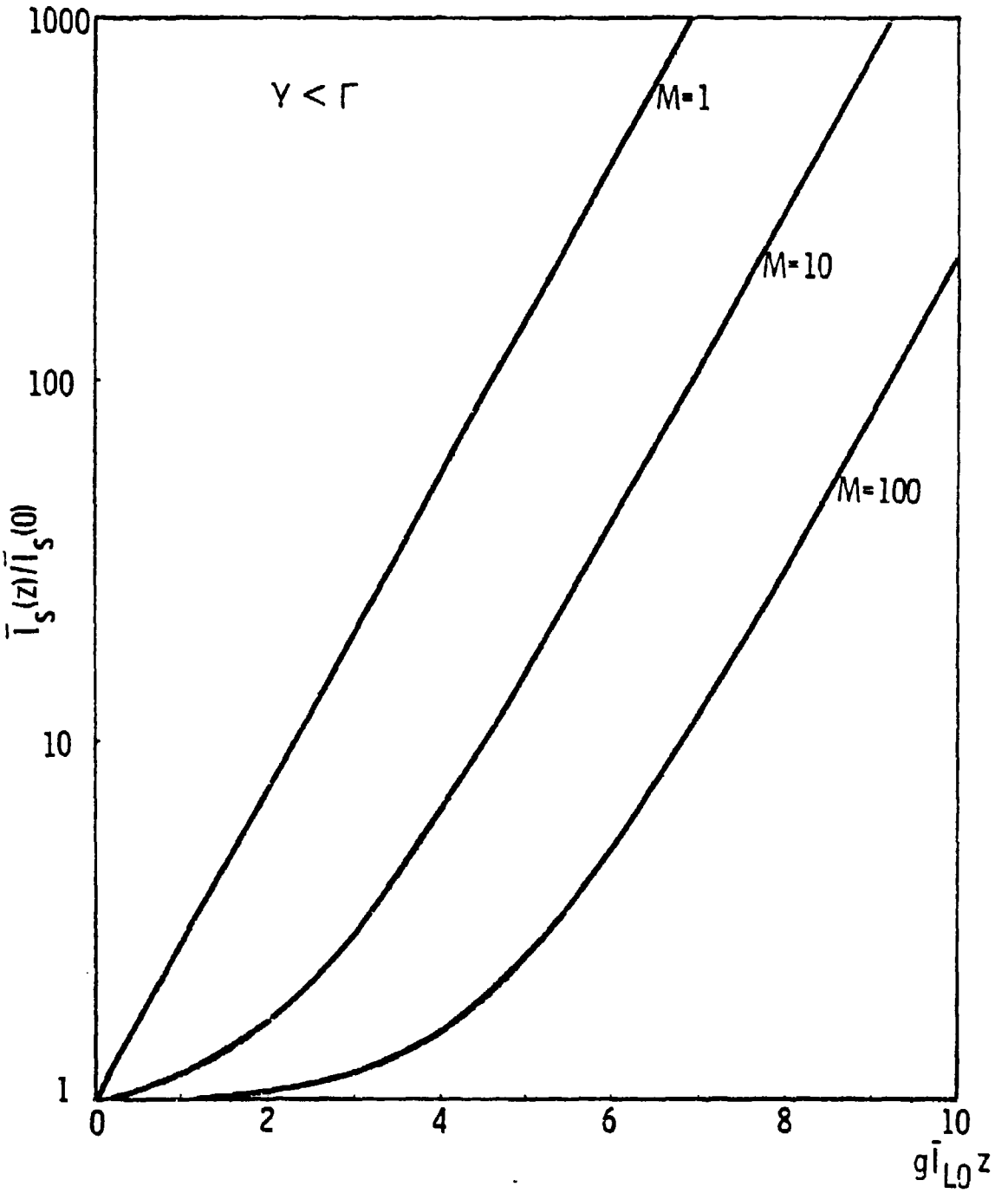

LASER-BANDWIDTH DEPENDENCE OF FORWARD GAIN IN A RAMAN AMPLIFIER WITH UNCORRELATED INJECTED PHASES.

NORTHROP
Research and Technology Center

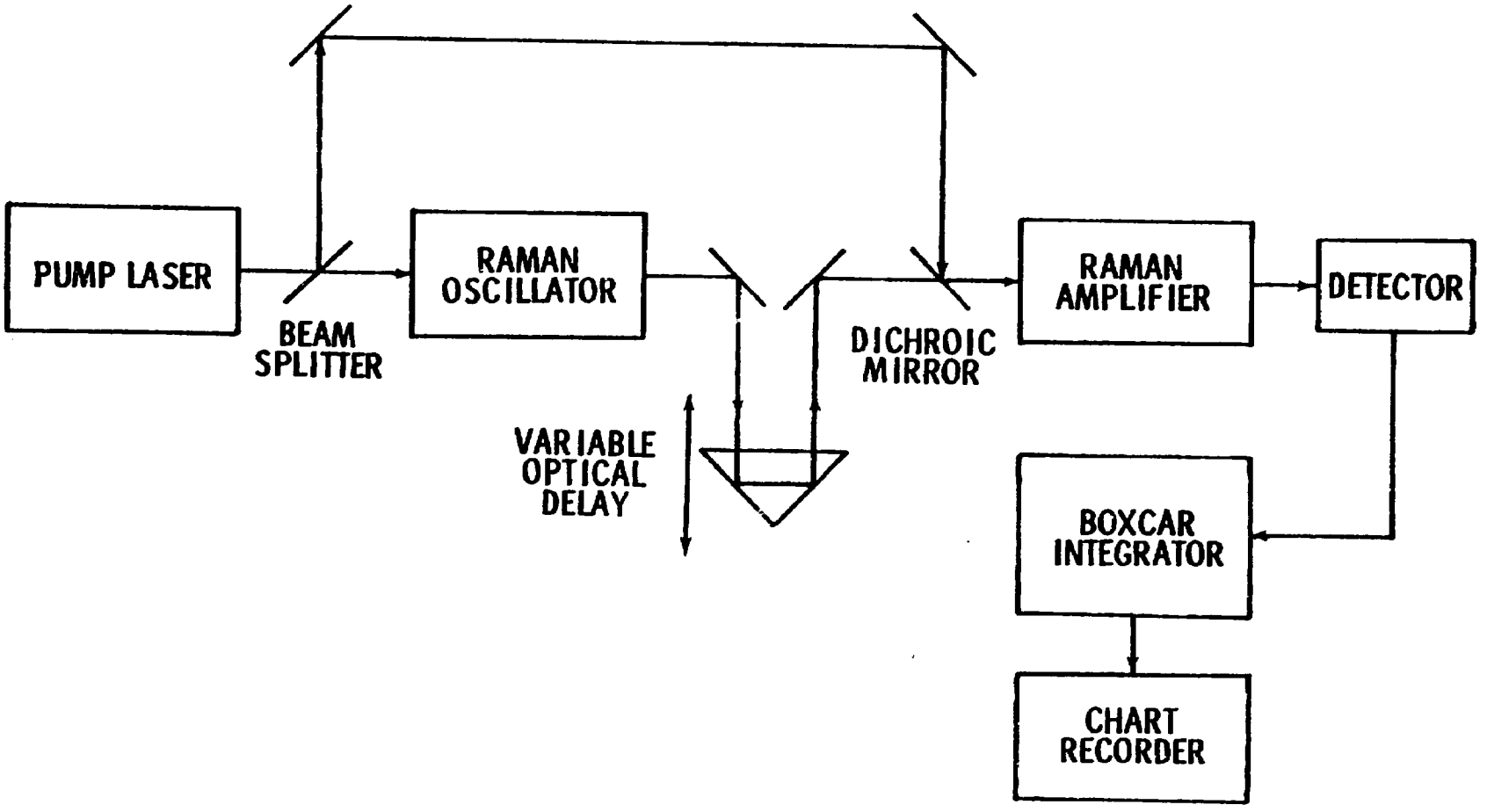

SCHEMATIC OF THE EXPERIMENTAL SETUP

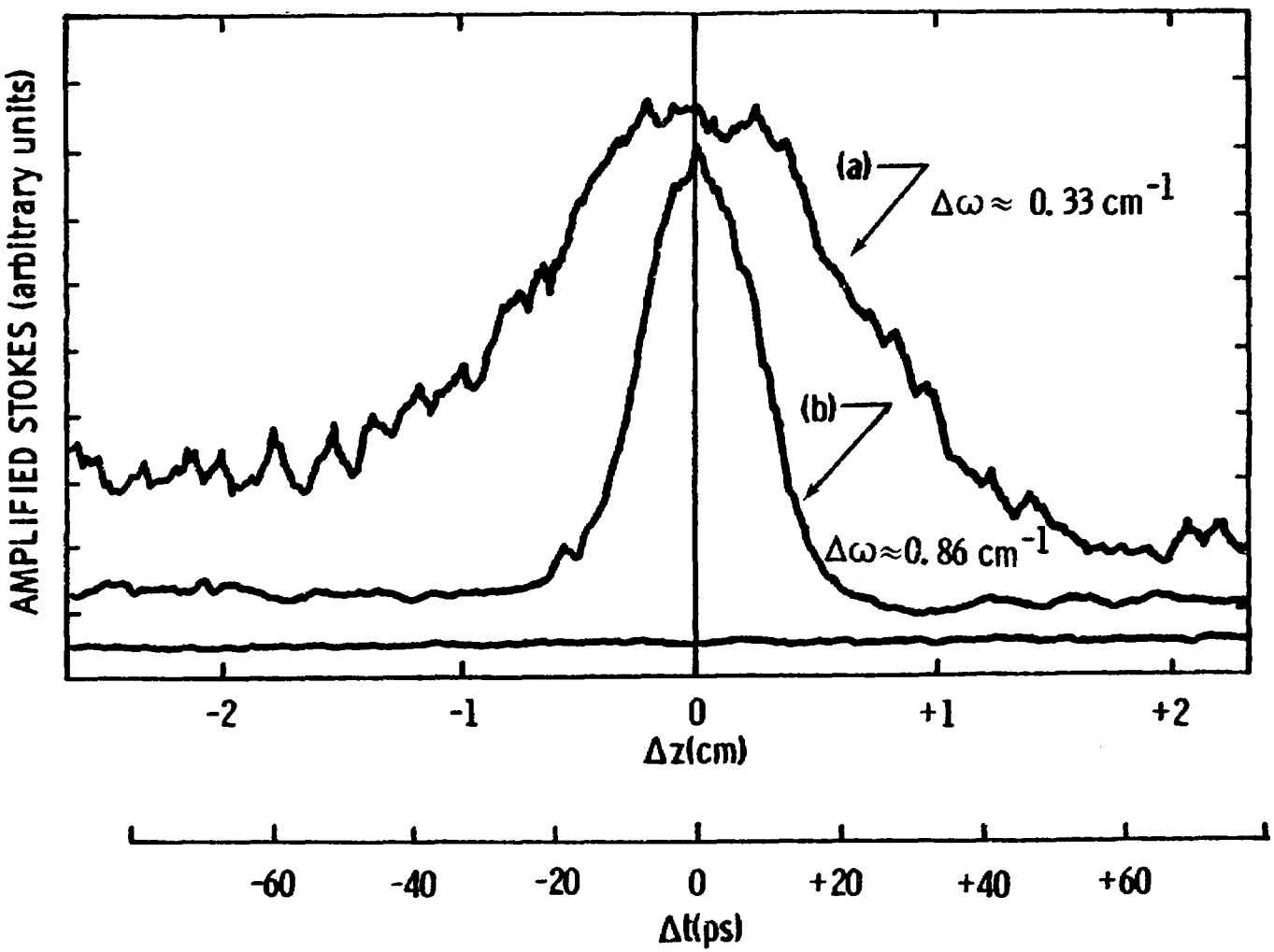

AMPLIFIED STOKES ENERGY VERSUS OPTICAL DELAY FOR (a) 0.33-cm^{-1} AND (b) 0.86-cm^{-1} PUMP BANDWIDTH. POSITIVE DELAYS CORRESPOND TO THE PUMP PRECEDING THE STOKES. PUMP ENERGY = 3 mJ. THE BASELINE CORRESPONDS TO THE INJECTED STOKES LEVEL.

NORTHROP
Research and Technology Center

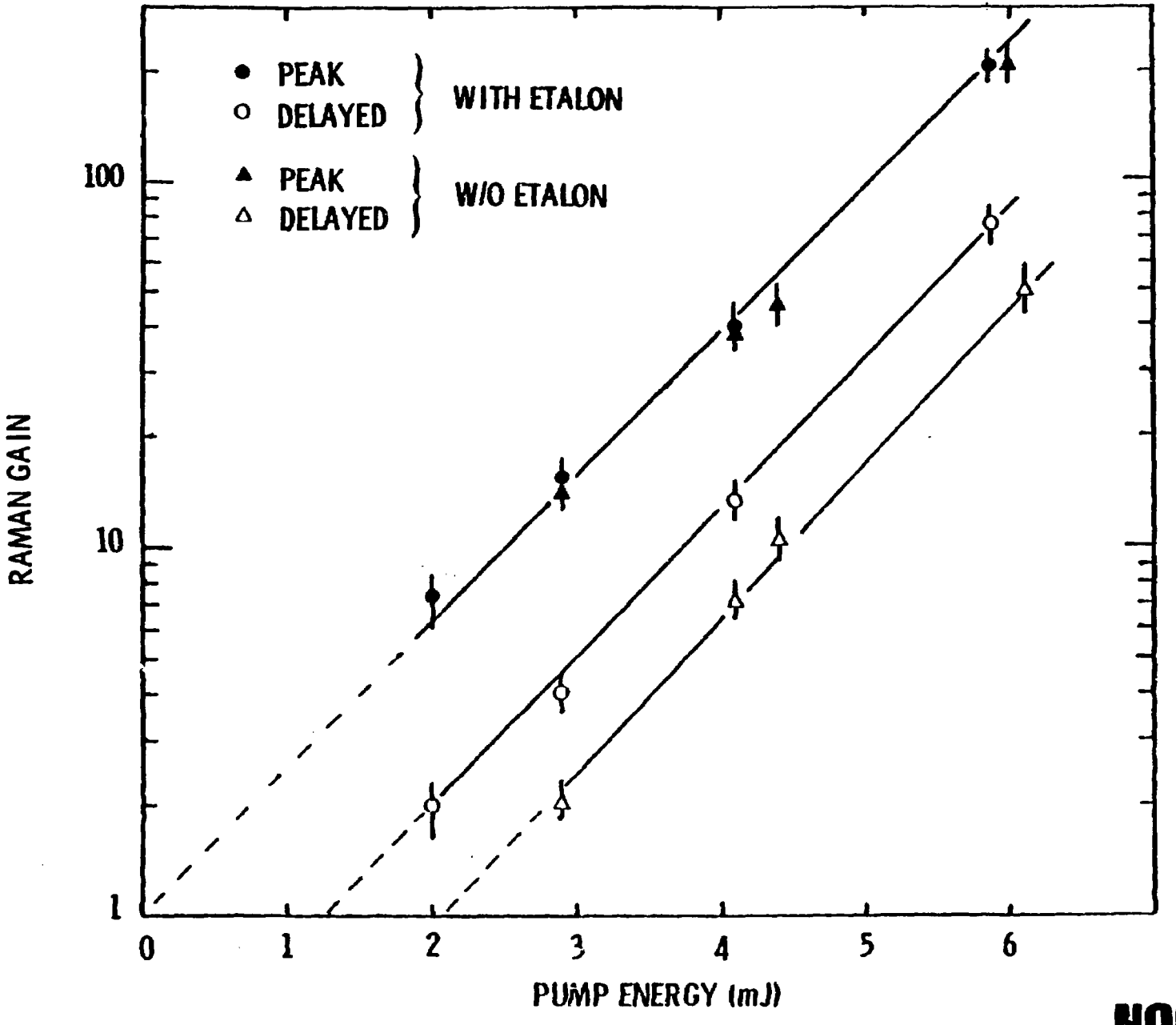

RAMAN AMPLIFIER GAIN VERSUS PUMP ENERGY

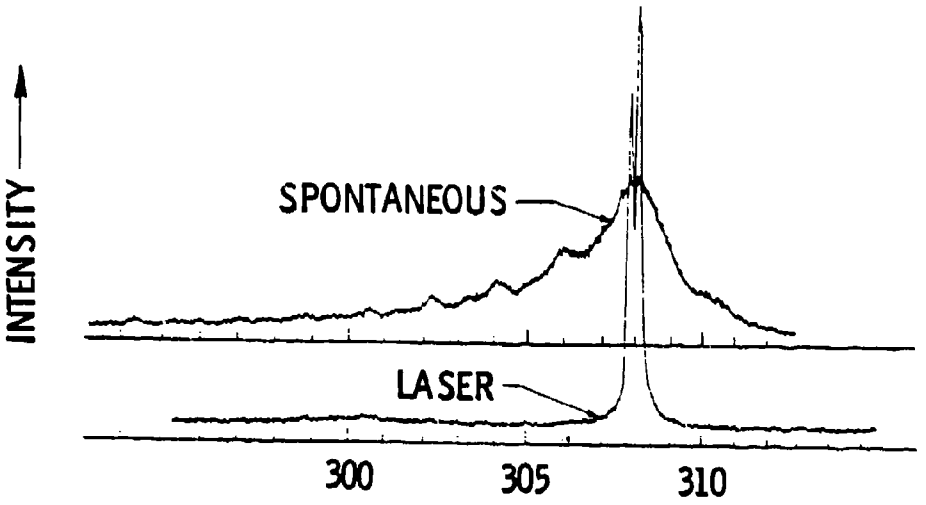

XeCl FLUORESCENCE AND LASER SPECTRA

NORTHROP
Research and Technology Center

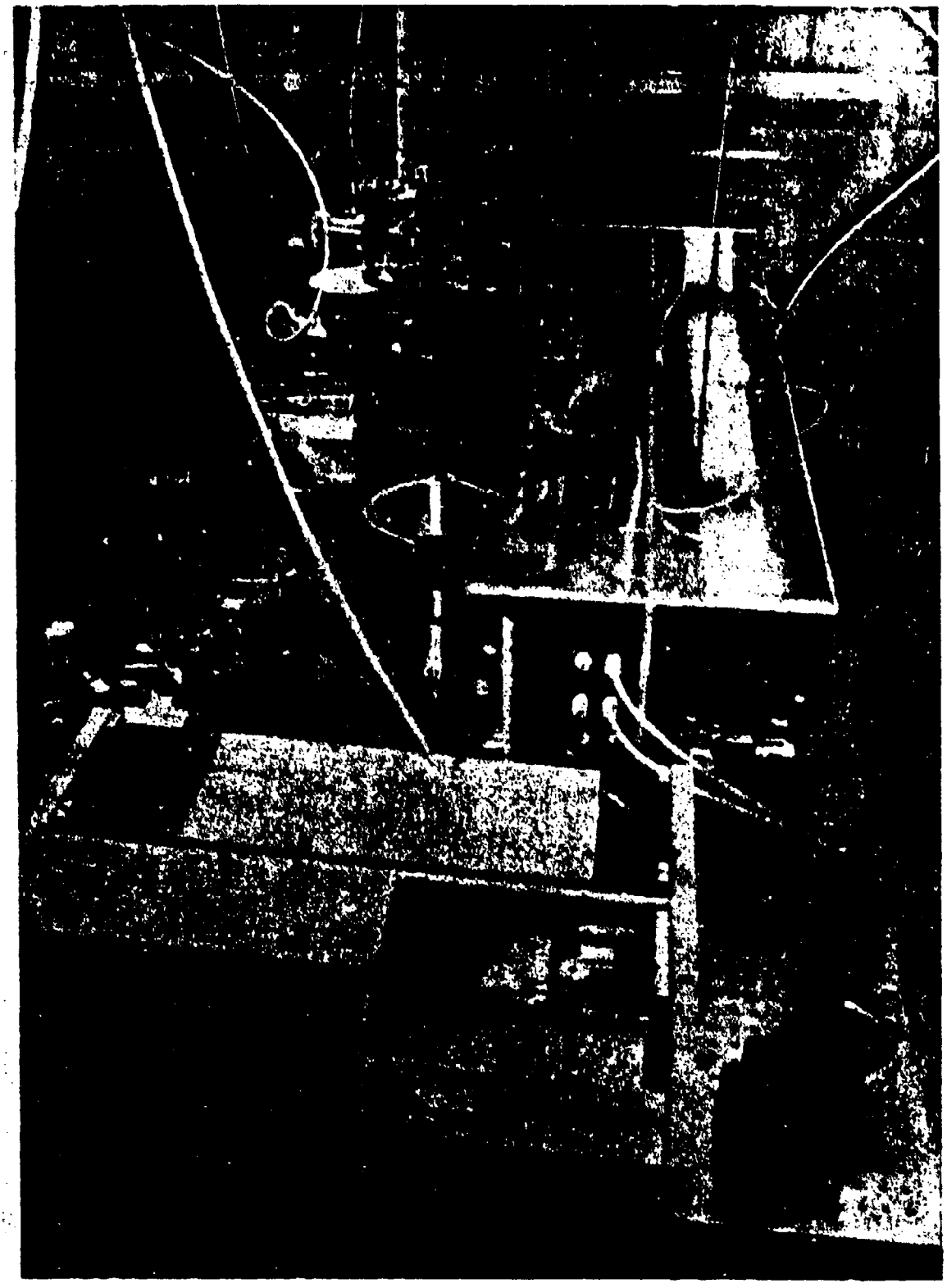

Tunable Narrow Bandwidth Injection-Locking Source

LEAD VAPOR CONVERSION OF AN X-RAY PREIONIZED XeCl LASER

J.I. LEVATTER & S.O. LIN
UCSD

I. NEW AVALANCHE DISCHARGE FORMATION MODEL

II. X-RAY PREIONIZED LASER SYSTEM

III. RAMAN DOWN CONVERSION IN Pb VAPOR

University of California
San Diego CA 92093

DISCHARGE FORMATION MODEL

(J. Appl. Phys. 51, 210, 1980)

NECESSARY CONDITIONS:

I. MINIMUM PREIONIZATION DENSITY, $n_{eo}(min)$

II. $n_{eo}(min)$ MUST BE VOLUMETRICALLY UNIFORM

III. $\vec{E}$ MUST BE UNIFORM

IV. MINIMUM $\frac{d(E/n)}{dt}$ (ie, VOLTAGE RISETIM. τ_r) ALLOWABLE

FUNCTIONAL DEPENDENCE OF CONDITIONS

I. $\propto$ GAS MIXTURE, $\frac{d(E/n)}{dt}$, & PRESSUE.

IV. $\propto$ GAS MIXTURE, & PRESSURE

SATISFACTORY OPERATING CONDITIONS FOR TYPICAL RARE GAS HALIDE LASERS

EXAMPLE 1: XeF ($He:Xe:F_2 = 94.5:5:0.5$)
Pressure – 1 atm.

$$n_{eo}\,(min) \geq 2 \times 10^{5}\ cm^{-3}$$
$$\tau_f \leq 16\ nsec$$

EXAMPLE 2: XeF ($He:Xe:F_2 = 94.5:5:0.5$)
Pressure – 6 atm.

$$n_{eo}\,(min) \geq 3 \times 10^{6}\ cm^{-3}$$
$$\tau_f \leq 6\ nsec$$

CONCLUSION OF THEORETICAL MODEL—

PROVIDED THE DISCHARGE IS PROPERLY INITIATED (i.e., CONDITIONS I → IV ARE SATISFIED) THERE IS NO INTRINSIC LIM TO THE VOLUME OR TEMPORAL SCALABILI OF RARE GAS HALIDE AVALANCHE DISCHARGES

RECENT EXPERIMENTAL VERIFICATION:
(APPL. PHYS. LETT. 34, 505, 1979)
XeF, KrF, & XeCl DISCHARGES AT ≥ 1 PRESSURE IN A 2.5 LITER VOLUME HA BEEN PRODUCED WITH NO ARCING O STREAMER FORMATION FOR A DURA OF 100 nsec

XeCl BURN PATTERN

XeCl DISCHARGE LUMINOSITY

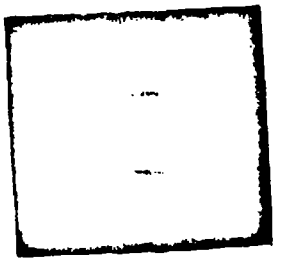

X-RAY PREIONIZED LASER SYSTEM BLOCK DIAGRAM

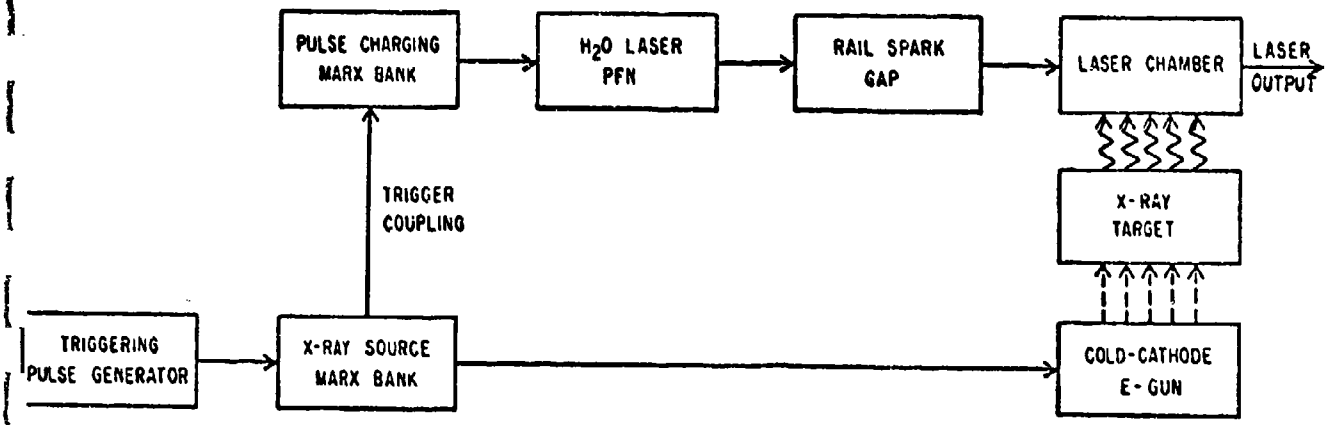

ELECTRICAL NETWORK

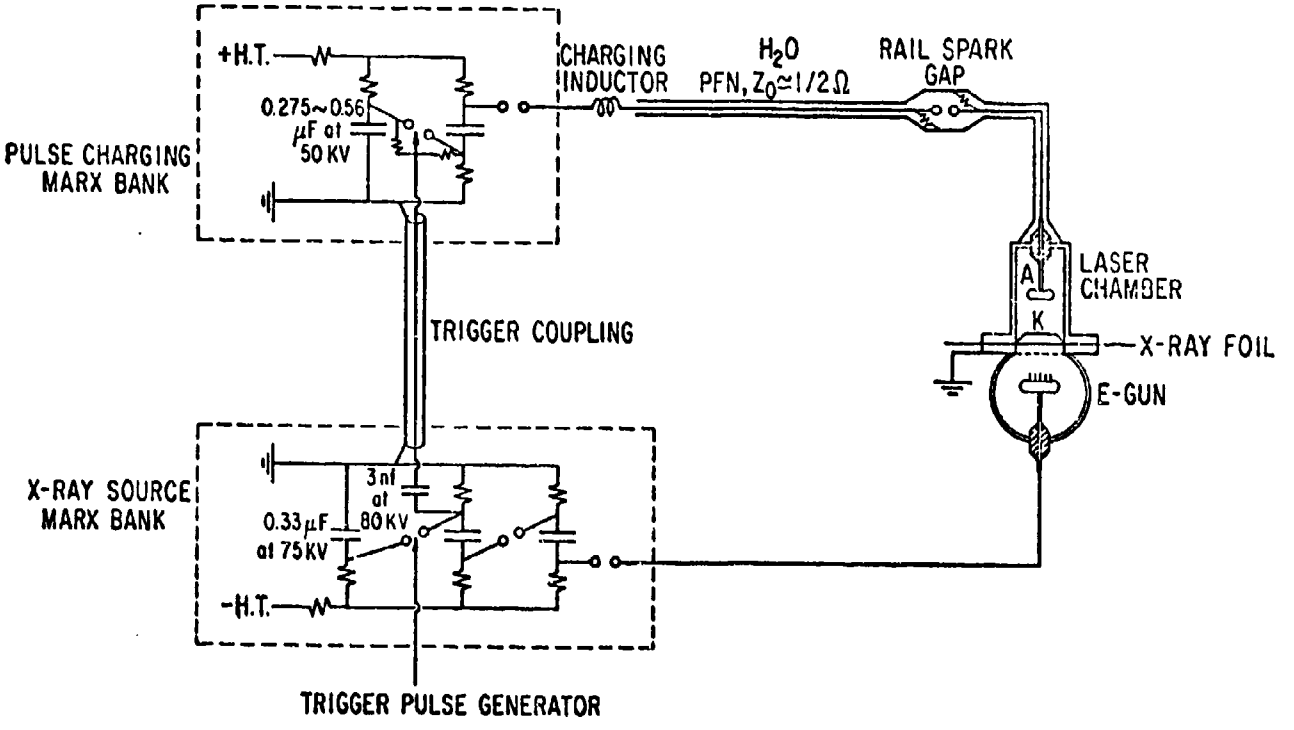

TYPICAL LASER PERFORMANCE - XeCl

1. LITER DISCHARGE VOLUME: 2.5 JOULE
2.5 LITER DISCHARGE VOLUME: > 5 JOULE

$$\text{LASER EFFICIENCY, } \eta \equiv \frac{\text{ENERGY STORED IN PRIMARY CAP}}{\text{LASER ENERGY OUT}}$$

$$\simeq 1.4\%$$

DISCHARGE VOLTAGE
35 kV/cm
50 nsec/cm

XeCl OUTPUT
20 nsec/cm
18 Mw/cm

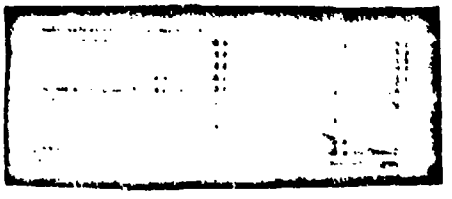

RAMAN DOWN CONVERSION

- REQUIRES GOOD BEAM QUALITY.
- REQUIRES HIGH OPTICAL DEINSITY.
- HOT SPOTS IN OPTICAL BEAM CAN EASILY DAMAGE OPTICS AT THE MULTI-JOULE LEVEL.

EXPERIMENTAL ARRANGEMENT

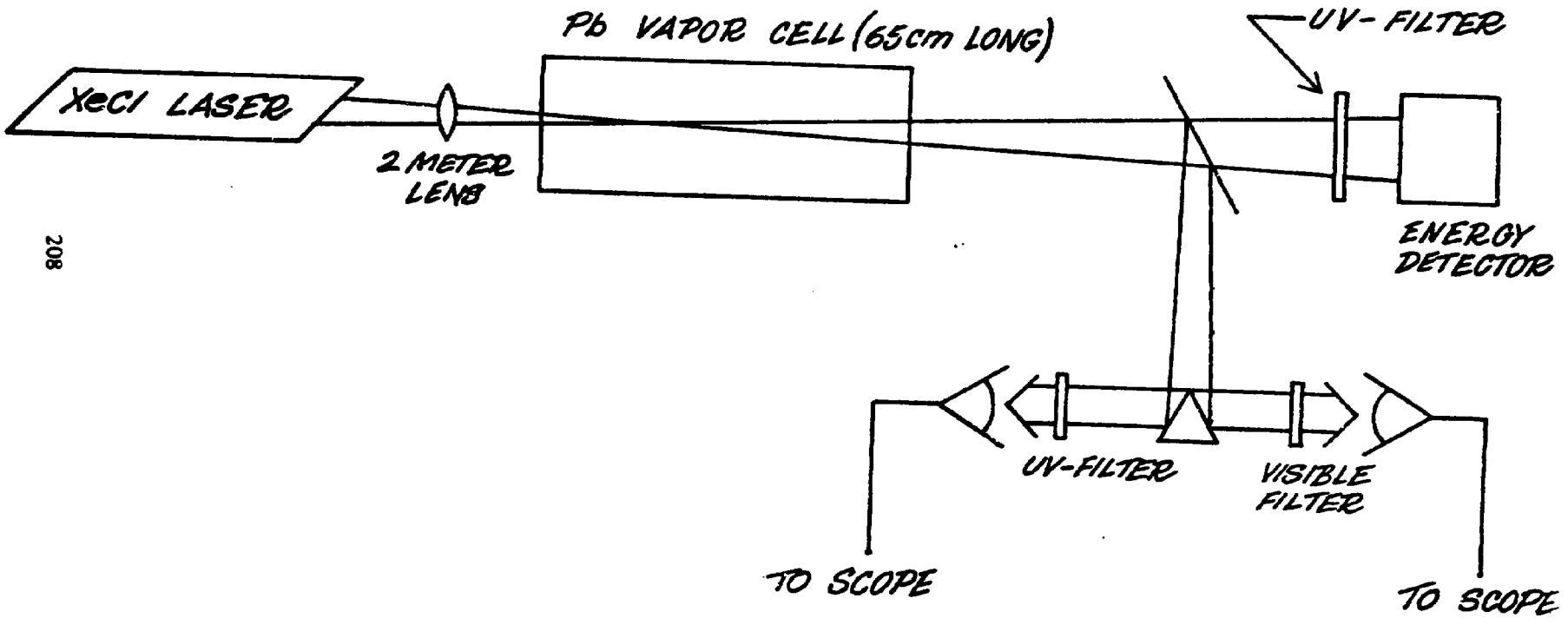

XeCl BEAM QUALITY (1 LITER DISCHARGE)

UNSTABLE RESONATOR USED ($M \simeq 1.4$)

NEAR FIELD

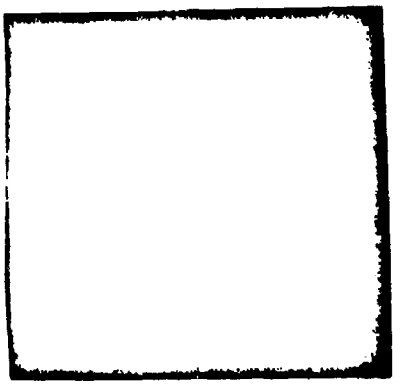

ENERGY $\simeq$ 1.5-2.5 J

FOCUS OF
2 METER
LENS

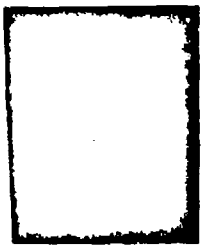

USABLE ENERGY
0.86 TO 1.5 J

INPUT-UV
E=0.86 J
20 nsec/cm

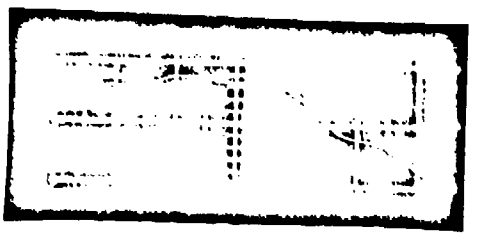

OUTPUT-459 nm
E=0.132 J
20 nsec/cm

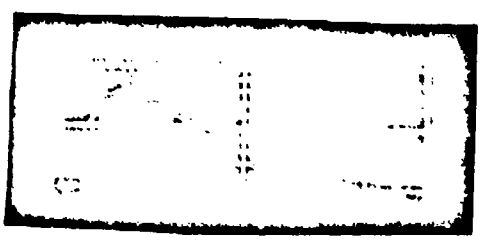

DEPLETED UV
20 nsec/cm
(~40% REMAINING)

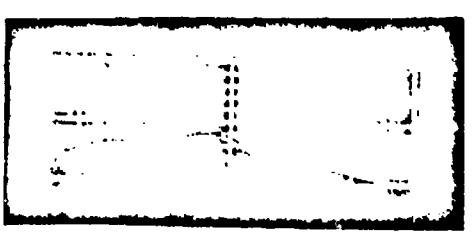

CONCLUSION

- CAN GENERATE MULTI-JOULE UV OUTPUT.
- EFFICIENT FREQUENCY CONVERSION REQUIRES HOMOGENEOUS DISCHARGE TO AVOID BEAM PARASITICS & HOT SPOTS WHICH CAN DAMAGE OPTICS.
- RESONATOR OPTICS SHOULD BE DESIGNED SO THAT THE LASER MODE STRUCTURE IS IN STEADY STATE.
- 50% ENERGY CONVERSION SEEMS POSSIBLE PROVIDED THE OPTICAL BEAM QUALITY IS SUFFICIENT TO ALLOW THE PROPAGATION OF A COLLIMATED INPUT BEAM.

LA-UR 80-665

TITLE: EXCIMER LASER ENGINEERING DEVELOPMENT AT LASL

AUTHOR(S): Phillip N. Mace, AP-1

SUBMITTED TO: Blue-Green Technical Interchange Meeting, NOSC, San Diego, CA

los alamos
scientific laboratory
of the University of California
LOS ALAMOS, NEW MEXICO 87545

EXCIMER LASER ENGINEERING DEVELOPMENT AT LASL

by
Phillip N. Mace, AP-1
Los Alamos Scientific Laboratory, University of California
Los Alamos, New Mexico 87545

The Molecular Laser Isotope Separation program under development in AP-Division, Los Alamos Scientific Laboratory, requires development of XeCℓ laser systems having specifications which differ from those required for the Blue-Green Strategic Communications Program satellite based laser only in energy/pulse and pulse repetition rate. There is thus clearly a high degree of overlap in the critical technology issues which must be addressed in order to be able to design efficient, long-life laser systems. Two areas are presented in this discussion; development of clean-up systems for XeCℓ closed loop lasers and predictions of future clean-up system requirements, and work underway to develop reliable, long-life pulse power components meeting voltage, peak current, and dI/dt requirements of discharge pumped excimer lasers. Other key technology issues which will be mentioned but not discussed in detail include flow system and acoustic attenuator design, discharge electrodynamics, laser kinetics and PFN design, preionization techniques, optical system design, optical damage, and advanced component concepts.

EXCIMER LASER ENGINEERING AT LASL

AREAS OF DEVELOPMENT

- PREIONIZATION
- KILOHERTZ SYSTEM STUDIES
- EFFICIENCY, ENERGY SCALING
- CHEMISTRY
- PULSE POWER COMPONENT DEVELOPMENT
- OPTICAL DAMAGE

LASER SYSTEM DEVELOPMENT

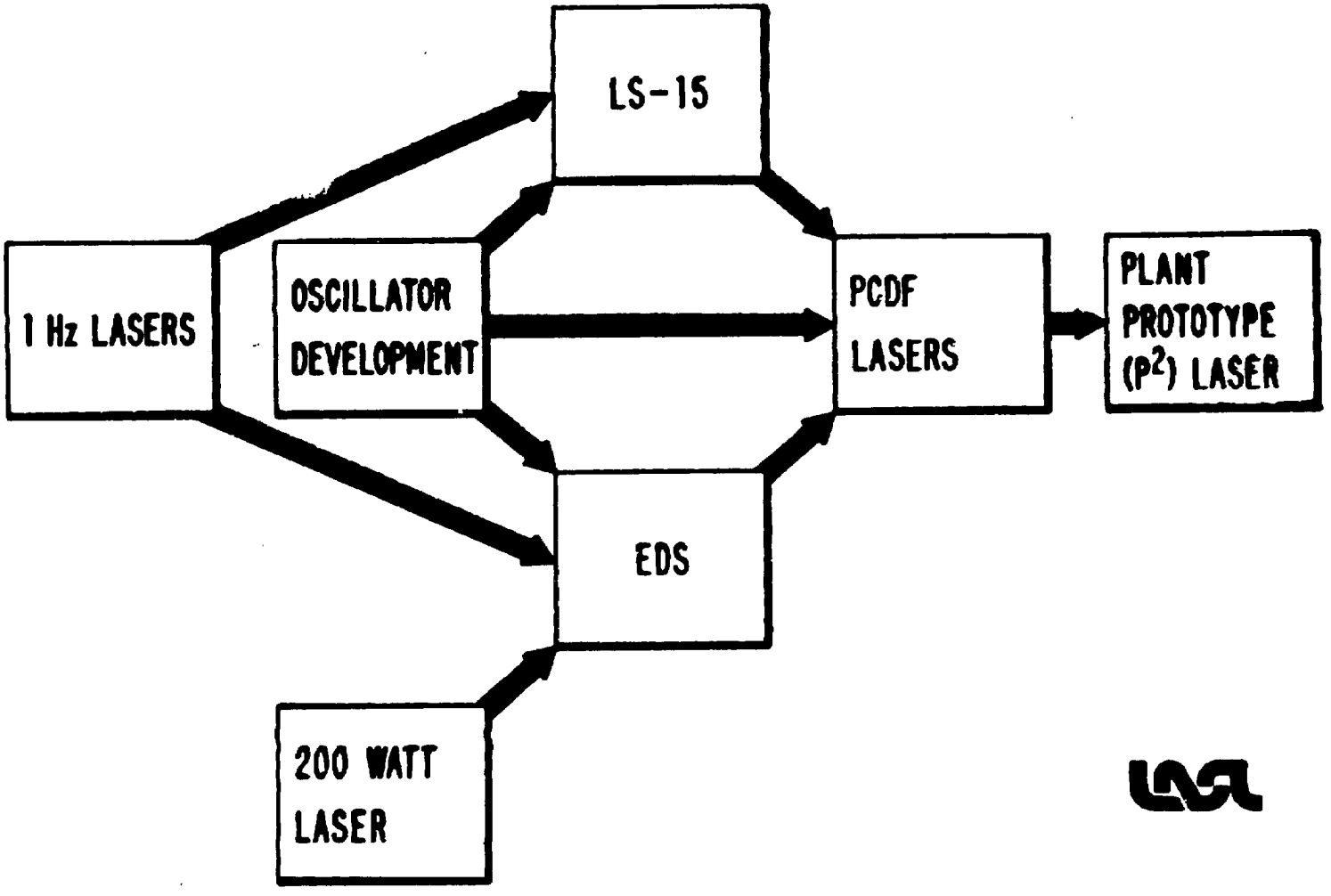

LASER GAS CHEMISTRY

- CLEAN–UP SYSTEMS HAVE BEEN DEVELOPED CAPABLE OF MAINTAINING INITIAL OUTPUT FOR LONG TIMES
- XeCℓ AT LEAST 200X LONGER LIFE THAN KrF
- NO PROBLEMS ANTICIPATED FOR 1984

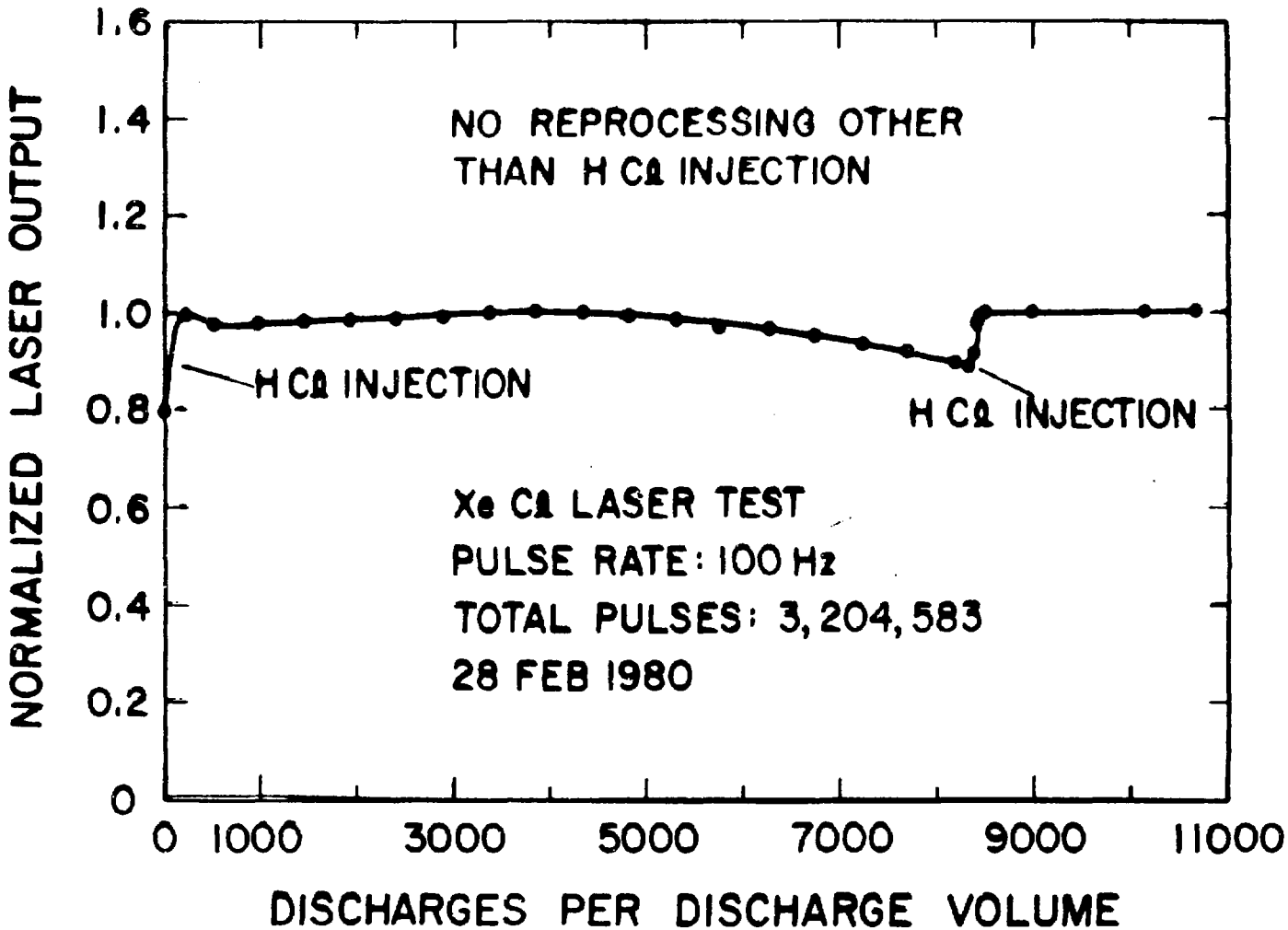
NORMALIZED LASER OUTPUT
1.6
1.4
1.2
1.0
0.8
0.6
0.4
0.2
0
NO REPROCESSING OTHER
THAN H Cℓ INJECTION
H Cℓ INJECTION
H Cℓ INJECTION
Xe Cℓ LASER TEST
PULSE RATE: 100 Hz
TOTAL PULSES: 3,204,583
28 FEB 1980
0
1000
3000
5000
7000
9000
11000
DISCHARGES PER DISCHARGE VOLUME

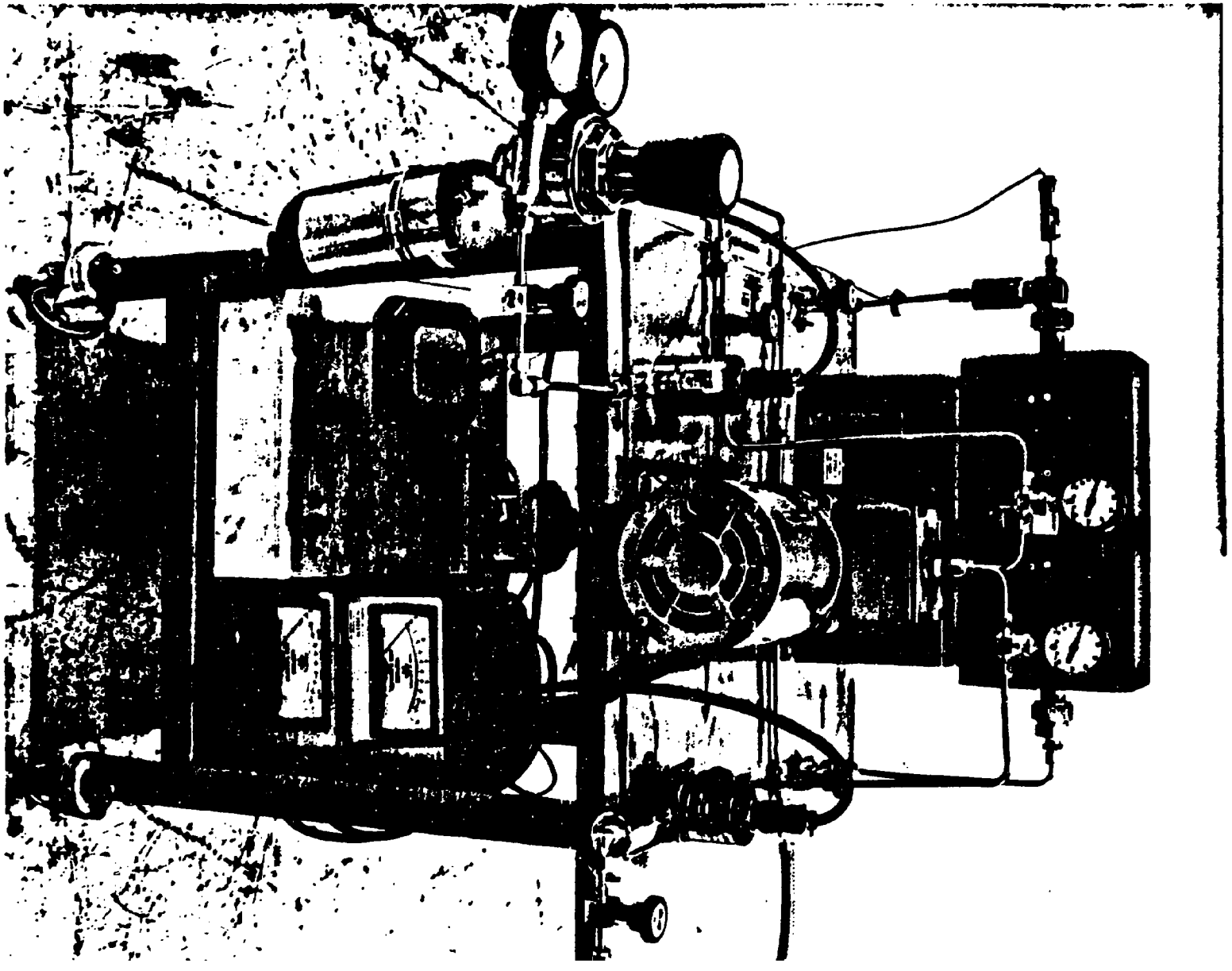

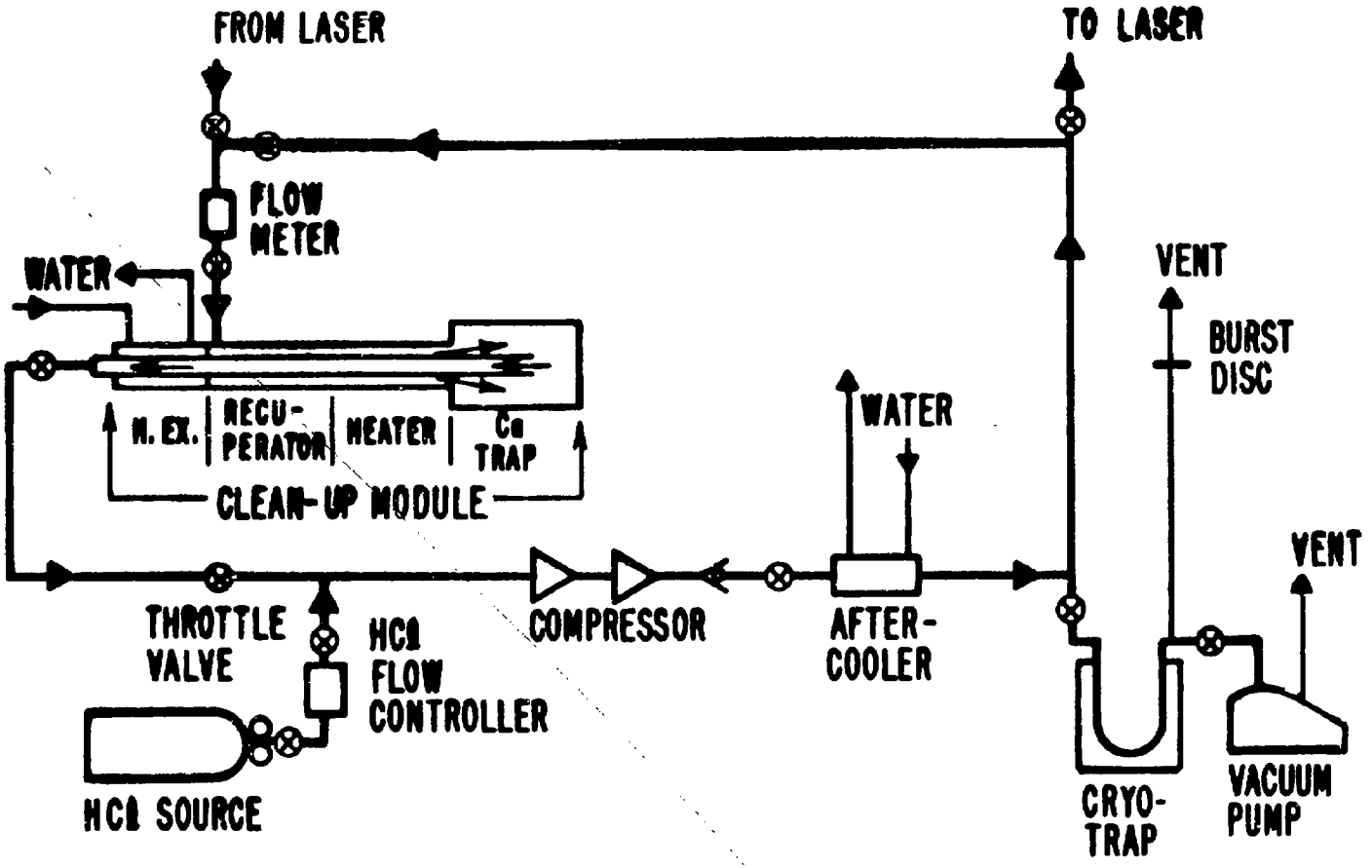

LS-15 GAS CLEAN-UP SCHEMATIC

LS-15
GAS CLEAN-UP
MODULE

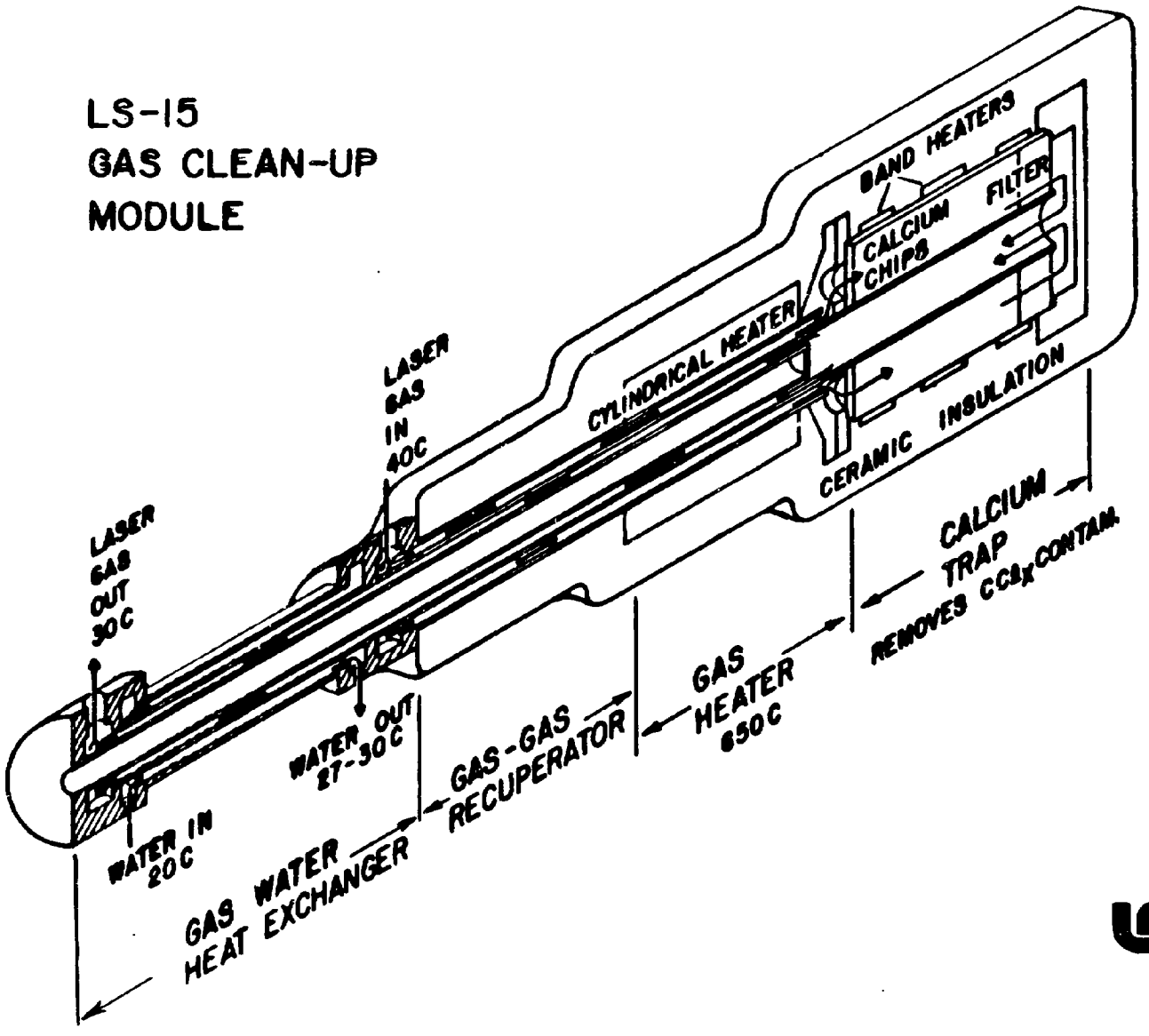

XeCl CLEAN–UP SYSTEM

REPROCESSING RATE: $\leqslant$ 0.75 SLM CONTINUOUS

GETTER TRAP TEMPERATURE: 650°C (TITANIUM)

HCℓ INJECTION RATE: ~0.3 SCCM

ESTIMATED SYSTEM LIFETIME: 10^{10} PULSES @ 100 Hz (~3.2 YEARS)

OVEN POWER CONSUMPTION : ~120 WATTS WITHOUT RECUPERATOR

AMOUNT OF TITANIUM REQUIRED: ~1 LITER

LASL

ADVANCED PULSE POWER TECHNOLOGY DEVELOPMENT

AP-1-VG-5117

COMPONENT DEVELOPMENT

IS THE KEY TO EFFICIENCY

AND SYSTEM RELIABILITY

THYRATRON DEVELOPMENT

- PRIME CONTRACTOR – EG&G
- MAJOR PROGRAM GOALS:
  1. INCREASE TOTAL CURRENT CAPABILITY
  2. INCREASE dI/dt CAPABILITY
  3. DEMONSTRATE SUB-NANOSECOND JITTER FOR PARALLEL OPERATION
  4. INVESTIGATE TUBE HEATING DURING LEADING EDGE
  5. INVESTIGATE TUBE RECOVERY
     – TIME REQUIRED
     – REVERSE VOLTAGE PROTECTION

AP-1-VG-2123A

RECENT PROGRESS IN THYRATRON DEVELOPMENT

- KEY SPECIFICATIONS ACHIEVED IN ONE TUBE
  - 50 kV OPERATING VOLTAGE
  - 20 kA PEAK CURRENT
  - $>10^{12}$ A/s DI/DT
- NO FUNDAMENTAL PHYSICS DISCOVERED WHICH WILL LIMIT ULTIMATELY REACHING LIFE OF >10,000 HOURS

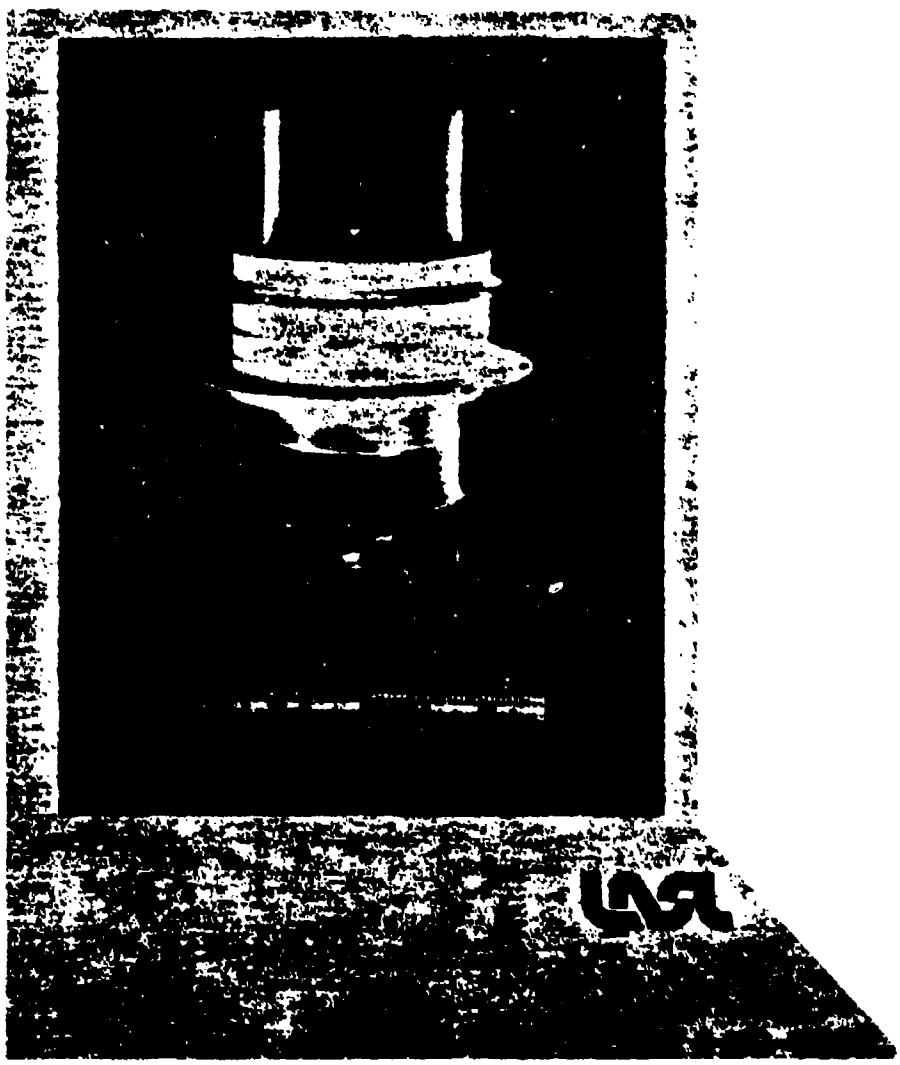

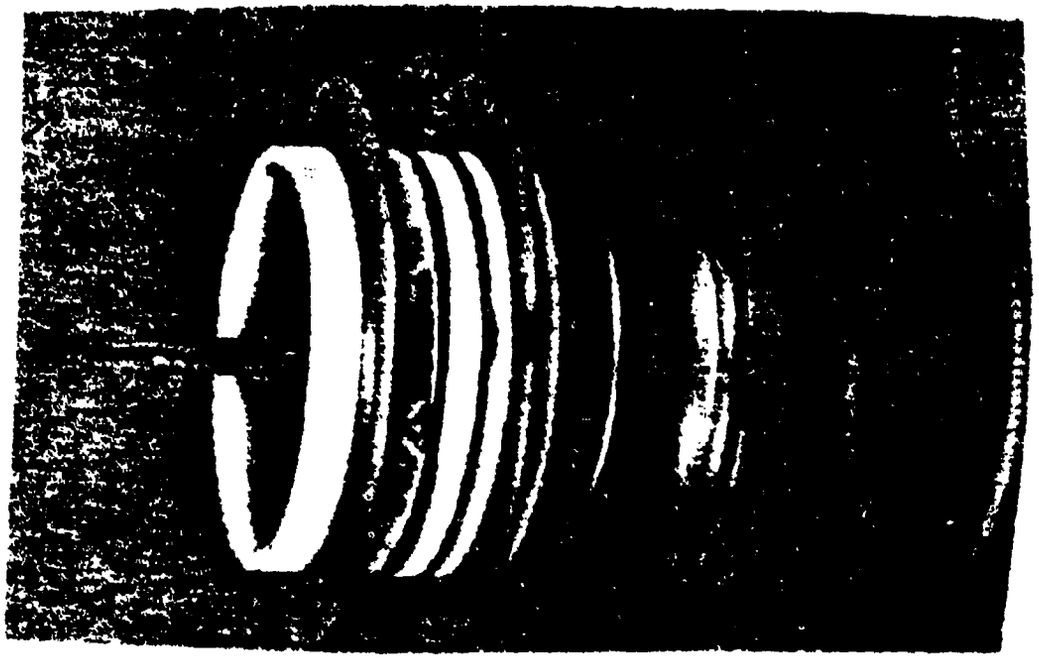

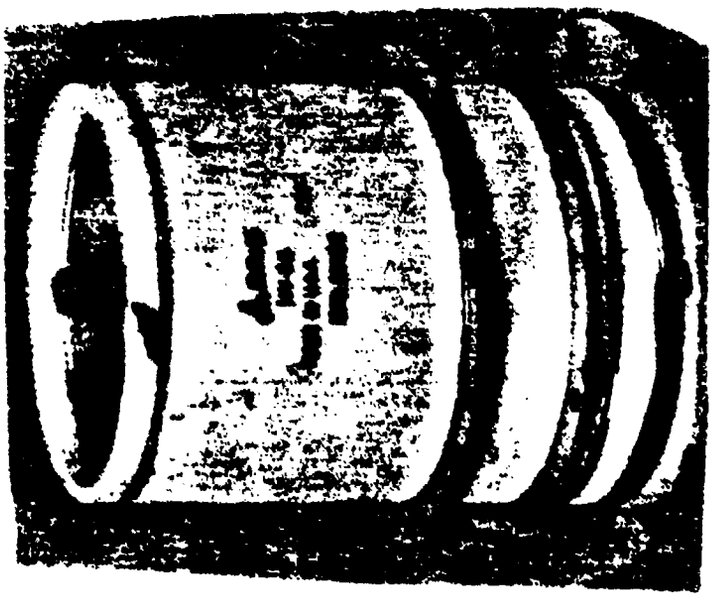

THYRATRON LIFE

- CATHODE – THERMAL EVAPORATION RATE OF CATHODE COATING
- RESERVOIR – GAS CLEANUP RATE
- MECHANICAL – SEAL FAILURE (OFTEN ACCIDENTAL)

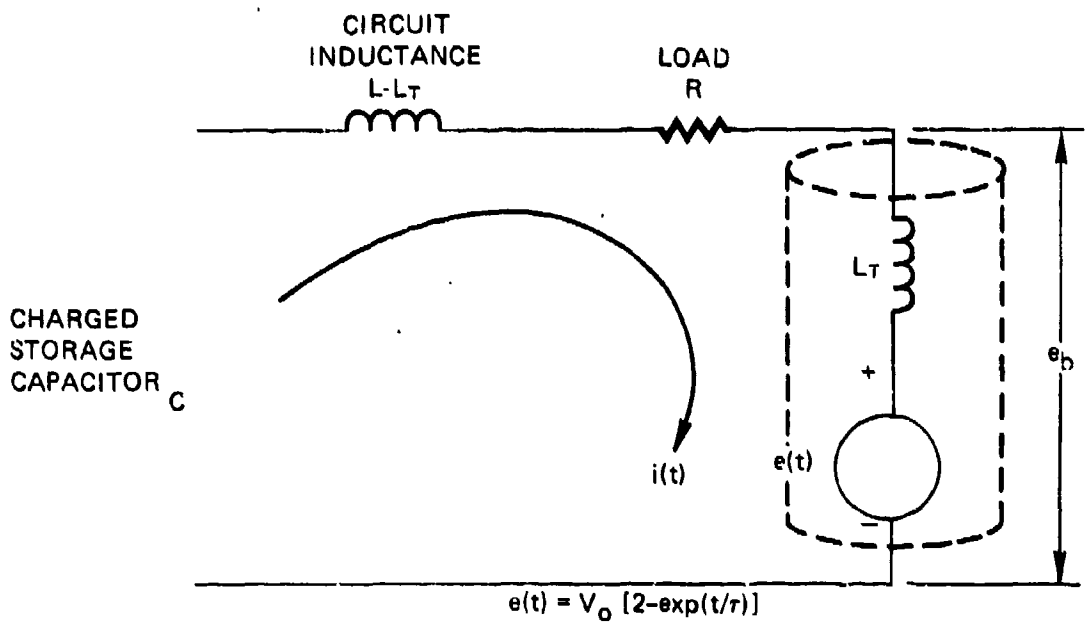
CIRCUIT
INDUCTANCE
L-LT
LOAD
R
CHARGED
STORAGE
CAPACITOR
C
LT
+
eb
e(t)
i(t)
−
e(t) = Vo [2-exp(t/τ)]

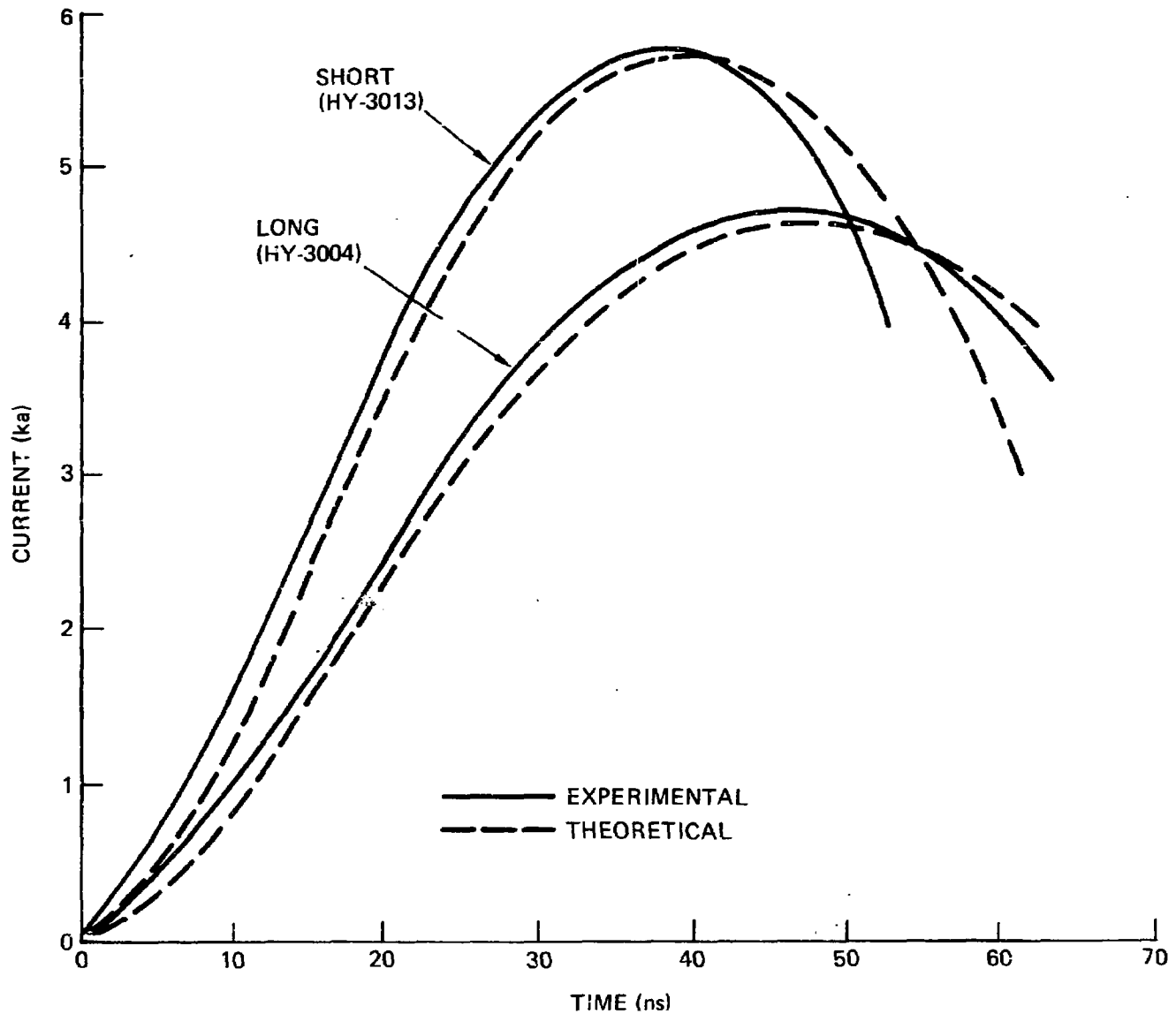
SHORT
(HY-3013)
LONG
(HY-3004)
EXPERIMENTAL
THEORETICAL
CURRENT (ka)
TIME (ns)
0
1
2
3
4
5
6
0
10
20
30
40
50
60
70

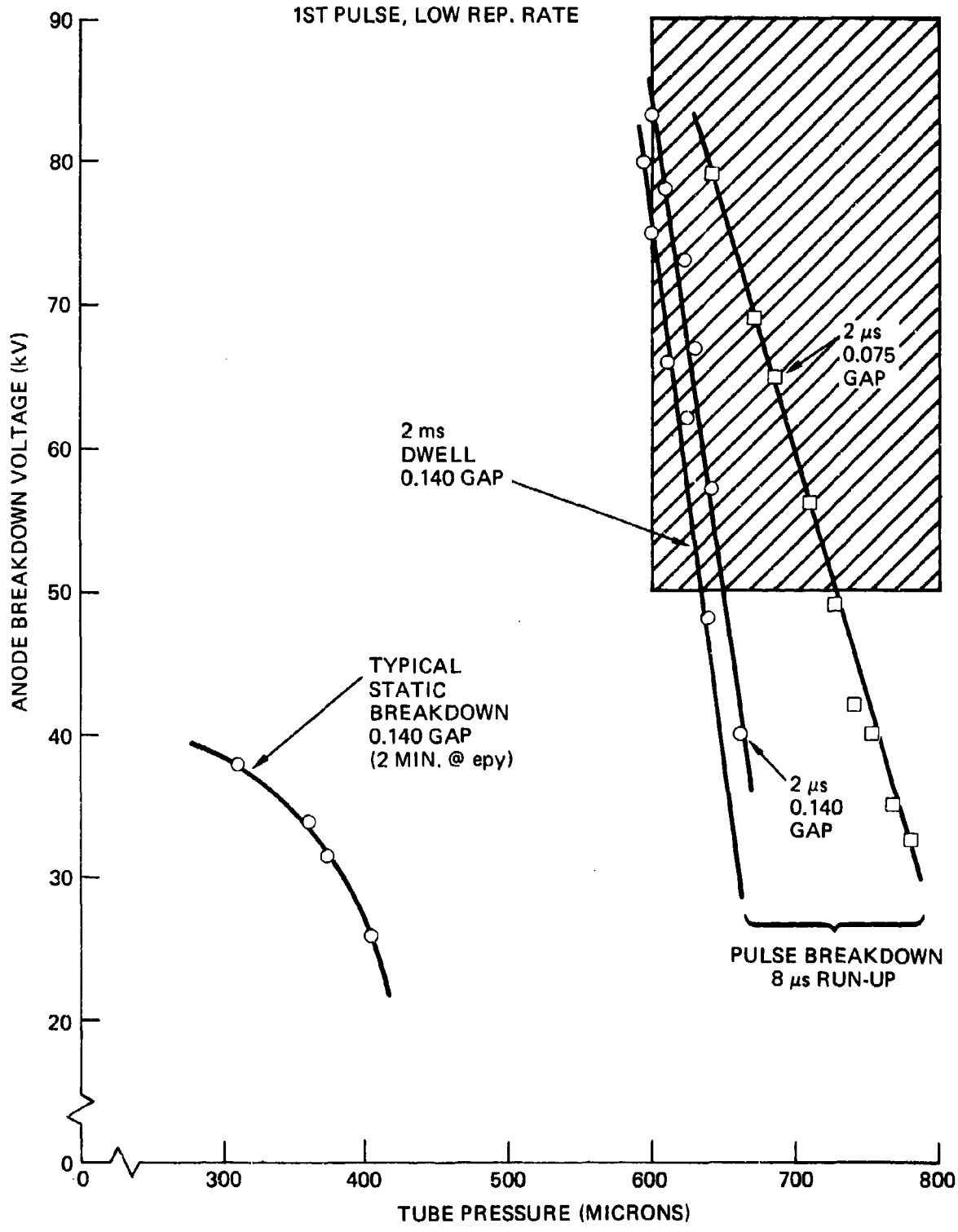
1ST PULSE, LOW REP. RATE
ANODE BREAKDOWN VOLTAGE (kV)
90
80
70
60
50
40
30
20
0
0
300
400
500
600
700
800
TUBE PRESSURE (MICRONS)
2 μs
0.075
GAP
2 ms
DWELL
0.140 GAP
TYPICAL
STATIC
BREAKDOWN
0.140 GAP
(2 MIN. @ epy)
2 μs
0.140
GAP
PULSE BREAKDOWN
8 μs RUN-UP

THYRATRON DEVELOPMENT

REMAINING TECHNOLOGY ISSUES:

- INCREASE PEAK CURRENT CAPABILITY TO 50 KA
- DEVELOP INVERSE VOLTAGE CAPABILITY
- DEMONSTRATE FULL POWER OPERATION UNDER DESIGN THERMAL LOAD

CAPACITOR DEVELOPMENT

- 1 kHz TEST FACILITY COMPLETE AND IN USE.

  FEATURES:

  - OPERATING VOLTAGE UP TO 80 kV.
  - AVERAGE POWER DURING TESTS OF 20 kW, TO BE UPGRADED TO 300 kW.
  - COMPLETE DATA ACQUISITION AND DATA REDUCTION SYSTEM.

- THIS IS THE ONLY MULTIKILOWATT HIGH REP RATE COMPONENT TEST SYSTEM IN EXISTENCE.

- THE LASL HIGH PULSE RATE PULSED POWER DEVELOPMENT PROGRAM IS UNIQUE IN THE NATION

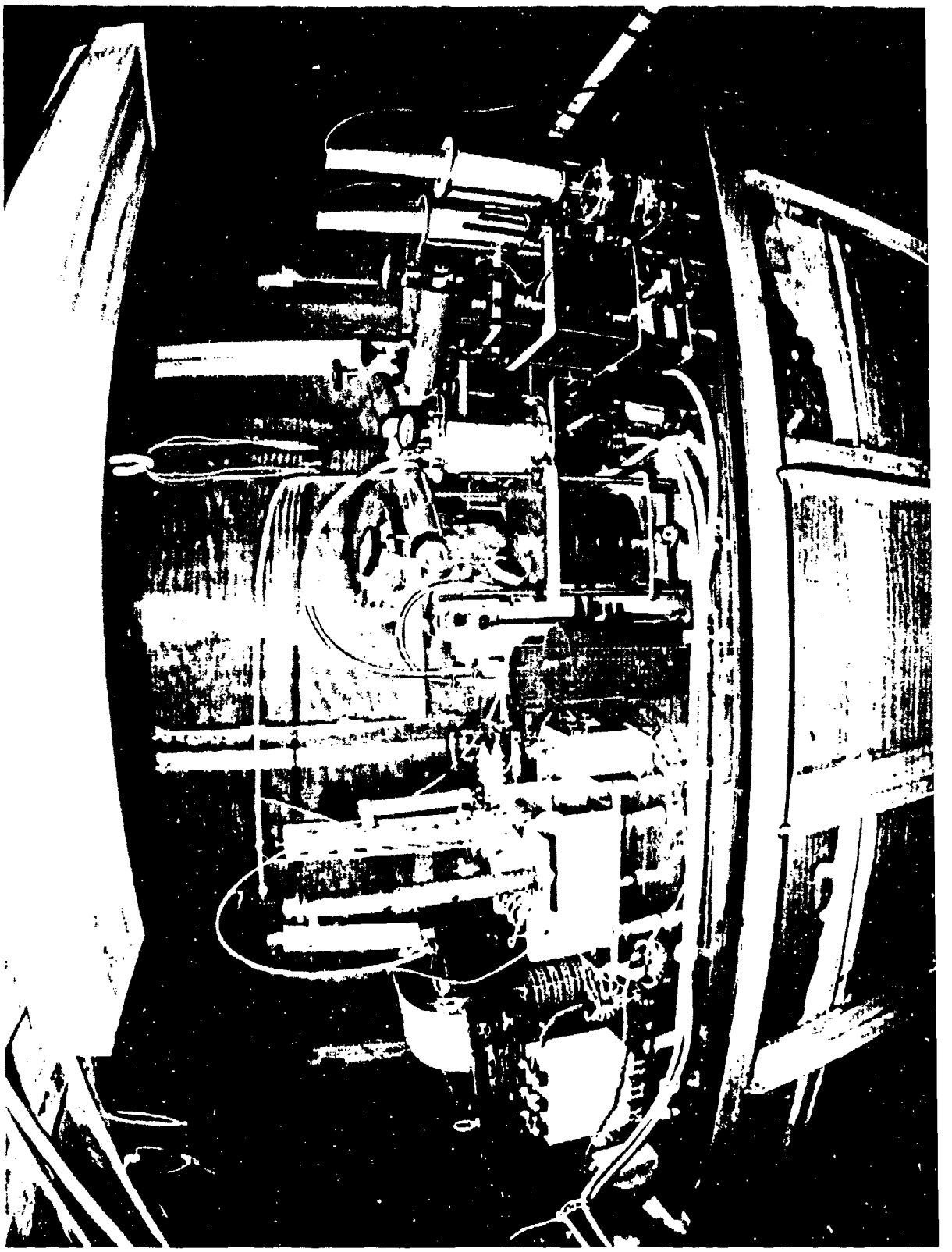

CAPACITOR DEVELOPMENT

- TESTING SIMULTANEOUSLY ASSESSES
  - CAPACITORS
  - SWITCHES
  - CHARGING TECHNIQUES
  - ADVANCED MODULATOR COMPONENTS
- FOR LIFETIME, RELIABILITY AND MAINTAINABILITY.

CAPACITOR DEVELOPMENT

MLIS REQUIREMENTS:

- 1–2 kHz PRF
- PEAK SYSTEM CURRENT >100 kA
- PEAK dI/dT > 1 MEGAMPERE/MICROSECOND
- LIFE $>10^{10}$, PREFERABLY $>10^{12}$ SHOTS
- TOTAL ENERGY STORED ~100 J
- OPERATING VOLTAGE 50–100 kV

CAPACITOR DEVELOPMENT

TWO PRIMARY APPROACHES:

- **RECONSTITUTED MICA, REDESIGNED FOR HIGH PEAK CURRENT, RMS CURRENT, & DI/dT**
- **PLASTIC FILM/LIQUID IMPREGNANT UNWICKED**

Capacitor Tests Include Development of New Diagnostic Aids

Measurement of Equivalent Series Resistance (ESR) During Test Gives Information on Failure Time

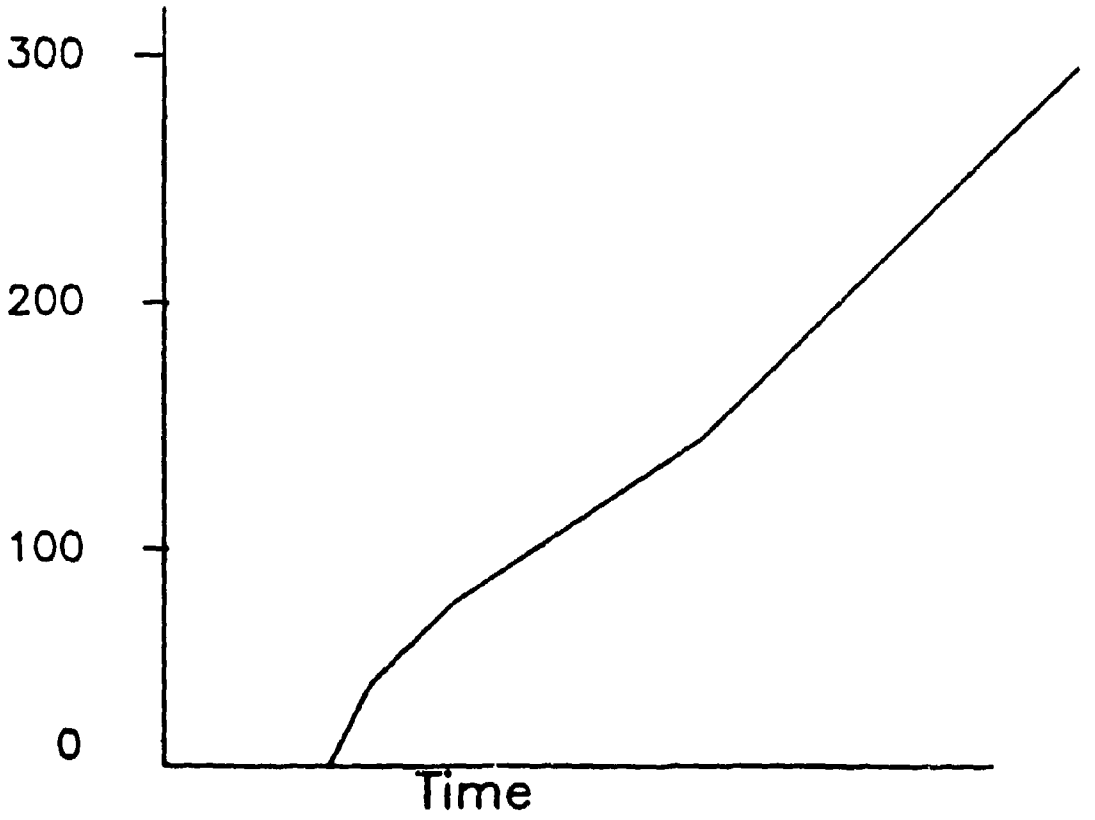

RECENT RESULTS FROM CAPACITOR TESTS

FAILURE RELATIONSHIP TO VOLTAGE STRESS GIVES A PREDICTIVE CAPABILITY OF TIME-TO-FAILURE

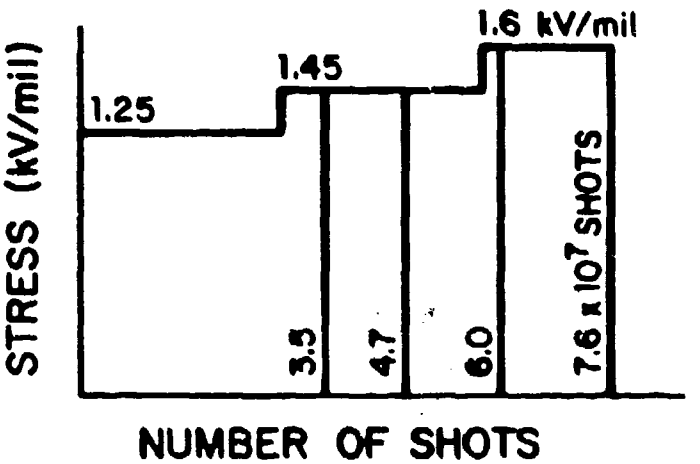

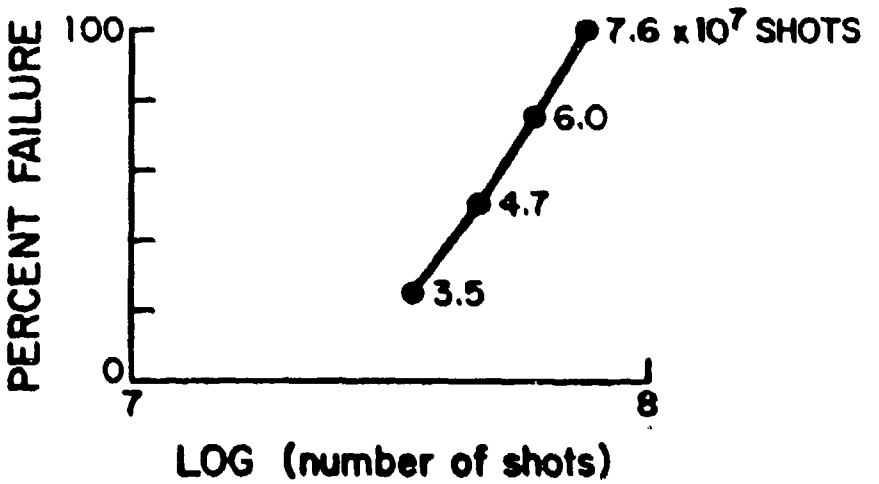

UV OPTICAL DAMAGE TESTS

LASER

- XeCl 308 nm
- 7 J/cm^2
- 100 Hz
- 700 W/cm^2

RESULTS

(1)	MgF_2	SURFACE GLOW FROM POLISHING COMPOUND NO DAMAGE IN 10^5 SHOTS
(2)	CaF_2	FLUORESCENCE FROM BULK MATERIAL BUT NO PERMANENT DAMAGE
(3)	SUPRASIL II	RED FLUORESCENCE BUT NO BULK DAMAGE AT 300 W/cm^2
(4)	Al_2O_3	VERY RAPID SURFACE DAMAGE

PRELIMINARY CONCLUSION IS 308 IS MUCH BETTER ON OPTICS THAN 248.

10^5 shots at 100 N_3

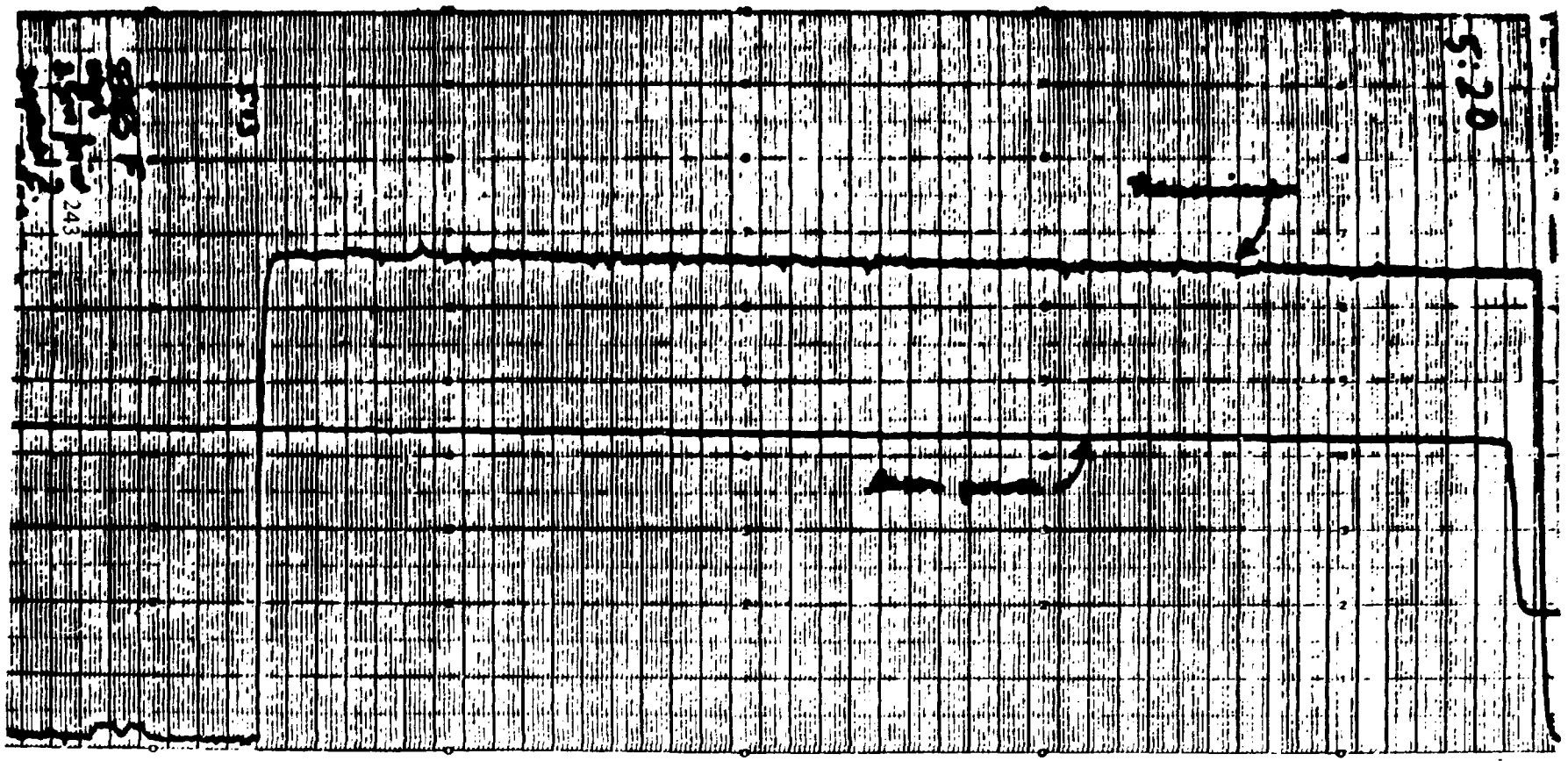

RARE GAS HALOGEN LASER MODEL

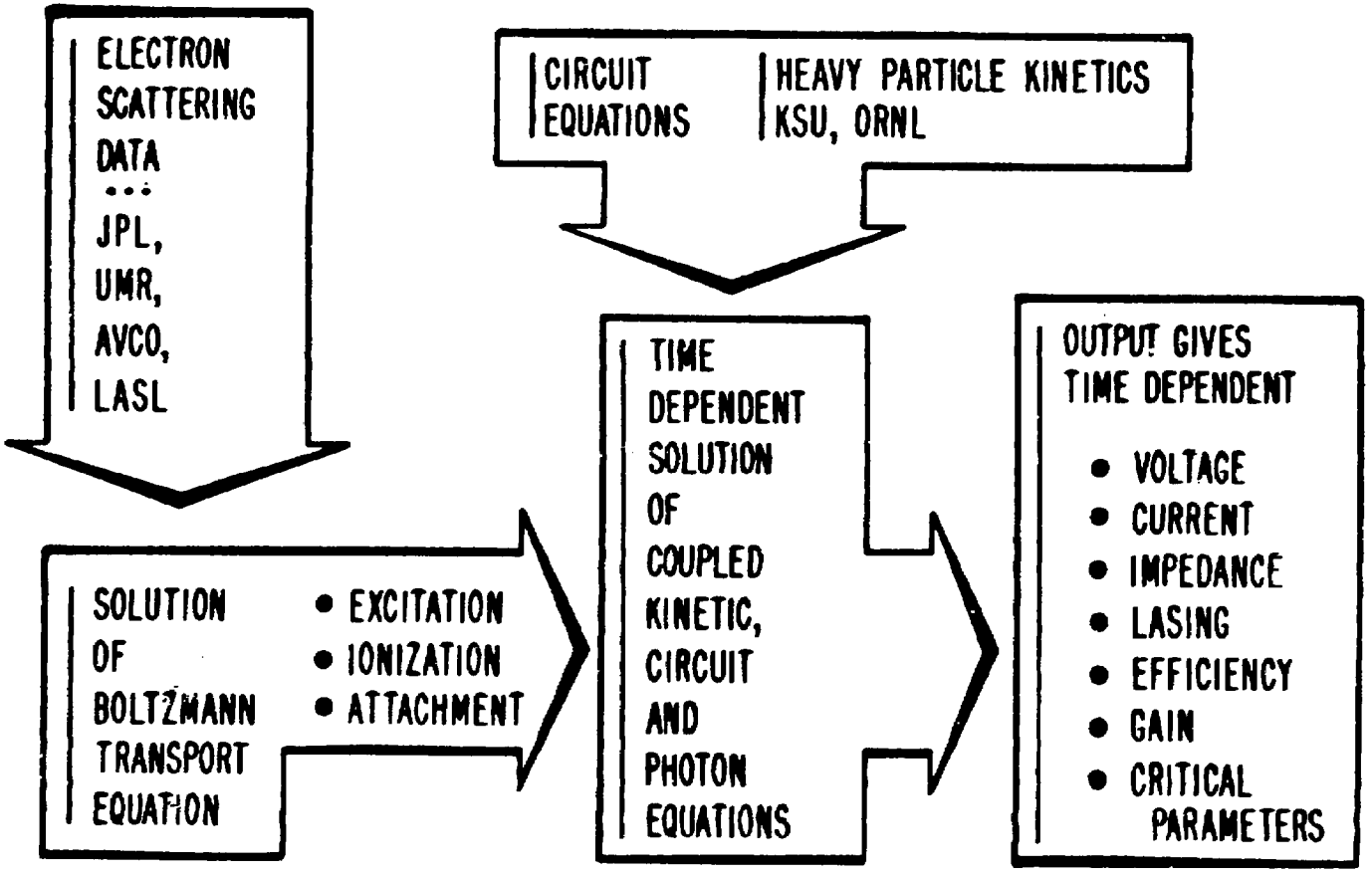

AP-I-VG-5005

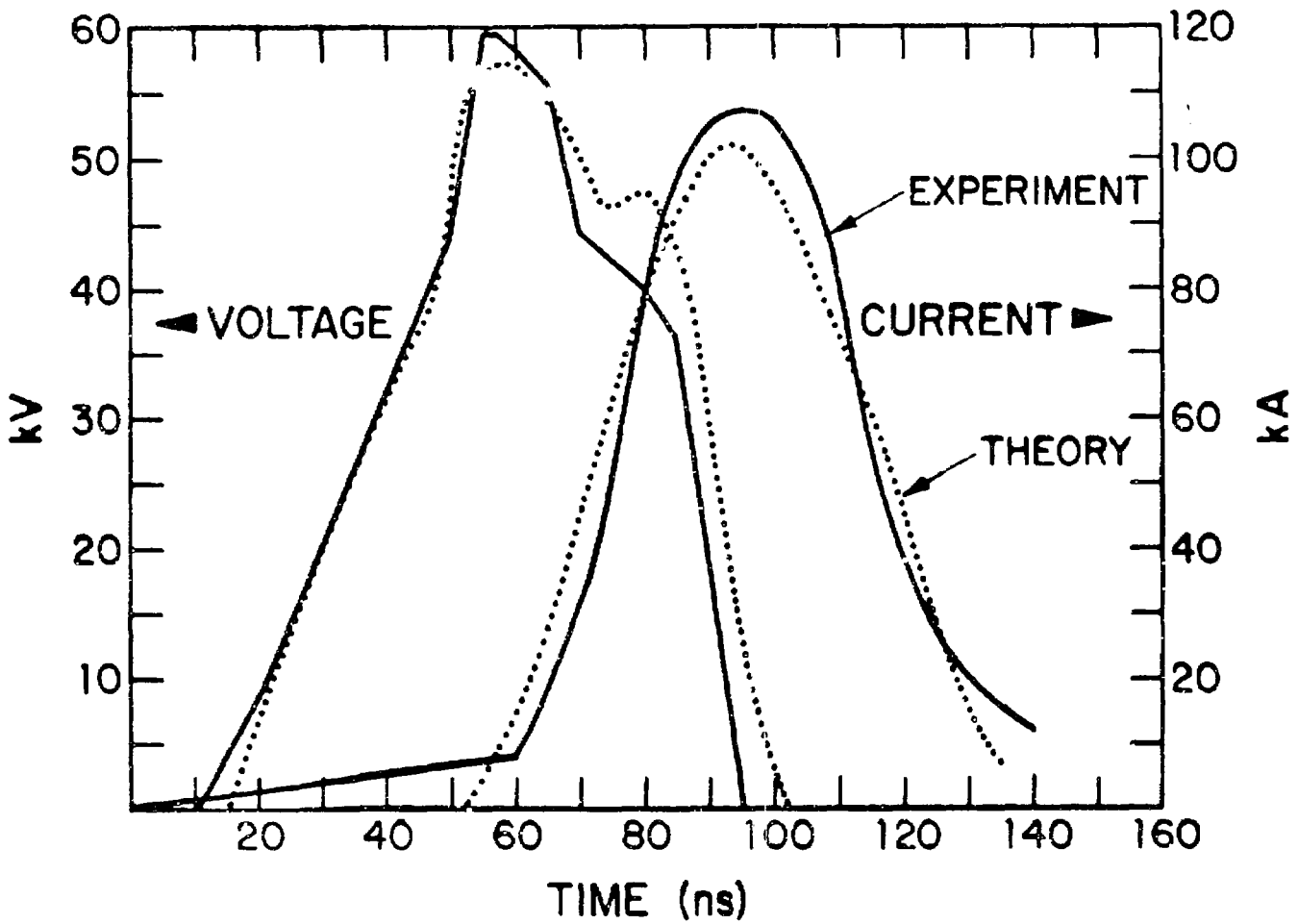
60
50
40
30
20
10
kV
120
100
80
60
40
20
kA
VOLTAGE
CURRENT
EXPERIMENT
THEORY
20
40
60
80
100
120
140
160
TIME (ns)

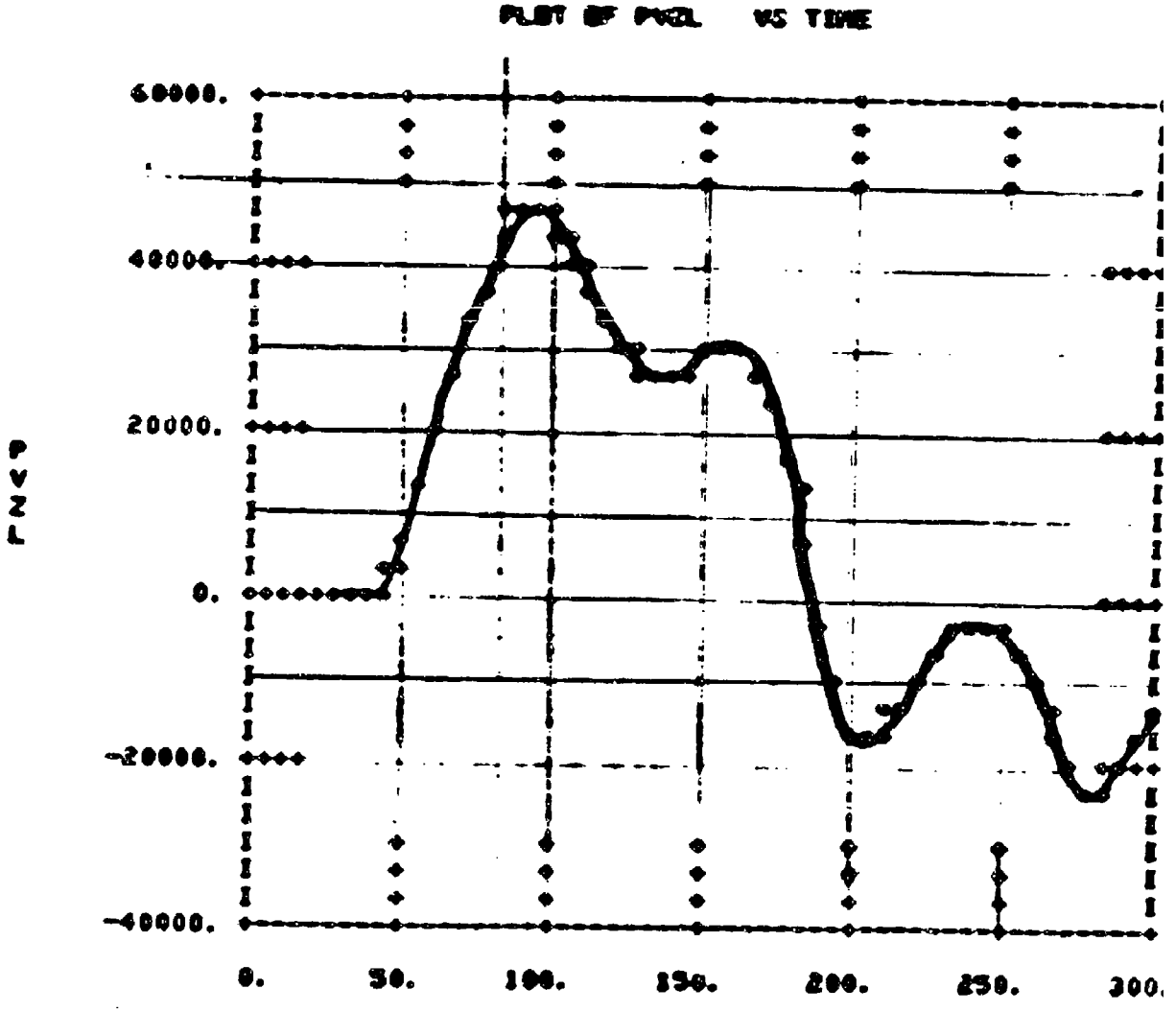
PLOT OF PVEL VS TIME
60000.
40000.
20000.
0.
-20000.
-40000.
PVEL
0.
50.
100.
150.
200.
250.
300.

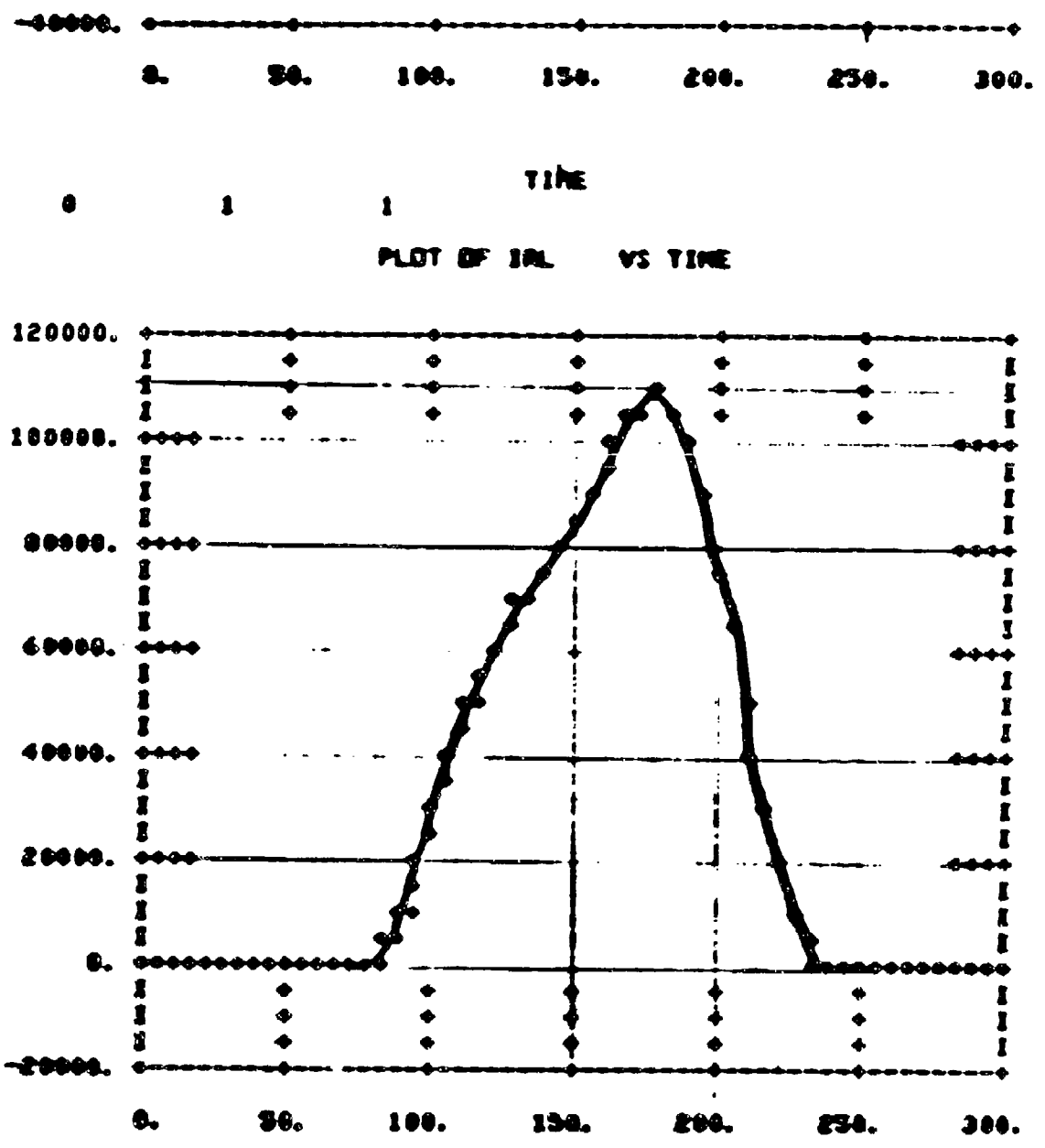
TIME
0 1 1
PLOT OF IRL VS TIME
120000.
100000.
80000.
60000.
40000.
20000.
0.
-20000.
IRL
0. 50. 100. 150. 200. 250. 300.

Shot # 51

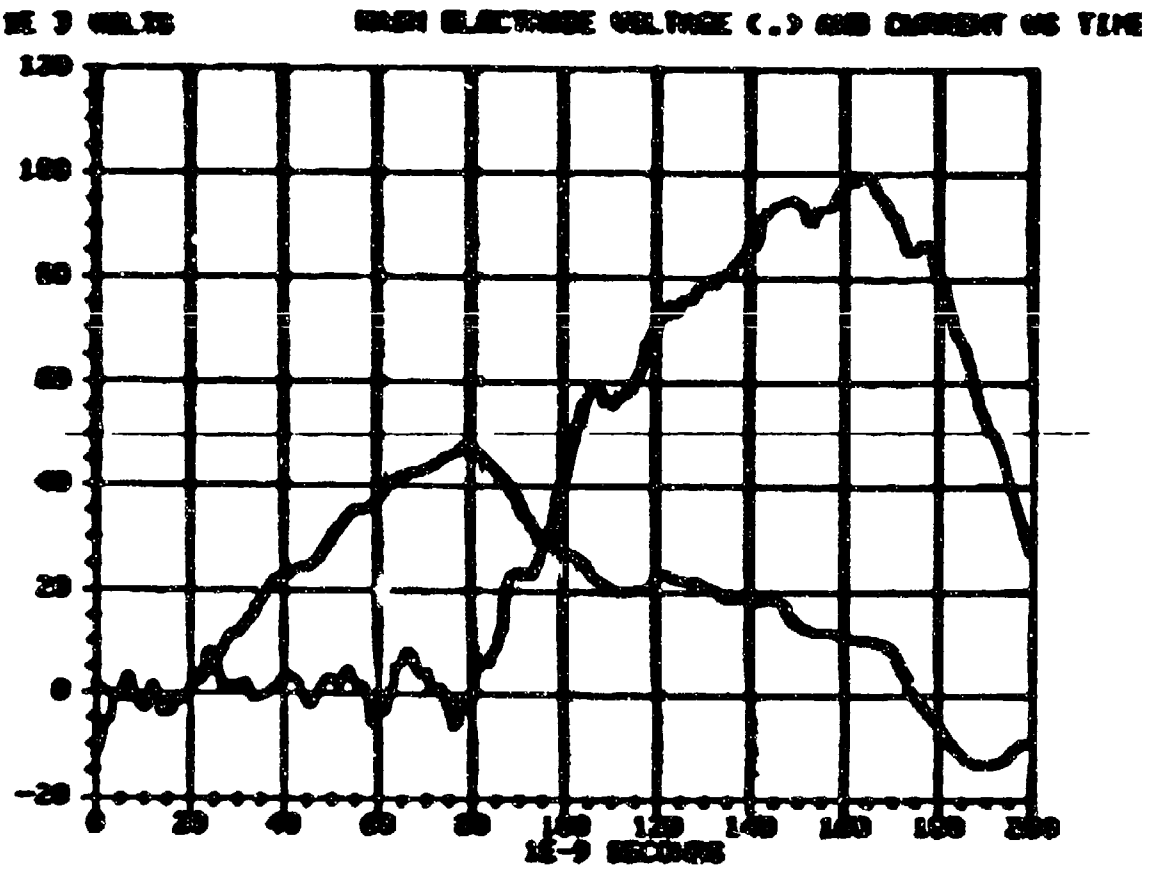

Strategic Blue-Green Optical Communications Program

Annual Technical Interchange Meeting 25-27 March 1980

Abstract For

UTRC Blue/Green Laser Research*

R. T. Brown and W. L. Nighan

Over the past two years UTRC has been carrying out a theoretical and experimental investigation of e-beam assisted XeCl(B) laser discharges[1]. Primary attention in this investigation has been focused in two areas: (1) development of techniques to enhance discharge stability, and (2) identification and evaluation of conditions compatible with high discharge : e-beam energy enhancement. The principal results of this study relevant to e-beam discharge excitation of the XeCl(B→X) laser will be presented.

Theoretical and experimental investigations of the HgBr(B)/$HgBr_2$ dissociation laser are also underway, with particular attention directed toward e-beam controlled discharge excitation[2]. Basic kinetic processes related to HgBr(B) formation in this laser will be discussed.

* Supported in part by NOSC under Contract N00014-78-C-0830 and by ONR under Contract N00014-76-C-0847.

1 W. L. Nighan and R. T. Brown, Appl. Phys. Lett. (April 1, 1980).

2 W. L. Nighan, Appl. Phys. Lett., 36, 173 (1980).

United Technologies Research Center
Silver Lane, MS 92
East Hartford CT 06108

UTRC BLUE/GREEN LASER RESEARCH

- E-beam controlled discharge excitation
  - XeCl(B)
  - HgBr(B)/$HgBr_2$
- R.T. Brown — XeCl results

  W.L. Nighan — HgBr(B)/$HgBr_2$ results

XeCl(B) FORMATION SEQUENCE IN DISCHARGE EXCITED MIXTURES

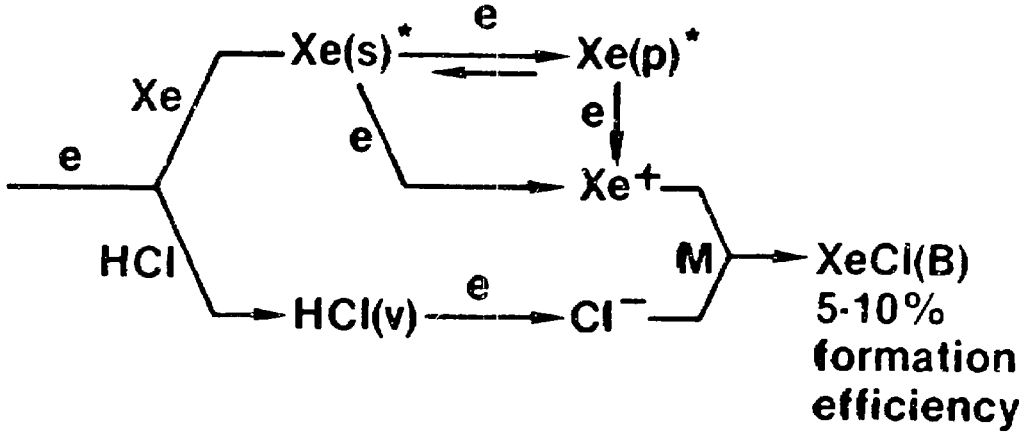

Rate Coefficients for HCl Vibrational Excitation and Attachment in an XeCl* Laser Mixture

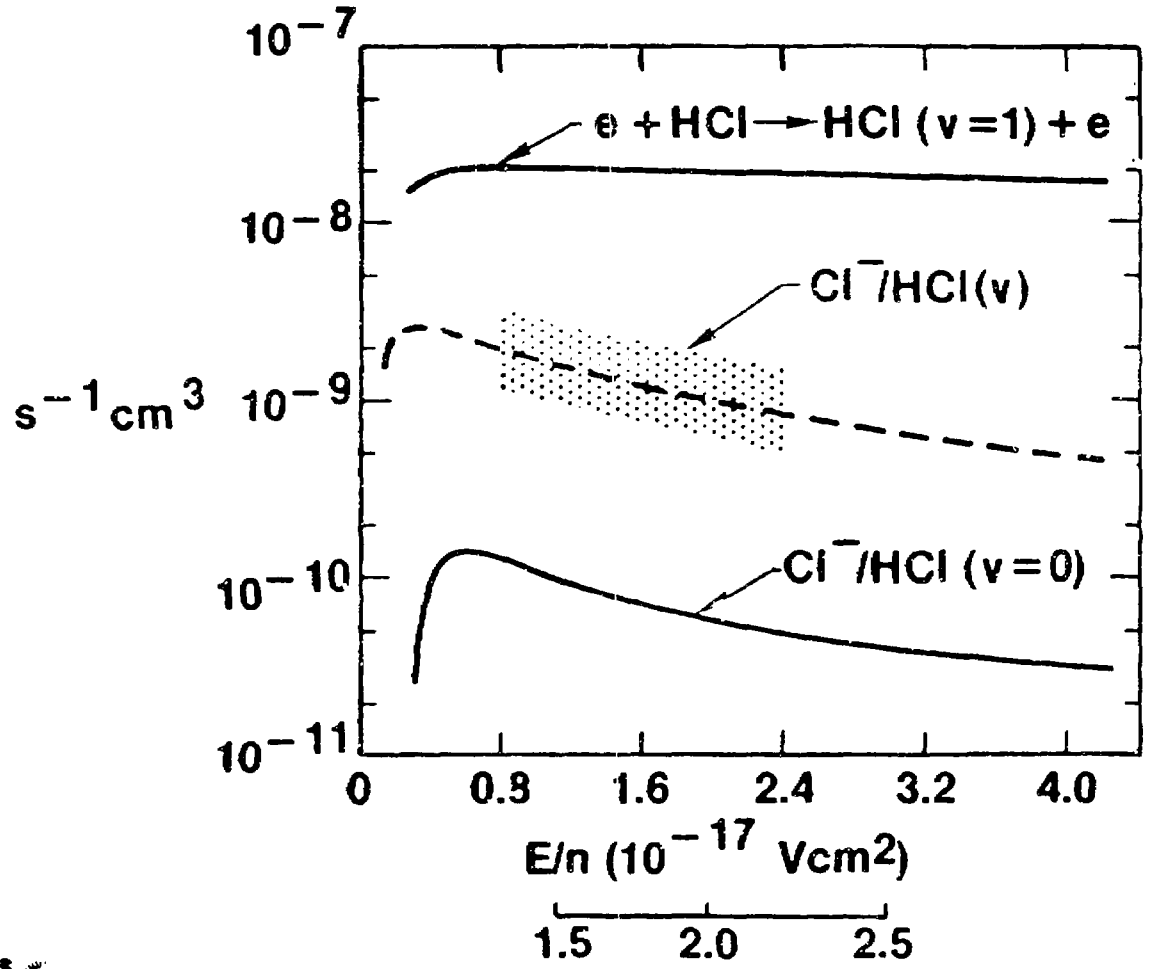

UNITED TECHNOLOGIES RESEARCH CENTER

79-10-7-2

E-BEAM-SUSTAINED DISCHARGE CHAMBER

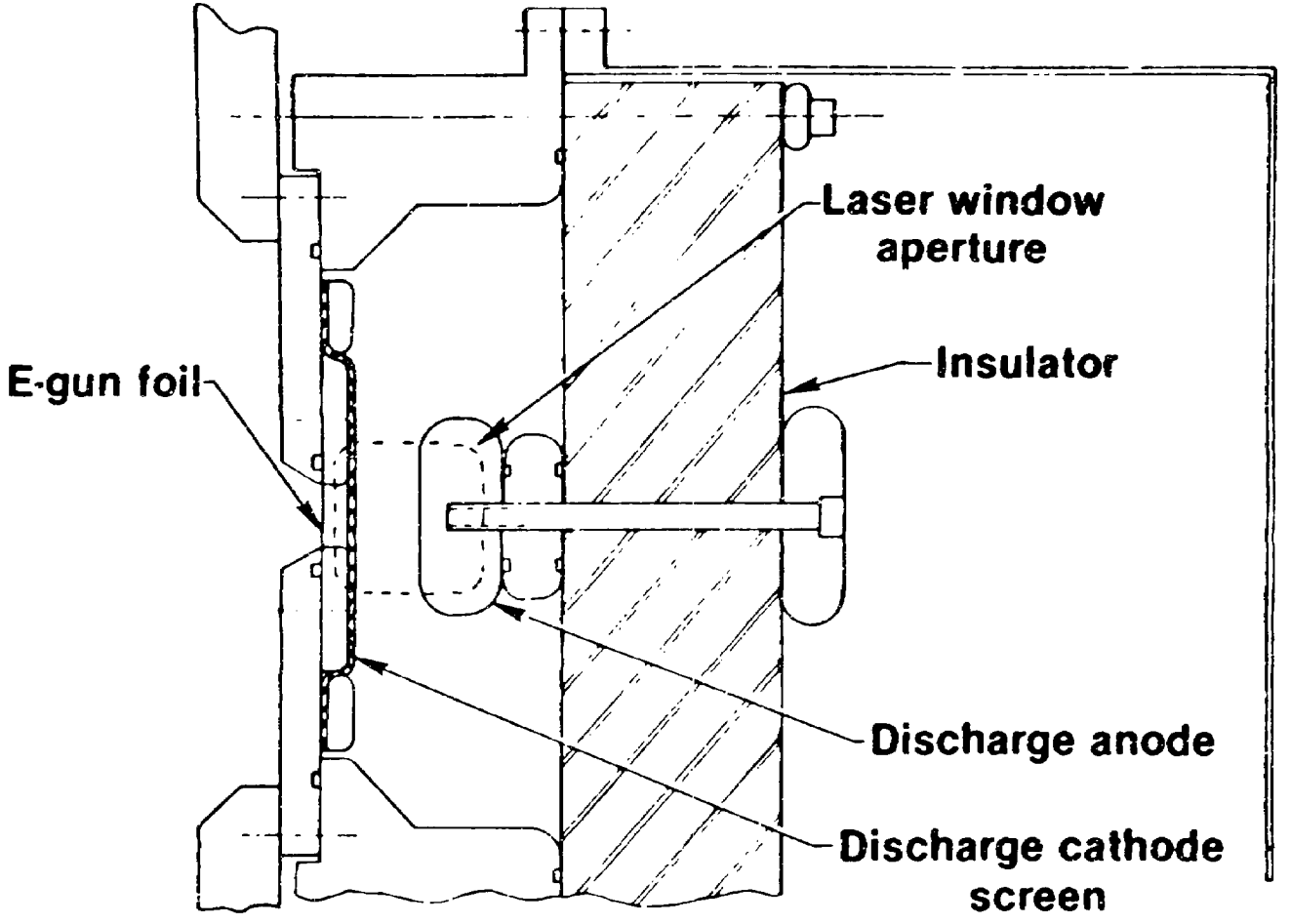

ELECTRON BEAM SUSTAINED DISCHARGE CELL

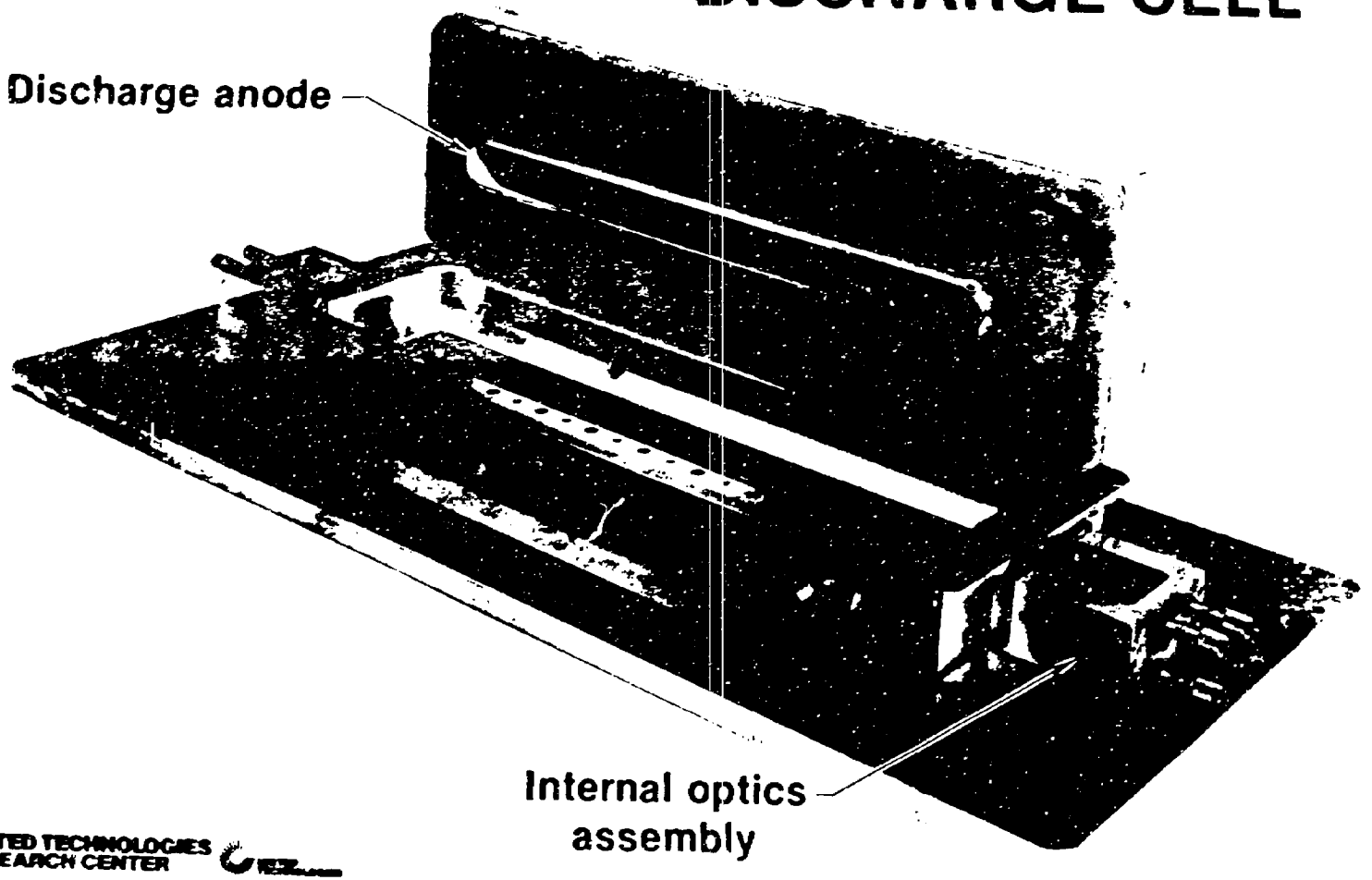

UNITED TECHNOLOGIES RESEARCH CENTER

Electron–Beam Sustained Discharge Experiment

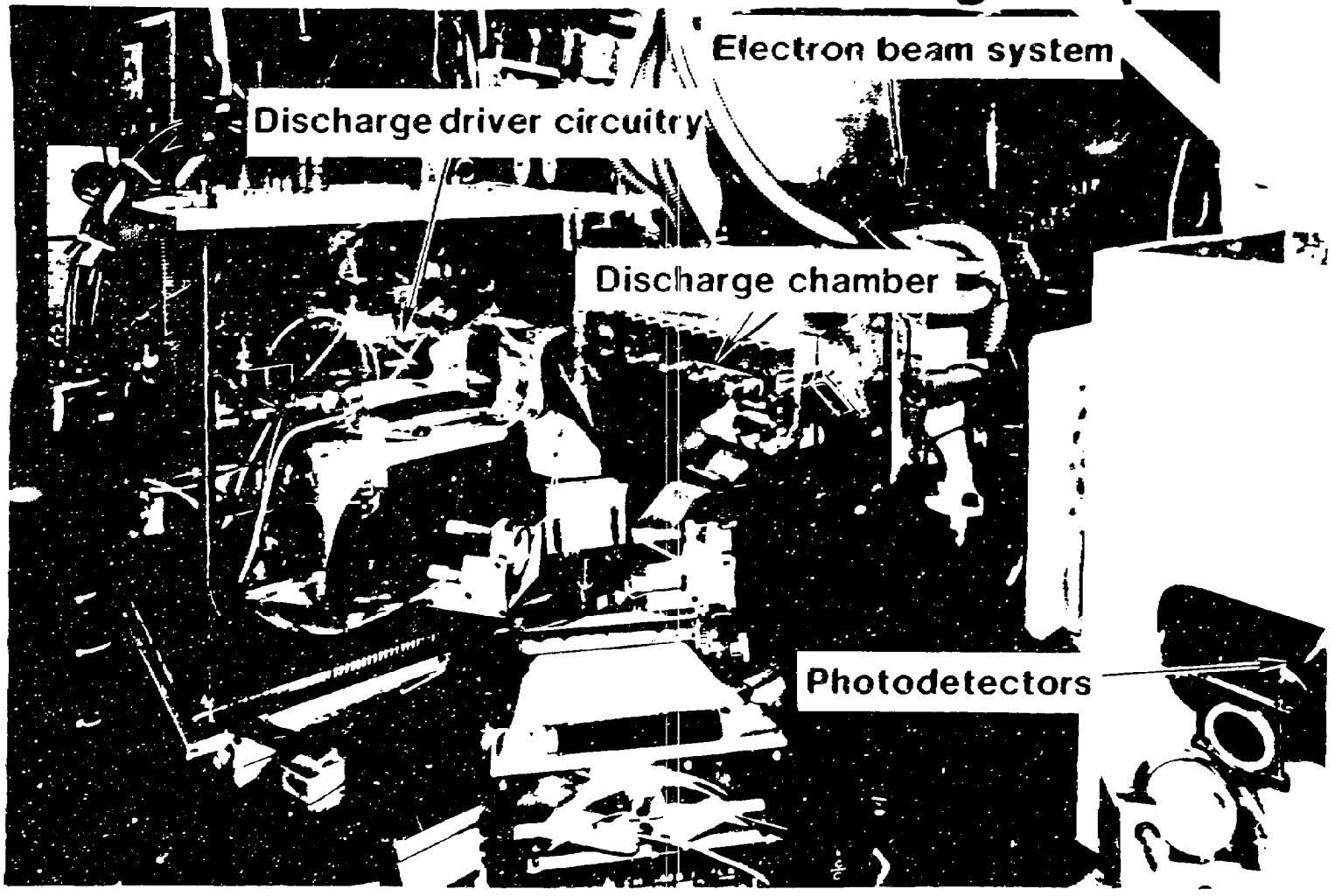

DISCHARGE DRIVING CIRCUIT

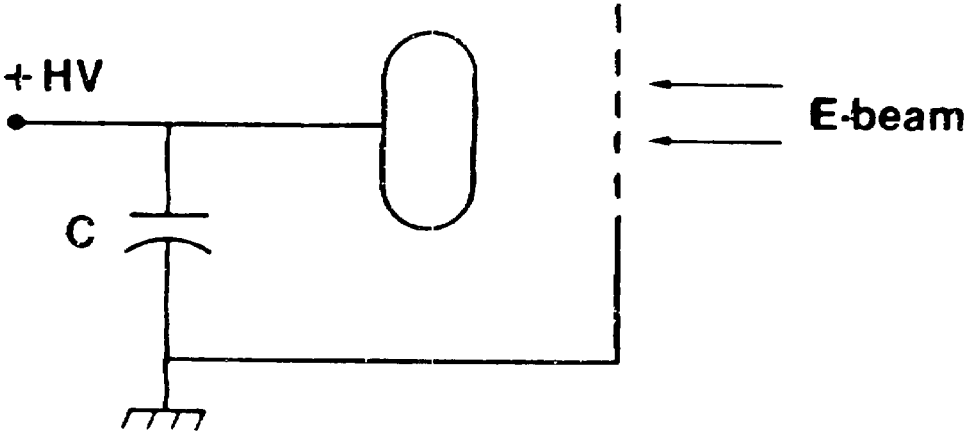

Measured XeCl* Discharge Characteristics

Ne/Xe/HCL: 0.99/0.01/0.0007; p=3.0 atm; S=50 + 2.5×10^7 t sec^{-1}

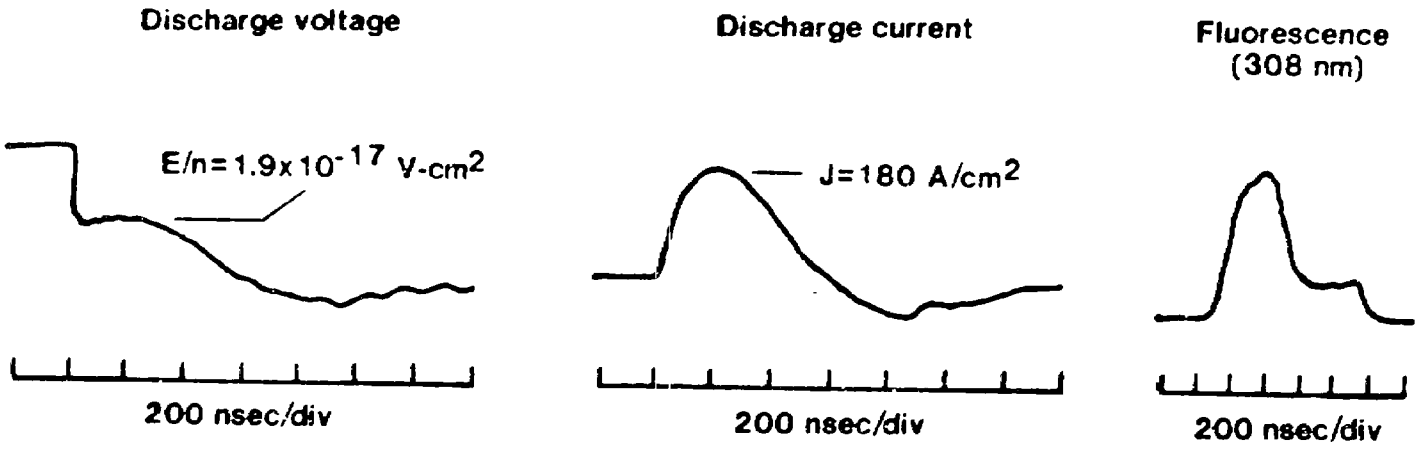

Energy enhancement factor = 6

Measured XeCl* Laser Characteristics

Ne/Xe/HCl: 0.99/0.01/0.0007; p=3.0 atm; $S=50+2.5\times10^{7}\ t\ sec^{-1}$

Fluorescence

200 nsec/div

Laser intensity

$R_1=0.99$; $R_2=0.50$

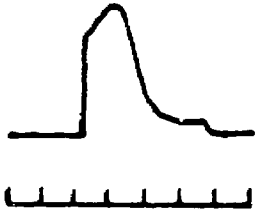

200 nsec/div

Laser spot

COMPUTED XeCl(B) MEDIUM PROPERTIES IN AN E-BEAM ASSISTED DISCHARGE

Ne/Xe/HCl = 0.989/0.01/0.001 P = 3 atm

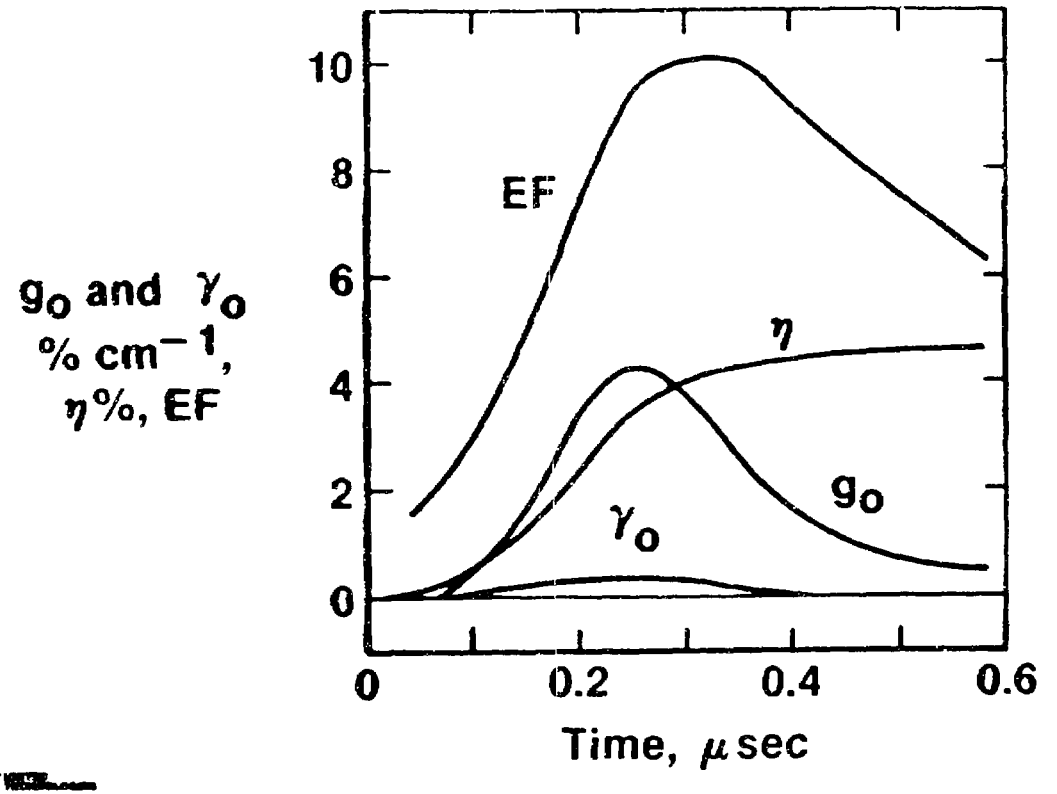

MEASURED CHARACTERISTICS IN AN E-BEAM ASSISTED XeCl LASER DISCHARGE

Ne/Xe/HCl = 0.989/0.01/0.001 p = 3 atm j_e = 0.8 A/cm^2

Etched screen cathode

Discharge current

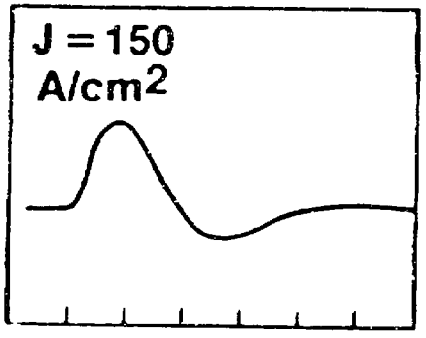

Fluorescence

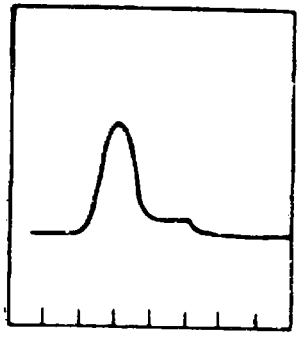

Discharge voltage

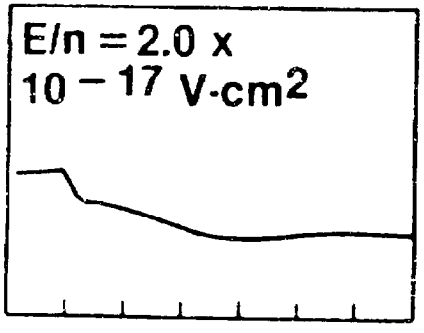

0.2 μsec/div

Laser intensity

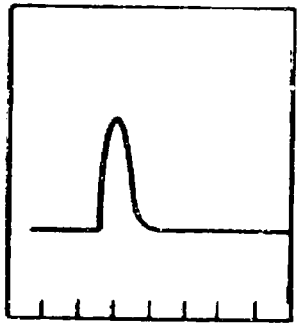

0.2 μsec/div

MEASURED XeCl* INTRINSIC LASER PROPERTIES

Gas mixture	Ne/Xe/HCl = 0.989/0.01/0.001
Pressure	3.0 atm
Temperature	25°C
Pulse length	300 nsec
E-beam current density	0.8 $A\text{-}cm^{-2}$
Input energy enhancement factor	10
Intrinsic laser efficiency	1.8%
Peak small signal gain	3.5%$\text{-}cm^{-1}$

MAJOR ACCOMPLISHMENTS

- Identification of vibrational excitation of HCl as a fundamental process in the XeCl(B) formation sequence

- Identification of $Xe^+ - Cl^-$ recombination as the XeCl(B) formation process in discharge excited XeCl lasers

- Development of an E-beam assisted discharge design permitting attainment of large volume, long duration, diffuse XeCl discharges having properties compatible with Navy requirements

489-505 nm $HgBr(B)/HgBr_2$ DISSOCIATION LASER

- Status
  - Discharge excitation of $N_2/HgBr_2$ mixtures
  - Electrical-optical conversion efficiency, 0.5-1.0%
  - Laser pulse energy, $\sim$ 1 joule/liter
- Potential
  - Conversion efficiency, 2-10%
  - Pulse energy, 2-10 joules/liter
  - Other mixtures, e.g., $Xe/HgBr_2$

Fractional Electron Power Transfer

Ne (0.95)-N_2 (0.05)-$HgBr_2$ (0.002)

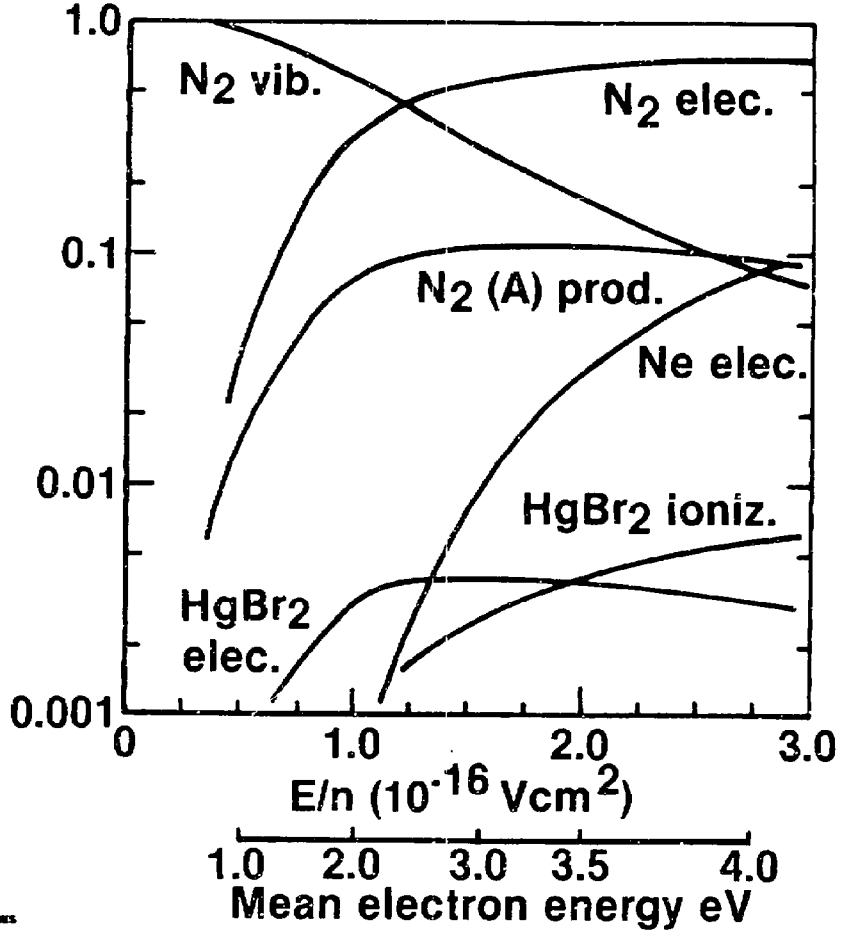

Schematic Energy Level Diagram

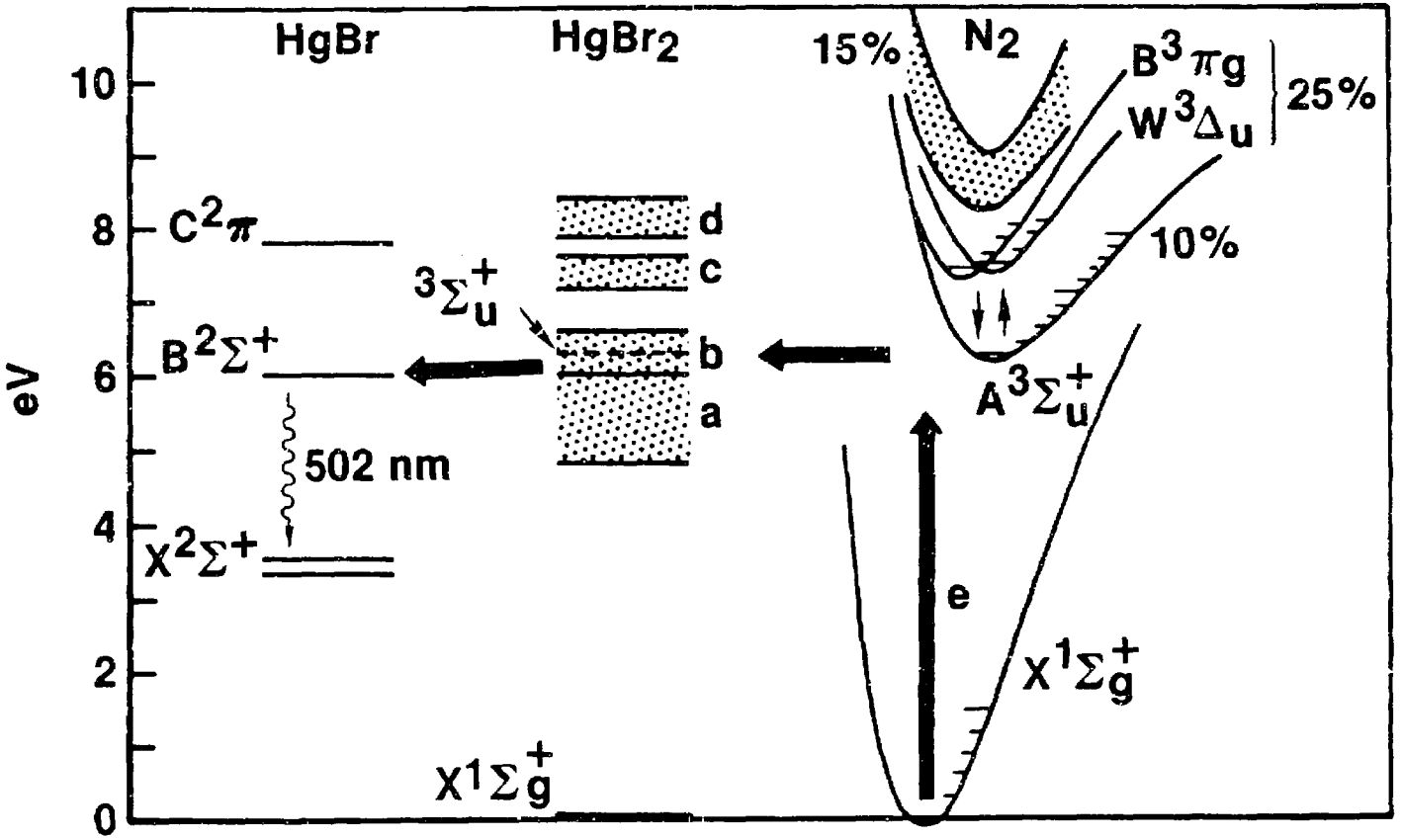

UNITED TECHNOLOGIES RESEARCH CENTER

79-08-164-3

N_2^* – $HgBr_2$ EXCITATION TRANSFER

$$N_2(A^3\Sigma_u^+) + HgBr_2 \longrightarrow HgBr_2(^3\Sigma_u^+) \longrightarrow HgBr(B^2\Sigma^+) \quad 1/3$$

$$\longrightarrow HgBr(A^2\pi, X^2\Sigma^+) \quad 2/3$$

$$N_2(B^3\pi_g) + HgBr_2 \longrightarrow HgBr_2(^3\pi_g) \longrightarrow HgBr(C^2\pi)$$

$$\longrightarrow HgBr(A^2\pi, B^2\Sigma^+, X^2\Sigma^+)$$

$$N_2(W^3\Delta_u) + HgBr_2 \longrightarrow HgBr_2(^3\Delta_u) \longrightarrow HgBr(A^2\pi, C^2\pi)$$

N_2^* energy utilization efficiency ~ 5 - 10 %

CURRENT DENSITY AND E/n VARIATION FOR FAST-PULSE DISCHARGE CONDITIONS

$N_e(0.95) - N_2(0.05) - HgBr_2(0.002)$; 2 atm, 155°C

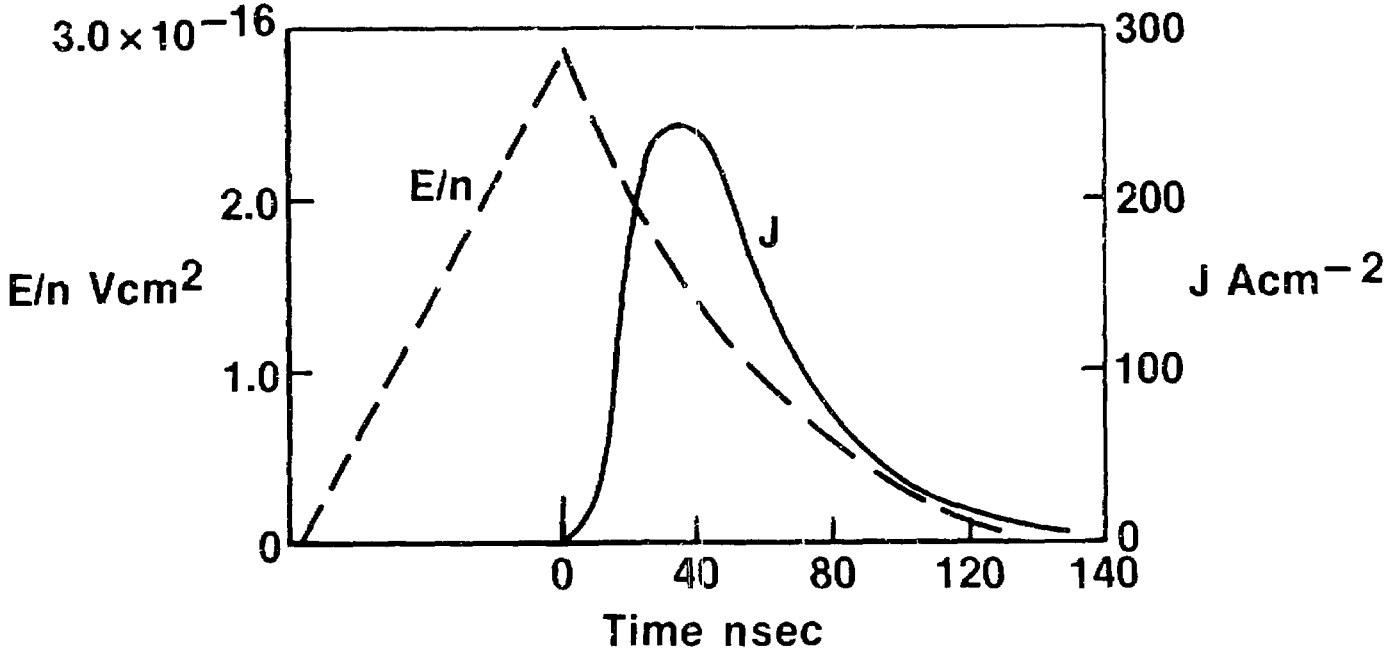

GAIN, HgBr(B) FORMATION EFFICIENCY AND ENERGY DENSITY FOR FAST-PULSE DISCHARGE CONDITIONS

$N_e(0.95) - N_2(0.05) - HgBr_2(0.002)$; 2 atm, 155°C

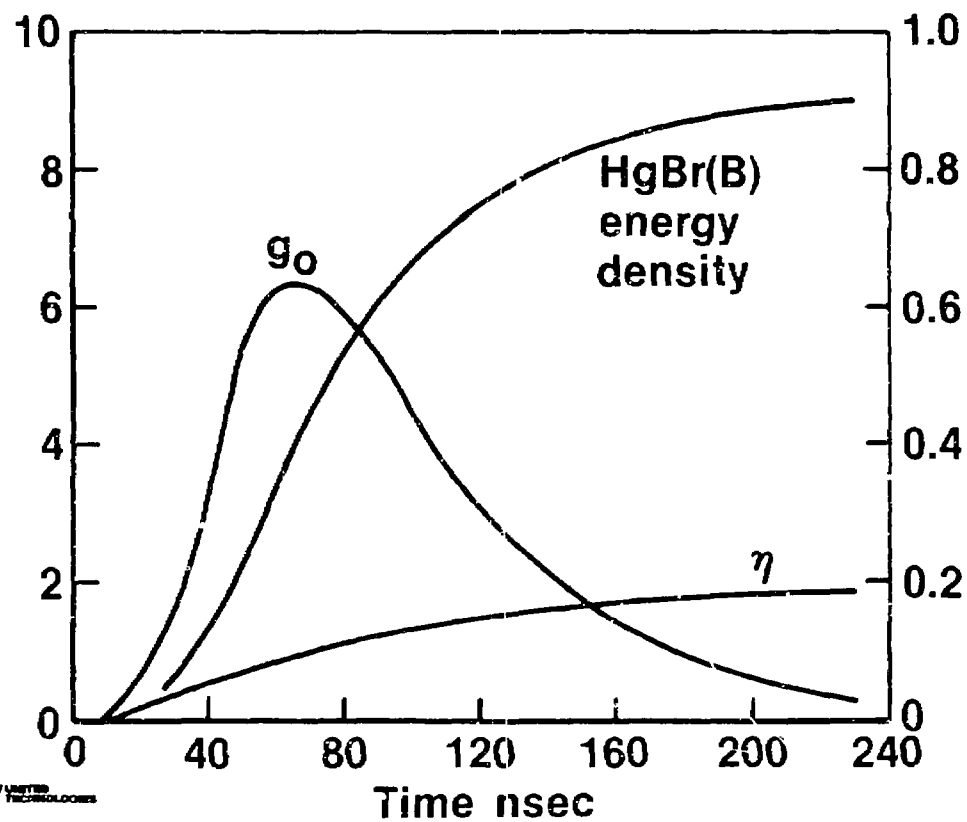

UNITED TECHNOLOGIES RESEARCH CENTER

80-3-82-7

DISCHARGE AND LASER PROPERTIES IN AN ELECTRON-BEAM CONTROLLED HgBr(B→X) LASER DISCHARGE: N_2 MIXTURE

$Ne/N_2HgBr_2 = 0.95/0.05/0.0025$; P = 2.0 atm, T = 163 °C

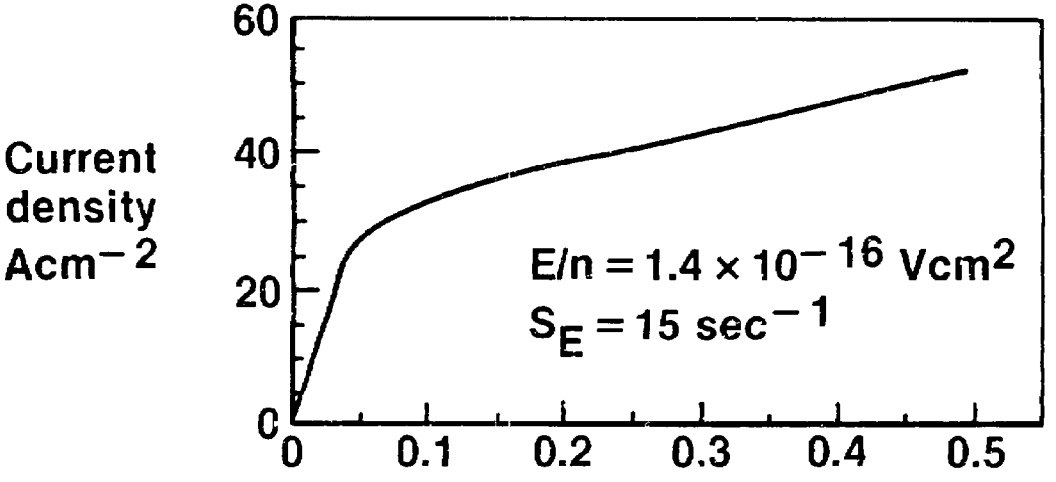

HgBr(B) prod. eff. %	1.0	1.4	1.6	1.6	1.7
Gain %/cm	1.3	2.0	2.3	2.6	2.9
HgBr(B) en. den. J/l	0.1	0.4	0.7	1.0	1.4
Enhancement factor	56	69	78	84	90

FRACTIONAL ELECTRON POWER TRANSFER

$Ne(0.90) - Xe(0.10) - HgBr_2(0.002)$

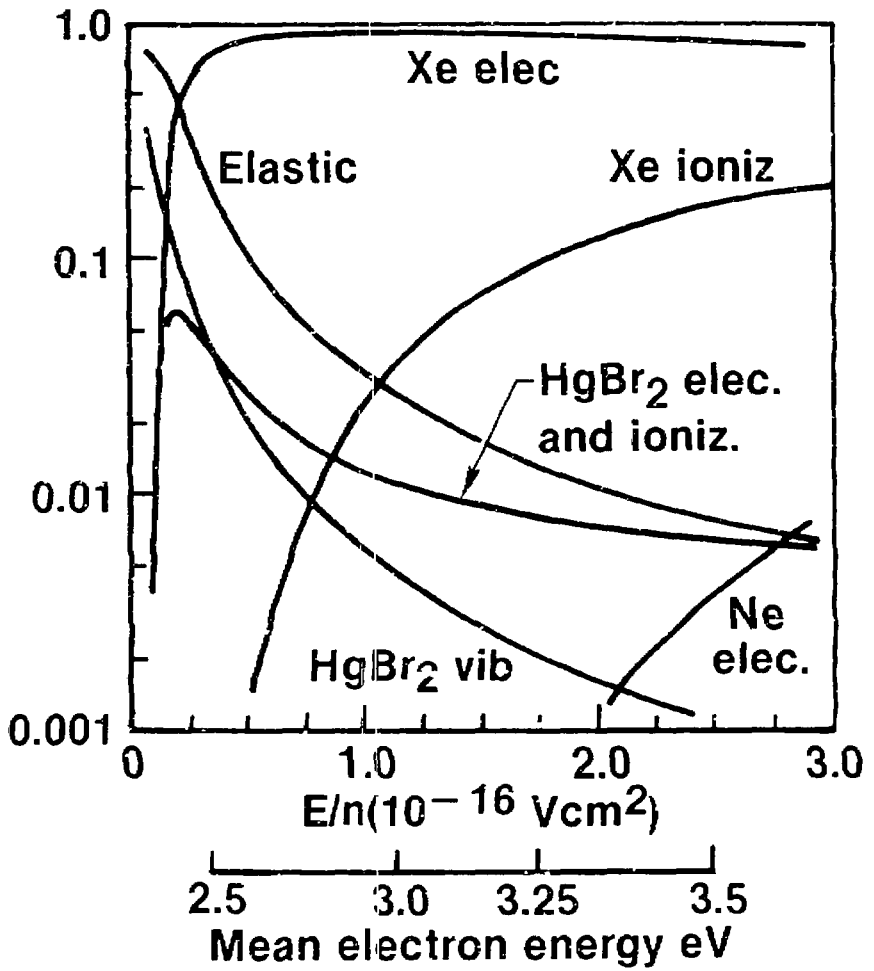

$Xe^* - HgBr_2$ EXCITATION TRANSFER

$$e + Xe \longrightarrow Xe(^3P_2) + e$$

$$Xe(^3P_2) + HgBr_2 \longrightarrow HgBr_2(^3\Sigma_u^+, ^3\pi_u) \longrightarrow HgBr(B^2\Sigma^+) \quad 5/6$$

$$\longrightarrow HgBr(C^2\pi) \quad 1/6$$

Xe^* energy utilization efficiency ~ 85 %

DISCHARGE AND LASER PROPERTIES IN AN ELECTRON-BEAM CONTROLLED HgBr(B→X) LASER DISCHARGE: Xe MIXTURE

$Ne/Xe/HgBr_2 = 0.90/0.10/0.0025$; P = 2.0 atm, T = 163°C

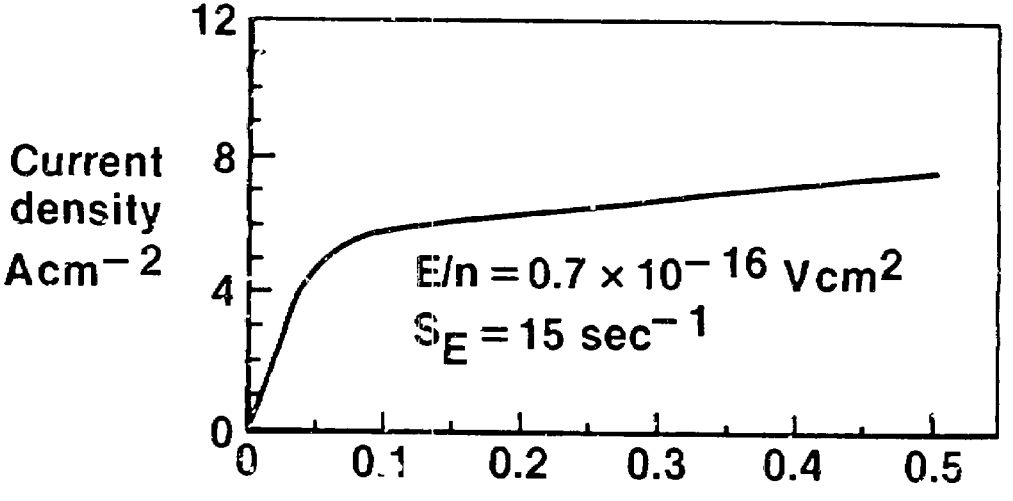

HgBr(B) prod. eff. %	10	15	16	17	17
Gain %/cm	1.6	1.9	2.0	2.1	2.2
HgBr(B) en. den. J/l	0.1	0.4	0.7	1.0	1.3
Enhancement factor	5.8	6.4	6.8	7.2	7.4

UNITED TECHNOLOGIES RESEARCH CENTER

80-3-82-4

SUMMARY

- $HgBr(B)/HgBr_2$ laser has the potential to meet the requirements of the Navy application
- Data base not yet complete
- Electronic energy utilization efficiency (N_2) and discharge stability (Xe) are key issues

MERCURY BROMIDE LASER SCALING APPROACHES

J.J. EWING, C. FISHER, S. MOODY, A. PINDROH, D. QUIMBY

WORK SUPPORTED BY NOSC/ONR AND MSNW IR&D

Mathematical Sciences Northwest
PO Box 1887
Bellevue WA 98009

MSNW

DISCHARGE EXCITED HgBr LASER SCALING

OBJECTIVE: EVALUATE METHODS FOR SCALING HgBr

- LENGTH : GAIN/LOSS
- APERTURE : PREIONIZATION METHOD
  UV OR X-RAY
- ENERGY DENSITY : PRESSURE
  ALTERNATE MIXTURES
  $HgBr_2$ DENSITY

MSNW MERCURY BROMIDE KINETICS CODE

- PREDICT HgBr PERFORMANCE AND SCALING
  - OVERALL EFFICIENCY
  - HIGH ENERGY OUTPUT

- BOLTZMANN ELECTRON KINETICS
- HEAVY BODY KINETICS
- LASER BUILDUP
- TEMPORAL E/N, GAIN
- CIRCUIT EQUATIONS

ENERGY FLOW IN THE DISCHARGE EXCITATION OF $Ne/N_2/HgBr_2$ MIXTURES

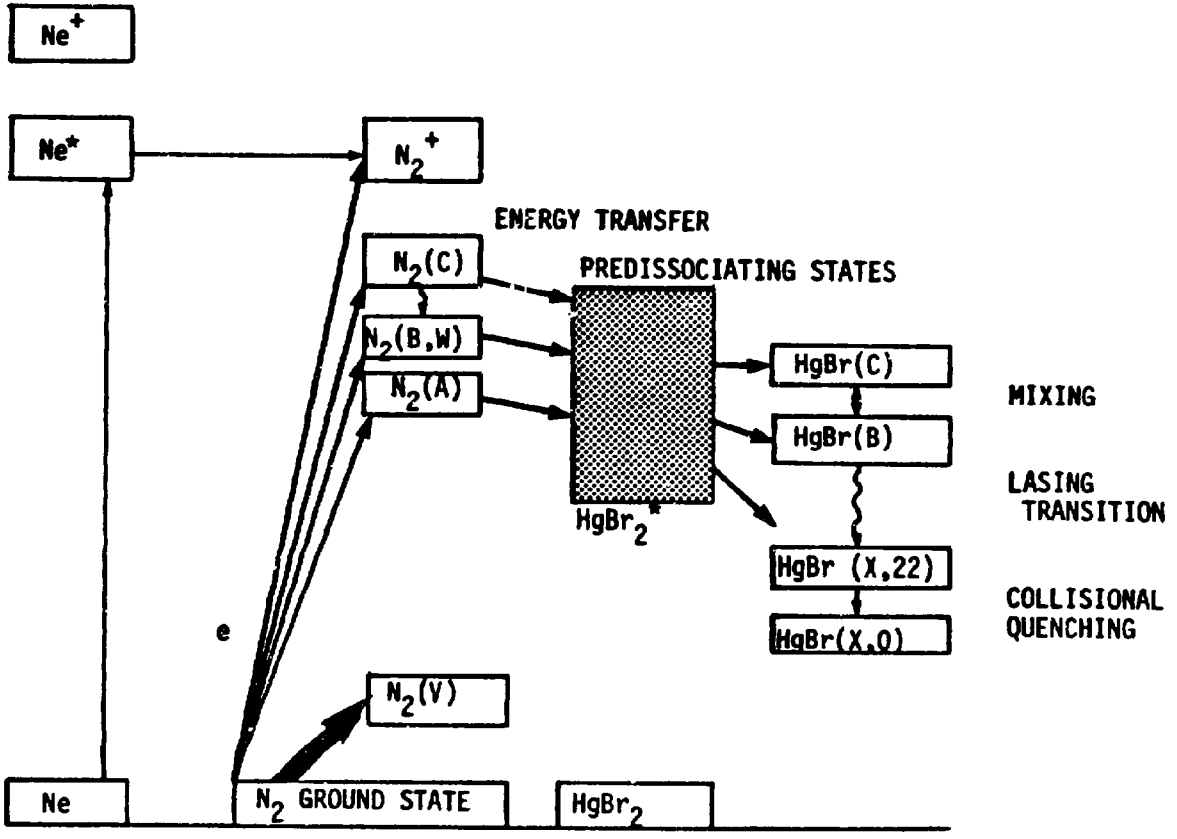

BOLTZMANN CODE PREDICTIONS FOR 10 PERCENT N_2, 90 PERCENT Ne

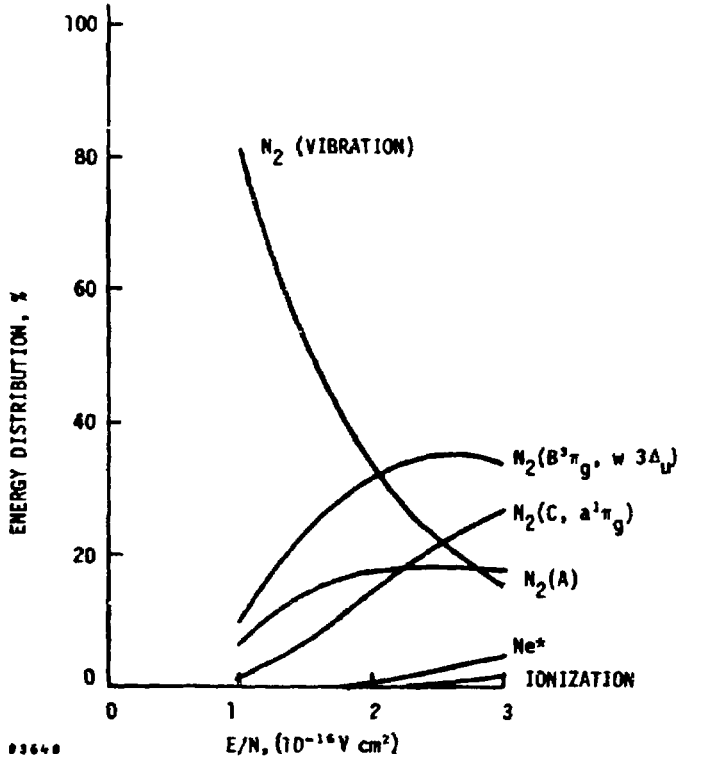

BOLTZMANN CODE PREDICTIONS FOR 5 PERCENT N_2, 95 PERCENT Ne

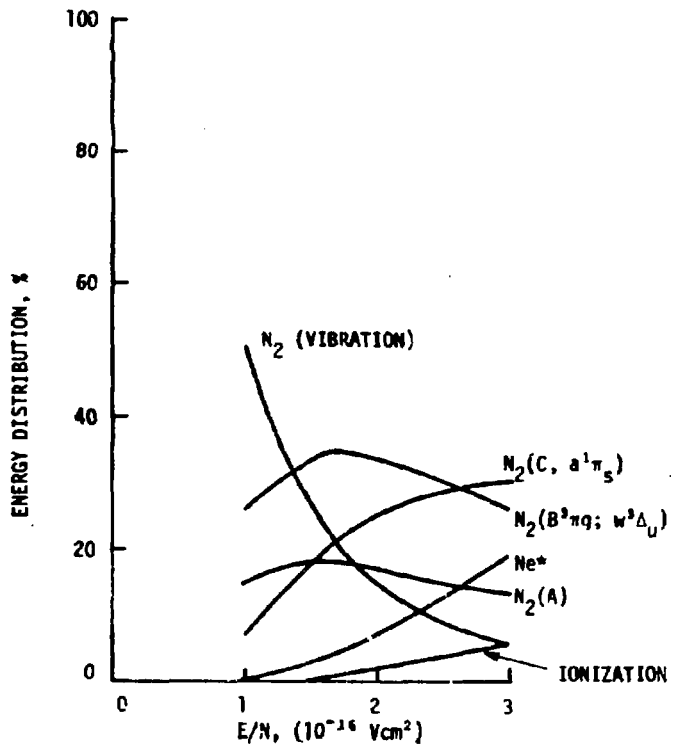

88 03647

CALCULATION OF GAIN AND CURRENT FOR HgBr LASER, USING THE PUBLISHED E/N PROFILE

$He/N_2/HgBr_2$ = 95/5/0.23

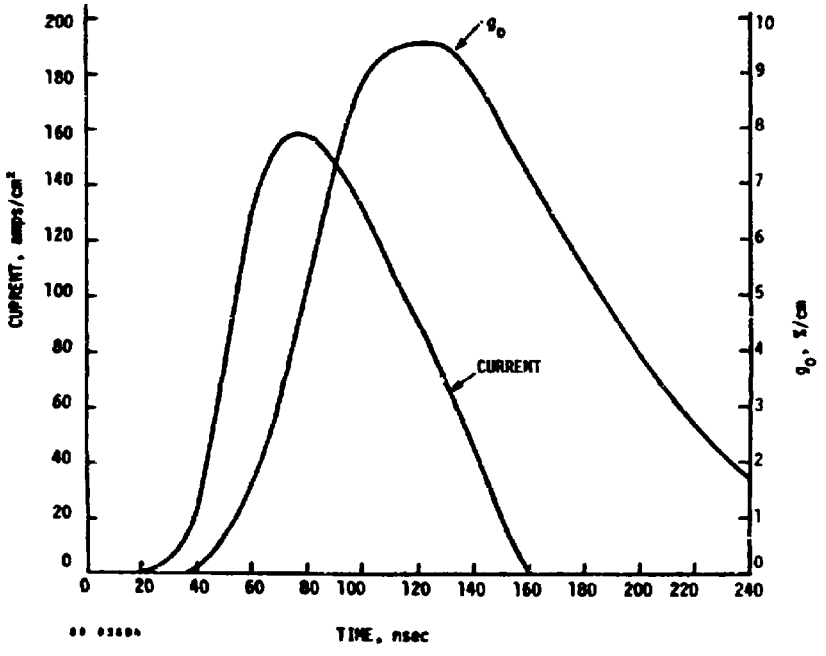

MSNW

MSNW MODEL PREDICTIONS OF HgBr(B→X) SMALL SIGNAL GAIN

$N_2/Ne/HgBr_2$ = 10/90/0.23

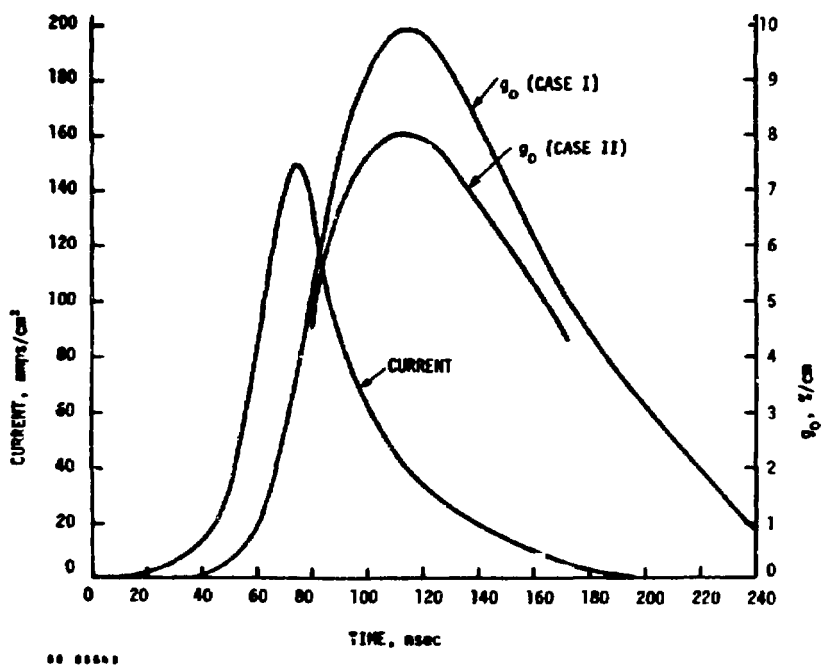

CASE I: HEAVY BODY MIXING OF HgBr C $\rightleftarrows$ B NEGLECTED
CASE II: HEAVY BODY AND ELECTRON MIXING OF HgBr C $\rightleftarrows$ B NEGLECTED, AND $N_2(A) + HgBr \rightarrow HgBr(B) + N_2$ NEGLECTED.

MSNW

MSNW MODEL PREDICTIONS OF HgBr(B→X) SMALL SIGNAL GAIN

$Ne/HgBr_2$ = 100/0.23

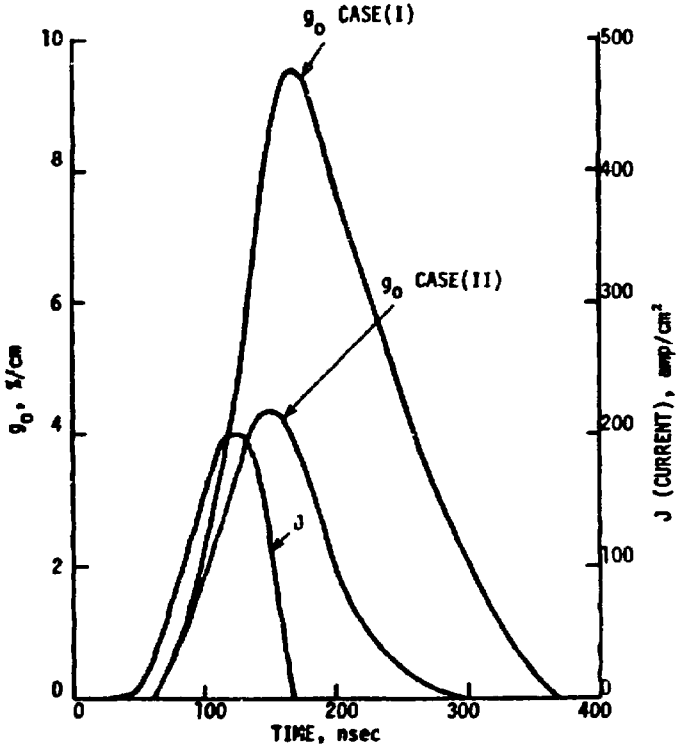

80 03650

CASE I: ELECTRON UP PUMPING RATE CONSTANT
$HgBr(X) + e \rightarrow HgBr(B) + e$, $K = 10^{-8}$ cm^3/sec

CASE II: $k = 10^{-10}$ cm^3/sec

MSNW

CALCULATED LASER OUTPUT AND SIDELIGHT FLUORESCENCE FOR 10 PERCENT N_2 HgBr LASER WITH 50 PERCENT FEEDBACK

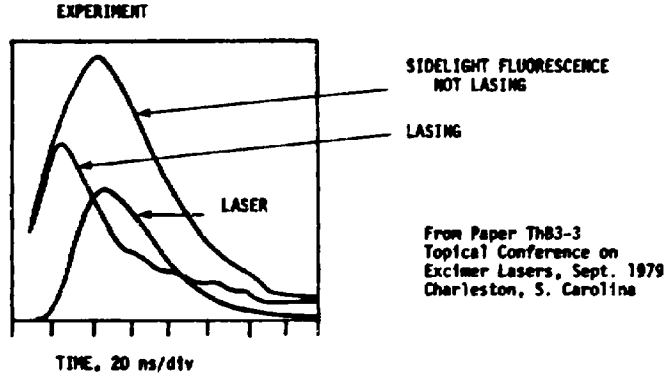

From Paper ThB3-3
Topical Conference on
Excimer Lasers, Sept. 1979
Charleston, S. Carolina

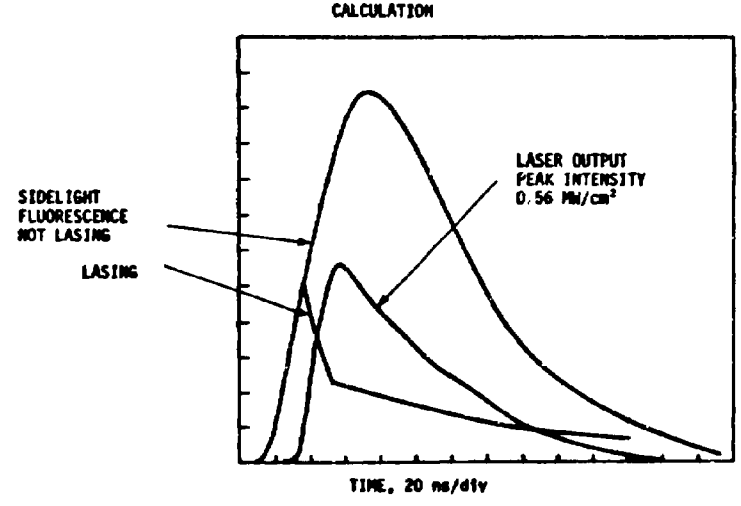

CALCULATIONS BASED ON THE E/N WAVEFORMS OF SCHIMITSCHEK AND CELTO, APPL. PHYS. LETT. 36, 176 (1980).

80 03685

MSNW

APERTURE SCALING DEPENDENT ON PREIONIZATION

- UV	SIMPLE, PENETRATION DEPTH? SPARKER SURVIVABILITY
- X-RAY	MINIMUM STOPPING - UNIFORM MINIMIZE E-BEAM CURRENT MORE COMPLEX
- E-BEAM	HIGH ELECTRON DENSITY POSSIBLE FOIL SURVIVABILITY

UV PREIONIZATION METHODS CURRENTLY UNDER INVESTIGATION

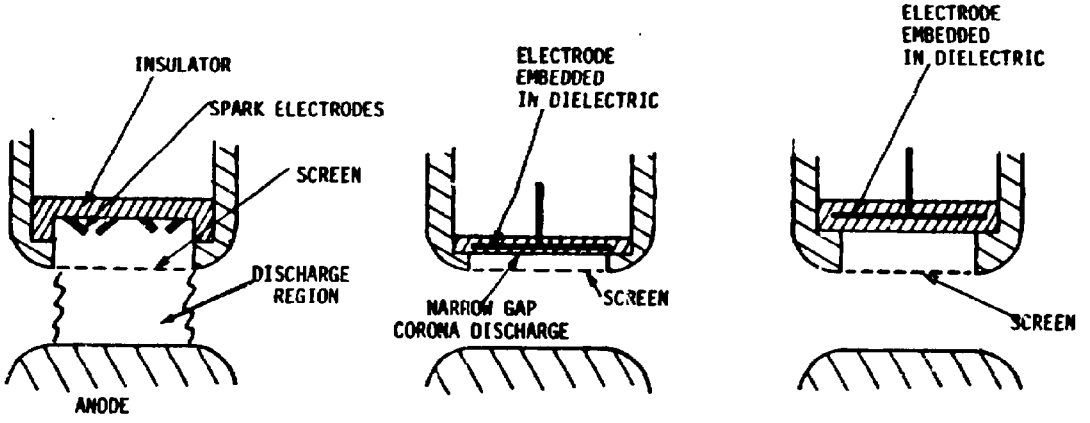

a) UV Sparks

b) Corona Discharge

c) Corona and Dielectric Surface Discharge

SCHEMATIC DIAGRAM OF MSNW X-RAY PREIONIZED XeCl DISCHARGE LASER

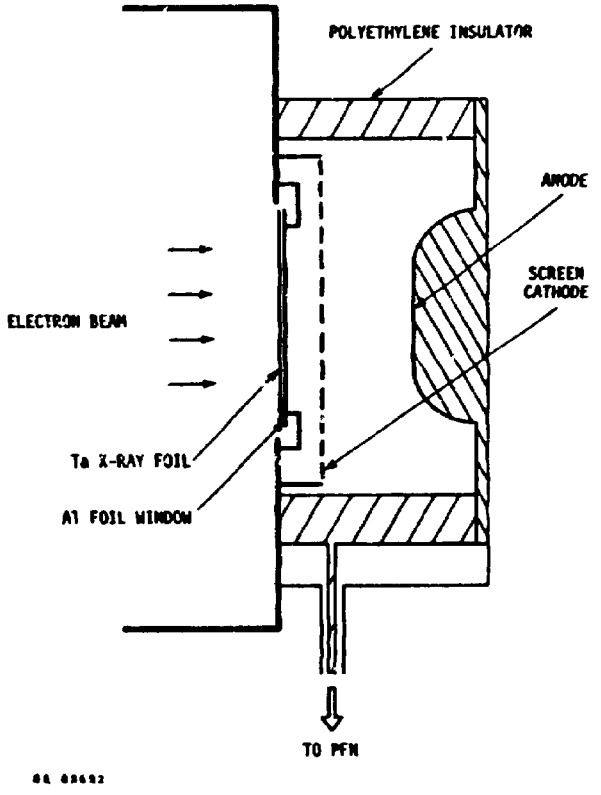

MSNW

DIAGNOSTIC TRACES OF MSNW X-RAY PREIONIZED XeCl DISCHARGE LASER

Ne = 2 atm
Xe = 45 torr
HCl = 3 torr
LASER ENERGY = 230 mJ

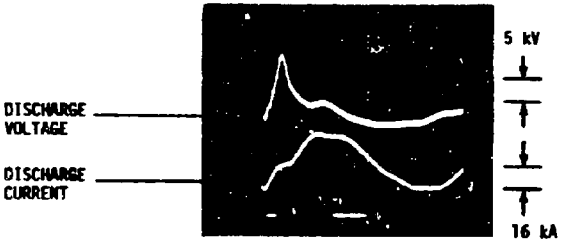

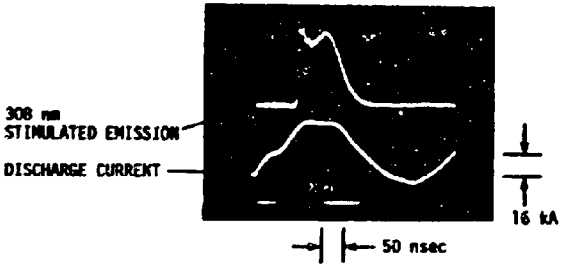

00 00642

MSNW

ENERGY DENSITY SCALING

- UTILIZE MIXTURES THAT HAVE HIGHER BRANCHING RATIOS
  - $Xe^* + HgBr_2 \rightarrow HgBr^* + Xe + Br$
  - DOESN'T WORK WELL WITH UV
    - X-RAY
    - E-BEAM
- PRESSURE SCALE

COMPARISON OF HgBr GAIN/LOSS MEASUREMENTS TO MSNW CODE PREDICTIONS

	Experiment[1]	Model	
Mixture	900 torr Ne 100 torr N_2 2.3 torr $HgBr_2$	900 torr Ne 100 torr N_2 2.3 torr $HgBr_2$	1800 torr Ne 200 torr N_2 4.6 torr $HgBr_2$
E/N($V\text{-}cm^2$)	1.5×10^{-16}	1.5×10^{-16}	1.5×10^{-16}
Current Density (A/cm^2)	150*	150	150
Small Signal Gain($\%cm^{-1}$)	6-6.6	8	16

*Discharge current in fringe of laser active volume assumed to be 50 percent of total.

MSNW UV PREIONIZED XeCl LASER PERFORMANCE

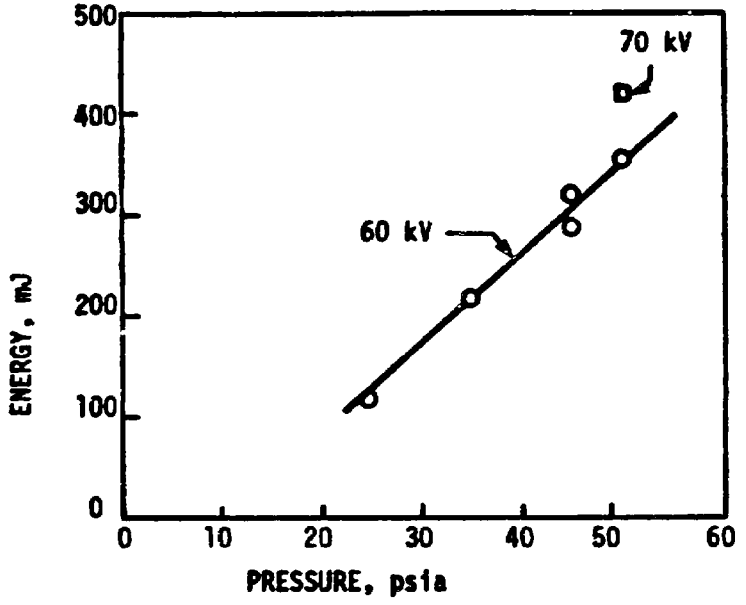

Ne + 3% Xe + 0.2% HCl; C = 25 nF; ELECTRODE GAP = 3 cm.

CROSS-SECTION VIEW OF MSNW X-RAY PREIONIZED 0.1 LITER HgBr LASER

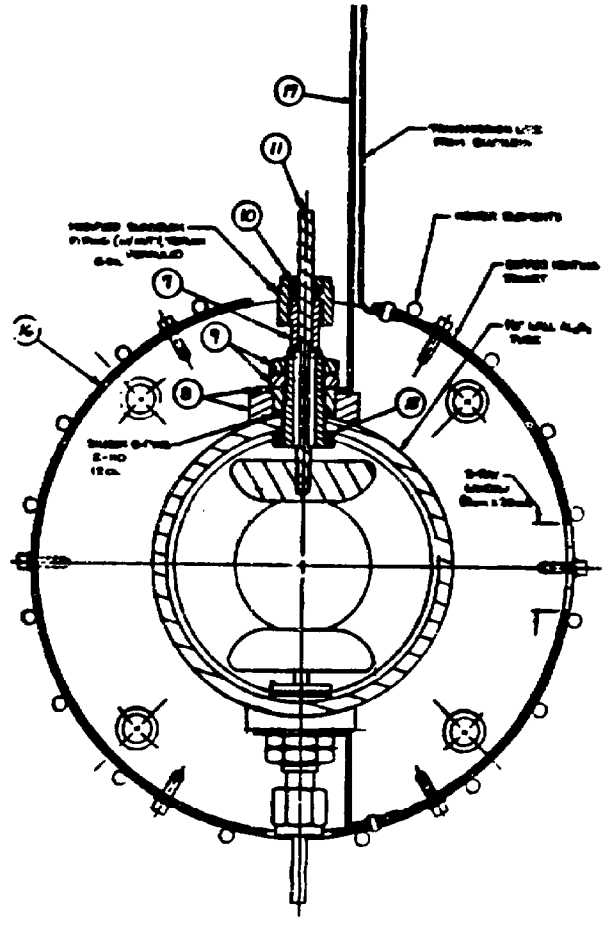

MSNW

HgBr LASER SCALING STATUS

- CODE UNDER DEVELOPMENT
  - REASONABLE AGREEMENT
- FABRICATED HIGH PRESSURE HgBr LASER
- DEMONSTRATED X-RAY PREIONIZED HgBr LASER
  - OPTIMIZATION IN PROGRESS

TITLE: PARAMETERIZATION STUDIES OF HgBr LASERS

CS LIU

SPONSOR: NOSC (MONITORED BY ONR)

CONTRACT PERIOD: MARCH 1980 - OCTOBER 1980
(8-MONTHS)

Westinghouse R&D Center
1310 Beulah Road
Pittsburgh PA 15235

PARAMETERIZATION STUDIES OF HgBr LASERS

During the past several years, mercury bromide has shown great promise as a high efficiency, high energy tunable laser in the blue-green region of the spectrum. Lasing in this medium has been demonstrated using a number of excitation techniques: optical pumping, E-beam, E-beam sustained discharge, and self-sustained discharge. The most promising technique thus far seems to be a UV-preionized self-sustained discharge, which has demonstrated energies of ~100 mJ, and efficiencies of ~1 percent.

Although there has been some speculation about the details of the excitation and lasing kinetics, optimization of this laser system still depends on empirical parameterizations. Optimization studies made to date were limited by the apparatus available. A number of important questions remain: for example, the independent effect of temperature and of $HgBr_2$ density, and the effect of buffer gas density on laser kinetics and discharge characteristics.

Attempts to establish parameters for a number of variables in the mercury bromide system have been severely limited in range. Buffer gas pressures have extended up to ~1 amagat, with temperatures up to ~230°C and $HgBr_2$ densities to $5 \times 10^{16}/cm^3$. This range of parameters has been determined basically by the type of apparatus used: that is, O-ring seals, simple Pyrex structures, and stainless steel electrode materials. The density of $HgBr_2$ has been adjusted by varying the temperature of the laser tube; thus the gas temperature and the $HgBr_2$ density were not independent variables. Both the temperature and pressure affect the laser kinetics, through the collision rates, for instance. In addition, the buffer gas density affects the discharge characteristics by changing both the E/N and the glow voltage. As the length of the discharge region is increased to produce larger volumes, the discharge impedance decreases; it would be advantageous to increase the impedance by increasing the buffer gas density.

Ideally, the buffer gas density, temperature, and energy loading would be varied independently, so as to optimize the performance of the HgBr laser. We have available at Westinghouse an apparatus which will enable us to make measurements over the required parameter range.

PROGRAM OBJECTIVE: TO OPTIMIZE THE LASER PERFORMANCE OF HgBr SYSTEMS

PROGRAM TASKS:

1. OPTIMIZE THE PERFORMANCE OF A HgBr LASER BY VARYING THE BUFFER GAS SPECIES AND PRESSURE (UP TO 10 ATM)
2. DETERMINE THE OPTIMUM VAPOR DENSITY OF THE $HgBr_2$ FOR THE BEST PERFORMANCE OF A HgBr LASER
3. DETERMINE THE OPTIMUM OPERATING TEMPERATURES FOR HgBr LASERS (UNDER SUPER-HEAT CONDITIONS)

LASER DISCHARGE TUBE REQUIREMENTS:

1. PRESSURE CAPABILITY: UP TO 10 ATM
2. TEMPERATURE CAPABILITY: ~300°C
3. CHEMICAL INERTNESS: SEALED OFF QUARTZ-MOLY TUBES

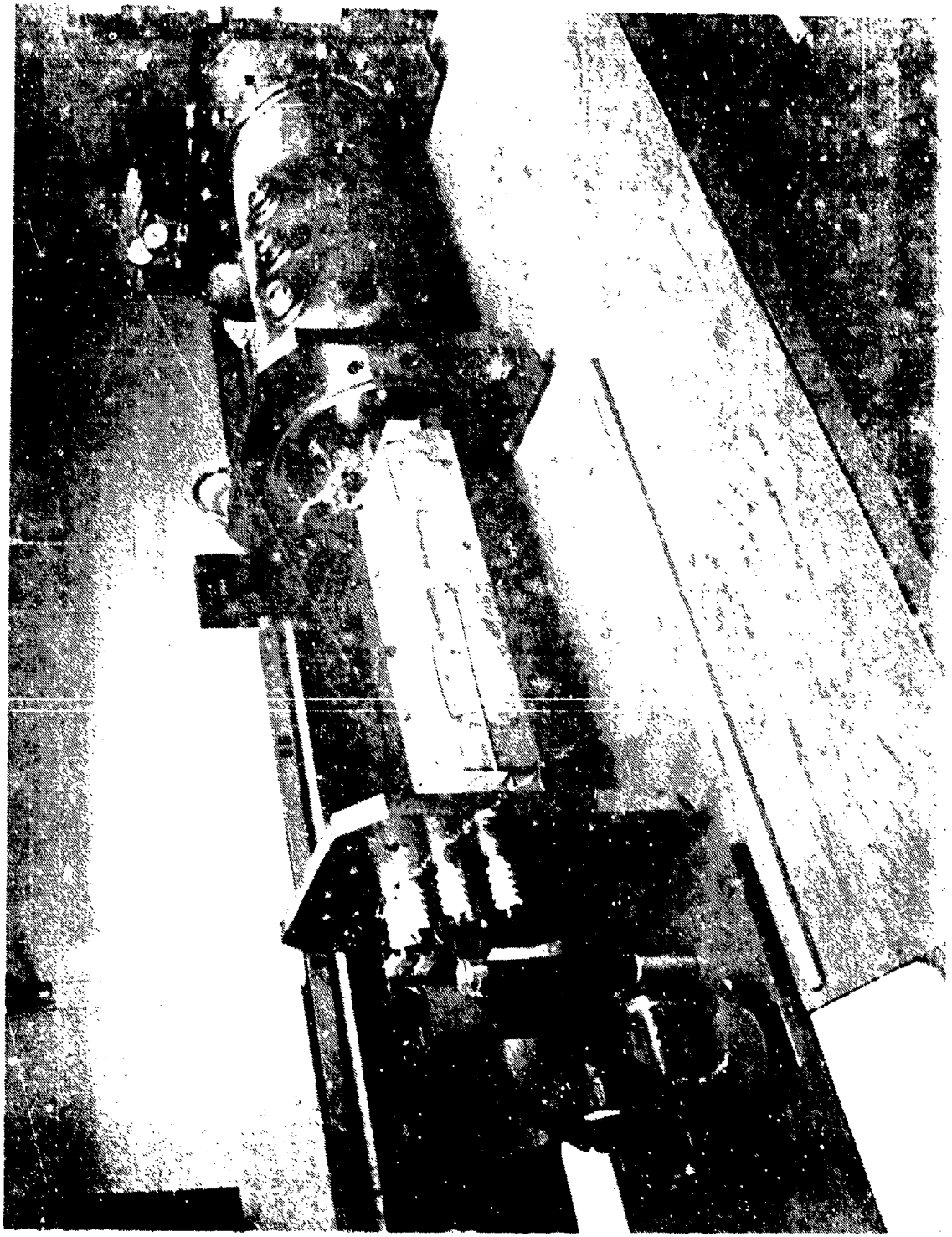

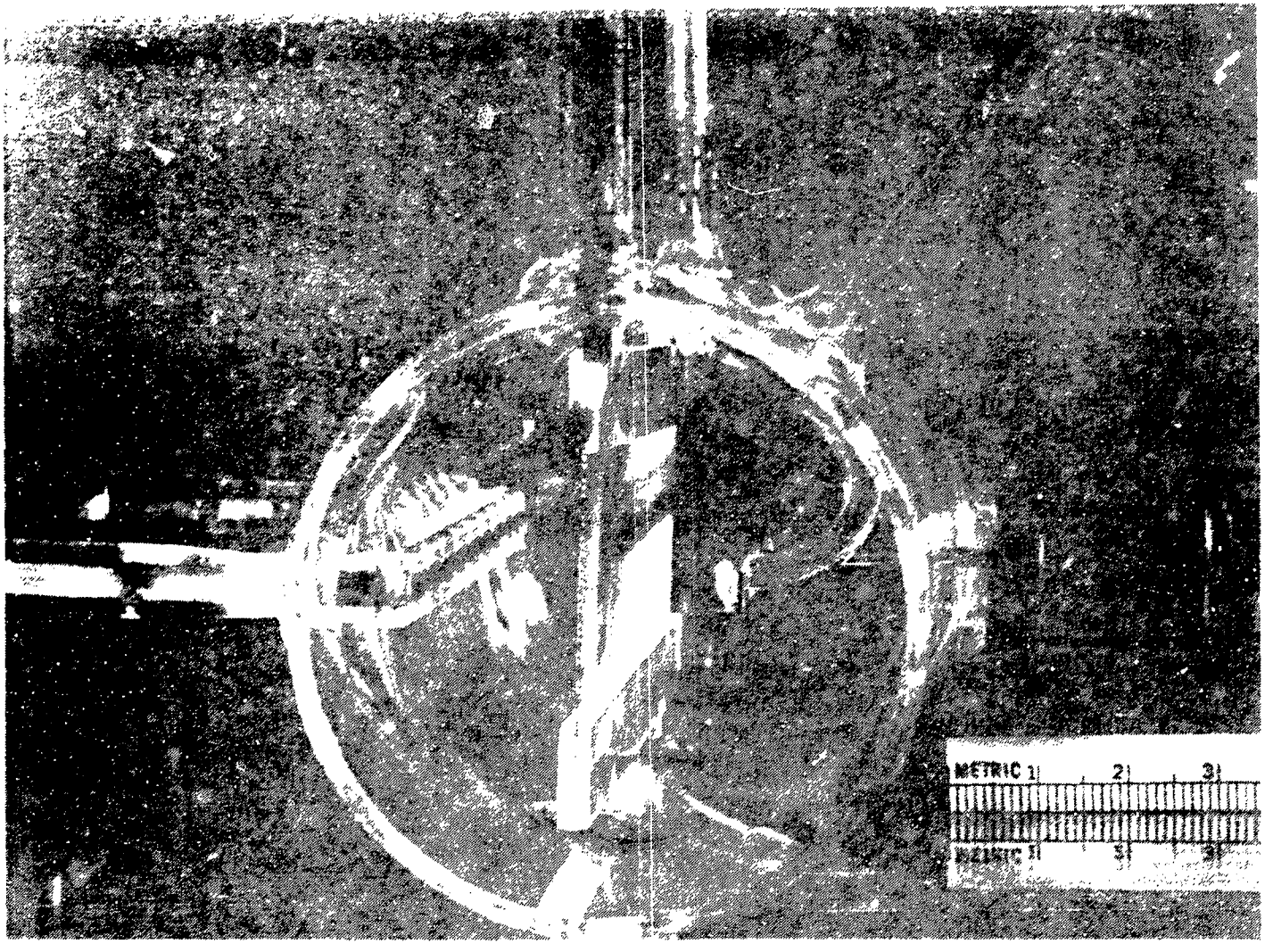
METRIC 1
2
3

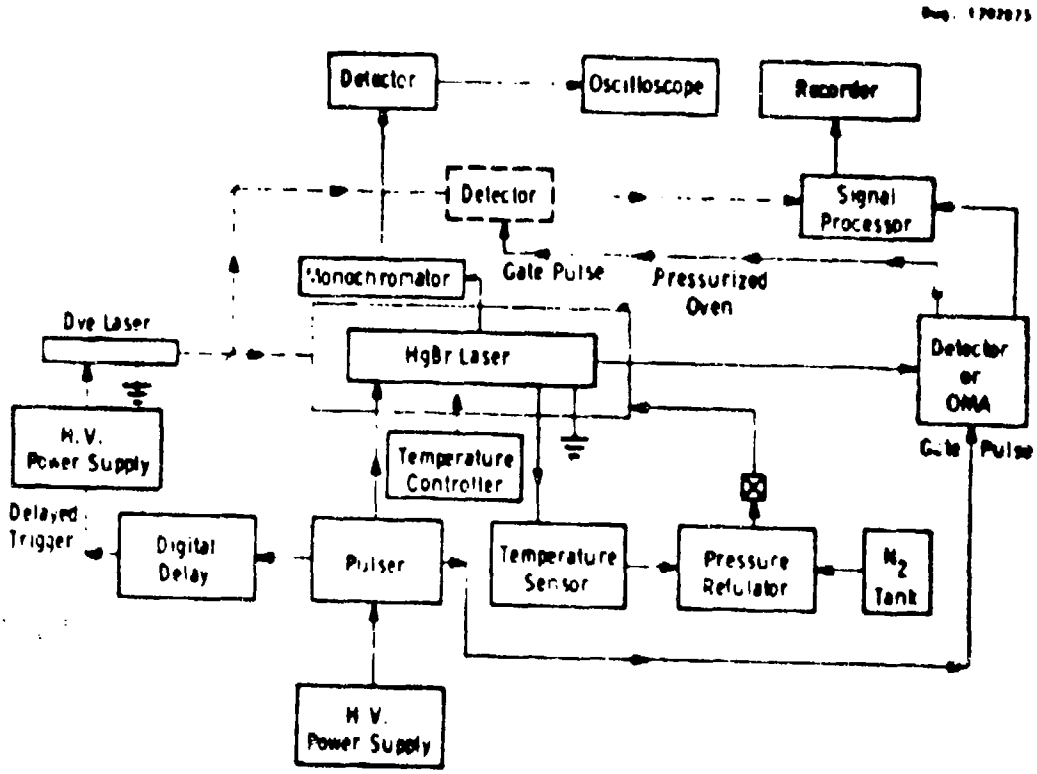

Figure 3 — Spectroscopic apparatus designed to measure the fluorescence and absorption of pulsed HgBr discharges.

TlHg EXCIMER LASER

Laser Medium: Hg + Tl
Temperature: ~ 900°C
Pressure: ~ 4 atm
Mercury Density: 3×10^{19} cm^{-3}
Thallium Density: ~ 10^{17} cm^{-3}

Discharge volume: $0.5 \times 1.0 \times 8.0 = 4$ cm^3
Peak Current: 50 A
Peak Current Density: 12.5 A cm^{-2}
Current Pulse Width: ~ 100 ns FWHM
Capacitor Charge Voltage: 15 kV
Glow Voltage: ~12 kV (est.)

Fluorescence: blue-green emission observed visually

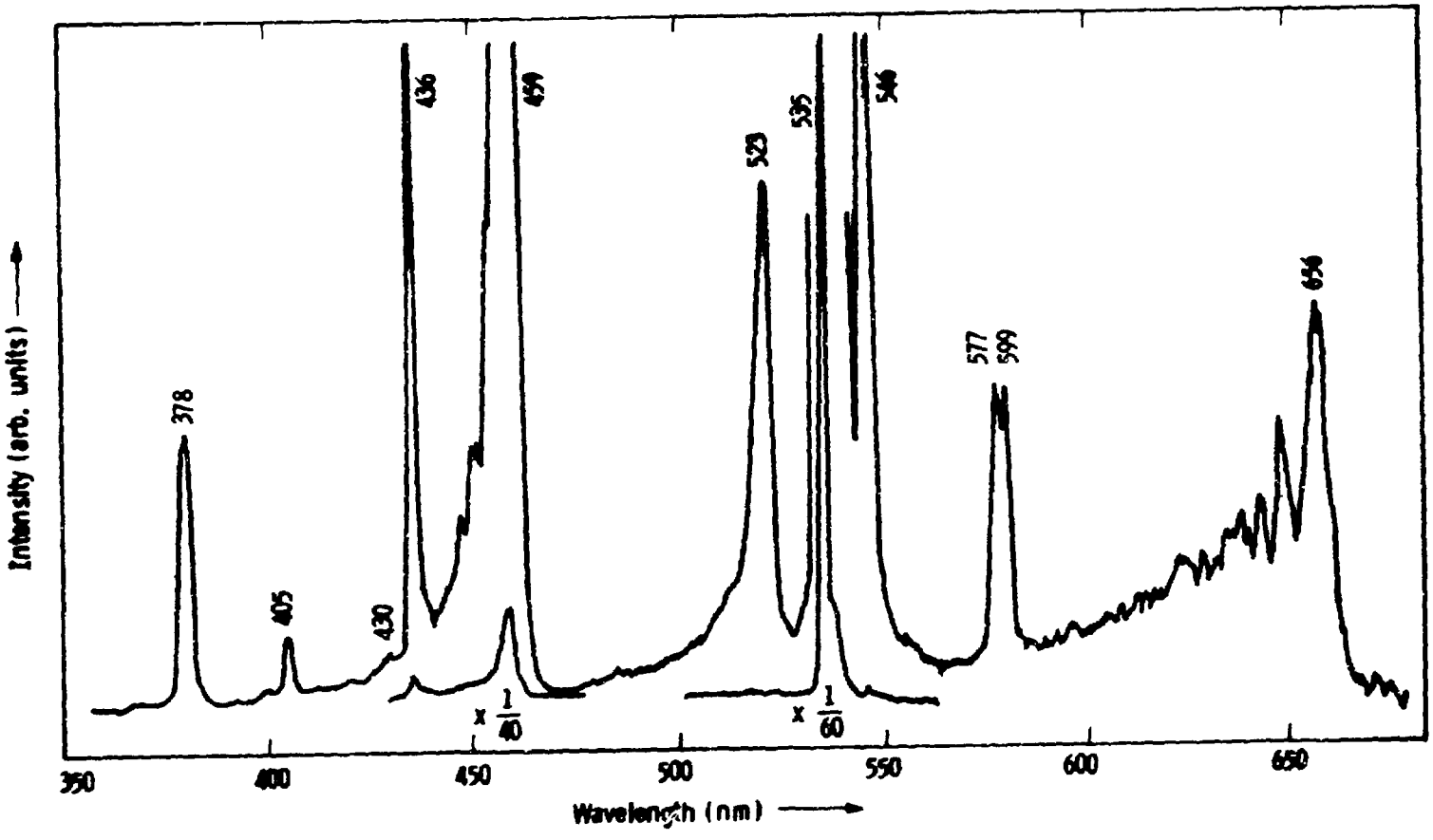

Fig. 2 – Time-integrated fluorescence from a pulsed glow discharge in Tl-Hg vapors at 900°C. Relative line intensities are uncorrected for S-20 spectral response

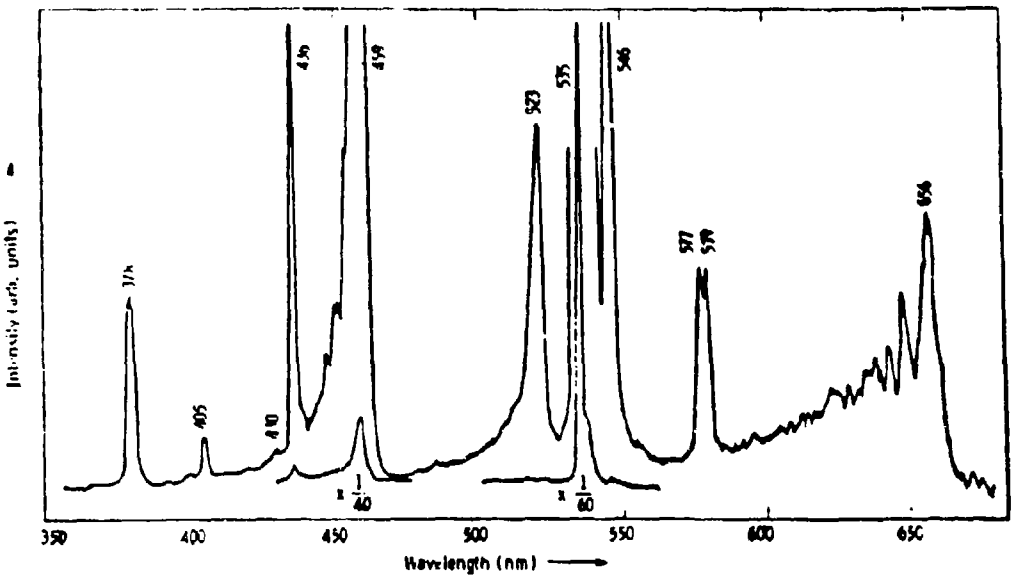

Fig 1- Time-integrated fluorescence from a pulsed glow discharge in Tl-Hg vapors at 900°C. Relative line intensities are uncorrected for S-20 spectral response

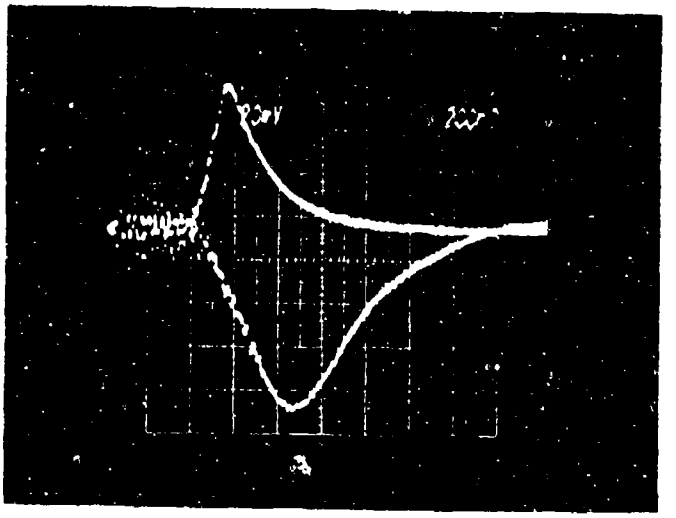

λ = 458 nm

920°C

Absorption

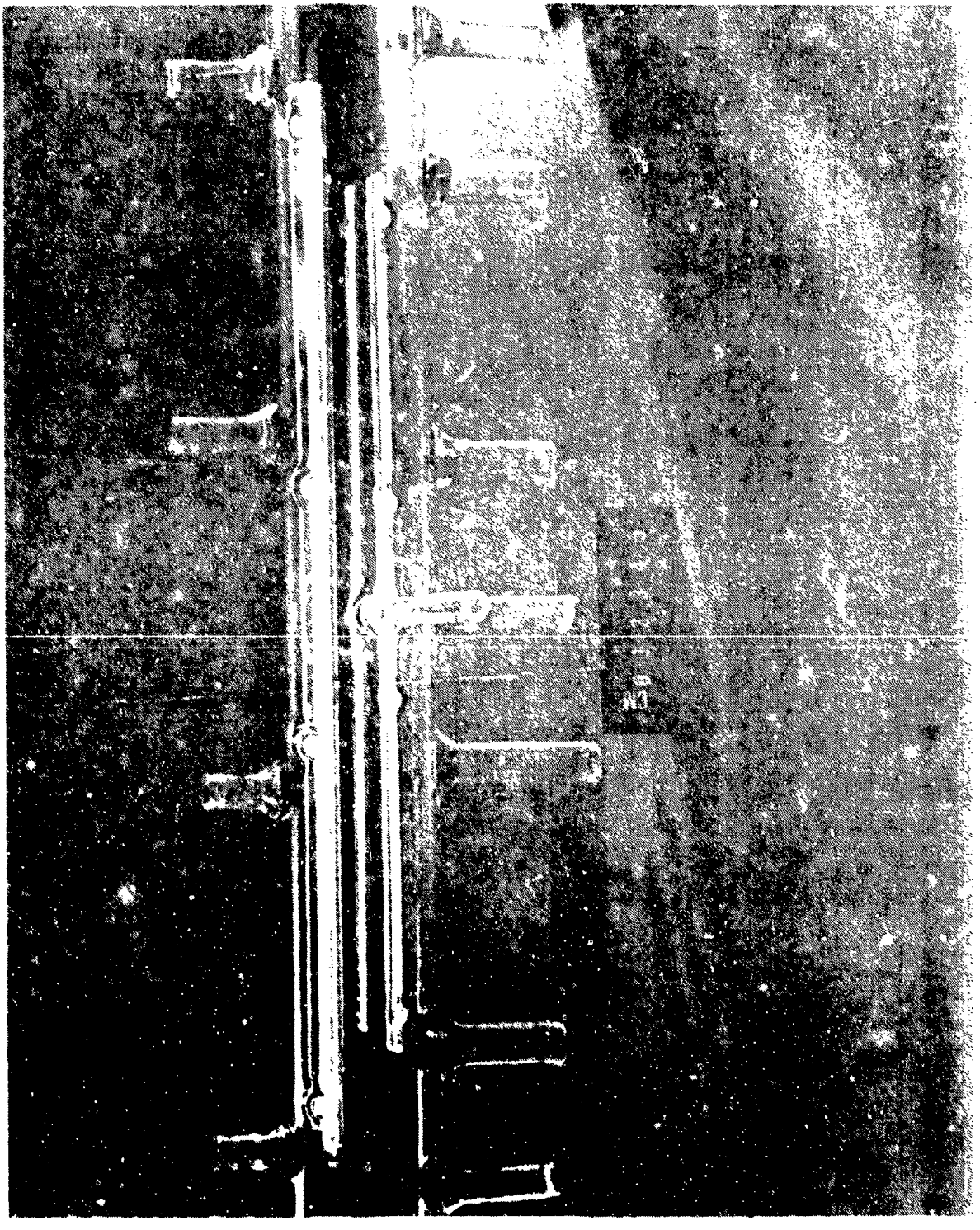

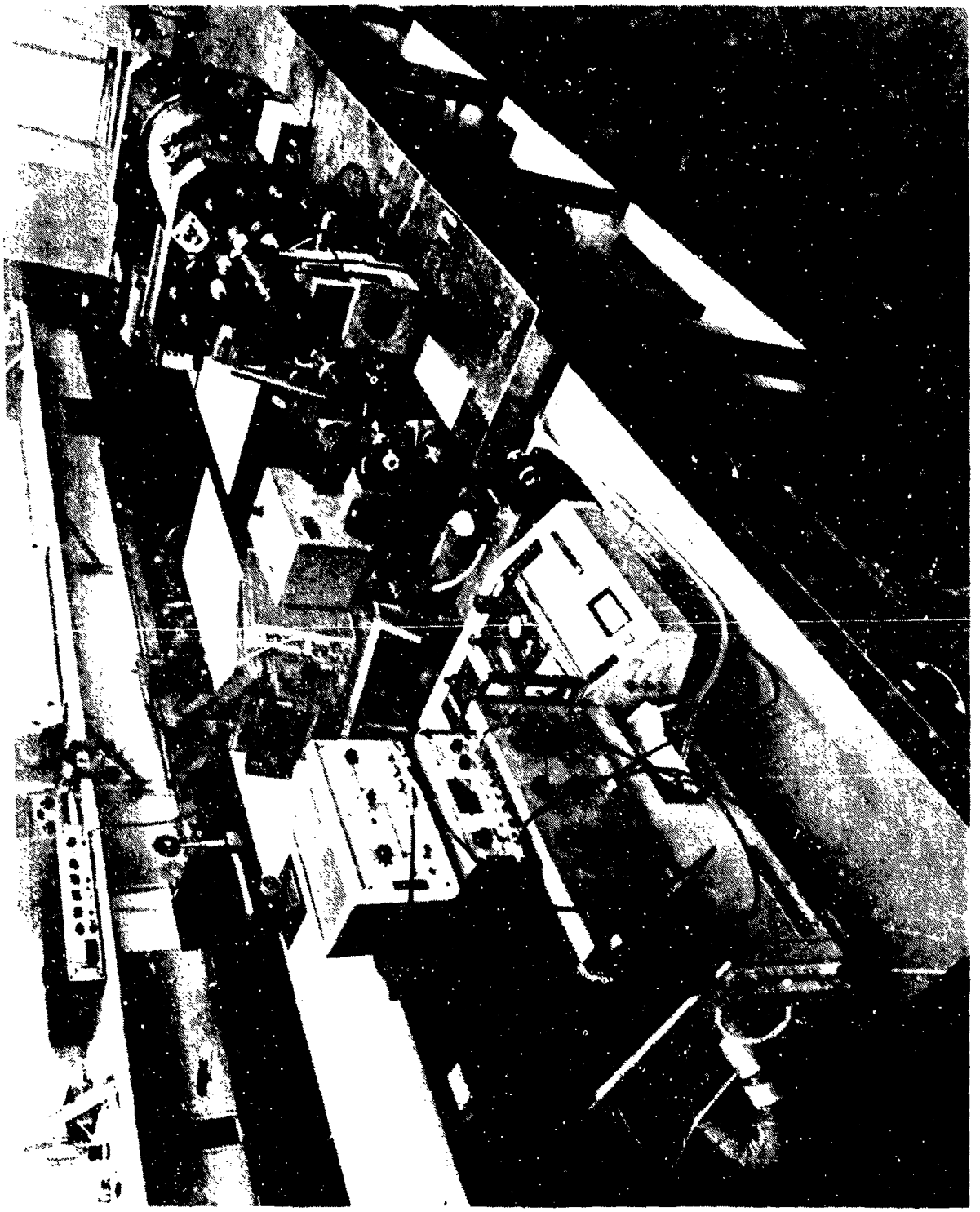

$HgBr_2$/HgBr Dissociation Laser

E. Schimitschek
Naval Ocean Systems Center
San Diego, CA 92152

During the past six months, work was performed to increase the pulse energy, and the repetition rate and to characterize gain and extraction efficiency at wavelengths within the B→X transition region.

To date, the following results were obtained:

1) a 1.2 liter, UV-preionized $HgBr_2$/HgBr discharge laser device has been constructed, with a driver energy of up to 100 Joules. Initial testing will begin in May 1980; the goal is to extract up to 1 Joule of laser energy

2) a 60 cm^3, UV-preionized $HgBr_2$/HgBr discharge laser was built with an interval cross-flow blower. This device was successfully operated up to 100 pps with no drop-off in pulse energy. The pulse energy measured so far is 30 mJ. Optimization now performed should bring the pulse energy up to 50 mJ. At that point, self-heated operation will begin.

3) gain has been measured as function of wavelength and N_2 partial pressure. Narrow-band extraction between 490-505 nm will be undertaken by injection-locking with a tunable dye laser.

$HgBr_2$/HgBr DISSOCIATION LASER EFFORTS AT NOSC

Work Performed By:

D. ALTMAN

J. CELTO

R. KRAUTWALD

E. SCHIMITSCHEK

T. SHAY

ON-GOING EFFORTS:

- MEASUREMENT OF GAIN, ABSORPTION, NARROW-LINE EXTRACTION EFFICIENCY
- REP. RATE UP-SCALING
- DISCHARGE VOLUME UP-SCALING

$HgBr_2$/HgBr CRITICAL ISSUES

- ENERGY/PULSE ⟶ 1 J
- REPETITION RATE ⟶ 100 PPS
- EFFICIENCY ⟶ 1%
- LIFETIME ⟶ 10^{10} SHOTS

ENERGY/PULSE

*90 MJ DEMONSTRATED WITH 0.8J/LITER AT 1.2 AMAGAT

*PRESENTLY UNDER CONSTRUCTION 1.2 LITER DEVICE WITH ENERGY STORAGE OF 100 JOULES

*PLANNED TO OPERATE MAY 80

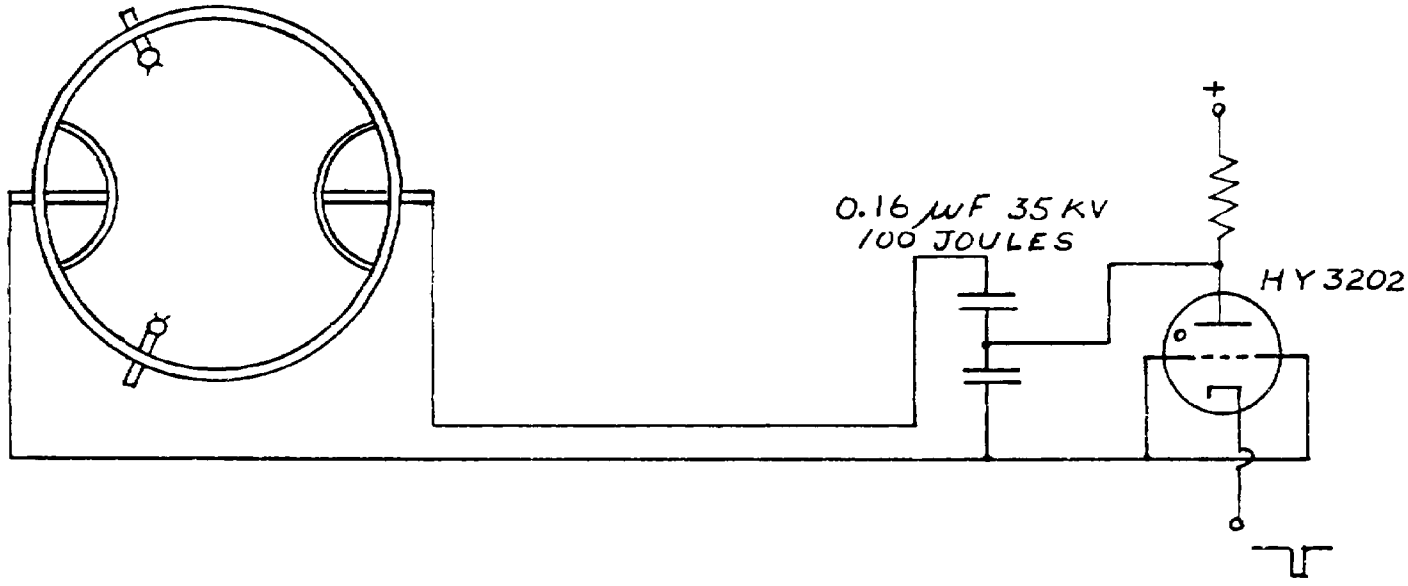

ONE LITER $HgBr_2/HgBr$ DISSOCIATION LASER

REPETITION RATE

- 60 CM^3 DEVICE WITH INTERNAL CROSS-FLOW BLOWER HAS BEEN CONSTRUCTED
- SUCCESSFULLY OPERATED AT UP TO 100 PPS WITH AVERAGE POWER OF ABOUT 1 WATT
- OPTIMIZATION (ENERGY/PULSE, EFFICIENCY) NOW IN PROGRESS
- FUTURE PLANS INCLUDE SELF-HEATED OPERATION

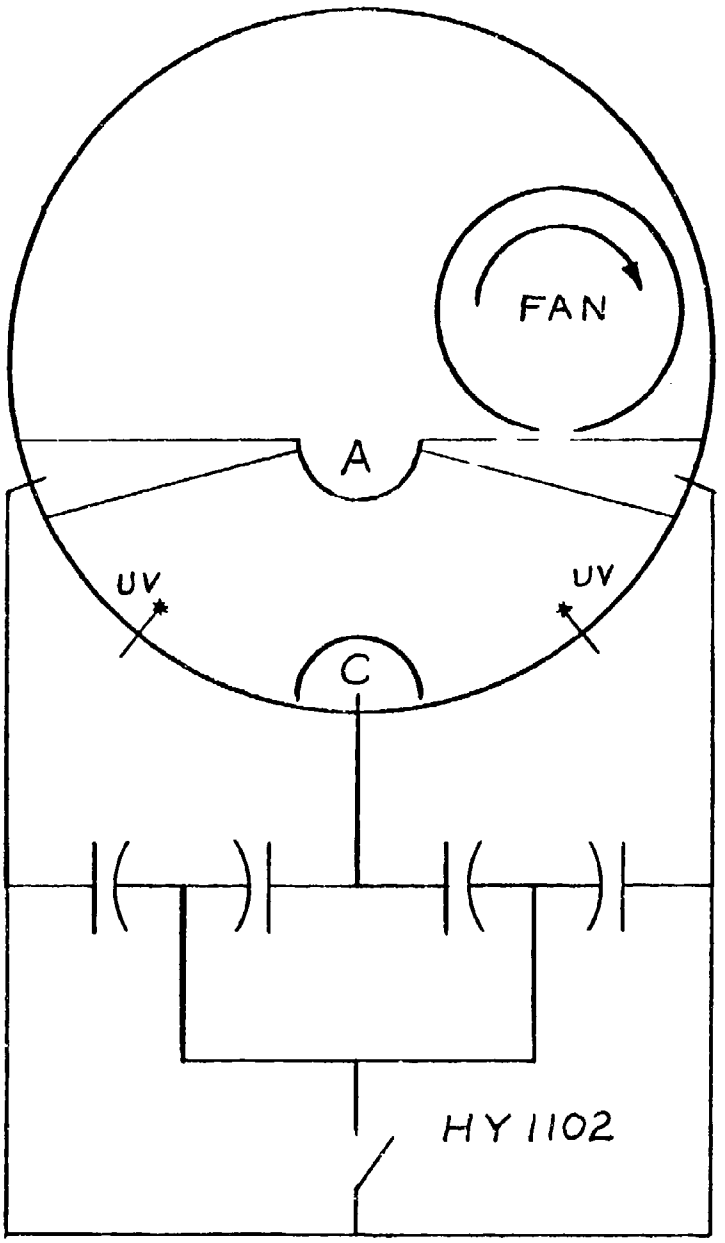

100 Hz $Hg\,Br$ LASER

EFFICIENCY

- 0.95% LASER EFFICIENCY AT 50 MJ DEMONSTRATED
- EFFICIENCY IS COMPLICATED FUNCTION OF TOTAL GAS PRESSURE, BUFFER GAS COMPOSITION, TEMPERATURE ($HgBr_2$ PRESSURE), PREIONIZATION, IMPEDANCE MATCH OF DRIVER/PLASMA
- EFFICIENCY HAS TO BE DEMONSTRATED UNDER CONDITION OF NARROW-BAND EXTRACTION
- EFFORTS UNDERWAY AT NOSC AND UNDER CONTRACT

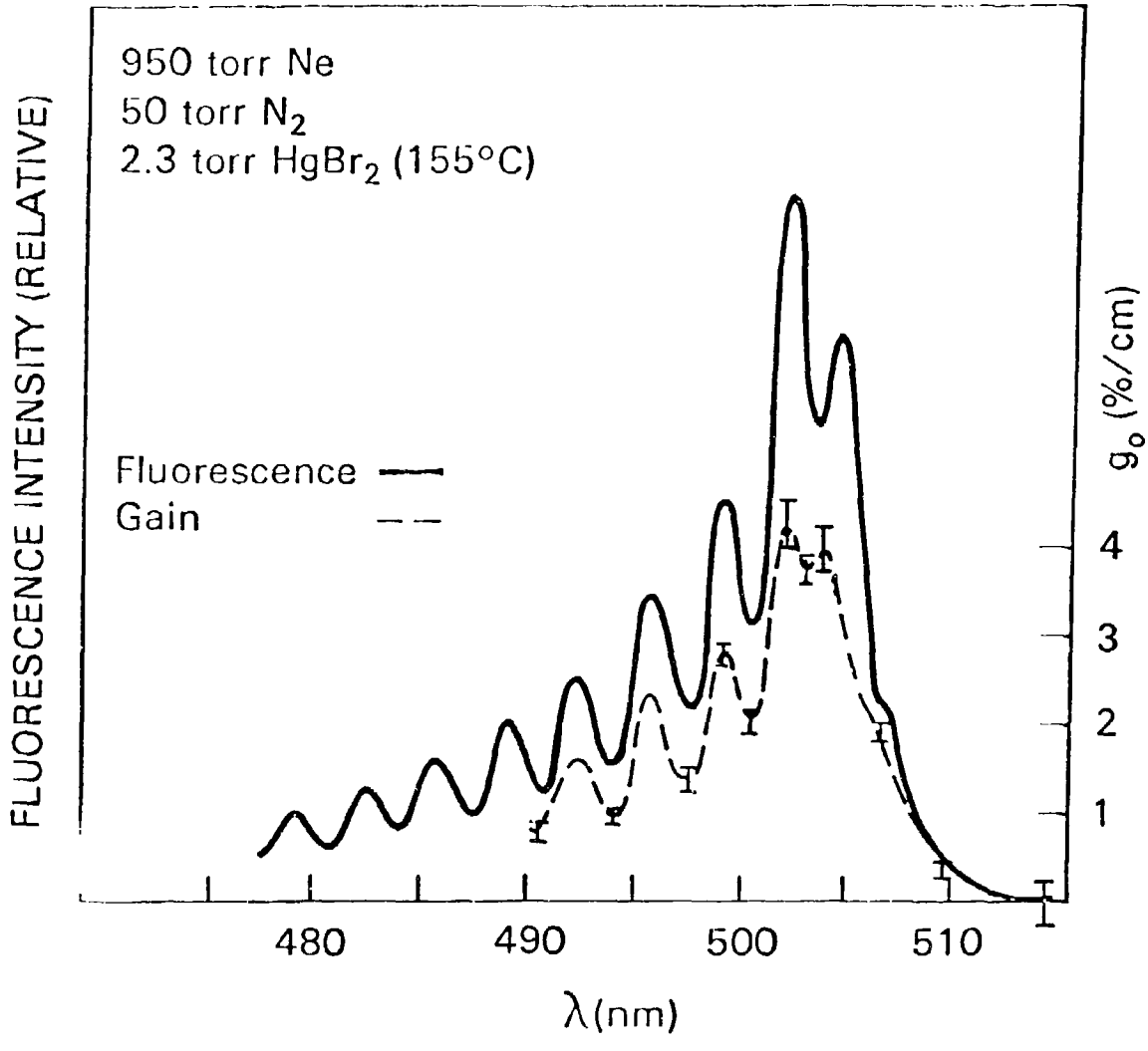

Gain and fluorescence profile of the HgBr B → X transition. Conditions as indicated.

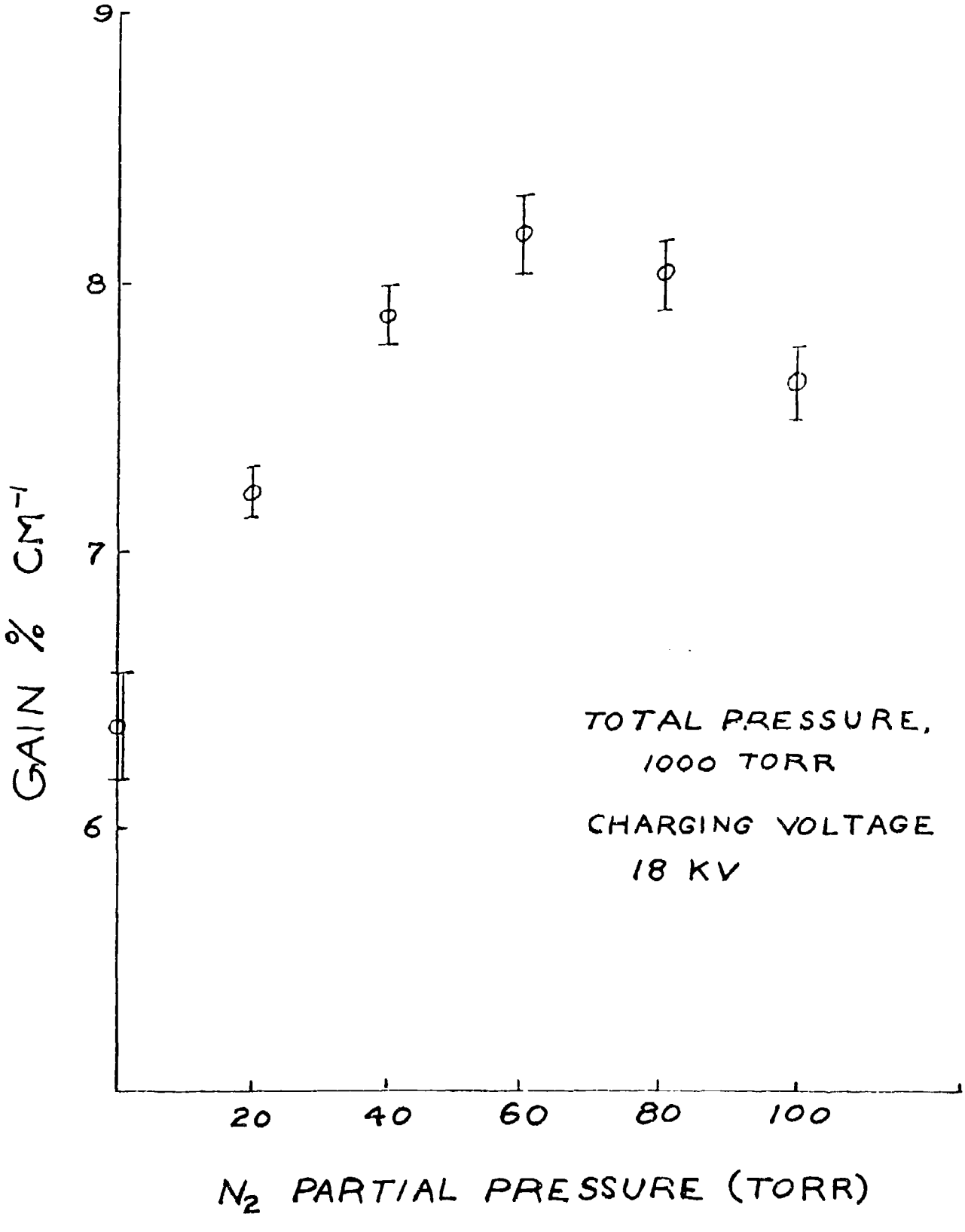
9
8
7
6
GAIN % CM⁻¹
TOTAL PRESSURE,
1000 TORR
CHARGING VOLTAGE
18 KV
20
40
60
80
100
N2 PARTIAL PRESSURE (TORR)

LIFETIME

- LIFETIME OF COMPONENTS OTHER THAN LASER MEDIUM: COMMON TO ALL FAST DISCHARGE LASERS
- LIFETIME OF LASER MEDIUM AND ITS EXCITED DISSOCIATION PRODUCTS IN CONTACT WITH METALS AND INSULATORS
- IN-DEPTH CONTRACTUAL STUDY BEING NEGOTIATED UNDER JOINT DARPA/NAVY FUNDING
- MOST CRITICAL ISSUE

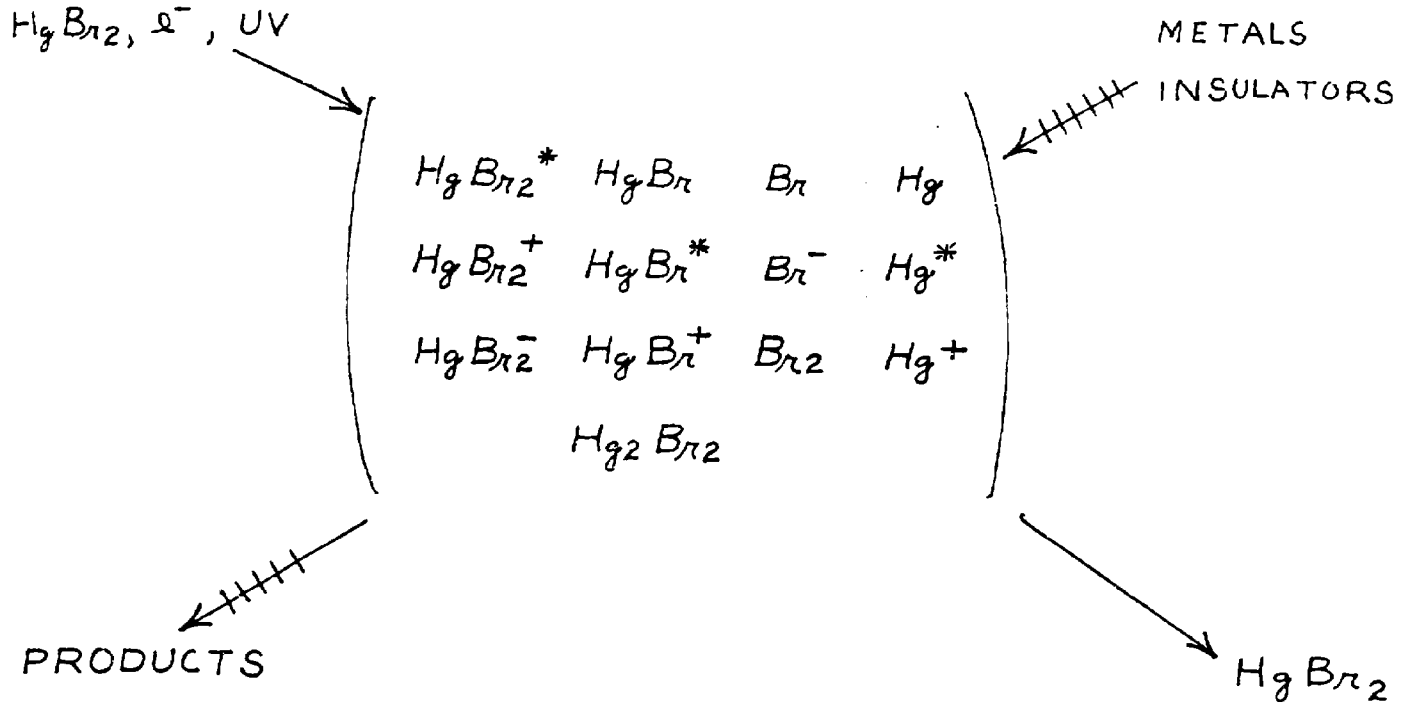
$HgBr_2$, e^-, UV
METALS
INSULATORS
$HgBr_2^*$ $HgBr$ Br Hg
$HgBr_2^+$ $HgBr^*$ Br^- Hg^*
$HgBr_2^-$ $HgBr^+$ Br_2 Hg^+
Hg_2Br_2
PRODUCTS
$HgBr_2$

BLUE-GREEN OPTICAL CONVERSION OF XeF*

(DARPA / ONR)

RICHARD HEINRICHS‡
HOWARD HYMAN
IRVING ITZKAN
DANIEL TRAINOR

‡ SUPPORTED BY AERL IRAD UNDER AERL/MIT COOPERATIVE PROGRAM

J3961

AVCO Everett Research Laboratory Inc
2385 Revere Beach Parkway
Everett MA 02149

AVCO EVERETT

EFFICIENT CONVERSION OF XeF* RADIATION TO THE BLUE-GREEN THROUGH SRS*

This presentation discussed the generation of blue-green laser radiation (λ~470nm) utilizing the technique of Stimulated Raman Scattering (SRS) of XeF* laser photons in molecular gases. Our specific approach involves sequential 1st Stokes conversion through two separate steps in H_2 and D_2.

The short pulse, low energy experiments were performed with a Lumonic Exciplex Laser (model TE-261). To achieve high laser flux, it was necessary to alter the supplied optics to include Brewster windows and an unstable cavity. In this modified configuration, typical output for XeF* was 10-20 mj in 6 nsec which, when focussed by a 50 cm f.L. plano convex lens, provided ~3 x 10^9 watts/cm^2.

Our high pressure hydrogen cells are constructed from two-inch diameter steel shock tube sections of approximately 40 cm path length. These cells are fitted with high grade optical quality UV quartz windows to allow the pump beam to enter and the resulting stimulated Raman emission to exit.

To date, we have performed stimulated Raman scattering experiments whereby XeF* laser photons (351 and 353 nm) have been efficiently converted to longer wavelengths using molecular hydrogen. For example, we have observed 1st Stokes energy conversion in a simple one pass configuration of ~44%, with peak power efficiencies of near 66%. This single pass one-step conversion to 411 and 414 nm

in hydrogen has been characterized with respect to gas pressure, laser intensity, and active cell length. These quantitative experimental observations are in reasonable agreement with theoretical expectations.

Experiments on the second step of the two-step Raman conversion processes showed us to be intensity limited. Experiments to test the approach were, therefore, performed with KrF and showed >70% pump depletion. Recently, experiments were performed with a 0.6J, 400 nsec laser in single step conversion utilizing H_2. These results showed ~35% conversion of XeF* radiation to 1st Stokes at 413nm in good agreement with our expectations. This work is in progress.

BLUE - GREEN OPTICAL CONVERSION OF XeF*

MOTIVATION

- PROVIDE ≥ 1% EFFICIENT BLUE – GREEN LASER FOR GROUND BASED SUBMARINE COMMUNICATION MISSION

GOAL

- DETERMINE FEASIBILITY OF UNIQUE TWO STEP MOLECULAR RAMAN APPROACH TO MEET EFFICIENCY REQUIREMENT
- DEMONSTRATE RAMAN CONVERSION TO THE BLUE – GREEN UTILIZING A 1 TO 10 J ONE METER XeF* LASER AS A PUMP

J3962

AVCO EVERETT

AERL APPROACH

- TWO STEP (SEQUENTIAL 1ST STOKES) MOLECULAR RAMAN CONVERSION

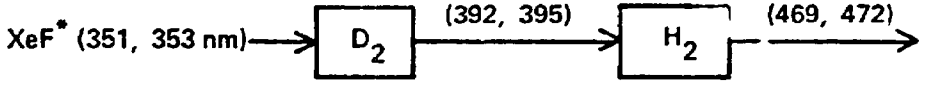

- KEY FEATURES

  TWO DIFFERENT MOLECULAR SPECIES ⇒ WAVELENGTH FLEXIBILITY

  OPTIMIZATION ON 1ST STOKES ⇒ MINIMIZE COMPETITIVE PROCESSES (HIGHER-ORDER STOKES, 4-WAVE)

J3964

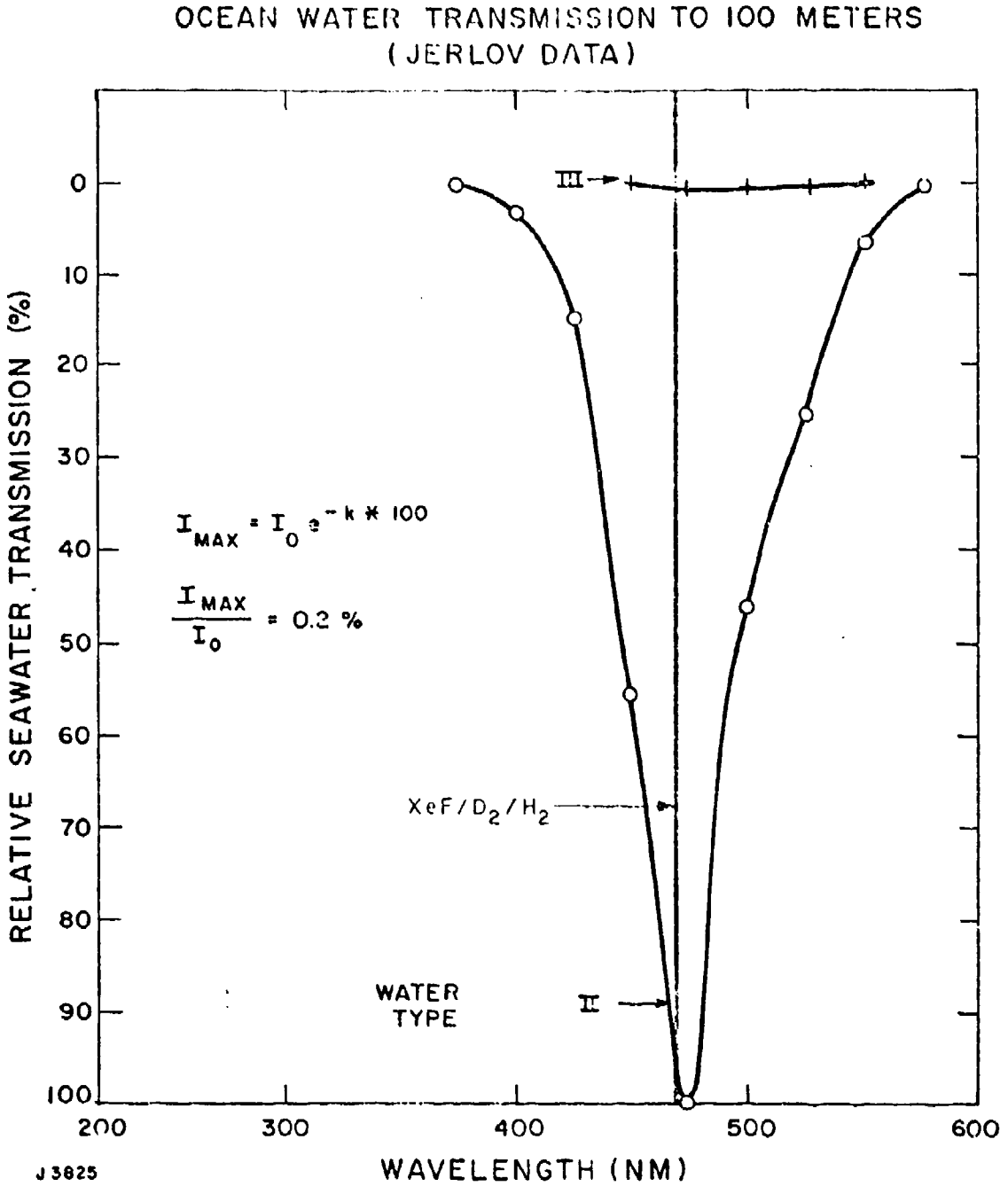

AVCO EVERETT

AVCO

SCHEMATIC OF EXPERIMENTAL TECHNIQUE
(SINGLE STEP EXPERIMENTS)

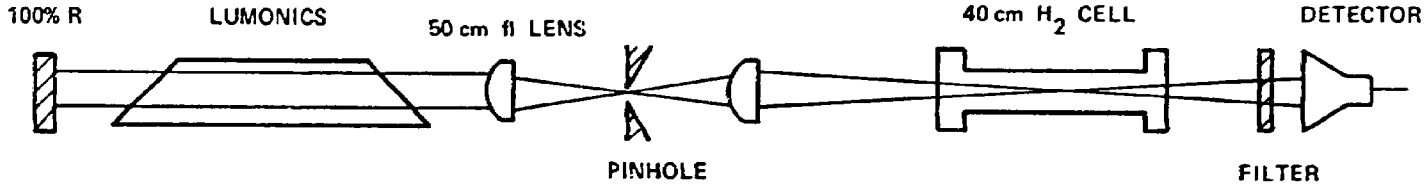

XeF* ~ 20 mJ

~ 3 x 10^9 W/cm^2

~ 0.5 x 10^9 W/cm^2

J-3959

FOCAL LENGTH VARIATION

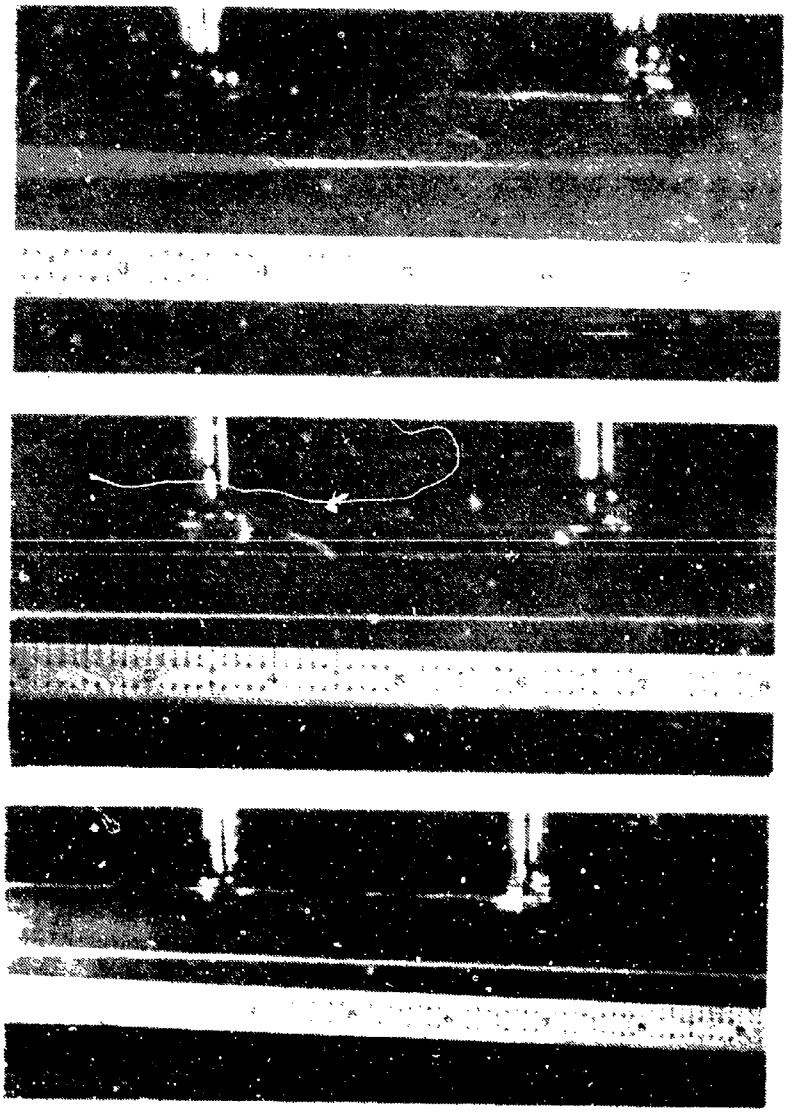

20 cm FOCUS

50 cm FOCUS

135 cm FOCUS

J3747

AVCO EVERETT

H_2 PRESSURE VARIATION (Xe F)

X - DEPLETED PUMP
□ - 1st STOKES
△ - 2nd STOKES

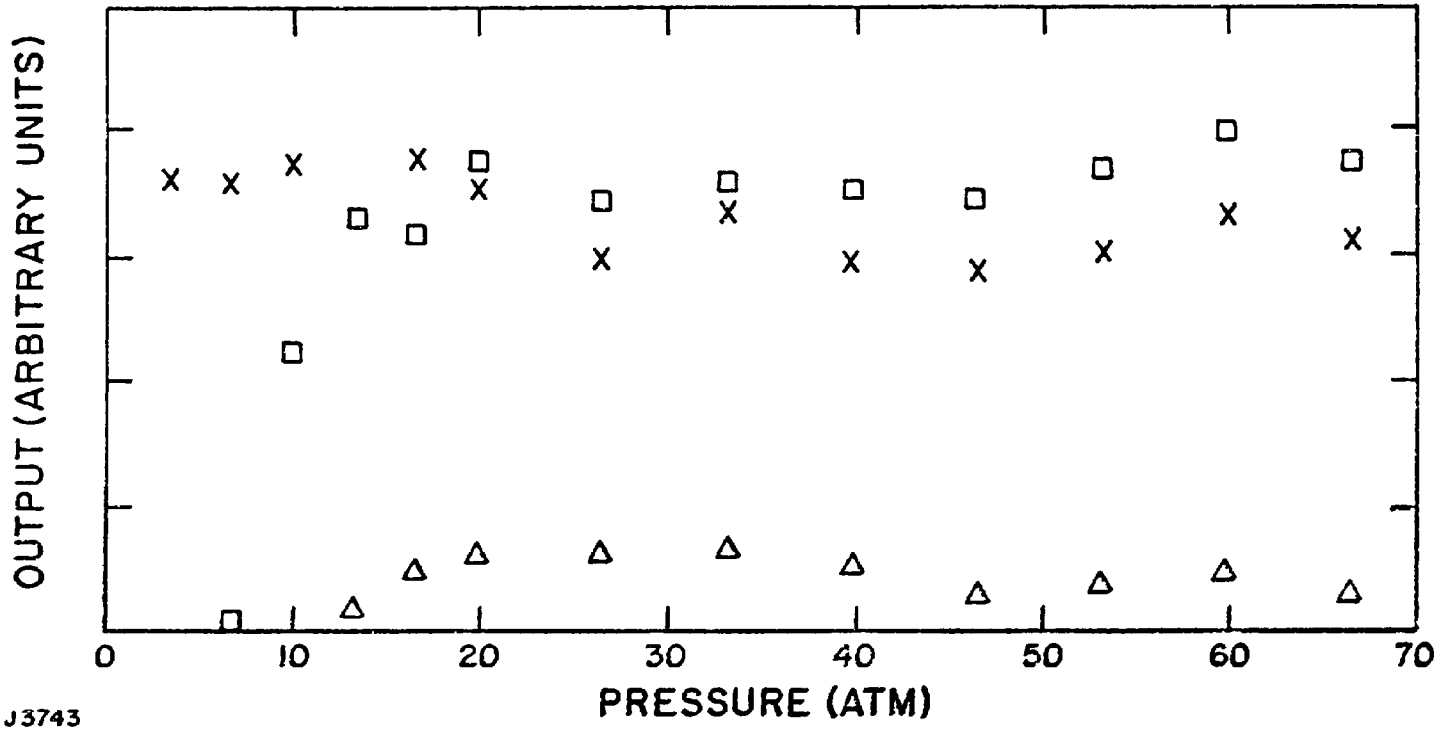

J3743

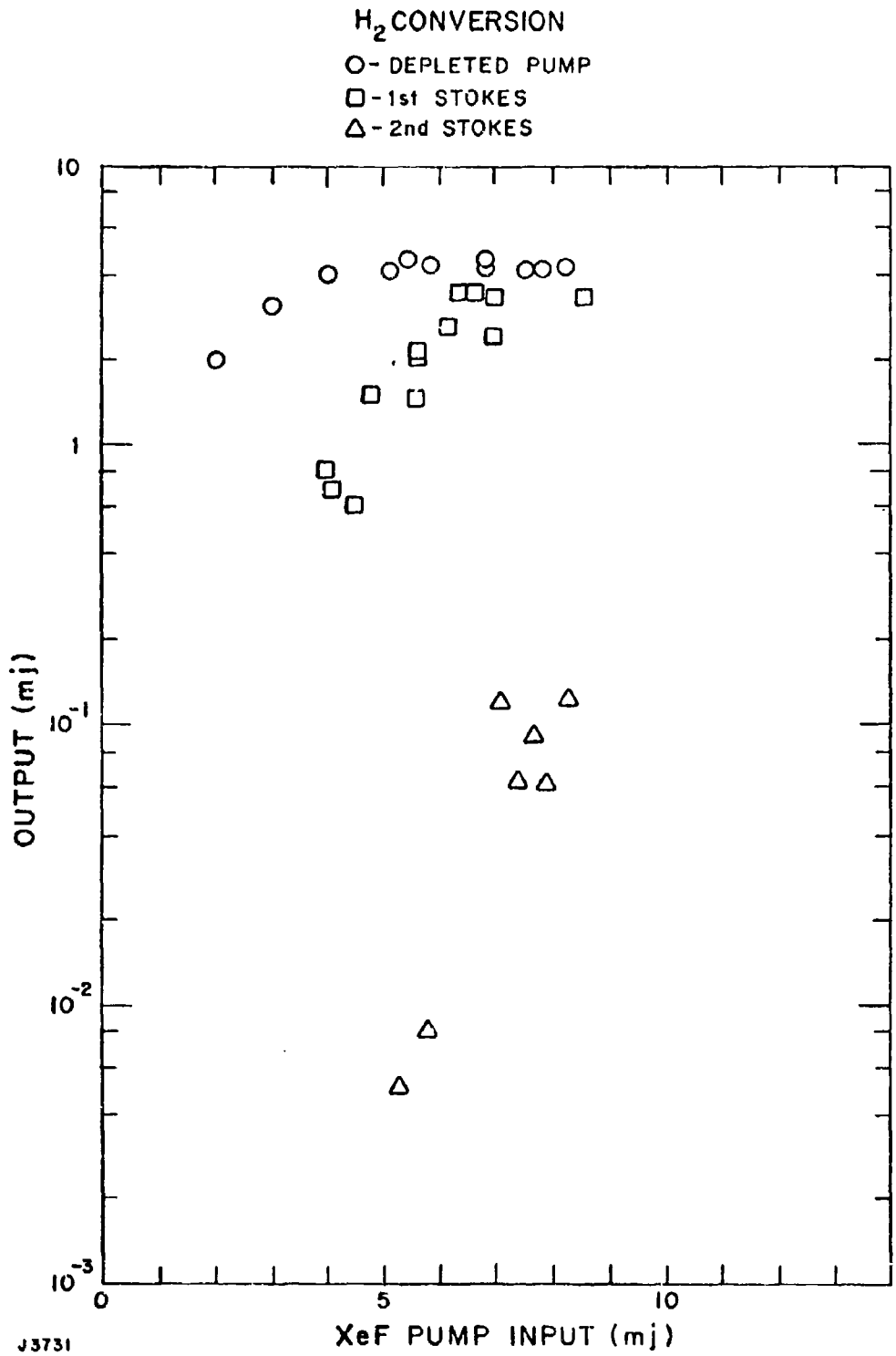

AVCO EVERETT

FIRST STOKES GAIN FOR FORWARD SRS IN H_2

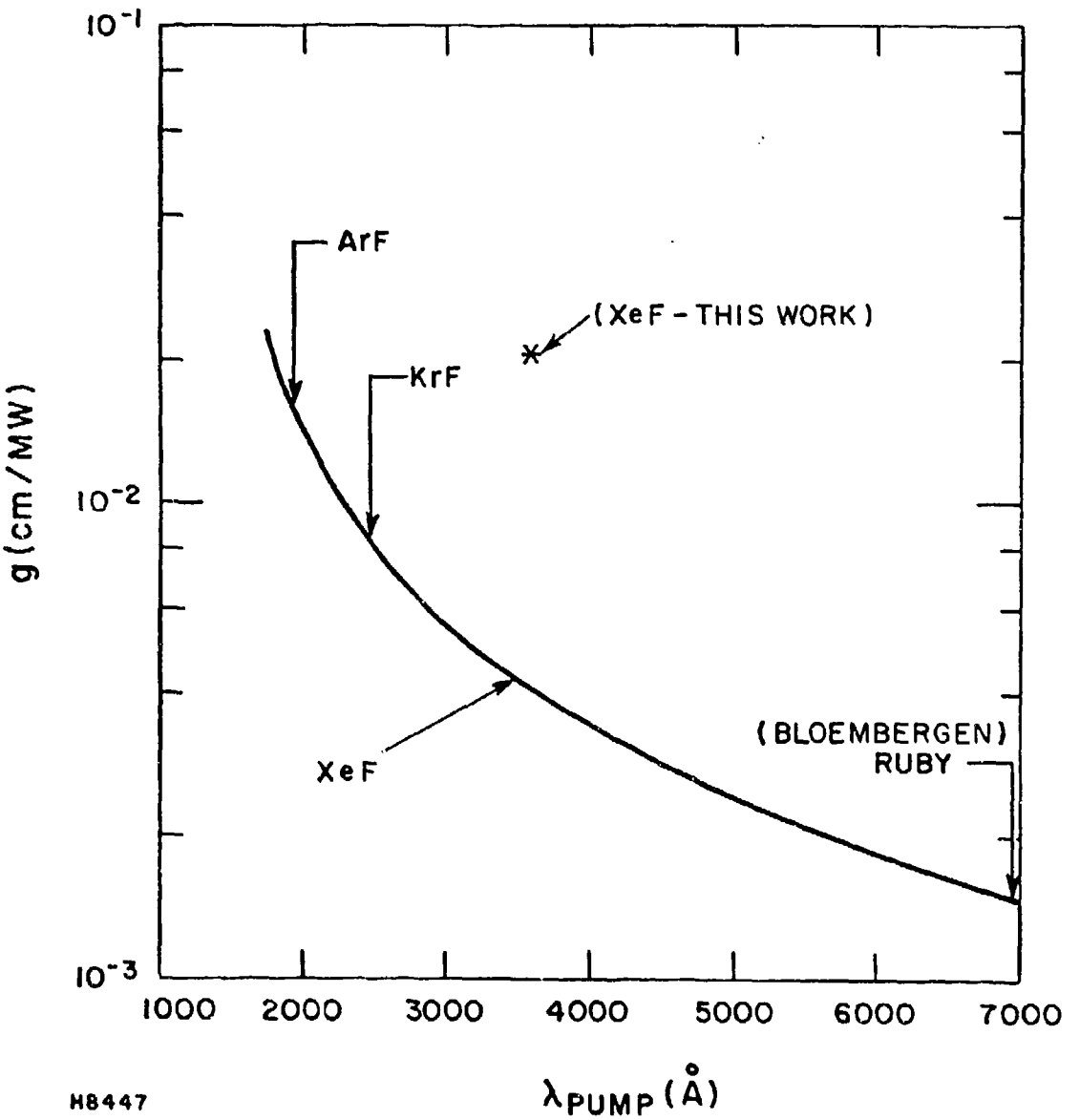

AVCO EVERETT

PULSE SHORTENING EFFECTS

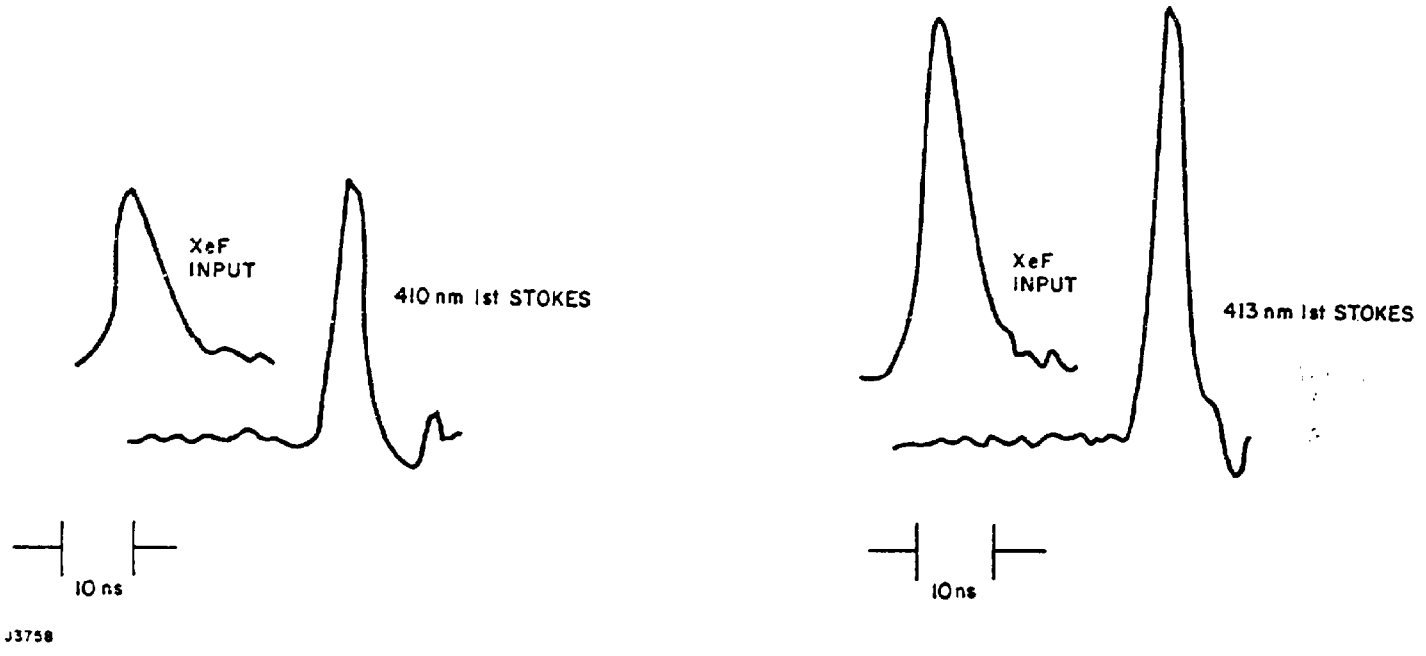

ONE STEP XeF/H_2 CONVERSION EFFICIENCIES

E_{IN} (mJ)	9.6
E_{OUT} (mJ)	4.2 (S_1), ~ 0 (S_2)
ENERGY EFF (%)	44
POWER EFF (%)	66
POWER PHOTON EFF (%)	76

J3960

AVCO EVERETT

PROGRAM STATUS
(MARCH 1980)

SMALL SCALE EXPERIMENTS (≤ 40 mJ, ~ 6 nsec)

- ONE STEP
  - EFFICIENT 1ST STOKES CONVERSION IN H_2 (66%)
- TWO STEP
  - $XeF/H_2/H_2$ (EFF ≃ 29% – PUMP POWER LIMITED)
  - $KrF/D_2/H_2$ (> 70% DEPLETION OF $S_1(D_2)$ IN H_2 CELL)

ONE METER DEVICE EXPERIMENTS (≥ 1 J, 0.4 μ sec)

- ONE STEP
  - XeF/H_2 (IN PROGRESS)

J3963

AVCO EVERETT

TWO STEP KrF/D_2/H_2 RAMAN CONVERSION

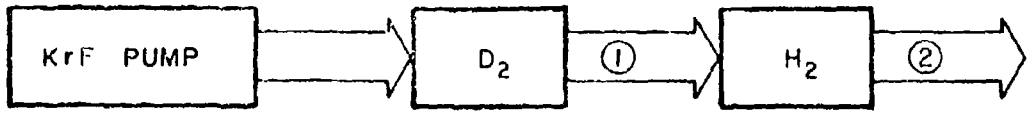

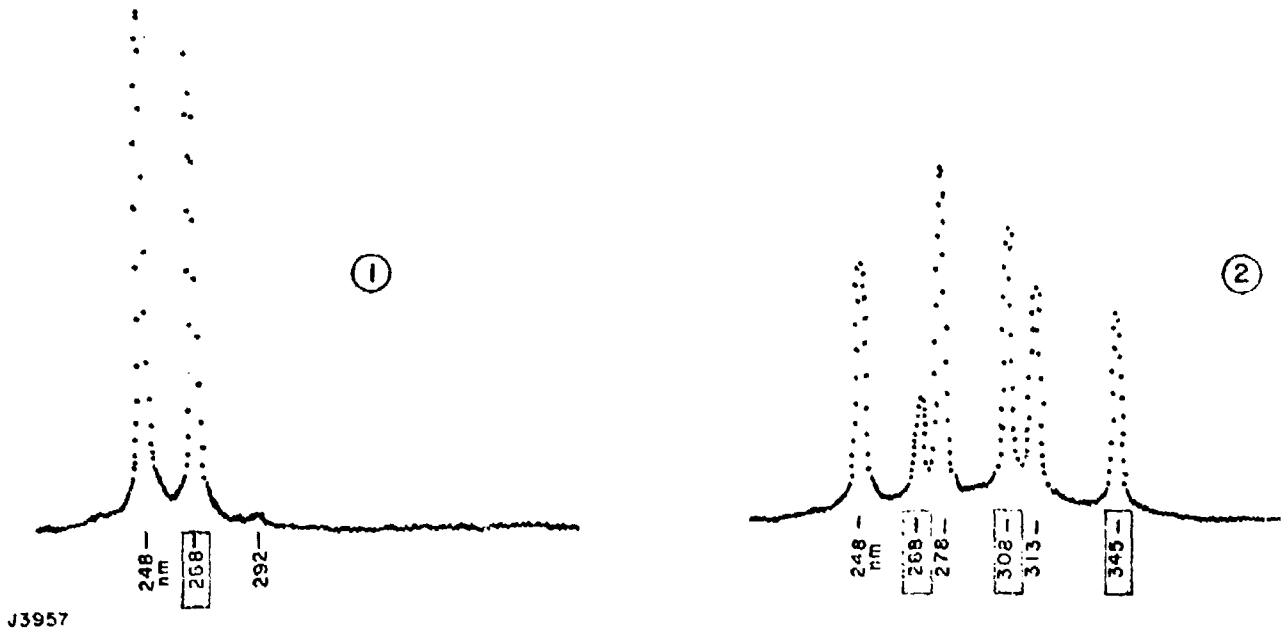

AVCO EVERETT

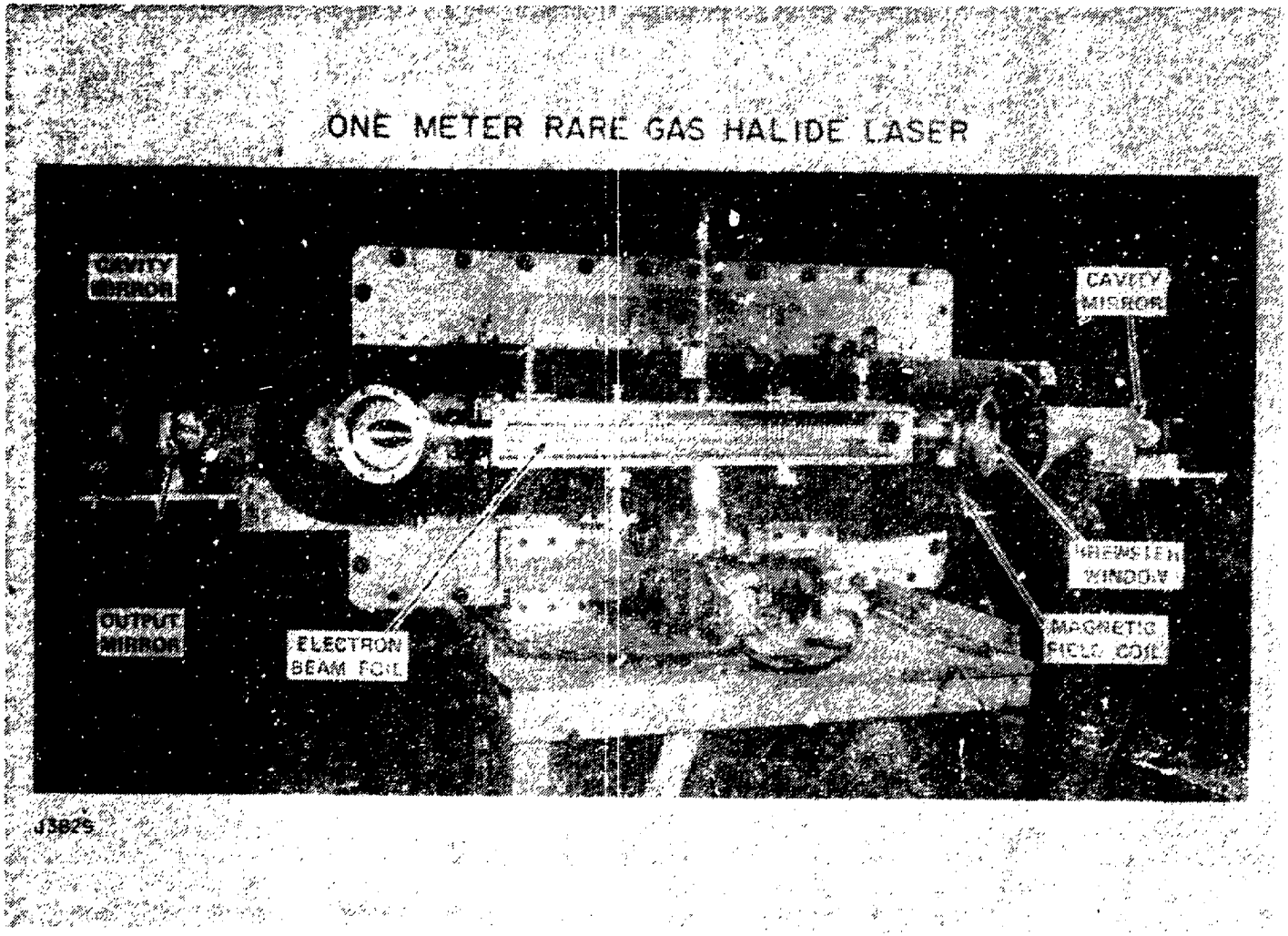
ONE METER RARE GAS HALIDE LASER
CAVITY MIRROR
CAVITY MIRROR
BREWSTER WINDOW
OUTPUT MIRROR
ELECTRON BEAM FOIL
MAGNETIC FIELD COIL
J3825

LONG PULSE LENGTH XeF* SRS EXPERIMENT (H_2)

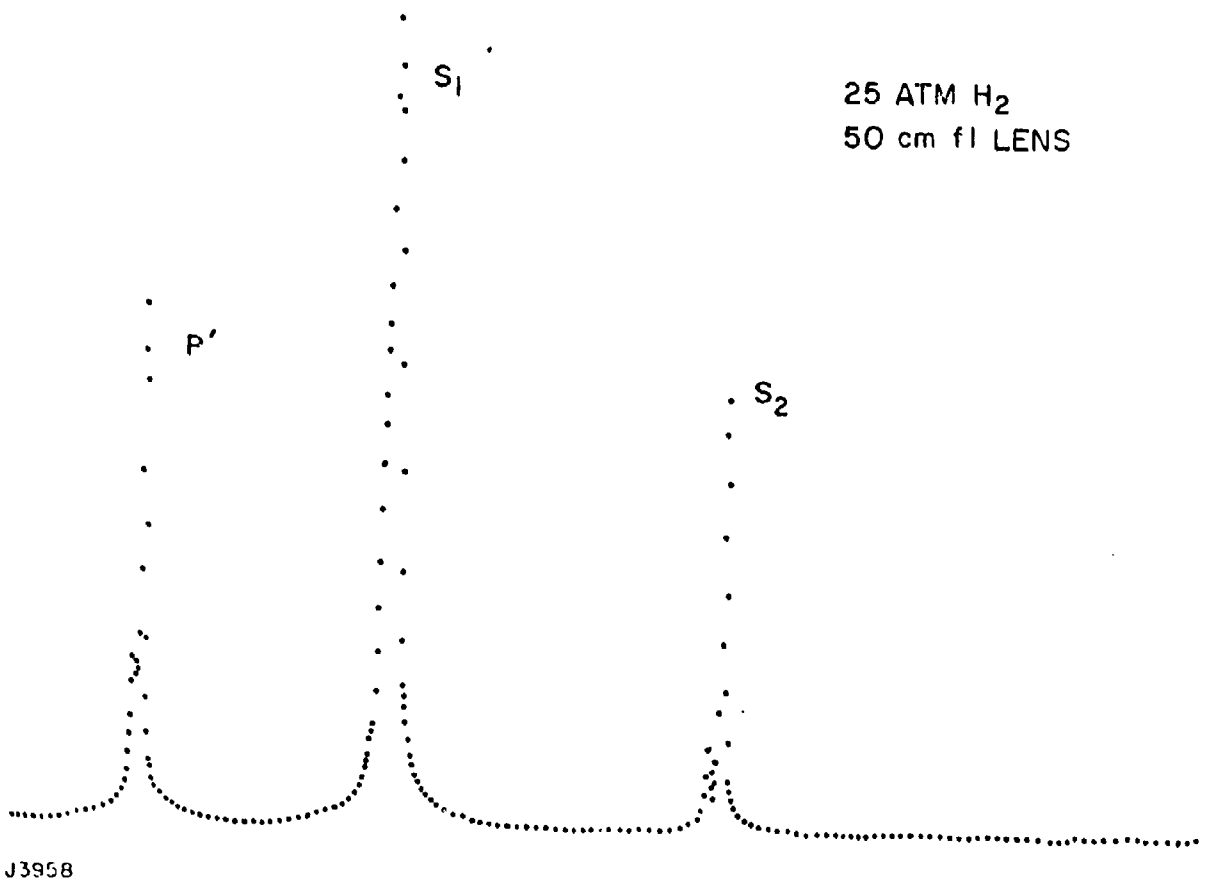

AVCO EVERETT

XeF^* PUMPED SRS EXPERIMENT (H_2)
(ONE METER DEVICE)

XeF^* in

353, (351) nm

400 nsec

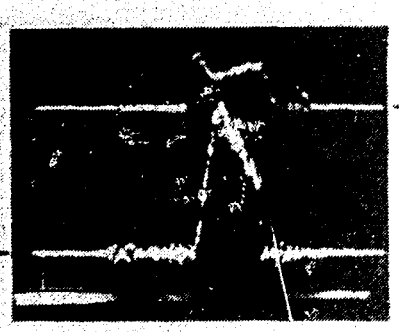

$S_1 + S_2$

DEPLETED XeF^*

STOKES RADIATION

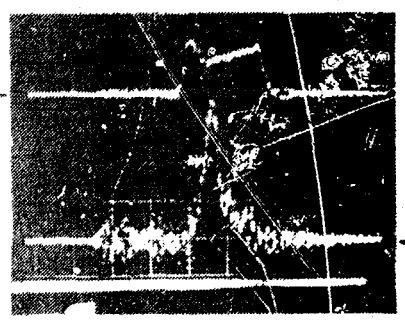

S_2 x 2.5

499, (495) nm

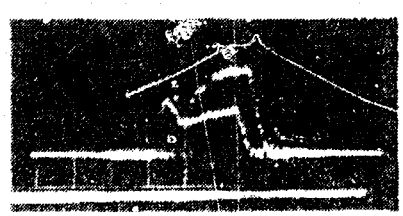

CONVERSION EFFICIENCY ~35%

J3982

AVCO EVERETT

BLUE-GREEN OPTICAL CONVERSION OF XeF^*

(1 METER DEVICE)

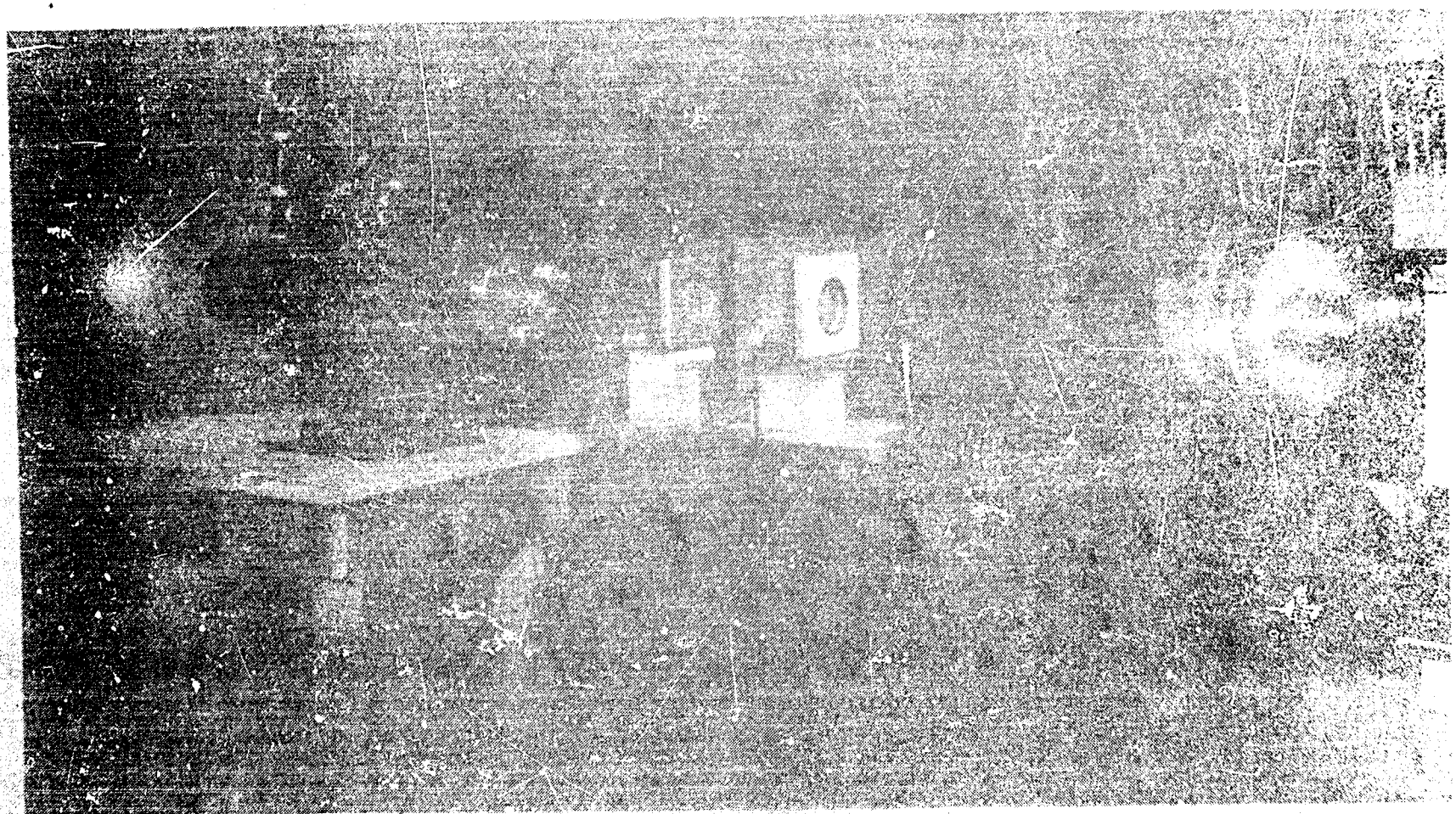

J3932

AVCO EVERETT

SCALING STUDIES OF EFFICIENT RAMAN CONVERTERS

E. A. STAPPAERTS, H. KOMINE, J. B. WEST, W. H. LONG, JR.

NORTHROP CORPORATION
NORTHROP RESEARCH AND TECHNOLOGY CENTER
One Research Park
Palos Verdes Peninsula CA 90274

ABSTRACT

A program of analytical and experimental investigations has been initiated recently with DARPA sponsorship to study the scalability of molecular Raman converters for the ground-based blue-green source. Based on existing data, preliminary design parameters are obtained for a Raman oscillator-amplifier system which converts the XeF laser wavelengths into blue-green. Thermal effects in Raman amplifiers are discussed together with gas flow characteristics needed for good beam quality.

The primary laser optical requirements with respect to Raman converter design are discussed in terms of spatial and temporal uniformity, beam divergence, and spectral characteristics. A series of experiments at an intermediate energy range (20-50J) will address various scaling issues including spectral narrowing of the primary laser and Raman conversion efficiency.

SCALING STUDIES OF EFFICIENT RAMAN CONVERTERS

March 1980

E. A. Stappaerts
H. Komine
J. B. West
W. H. Long, Jr.

Northrop Corporation
Northrop Research and Technology Center
One Research Park
Palos Verdes Peninsula, California 90274

OBJECTIVE:

INVESTIGATE THE SCALABILITY OF EFFICIENT RAMAN CONVERSION OF XeF (XeCl) LASER WAVELENGTH INTO THE BLUE-GREEN REGION

APPROACH:

NOVEL RAMAN OSCILLATOR-AMPLIFIER SYSTEM BASED ON SELECTIVE MULTIPLE-STOKES-ORDER CONVERSION IN MOLECULAR GASES

NORTHROP
Research and Technology Center

TABLE OF RAMAN SHIFTED XeF/XeCl LASER
WAVELENGTH IN THE BLUE-GREEN REGION

	WAVELENGTH (nm)	
PUMP / RAMAN SHIFT	XeF 351 / 353	XeCl 308
$2H_2$	496 / 500	
$H_2 + D_2$	468 / 472	
$2D_2$	444 / 447	
$3H_2$		500
$2H_2 + D_2$		472
$H_2 + 2D_2$		447

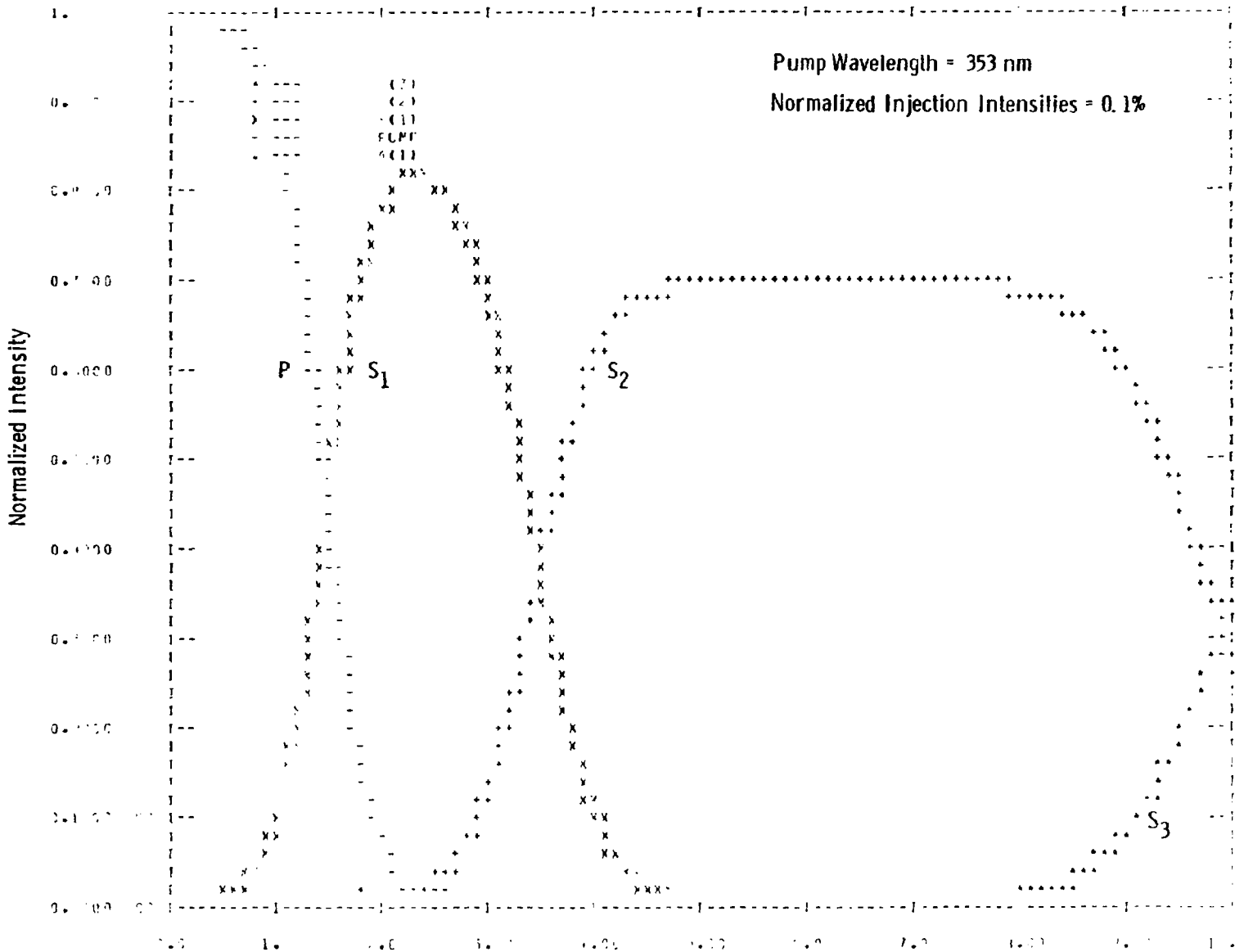
Pump Wavelength = 353 nm
Normalized Injection Intensities = 0.1%
Normalized Intensity
P
S_1
S_2
S_3

PROGRAM ELEMENTS

RAMAN CONVERTER SYSTEM ANALYSIS

- DESIGN CONSTRAINTS
- NOMINAL OPERATING PARAMETERS
- THERMAL EFFECTS

PRIMARY LASER SYSTEM REQUIREMENTS

- BEAM QUALITY AND PULSE SHAPE
- SPECTRAL WIDTH CONTROL

INTERMEDIATE ENERGY SCALING EXPERIMENTS

- FY 80-81

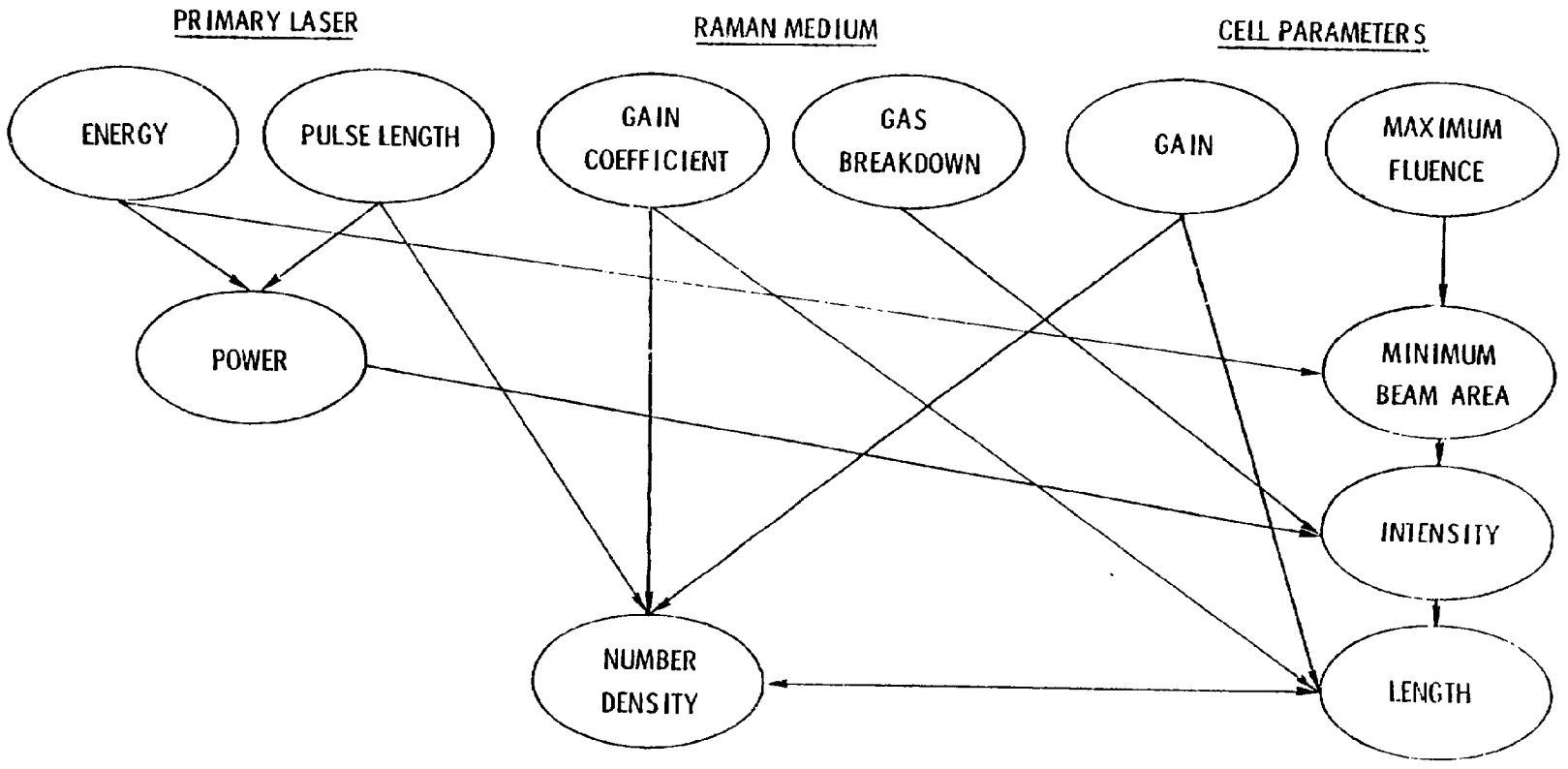

RAMAN OSCILLATOR-AMPLIFIER SYSTEM
DESIGN CONSTRAINTS

NORTHROP
Research and Technology Center

SUMMARY OF DESIGN PARAMETERS

	H_2	
	OSC	AMP
PUMP ENERGY (J)	.2	1000
INJECTED ENERGY (J)	---	.050*
LENGTH (m)	2	4
BEAM AREA (cm^2)	$1.7 * 10^{-4}$	200
TEMPERATURE (K)	300	300
PRESSURE (atm)	10	3
GAIN g (cm/W)	$2 * 10^{-8}$	$2 * 10^{-8}$
WINDOW FLUENCE (J/cm^2)	5	5

*PER STOKES ORDER

THERMAL EFFECTS IN RAMAN AMPLIFIERS

MOLECULAR VIBRATION RELAXATION

- QUENCHING RATE [F. DeMartini and J. Ducing, Phys. Rev. Lett., 17, 117 (1966)]:

$$p\tau = (1060 \pm 100) \times 10^{-6} \text{ atm-sec @ } T = 300 \text{ K}$$

$$p = 3 \text{ atm} \rightarrow \tau = 0.35 \text{ ms} \ll 1/\text{PRF (100 Hz)}$$

TEMPERATURE RISE/DENSITY GRADIENT

- UP TO ~ 40% AVERAGE POWER DEPOSITION IN RAMAN MEDIUM
- THERMAL LENS/BEAM DISTORTION EFFECTS WITHOUT FLOW

NORTHROP
Research and Technology Center

RAMAN AMPLIFIER FLOW SYSTEM CHARACTERISTICS

- GAS TEMPERATURE RISE PER PULSE ~ 2 K OVER 0.35 ms
- NEGLIGIBLE PRESSURE (SHOCK) WAVES → FLUSH FACTOR ~ 1
- NO CHEMICAL CLEANUP PROBLEMS
- LOWER HEAT LOADING COMPARED TO PRIMARY LASER SYSTEM
- SIMPLER FLOW SYSTEM COMPARED TO PRIMARY LASER SYSTEM
- COMPRESSOR POWER ≤ 10% OF PRIMARY LASER POWER SUPPLY

PRIMARY LASER OPTICAL REQUIREMENTS

- BEAM DIVERGENCE: NEAR DIFFRACTION LIMIT
- SPATIAL BEAM UNIFORMITY: $\leqslant \pm 20\%$ VARIATION
- TEMPORAL PULSE UNIFORMITY: NEARLY RECTANGULAR PULSE $\leqslant \pm 20\%$ DISTORTION
- WAVELENGTH: SINGLE LINE
- SPECTRAL WIDTH: $\leqslant 0.2$ Å ($\Delta\nu \leqslant 0.8\ cm^{-1}$ @ $\lambda = 500$ nm)

INTERMEDIATE ENERGY SCALING EXPERIMENTAL PROGRAM

PRIMARY LASER

- DARPA/NRTC SHORT WAVELENGTH ADVANCED TEST BED (SWAT) LASER
- ELECTRON BEAM PUMPING/MAGNETIC GUIDE FIELD
- XeF (XeCl) OPERATION AT 20-50 J

SPECTRAL CONTROL

- SINGLE LINE OUTPUT VIA INJECTION-LOCKING
- NARROW LINEWIDTH

RAMAN CONVERSION

- SECOND-ORDER RAMAN OSCILLATOR-AMPLIFIER SYSTEM
- H_2 GAS

SWAT LASER CHARACTERISTICS

ELECTRON GUN

- TYPE: COLD CATHODE FIELD EMISSION DIODE
- CIRCUIT: THREE-STAGE MARX BANK WITH PEAKING CAPACITOR
- BEAM VOLTAGE: 360 kV NOMINAL
- BEAM CURRENT: 22 A FOR 400 ns PULSE
  12 A FOR 800 ns PULSE
  8 A FOR 1.2 μs PULSE

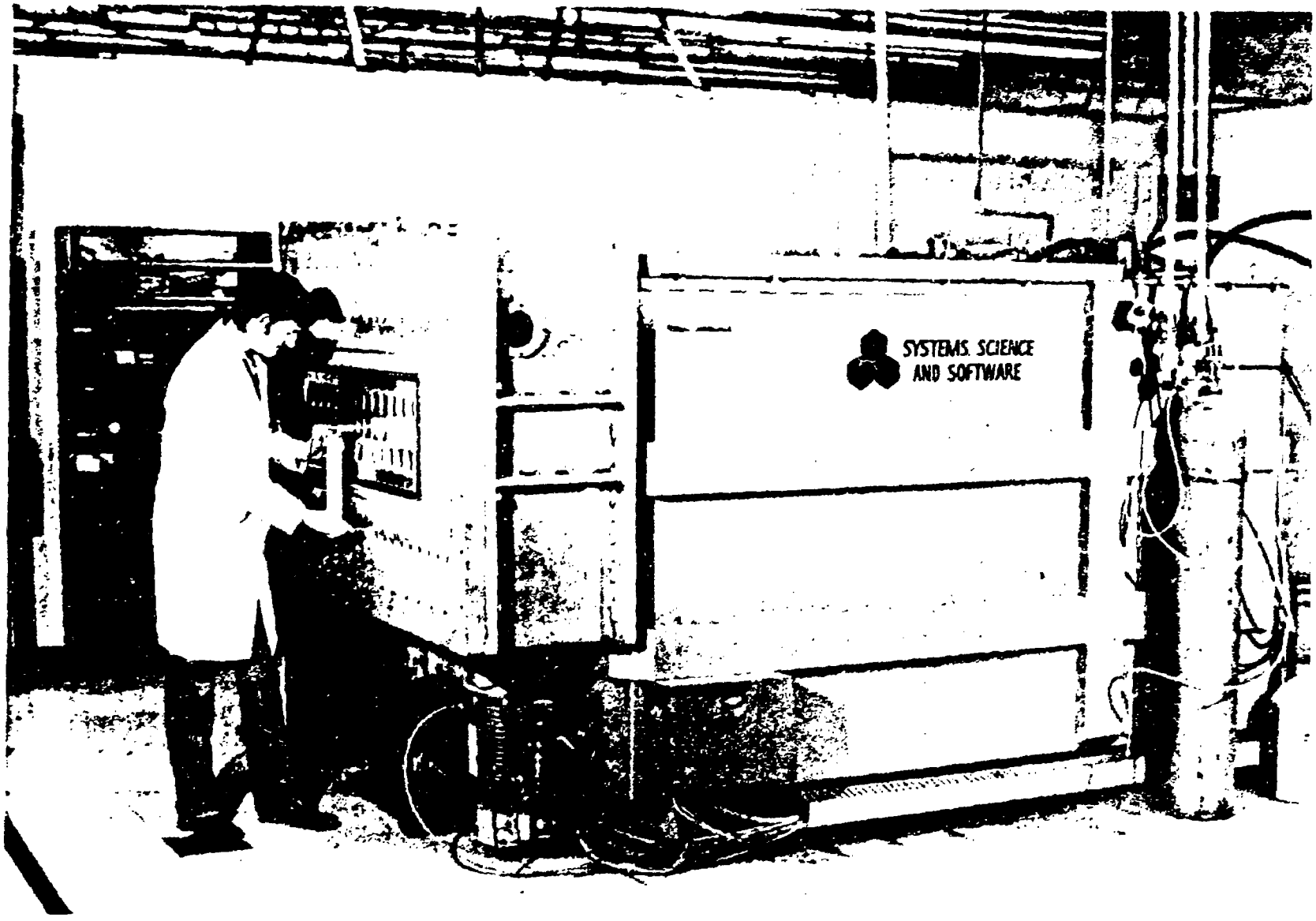

Swat Laser Electron Gun

SWAT LASER CHARACTERISTICS

LASER PERFORMANCE

- ACTIVE VOLUME: 10 LITERS
- KrF (50 J; 800 ns) WITH [1290 Ar, 100 Kr, 2 F_2] MIXTURE @ 10 A/cm^2
- XeF (1.7 J/ℓ; 700 ns) WITH [2280 Ne, 7.5 Xe, 2.5 NF_3] MIXTURE @ 15 A/cm^2

OPTICAL SYSTEM

- POSITIVE BRANCH CONFOCAL UNSTABLE RESONATOR
- NARROW LINEWIDTH INJECTION-LOCKING

NORTHROP
Research and Technology Center

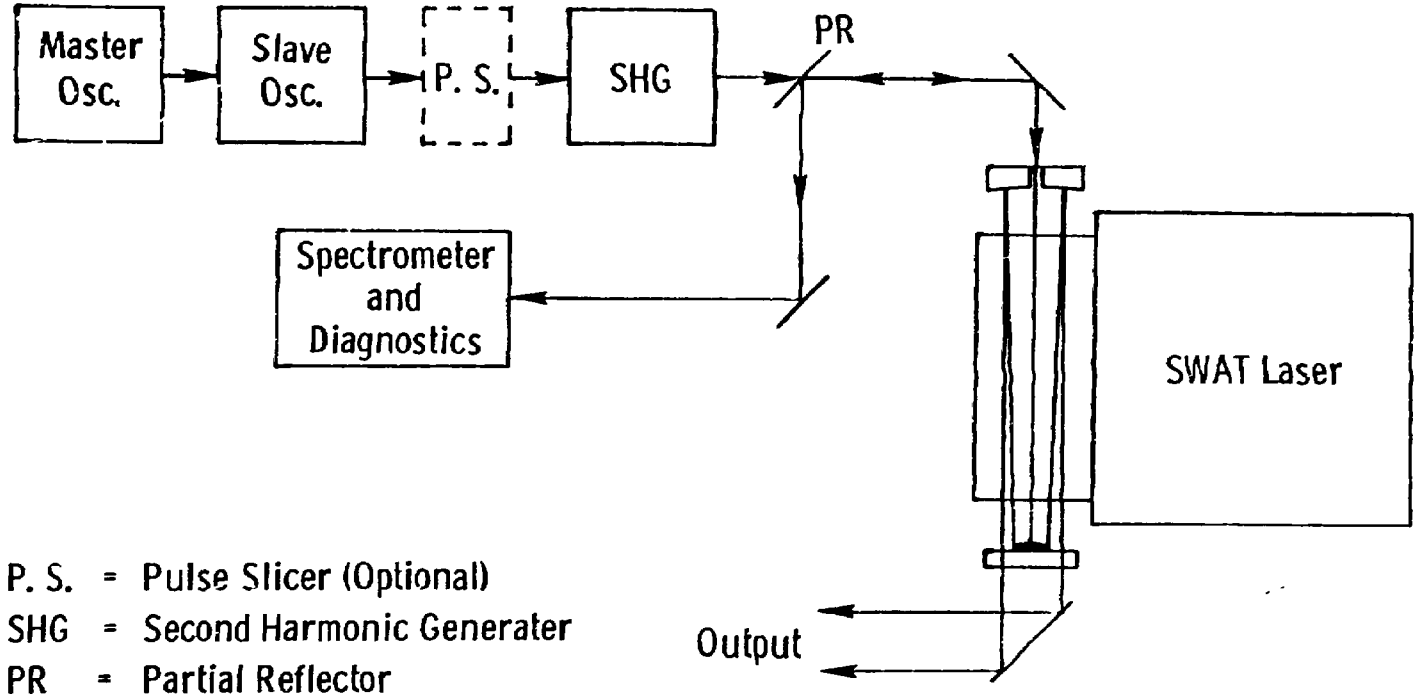

P. S. = Pulse Slicer (Optional)
SHG = Second Harmonic Generater
PR = Partial Reflector

SWAT Laser Injection-Locking

NORTHROP
Research and Technology Center

Ground Based Xe Cl-Pb Blue Green Source

N. Djeu

Naval Research Laboratory
Washington, D. C. 20375

ABSTRACT

The Pb vapor Raman converted XeCl laser is a potential candidate for a ground based blue-green strategic communications system. In addition to having an intrinsic efficiency of 6%, the e-beam pumped Xe Cl laser can deliver high energy pulses in a narrow bandwidth. Coupled with high efficiency for Raman conversion, the overall system should be capable of producing the required power at the specified efficiency and output bandwidth.

In earlier experiments high conversion efficiency (~50%) was observed with short (~20nsec) Xe Cl laser pump pulses. Here we report the efficient conversion of 400 nsec long XeCl pump pulses. With an oscillator-amplifier configuration, an initial XeCl pulse of 200 mJ produced 80 mJ in the blue-green, giving an energy conversion efficiency of 40%. Scale-up demonstrations at the 10 J level will be pursued jointly by NRL and Maxwell Laboratories in the near future.

The question concerning the acoustic waves set up by the de-excitation of metastable Pb atoms has been examined through some order of magnitude calculations. The results show that the amplitude of the initial pressure waves has a quadratic dependency on the rate of heat release. To obtain a realistic assessment of the magnitude of the acoustic waves in the Pb vapor cell, one must know the rate of electronic quenching in Pb as well as the mechanical impedance of the wall material.

GROUND BASED

XeCl-Pb BLUE-GREEN SOURCE

- Summary of status of e-beam pumped XeCl laser
- Results on conversion of 400 nsec XeCl pump pulse
- Plans for conversion of 10 J XeCl pump pulse
- Estimates of magnitude of acoustic waves in Pb vapor cell

NRL

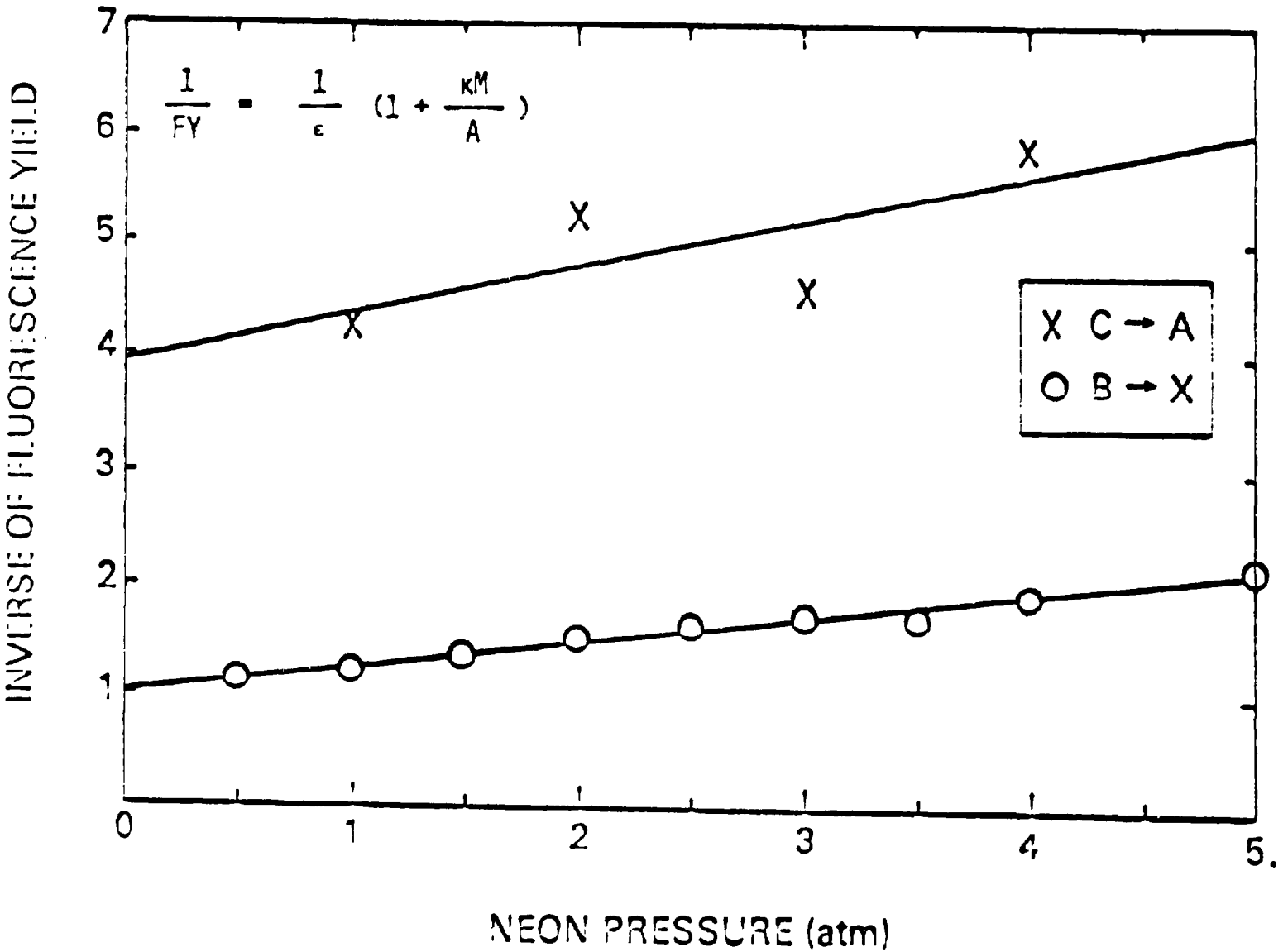
$\frac{1}{FY} = \frac{1}{\epsilon}\left(1 + \frac{KM}{A}\right)$
INVERSE OF FLUORESCENCE YIELD
NEON PRESSURE (atm)
X C → A
O B → X
0
1
2
3
4
5.
1
2
3
4
5
6
7

TEMPERATURE MODIFICATION

OF E-BEAM PUMPED XeCl LASER

- PERFORMANCE OF THE XeCl LASER IN THE RANGE OF -20°C TO 160°C HAS BEEN INVESTIGATED.
- WITHIN EXPERIMENTAL ERROR, NO CHANGE IN THE OUTPUT OF THE XeCl LASER WAS OBSERVED.
- THE USE OF DCl GIVES 15% IMPROVEMENT OVER HCl THROUGHOUT THE TEMPERATURE RANGE.

NRL

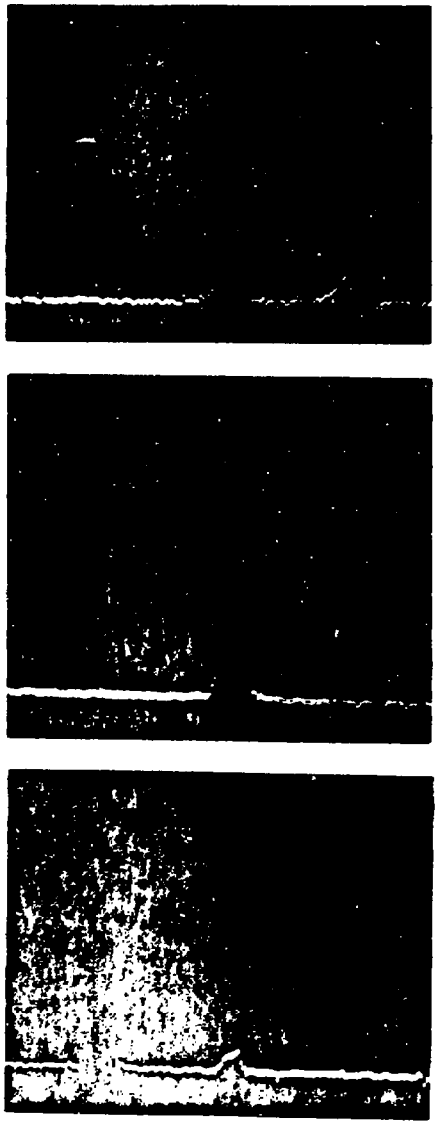

E-BEAM PUMPED XeCl LASER

- FORMATION INTO B AND C STATES TAKES PLACE AT AN EFFICIENCY OF 17%
- BEST INTRINSIC LASER EFFICIENCY OBSERVED TO DATE IS 6% MAINLY BECAUSE OF TRANSIENT ABSORPTION (~0.1 GAIN)
- LASER OPTIMIZES AT ROOM TEMPERATURE AT A TOTAL PRESSURE OF 4 ATM (Ne:Xe:HCl = 98.9:1.0:0.067)
- EXTRACTION IN BANDWIDTH < 0.1 cm^{-1} SHOULD BE POSSIBLE IN A LARGE PORTION OF 307.8-308.4 NM

NRL

Pb VAPOR RAMAN CONVERTER

Pump	XeCl at 308 nm
Output	459 nm
Temperature	1200° C
Density	10^{17} cm^{-3}
Gain	3×10^{-8} cm W^{-1}

NRL

PHOTON TRANSPORT IN SRS

$$\frac{\partial N_s}{\partial z} + \frac{1}{c}\frac{\partial N_s}{\partial t} = g_o (N_1 - N_f) N_p N_s$$

$$\frac{1}{c}\frac{\partial N_1}{\partial t} = -g_o (N_1 - N_f) N_p N_s$$

$$N_s + N_p = N_{so} + N_{po}$$

$$N_1 + N_f = N$$

NRL

APPROXIMATE SCALING OF SATURABLE RAMAN CONVERTER

- ASSUME CONSTANT PUMP ENERGY AND CONSTANT RAMAN MEDIUM NUMBER DENSITY

- LENGTH REQUIRED FOR EFFICIENT CONVERSION SCALES WITH PULSE DURATION APPROXIMATELY AS FOLLOWS

  GAIN CONSIDERATION: $t^{-1} A^{-1} \ell \sim$ CONST.

  VOLUME CONSIDERATION: $A\ell \sim$ CONST.

  THEREFORE: $\ell \sim t^{\frac{1}{2}}$

NRL

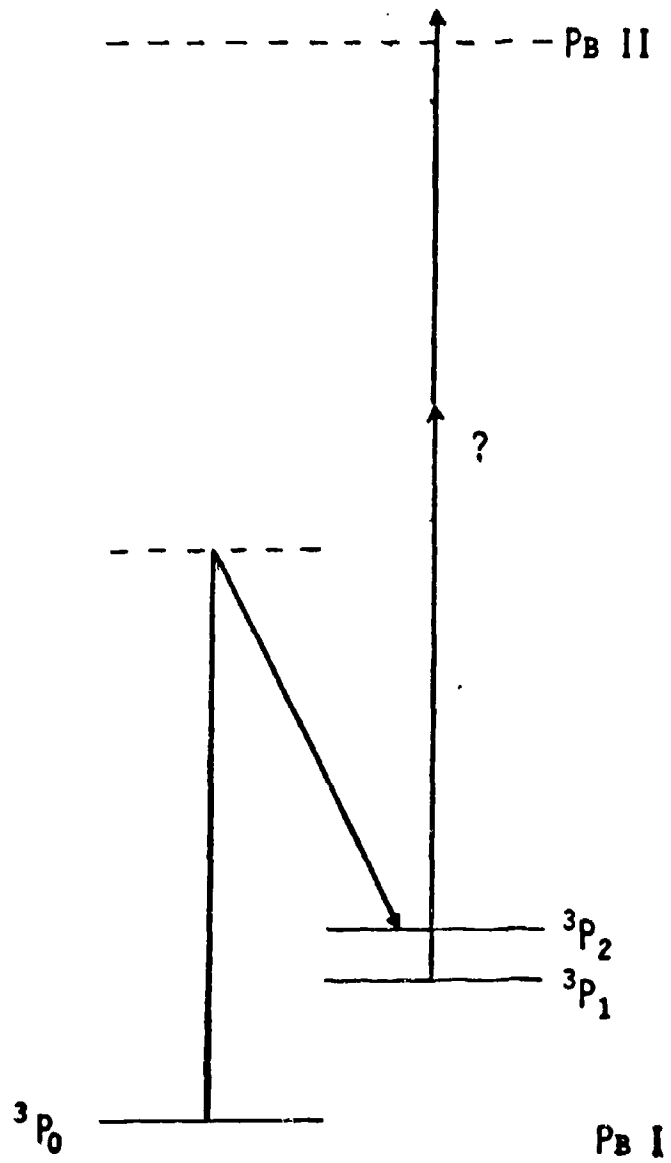
Pb II
?
$^3P_2$
$^3P_1$
$^3P_0$
Pb I

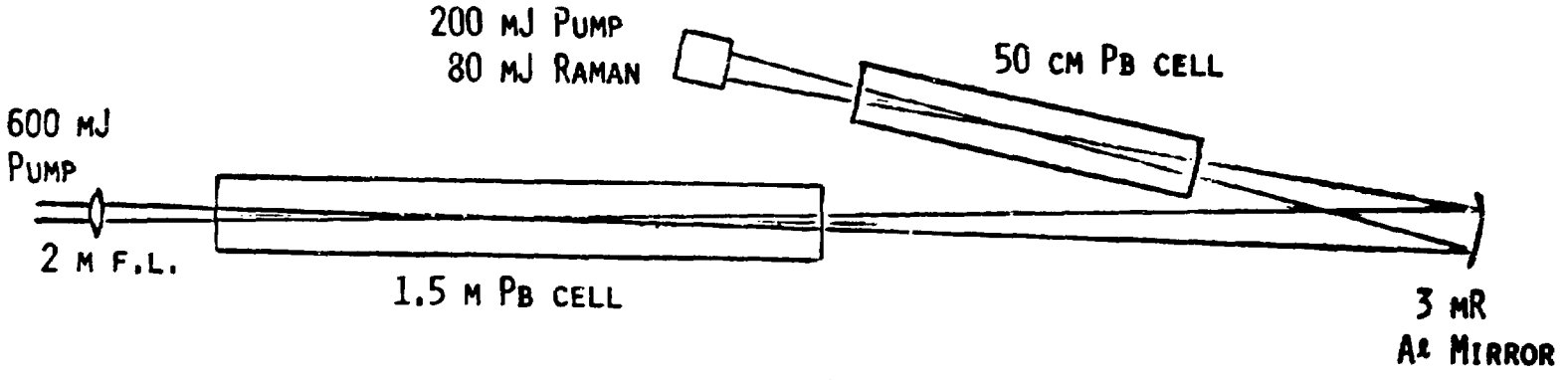
200 MJ PUMP
80 MJ RAMAN
50 CM PB CELL
600 MJ
PUMP
2 M F.L.
1.5 M PB CELL
3 MR
Al MIRROR

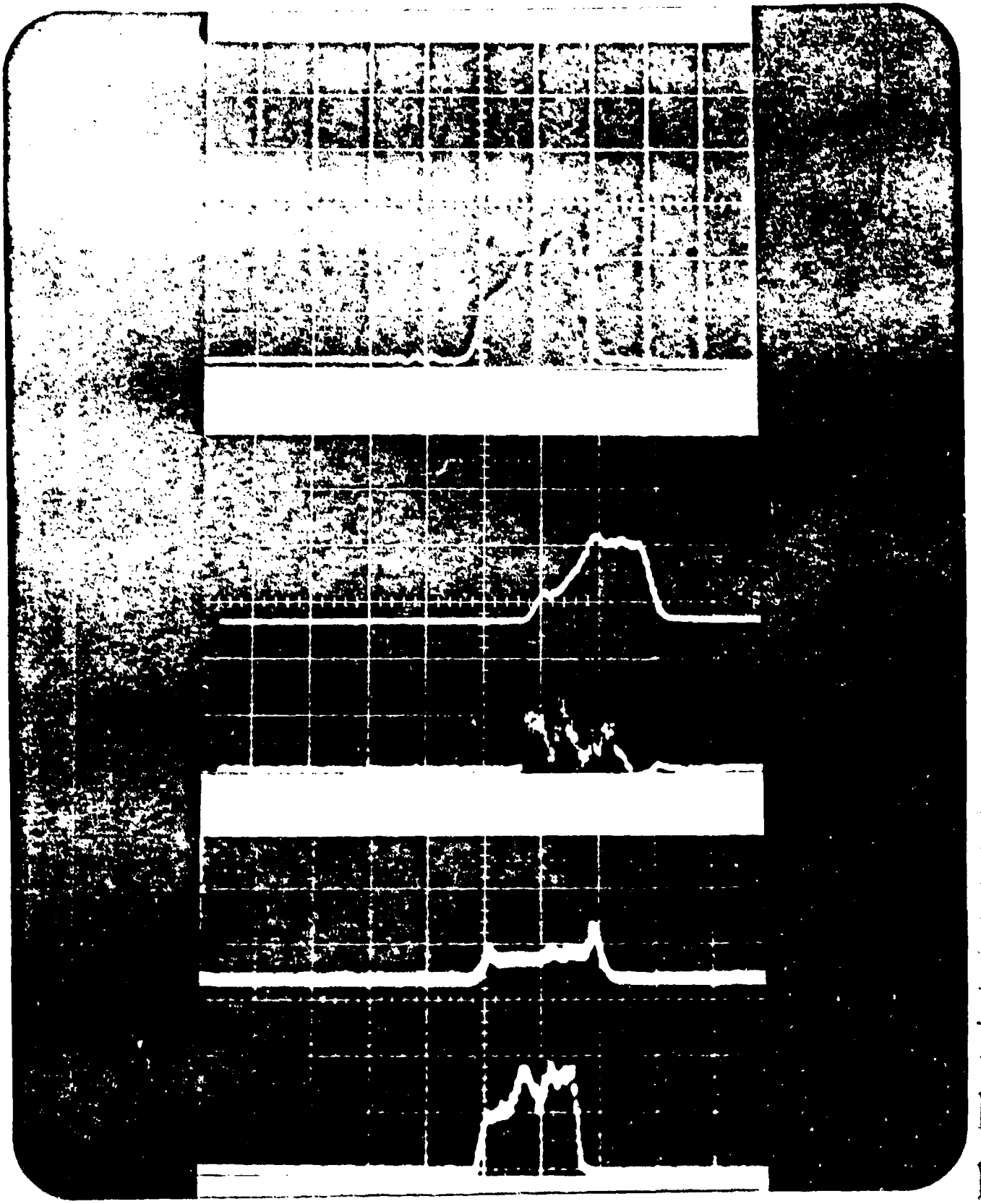

CONCLUSIONS FROM LONG PULSE CONVERSION EXPERIMENT

- ENERGY CONVERSION EFFICIENCY OF 40% DEMONSTRATED FOR 400 NSEC PUMP PULSE
- NO ANAOMALOUS BEHAVIOR OBSERVED
- Pb VAPOR CELLS OF REASONABLE LENGTH ARE ADEQUATE FOR CONVERTING LONG XeCl PUMP PULSE

NRL

SCALING TO 10 J XeCl PUMP

- JOINT NRL/MAXWELL EXPERIMENT TO BE CARRIED OUT WITH MLI'S 40 1 DEVICE
- TWO 3 M Pb VAPOR CELLS AND A COLLIMATED BEAM OF 1.5-2 CM DIAMETER WILL BE USED
- RESULTS WILL BE COMPARED WITH PREDICTIONS TO CHECK ADEQUACY OF UNDERSTANDING

NRL

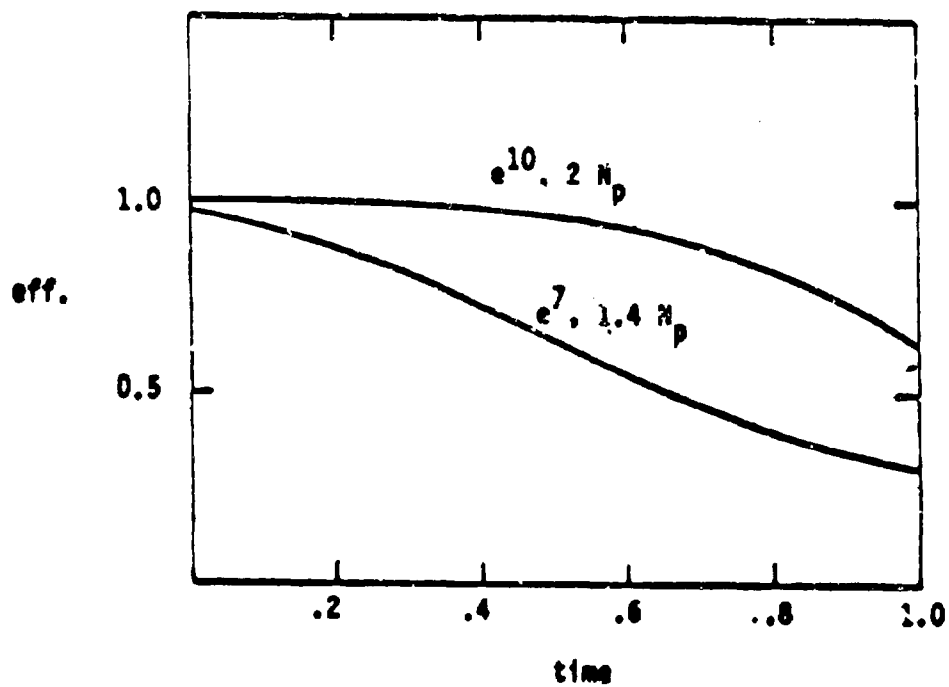
1.0
0.5
eff.
e^{10}, 2 N_p
e^{7}, 1.4 N_p
.2
.4
.6
.8
1.0
time

ESTIMATES OF PRESSURE WAVES

- ACOUSTIC PRESSURE PROPAGATION EQUATION:

$$\nabla^2 p - \frac{1}{c^2}\frac{\partial^2 p}{\partial t^2} = -\frac{\beta}{c_p}\frac{\partial H}{\partial t}$$

- IN UNBOUNDED SPACE

$$p(\bar{r},t) = \frac{\beta}{4\pi c_p}\int dV_o \frac{H'(\bar{r}_o, t - R/c)}{R}$$

- CONVERSION OF 1 KJ PULSE IN 10 M X 20 CM DIA. CELL DEPOSITS APPROXIMATELY 1 MJ CM^{-3} IN MEDIUM.

- IN MIXTURE OF (HE: P_B = 10:1) AND FOR $H(t) = H_o (e^{-kt} - e^{-2kt})$, INITIAL AMPLITUDE OF PRESSURE WAVE SCALES WITH k AS

$$\Delta p \text{ (torr)} \sim 10^{-8} \; k^2 \; (\text{sec}^{-2})$$

- IN 10 MSEC, PRESSURE WAVE HITS WALL ~ 30 TIMES

CONCLUSIONS FROM

P_B VAPOR MEDIUM QUALITY ANALYSIS

- FOR N (P_B) = 10^{17} CM^{-3} AND N (HE) = 2 x 10^{18} CM^{-3}, 1.3 D.L. BEAM IMPLIES $\Delta\rho/\rho$ = 10^{-3} (RANDOM) TO 10^{-4} (ORDERED) FOR 10 M LENGTH.
- PRELIMINARY ANALYSIS INDICATES THAT MEDIUM UNIFORMITY IN P_B VAPOR CELL SHOULD BE ADEQUATE AT $\sim$ 100 Hz.
- DETAILED MODELING OF ACOUSTIC WAVES WOULD REQUIRE KNOWLEDGE OF RATE OF HEAT DEPOSITION AND BOUNDARY CONDITIONS.

NRL

SRI International

TUNABLE BLUE-GREEN LASER DEVELOPMENT

At

SRI INTERNATIONAL

Research Staff

W. K. Bischel
G. Black
D. J. Eckstrom
D. L. Huestis
D. C. Lorents*
H. H. Nakano*
K. Y. Tang
R. A. Tilton**
H. C. Walker, Jr.

*Present Address: Hewlett Packard, Palo Alto CA

**Permanent Address: Miami University, Ohio

MP 80-36

Presented at the Fourth Strategic Blue-Green Laser Communication Meeting, San Diego, CA March, 1980

SRI International

333 Ravenswood Ave. • Menlo Park, California 94025
(415) 326-6200 • Cable: SRI INTL MPK • TWX: 910-373-1246

PHOTOLYTICALLY PUMPED XeF(C-A) BLUE-GREEN LASER DEVELOPMENT

Presented by D. J. Eckstrom

Background and Review

Summary of Supporting Kinetics Experiments

New Measurements

- Fluorescence Spectrum and Intensities
- Gain/Absorption Results
- New Laser Experiments

Conclusions and Status

Scale-up Design

Open Discharge Photolytic Pumping Concept

SCHEMATIC XeF POTENTIAL CURVES
SHOWING B 1/2 – C 3/2 SPLITTING

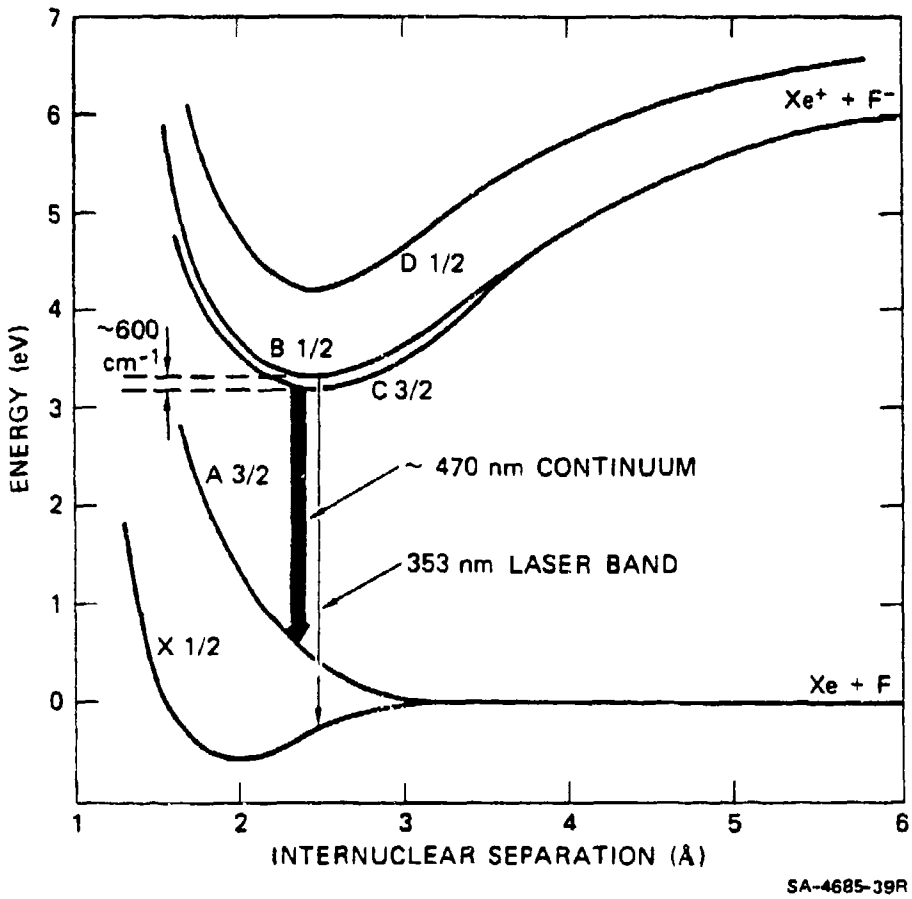

XeF(C-A) LASER DEMONSTRATIONS

Photolytic	Bischel, et al. A.P.L. 34, 565 (1979)	SRI
	Zuev, et al.	Lebedev Inst.
	Powell, et al.	LLL
Discharge	Burnham A.P.L. 35, 48 (1978)	NRL
	Fisher, et al. A.P.L. 35, 26 (1979)	MSNW
E-Beam	Ernst and Tittel A.P.L. 35, 36 (1979)	Rice U.

Why Photolytic?

- No electrons
  - Favorable C/B population ratio
  - No ionic absorbers
- Clean excitation, simplified kinetics

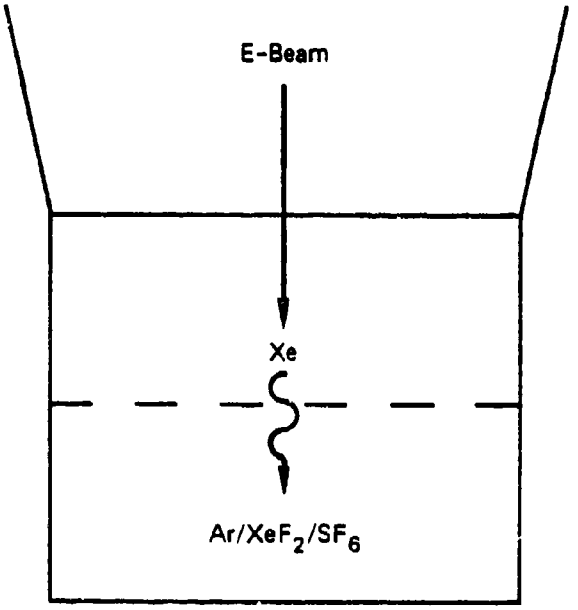

SA-6158-122

FLUORESCENCE PUMPING

$e\text{-BEAM} + Xe \rightarrow Xe^{+} \rightarrow Xe_2^{*} \rightarrow h\nu(172\ nm)$

$h\nu(172\ nm) + XeF_2 \rightarrow XeF^{*} + F$

$XeF^{*} + M \rightarrow XeF(C) + M$

$XeF(C) + h\nu(483\ nm) \rightarrow Xe + F + 2h\nu$

3

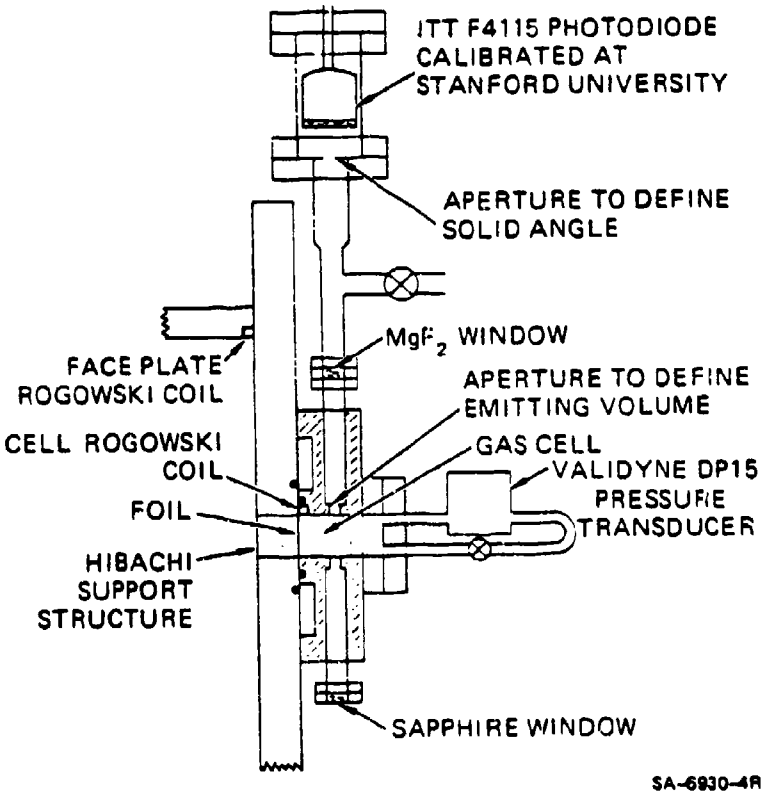
ITT F4115 PHOTODIODE
CALIBRATED AT
STANFORD UNIVERSITY
APERTURE TO DEFINE
SOLID ANGLE
MgF_2 WINDOW
FACE PLATE
ROGOWSKI COIL
APERTURE TO DEFINE
EMITTING VOLUME
CELL ROGOWSKI
COIL
GAS CELL
VALIDYNE DP15
PRESSURE
TRANSDUCER
FOIL
HIBACHI
SUPPORT
STRUCTURE
SAPPHIRE WINDOW
SA-6930-4R

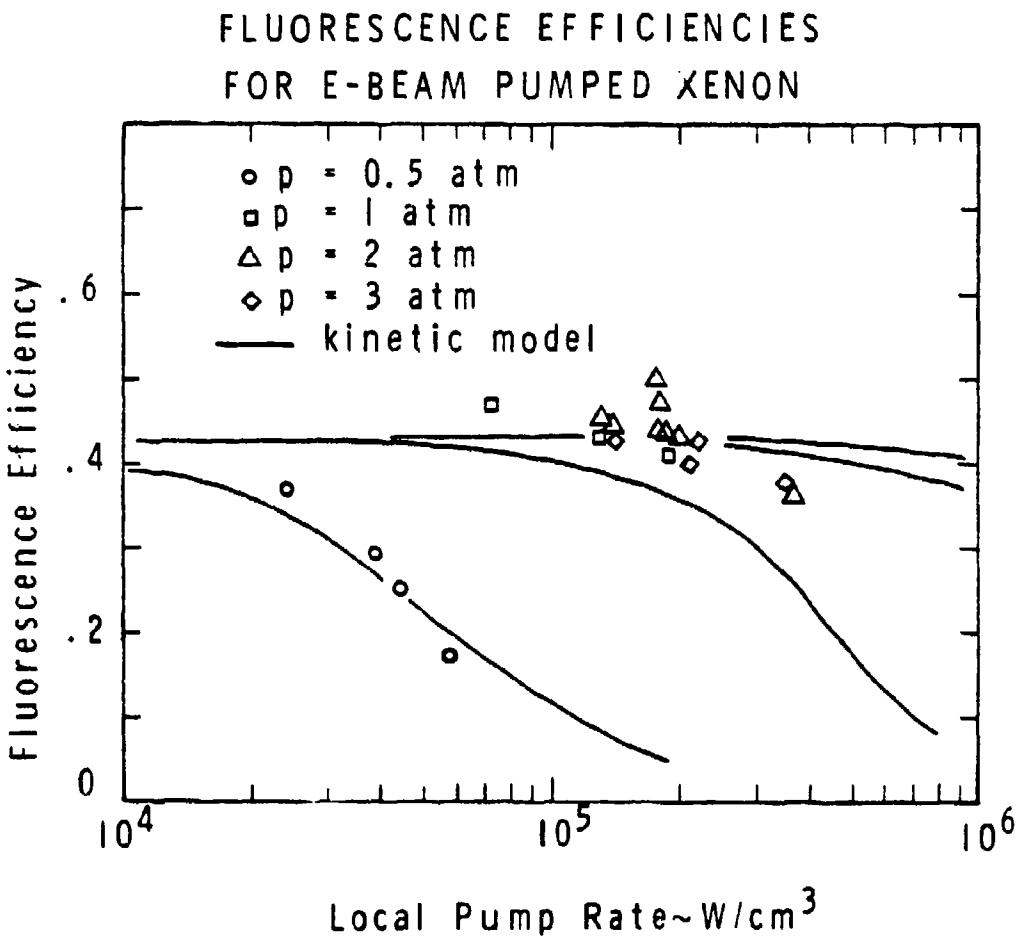
FLUORESCENCE EFFICIENCIES
FOR E-BEAM PUMPED XENON
p = 0.5 atm
p = 1 atm
p = 2 atm
p = 3 atm
kinetic model
Fluorescence Efficiency
.6
.4
.2
0
10^4
10^5
10^6
Local Pump Rate~W/cm^3

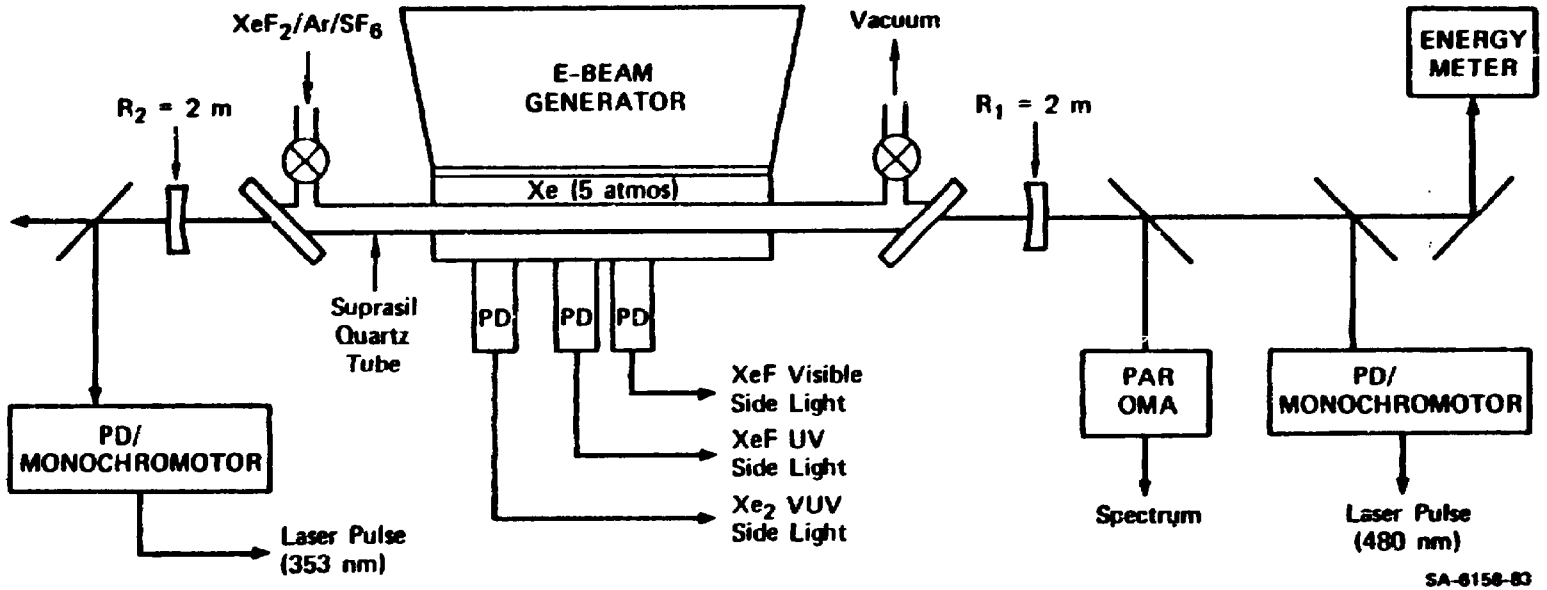
$XeF_2/Ar/SF_6$
E-BEAM GENERATOR
Vacuum
ENERGY METER
R_2 = 2 m
R_1 = 2 m
Xe (5 atmos)
Suprasil Quartz Tube
PD
PD
PD
XeF Visible Side Light
XeF UV Side Light
Xe_2 VUV Side Light
PD/ MONOCHROMOTOR
Laser Pulse (353 nm)
PAR OMA
Spectrum
PD/ MONOCHROMOTOR
Laser Pulse (480 nm)
SA-6158-83

XeF(C-A) LASER ISSUES - 1979

KINETICS ISSUES

- XeF_2 Absorption Cross Sections
- Excited State Quantum Yield
- XeF(C) Lifetime, Quenching, Mixing

LASER CHARACTERIZATION

- Fluorescence Intensities (B and C) and Spectrum
  - B/C Laser Competition
  - Quenching (XeF_2, F)
  - Gain Cross-sections, Calculated
  - Electron mixing effects (photoionization)
- Gain/Absorption
  - Background Absorptions (extraction efficiency)
- Laser Demonstrations
  - Time Histories
  - B/C Competition
  - Absorptions
  - Tunability

OVERLAP BETWEEN XeF_2 ABSORPTION AND Xe_2^* FLUORESCENCE

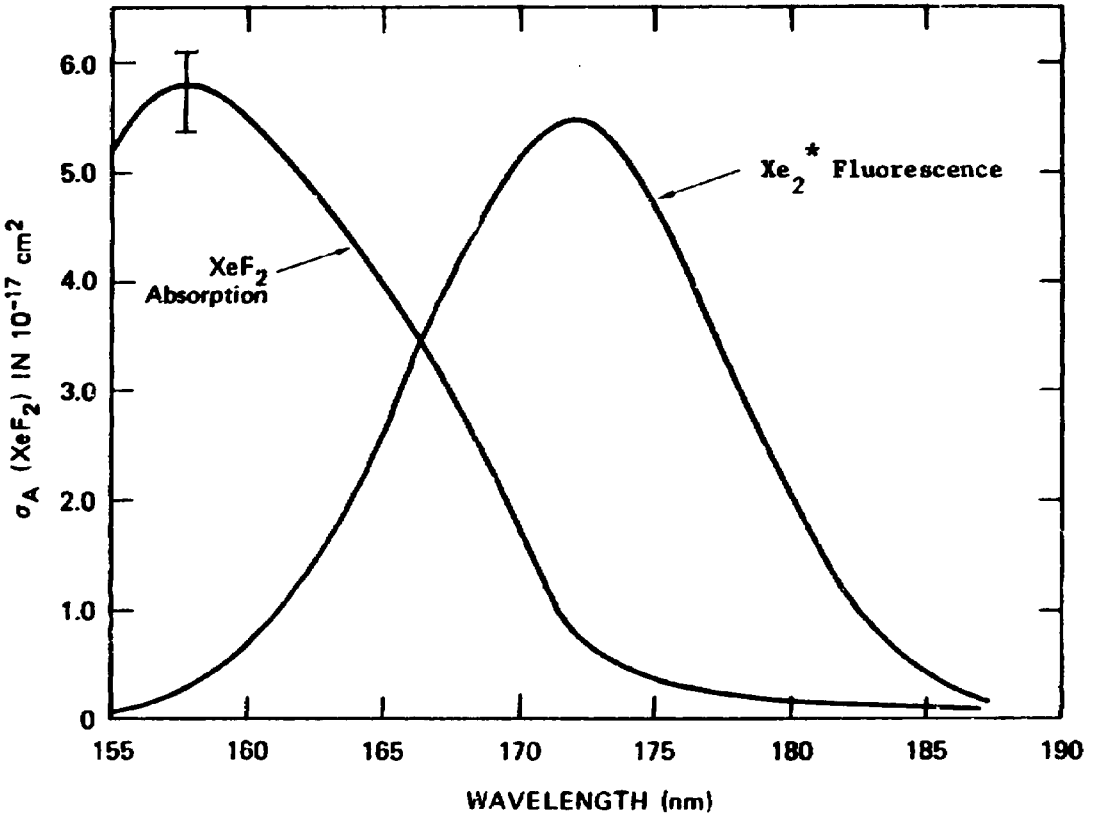

QUANTUM YIELDS

Measurements normalized to $O(^1S)$ from N_2O *
(in presence of Xe)

B state

$QY = 0.9^{+0.1}_{-0.2}$

Constant 145 nm < λ < 175 nm

C state

QY = 0.08 ± 0.02 at 157.5 nm

Decreases by ~40% between 146 and 172 nm

[Previous work QY(C) <0.1 QY(B)]

D state

QY = 0.028 ± 0.005 at 155 nm

Decreases by factor of at least 2 between 155 and 165 nm

*G. Black, R. L. Sharpless, T. G. Slanger, and D. C. Lorents, J. Chem. Phys. 62, 4266 (1975)

SUMMARY OF MEASURED RATES FOR XeF^*

Radiative Lifetimes

C state: $\tau_C = 101 \pm 5$ sec

B state: $\tau_B = 13.3 \pm 0.2$ sec

Quenching / B-C Mixing

Rate / Gas	Quenching		Mixing
	B State (cm^3/sec)	C State (cm^3/sec)	B→C (cm^3/sec)
XeF_2	7.4×10^{-10}	4.75×10^{-10}	---
Ar	---	$7 \pm 7 \times 10^{-15}$	$1.4 \pm 0.2 \times 10^{-11}$
N_2	---	$\leq 2.5 \times 10^{-14}$	$5.7 \pm 0.3 \times 10^{-11}$
SF_6	---	$\leq 9 \times 10^{-14}$	$8 \pm 1 \times 10^{-11}$
Xe	1.9×10^{-10}		1.5×10^{-10}

TYPICAL DATA SET
2 torr XeF, 30 psia Ar
Time scale - 0.2 μsec/cm

E-BEAM PARAMETERS

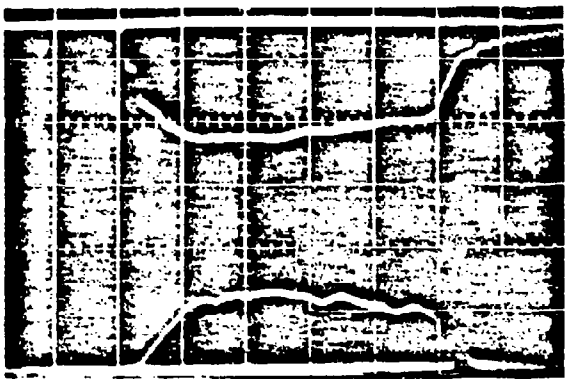

Voltage = 350 kV

Current = 12 A/cm^2

FLUORESCENCE

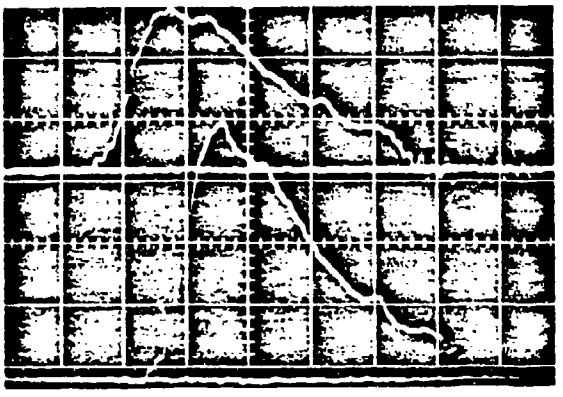

UV
$340 < \lambda < 360$
$\dot{F}_{uv} = 1.2 \times 10^{22}$ photons/cm^3 sec

Visible
$\lambda > 400$ nm
$\dot{F}_{vis} = 1.4 \times 10^{22}$ photons/cm^3 sec

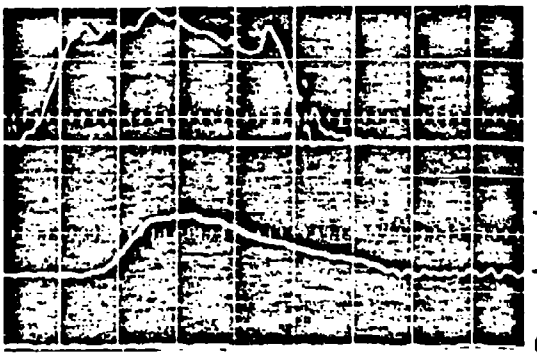

VUV
$\lambda < 250$ nm
$\dot{F}_{vuv} = 8 \times 10^{23}$ photons/cm^3 sec
$\sim 3 \times 10^5$ W/cm^2 on tube

GAIN MEASUREMENT

$-I$

$-I_o$

0

$\lambda = 501.7$ nm
$g = 5.8 \times 10^{-3}$/cm

SA-6158-116

B/C STATE FLUORESCENCE INTENSITY RATIOS

- Intensity ratio from kinetic theory

$$\frac{I(B)}{I(C)} = \frac{A_B}{A_C}\frac{k_{CB}}{k_{BC}} + \frac{A_B}{k_{BC}}\frac{1}{[R_g]}\left(1 + \frac{k_C}{A_C}[XeF_2]\right)$$

$A_B = 7.5\times10^7$/sec, $A_C = 9.9\times10^6$

$k_C = 4.75\times10^{-10}$ cm^3/sec

$k_{BC}/k_{CB} = 22.8$

- Argon Buffer $K_{BC} = 1.3\times10^{-11}$ cm^3/sec

$$\frac{I(B)}{I(C)} = 0.333 + \frac{14.5}{[R_g]}$$

- N_2 Buffer $K_{BC} = 5.7\times10^{-11}$ cm^3/sec

$$\frac{I(B)}{I(C)} = 0.333 + \frac{3.3}{[R_g]}$$

-$[R_g]$ in units of PSIA-

B/C STATE FLUORESCENCE RATIOS

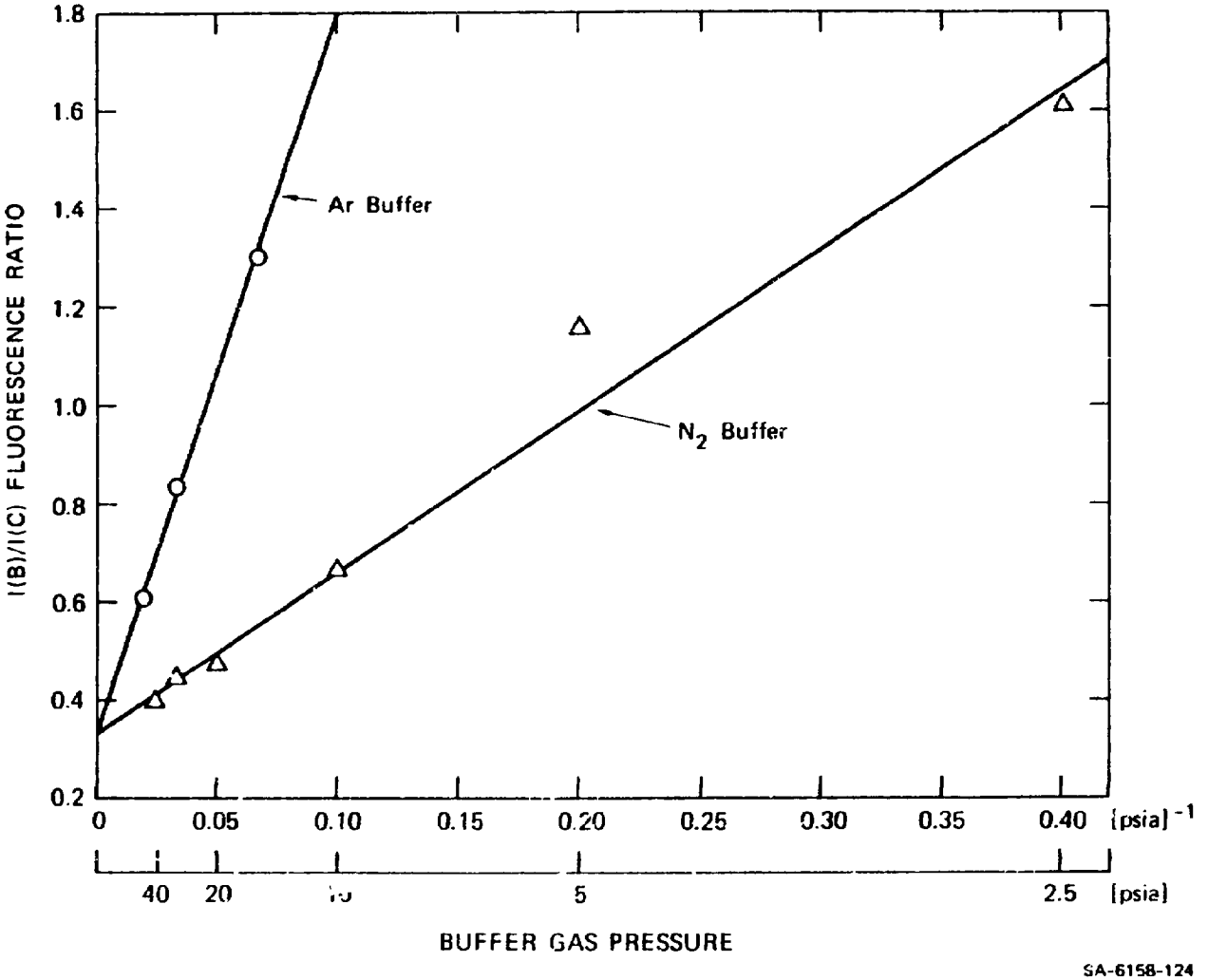

SA-6158-124

FLUORESCENCE RATIO VERSUS TIME

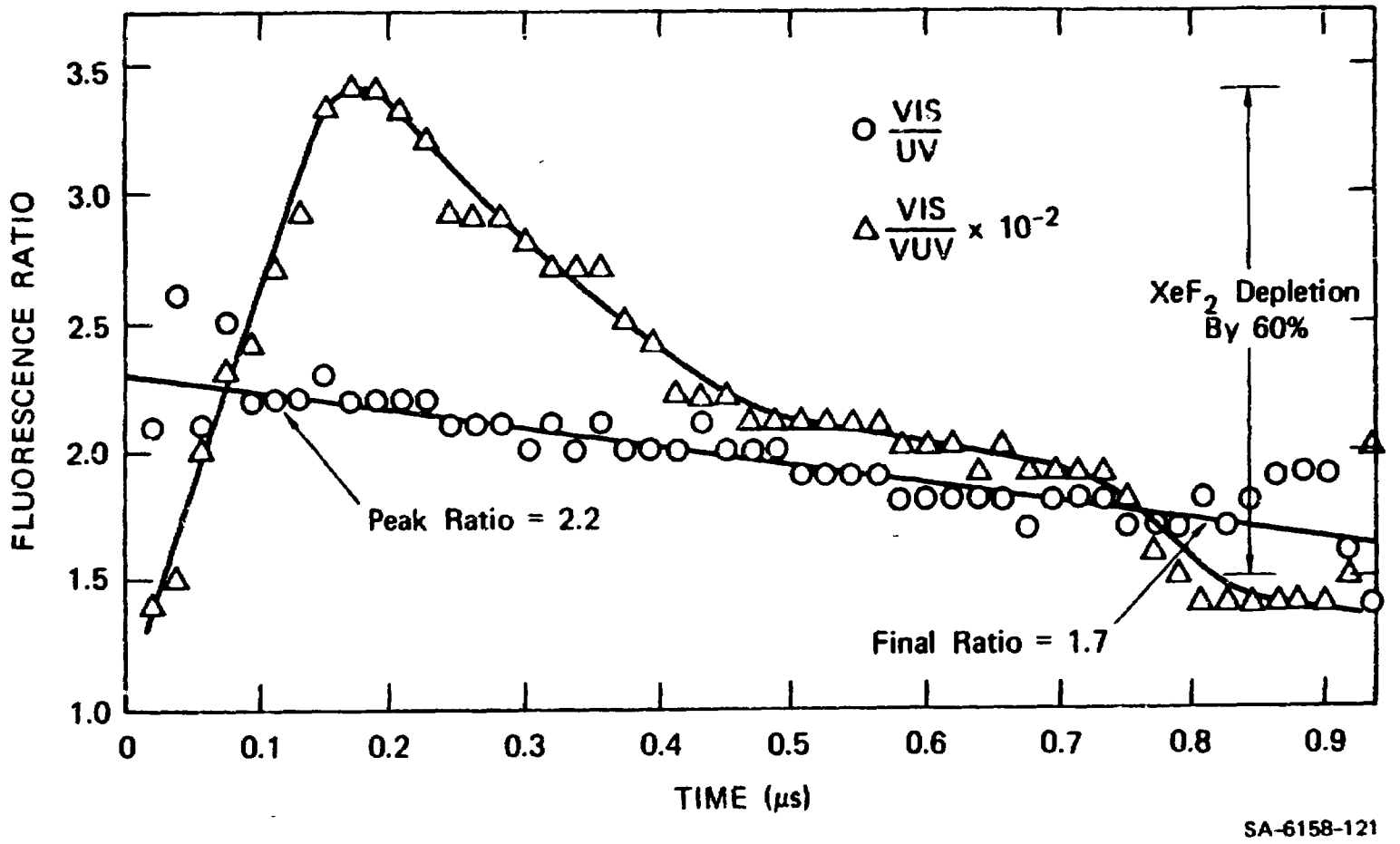

EXPERIMENTAL APPROACH

- Gain cross section

$$\sigma_g = \ell n\ (I/I_0)/L\ N^*$$

where

$N^* = \dot{F}_{vis}$ (#/cm^3-sec)/A

A = 10^7/sec

L = 100 cm

- Calculated gain cross section

$$\sigma_g = \frac{A}{8\pi c}\ \lambda^4\ \frac{f(\lambda)}{\int f(\lambda)\, d\lambda}$$

FLUORESCENCE SPECTRUM WITH ARGON AND NITROGEN BUFFER

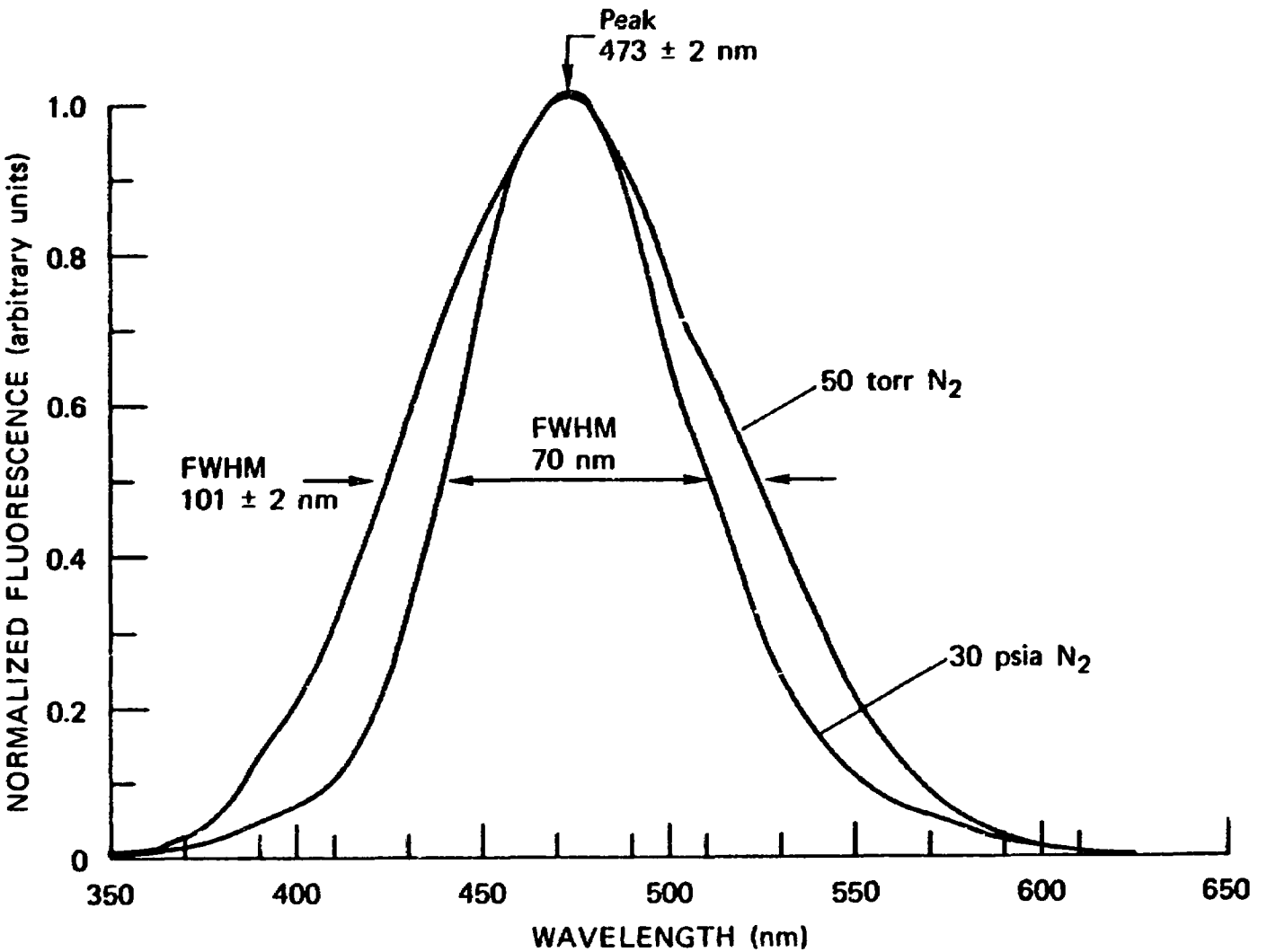

SA-6158-120

FLUORESCENCE SPECTRUM WITH ARGON AND ARGON BUFFER

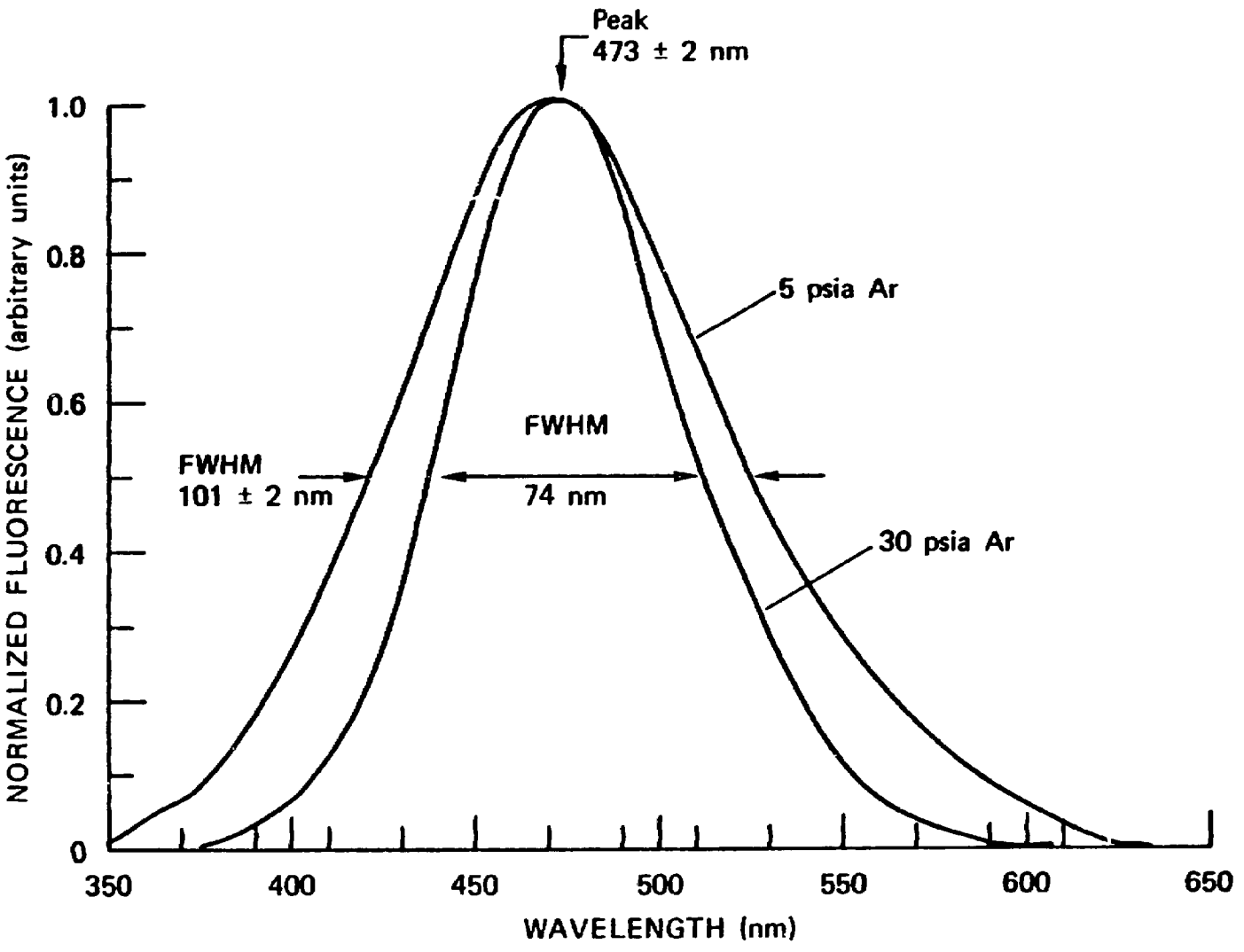

SA-6158-120

CALCULATED AND MEASURED CROSS SECTION

NITROGEN BUFFER

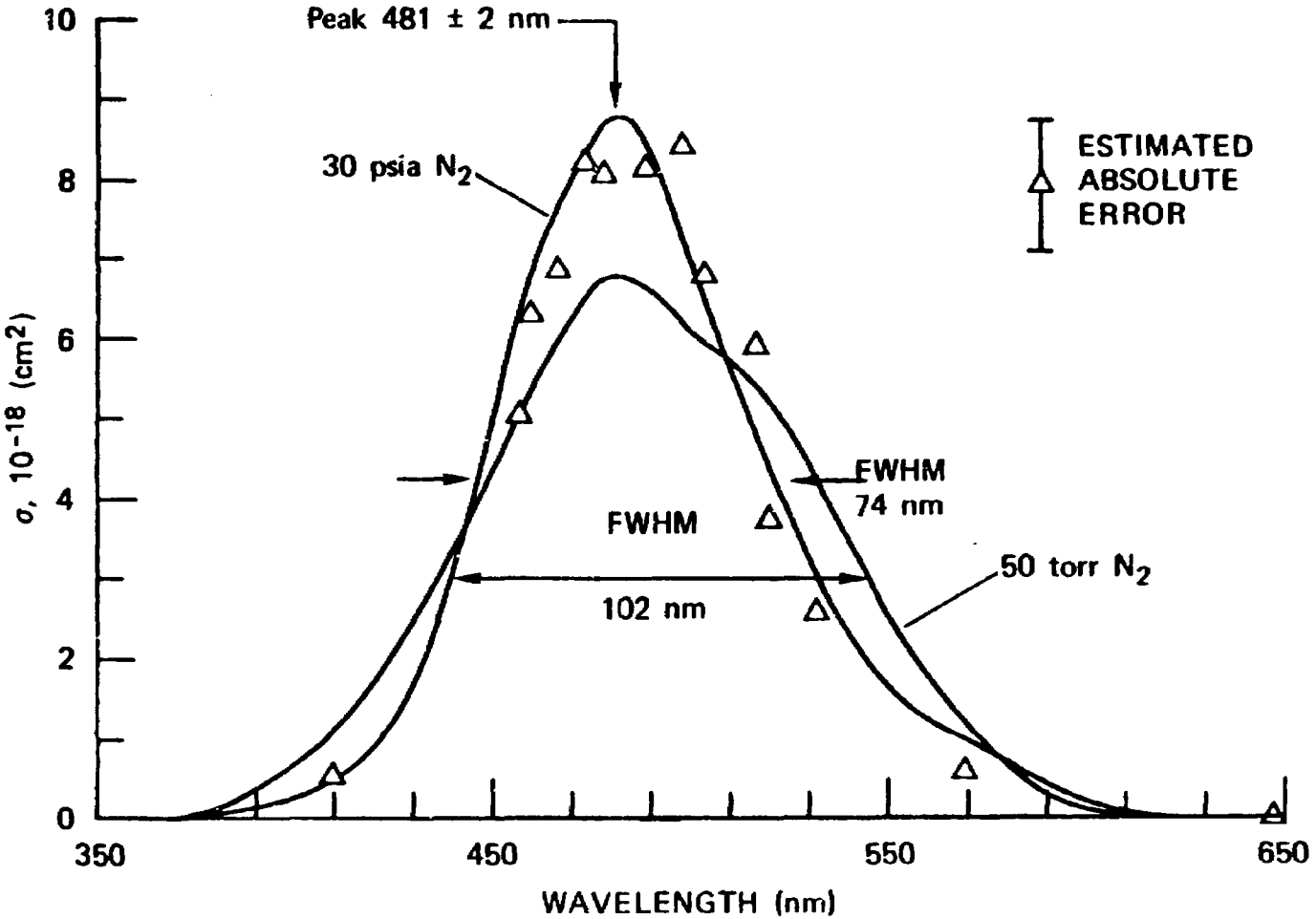

SA-6158-119

CALCULATED AND MEASURED CROSS SECTION
ARGON BUFFER

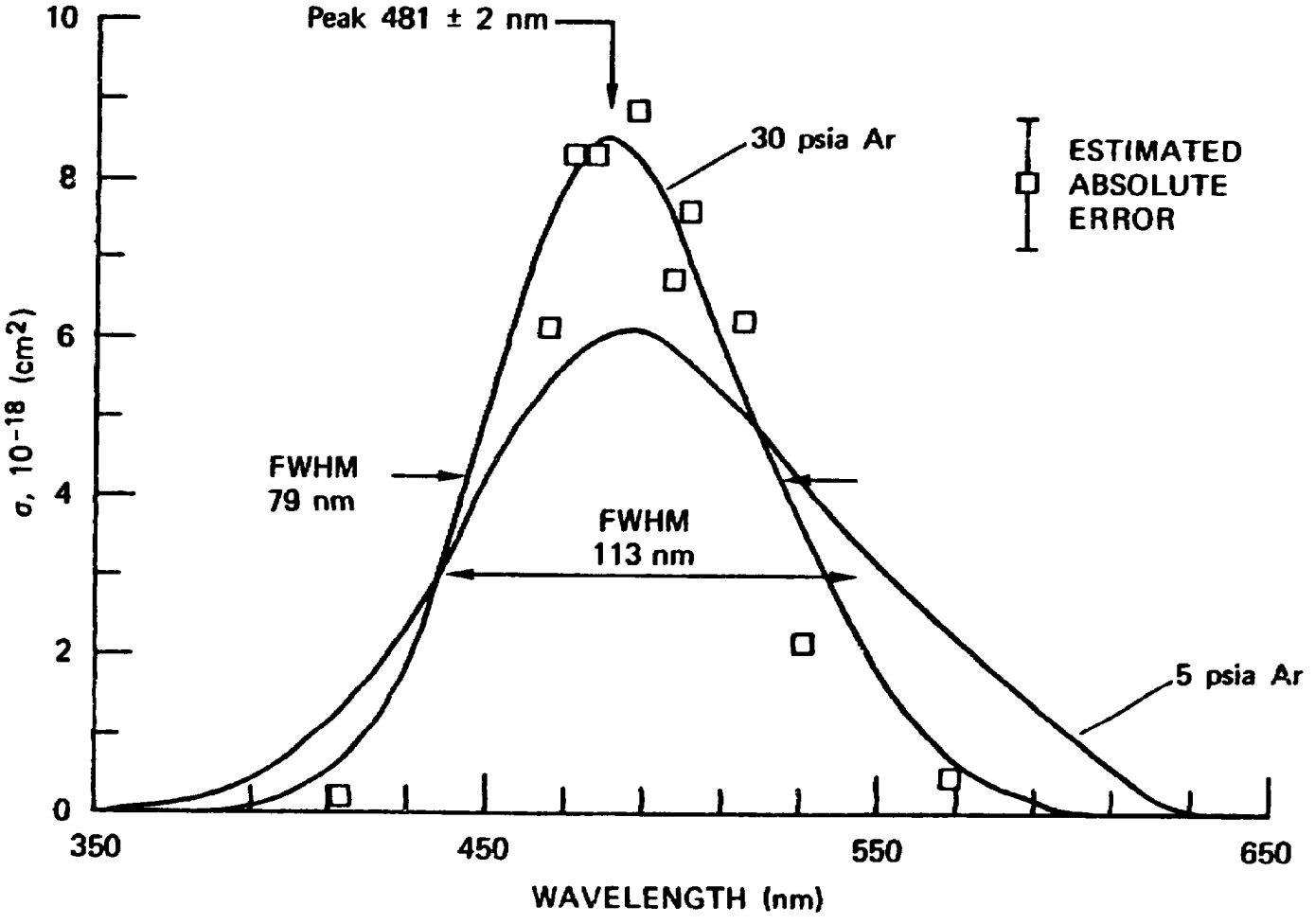

SA-6158-119

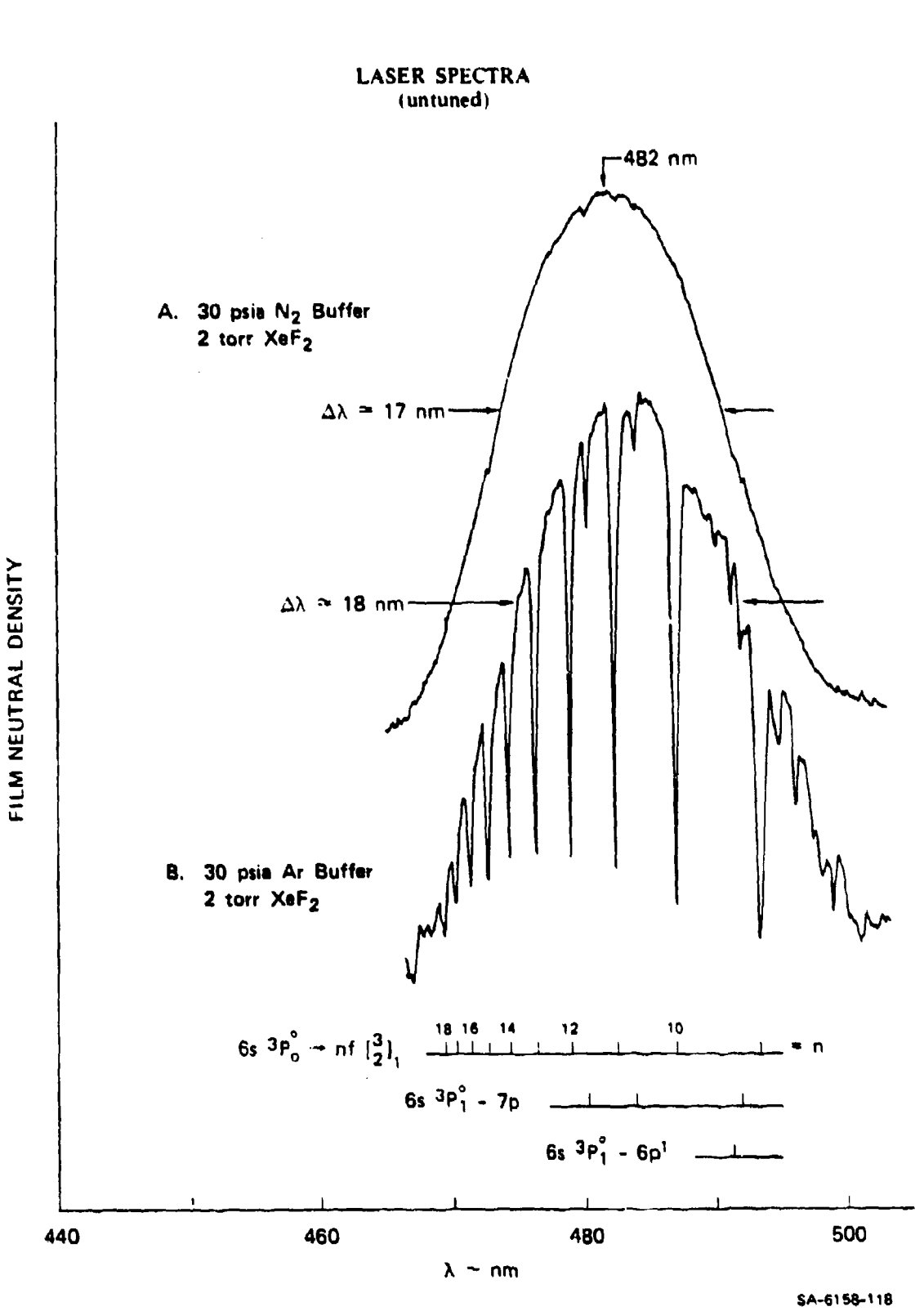
LASER SPECTRA
(untuned)
482 nm
A. 30 psia N_2 Buffer
2 torr XeF_2
$\Delta\lambda \simeq 17$ nm
$\Delta\lambda \simeq 18$ nm
B. 30 psia Ar Buffer
2 torr XeF_2
FILM NEUTRAL DENSITY
18 16 14 12 10
$6s\ ^3P_0^\circ \rightarrow nf\ [\frac{3}{2}]_1$
= n
$6s\ ^3P_1^\circ$ - 7p
$6s\ ^3P_1^\circ$ - $6p^1$
440
460
480
500
λ ~ nm
SA-6158-118

PARTIAL ENERGY LEVEL DIAGRAM FOR XeF_2, XeF, AND Xe

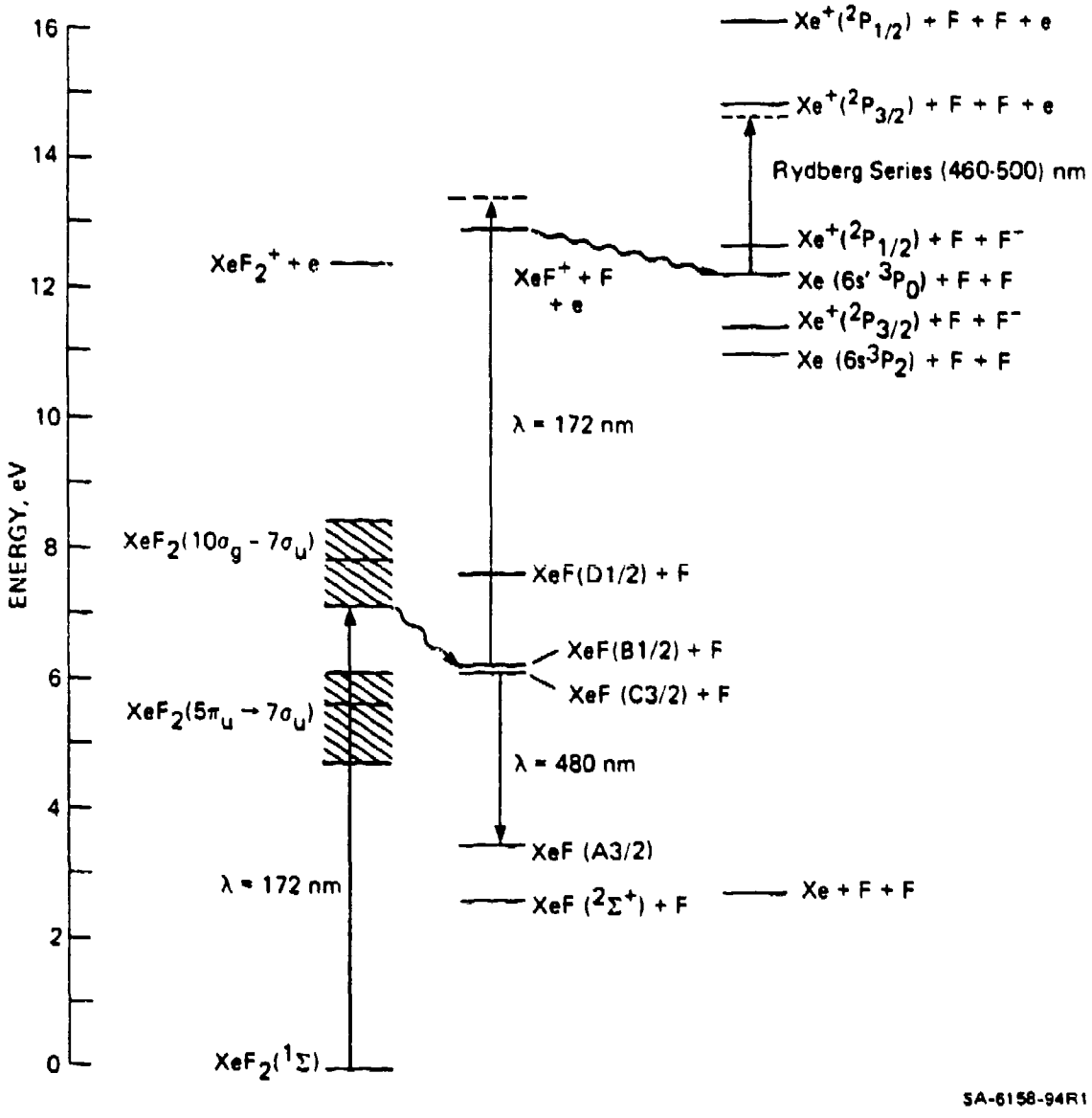

SA-6158-94R1

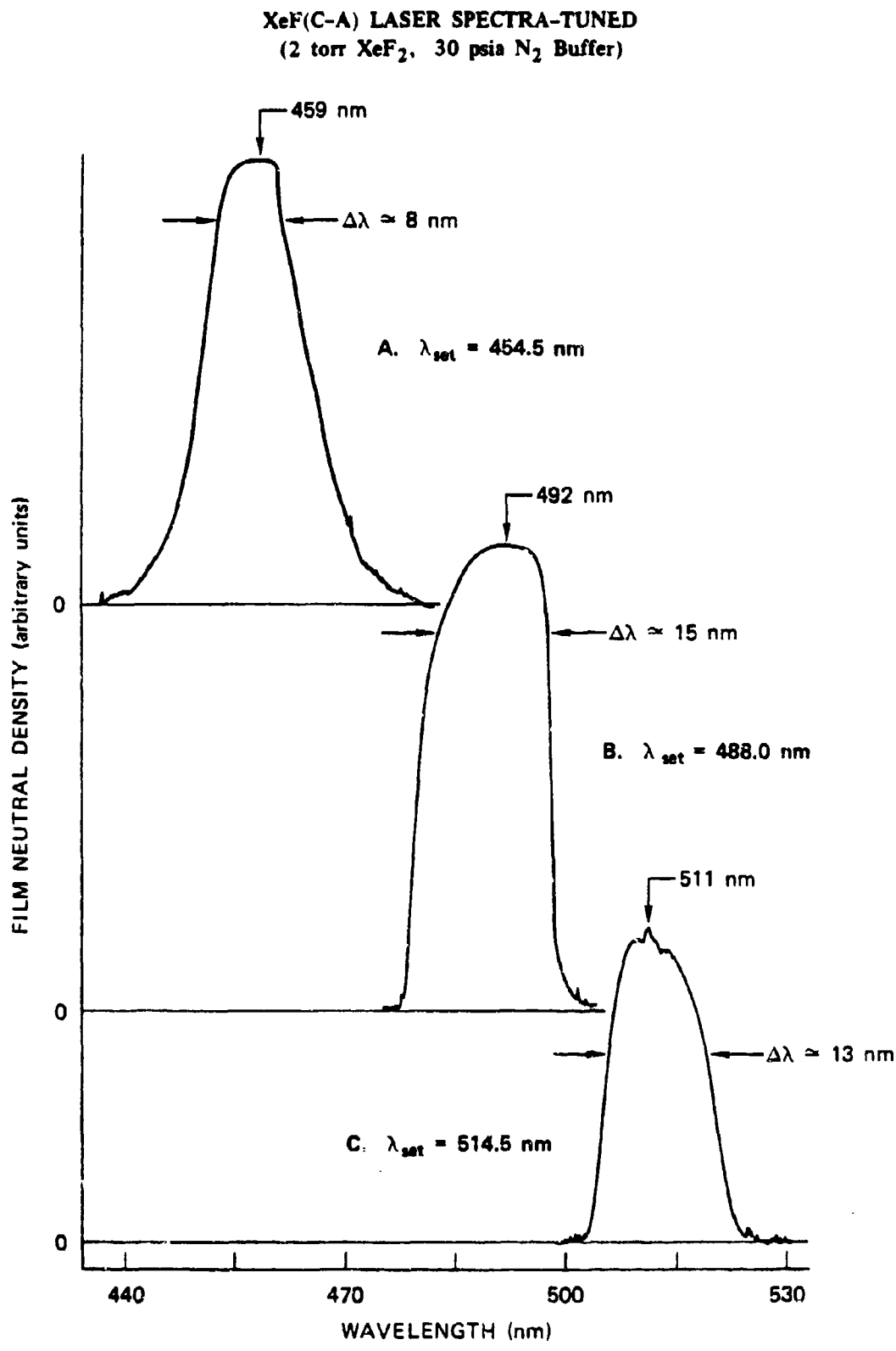
XeF(C-A) LASER SPECTRA-TUNED
(2 torr XeF2, 30 psia N2 Buffer)
459 nm
Δλ ≃ 8 nm
A. λset = 454.5 nm
492 nm
Δλ ≃ 15 nm
B. λset = 488.0 nm
511 nm
Δλ ≃ 13 nm
C. λset = 514.5 nm
FILM NEUTRAL DENSITY (arbitrary units)
0
0
0
440
470
500
530
WAVELENGTH (nm)
SA-6158-117

CONCLUSIONS

Gain/Absorption

- May be weak background continuum absorption with Ar buffer
- No background continuum absorption with N_2 buffer
- Discrete line absorptions suppressed with N_2 buffer

Photoionization

- Does not affect intensity ratios at low pump rates
- Discrete line absorptions suppressed with N_2 buffer

Quenching

- Some evidence that F-atom quenching is important

B/C Competition

- No B - X lasing observed in these experiments

Tunability

- Demonstrated lasing from 454 to 525 nm

STATUS

Kinetics Issues

- Quenching of XeF^* by F atoms and electrons
- Photoionization cross sections for XeF^* near 170 nm

Laser Issues

- Coupling of VUV to laser medium (spatial and spectral)
- Energy extraction from medium with spatial and temporal nonuniformities
- Competition from B-X superfluorescence

Systems Issues

- Recycling of XeF_2/N_2 mixture
- Laser tuning and frequency narrowing to match detector characteristics

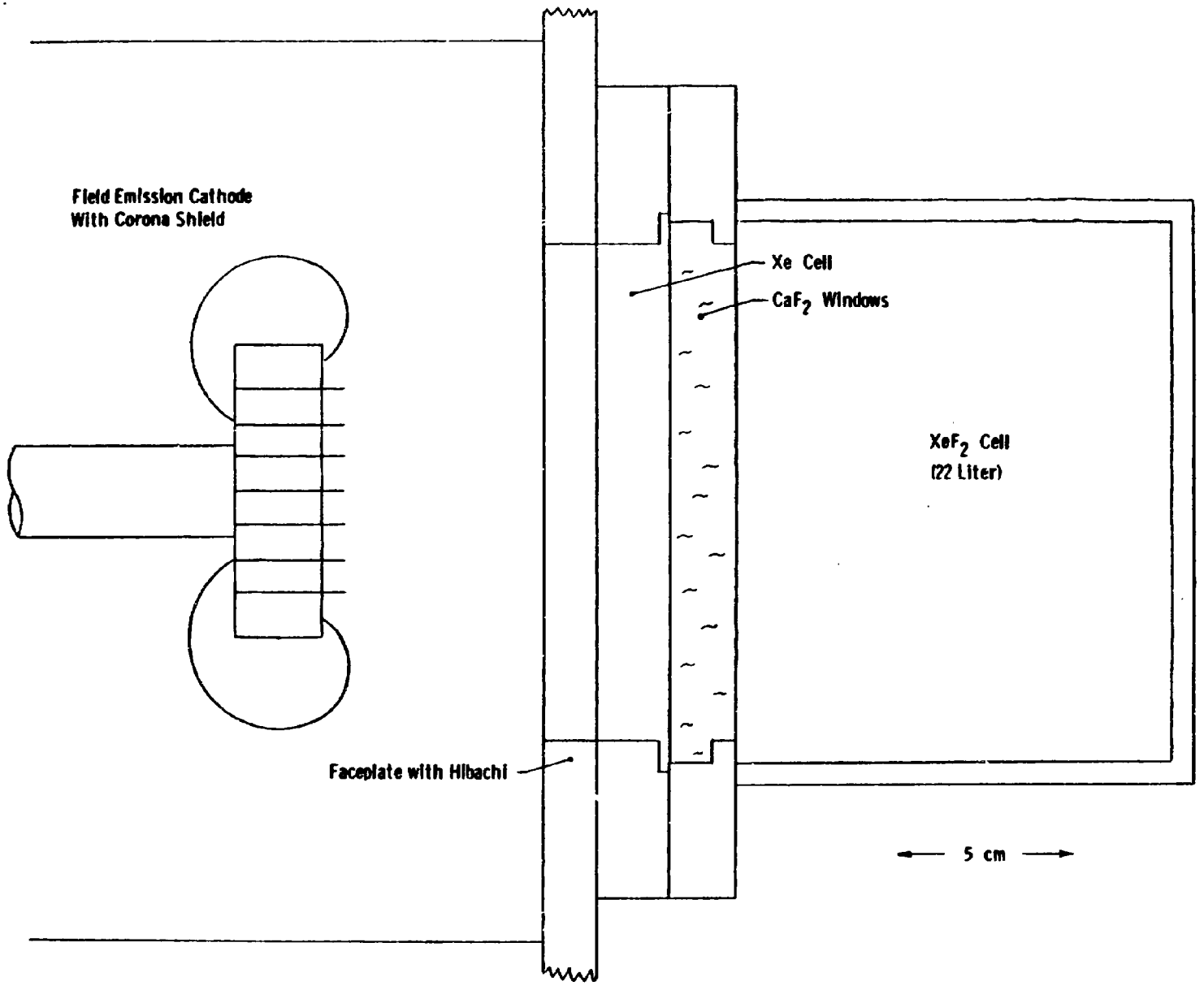
Field Emission Cathode
With Corona Shield
Xe Cell
CaF_2 Windows
XeF_2 Cell
(22 Liter)
Faceplate with Hibachi
5 cm

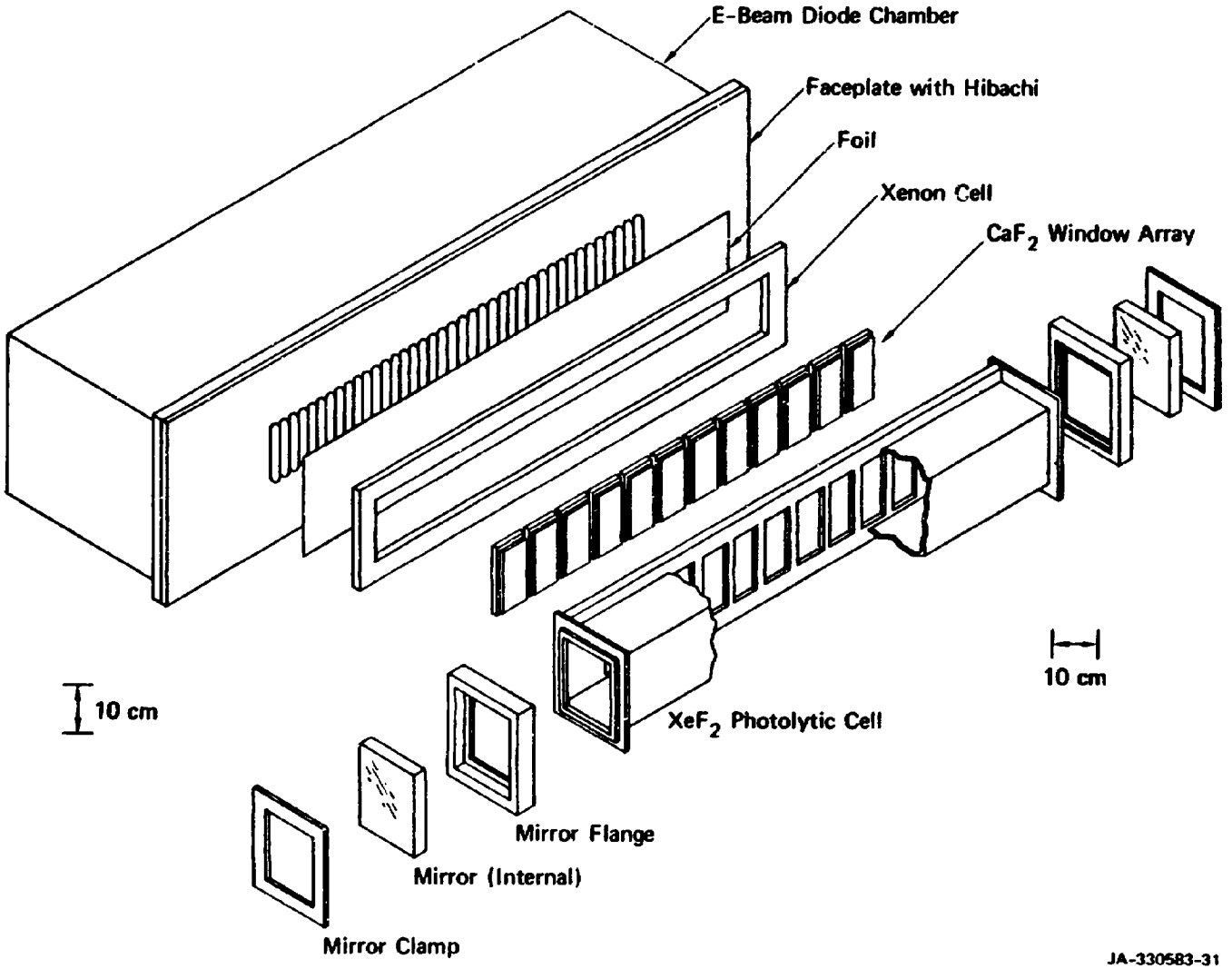

FIGURE SRI LARGE APERTURE PHOTOLYTICALLY PUMPED LASER

The Xe_2Cl Blue-Green Laser the first of a new class of lasers based on the triatomic rare gas halides

K. Y. Tang and D. L. Huestis
Molecular Physics Laboratory
SRI International
Menlo Park, CA 94025

DISCOVERY OF THE TRIATOMIC RARE GAS HALIDES, Rg_2X

- Companion Emission in RgX Laser Media

  ArF (193 nm) - Ar_2F (290 nm)
  KrF (248 nm) - Kr_2F (400 nm)
  XeCl (308 nn) - Xe_2Cl (490 nm)

- Products of Interception and Quenching

  $Rg_2^* + X_2 \longrightarrow Rg_2X^* + X$

  $RgX^* + 2Rg \longrightarrow Rg_2X^* + Rg$

A NEW CLASS OF LASER CANDIDATES: THE TRIATOMIC RARE GAS HALIDES, Rg_2X

Laboratory Observation	Laser Implication
• Selective Formation Pathway	Choice of Excitation Methods
• High Production Yield ($\Phi \sim 0.9$)	Potential High Efficiency
• Dissociative Lower State	No Bottle-necking
• Broad-band Emission ($\Delta\lambda > 50$ nm)	Wide Frequency Tunability
• Small Stimulated Emission Cross-section ($\sigma \leq 10^{-17}$ cm^2)	Potential High Power Interference by Absorption • Rg_2X^* • Background

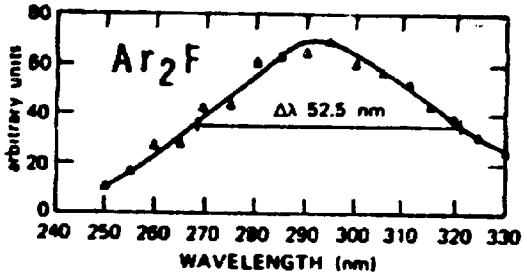

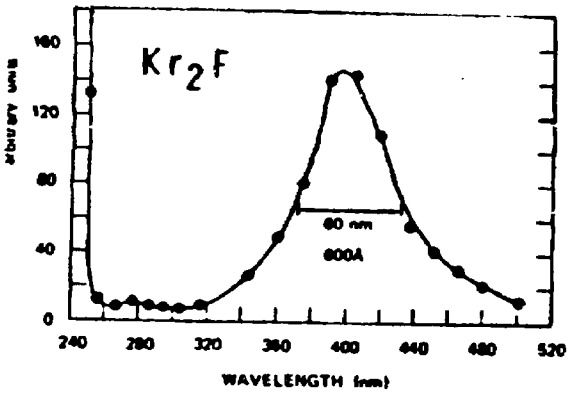

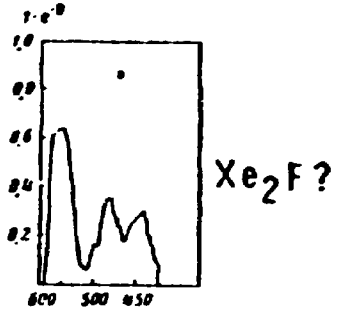

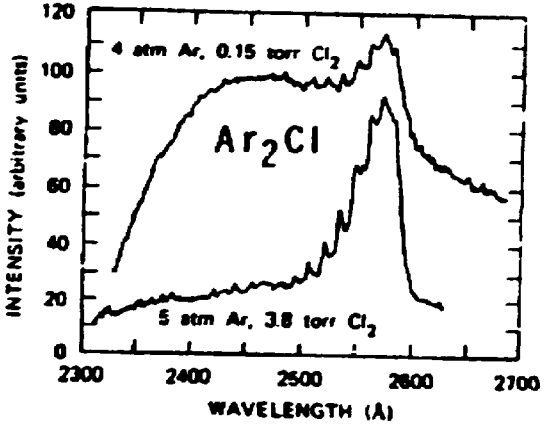

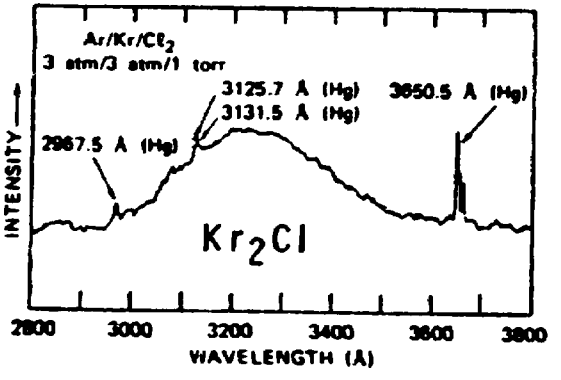

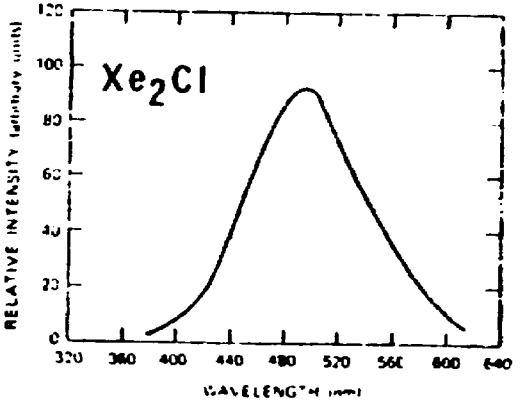

EMISSION SPECTRA OF THE TRIATOMIC RARE GAS HALIDES

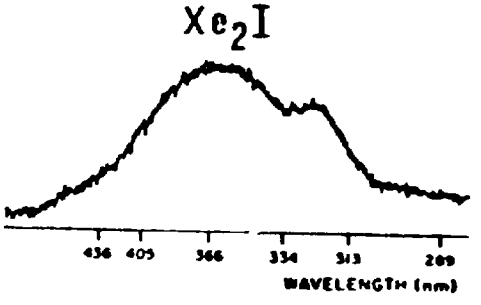

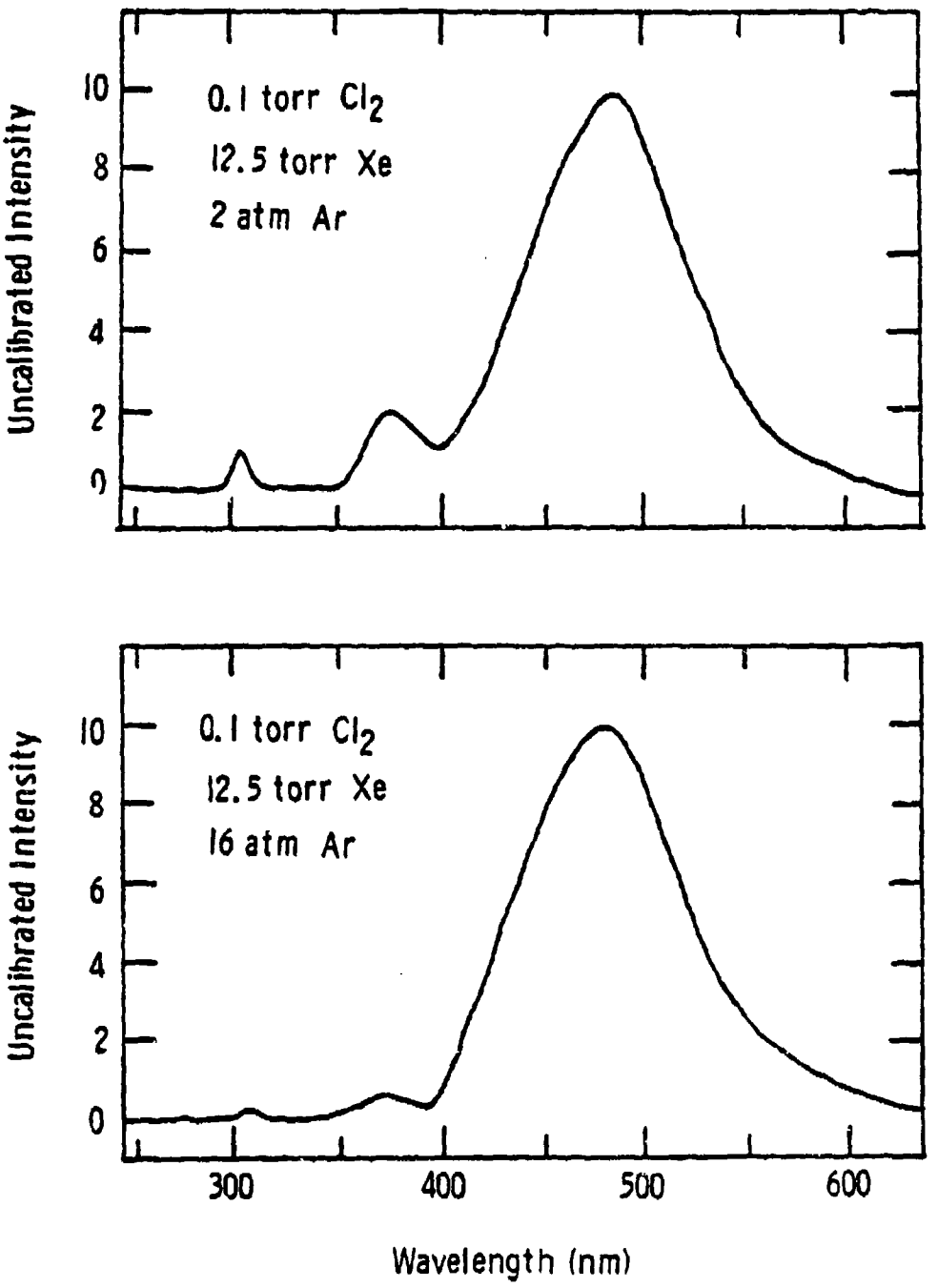
Uncalibrated Intensity
10
8
6
4
2
0
0.1 torr Cl_2
12.5 torr Xe
2 atm Ar
Uncalibrated Intensity
10
8
6
4
2
0
0.1 torr Cl_2
12.5 torr Xe
16 atm Ar
300
400
500
600
Wavelength (nm)

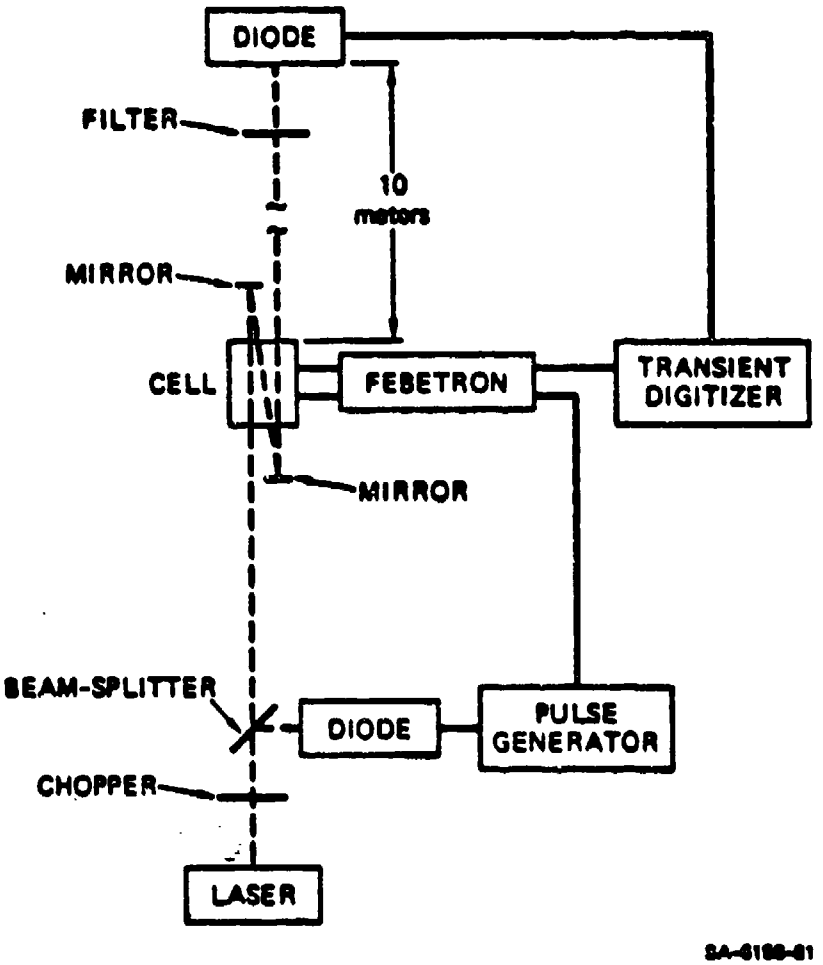
DIODE
FILTER
10
meters
MIRROR
CELL
FEBETRON
TRANSIENT
DIGITIZER
MIRROR
BEAM-SPLITTER
DIODE
PULSE
GENERATOR
CHOPPER
LASER

Figure 1

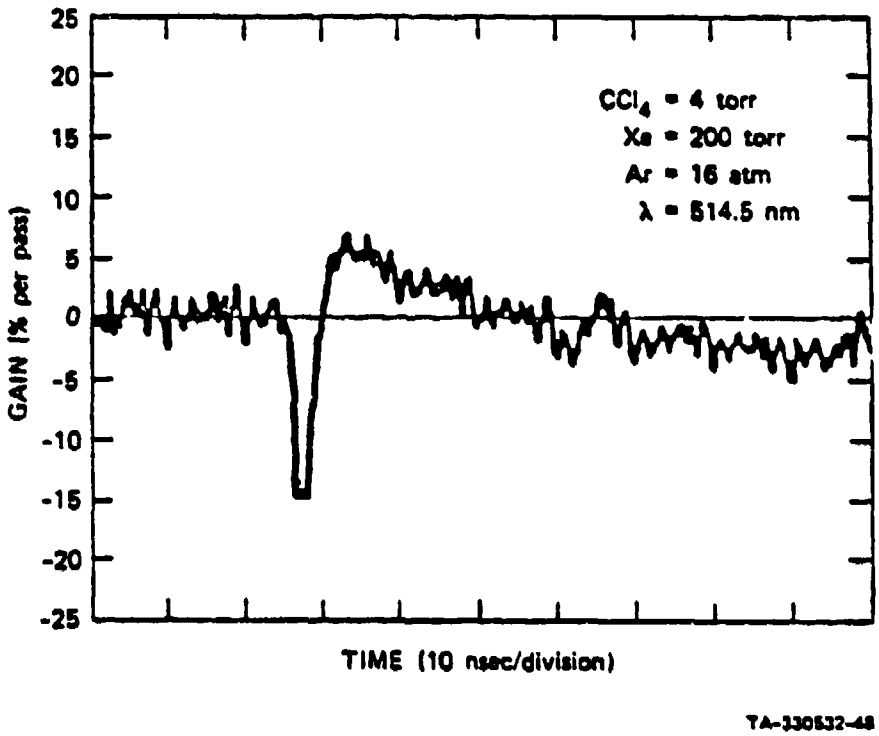

Weaker gain also observed at 488 and 498 nm.

By F. K. Tittel, W. L. Wilson, R. E. Stickel, G. Marowsky and W. E. Ernst

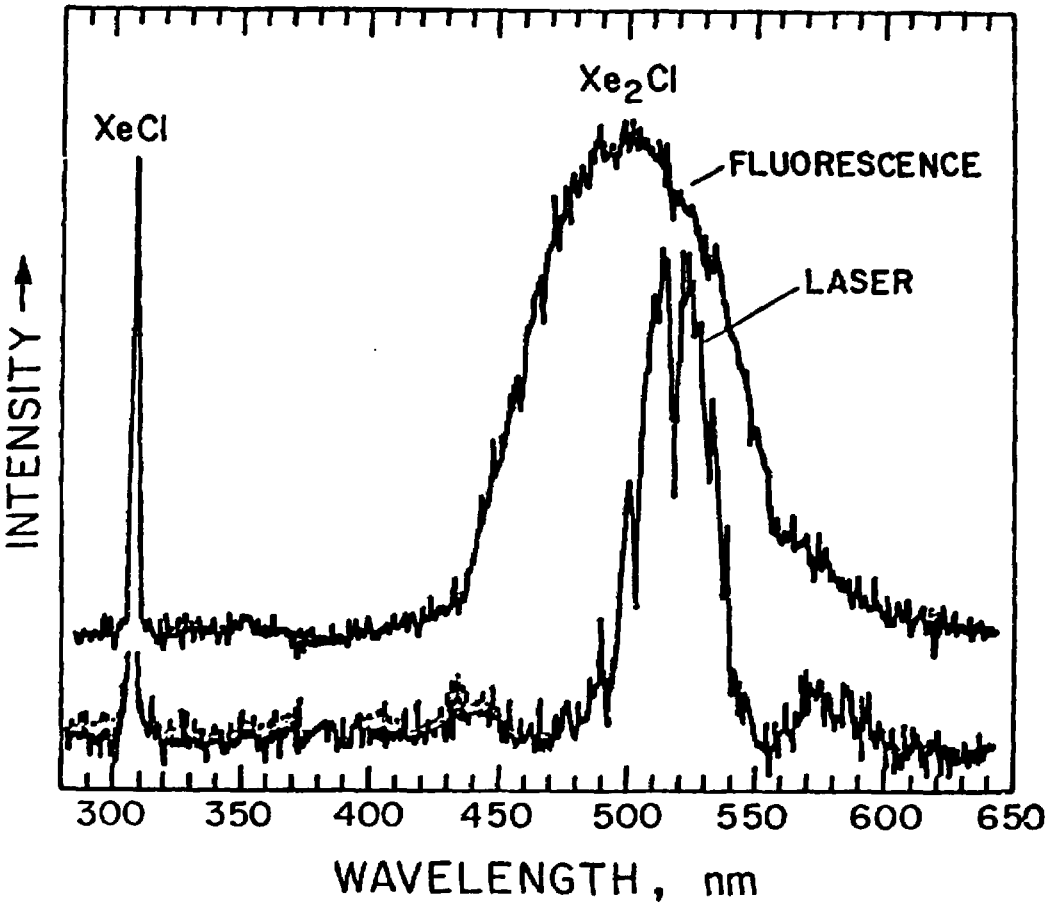

Summary of Rg_2X Laser Study

Status

- Spectroscopy -
  - Most Rg_2X^* Emission Observed
  - Electronic Structure Understood
- Kinetics -
  - High Production Efficiency Verified
- Laser -
  - Gain Observed in Xe_2Cl
  - Self-absorption not Important
  - Laser Action of Xe_2Cl Achieved via Direct e-beam Excitation

Current Xe_2Cl Laser Work at SRI

- Small Scale Laser Demonstration via Incoherent vuv Photolytic Pumping
- Detailed Understanding of the Kinetics

XeCl LASERS FOR BLUE-GREEN CONVERSION

J Asmus

Maxwell Labs
8835 Balboa Avenue
San Diego CA 92123

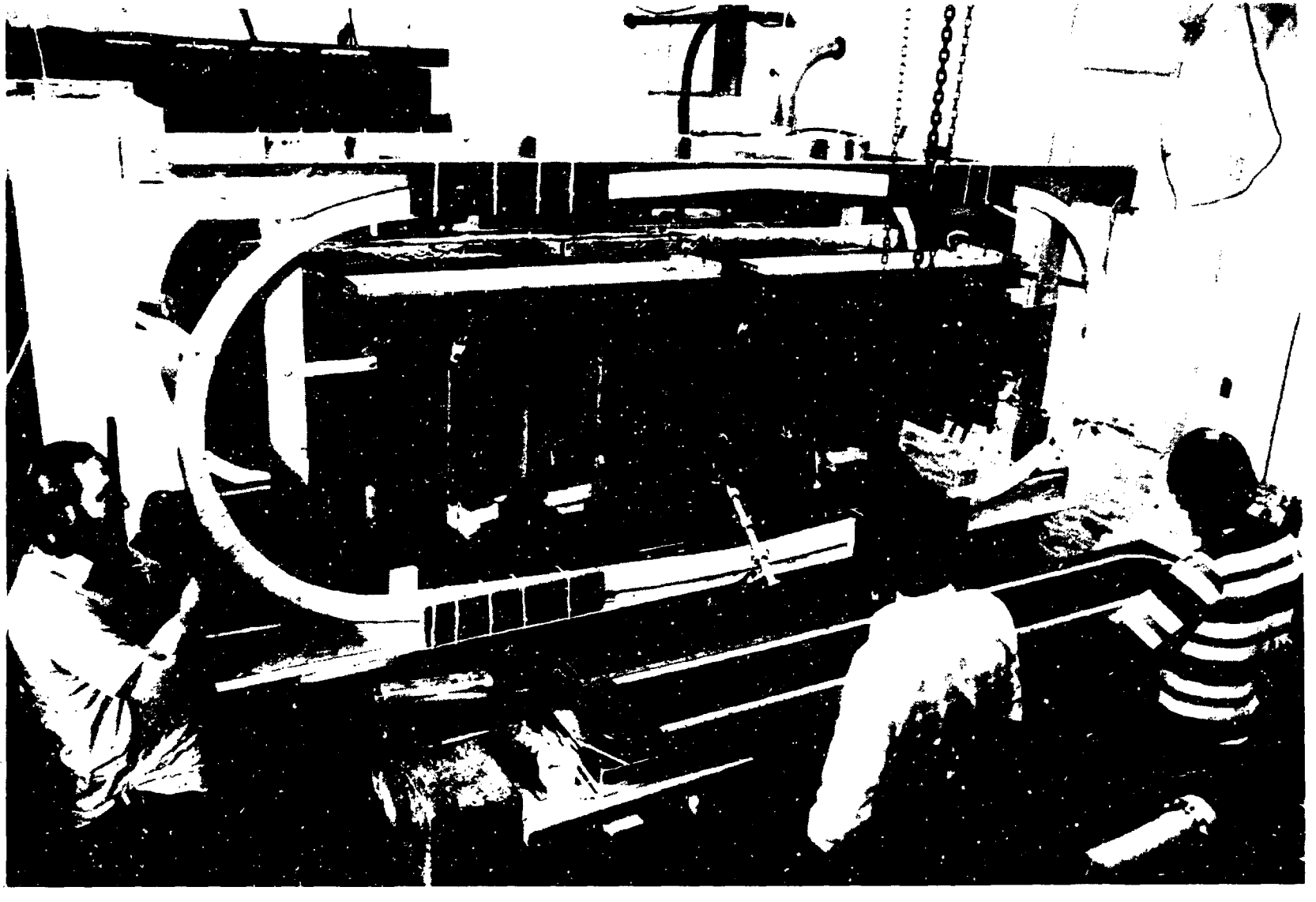

UPPER TRACE ELECTRON BEAM VOLTAGE, 88 KV/DIV, 200 NS/DIV

LOWER TRACE ELECTRON BEAM CURRENT, 27.4 KA/DIV, 200 NS/DIV

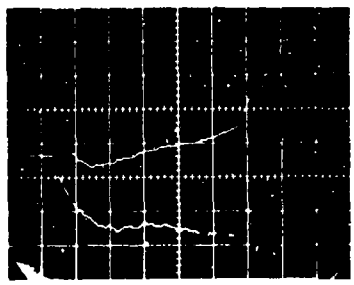

LASER LOADED FLUORESCENCE, 200 NS/DIV

MAXWELL

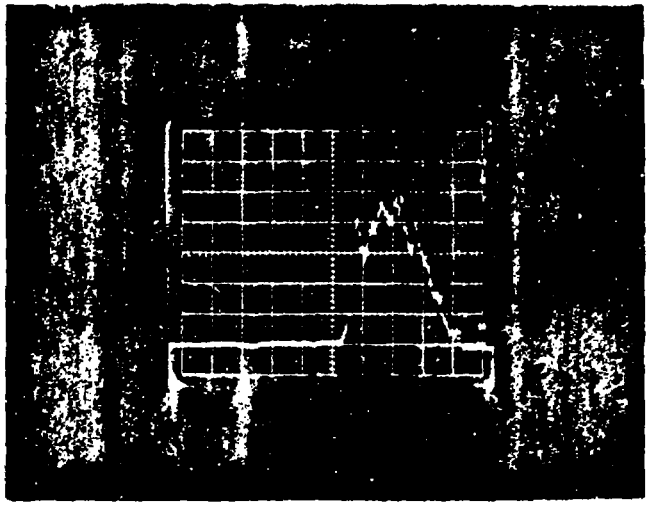

2 METER LASER E-BEAM PERFORMANCE

BEAM PATTERNS vs GUIDE FIELD STRENGTHS

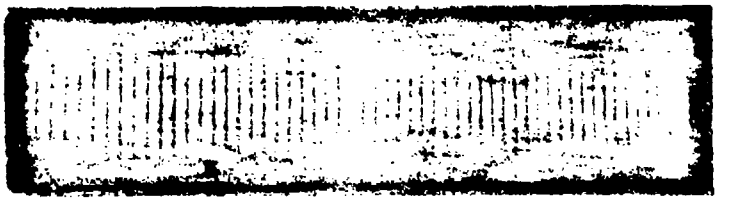

4/13-3
NO FIELD
5-BLADE CATHODE
45kV

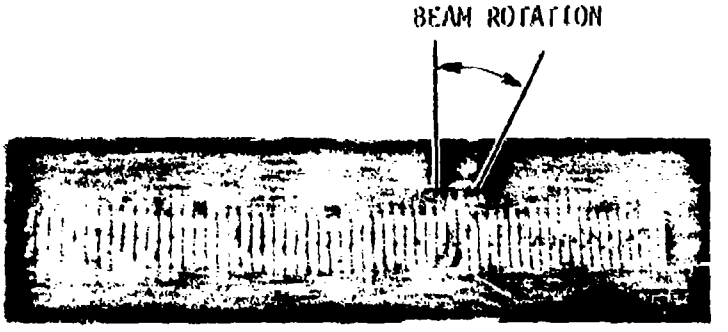

4/4-7
278 GAUSS GUIDE FIELD
5-BLADE CATHODE
45kV

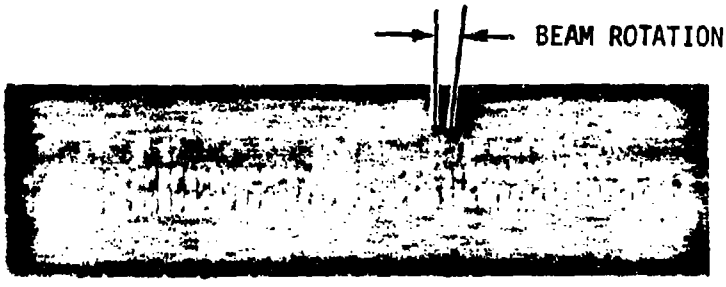

4/13-4
436 GAUSS GUIDE FIELD
5-BLADE CATHODE
45kV

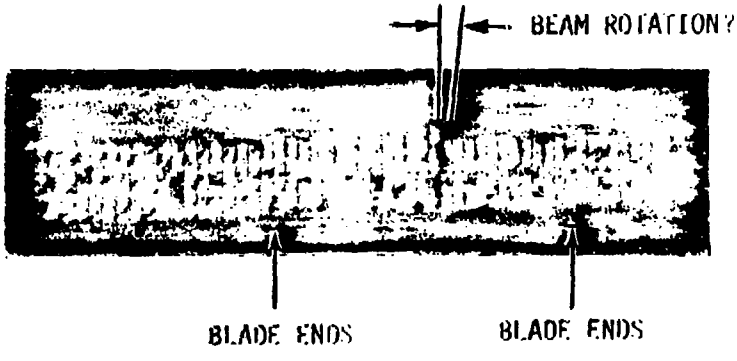

4/17-2
436 GAUSS GUIDE FIELD
SKEWED CATHODE
45kV

CATHODE BLADE ARRANGEMENTS--COMPARISON

NORMAL CATHODE ARRAY, 11 FULL BLADES

SKEW CATHODE ARRAY, 7 FULL BLADES AND 4 STEPPED BLADES

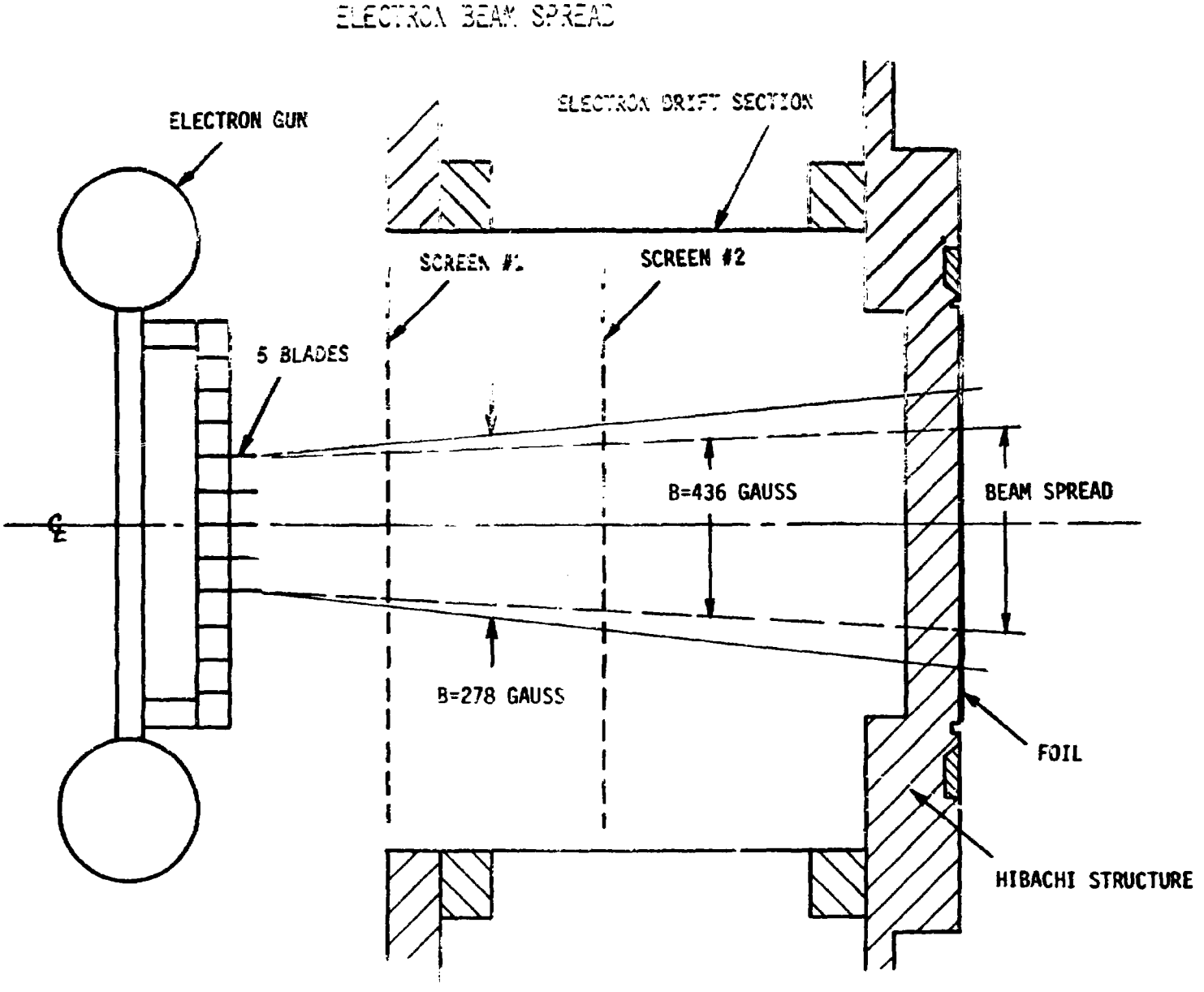
ELECTRON BEAM SPREAD
ELECTRON GUN
ELECTRON DRIFT SECTION
SCREEN #1
SCREEN #2
5 BLADES
B=436 GAUSS
BEAM SPREAD
B=278 GAUSS
FOIL
HIBACHI STRUCTURE

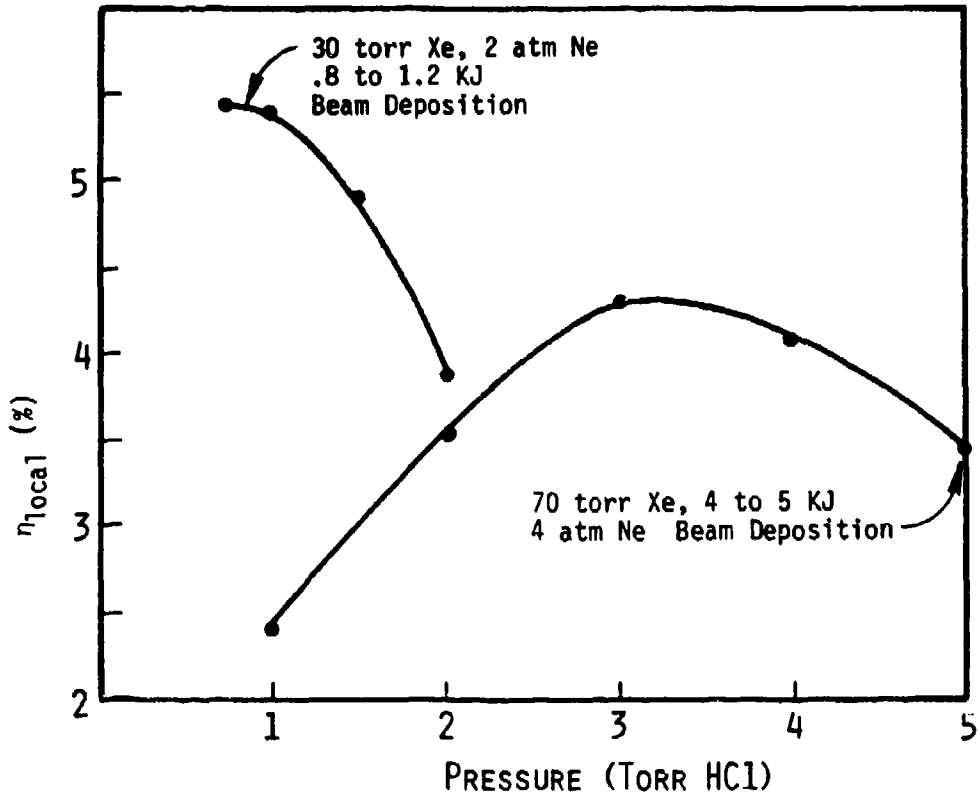
30 torr Xe, 2 atm Ne
.8 to 1.2 KJ
Beam Deposition
70 torr Xe, 4 to 5 KJ
4 atm Ne Beam Deposition
η_{local} (%)
5
4
3
2
1
2
3
4
5
PRESSURE (TORR HCl)

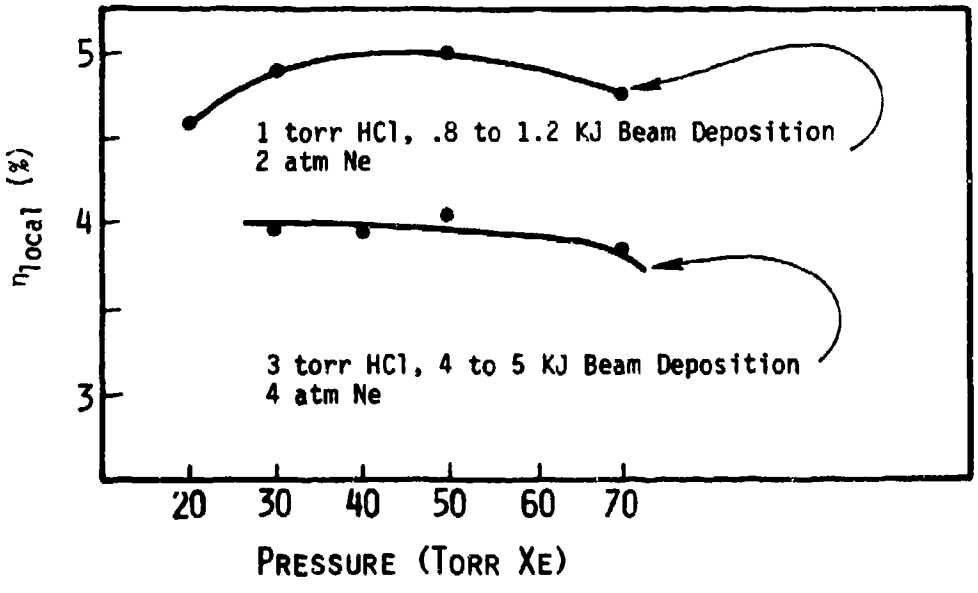
1 torr HCl, .8 to 1.2 KJ Beam Deposition
2 atm Ne
3 torr HCl, 4 to 5 KJ Beam Deposition
4 atm Ne
η_{local} (%)
5
4
3
20
30
40
50
60
70
PRESSURE (TORR XE)

MAXWELL

40 L LASER OPERATION (JUNE-AUG)

XeF

ENERGY/PULSE	25
TEMPERATURE	25° C
DENSITY	2.5 AMAGAT
ELECTRICAL EXCITATION	75%
NEAR FIELD DISTRIBUTION	±10% (APERTURE)
COATING DAMAGE TESTS (6 J)	±5% (APERTURE/4)
NUMBER OF TEST SHOTS	650

	Laser Volume (liters)	E beam Deposition (KJ)	Laser Output (J)	Local[1] Efficiency	Specific Laser Output (J/L)
KrF	60	6	300	5%	5
XeF	60	6	200	3.3%	3
XeCl	40	4	200	5%	5

[1] Local efficiency = Laser output/Deposited beam energy

MAXWELL

COATING DAMAGE TESTS

XeF, N ON ONE

	FLUX (J/CM^2)	SHOTS TO DAMAGE
TM 2 (6 INCH MOLY, 99.5%)	0.6	>50
	1.2	>50
	2.5	24-40
	6.7	8-10
	9.6	1-2
TM 1 (6 INCH MOLY, 98.5%)	0.6	>50
	1.2	>50
	2.5	>50
	4.2	28
	6.7	20

E-BEAM TO 40 LITER LASER INTERFACE

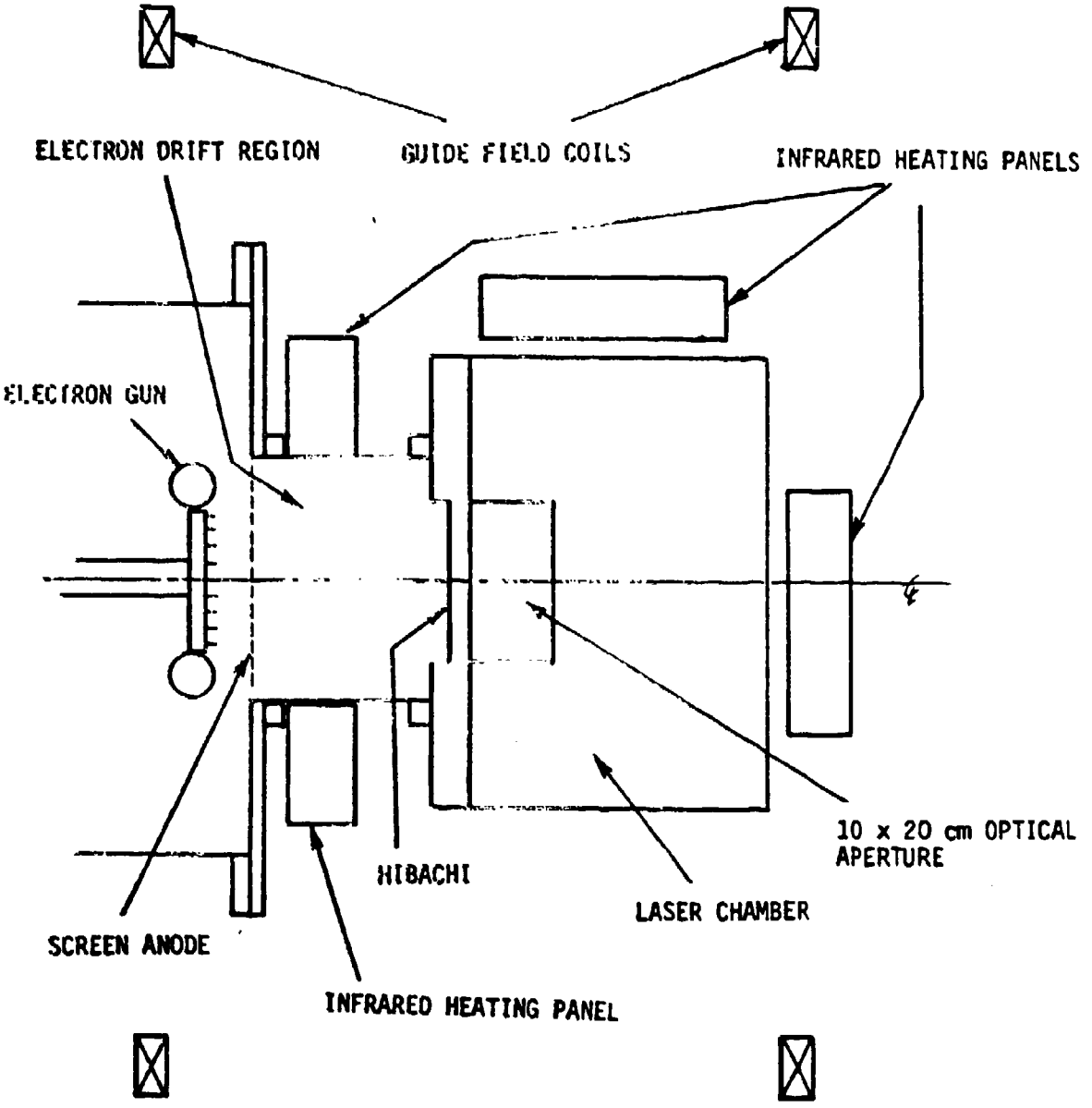

LASER GAS DEGRADATION

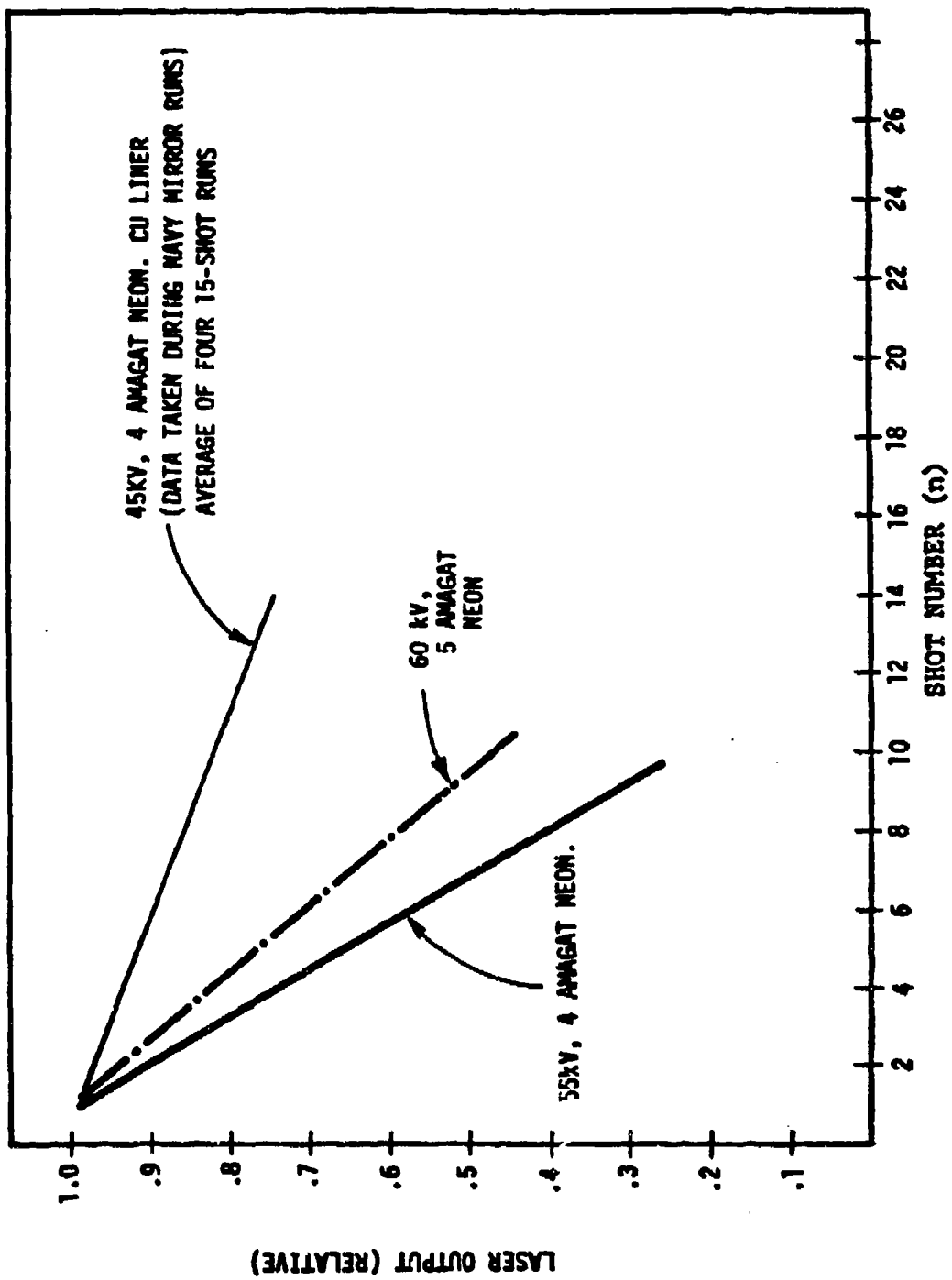

E-BEAM TO 40 LITER LASER INTERFACE

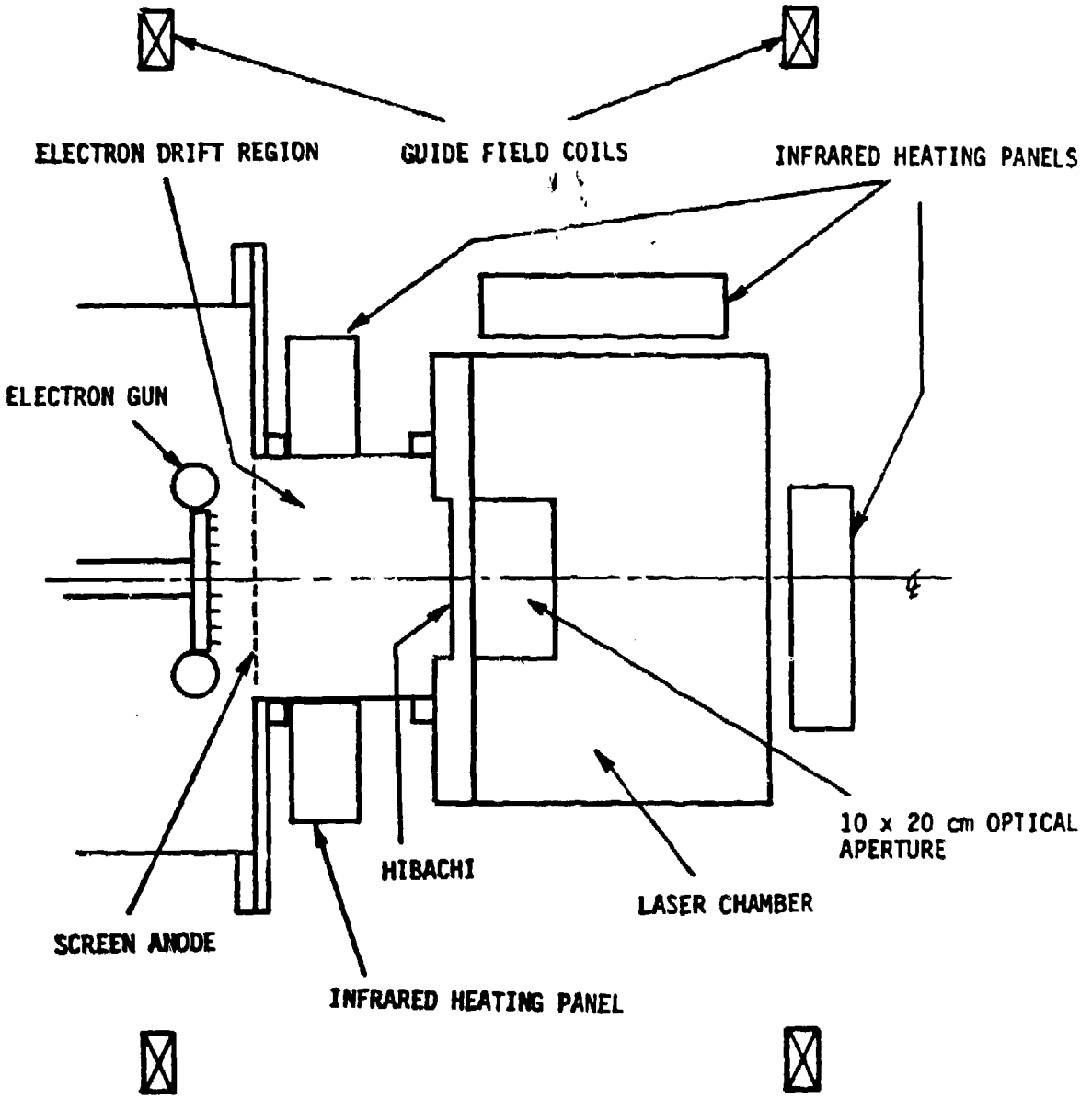

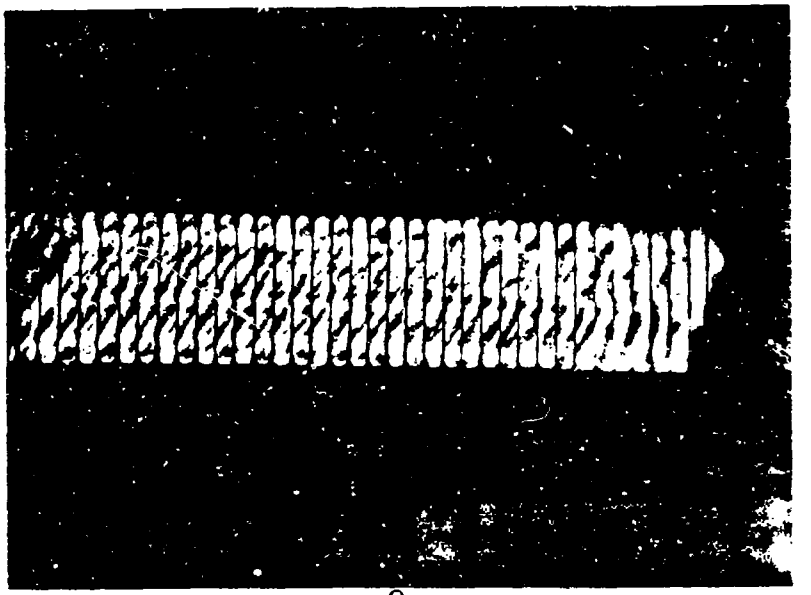

CARBON FELT CATHODE WITH 2 DIMENSIONAL E-BEAM NEUTRALIZATION (ONE-HALF OF 20CM X 2 METER E-BEAM)

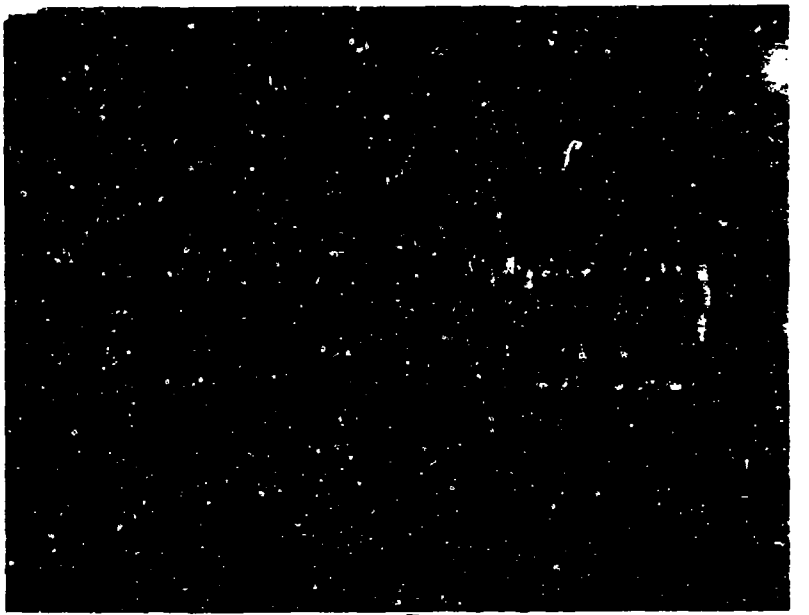

CARBON FELT CATHODE WITH 3 DIMENSIONAL E-BEAM NEUTRALIZATION (ONE-HALF OF 20CM X 2 METER E-BEAM)

ELECTRON BEAM EXCITED BLUE-GREEN XeF

J.D. CAMPBELL

C.H. FISHER

R.E. CENTER

A.L. PINDROH

(SUPPORTED BY DARPA)

Mathematical Sciences Northwest
PO Box 1887
Bellevue WA 98009

MSNW

ELECTRON BEAM EXCITED BLUE-GREEN XeF

OBJECTIVE: INVESTIGATE FEASIBILITY OF A BLUE-GREEN XeF LASER USING ELECTRON BEAM PUMPING

PROGRAM: DETERMINE GAIN OR ABSORPTION ON XeF 460 nm BAND AS FUNCTION OF

- -- GAS PRESSURE
- -- GAS MIXTURE
- -- GAS TEMPERATURE

DEVELOP KINETIC MODEL TO PREDICT LASER PERFORMANCE

PERFORM OSCILLATOR EXPERIMENTS FOR HIGHEST GAIN CONDITIONS

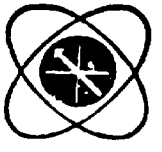

XeF FORMATION KINETICS

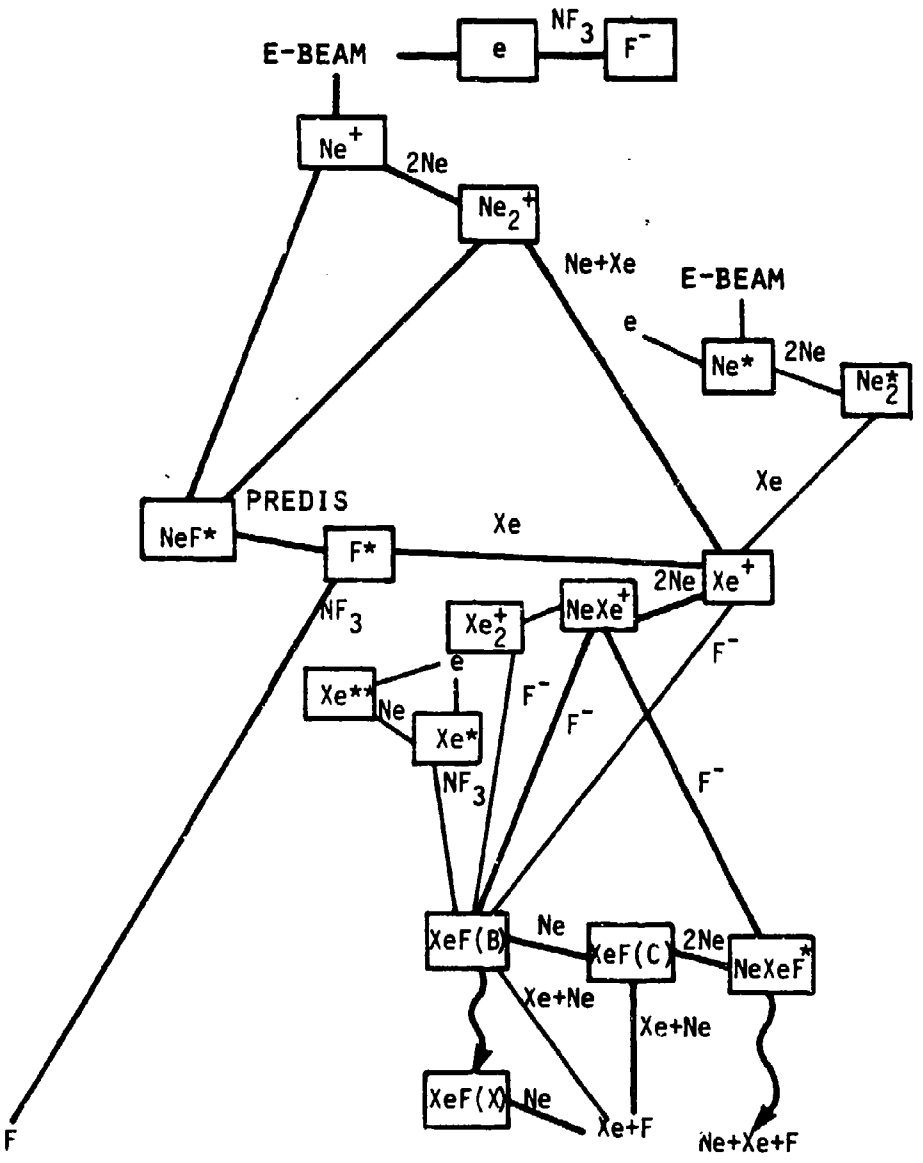

80 03699

XeF FORMATION KINETICS

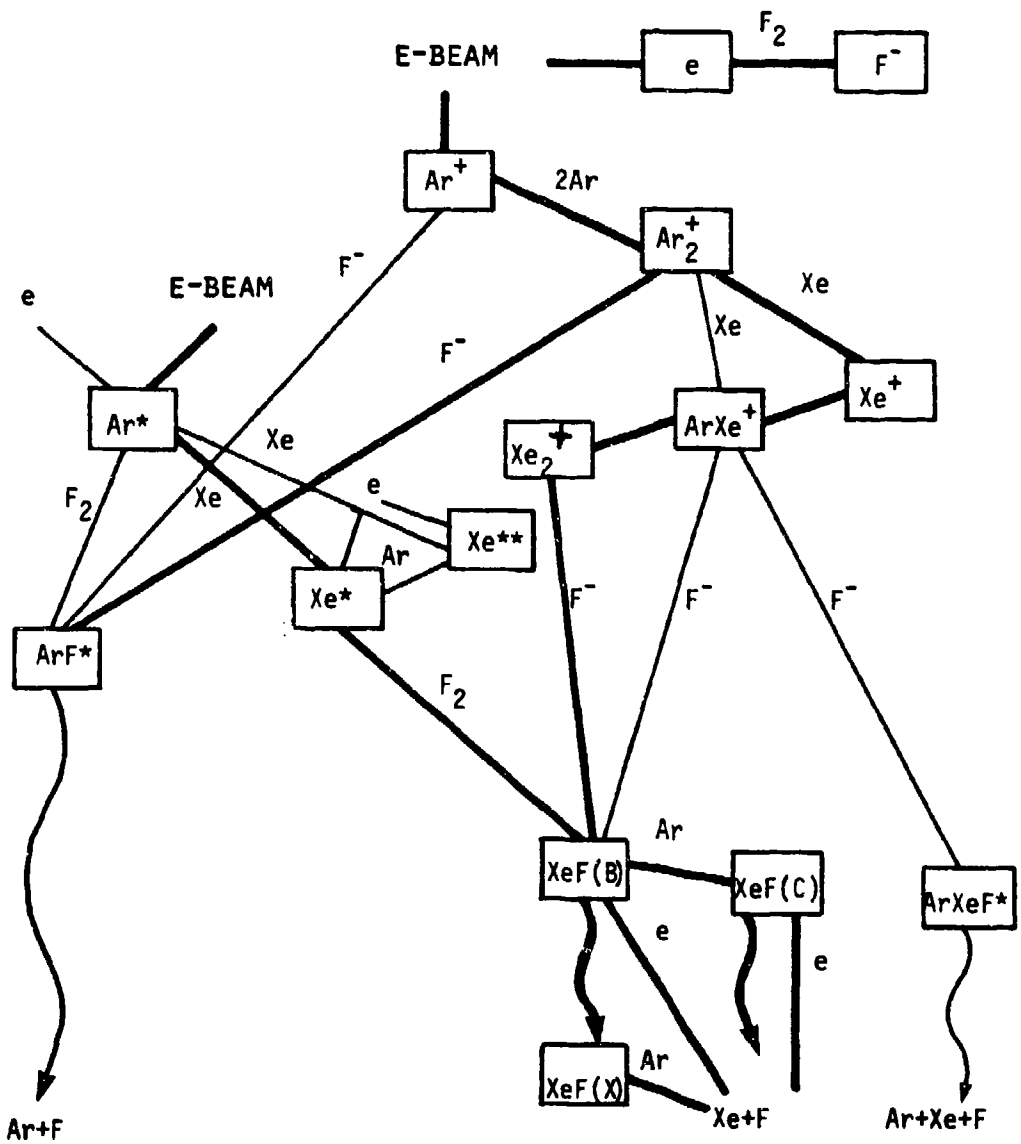

80 Q3698

CODE PREDICTIONS FOR $Ne/Xe/NF_3$ MIXTURES

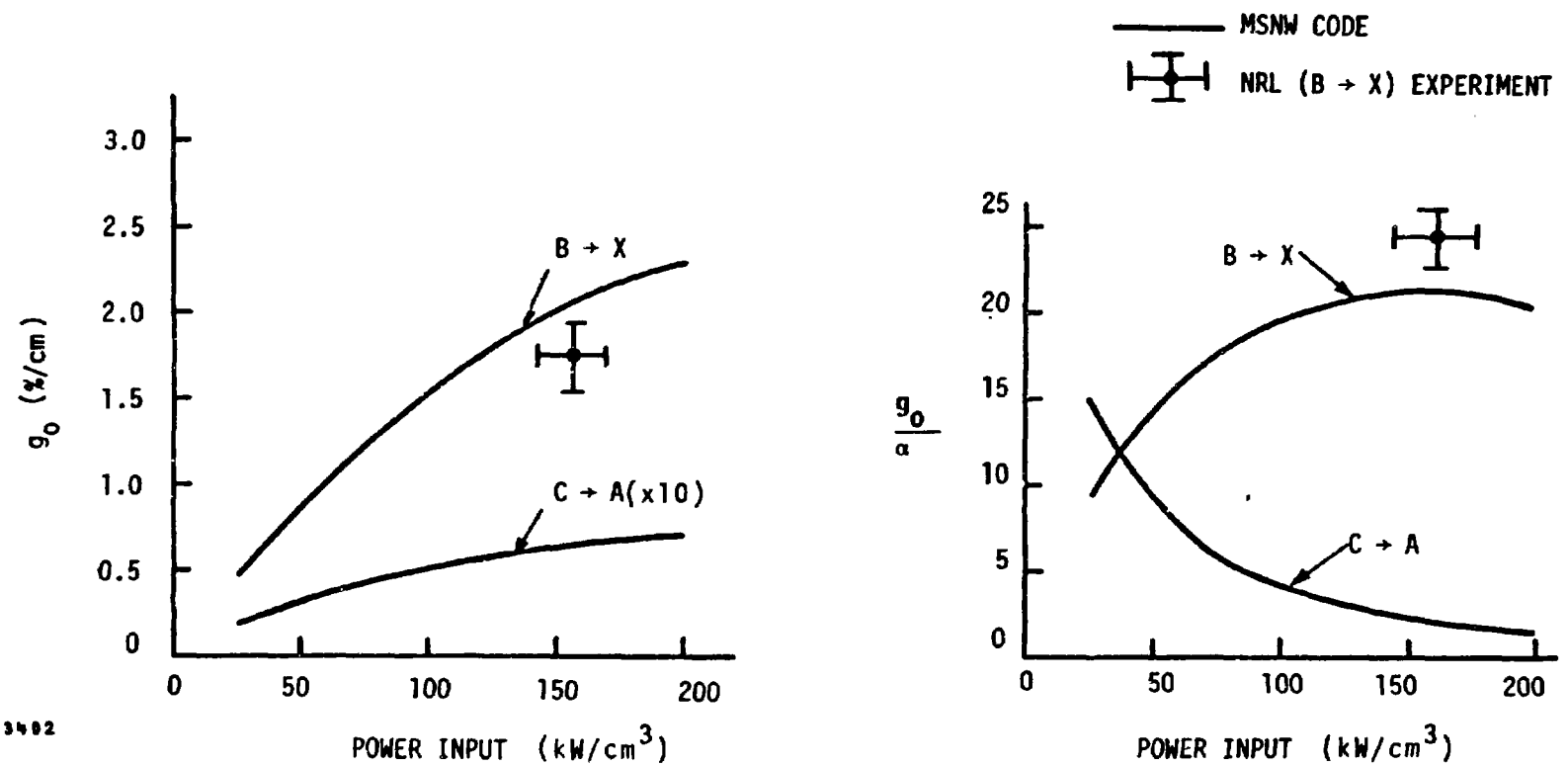

79 03402

MSNW

XeF^* (B→X) POWER EXTRACTION

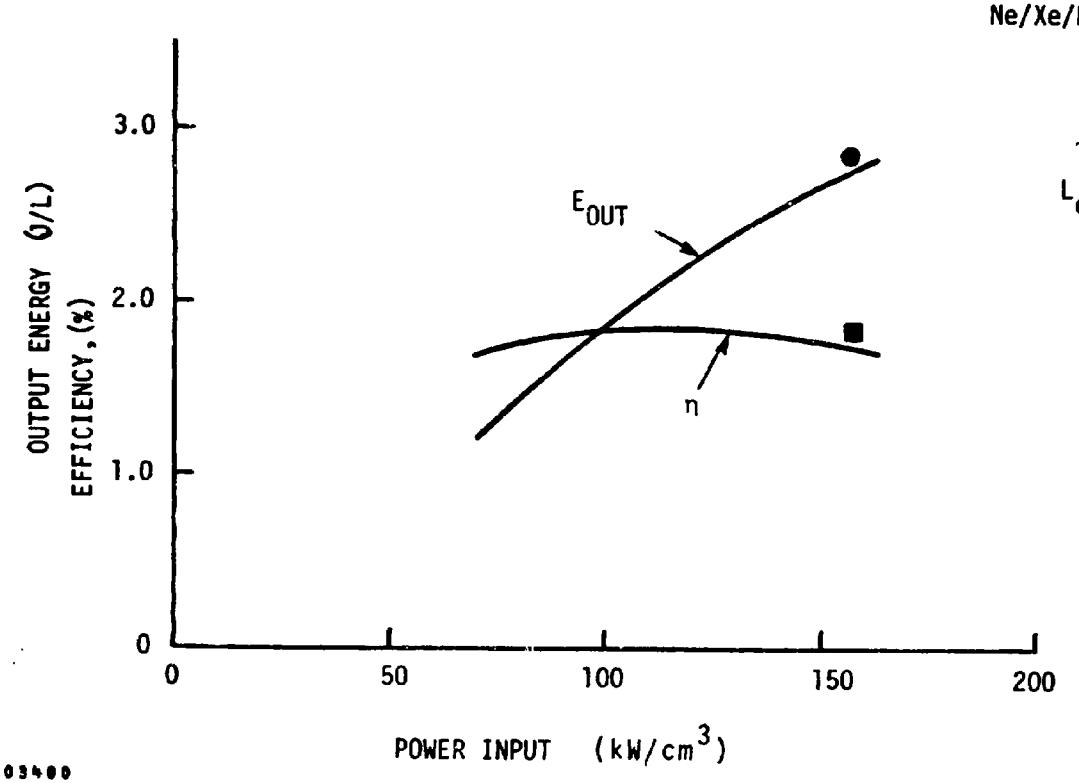

$Ne/Xe/NF_3$ = 99.76/0.18/0.06
P = 5 atm
T_o = 300 °K
τ_{eb} = 1 μsec
L_{cav} = 100 cm
T_m = 50%

MSNW CODE

● E_{OUT} CHAMPAGNE EXPERIMENT

■ η

79 03400

MSNW

CODE PREDICTIONS FOR XeF PERFORMANCE -Ar DILUENT

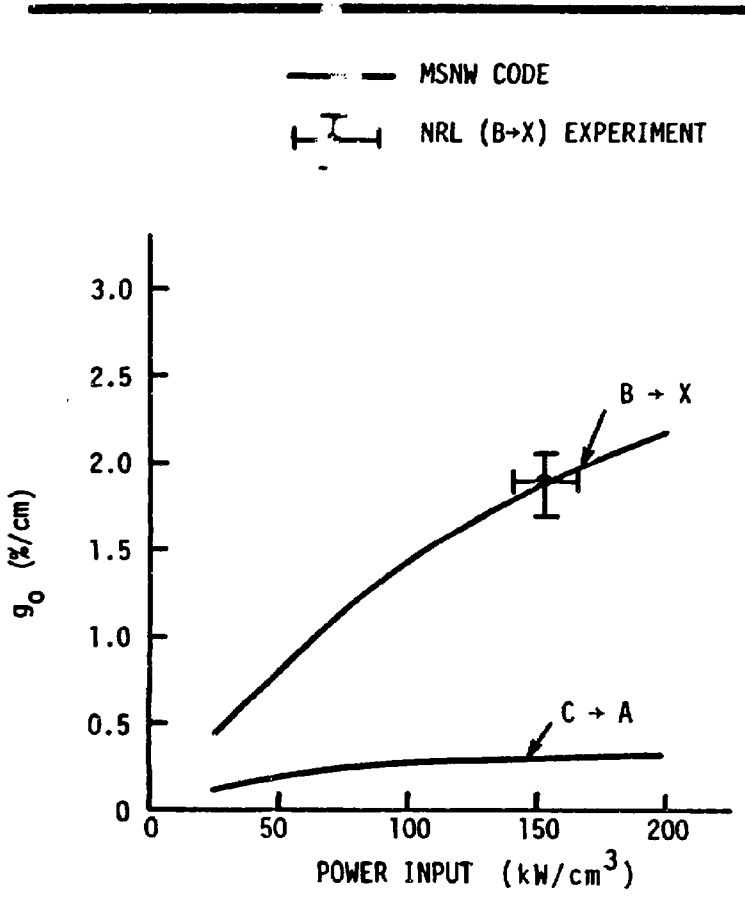

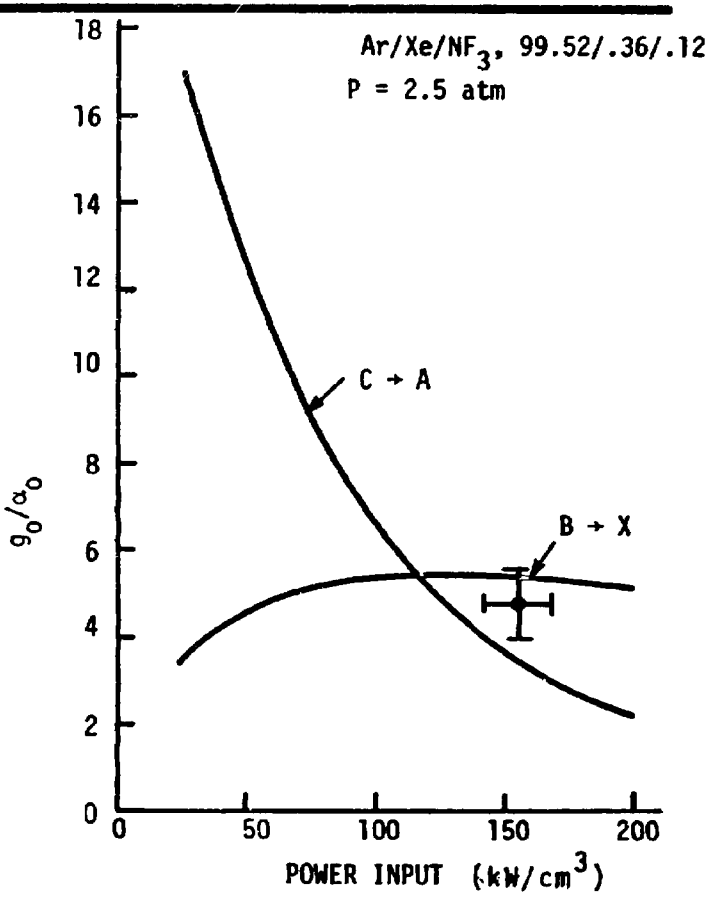

79 03399

MSNW

EXPERIMENTAL SETUP FOR XeF(C→A) GAIN MEASUREMENTS

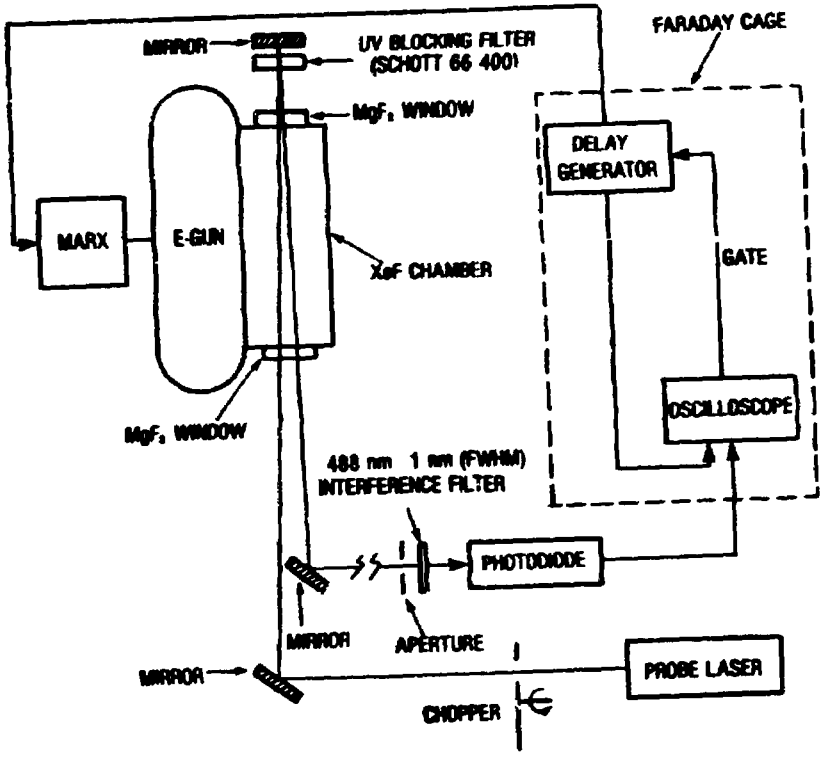

ROOM TEMPERATURE GAIN/ABSORPTION DATA OBTAINED USING A CW Ar^+ LASER PROBE

MIXTURE COMPOSITION: 0.12% NF_3, 0.24% Xe, Neon

(A) PROBE LASER INTENSITY

(B) E-GUN CURRENT PROFILE

200 ns/div

(A)

(B)

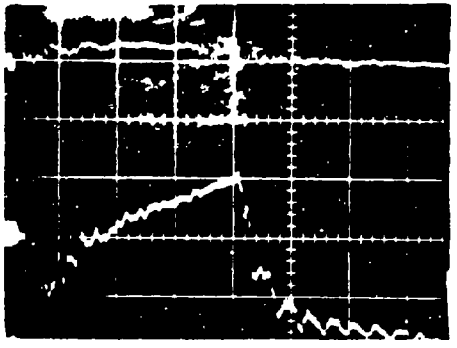

5 ATM MIXTURE

488 nm PROBE

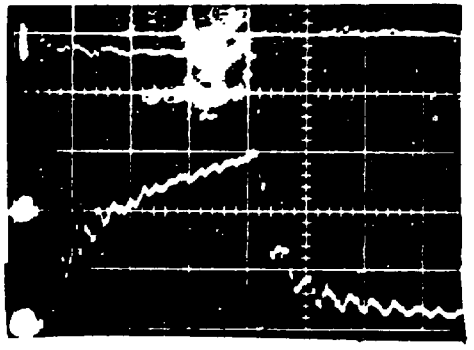

5 ATM MIXTURE

514.5 nm PROBE

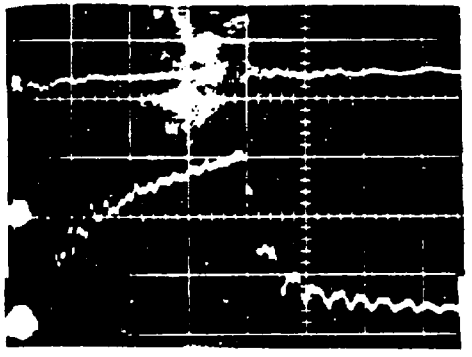

2 ATM MIXTURE

488 nm PROBE

SUMMARY OF XeF (C→A) GAIN/ABSORPTION DATA

Xe	NF_3	F_2	DILUENT	P(atm)	t(°C)	λ(nm)	NET GAIN (cm^{-1})	NET ABS (cm^{-1})
0.25%	0.12%		Ne	4-5	20	488.0	$5x10^{-4}$	
						514.5		$5x10^{-4}$
0.5%	0.12%		Ne	5	20	488.0	$<5x10^{-4}$	
						514.5		$5x10^{-4}$
0.25%		0.12	Ne	4	20	488.0	$\sim3x10^{-4}$	
0.25%		0.12	Ne	4	-20	488.0	$\sim6x10^{-4}$	
0.25%		0.12	Ar	1.5	20	488.0	$<5x10^{-4}$	
0.25%		0.12		1.5	-24	488.0		$5x10^{-4}$

TEMPORAL DEPENDENCE OF XeF(C→A) LASER EMISSION

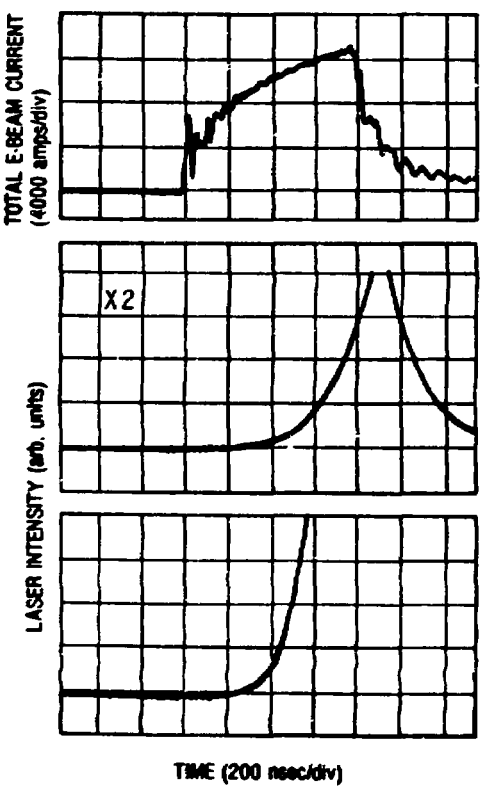

$Ar/Xe/F_2$
100/0.25/0.12
p = 2 atm

$Kr/Xe/F_2$
99/0.5/0.25
p = 1 atm

80 03697

TEMPORAL DEPENDENCE OF XeF(C→A) STIMULATED EMISSION

Kr = 1 atm
Xe = 4 torr
F_2 = 2 torr

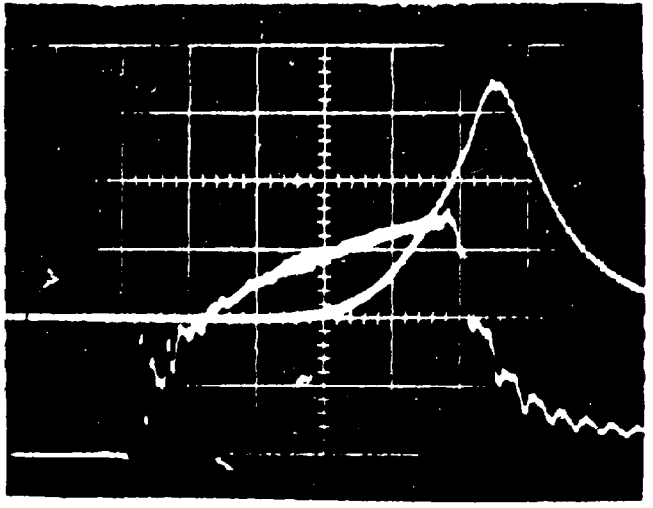

480 nm STIMULATED EMISSION

E-BEAM CURRENT (4 kA/div)

BD 03695

TIME (200 nsec/div)

MSNW

E-BEAM EXCITED XeF(C→A) LASER AND FLUORESCENCE SPECTRA

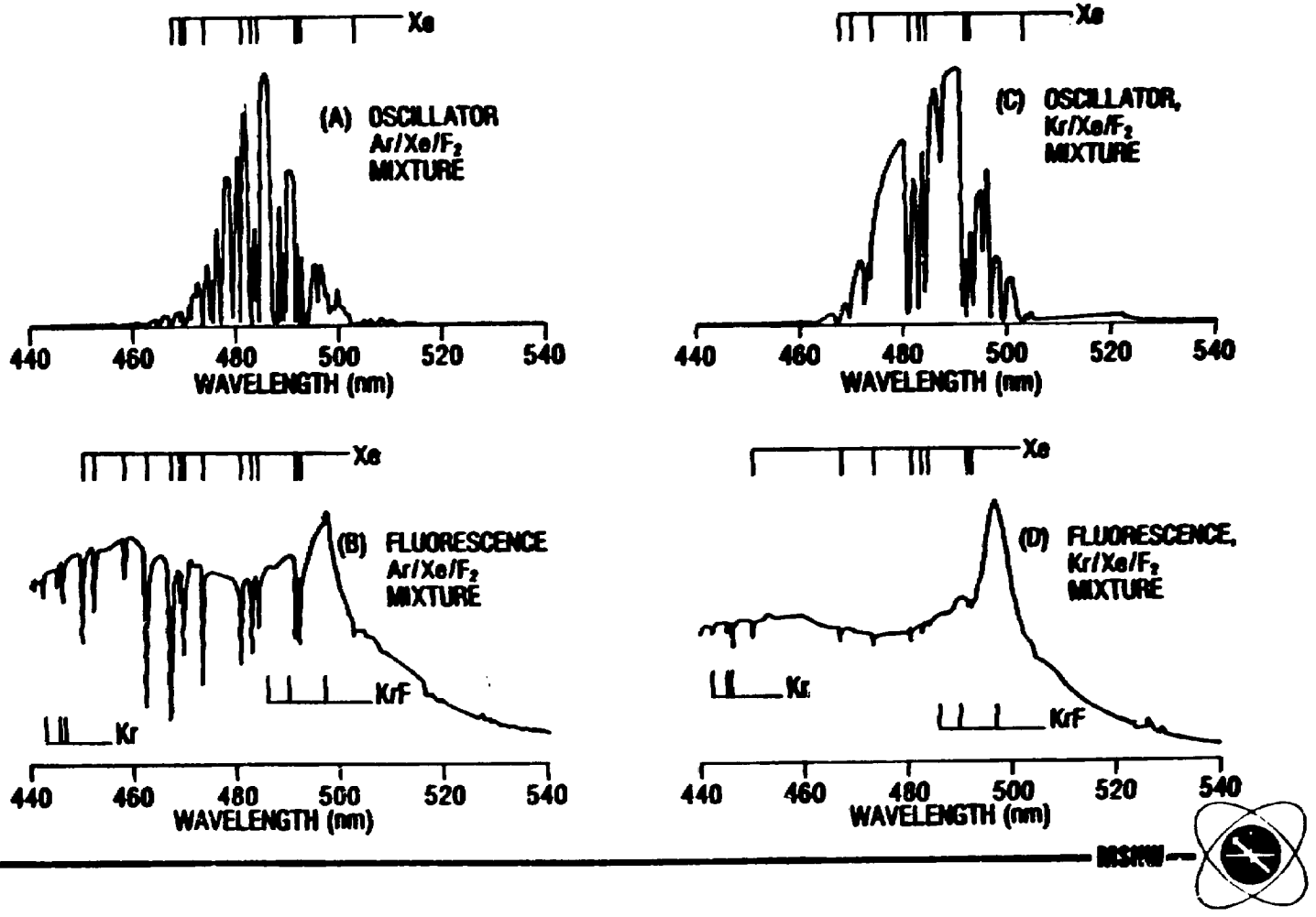

BLUE GREEN XeF STATUS

LASING DEMONSTRATED USING SCALABLE E-BEAM EXCITATION

TUNABILITY DEMONSTRATED USING INJECTED DYE LASER PULSE

Kr DILUENT GIVES BEST PERFORMANCE

EXPERIMENTAL NET GAINS ARE SMALL ($\sim 5 \times 10^{-4}$ cm^{-1})

THE CURRENT STATUS OF COPPER LASER DEVELOPMENT

RE Grove

Summary

The applicability of copper vapor lasers to many military and industrial problems has been limited in the past due to a lack of engineering development, demonstration of high average power operation, or scaling capability. Recent work at the Lawrence Livermore Laboratory has changed considerably the outlook for copper vapor lasers. A copper laser system is presently nearing completion which will have a total power capability of 400 - 500 W at a prf of 6 kHz. The laser system has already demonstrated single aperture powers from individual master oscillator-power amplifier chains of over 100 W with efficiencies of ~0.7 percent. The individual MOPA chains are made up of an oscillator and five amplifiers, and produce about 16 mj/pulse at 6 kHz. Both the laser heads and their associated electronics have been engineered to achieve a high degree of maintainability and reproducibility.

In addition to this successful demonstration of the use of copper lasers in a MOPA configuration, recent experiments at LLL have confirmed that under certain operating conditions, volumetric deactivation of the lower laser level in copper can be achieved. This permits simple bore diameter scaling of the active volume of a copper laser and thus allows substantial increases in both the pulse energy and average power. A large bore copper laser with a 7.3 cm I.D. has recently been operated at output average powers of 55 W at 5 kHz (11 mj per pulse). Based on earlier experiments at General Electric Company at low repetition rates, the pulse energy for this bore diameter is expected to increase by about a factor of three as the prf is reduced to ~1 kHz.

Finally, recent work in the Soviet Union over the past two years has resulted in the achievement of energy densities of about 500 $\mu j/cm^3$ using transverse discharges and extremely high copper densities ($\sim 10^{17}$ to 10^{18} per cm^3). Attainment of specific energies around this value would, of course, result in extremely large pulse energies in small active volumes. However, the specific energies achieved at LLL to date in engineered, scalable copper laser designs, when considered in the context of simple bore diameter scaling and efficient MOPA operation, could result in copper lasers of reasonable size which have the pulse energies and other performance parameters required for many military and industrial applications.

Lawrence Livermore Laboratory
PO Box 5508
Livermore CA 94550

COPPER VAPOR LASERS

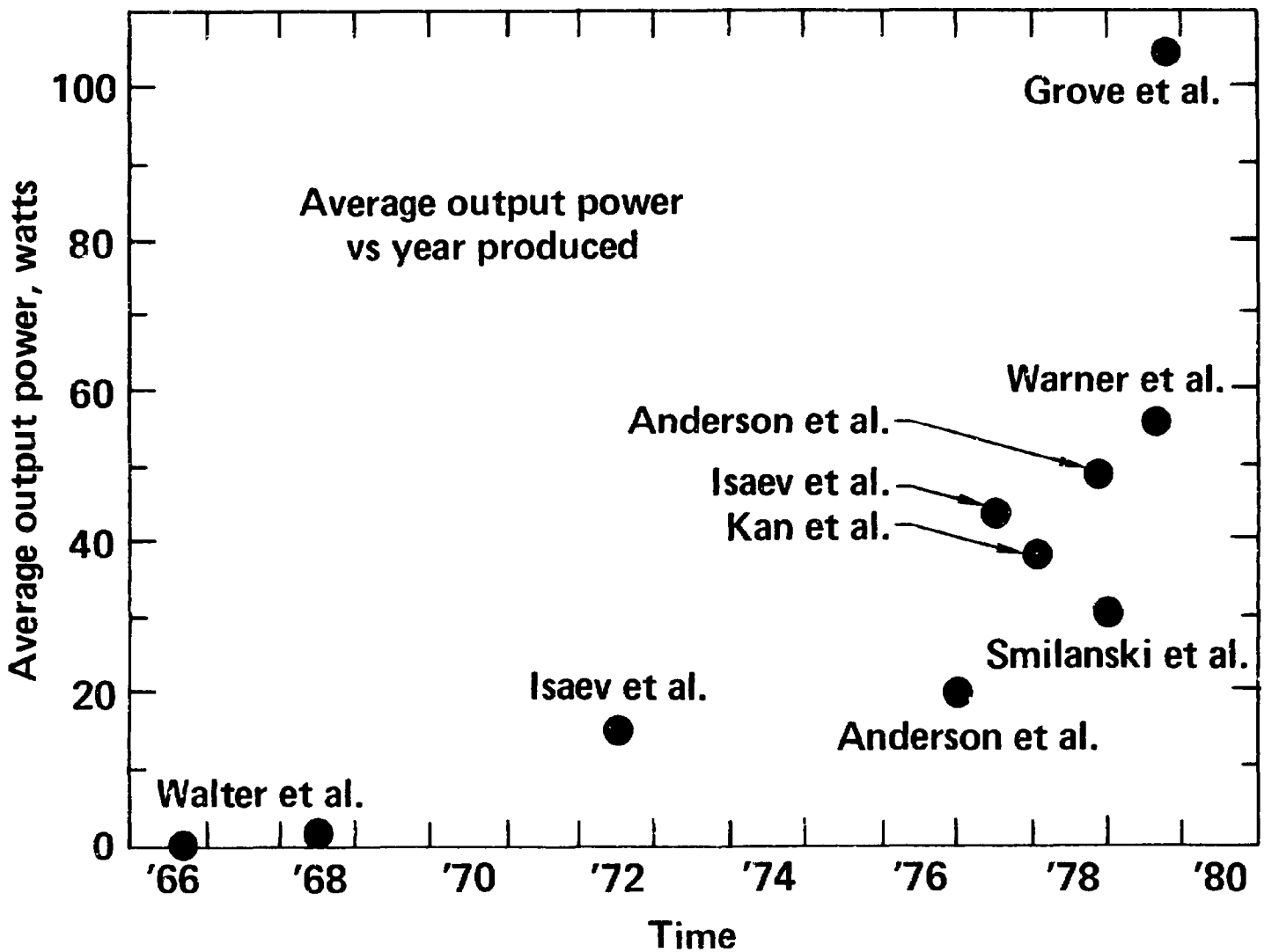

30-17-0280-0636

METHODS FOR INCREASING SINGLE APERTURE POWER

- Increase active length
  - Increase hot zone
  - Use master oscillator-power amplifier (MOPA) configuration
- Increase bore diameter
  - Not thought possible until recently
  - Preliminary results very promising
- Increase output energy density

30-05-0380-1030

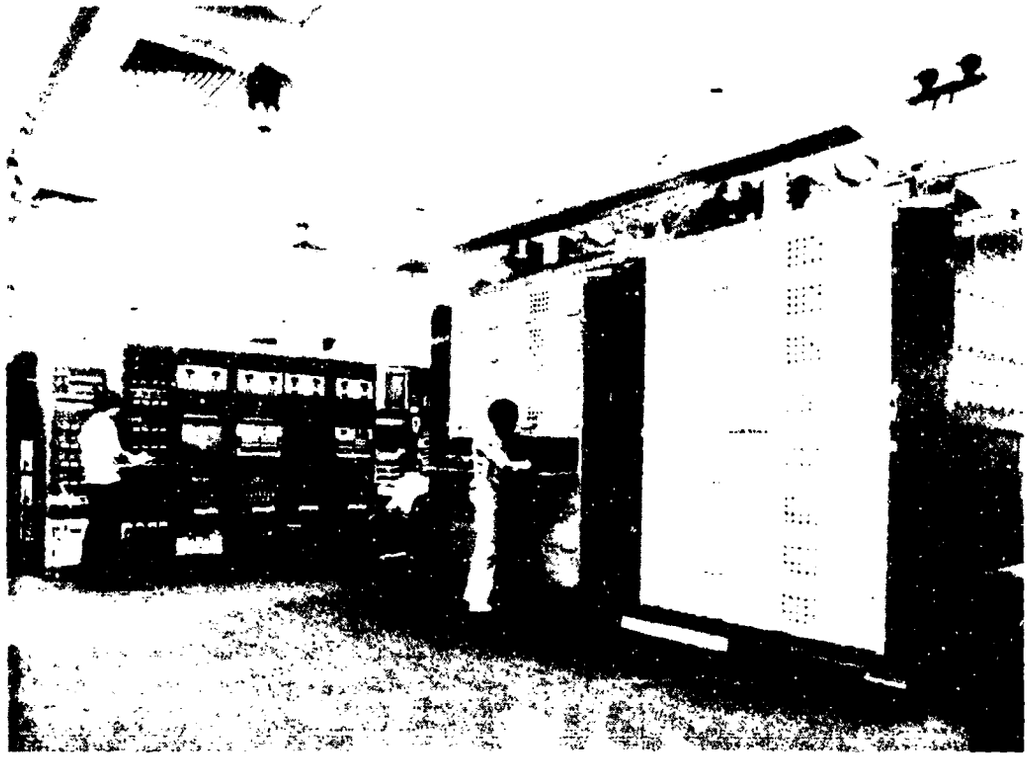

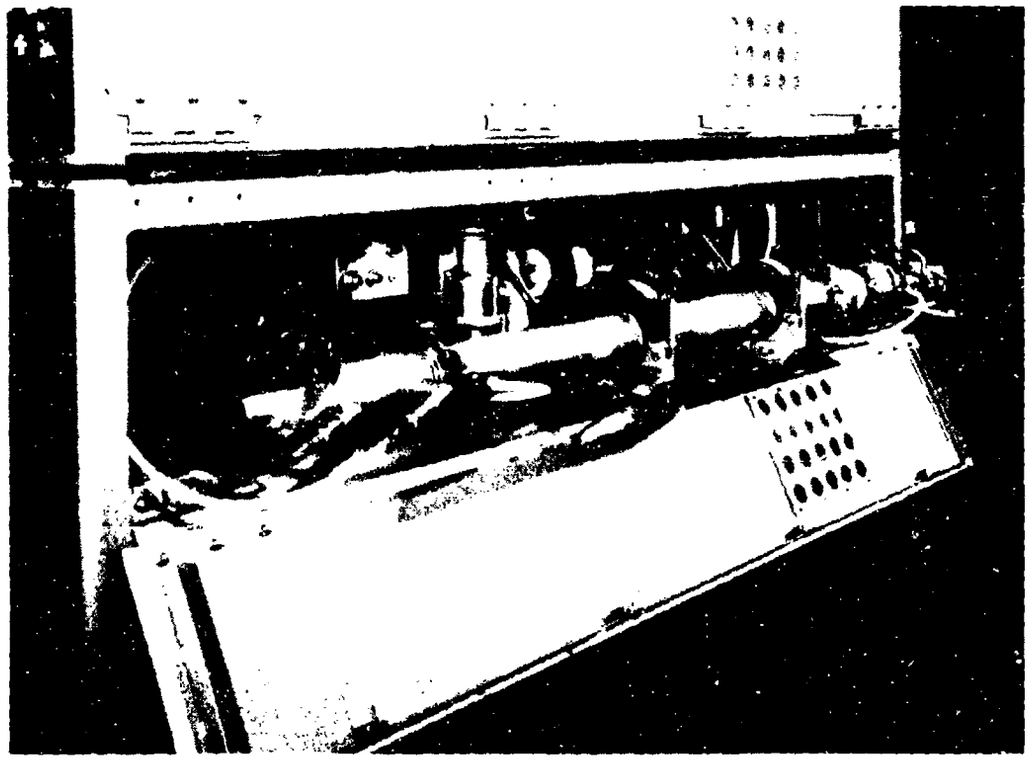

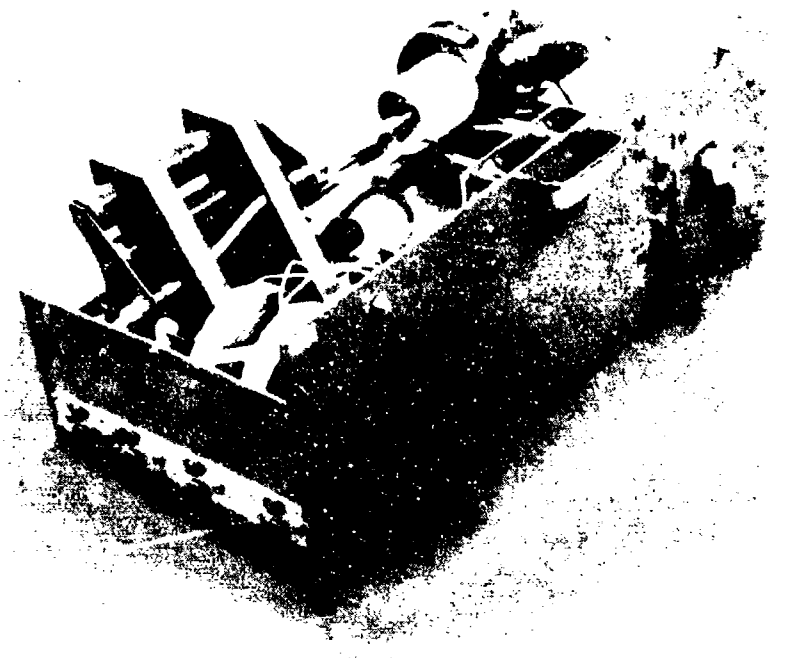

SIX HEAD MOPA CONFIGURATION

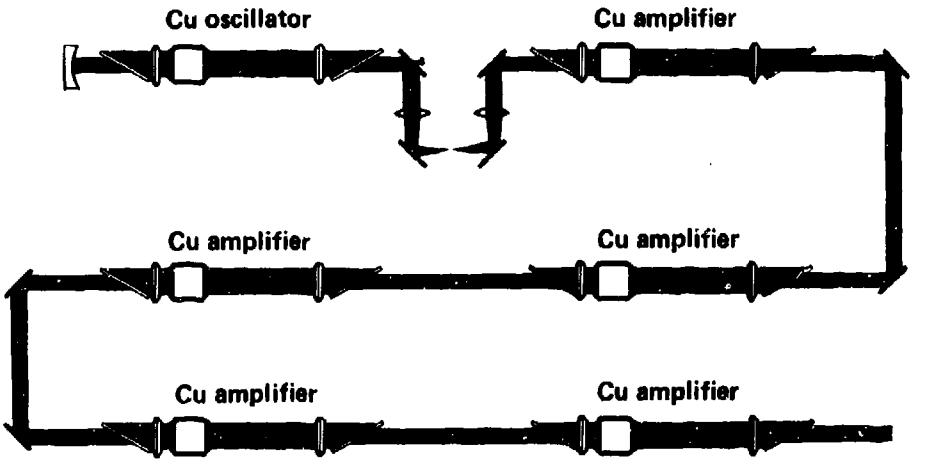

30-01-1279-5092

SIX HEAD MOPA CHAIN – PERFORMANCE

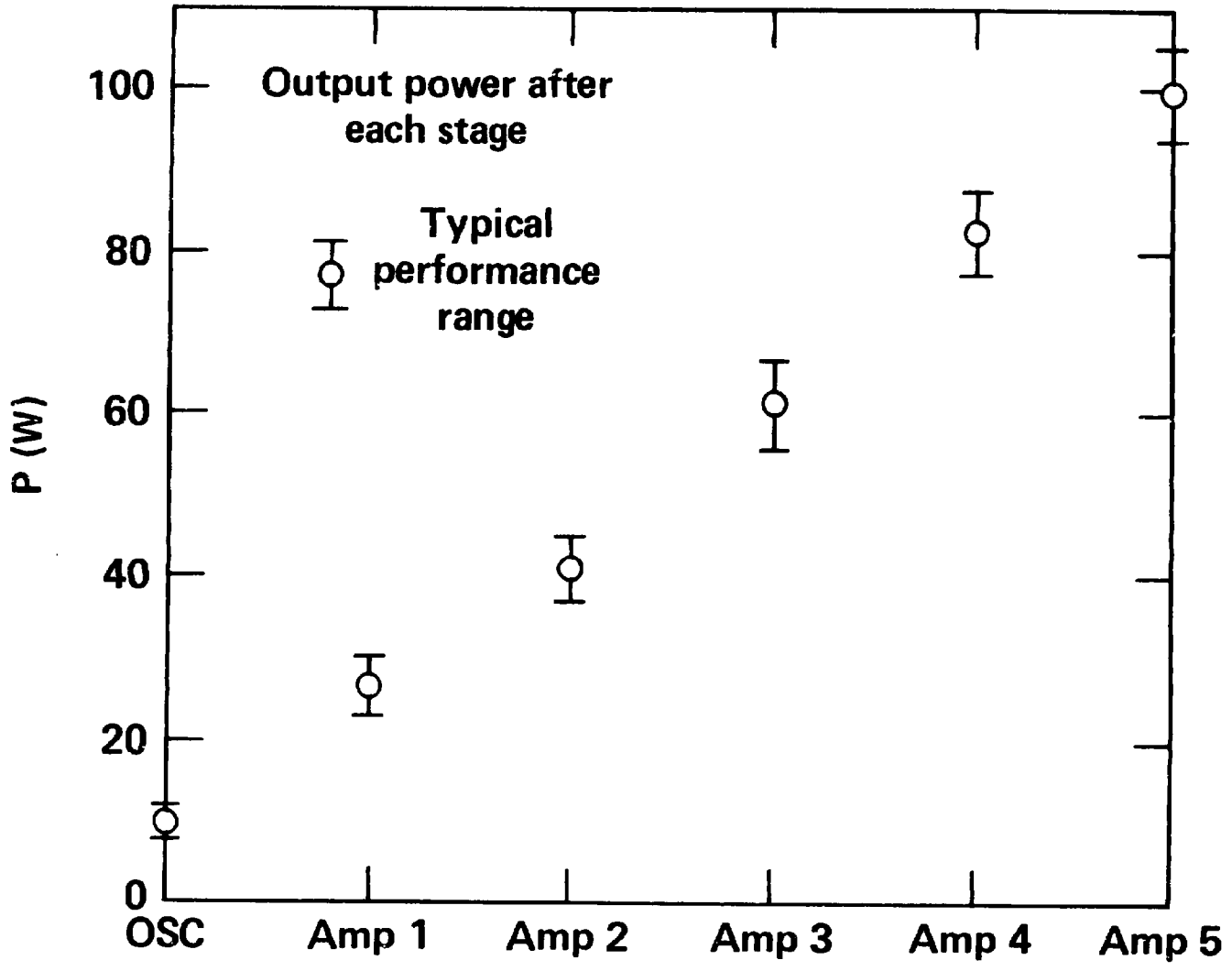

30-05-1279-5115

LARGE BORE COPPER VAPOR LASER

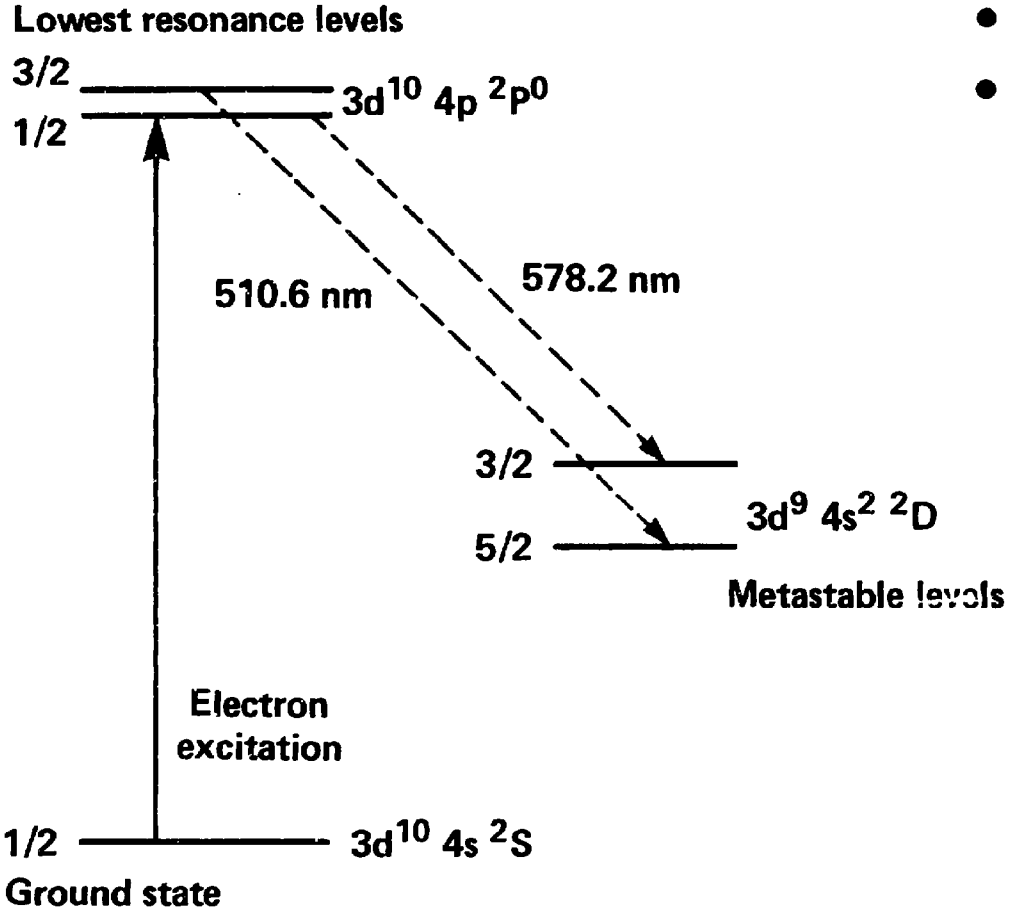

- Self terminating laser
- Repetition rate dependent on rate of deactivation of metastable

30-17-0280-0434

CVL – OPERATION IN HELIUM AND NEON

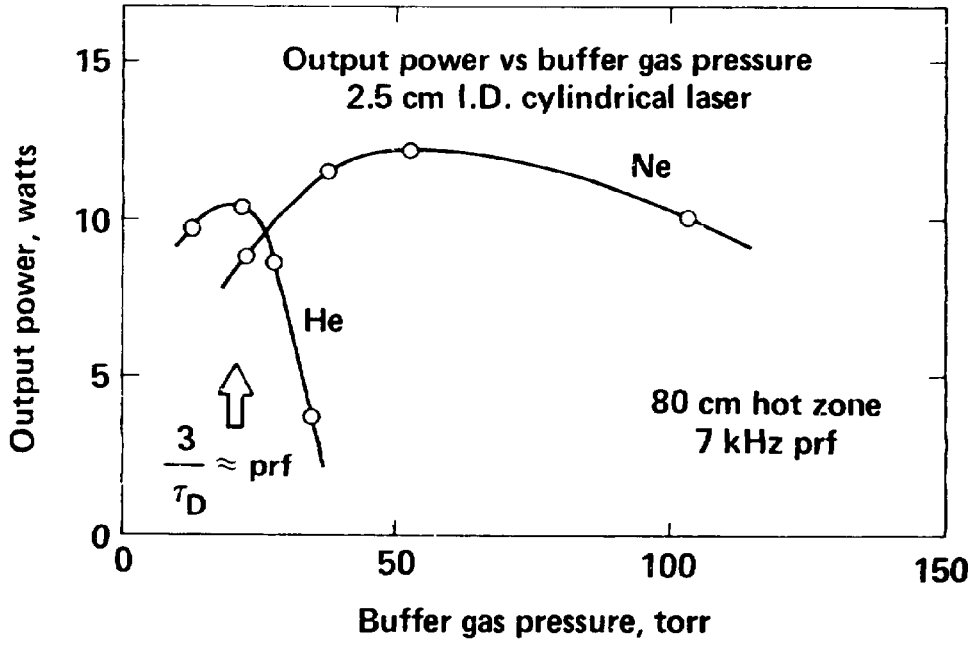

- Deactivation of Cu metastable in Cu-helium laser is due to diffusion:
  - $PRF \approx 3/\tau_D$
  - $\tau_D \propto P \cdot r^2$
- Deactivation of Cu metastable in Cu-neon laser has characteristics of a volumetric process

LARGE BORE CYLINDRICAL LASER

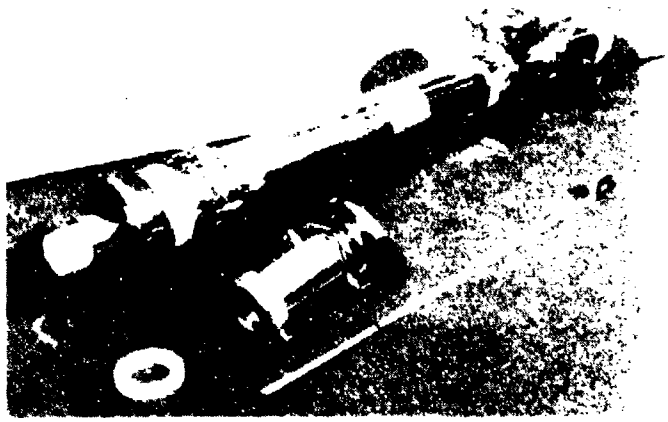

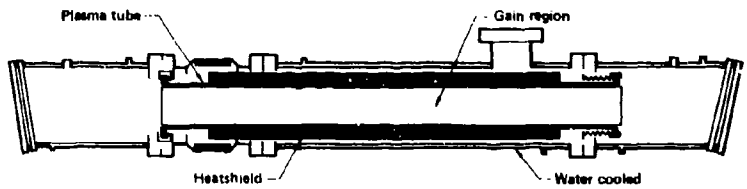

30-01-0180-0064

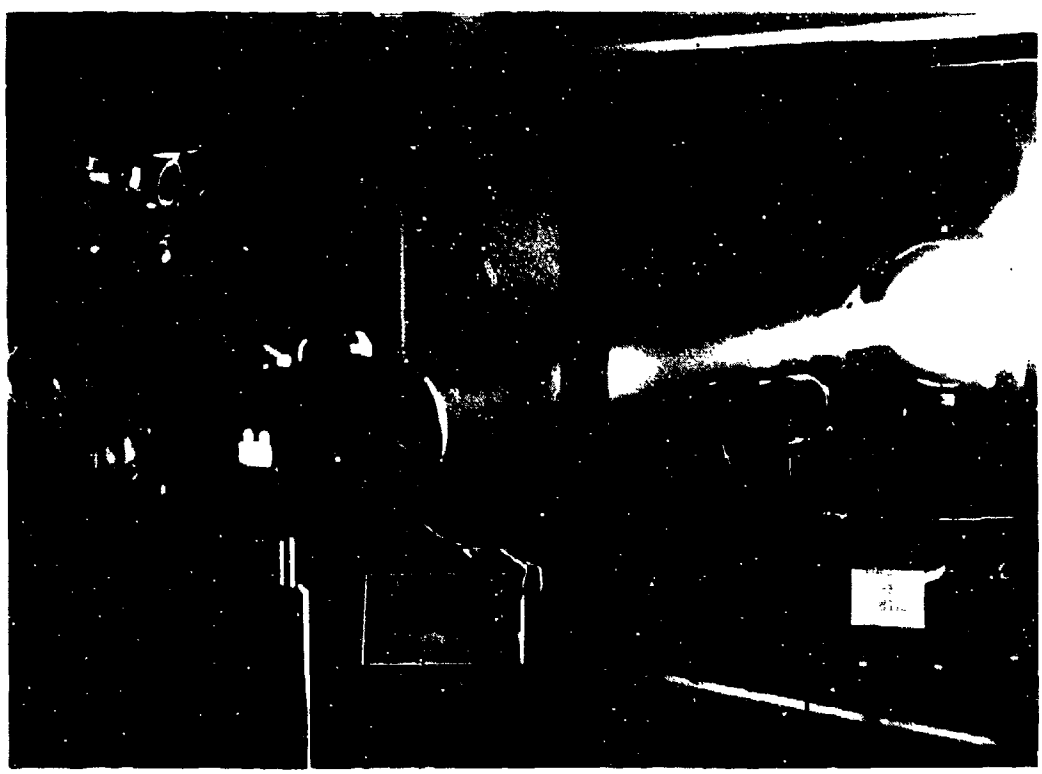

OSCILLATOR PERFORMANCE

Discharge tube I.D.	7.3 cm (2.9 in.)
Tube length	122 cm (48 in.)
Hot zone	60 cm (23 in.)
Neon pressure	33 torr
PRF	4 – 5 kHz
Efficiency (as osc)	0.6%

Output power	55 W

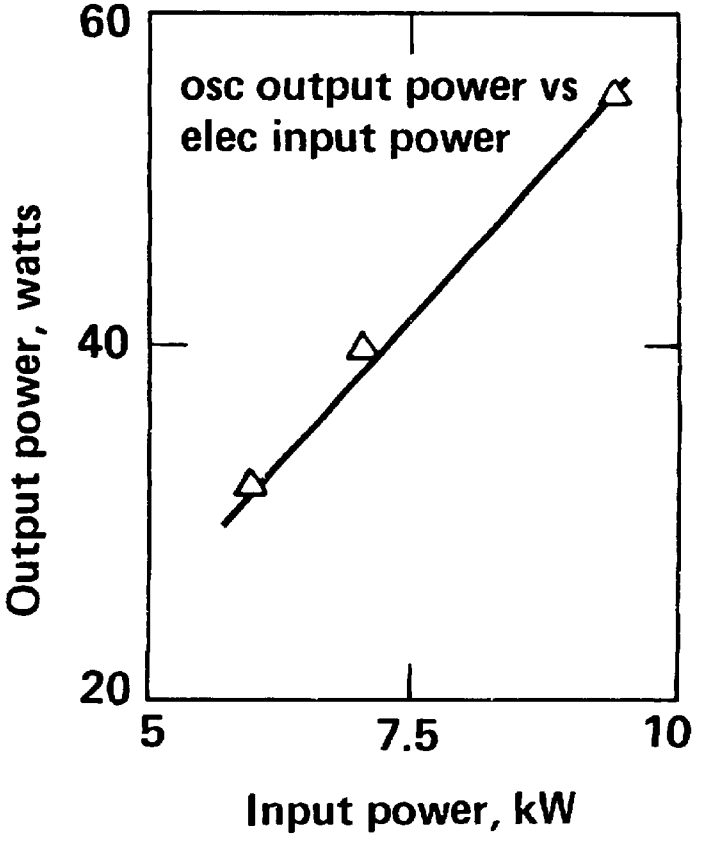

OUTPUT ENERGY DENSITY

Location	Date	Discharge	PRF	Output Energy Density	$\frac{\text{Estored}}{\text{Eosc}}$	Stored Energy Density
US-LLL	1977	Longitid (2.5 cm)	6 kHz	11 $\mu J/cm^3$	1.5	17 $\mu J/cm^3$
US-GE	1977	Longitud (2.5 – 4 cm)	1 – 2 kHz	30 $\mu J/cm^3$	1.5*	45 $\mu J/cm^{3*}$
US-LLL	1979	Longitud (7.3 cm)	5 kHz	6 $\mu J/cm^3$	1.8	10 $\mu J/cm^{3*}$
USSR	1976	Transv	Single shot	400 $\mu J/cm^3$	–	–
USSR	1977	Transv	Single shot	640 $\mu J/cm^3$	–	–

* Estimated

COPPER VAPOR LASER DEVELOPMENT – SUMMARY

- Copper lasers in 15-100 W (2-16 mJ) range are now well into engineering phase
- Effective use of MOPA configuration demonstrated
- Large bore (7.3 cm) Cu laser operated at 55 W
- Volumetric deactivation permits simple bore diameter scaling

⇨ Applicability of copper vapor lasers to many strategic and tactical problems should be reevaluated

30-17-0380-1032

CHANNEL CHARACTERIZATION SESSION

DOWNLINK LASER CLOUD PROPAGATION EXPERIMENTS

G. R. Hostetter

GTE Sylvania
PO Box 188
Mountain View, CA 94042

During the months of August-September 1979 the Downlink Lase Cloud Experiment was conducted by GTE for DARPA and the Navy. It was designed to obtain the first data on the stretching of a lase pulse resulting from vertical propagation through a cloud layer. The pulse stretching data is needed to design systems that can communicate between satellites and submarines using high intensit short pulse lasers.

GTE SYLVANIA

DOWNLINK LASER CLOUD EXPERIMENT

SPONSORS-DARPA/NAVY

CLOUD EXPERIMENT

GTE Systems

OBJECTIVE

OBTAIN FIRST REAL WORLD DATA FOR
LASER PULSES PROPAGATING VERTICALLY
THROUGH CLOUDS

DOWNLINK LASER CLOUD EXPERIMENT

GTE SYLVANIA

- KEY ISSUES
  - OPTICAL TRANSMISSION
  - PULSE STRETCHING AND SHAPE

TEST SET-UP
(DOWNLINK LASER CLOUD EXPERIMENT)

GTE SYLVANIA

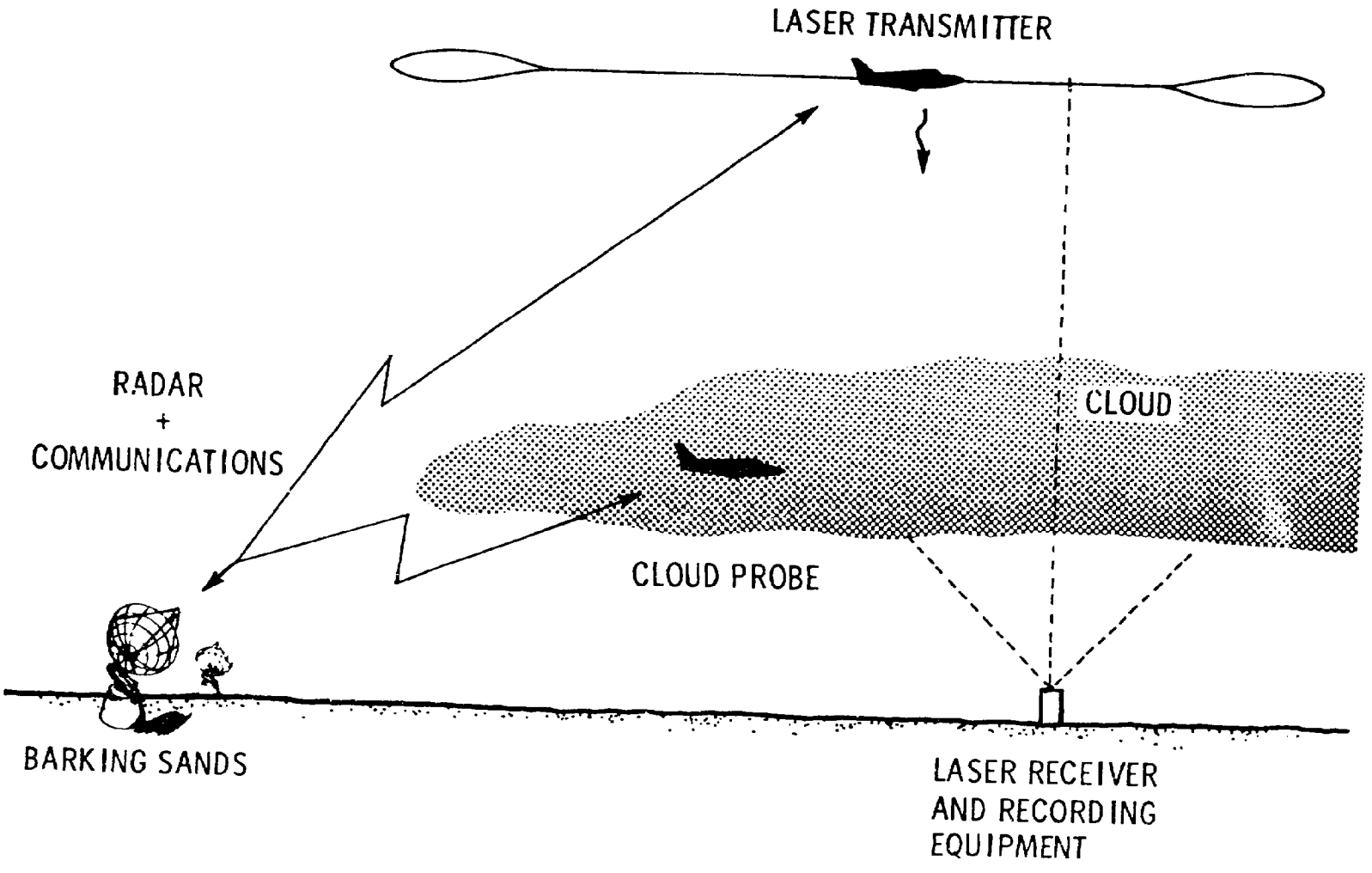

DATA COLLECTION AND REDUCTION

GTE Systems

COORDINATION FOR TESTS	SOURCE FOR DATA	BASIC DATA	REDUCED DATA	DATA EVALUATION
GTE	GTE	RECEIVED LASER SIGNAL AMPLITUDE	• TRANSMISSION • PULSEWIDTH • PULSE SHAPE	GTE
GTE	BARKING SANDS	AIRCRAFT POSITION	VS	
GTE	NOSC	PARTICLE SIZE AND DENSITY OF CLOUDS (EXTINCTION COEFFICIENT) BASE AND HEIGHT OF CLOUDS	OPTICAL THICKNESS OF CLOUD	
GTE	HSS/NOSC	PATH LENGTH DATA FROM MOONLIGHT	• PULSEWIDTH • PULSE SHAPE VS OPTICAL THICKNESS OF CLOUD	HSS/NOSC

PULSE SHAPE DATA: RUN NO. 182; SEPT 9, 0:55 AM (LOCAL TIME) (DOWNLINK LASER CLOUD EXPERIMENT)

GTE Systems

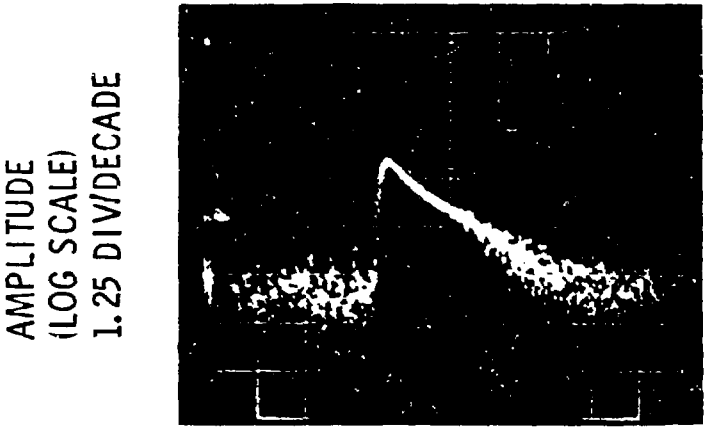

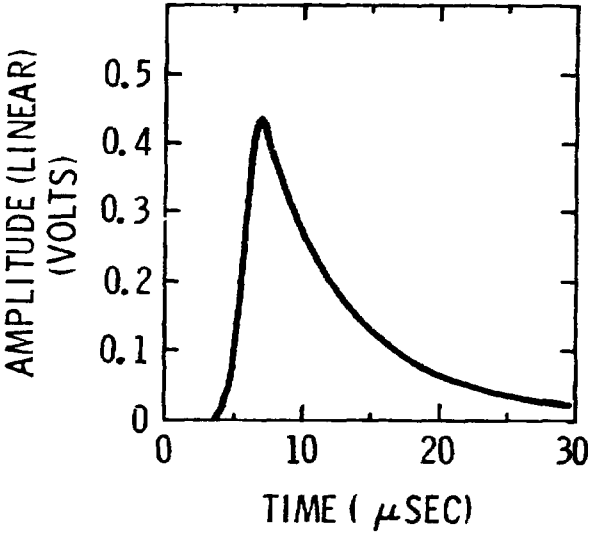

PULSEWIDTH (1/2 POWER)--6 MICROSECONDS

TIME TO PEAK--2 MICROSECONDS

CLOUD GEOMETRIC THICKNESS--≈ 4000 FT

OPTICAL THICKNESS--TBD

PULSE SHAPE DATA: RUN #082; AUG 30, 21:16 (PM) (LOCAL TIME) (DOWNLINK LASER CLOUD EXPERIMENT)

GTE Systems

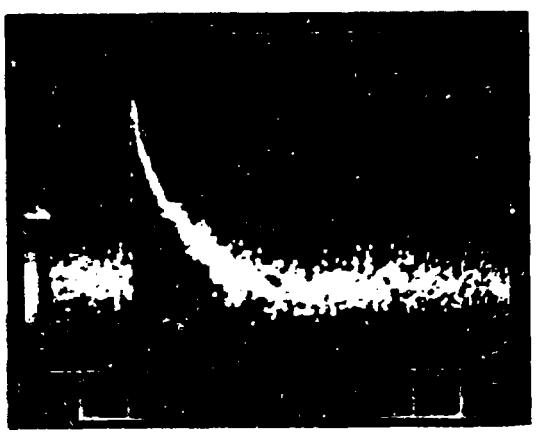

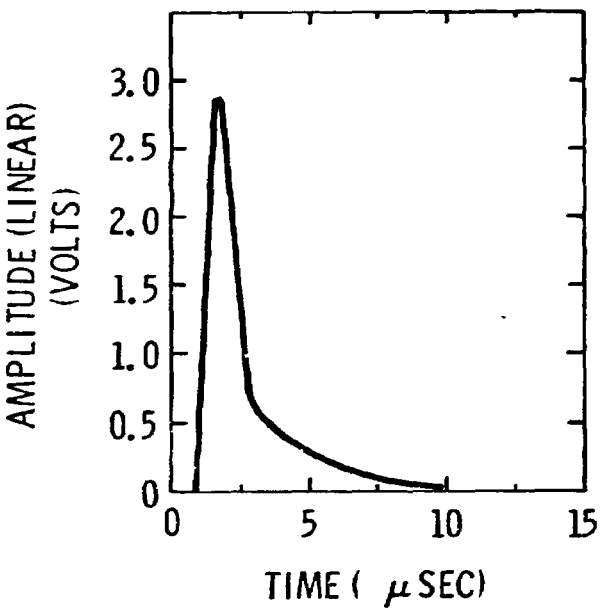

PULSE WIDTH (1/2 POWER)--1 MICROSECOND

TIME TO PEAK--1 MICROSECOND

CLOUD GEOMTRIC THICKNESS-- ≈1500

OPTICAL THICKNESS--TBS

PULSE SHAPE DATA: RUN #352; SEPT 21, 22:28 PM (LOCAL TIME)
(DOWNLINK LASER CLOUD EXPERIMENT)

GTE Systems

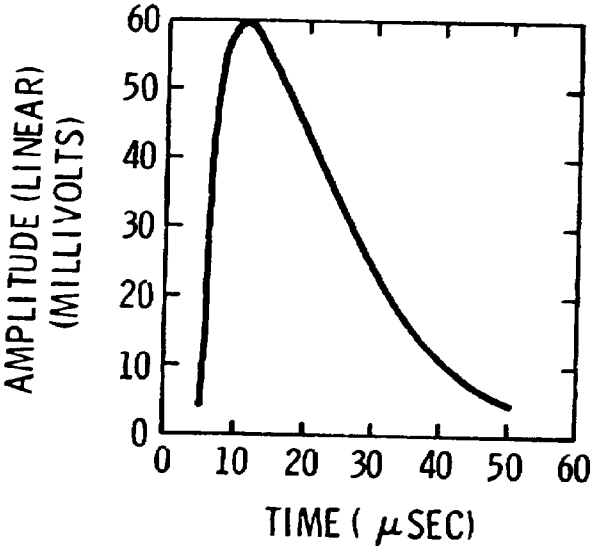

PULSEWIDTH (1/2 POWER)--22 MICROSECONDS

TIME TO PEAK--5 MICROSECONDS

CLOUD GEOMETRIC THICKNESS-- ≈8000 FT

OPTICAL THICKNESS--TBD

PULSE SHAPE DATA: RUN #129; SEPT 7, 1:53 AM (LOCAL TIME)
(DOWNLINK LASER CLOUD EXPERIMENT)

GTE Systems

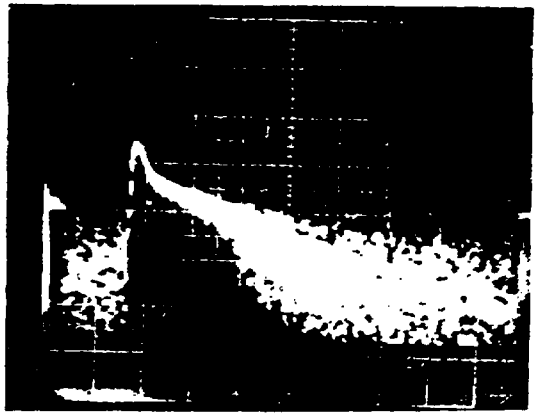

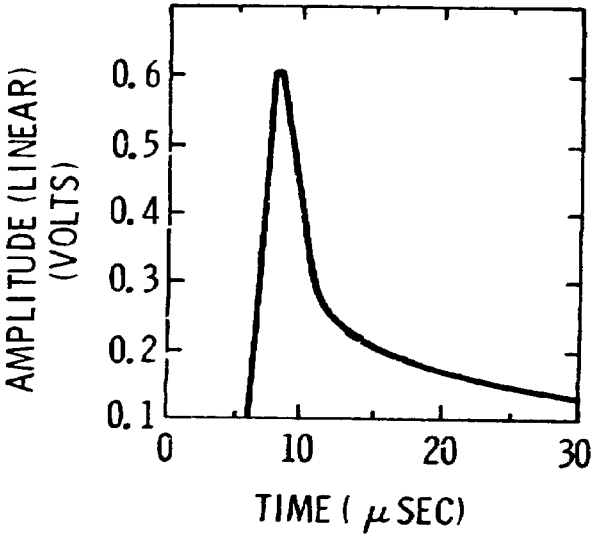

PULSEWIDTH (1/2 POWER)--3 MICROSECONDS

TIME TO PEAK--2 MICROSECONDS

CLOUD GEOMETRIC THICKNESS-- ≈5000 FT

OPTICAL THICKNESS--TBD

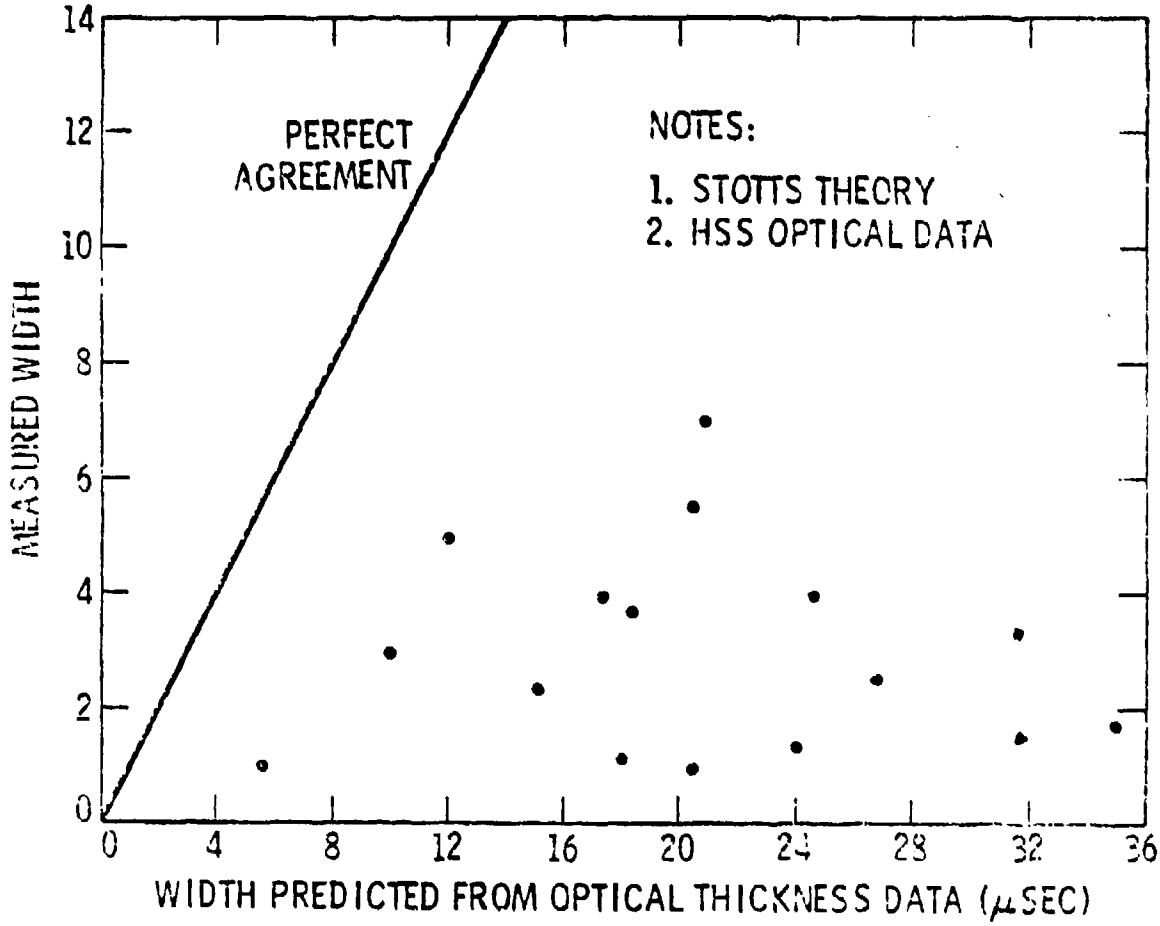

Data Analysis: Pulse Width-Predicted Vs Measured

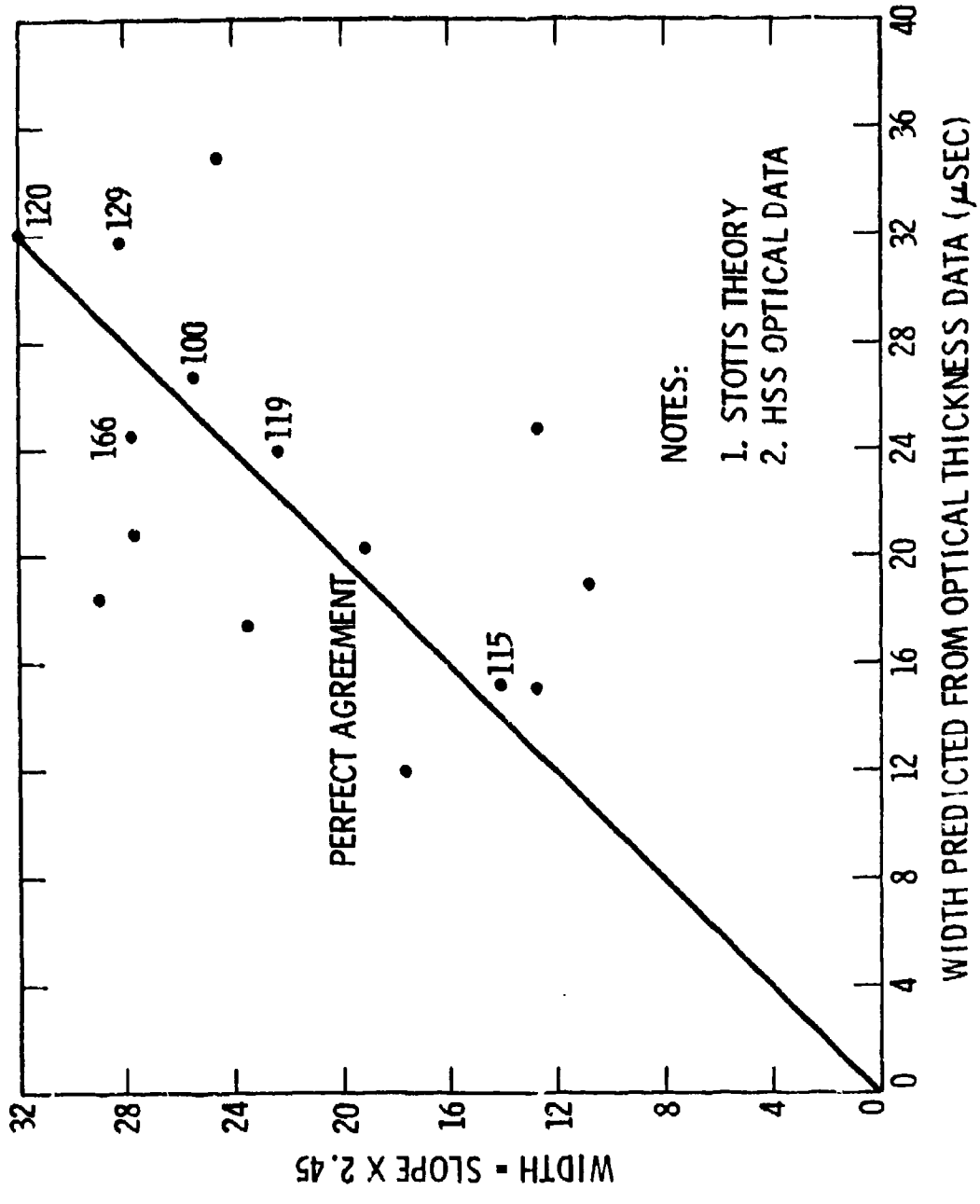

Data Analysis: Pulse Width-Predicted VS Inferred From Slope

CONCLUSIONS:
(DOWNLINK CLOUD EXPERIMENT)

GTE Systems

- PULSE WIDTH LESS THAN PREDICTED
- ANALYTICAL MODELS SHOULD BE IMPROVED TO INCLUDE REAL WORLD CLOUD GEOMETRIES
- DO MORE EXPERIMENTATION

EXPERIMENT DETAILS
(DOWNLINK CLOUD EXPERIMENT)

GTE Systems

- TEST DESCRIPTION
  - EQUIPMENT
  - TEST SITE
  - TEST SCHEDULE
- DATA REDUCTION
  - DATA AND SOURCES
  - ANALYSIS STEPS
  - CLOUD DATA
  - ADDITIONAL ANALYSIS


GTE SYLVANIA
GTE SYLVANIA

HIGH ALTITUDE AIRCRAFT
(DOWNLINK LASER CLOUD EXPERIMENT)

GTE Systems

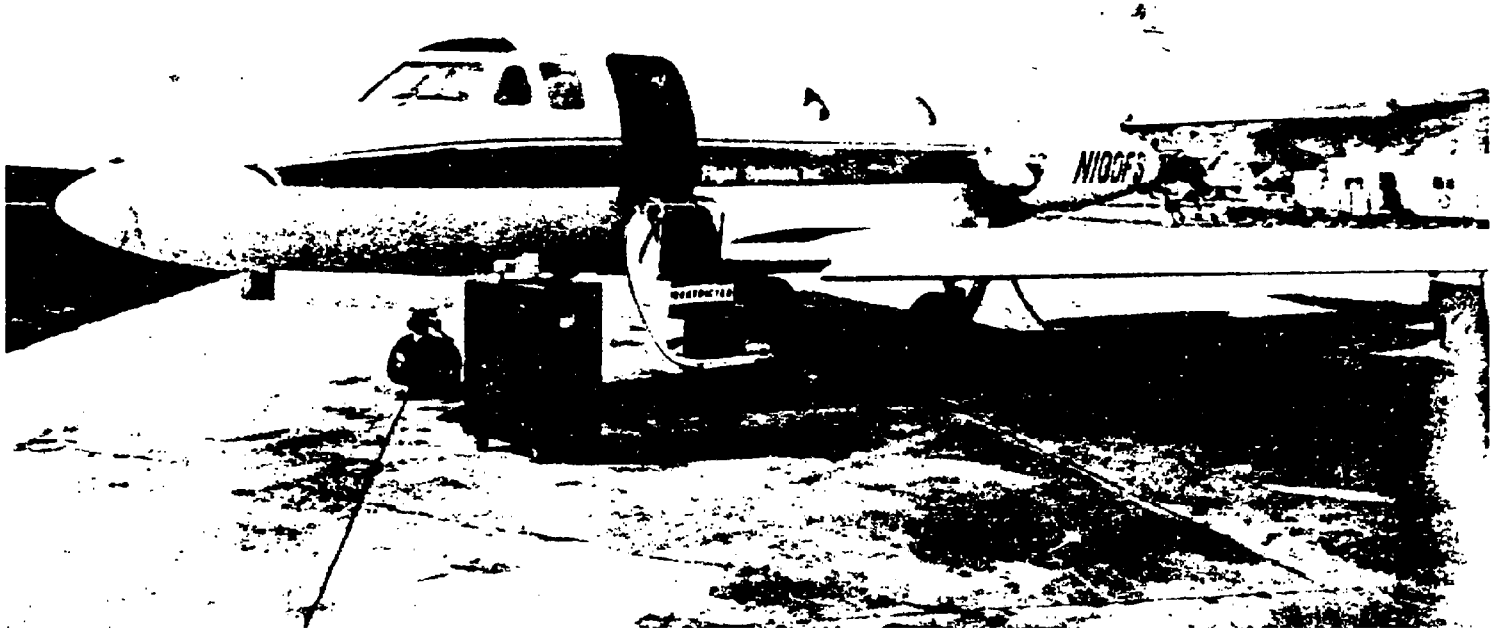

LASER MOUNTED IN AIRCRAFT (DOWNLINK LASER CLOUD EXPERIMENT)

GTE Systems

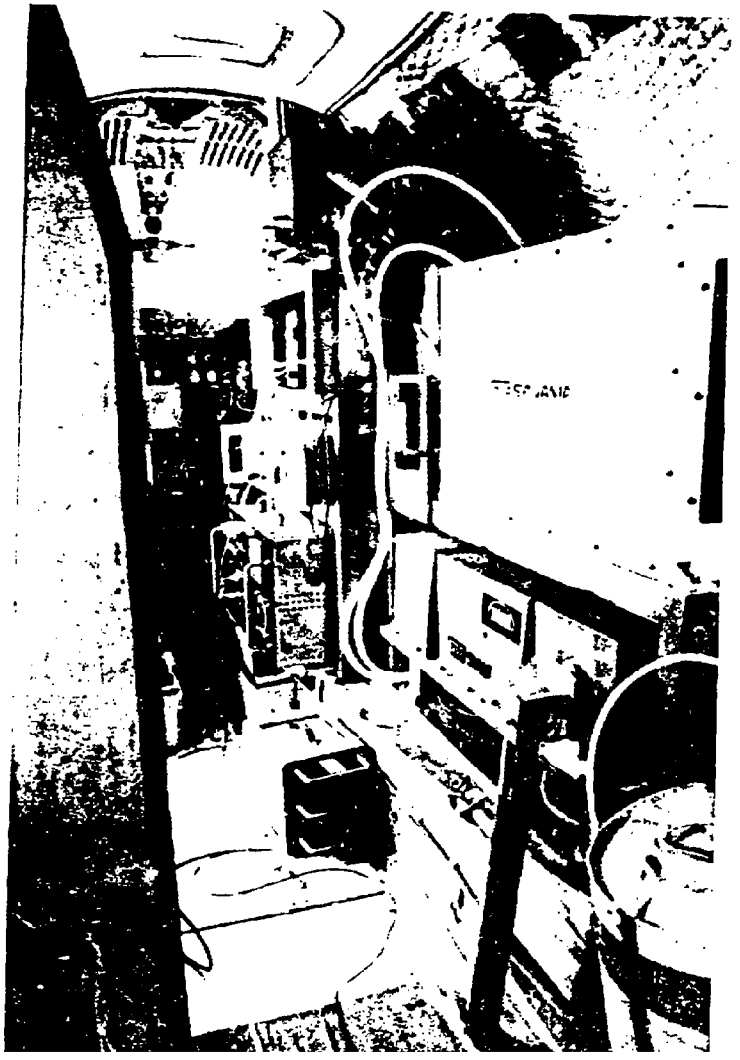

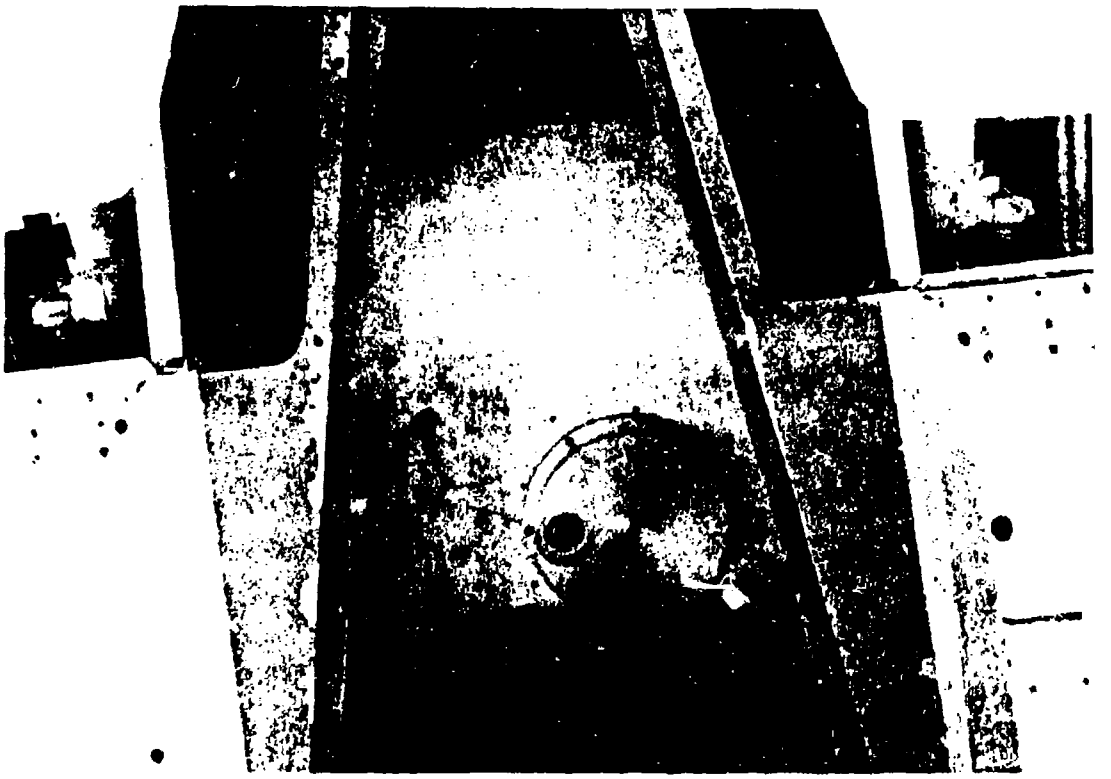

Aircraft Window For Laser Output

PREFLIGHT LASER TEST
(DOWNLINK LASER CLOUD EXPERIMENT)

GTE Systems

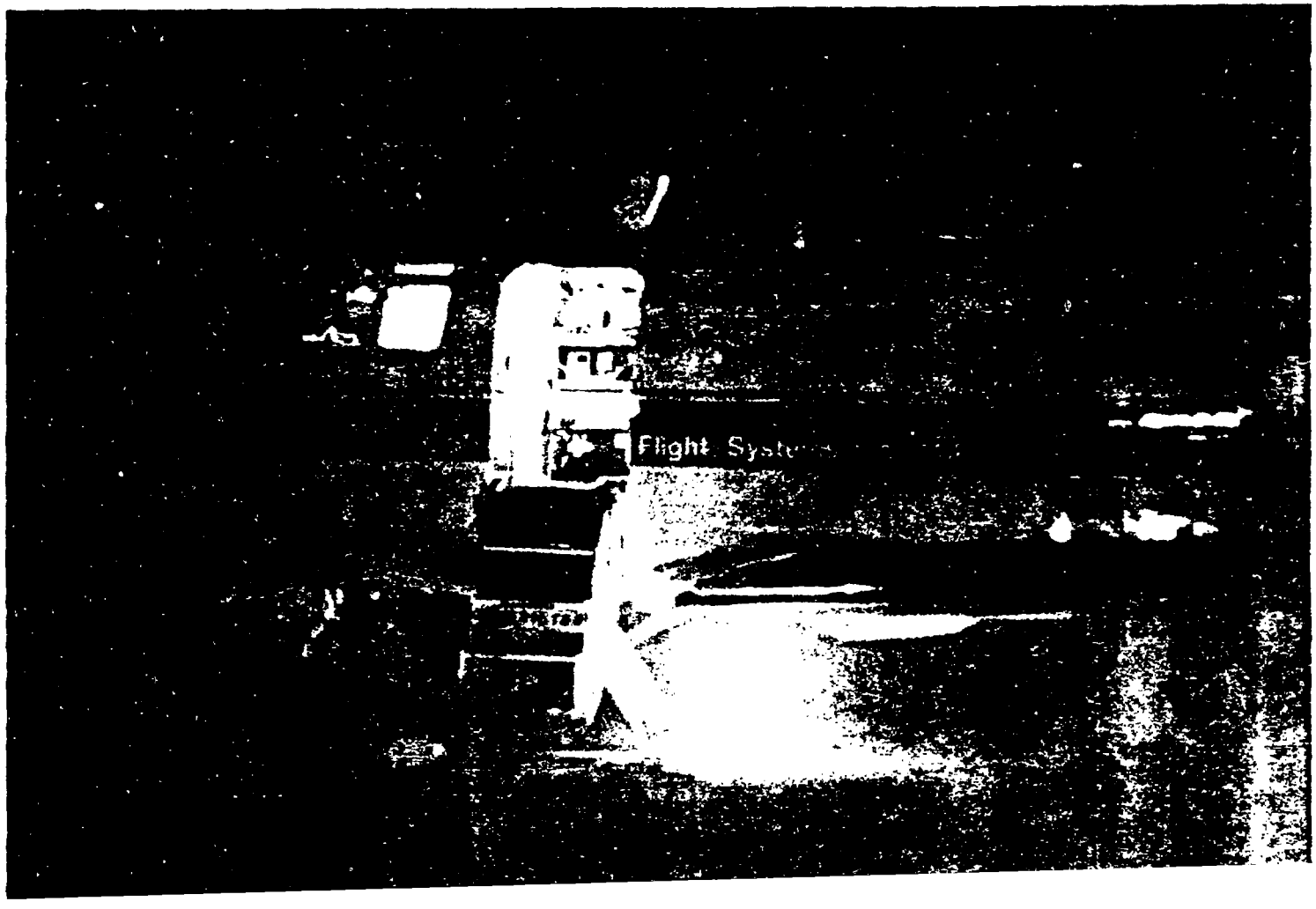

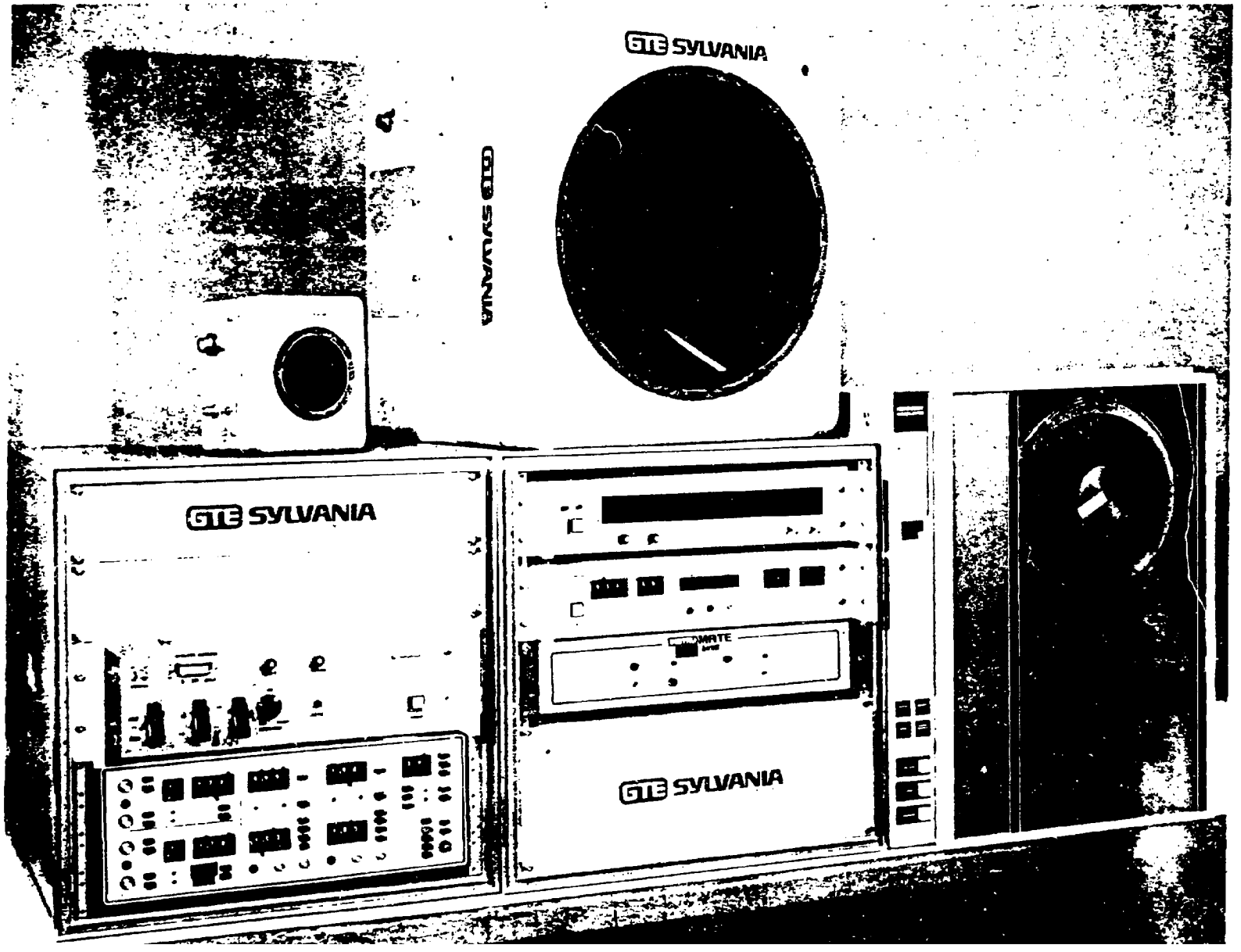
GTE SYLVANIA
GTE SYLVANIA
GTE SYLVANIA
GTE SYLVANIA

RECEIVER: WITHIN TRAILER
(DOWNLINK LASER CLOUD EXPERIMENT)

GTE Systems

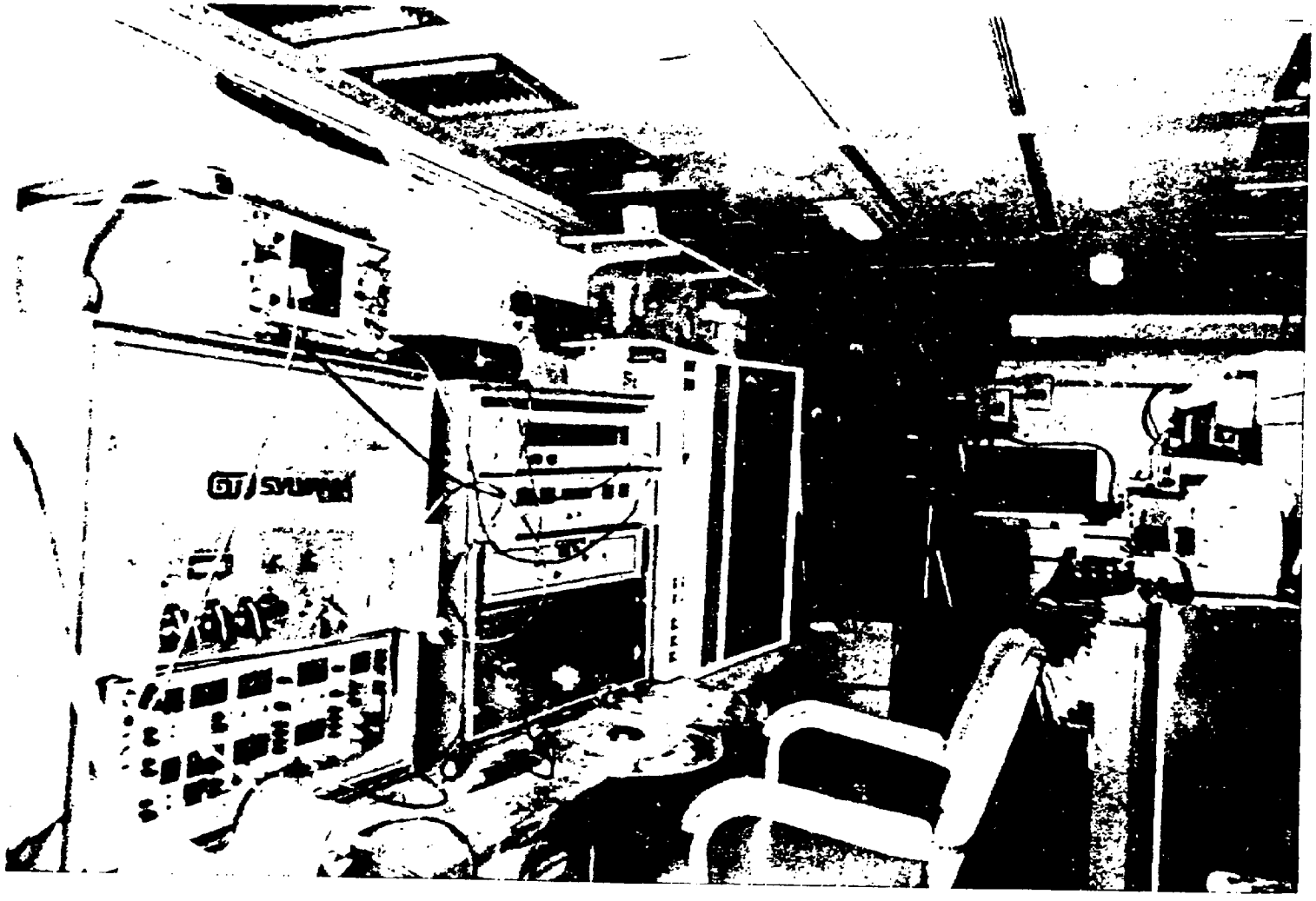

CLOUD FORMATIONS AT KAUAI

GTE SYLVANIA

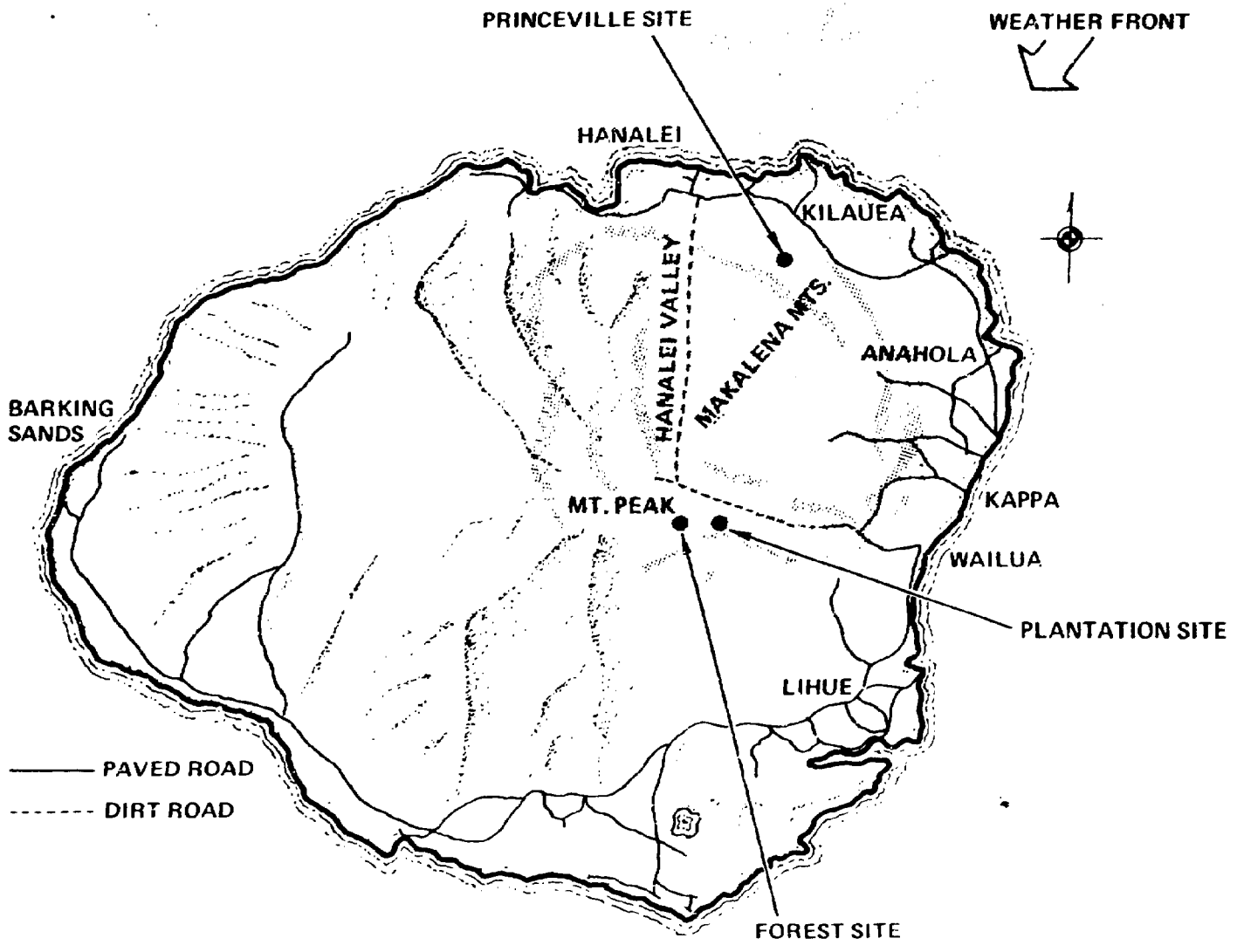

TEST SITE: AERIAL VIEW
(DOWNLINK LASER CLOUD EXPERIMENT)

GTE Systems

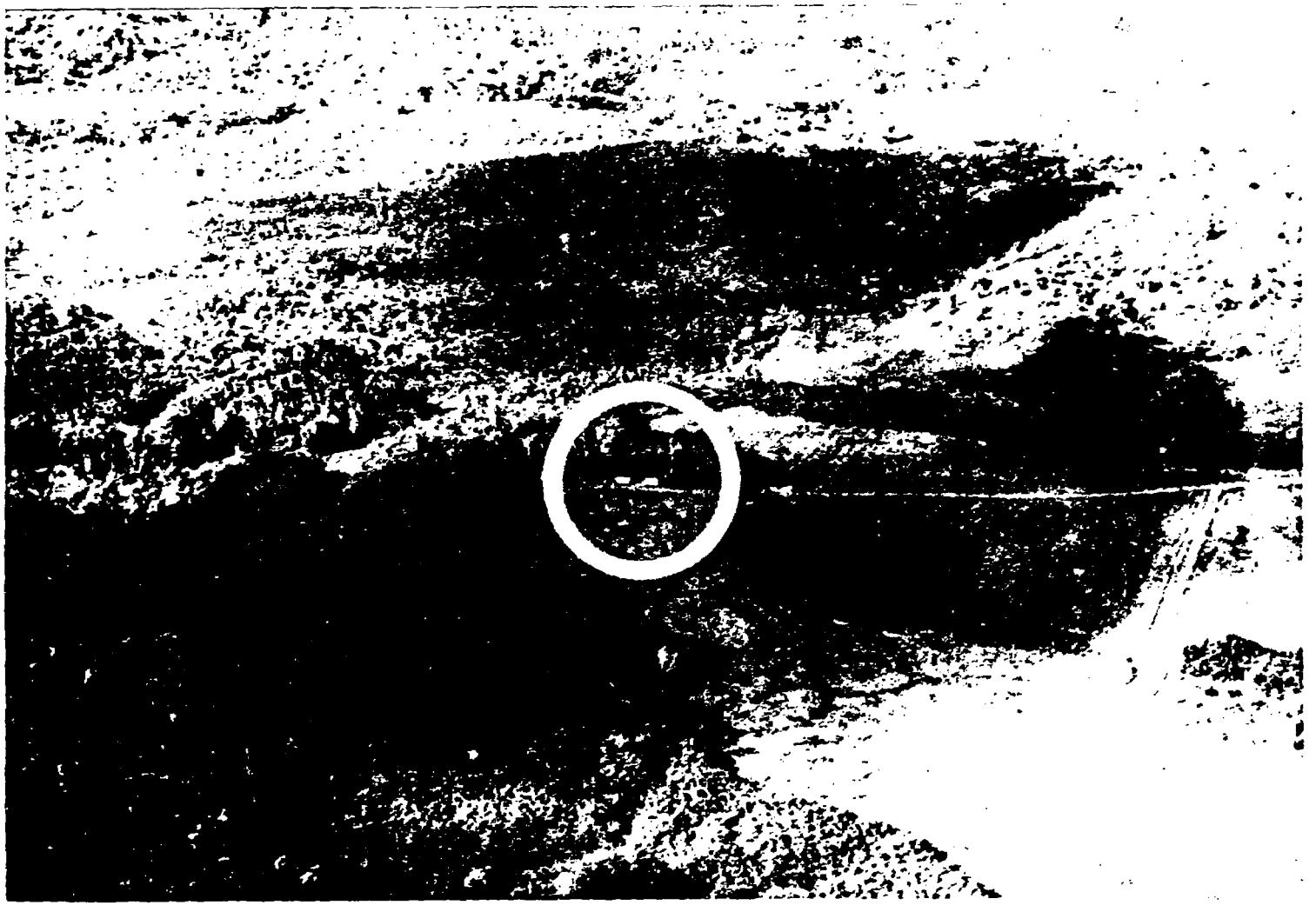

TEST SITE
(DOWNLINK LASER CLOUD EXPERIMENT)

GTE Systems

TEST SITE LAYOUT
(DOWNLINK LASER CLOUD EXPERIMENT)

GTE Systems

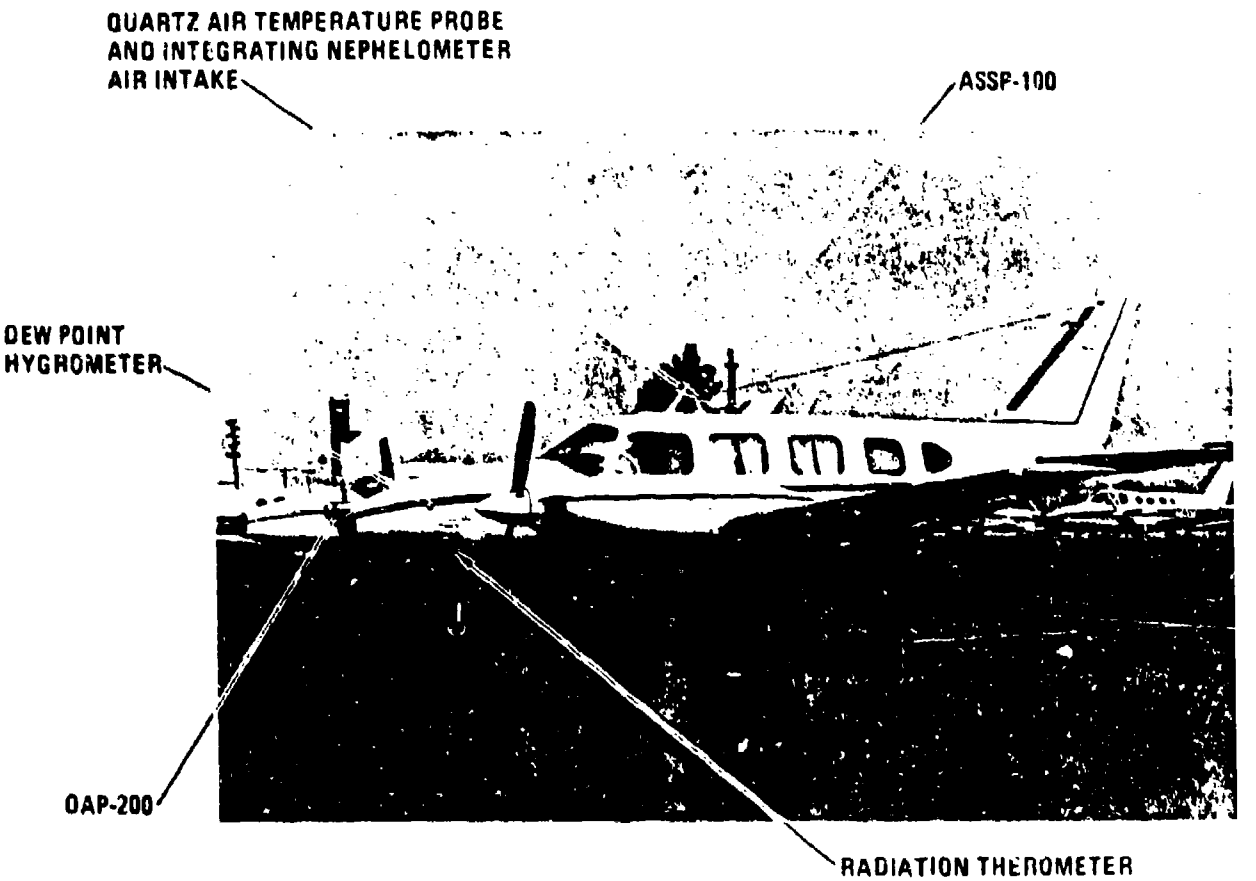

Instrumented Cloud Probe Aircraft

FLIGHT PATH OF CLOUD PROBE AIRCRAFT (DOWNLINK LASER CLOUD EXPERIMENT)

GTE Systems

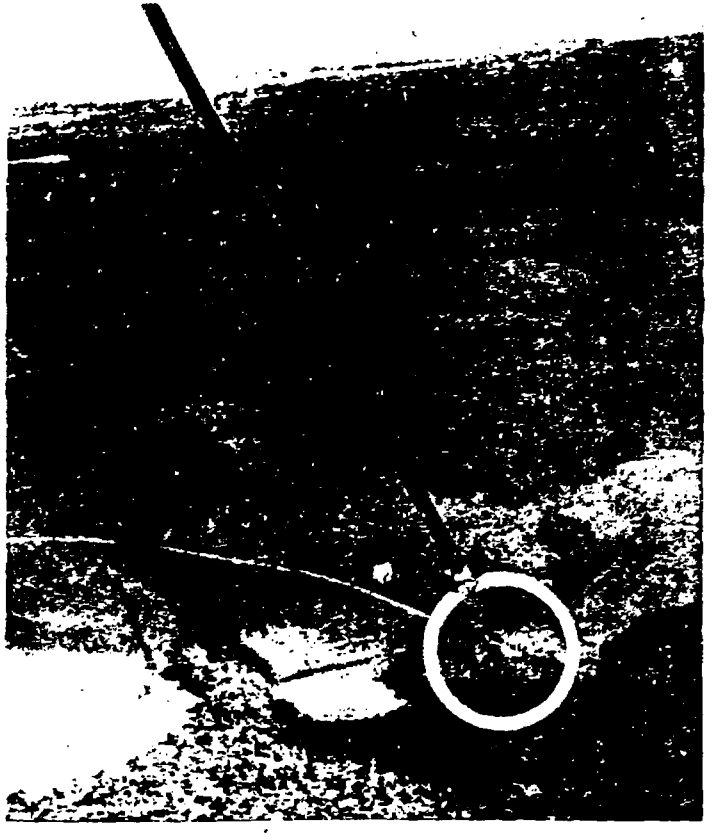

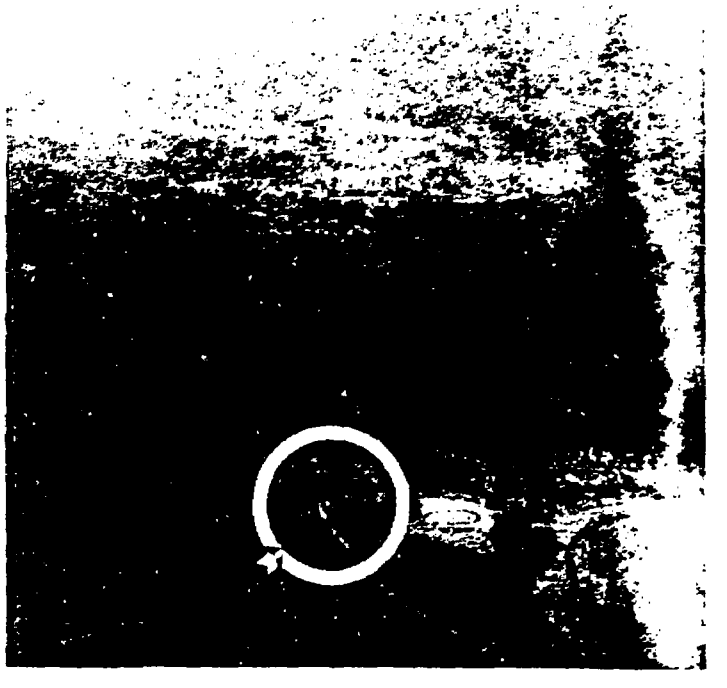

MT. WAIALEALE, KAUAI
(DOWNLINK LASER CLOUD EXPERIMENT)

GTE Systems

CLOUD PATTERNS
(DOWNLINK LASER CLOUD EXPERIMENT)

GTE Systems

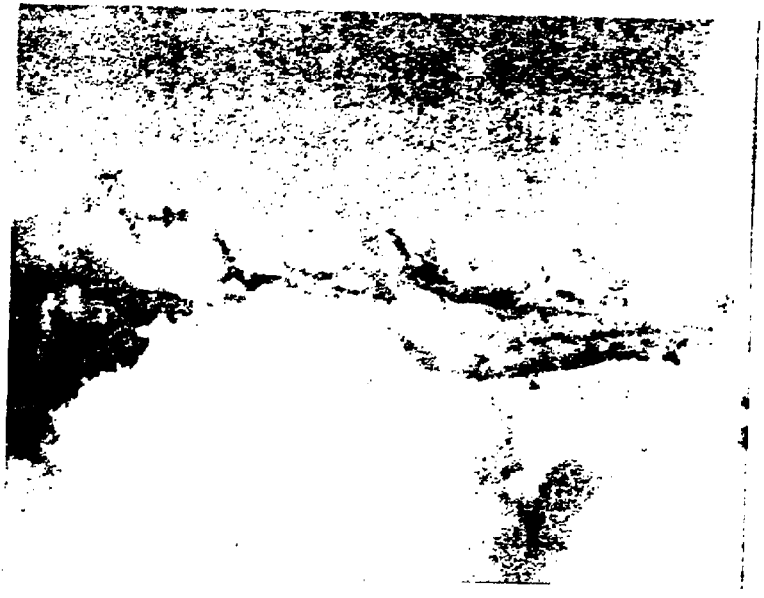

PLOT BOARD PLOT, LARGE SCALE (DOWNLINK CLOUD EXPERIMENT)

GTE Systems

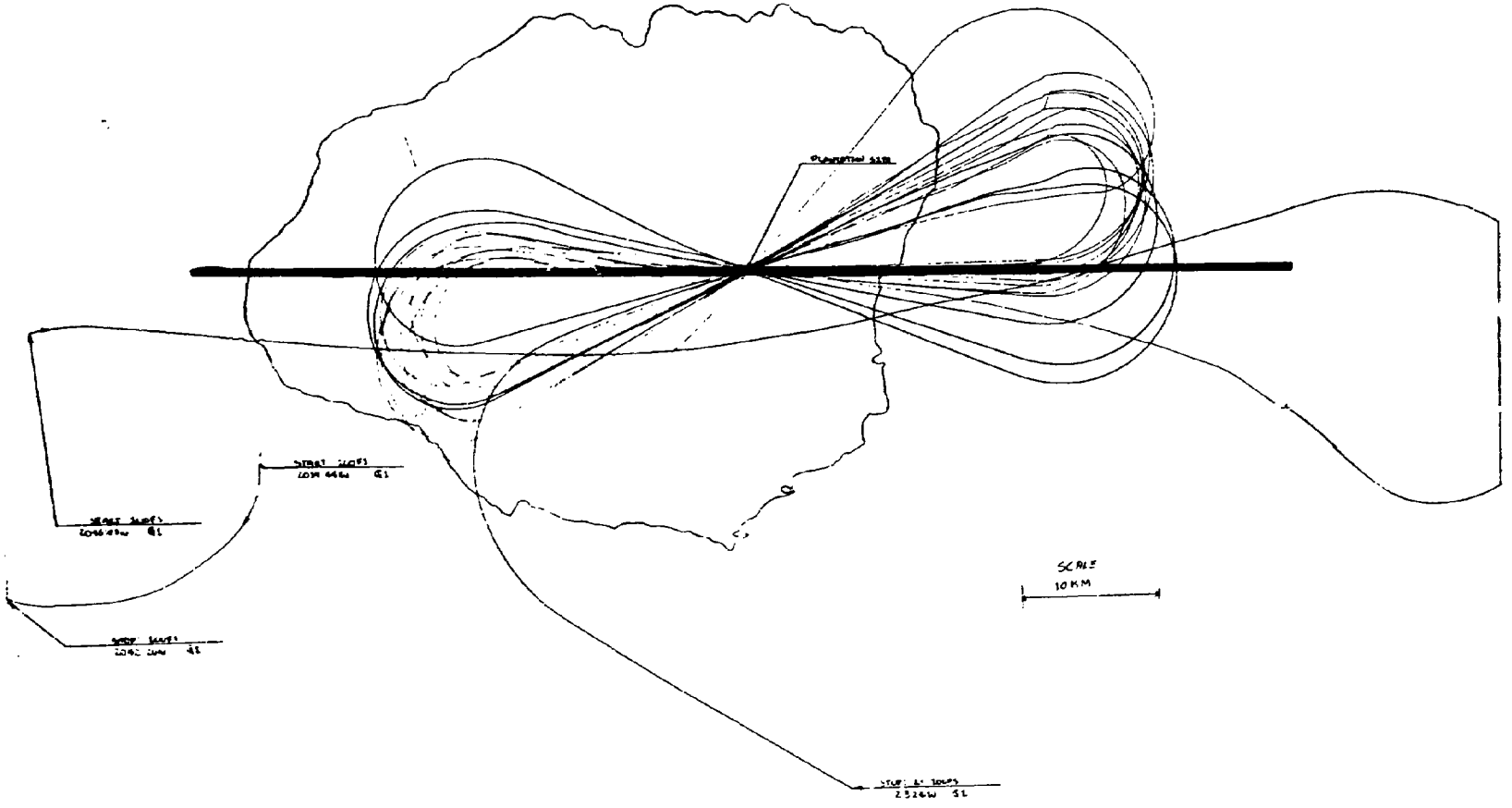

Sylvania Systems Group
Western Division

PLOT BOARD PLOT, FINE SCALE (DOWNLINKCLOUD EXPERIMENT)

GTE Systems

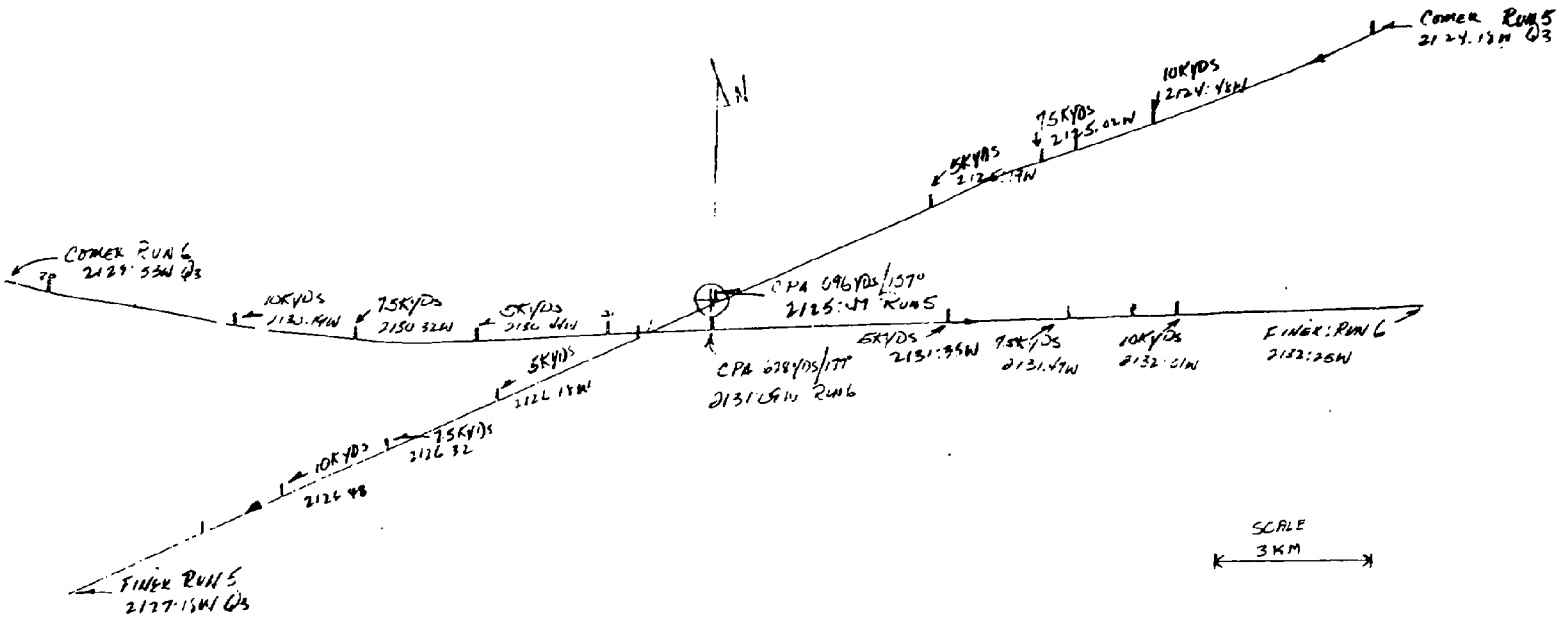

Sylvania Systems Group
Western Division

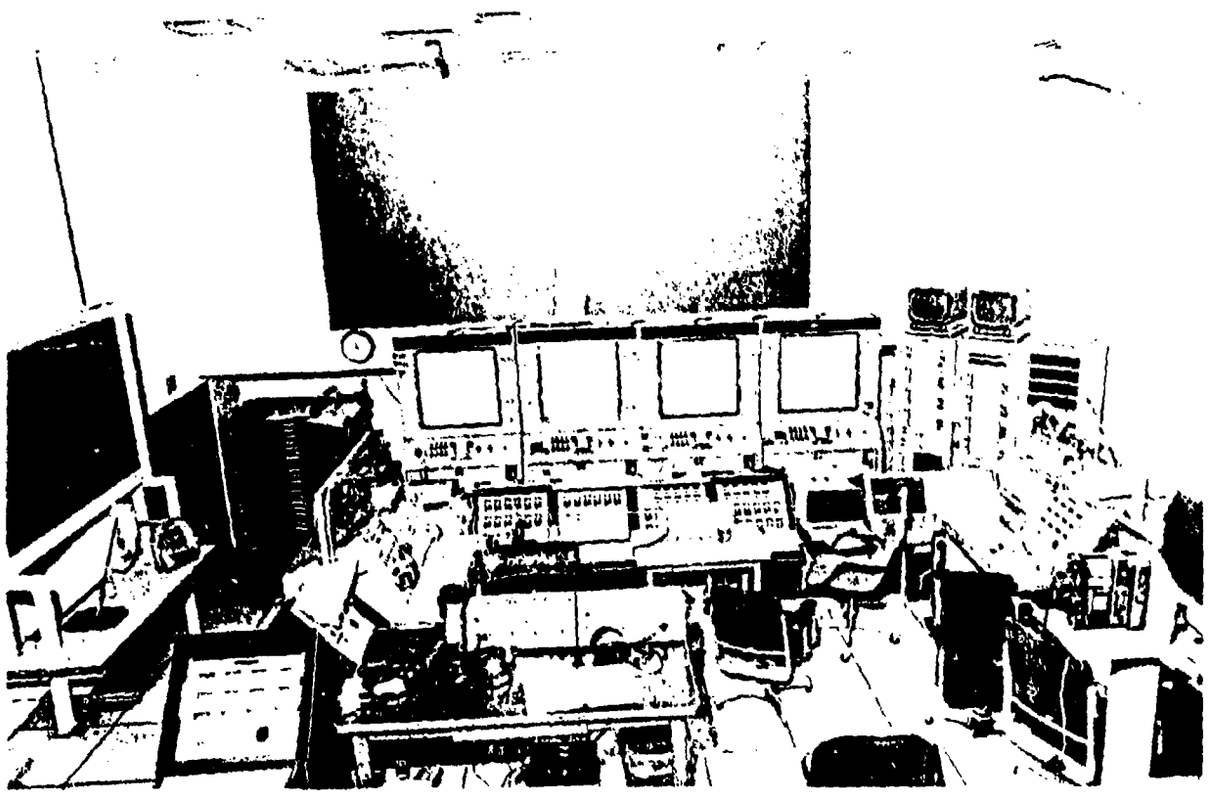

Control Room "BRAVO" at PMRF

AIRCRAFT FLIGHT PATH ABOVE SITE (DOWNLINK LASER CLOUD EXPERIMENT)

GTE Systems

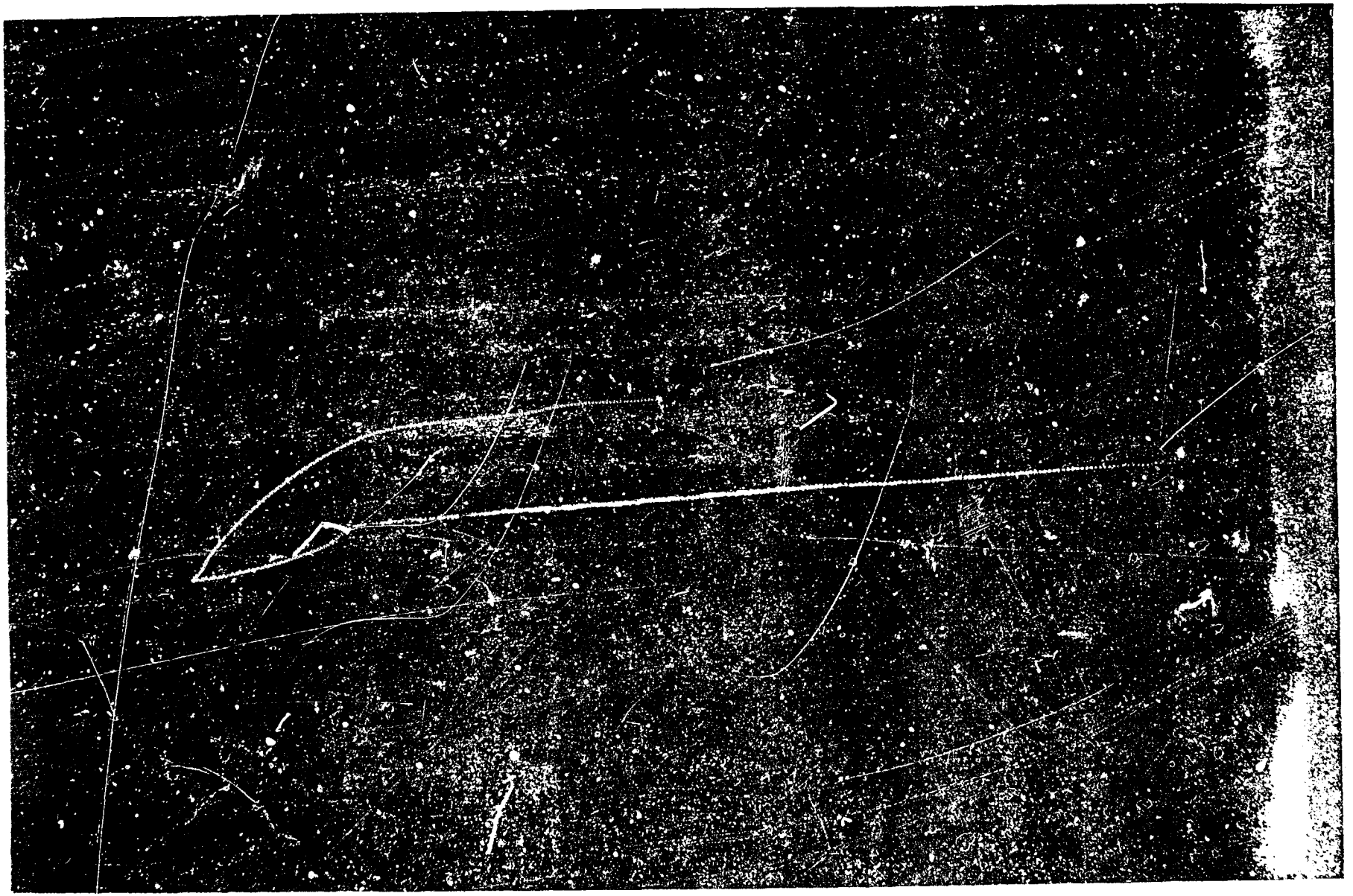

MONTHLY SCHEDULE
(DOWNLINK CLOUD EXPERIMENT)

GTE Systems

AUGUST 1979

SUN	MON	TUES	WED	THURS	FRI	SAT
			1	2	3	4
5	6	7	8	(9) FLIGHT TEST	10	11
12 GTE/HSS ARRIVE	13	14 PMRF INTERFACE	15	16	17	18
19 AIRCRAFT ARRIVE	(20) BEGIN EXPERIMENT	(21)	22	23	(24)	25
26	27	28	29	(30)	31	

SEPTEMBER 1979

SUN	MON	TUES	WED	THURS	FRI	SAT
						1
2	3	4	(5) (BEST TWO NIGHTS FOR HSS)	(6)	(7)	(8)
9	10	(11)	(12)	(13)	(14)	15
16	(17)	(18)	(19)	(20)	(21) LAST NIGHT	22
23 RETURN TO CONUS	24	25	26	27	28	29

DATA TAKING OVERVIEW (DOWNLINK CLOUD EXPERIMENT)

GTE Systems

- 19 TOTAL FLIGHTS, TEST OR DATA
- 13 FLIGHTS WITH GOOD DATA, 3 WITH ONLY MARGINAL DATA
- 360 DATA RUNS (200,000 DATA PULSES X 4,000 BITS/PULSE = 800 MILLION BITS INFO)
- 80 RUNS, HIGHEST PRIORITY (GOOD DATA)
- 84 RUNS, SECOND PRIORITY (MARGINAL DATA)

DATA ANALYSIS PROCEDURE (DOWNLINK CLOUD EXPERIMENT)

- INITIAL SURVEY OF DATA
- DATA AVERAGING
- PULSE PARAMETER EVALUATION
- SLOPE EVALUATION

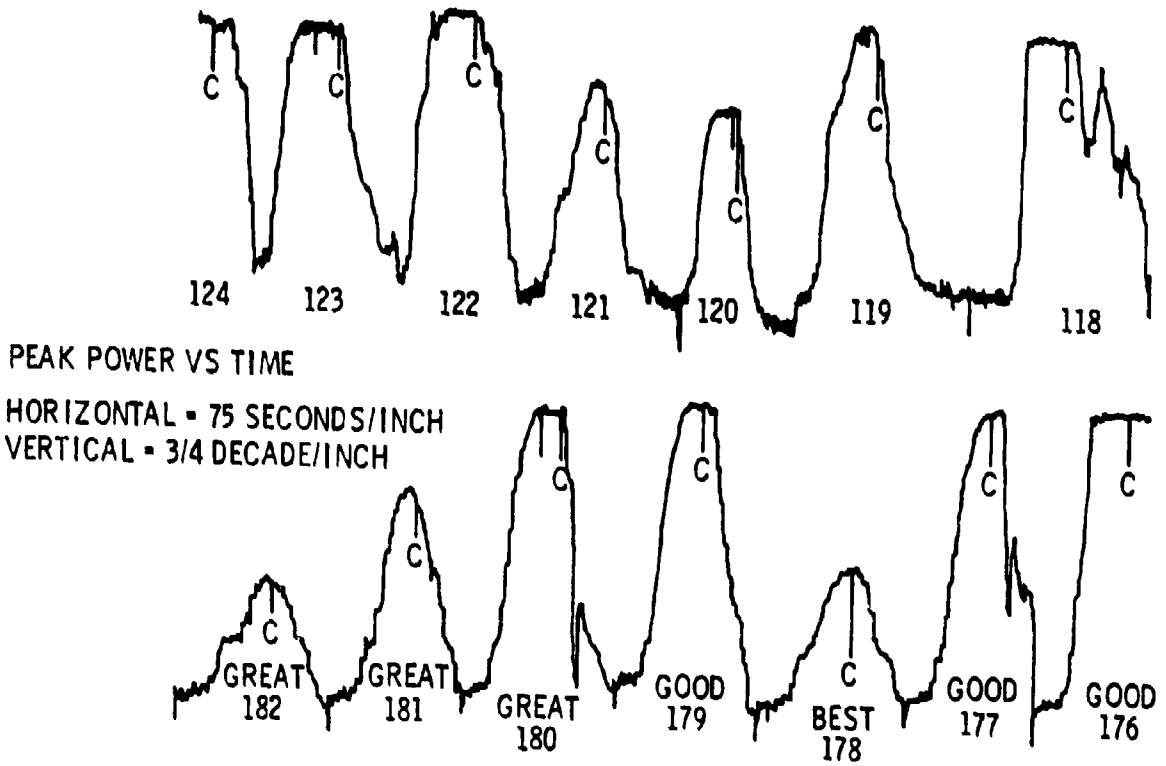

Data Survey, Typical Plot

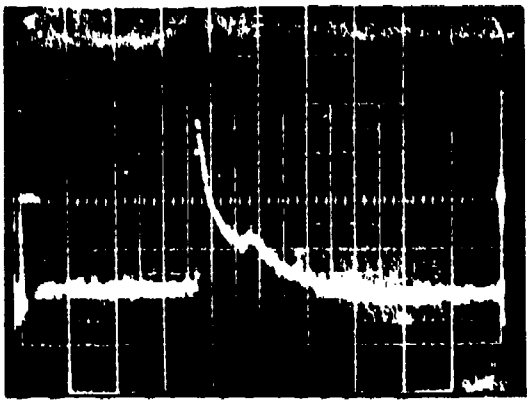

32

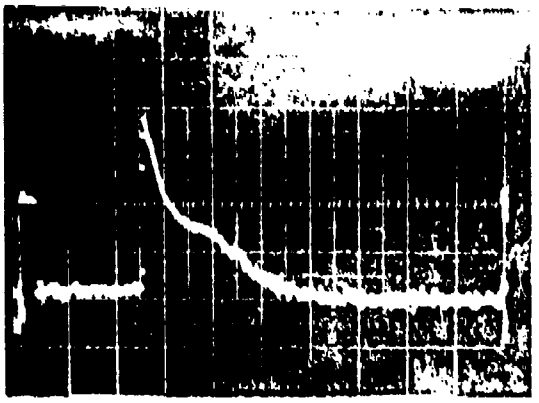

38

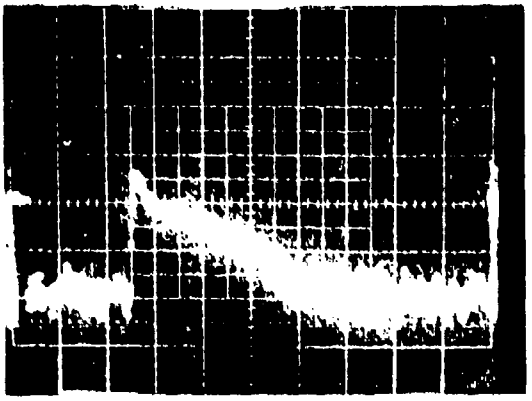

100

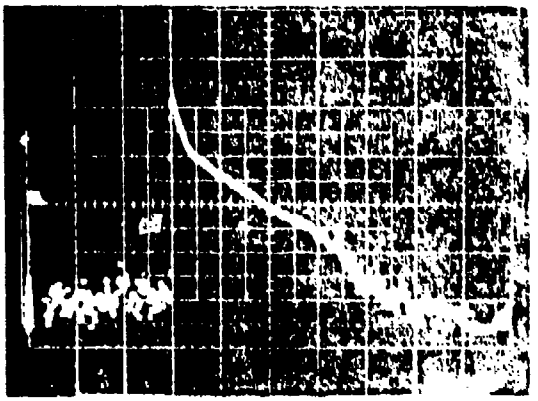

119

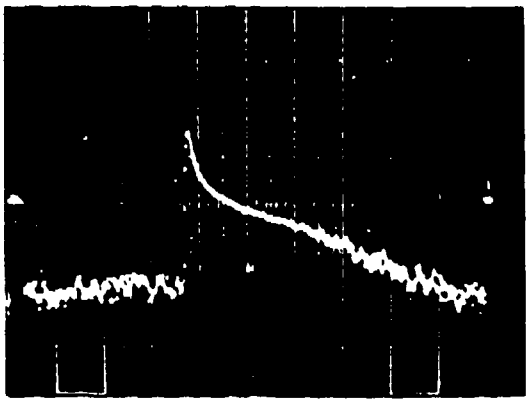

120

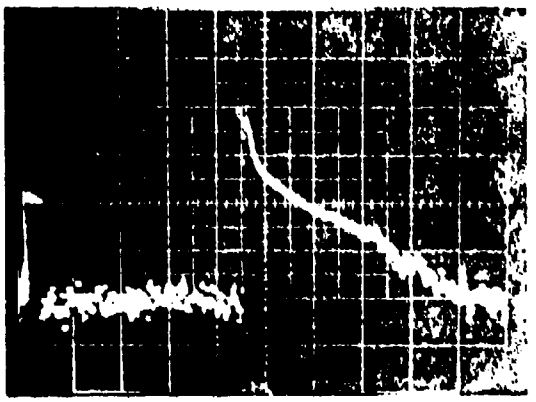

121

Typical Data From Six Runs

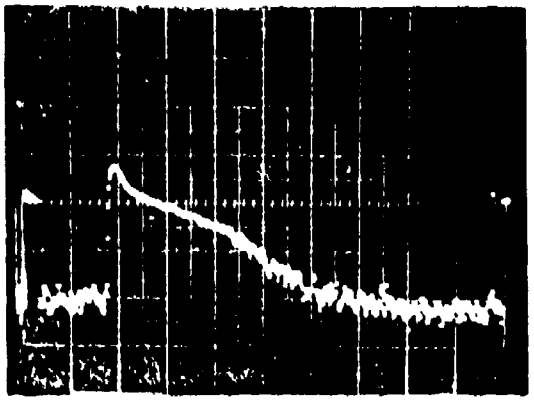

129

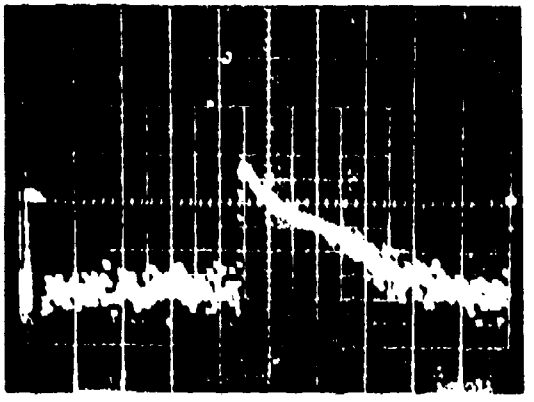

166

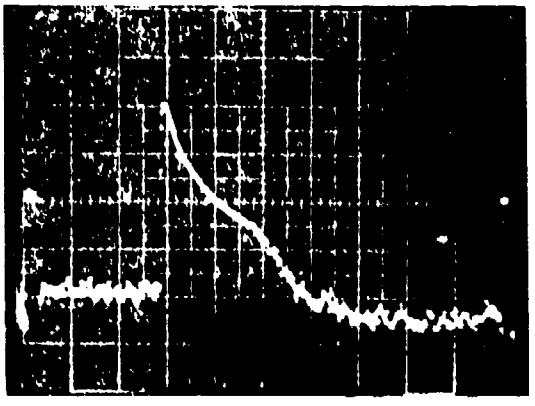

175

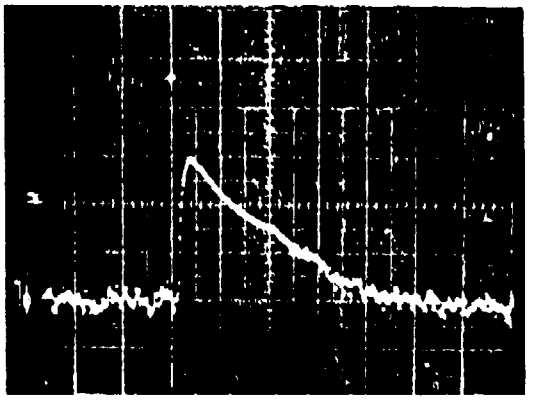

178

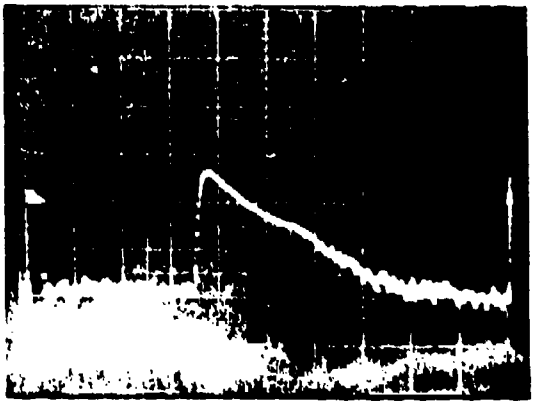

182

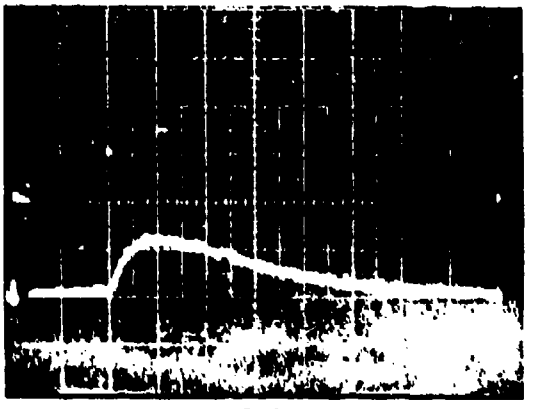

260

Typical Data From Six Runs

GTE

PULSE SHAPE PARAMETERS

GTE RUN UMBER	(μsec) WIDTH	TIME TO PEAK	MEAN DELAY	10^{-6}W PEAK POWER	10^{-12}WS ENERGY	ATTENU-ATION	μsec/1/e SLOPE 1	μsec/1 SLOPE 2
190	Bomb							
191	2.2	1.4	1.4	1.12	2.63	.033	1	6
192	1.8	.8	1.34	2.4	5.9	.039	1	6
193	2.0	1.0	4.5	1.19	4.67	.058	1,5	9
200				.209				
225				.209				
231	.8	.4		11.9	11.5	.14		
232	1.0	.4		6.5	8.81	.11		
233	1.0	.6		4.9	6.56	.082		
234	2.2	1.0	3.9	.94	3.95	.049	2	6
235	.8	.4		12.8	13.9	.17		
236	1.8	1.0		2.47	6.89	.086		
237	2.0	1.2	.8	11.2	35.6	.45	1	5
238	.6	.4		14.6	10.7	.133		
249	1.0	.6		11.9	20.6	.26		
250								
252				.178				

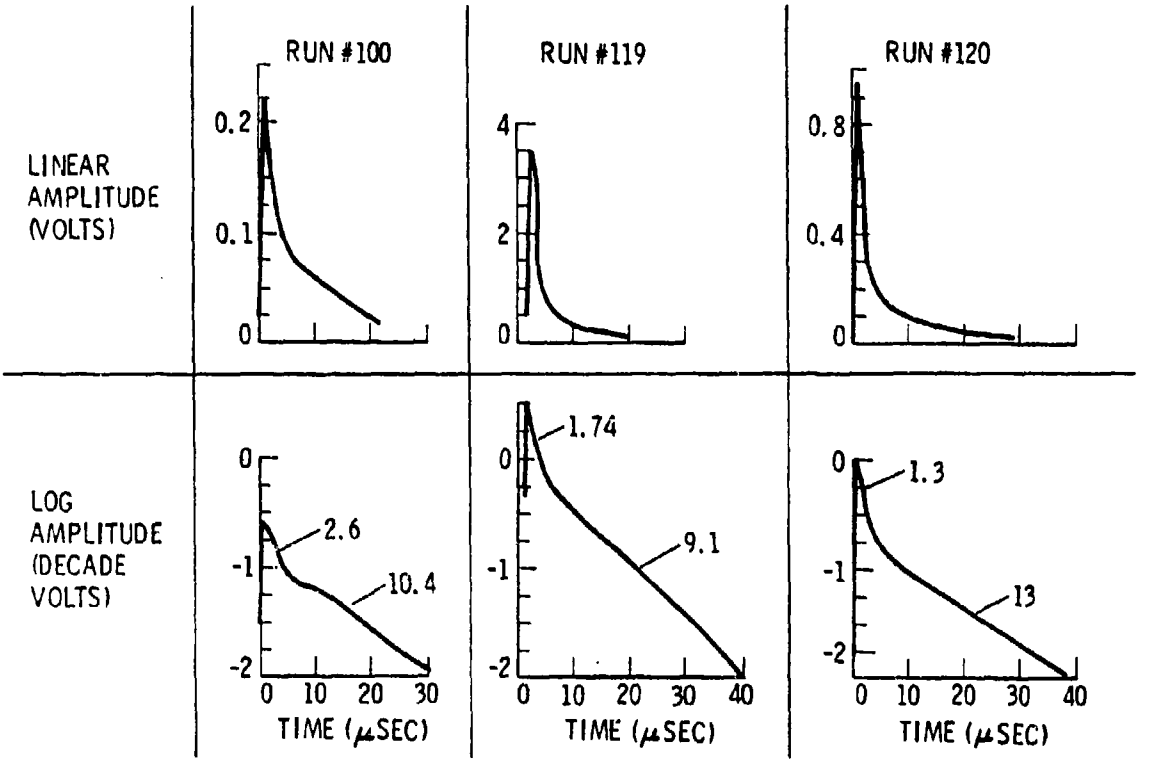

Reduced Data Plots

SLOPE EVALUATION (DOWNLINK CLOUD EXPERIMENT)

GTE Systems

- FOR DIAGNOSTIC PURPOSES, CALCULATE SLOPE OF LOG PLOTS - TIME CONSTANT
- MANY CURVES WITH TWO DISTANT TIME CONSTANTS

WEATHER CHARACTERISTICS (DOWNLINK CLOUD EXPERIMENT)

GTE Systems

- CLOUDY TIMES CYCLIC
  - 8 - 8:30 PM
  - 10 - 10:30 PM
  - 12:30 - 1:00 AM
- TYPICAL OPTICAL THICKNESS CALCULATED BY HSS = 15 - 80
- CLOUD PROBE DATA CALCULATE OPTICAL THICKNESS = 1 - 10

501

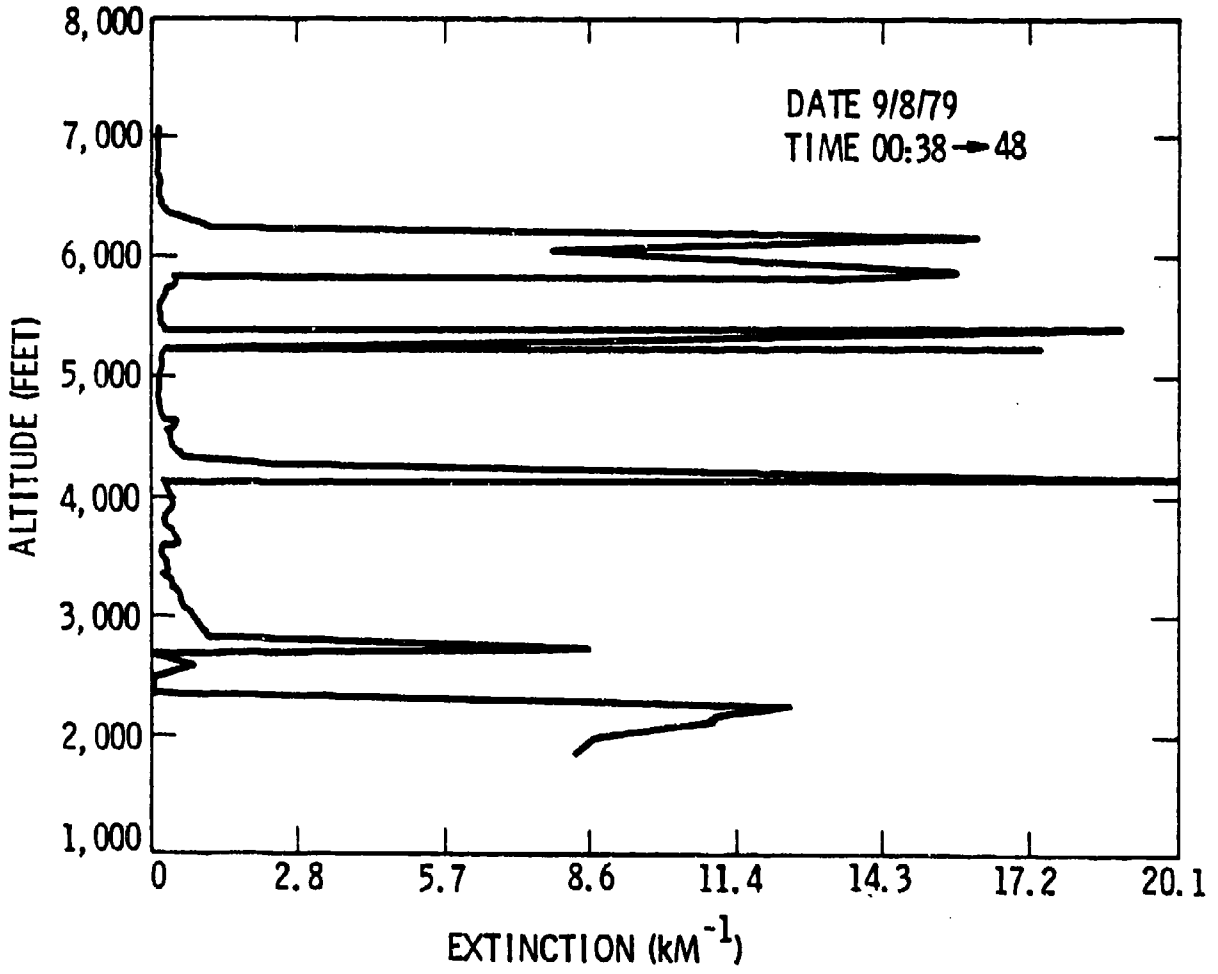

Typical Extinction Coefficient Vs Altitude Plot

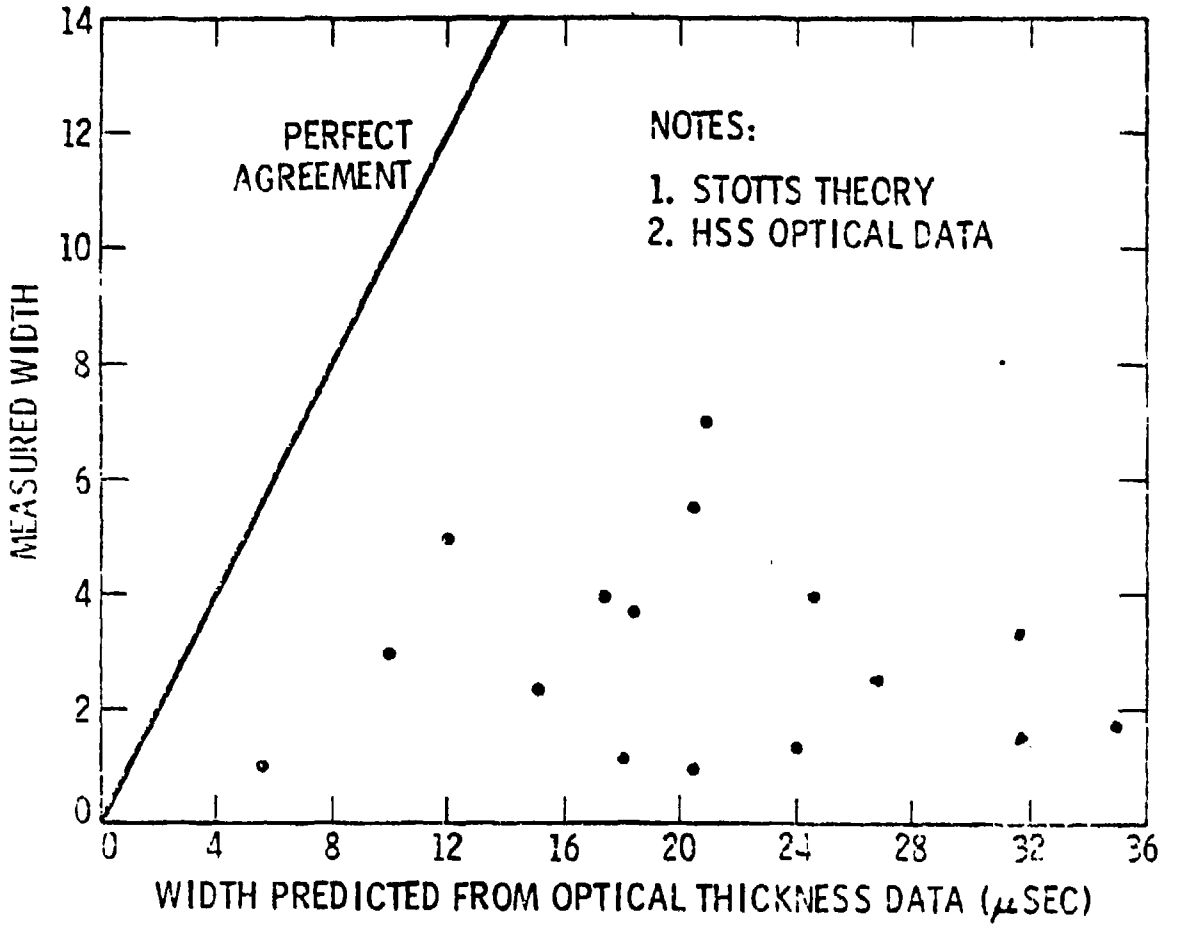

Data Analysis: Pulse Width-Predicted Vs Measured

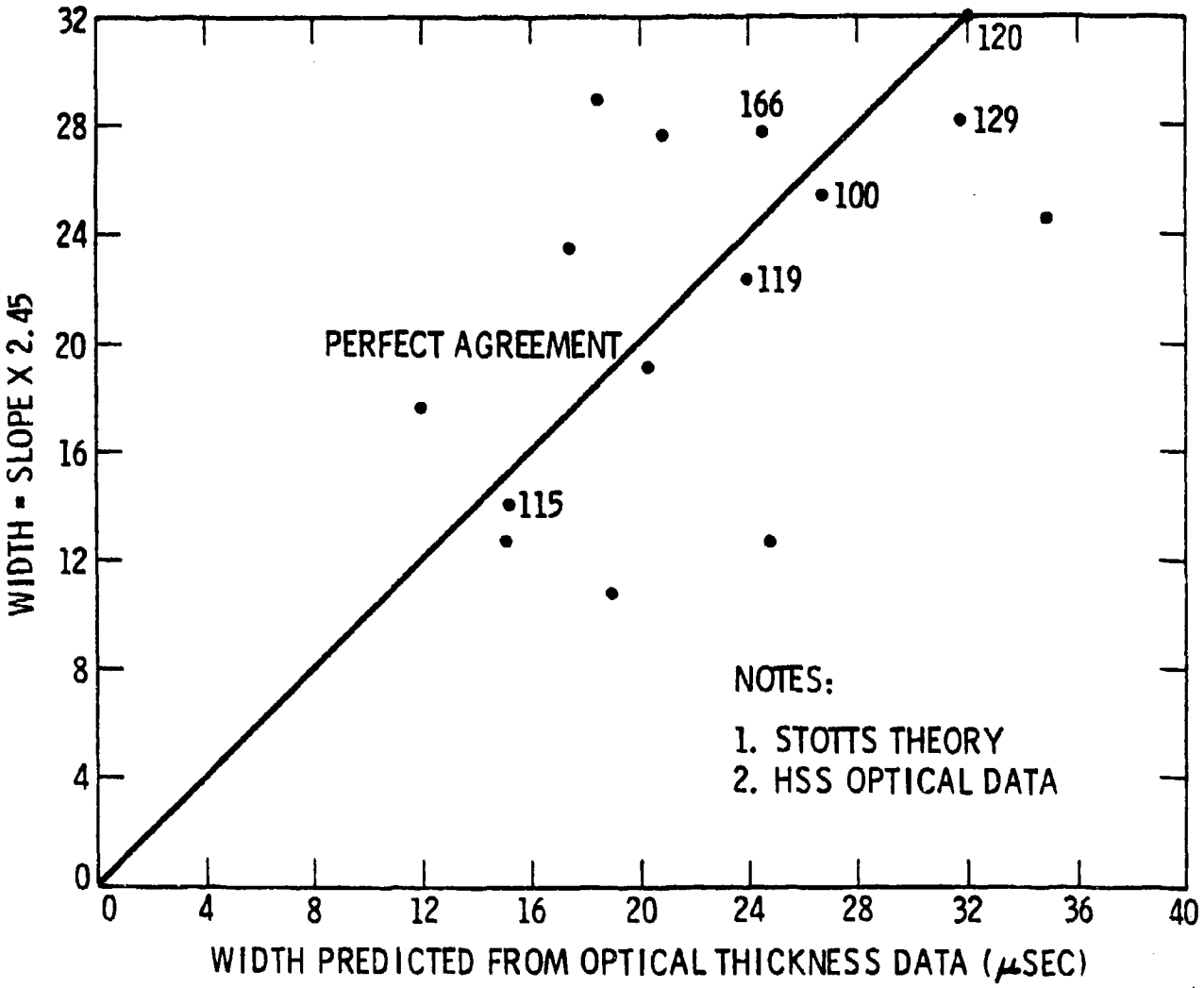

Data Analysis: Pulse Width-Predicted VS Inferred From Slope

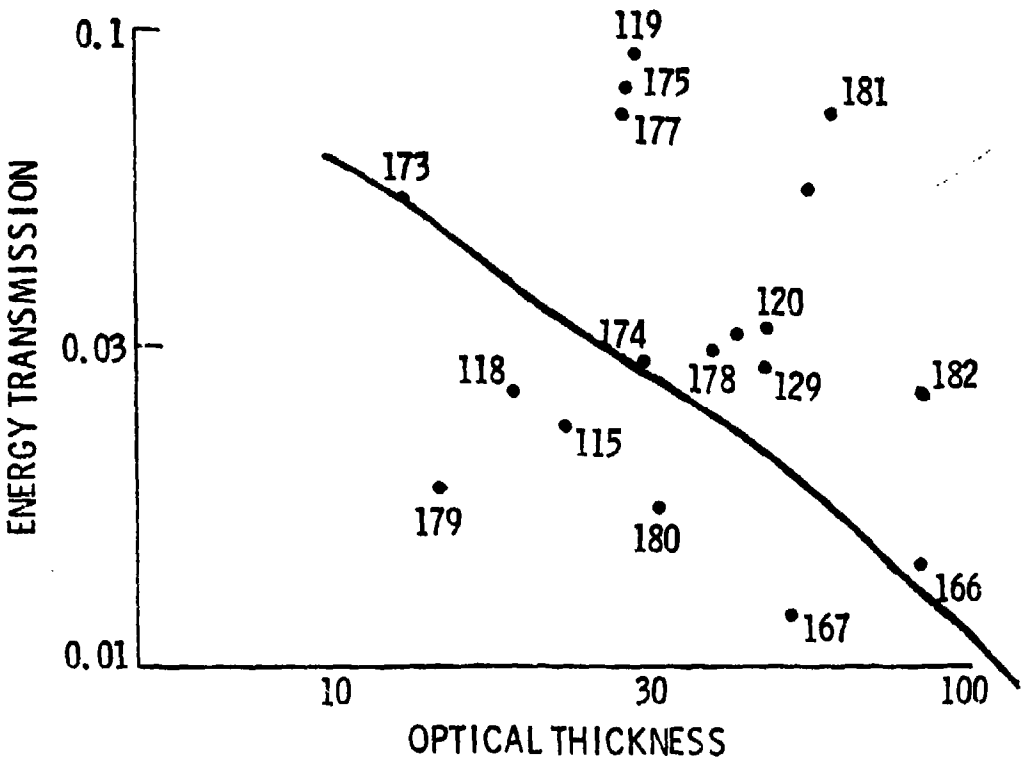

Data Analysis: Transmission As Optical Thickness

REPORT OUTLINE
(DOWNLINK CLOUD EXPERIMENT)

GTE Systems

FINAL REPORT

1. INTRODUCTION AND SUMMARY
2. EXPERIMENT DESCRIPTION
3. DATA REDUCTION AND ANALYSIS

APPENDICES

A PULSE SHAPE RAW DATA OVERVIEW

B RAW CLOUD DATA AND RUN PRIORITIES

C LASER AND LASER PLATFORM

D PULSE SHAPE PARAMETERS

E CLOUD CHARACTERISTICS

F TYPICAL RAW DATA PHOTOGRAPHS

G REDUCED DATA PLOTS

DATA ANALYSIS SUMMARY
(DOWNLINK CLOUD EXPERIMENT)

GTE Systems

- PULSE WIDTH LESS THAN PREDICTED
- STABLE PULSE SHAPES
- ATTENUATION LESS THAN WHAT PREDICTED
- DUAL MODE OF PROPAGATION THROUGH CLOUDS INDICATED BY DATA

S07

RECOMMENDATIONS (DOWNLINK CLOUD EXPERIMENT)

- IMPROVE ANALYTICAL MODELS TO INCLUDE REAL WORLD CLOUD GEOMETRIES
- CONDUCT ADDITIONAL EXPERIMENTS IN REAL WORLD ENVIRONMENT

THE TEMPORAL AND SPATIAL SMEARING OF BLUE-GREEN PULSES IN CLOUDS

G. C. Mooradian and M. Geller
NOSC

The time history of large diameter (approximately 6 km) blue-green laser pulses propagating through clouds in Kauai was measured as function of receiver field of view (FOV). Analyses of the data showed that the transmitted power of each pulse could be represented by a linear combination of two modified Gamma functions: $P(t) = C_1 \exp(-k_1 t) + C_2 (\exp -k_2 t)$. One term is the diffusion component, and the other term is a lower order multiple scattering part, which may even be a direct, non-scattered portion of the transmitted beam. Some data showed that for wide FOV, the received pulse consisted of a large diffusion component, and that as the FOV decreased, the pulse energy in the diffusion component decreased and the non-diffusion part increased. In the limit of the smallest FOV, only the non-diffusion component was obtained. Other examples show that for very dense clouds, the only component received was the diffusion type. Data was presented for the power received as a function of FOV of the receiver for various values of optical thickness, and for the case where the transmitting aircraft was not directly overhead, but 5000 yards distant, and for the cases where the receiver was intentionally directed 5 and 10 degrees from the vertical. The measured pulse widths were consistently smaller than the theoretical values derived from Stotts** using the value of optical thickness as inferred by the HSS moon radiometric data. This discrepancy may be explained by the overestimation in the values of cloud physical thickness measurements made by the meteorological aircraft.

**Stotts: Applied Optics, 17, 504 (1978)

NOSC

VARIABLE FIELD OF VIEW RECEIVERS AND DATA RECORDING SETUP

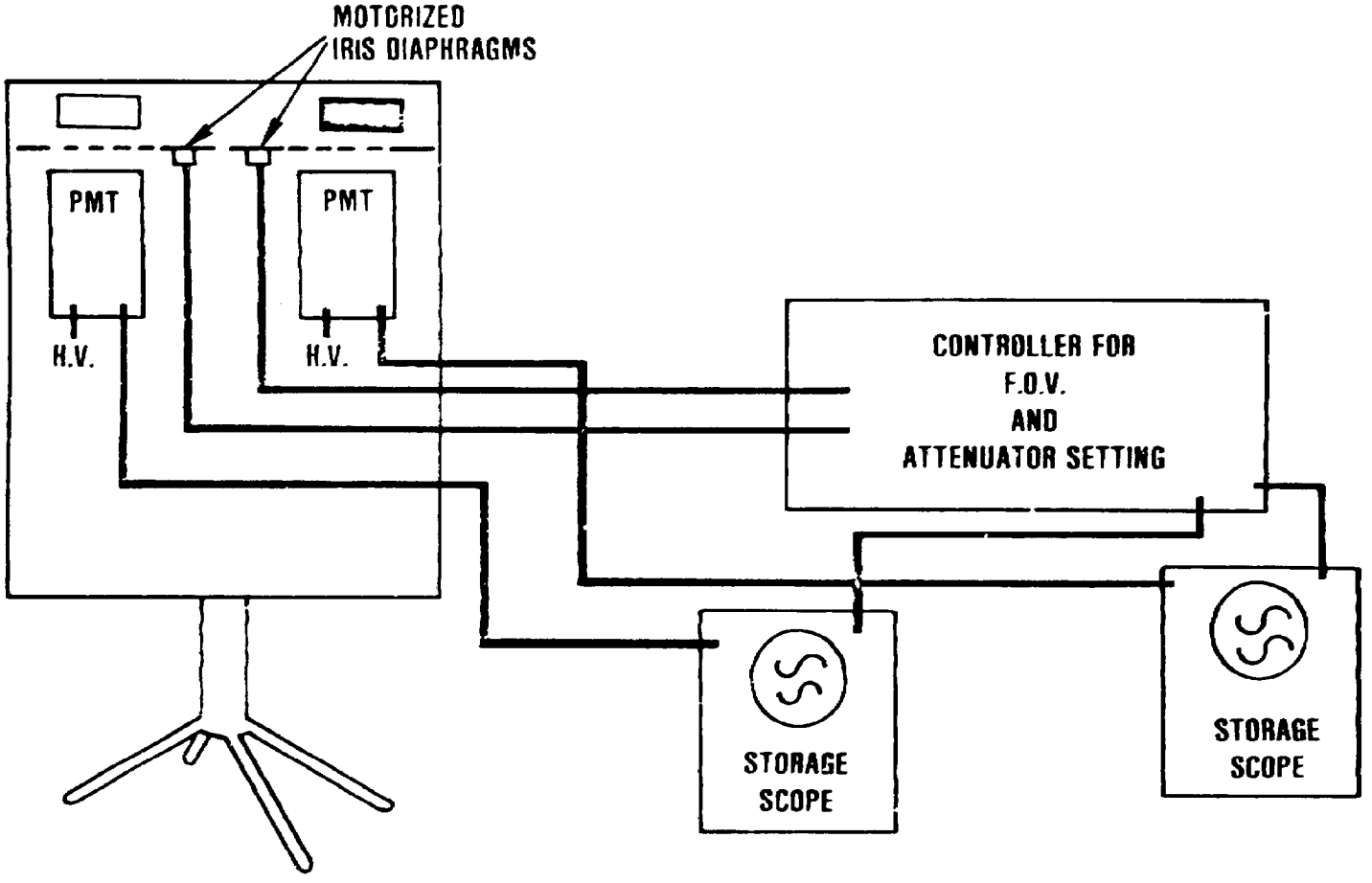

REPRESENTATIVE NORMALIZED PULSE SHAPES AS A FUNCTION OF CLOUD OPTICAL THICKNESS

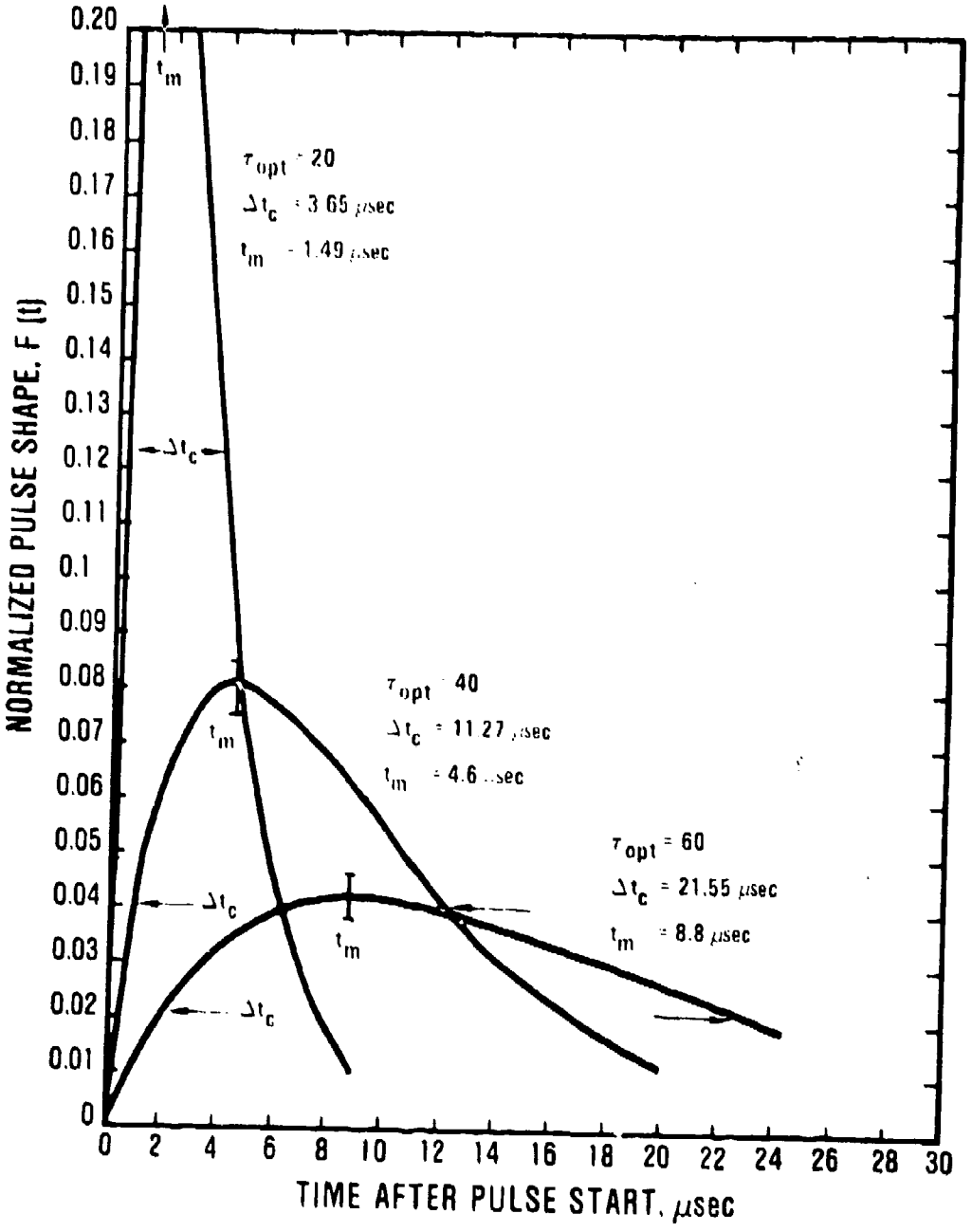

NOSC 64

DIFFUSION COMPONENT $f(t) = Cte^{-Kt}$

PULSE WIDTH (FWHM) = $\frac{2.45}{K}$

PEAK POWER ($t = 1/K$) = $0.368\ C/K$

AVERAGE TIME DELAY = $\frac{2}{K}$

ENERGY PER PULSE (AREA UNDER CURVE) = $\frac{C}{K^2}$

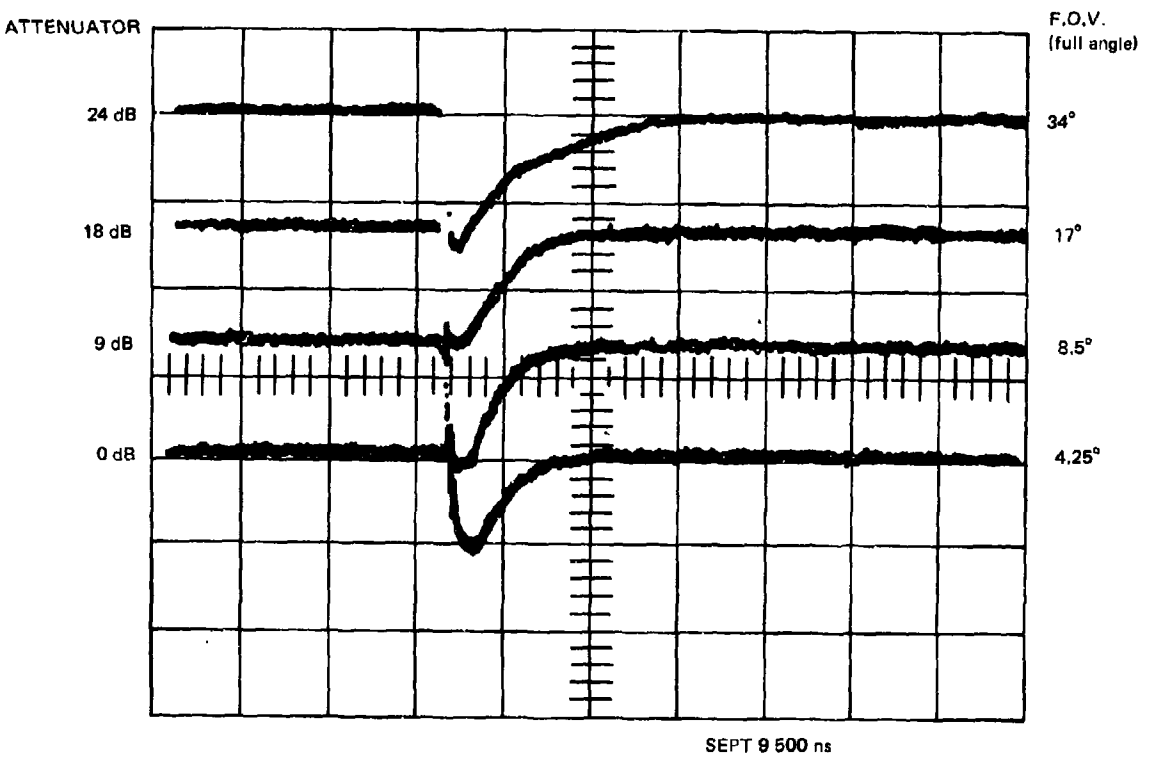
ATTENUATOR
F.O.V.
(full angle)
24 dB
34°
18 dB
17°
9 dB
8.5°
0 dB
4.25°
SEPT 9 500 ns

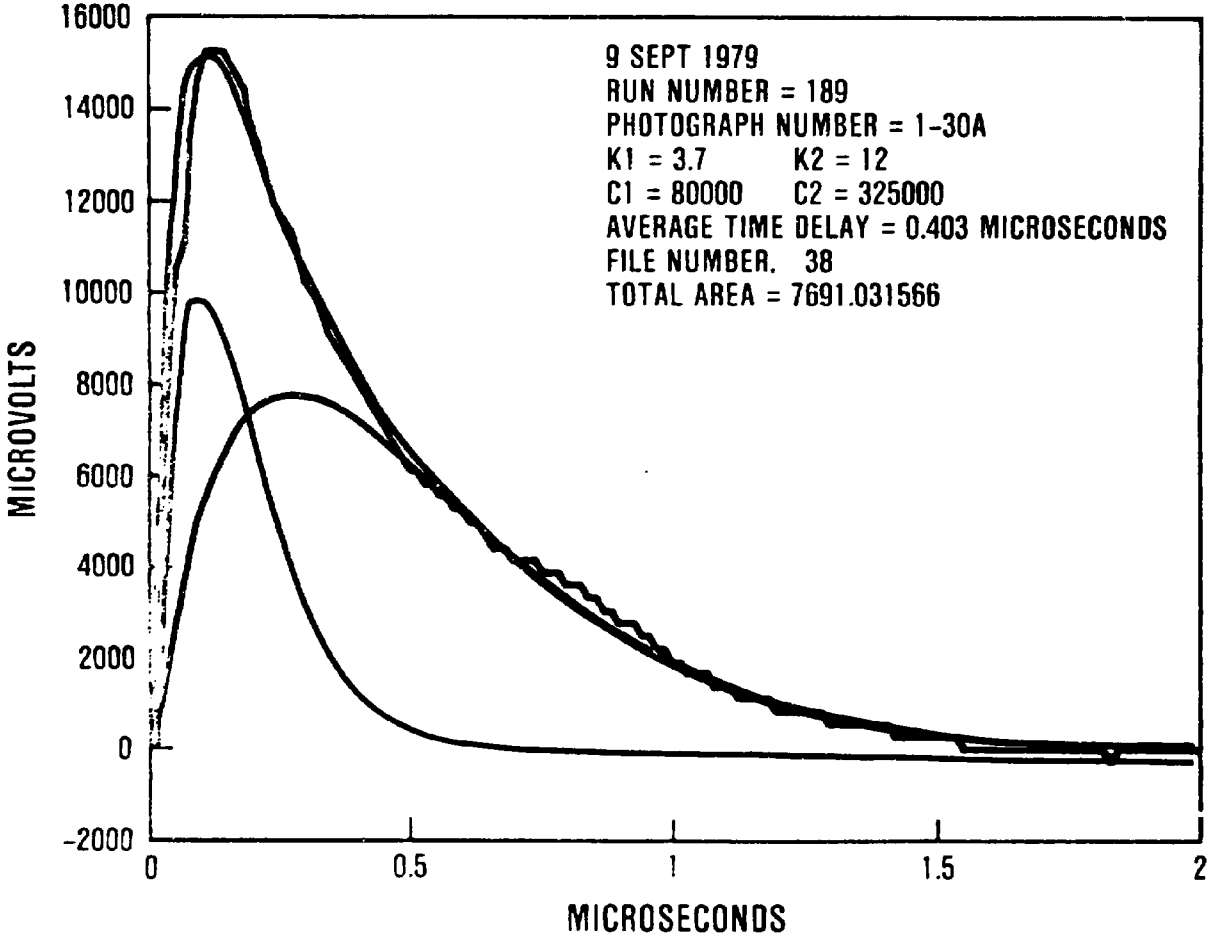
9 SEPT 1979
RUN NUMBER = 189
PHOTOGRAPH NUMBER = 1-30A
K1 = 3.7 K2 = 12
C1 = 80000 C2 = 325000
AVERAGE TIME DELAY = 0.403 MICROSECONDS
FILE NUMBER. 38
TOTAL AREA = 7691.031566
MICROVOLTS
16000
14000
12000
10000
8000
6000
4000
2000
0
-2000
0
0.5
1
1.5
2
MICROSECONDS

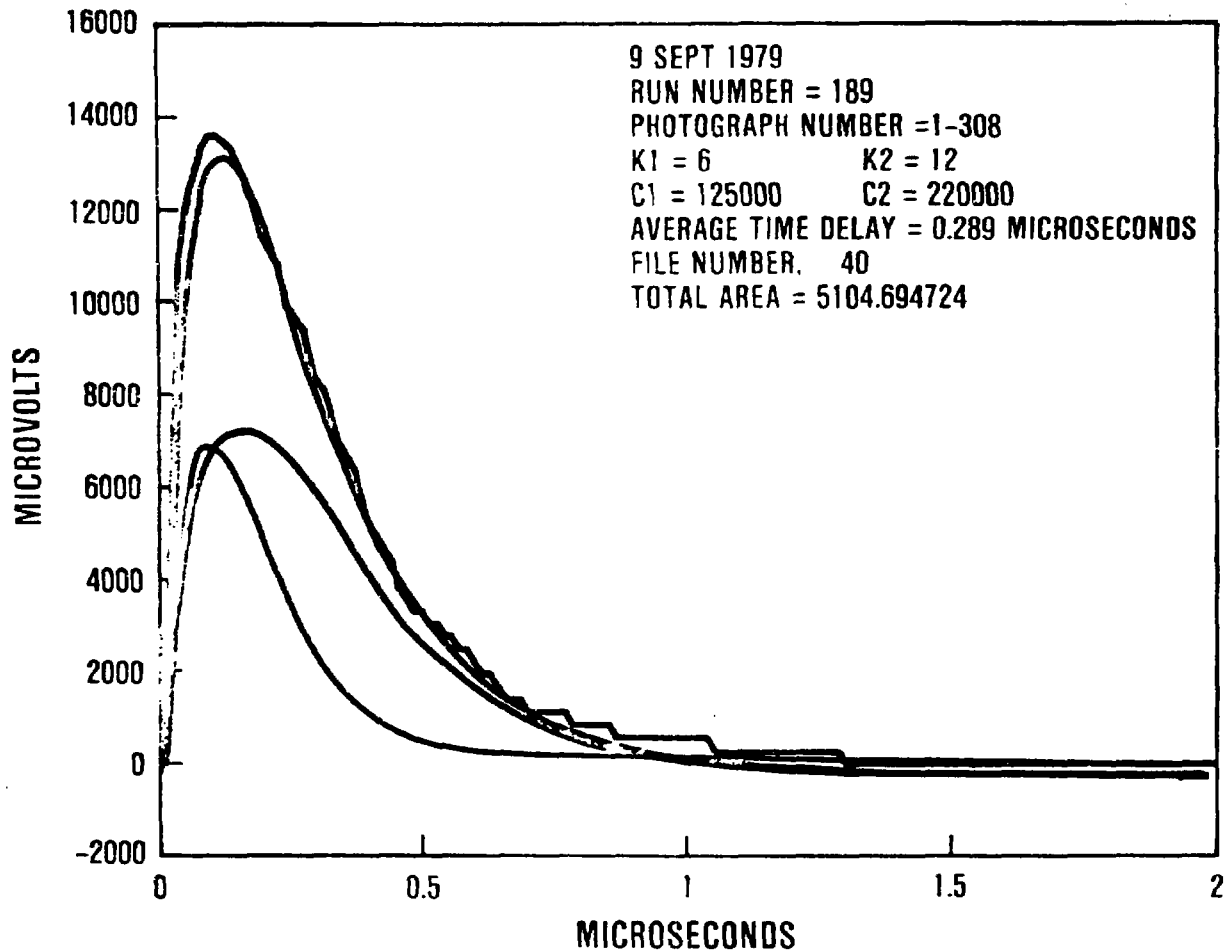
9 SEPT 1979
RUN NUMBER = 189
PHOTOGRAPH NUMBER =1-308
K1 = 6 K2 = 12
C1 = 125000 C2 = 220000
AVERAGE TIME DELAY = 0.289 MICROSECONDS
FILE NUMBER. 40
TOTAL AREA = 5104.694724
MICROVOLTS
16000
14000
12000
10000
8000
6000
4000
2000
0
-2000
0
0.5
1
1.5
2
MICROSECONDS

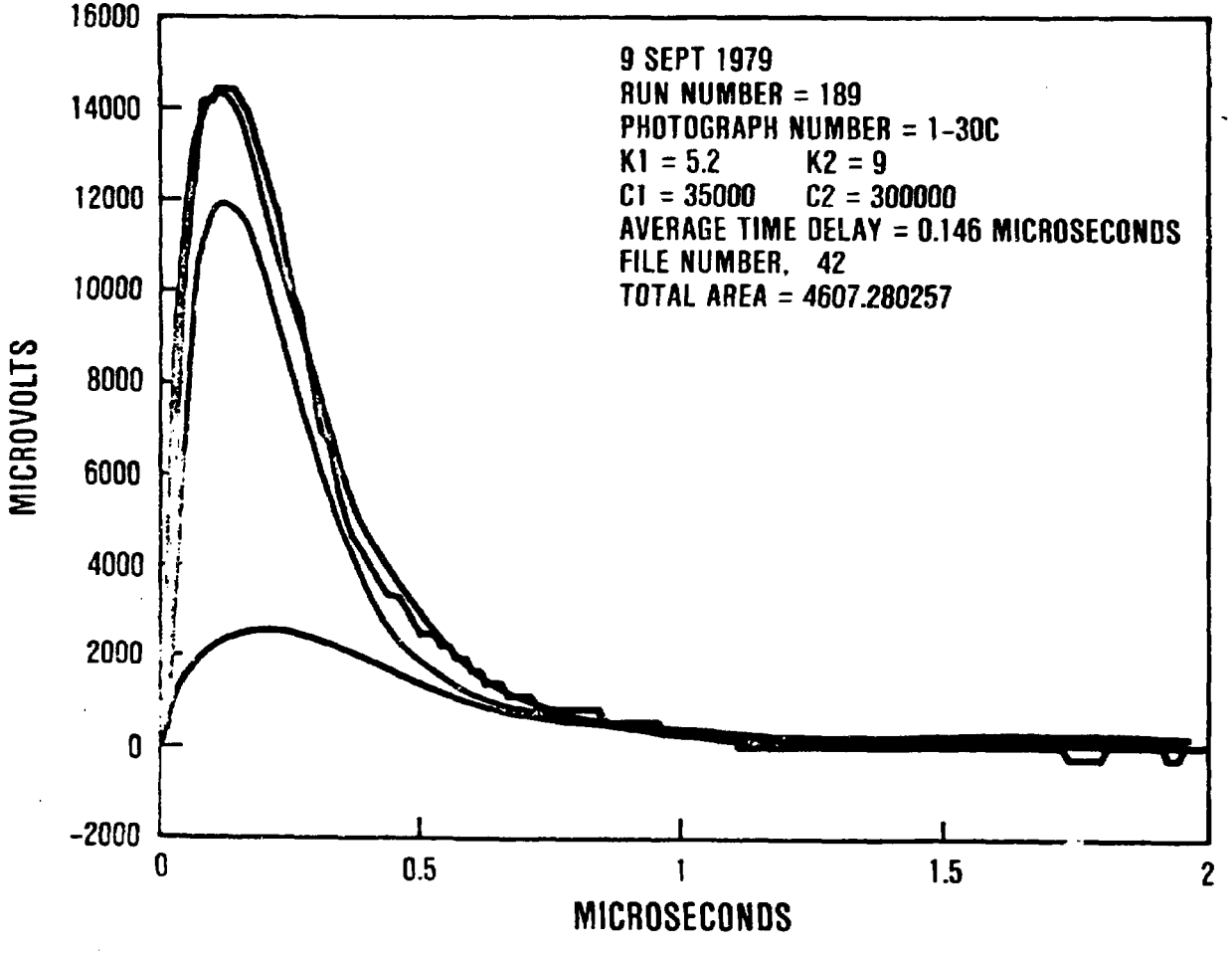
9 SEPT 1979
RUN NUMBER = 189
PHOTOGRAPH NUMBER = 1-30C
K1 = 5.2 K2 = 9
C1 = 35000 C2 = 300000
AVERAGE TIME DELAY = 0.146 MICROSECONDS
FILE NUMBER, 42
TOTAL AREA = 4607.280257
MICROVOLTS
16000
14000
12000
10000
8000
6000
4000
2000
0
-2000
0
0.5
1
1.5
2
MICROSECONDS

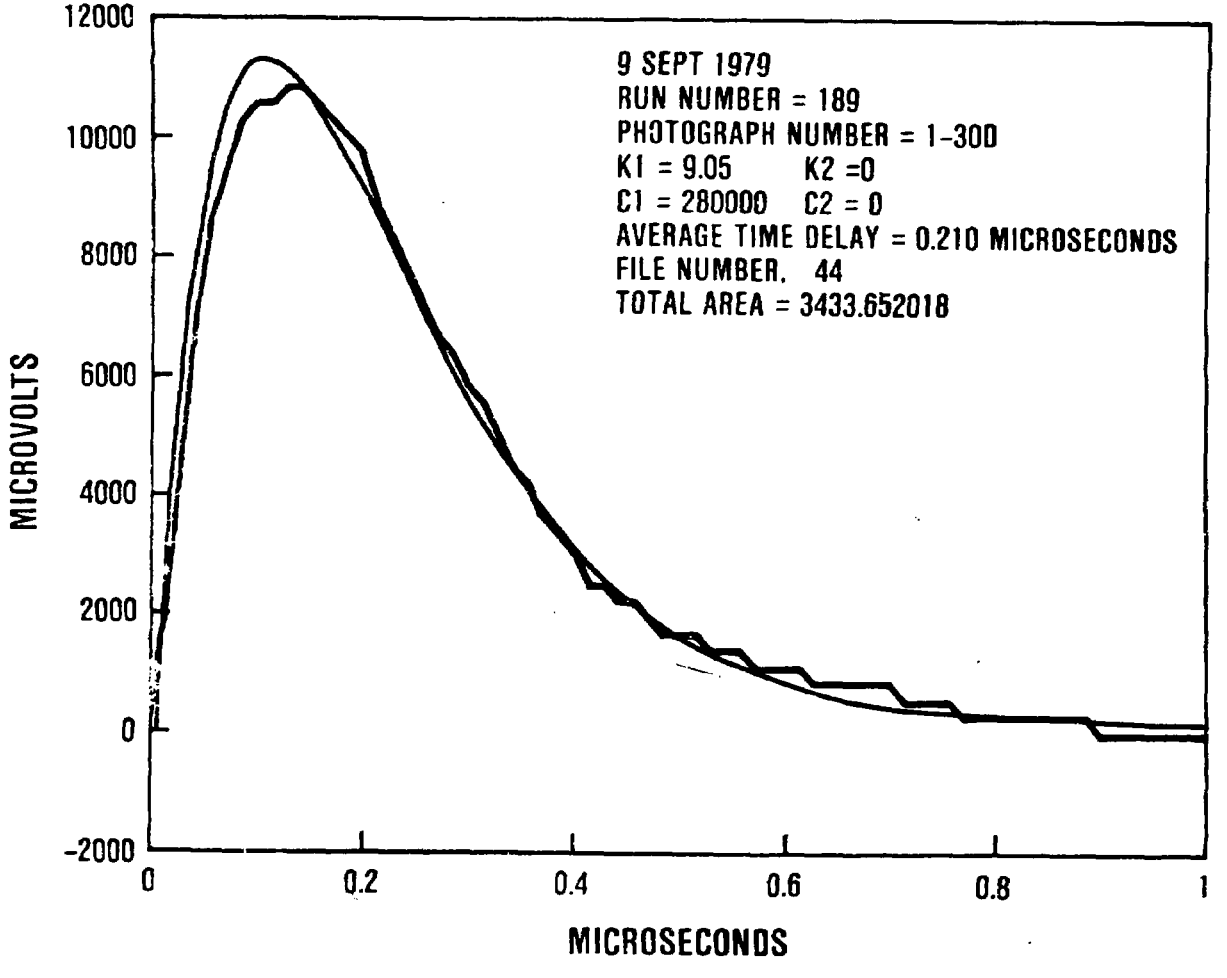
9 SEPT 1979
RUN NUMBER = 189
PHOTOGRAPH NUMBER = 1-300
K1 = 9.05 K2 =0
C1 = 280000 C2 = 0
AVERAGE TIME DELAY = 0.210 MICROSECONDS
FILE NUMBER. 44
TOTAL AREA = 3433.652018
MICROVOLTS
12000
10000
8000
6000
4000
2000
0
-2000
0
0.2
0.4
0.6
0.8
1
MICROSECONDS

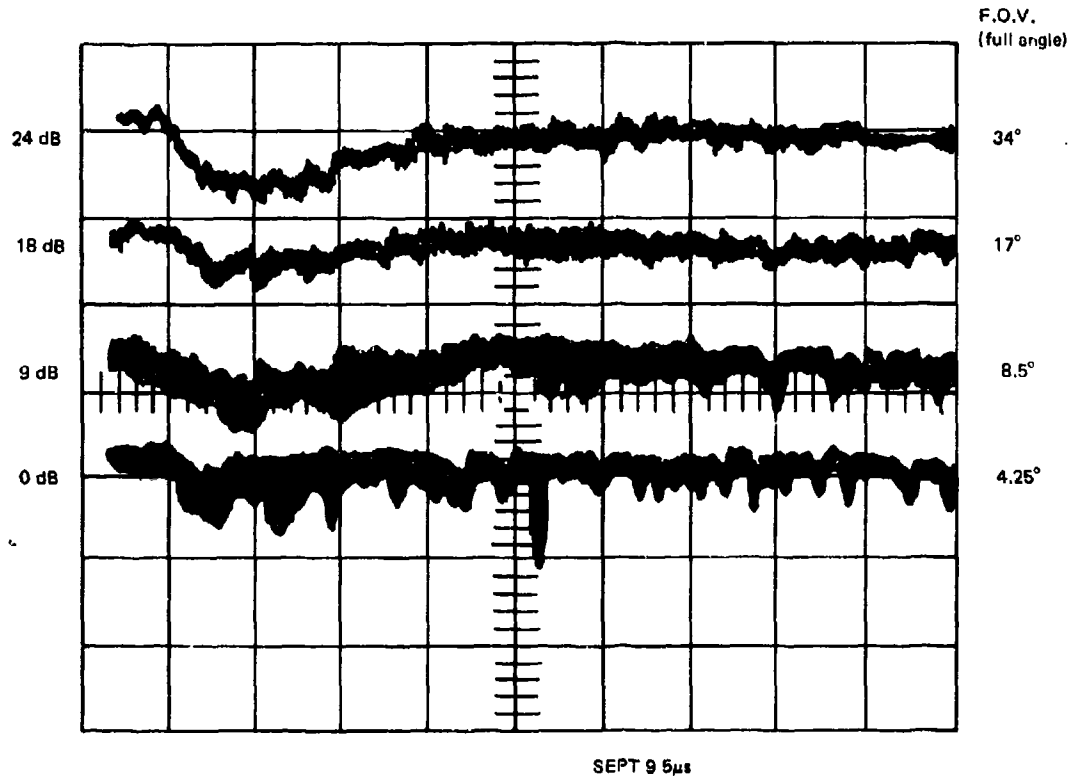
F.O.V.
(full angle)
24 dB
18 dB
9 dB
0 dB
34°
17°
8.5°
4.25°
SEPT 9 5μs

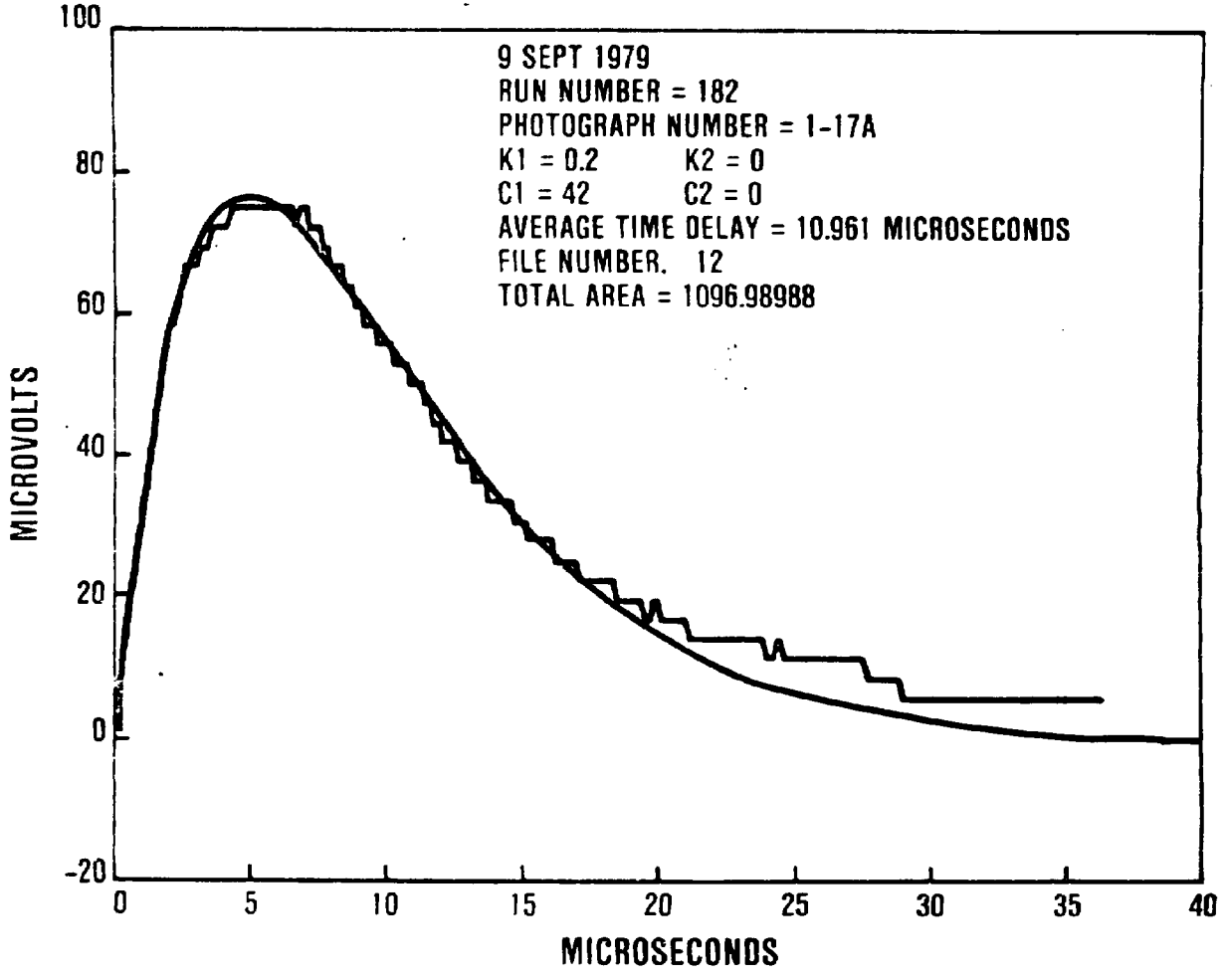
9 SEPT 1979
RUN NUMBER = 182
PHOTOGRAPH NUMBER = 1-17A
K1 = 0.2 K2 = 0
C1 = 42 C2 = 0
AVERAGE TIME DELAY = 10.961 MICROSECONDS
FILE NUMBER. 12
TOTAL AREA = 1096.98988
MICROVOLTS
MICROSECONDS
100
80
60
40
20
0
-20
0
5
10
15
20
25
30
35
40

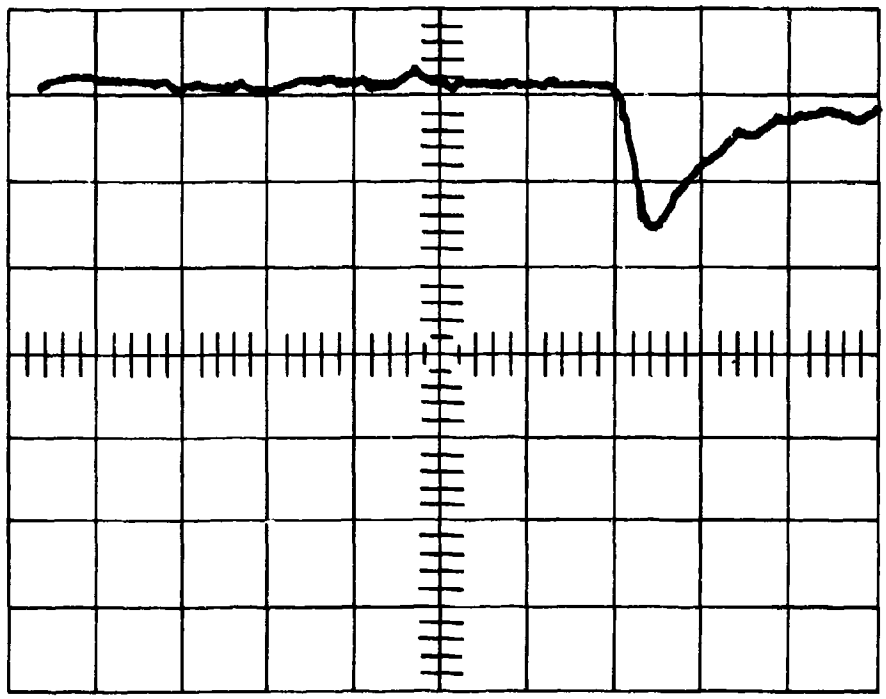
FOV 34°
SEPT 7 1μs

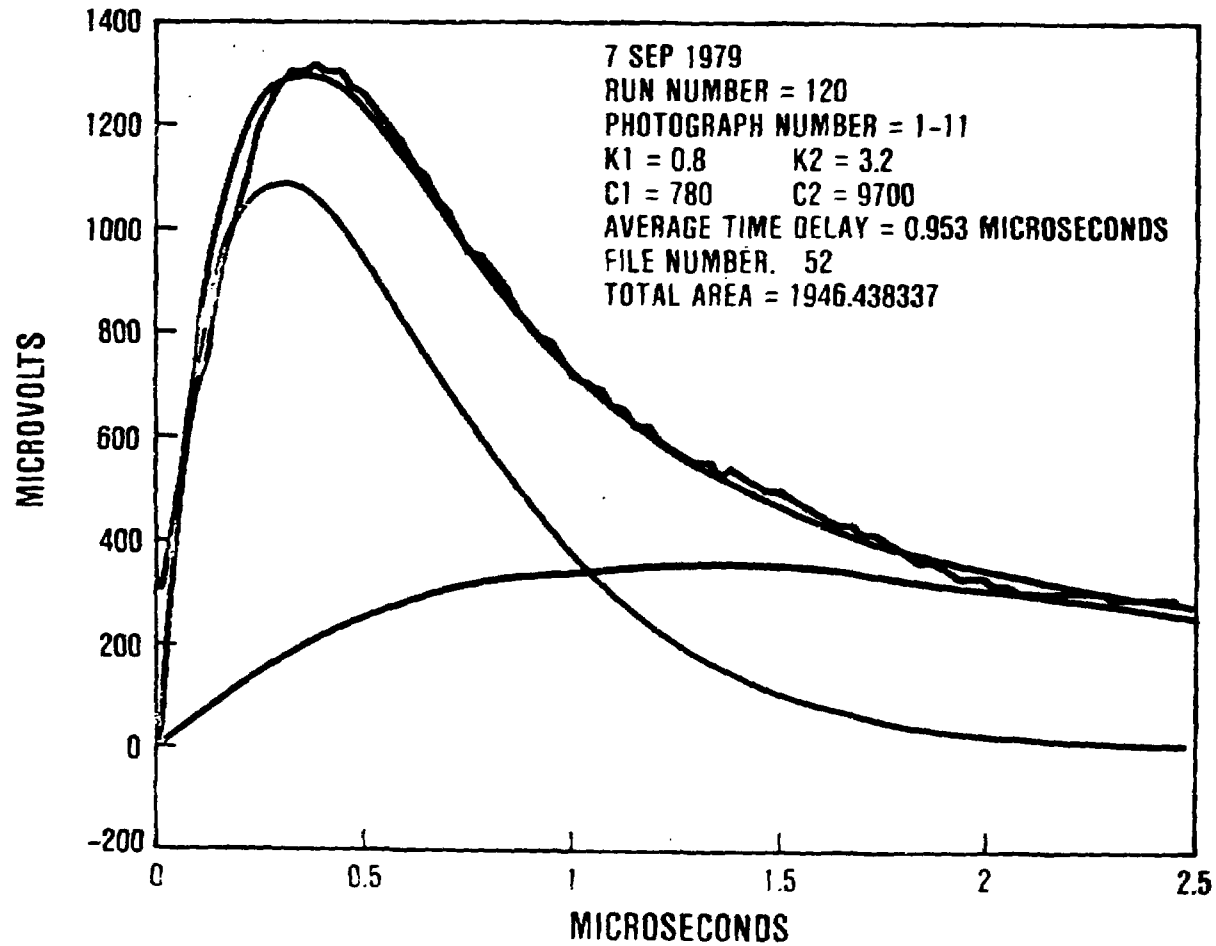
7 SEP 1979
RUN NUMBER = 120
PHOTOGRAPH NUMBER = 1-11
K1 = 0.8 K2 = 3.2
C1 = 780 C2 = 9700
AVERAGE TIME DELAY = 0.953 MICROSECONDS
FILE NUMBER. 52
TOTAL AREA = 1946.438337
MICROVOLTS
1400
1200
1000
800
600
400
200
0
-200
0
0.5
1
1.5
2
2.5
MICROSECONDS

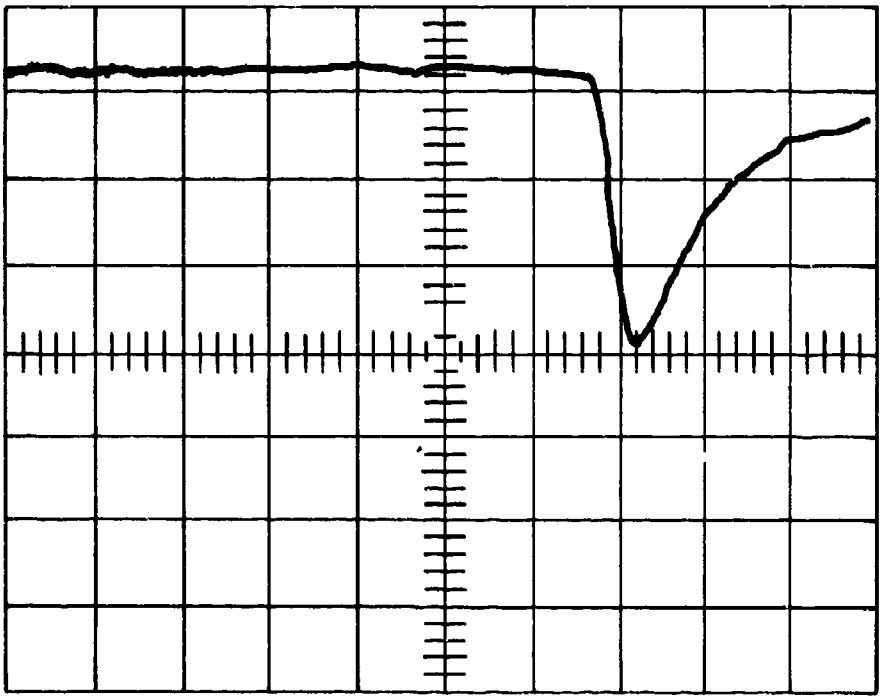
FOV 34°
SEPT 7 1μs

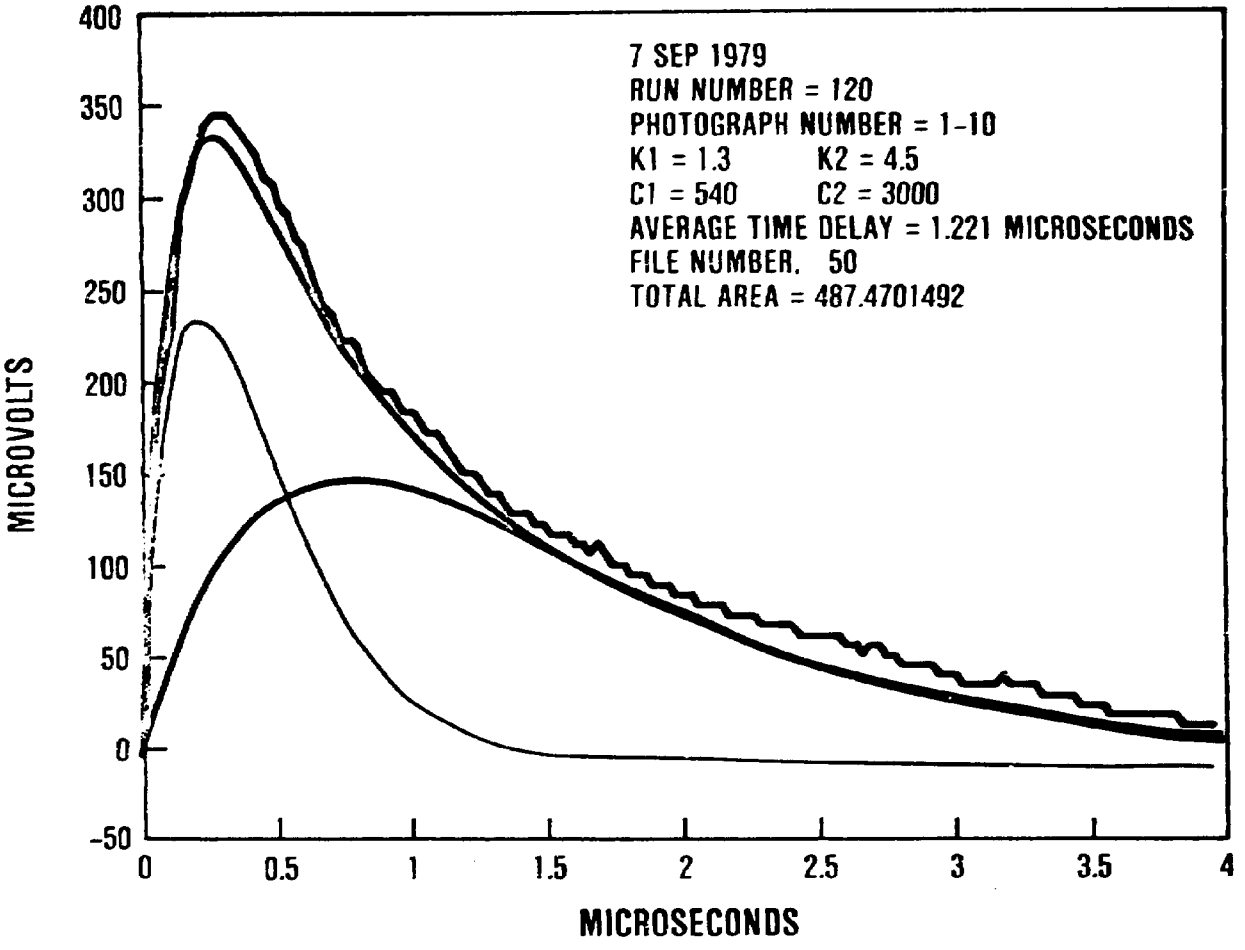
7 SEP 1979
RUN NUMBER = 120
PHOTOGRAPH NUMBER = 1-10
K1 = 1.3 K2 = 4.5
C1 = 540 C2 = 3000
AVERAGE TIME DELAY = 1.221 MICROSECONDS
FILE NUMBER. 50
TOTAL AREA = 487.4701492
MICROVOLTS
400
350
300
250
200
150
100
50
0
-50
0
0.5
1
1.5
2
2.5
3
3.5
4
MICROSECONDS

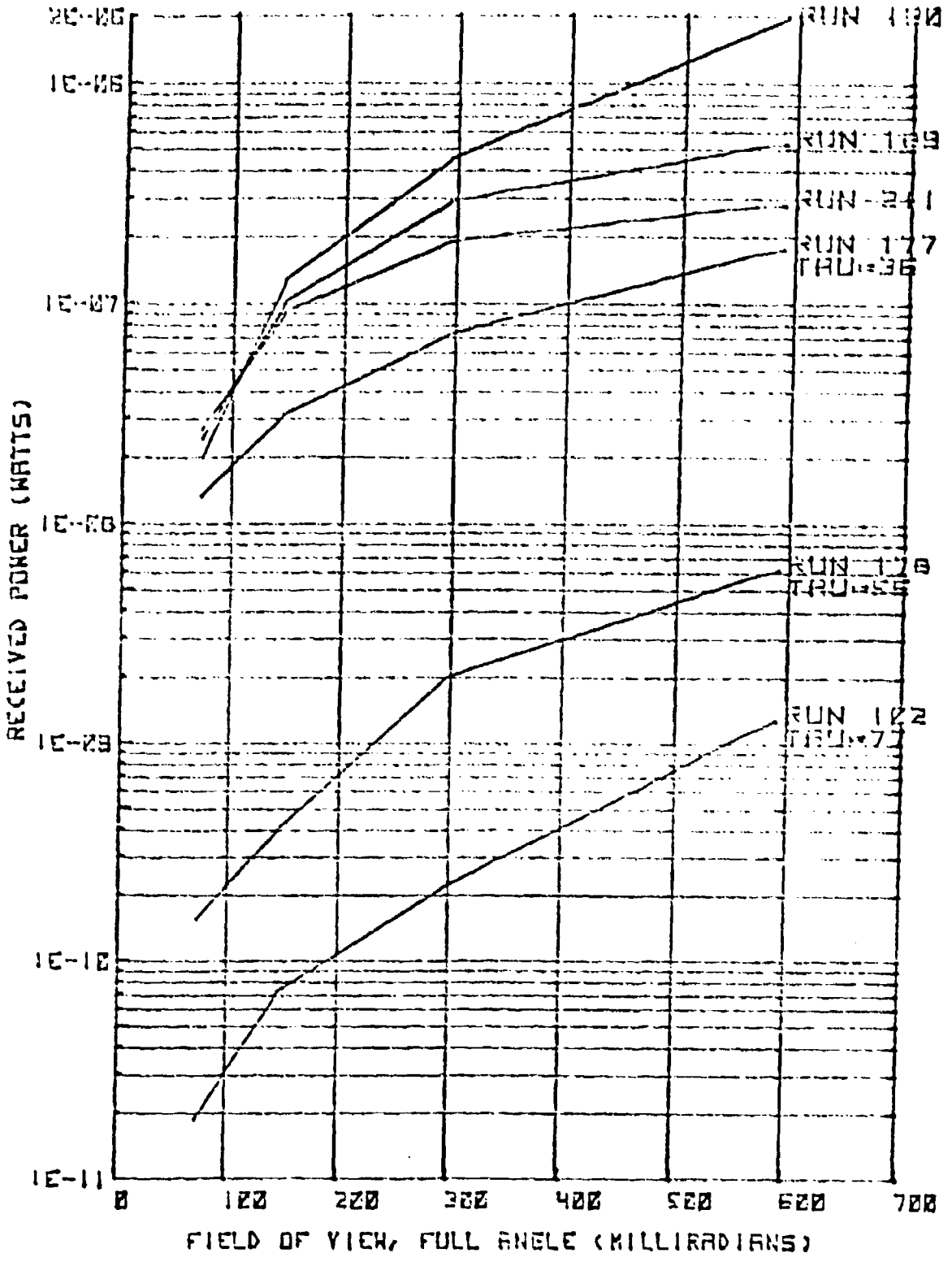
1E-05
1E-06
1E-07
1E-08
1E-09
1E-10
1E-11
RECEIVED POWER (WATTS)
0
100
200
300
400
500
600
700
FIELD OF VIEW, FULL ANGLE (MILLIRADIANS)
RUN 177
THRU=36
RUN 122
THRU=72

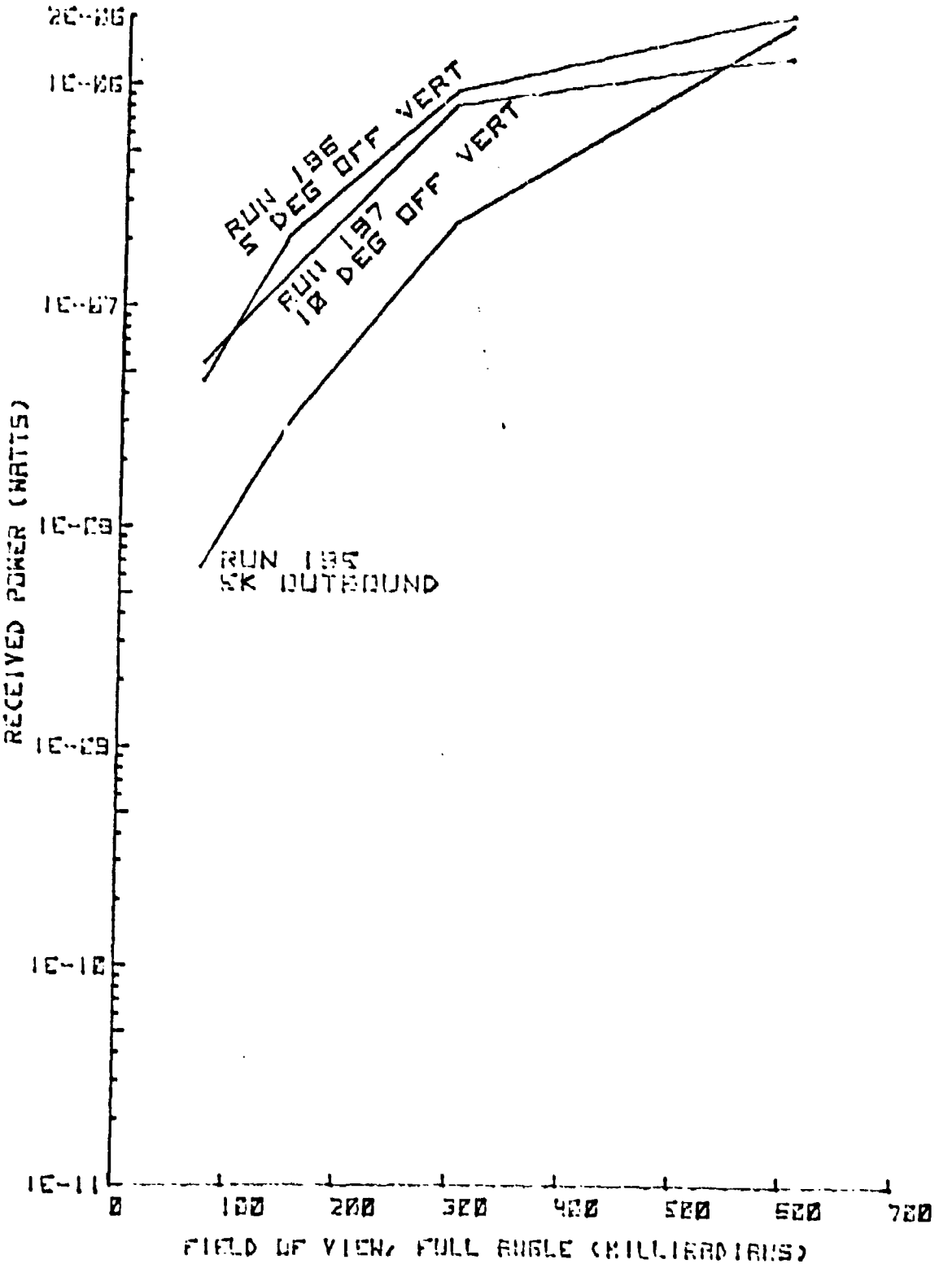
RECEIVED POWER (WATTS)
1E-06
1E-07
1E-08
1E-09
1E-10
1E-11
0
100
200
300
400
500
600
700
FIELD OF VIEW, FULL ANGLE (MILLIRADIANS)
RUN 196
5 DEG OFF VERT
RUN 197
10 DEG OFF VERT
RUN 195
5K OUTBOUND

NOSC 64

Stotts:

Multipath time spread

$$= \frac{Z}{C} \left\{ \frac{0.30}{\omega_0 \tau \gamma_0^2} \left[\left(1 + 2.25\, \omega_0 \tau \gamma_D^2 \right)^{3/2} - 1 \right] - 1 \right\}$$

γ_0 = RMS SCATTER ANGLE

τ = OPTICAL THICKNESS

Z = PHYSICAL THICKNESS

$\omega_0 = 1$

COMPARISON OF EXPERIMENTAL AND THEORETICAL PULSE WIDTHS

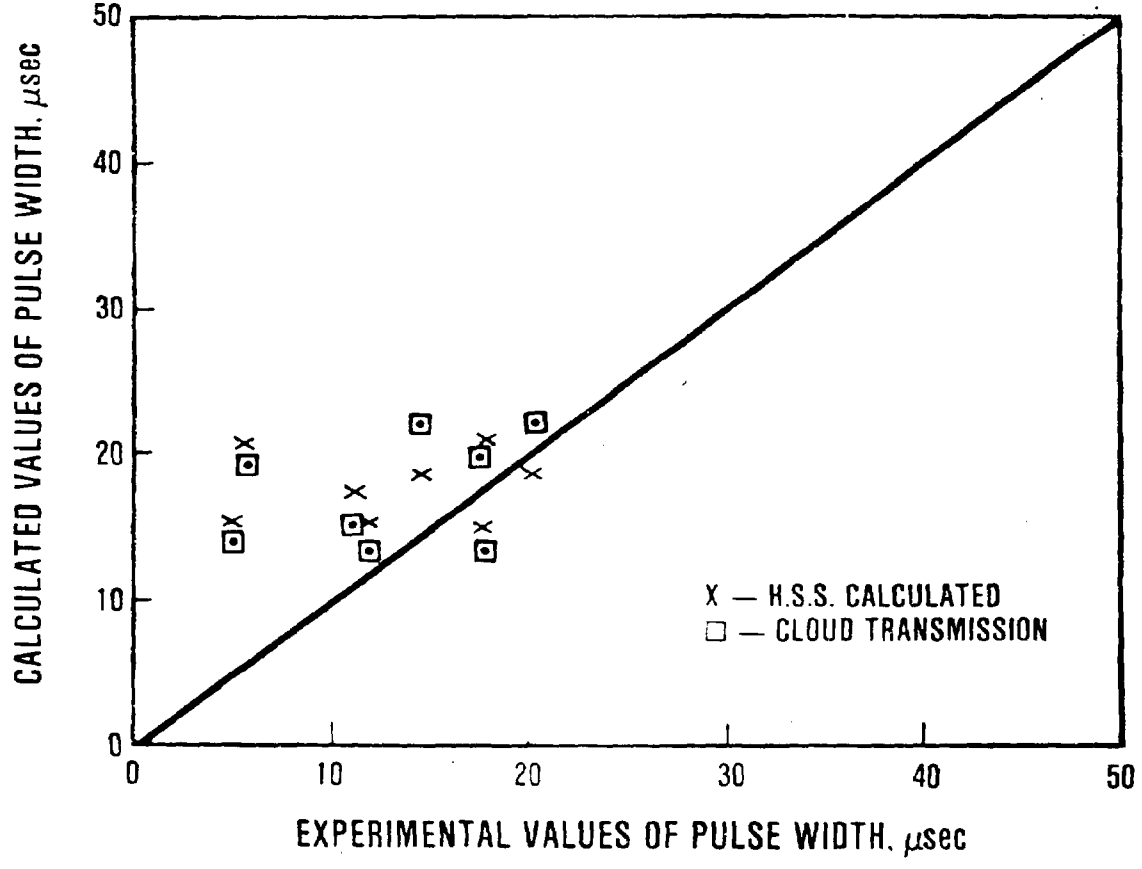

KAUAI CLOUD EXPERIMENT MEASUREMENTS: O_2 ABSORPTION TECHNIQUES

H.S. Stewart and D. F. Hansen

A. Discussion of Basic Technique and Pre-Kauai Experimental Measureme by H.S. Stewart.

Slide 1. States the purpose of the technique

Slide 2. States the basic concept of the technique

Slide 3. States the method of concept implementation

Slide 4. Lower half of slide shows how resolution spectrum of sunlight as transmitted by one, two and three air masses. The selected wavelength for measuring O_2 absorption, 0.7606μ is shown as "on" and the wavelength for O_2 free observation, 0.7530μ, is marked as "off". Top of slide shows zenith angles for one, two and three air mass observations.

Slide 5. Illustrates concept of diffuse transmission as compared to specular transmission, $I_0 S(Z)/I_0$.

Slide 6. The 0.5° field-of-view teleradiometer and its on and off band filters used for measurements of O_2 absorption in clouds.

Slide 7. San Nicolas Island, CA. Observations of O_2 absorption in overcasts were made at NW corner near the NRL Tower Site.

Slide 8. Calibration of the teleradiometer made against setting sun. In this plot log (on-band reading) -log (off-band reading) is plotted against (path through atmospheric $O_2)^{1/2}$ and gives a straight line.

Slide 9. Reduced data for May 3, 1979 overcast. Readings are made at zenith angles 30°, 45°, and 60° and azimuth values north, east, south and west. On the figure for each direction the time delay in the overcast in microseconds is printed above the transmission of the overcast.

Slide 10. The same as Slide 9 but for May 4.

Slide 11. The left hand side of the slide shows a camera system for recording the on-band/off-band ratio simultaneously for many lines-of-sight. The camera views the whole hemisphere of the sky via the reflecting sphere. Separate

HSS Inc
2 Alfred Circle
Bedford MA 01730

Slide 11 (cont.) pictures are taken through the on-band and the off-band filters. Data is reduced separately for each of 125000 lines-of-sight giving time delay in O_2 and cloud and overcast transmission.

Slide 12. From data taken as in Slide 11 a curve of probability of geometric plus diffusion delay as a function of delay time is generated. Slide 12 shows such a curve for 0937 3 August 1977.

Slide 13. It is possible that future observations may involve multiple lines-of-sight but not as many as 125,000. The slide shows a possible subdivision of the hemisphere of the sky into 25 elements giving equal signals from a uniform overcast. Some radiometric gadget might be used for such observations.

B. KAUAI EXPERIMENT; by D. F. Hansen.

Slide 14. This is a photograph of the two-channel teleradiometer used during Kauai experiment. Use of the moon, instead of the sun as the source of illumination required the instrument to have high sensitivity. This sensitivity was provided by use of thermoelectrically cooled photomultiplier tubes and six-inch diameter collecting apertures. Each channel was equipped with a six-inch diameter interference filter; the center wavelength of the on-band channel was 7608 Å, with a half-peak bandwidth of 15 Å; the center wavelength of the off-band channel was 7530 Å with a bandwidth of 30 Å. A circulating fluid heat-exchanger unit, also shown in the photograph was used to extract the heat from the thermoelectric coolers.

Slide 15. Photograph of the electronic controls and PAR photon counting systems used in conjunction with the two-channel teleradiometer.

Slide 16. Summary of data-run participation using the two-channel teleradiometer during the KAUAI Experiment.

Slide 17. Calibration curve for the two-channel teleradiometer generated prior-to the experiment, with cloud-free lines of sight at Barking Sands, Kauai using sunlight (greatly attenuated) as the source of illumination; and also using cloud-free lines of sight and the moon as the source, during the evenings when the experiments were conducted.

Slide 18. Visual observations of overcast and precipitation which were present during each of the data runs for two evenings when the teleradiometer participated in the KAUAI experiment.

Slide 19. Typical Data-Results. Table summarizing the measurements made with the two-channel teleradiometer on each data run and the data derived from the measurements.

Slide 20. Comparison of mean-time-delays measured by GTE-Sylvania with mean-time delays measured with the two-channel teleradiometer for Aircraft Run No. 120. The zenith angle changes for the Sylvania data as the aircraft passes overhead whereas for any given run the zenith angle to the moon is fixed for the teleradiometer measurement.

Slide 21. Comparison of mean-time-delays measured by GTE-Sylvania with mean-time-delays measured with the two-channel teleradiometer for Aircraft Run No. 119.

Slide 22. Comparison of mean-time-delays measured by GTE-Sylvania with mean time delays measured with the two channel teleradiometer for Aircraft Run No. 100. Note the large change in mean-time-delays which occured in the Sylvania data when the rain shower commenced over the site.

The major differences between the Sylvania and HSS Inc measurements of mean-time-delay are attributed to the fact that the zenith angle to the moon was quite different than the zenith angle to the aircraft for all data runs.

Slide 23. Scatter diagram of correlation between NOSC and HSS Inc. Values of Optical Thickness--obtained on eighteen data runs.

Slide 24. Plot of mean-time-delay vs product of optical thickness and geometric thickness of the clouds for 23 data runs.

PURPOSE

TO DEDUCE THE DELAY AND SMEARING OF A LIGHT PULSE IN ITS TRANSIT OF A CLOUD OR OVERCAST USING STEADY STATE OBSERVATIONS OF SUNLIT CLOUDS.

Slide 1

BASIC CONCEPT

THE LONGER A PHOTON TAKES IN GETTING THROUGH A SCATTERING AND ABSORBING CLOUD THE GREATER THE PROBABILITY THAT IT WILL BE ABSORBED.

CONCEPT IMPLEMENTATION

THE STRENGTH OF OXYGEN ABSORPTION AT ABOUT

$\lambda = 0.7606\,\mu$ IS MEASURED FOR THE SUNLIGHT

TRANSMITTED BY AN OVERCAST AND THIS IS CORRELATED

TO THE MEAN PATH LENGTH IN THE OVERCAST AND

THE MEAN TIME OF TRANSIT.

Slide 3.

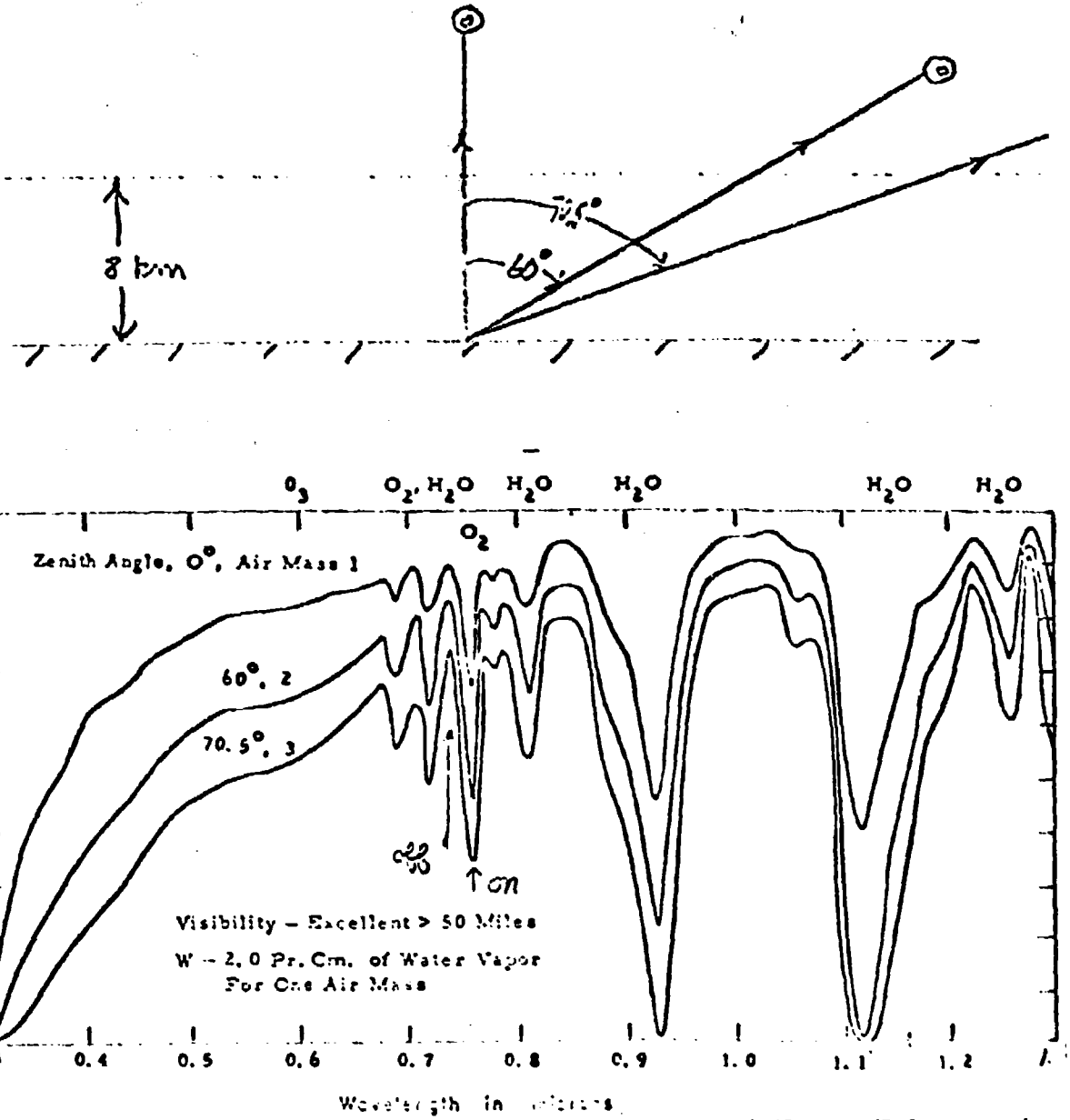

Fig. 6. Transmission of the atmosphere in the near ultraviolet, visible, and near infrared. (From R. O'B. Carpenter and R. M. Chapman, in "Effects of Night Sky Backgrounds on Optical Measurements," p. 25. Geophysics Corp. of America, March 6, 1959.)

Slide 4

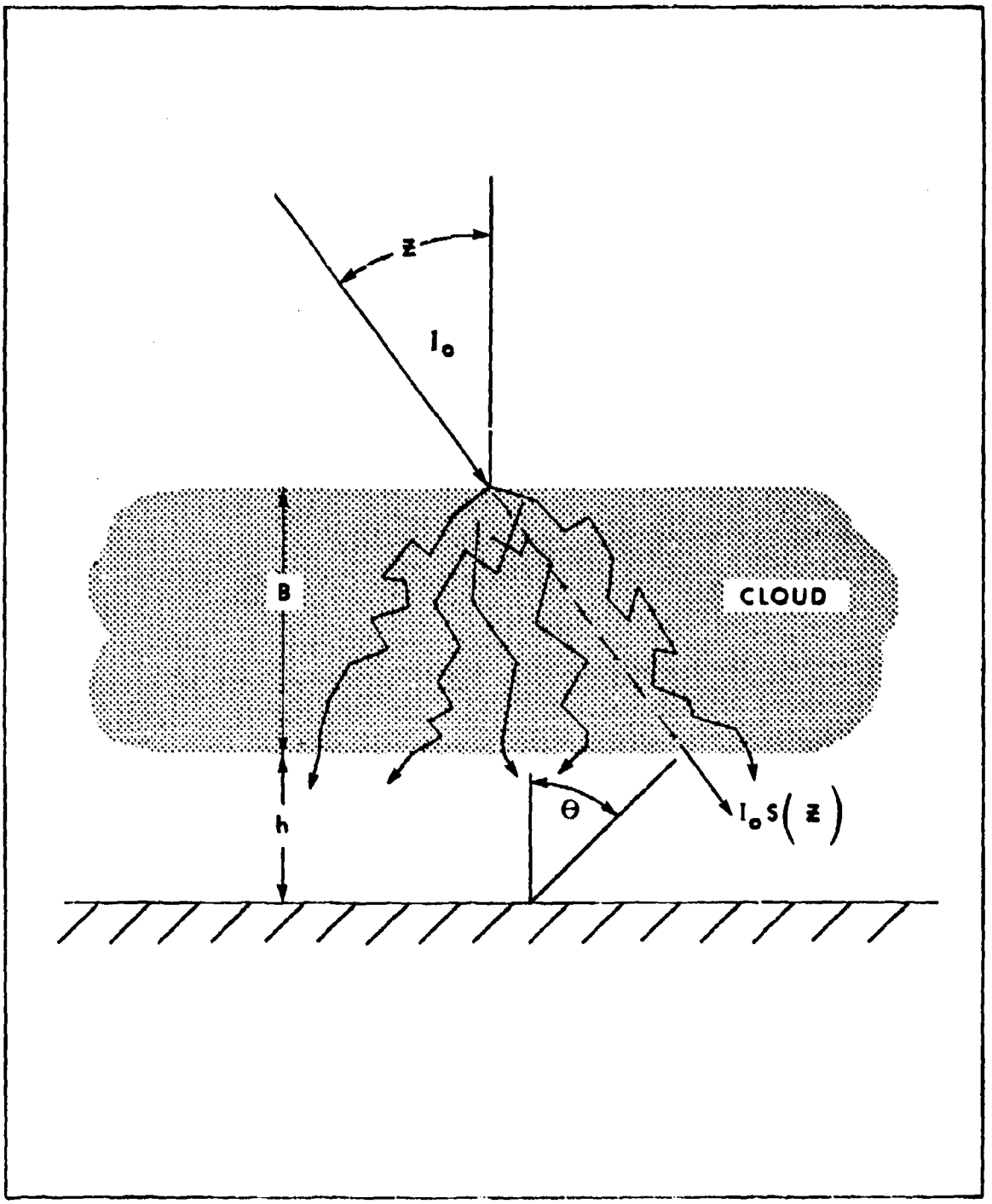

Figure 7. Diffuse and specular transmission.

Slide 5.

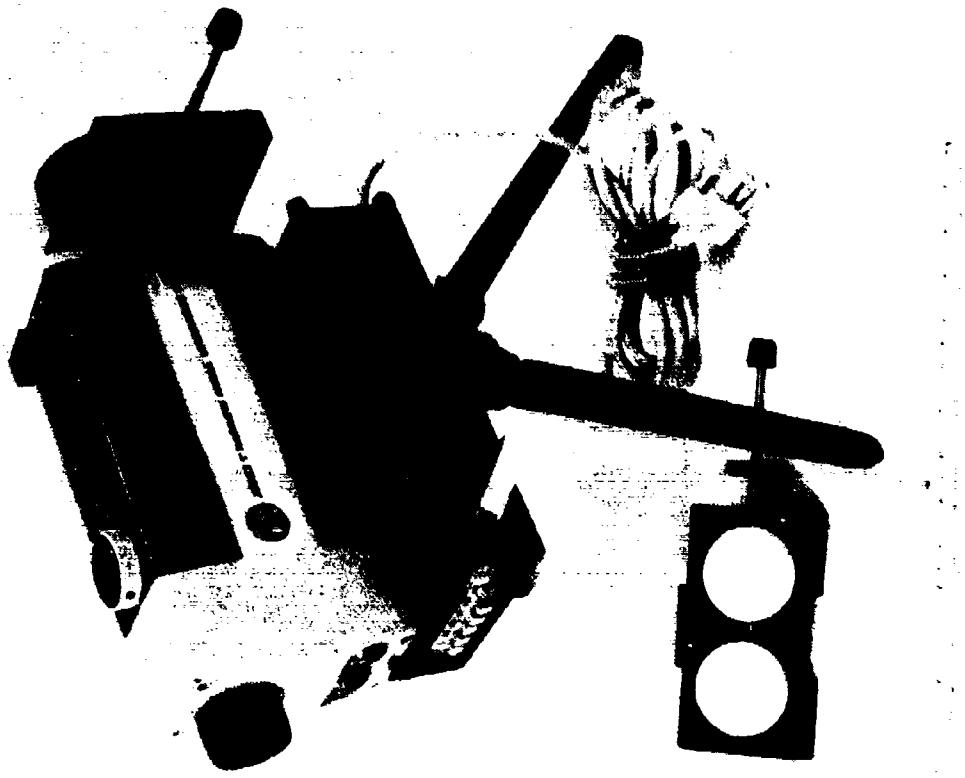

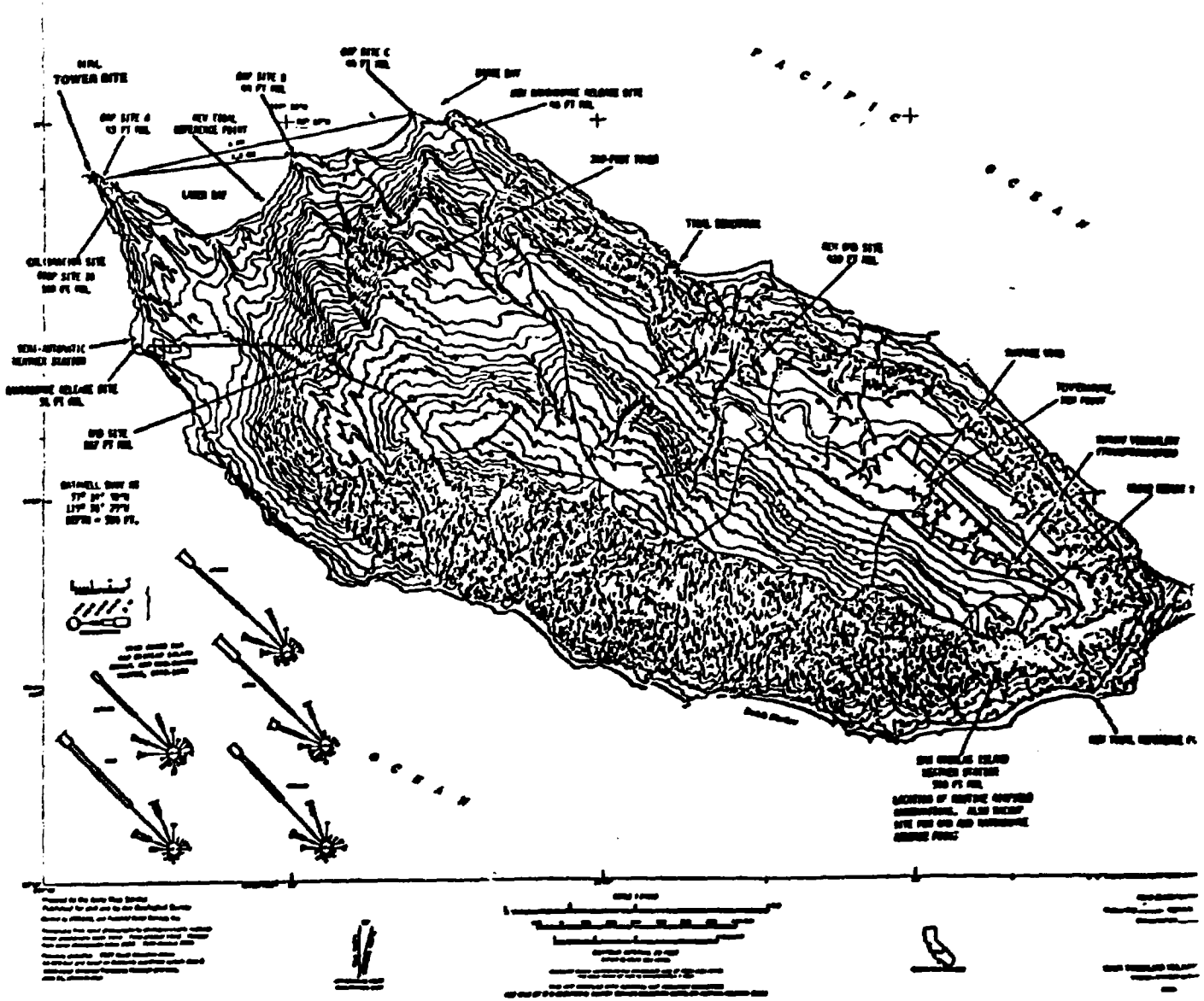

Slide 7.

Fig. 2 - Map of San Nicolas Island showing the location of various installations, including the NRL tower site and OSP Site A on the northwest point of the island

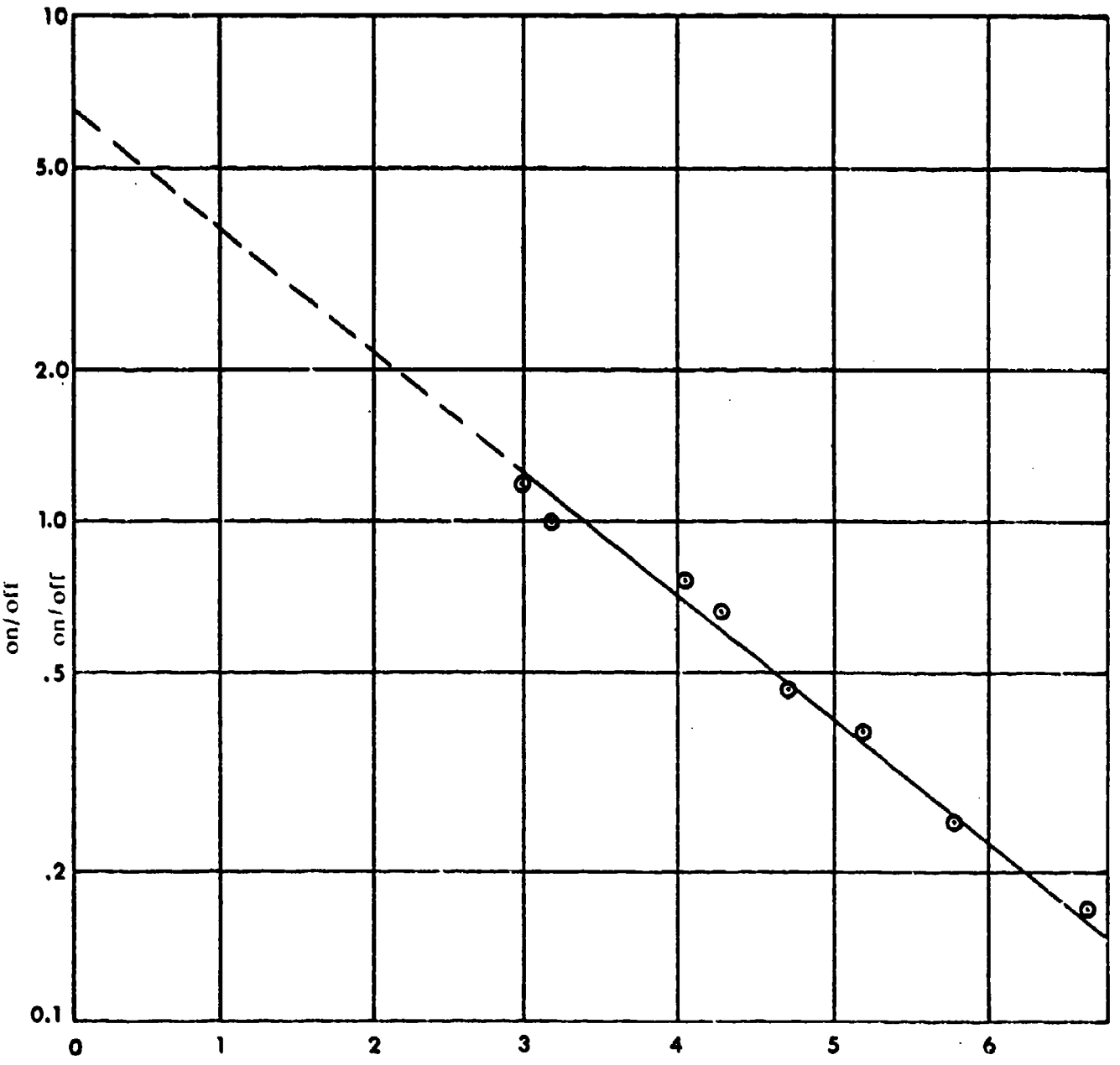

$$L = \sqrt{8 \sec z} \ , \ km^{-1}$$

$$\frac{on}{off} = 6.54\, e^{-0.558\sqrt{L}}$$

$$L = \left\{ \frac{\ln \frac{on}{off} - \ln 6.54}{-0.558} \right\}^2$$

on = Radiance at 7606 Å

off = Radiance at 7530 Å

L = Path Length through O_2 at STP

Figure 5. Calibration of two wavelength teleradiometer, 18 March 1979.

Slide 8.

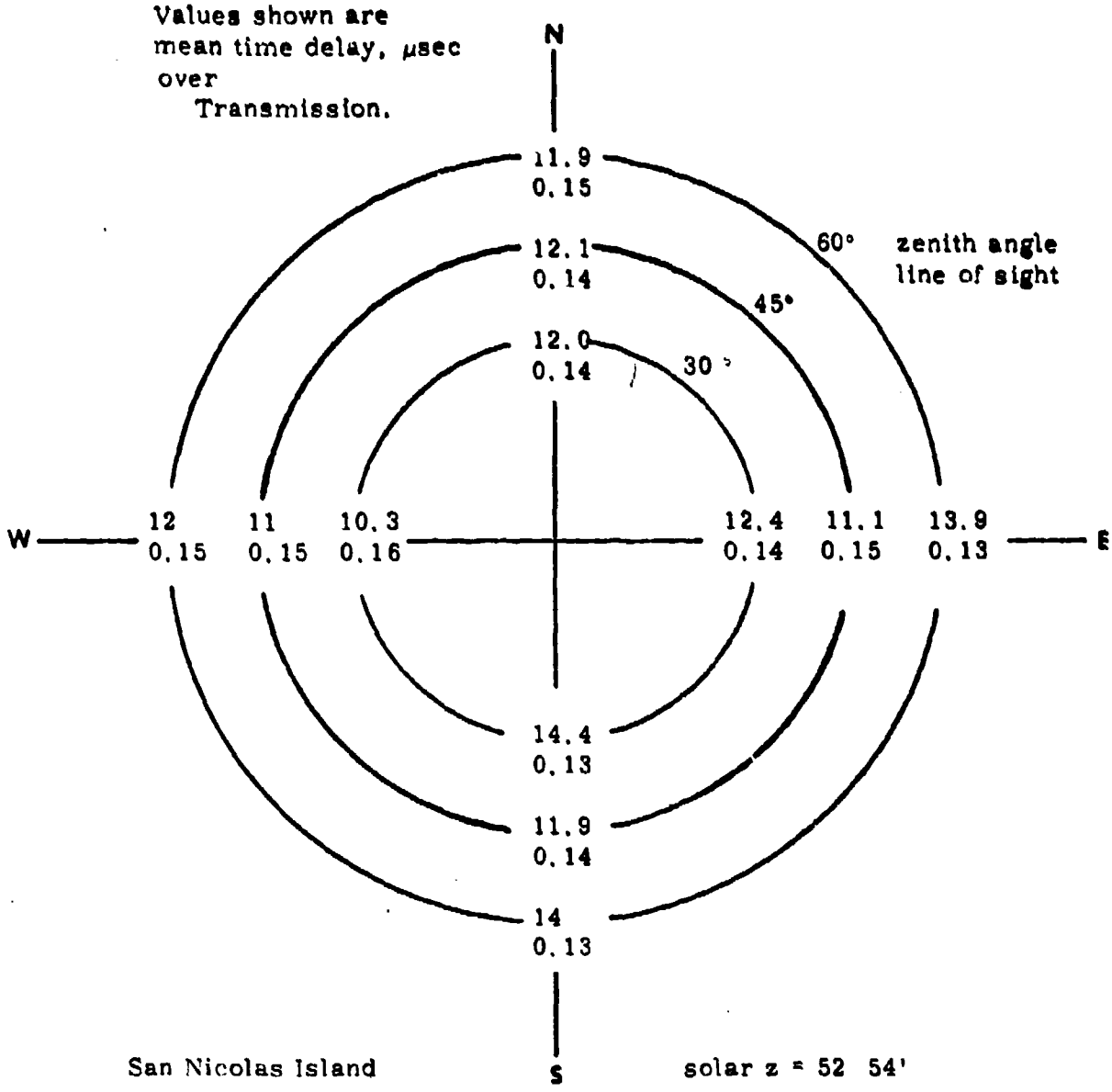

Figure 8. OVERCAST TIME DELAY AND TRANSMISSION

Slide 9.

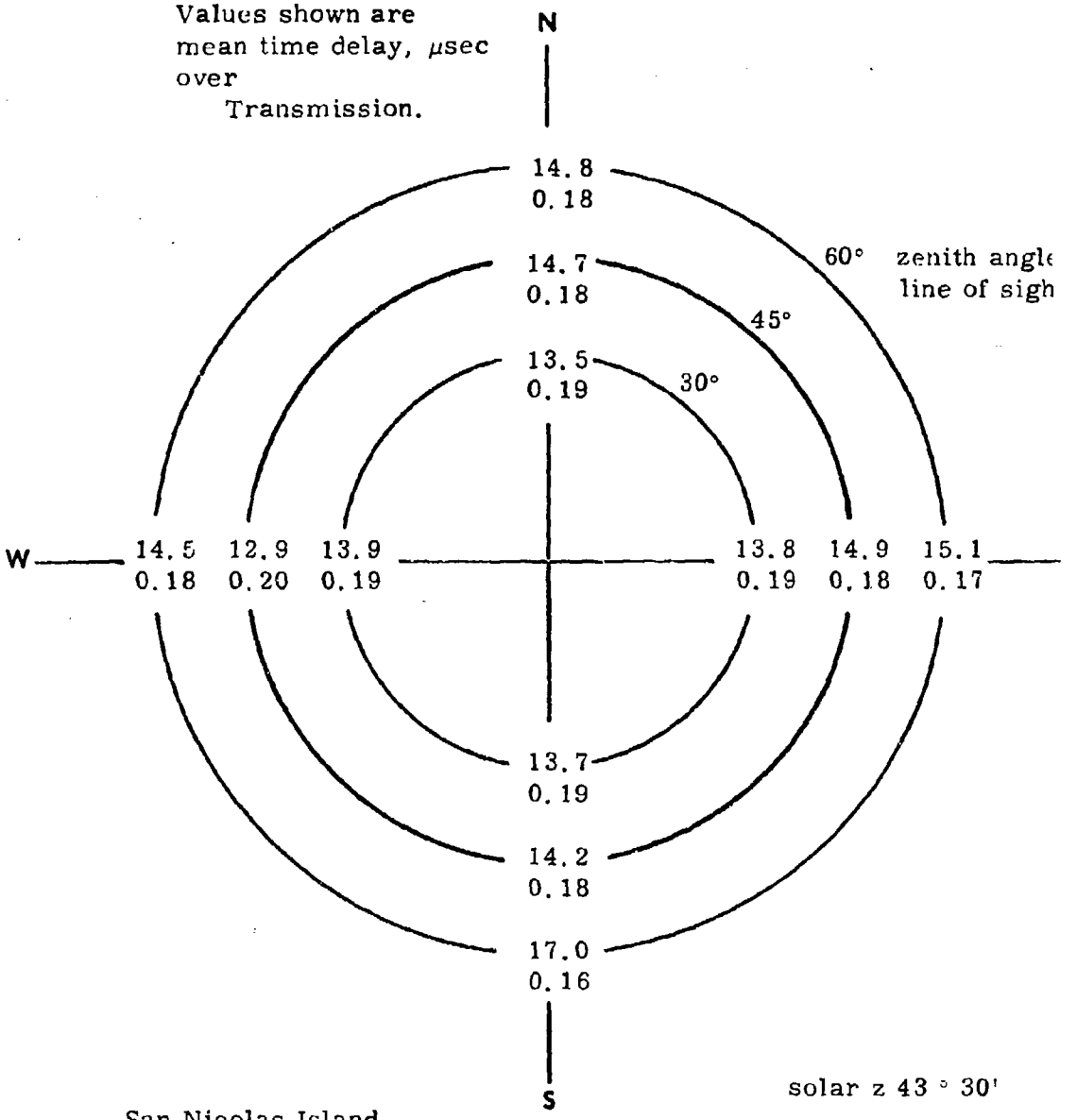

Figure 9. OVERCAST TIME DELAY AND TRANSMISSION

Slide 10.

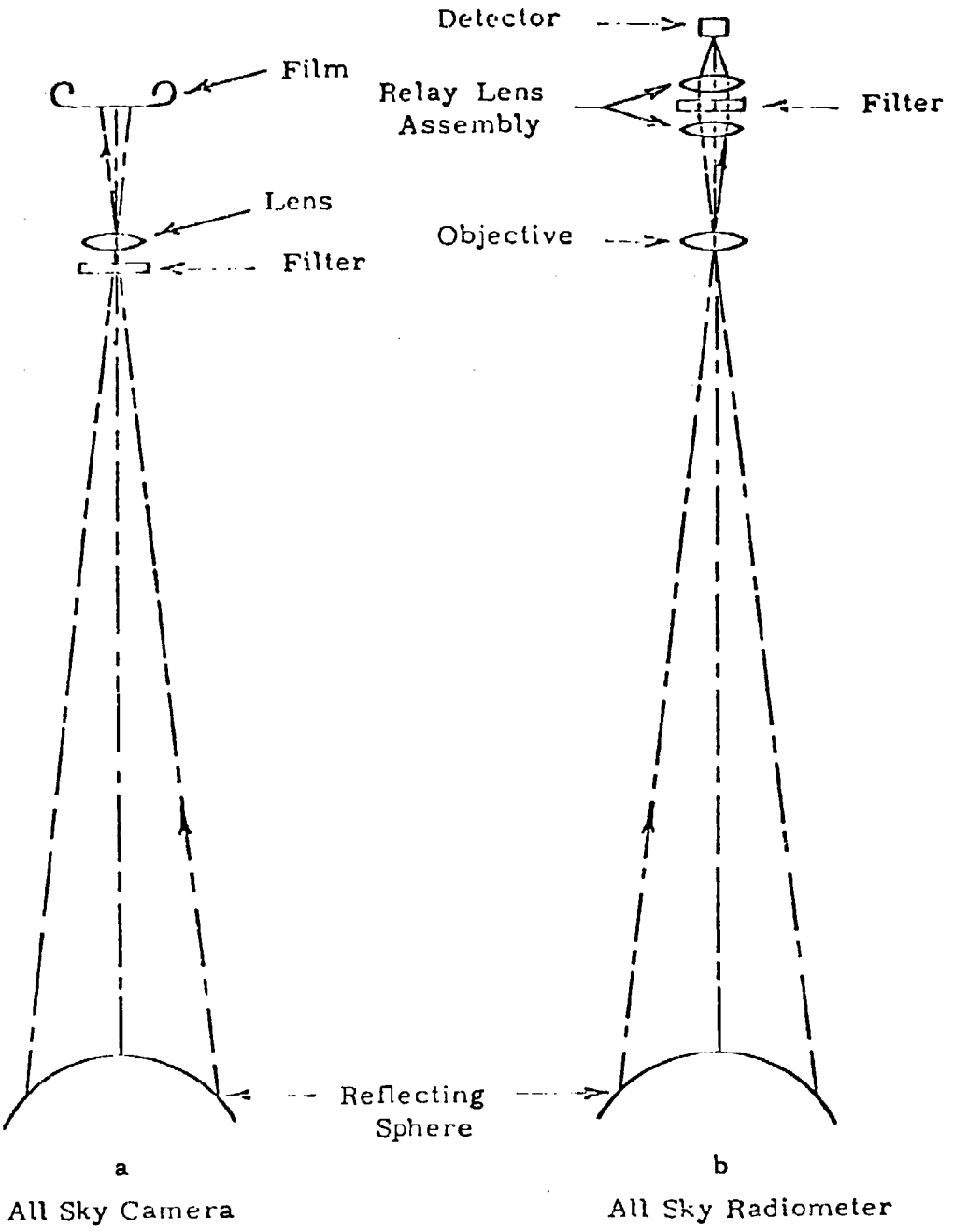

Figure 4.6. All sky detectors using reflections from a spheric surface.

Slide 11.

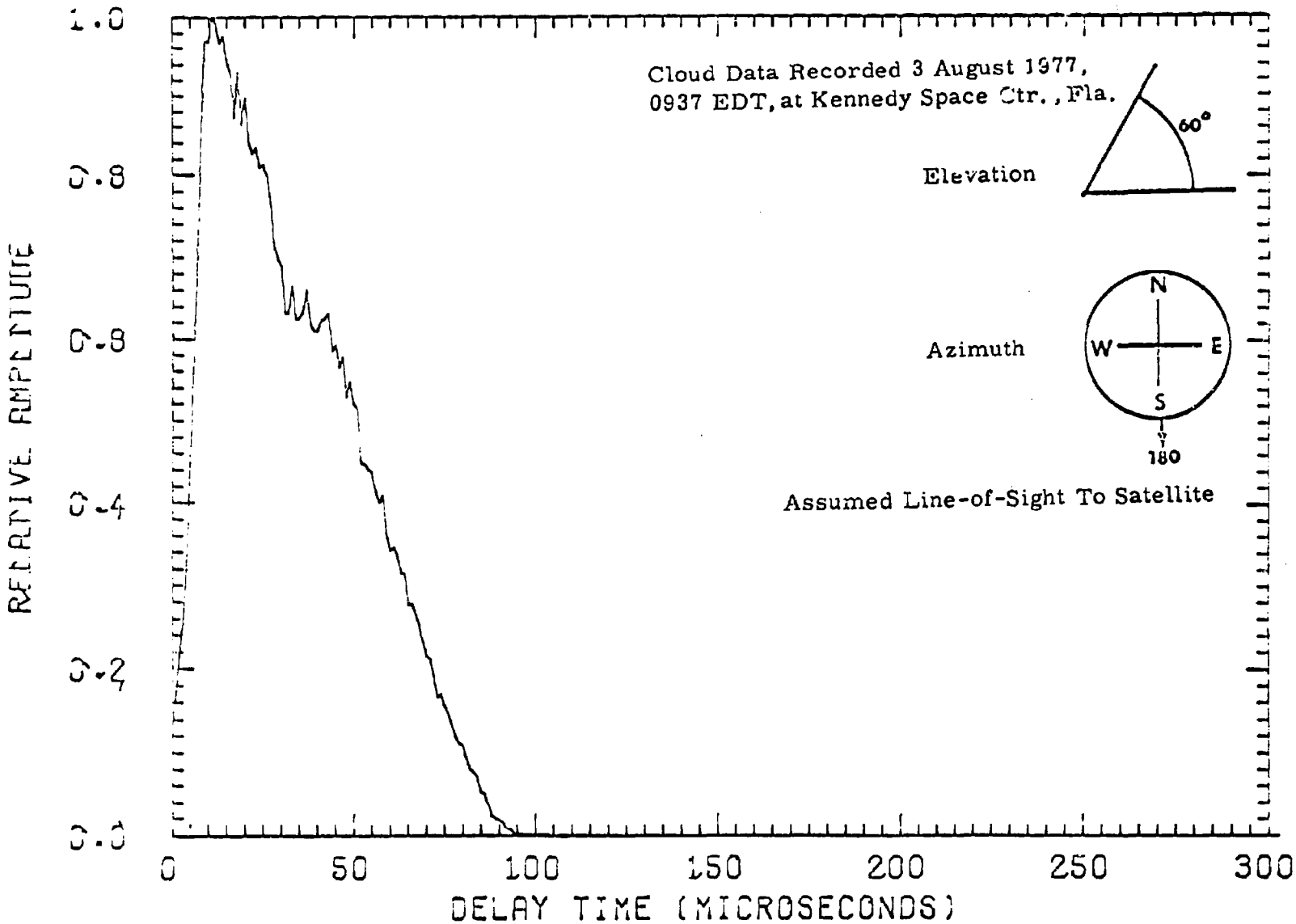
1.0
0.8
0.6
0.4
0.2
0
RELATIVE AMPLITUDE
0
50
100
150
200
250
300
DELAY TIME (MICROSECONDS)
Cloud Data Recorded 3 August 1977,
0937 EDT, at Kennedy Space Ctr., Fla.
Elevation
60°
Azimuth
N
W
E
S
180
Assumed Line-of-Sight To Satellite

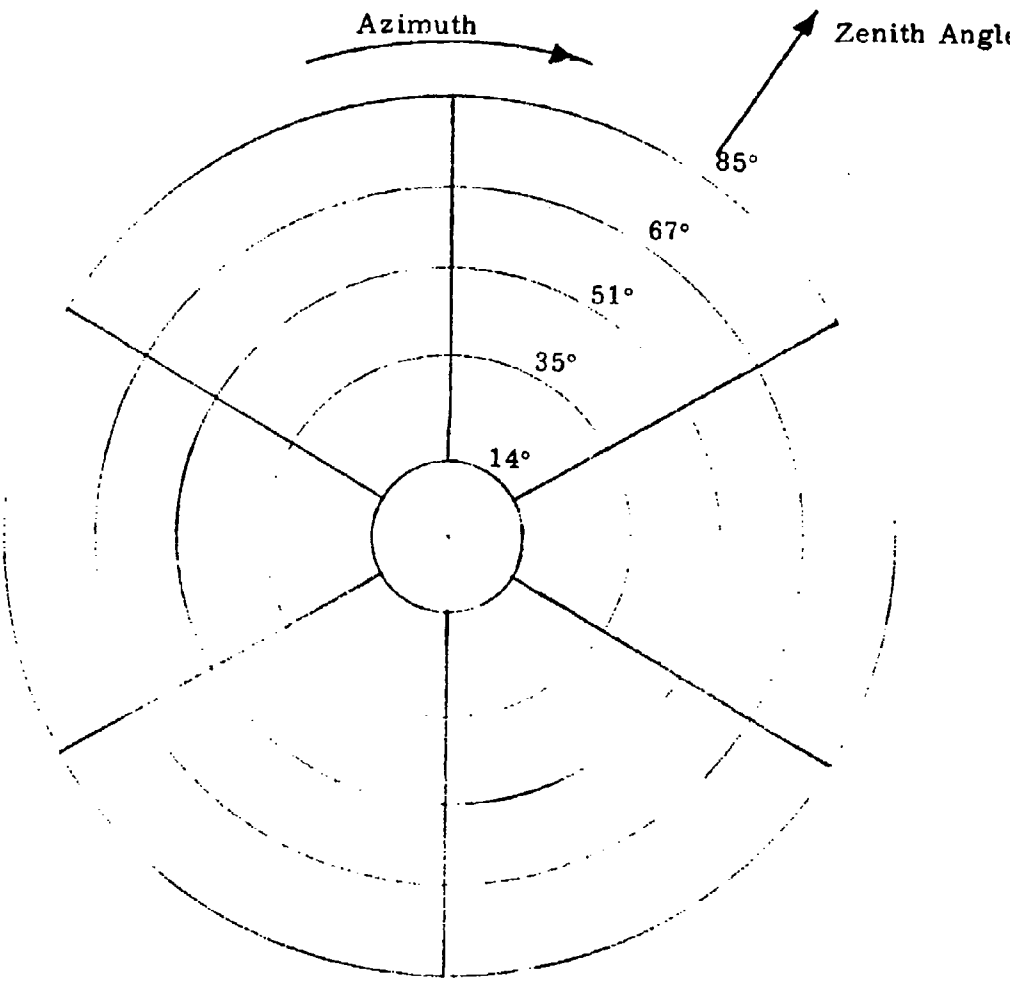

Figure 3. Solid angles receiving equal power from uniform overcast.

Slide 13.

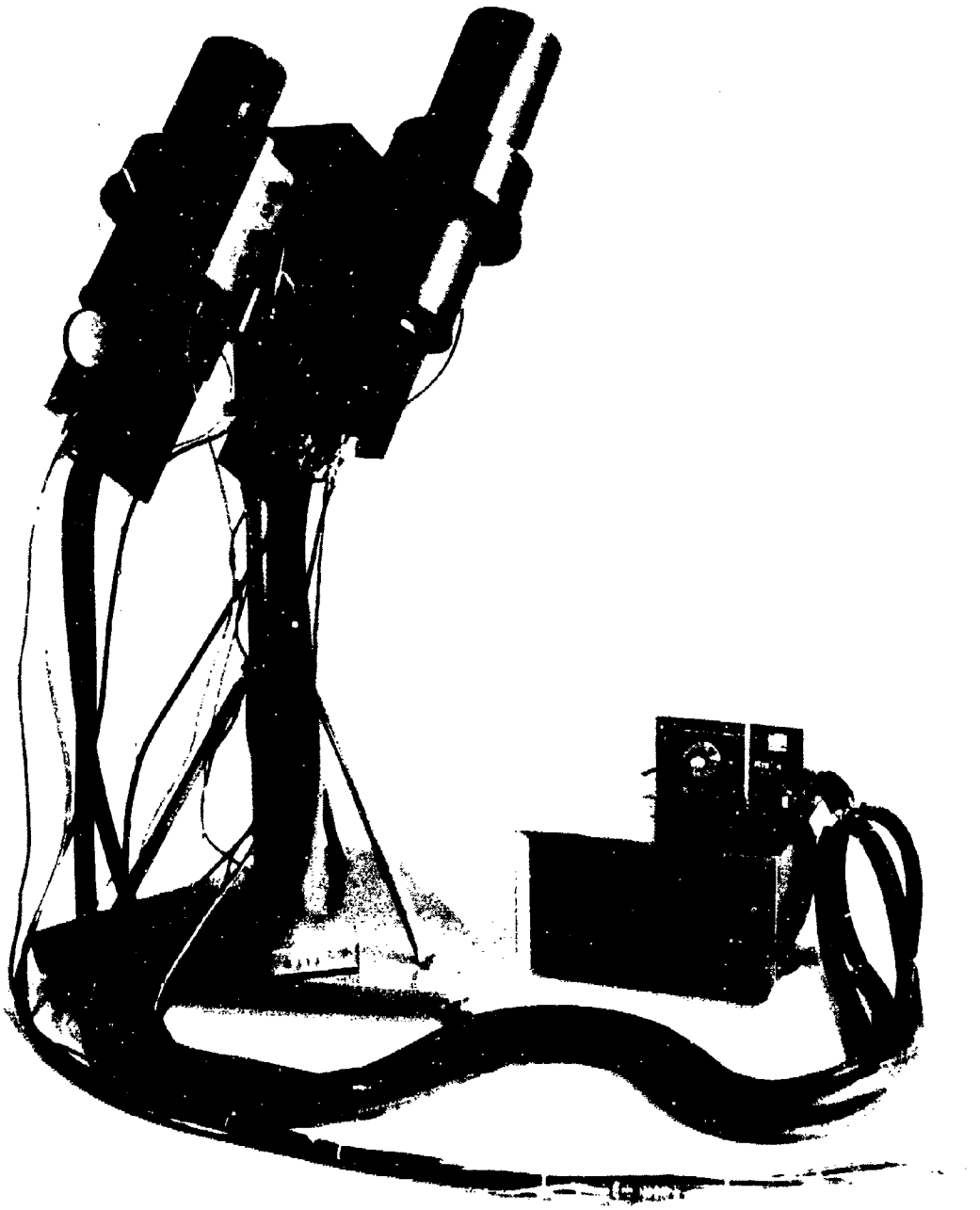

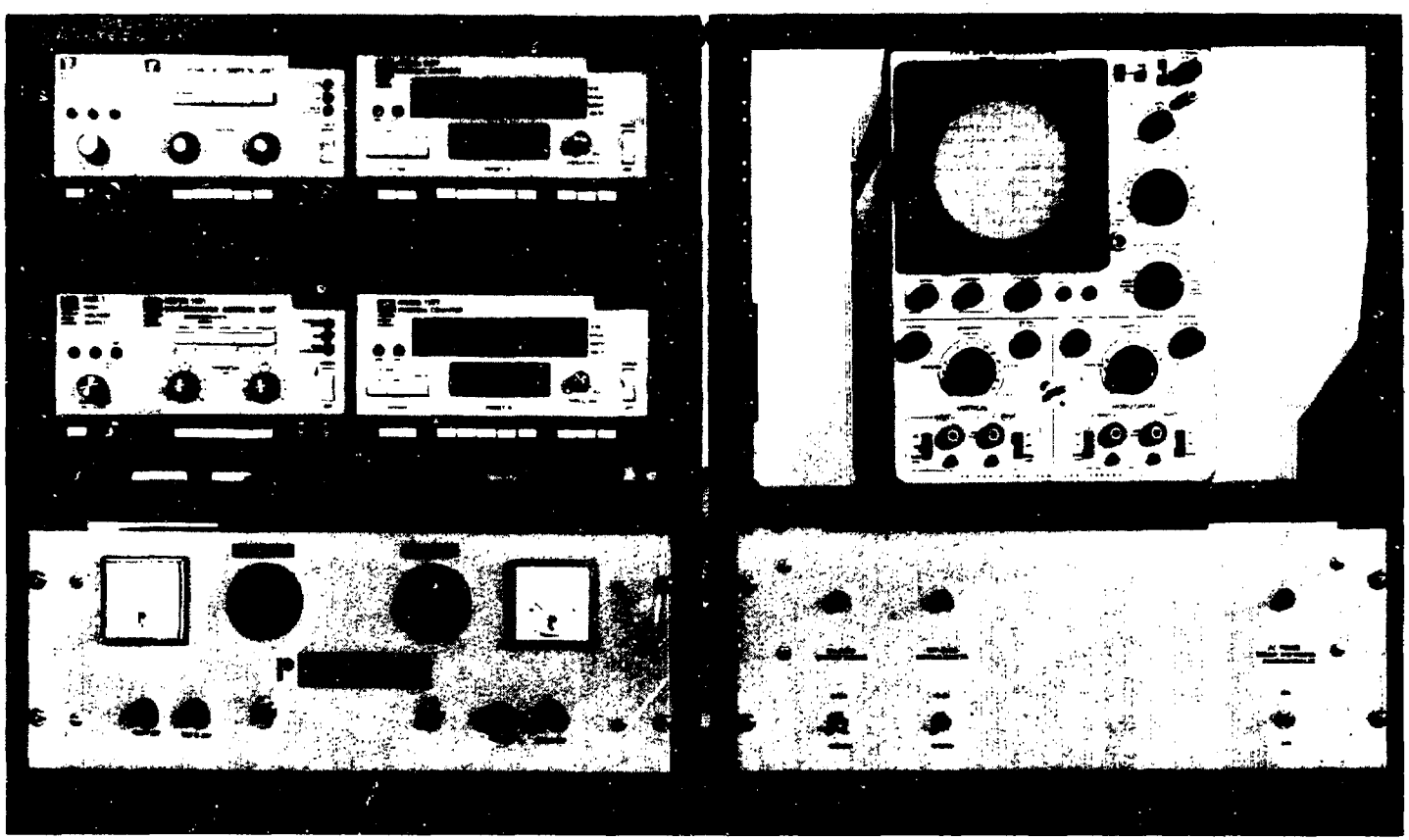

Slide 15

KAUAI LASER - CLOUD EXPERIMENT

TELERADIOMETER PARTICIPATION

NUMBER OF AIRCRAFT RUNS	~336
TELERADIOMETER PARTICIPATION	117
A/C RUNS SELECTED FOR ANALYSIS **	28
A/C RUNS WITH SIGNIFICANT MEAN-TIME-DELAY	12

**BASIS OF SELECTION

(1) CLOUDS IN OVERHEAD DIRECTION

(2) CLOUDS IN LOS TO MOON

(3) GTE-SYLVANIA DATA SHOWS PULSE STRETCHING

(4) TELERADIOMETER DATA SHOWS MEAN-PATH-DELAY

Slide 16.

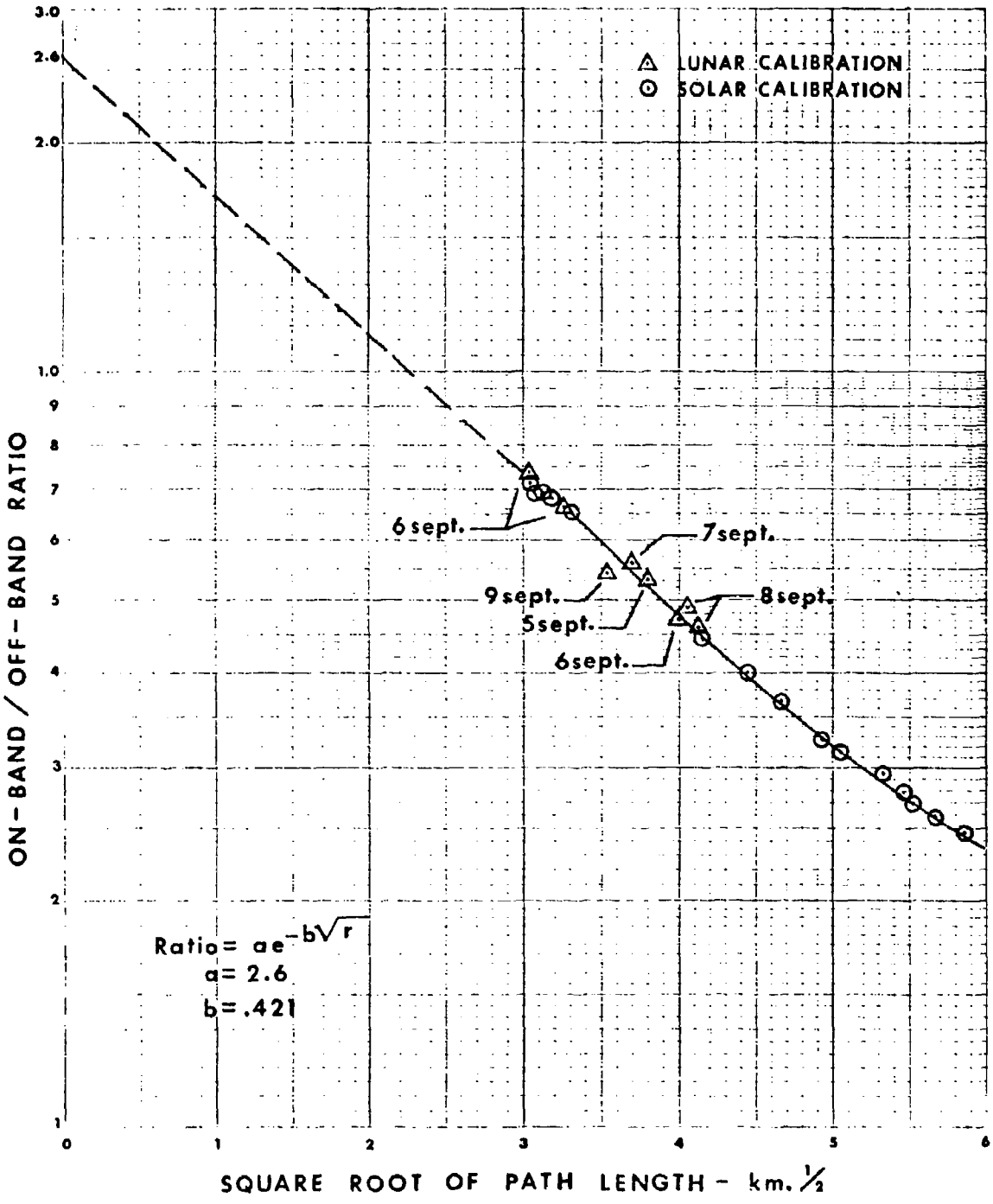
LUNAR CALIBRATION
SOLAR CALIBRATION
6 sept.
7 sept.
9 sept.
8 sept.
5 sept.
6 sept.
Ratio = $ae^{-b\sqrt{r}}$
a = 2.6
b = .421
ON-BAND / OFF-BAND RATIO
SQUARE ROOT OF PATH LENGTH - km.$^{1/2}$

Slide 17.

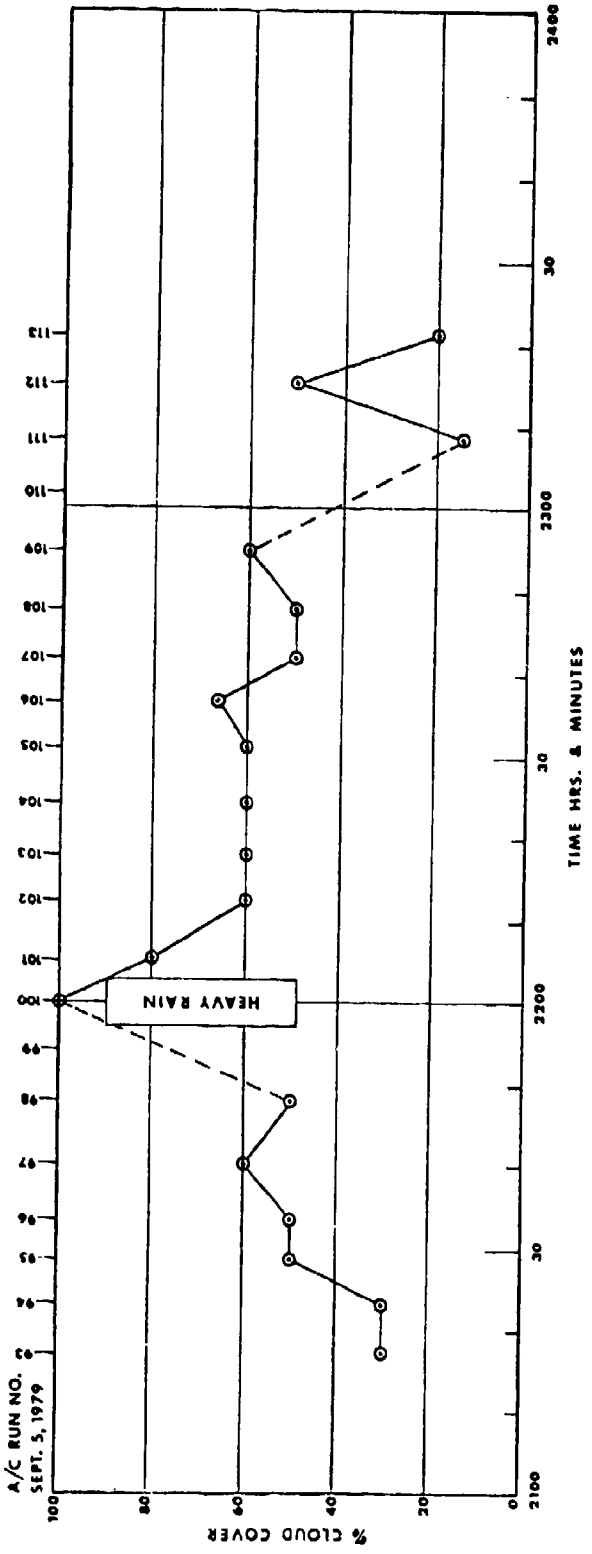
A/C RUN NO.
SEPT. 5, 1979
% CLOUD COVER
TIME HRS. & MINUTES
HEAVY RAIN
2100
2200
2300
2400
30

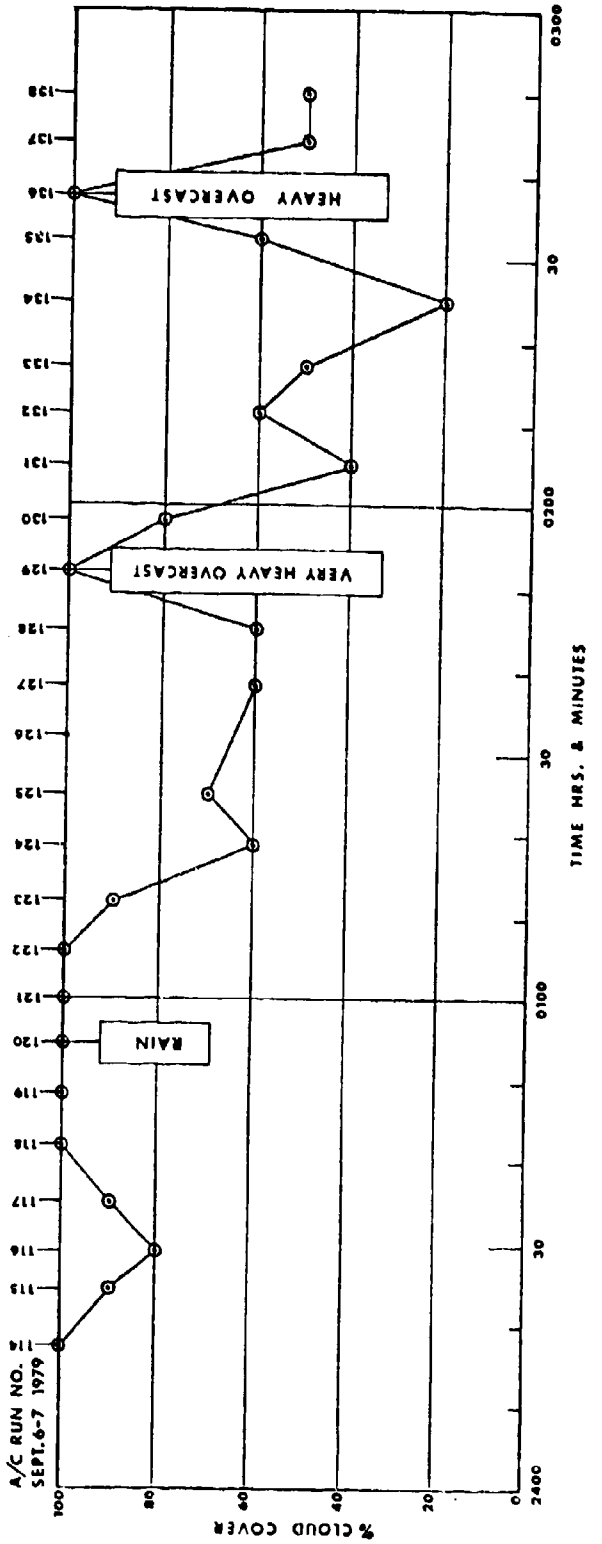
A/C RUN NO.
SEPT. 6-7 1979
% CLOUD COVER
TIME HRS. & MINUTES
RAIN
VERY HEAVY OVERCAST
HEAVY OVERCAST
0100
0200
0300
30

KAUAI CLOUD EXPERIMENT - 1979
TELERADIOMETER MEASUREMENTS

RUN NO: 166	AIRCRAFT PARAMETERS	CLOUD STATUS	LUNAR INFO.
Date: 7/8 Sept	Altitude: 41,869 ft.	Bottom Heights: 2200 ft.	Elevation Angle 61.8 deg.
Time: 0104	Direction: 057 °	Tops (Max): 6500 ft.	Zenith Angle 28.2 deg.
Site: Plantation	Speed: 452 mph.	Tops (Mean): ft.	Azimuth Angle 131 deg.
Site Elev: 600 ft.			

		← Distance From O.H. Position (Yds) →						
PARAMETER	Units	-10,000	-7,500	-5,000	O.H.	+5,000	+10,000	+15,000
MEASURED OR DERIVED								
On-Band/Off-Band Ratio	--	.489	.469	.461	.438	.435	.425	.415
Total Pathlength in O_2	km	15.76	16.56	16.89	17.91	18.05	18.52	19.01
Cloud Free Pathlength in O_2	km	9.08	9.08	9.08	9.08	9.08	9.08	9.08
Mean Path Delay	km	6.68	7.48	7.81	8.83	8.97	9.44	9.93
Mean Time Delay (uncorrected)	μsec	22.3	24.9	26.1	29.4	29.9	31.5	33.1
CALCULATED (Cloud Model)								
Mean Time Delay (Corrected)	μsec	26.2	29.3	30.5	34.4	35.0	36.8	38.7
Cloud Transmission	%	11.5	10.3	9.9	8.8	8.7	8.2	7.8
Mean Free Path (Transport)	meter	118	106	101	89	88	83	79
Mean Free Path (Optical)	meter	20	18	17	15	15	14	13
Optical Thickness	--	65.1	73.0	76.4	86.5	87.9	92.8	97.7
Time A/C At Position	min:sec							

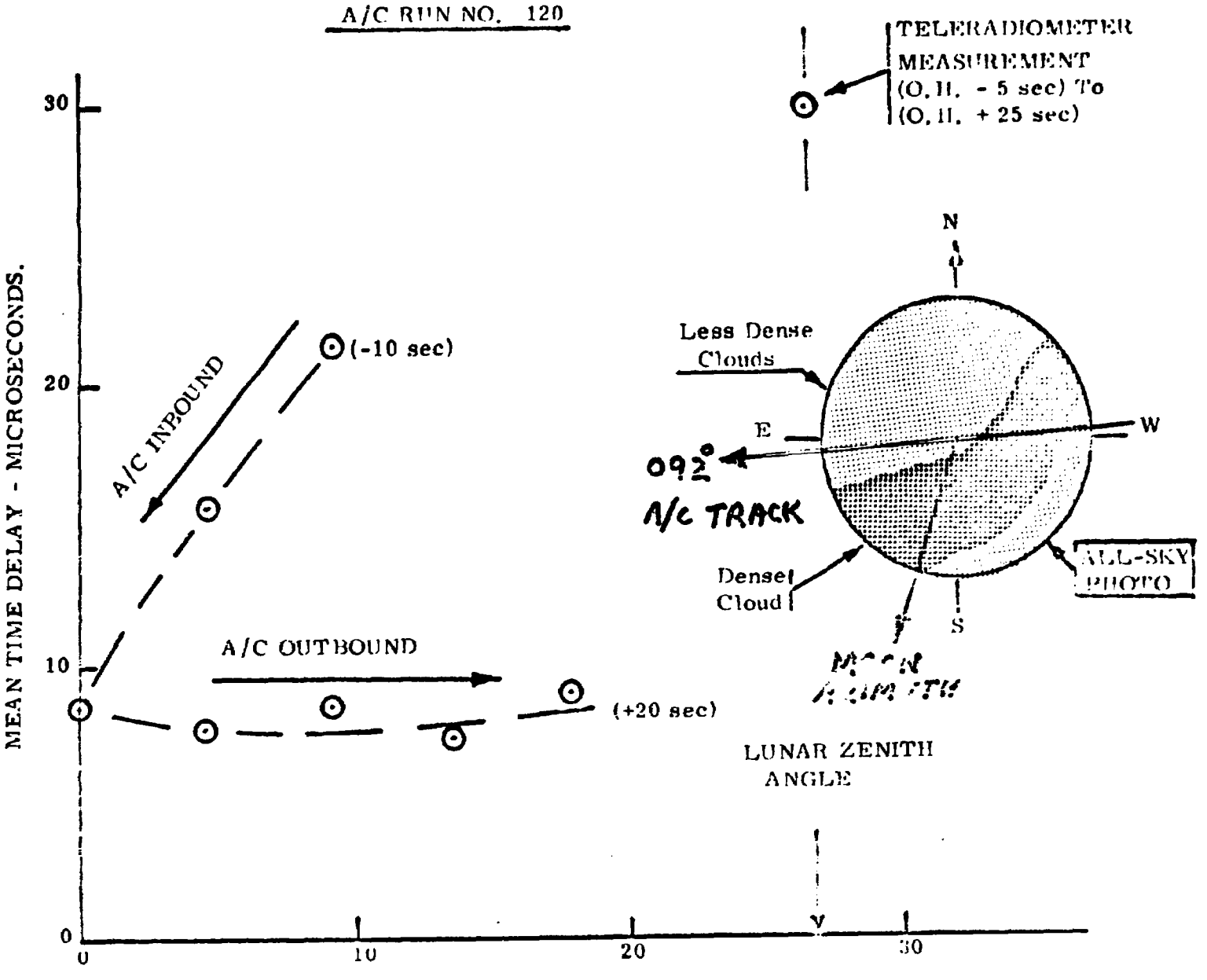
A/C RUN NO. 120
TELERADIOMETER
MEASUREMENT
(O. H. - 5 sec) To
(O. H. + 25 sec)
MEAN TIME DELAY - MICROSECONDS.
30
20
10
0
(-10 sec)
A/C INBOUND
A/C OUTBOUND
(+20 sec)
N
E
W
S
Less Dense
Clouds
Dense
Cloud
092°
A/C TRACK
ALL-SKY
PHOTO
LUNAR ZENITH
ANGLE
0
10
20
30
ZENITH ANGLE - DEGREES.

Slide 20.

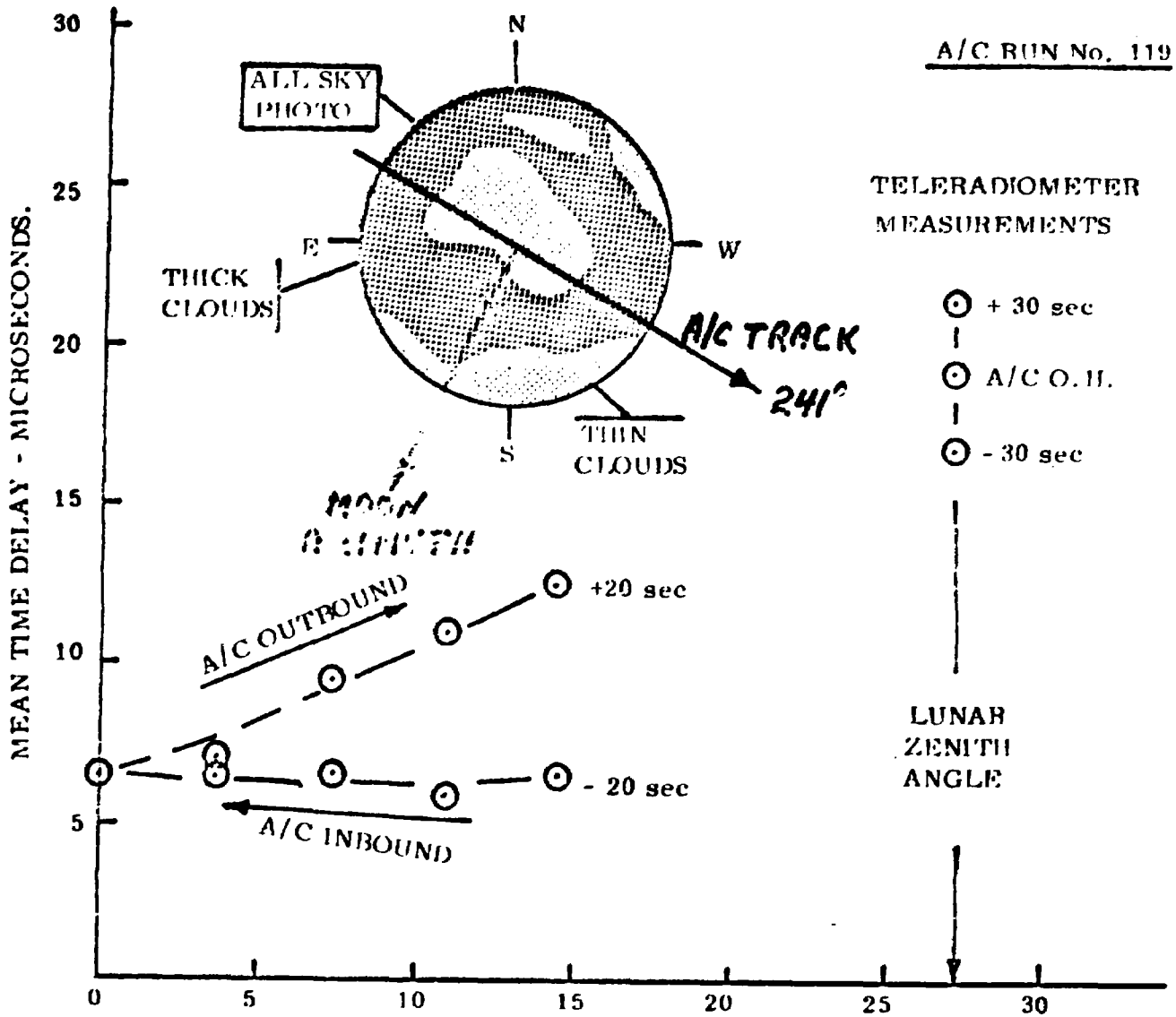
A/C RUN No. 119
ALL SKY PHOTO
N
E
W
S
THICK CLOUDS
THIN CLOUDS
A/C TRACK
241°
TELERADIOMETER MEASUREMENTS
+ 30 sec
A/C O. H.
- 30 sec
LUNAR ZENITH ANGLE
+20 sec
- 20 sec
A/C OUTBOUND
A/C INBOUND
MEAN TIME DELAY - MICROSECONDS.
ZENITH ANGLE - DEGREES.
0
5
10
15
20
25
30

Slide 21.

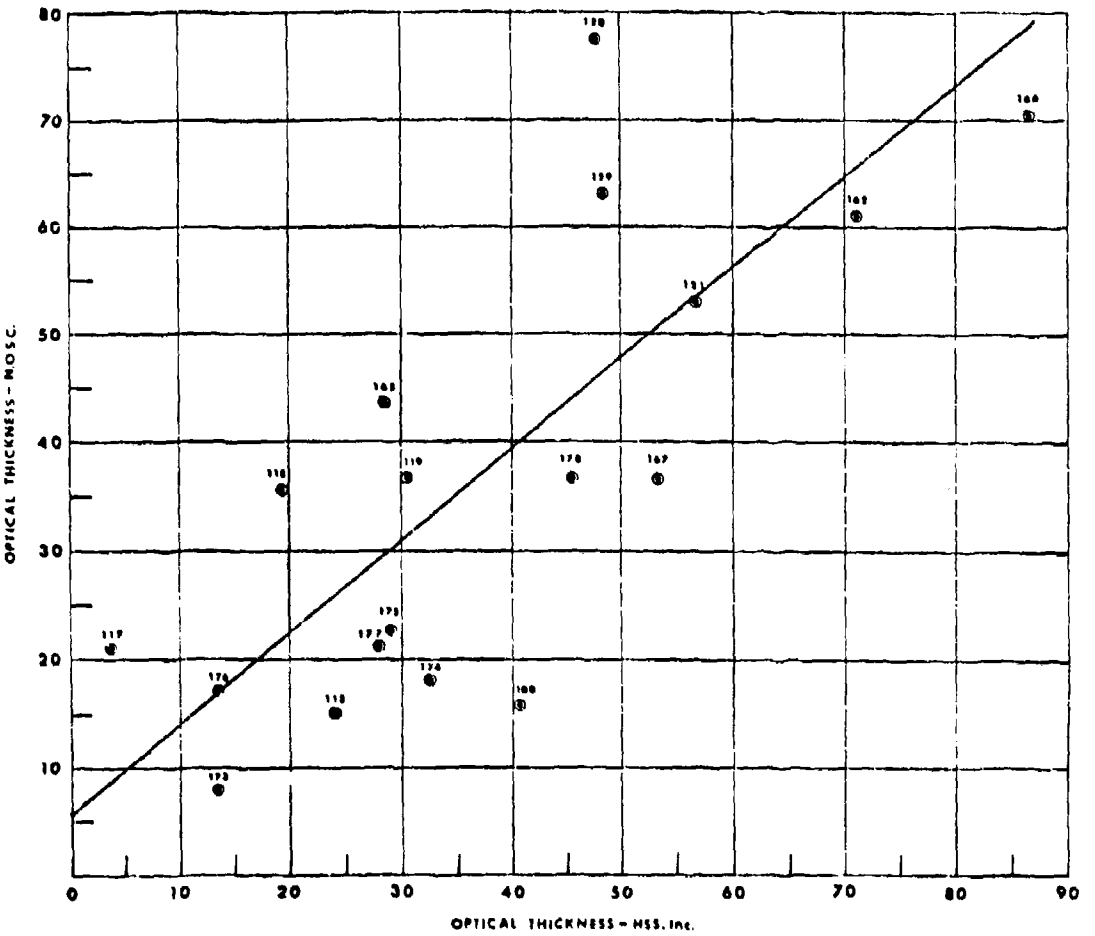

Figure . Scatter diagram of correlation between NOSC and HSS Inc Values of Optical Thickness for eighteen data runs; the Coefficient of Determination $r^2 = 0.89$ and the Correlation Coefficient $r = 0.94$.

Slide 23.

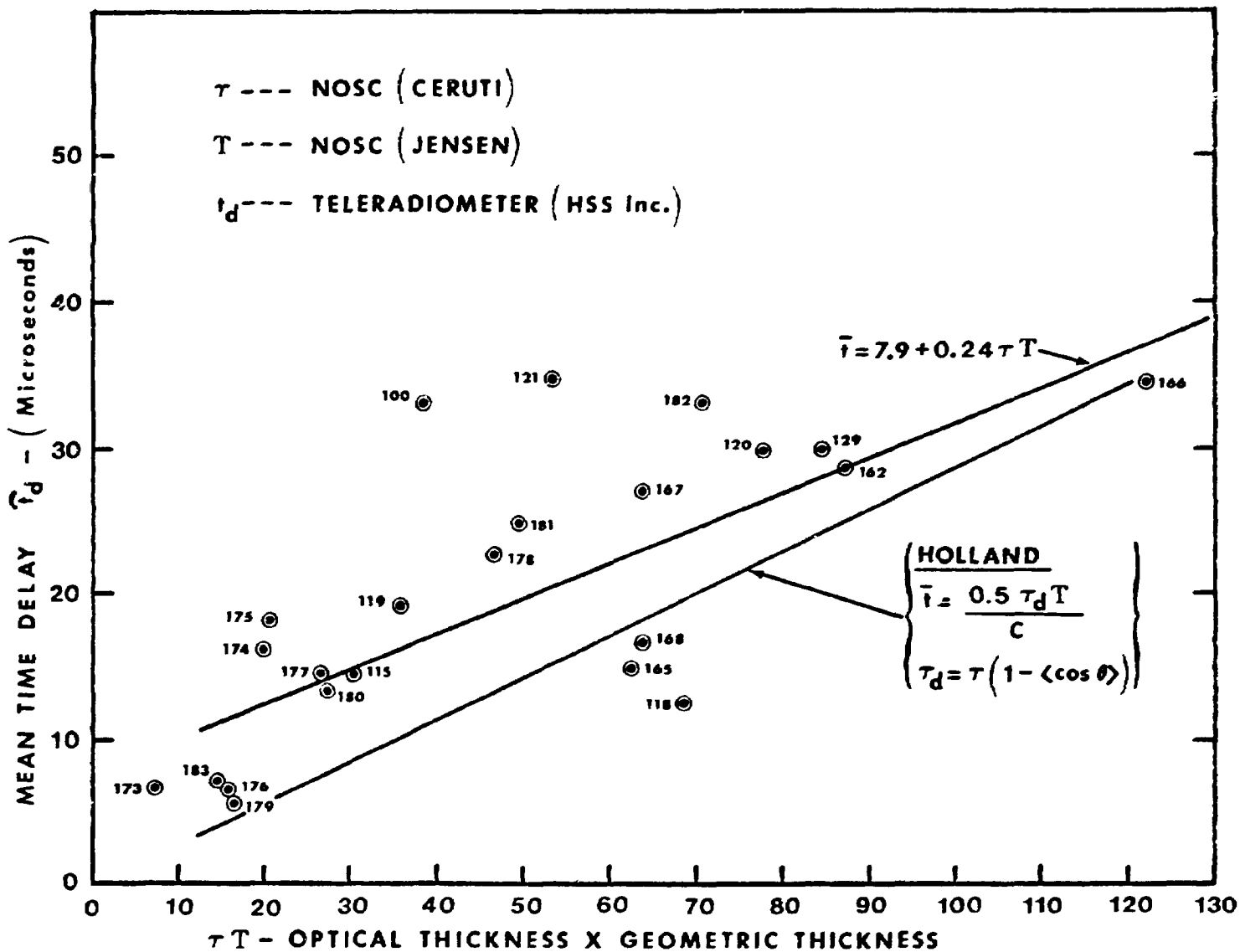
τ --- NOSC (CERUTI)
T --- NOSC (JENSEN)
t_d --- TELERADIOMETER (HSS Inc.)
$\bar{t} = 7.9 + 0.24\,\tau T$
HOLLAND
$\bar{t} = \frac{0.5\,\tau_d T}{C}$
$\tau_d = \tau\left(1 - \langle\cos\theta\rangle\right)$
MEAN TIME DELAY $\bar{t}_d$ - (Microseconds)
τT - OPTICAL THICKNESS X GEOMETRIC THICKNESS
0
10
20
30
40
50
60
70
80
90
100
110
120
130
100
121
182
166
120
129
162
167
181
178
119
175
174
177
115
180
168
165
118
173
183
176
179

Slide 24.

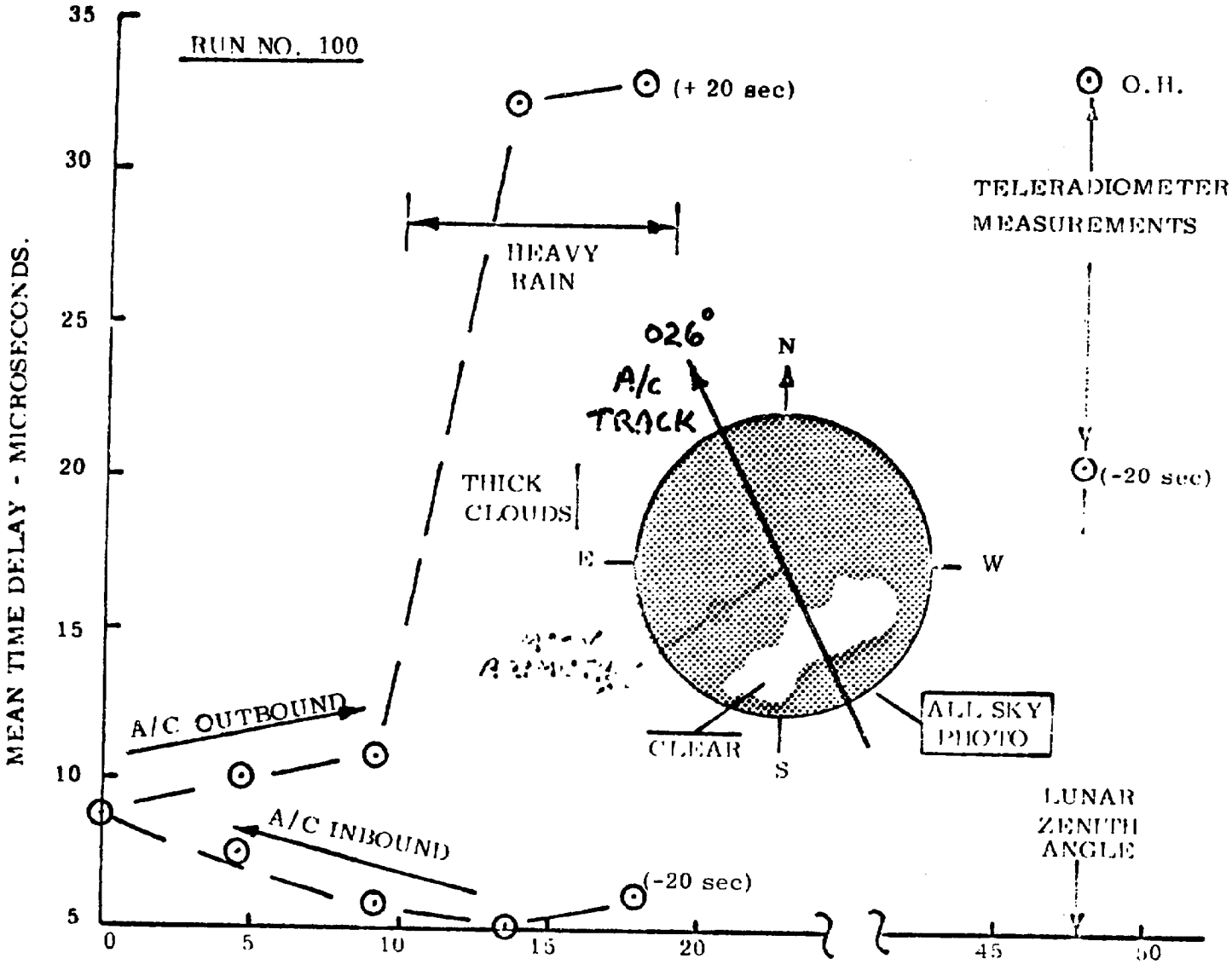
RUN NO. 100
MEAN TIME DELAY - MICROSECONDS
35
30
25
20
15
10
5
0
5
10
15
20
45
50
(+ 20 sec)
HEAVY RAIN
026°
A/c TRACK
N
THICK CLOUDS
E
W
S
CLEAR
ALL SKY PHOTO
A/C OUTBOUND
A/C INBOUND
(-20 sec)
O.H.
TELERADIOMETER MEASUREMENTS
(-20 sec)
LUNAR ZENITH ANGLE

UPLINK PROPAGATION AND ADAPTIVE OPTICS*

D.P. Greenwood

27 March 1980

Massachusetts Institute of Technology
Lincoln Laboratory
P.O. Box 73
Lexington, Massachusetts 02173

ABSTRACT

The basic limitation to propagating a laser beam from ground to space for the Blue Green communication application is atmospheric turbulence. Also, thermal blooming is beginning to be significant for laser power levels above approximately 100 kWatt, average power, for a wavelength of 0.48 μm. We have addressed the degree to which the beam is spread by these aberrating effects, and also the effectiveness of adaptive optics in correcting for the induced phase errors. Adaptive optics appear feasible in reducing the beam spread to near diffraction-limited performance, however, there are a number of residual errors: amplitude, fitting, isoplanatism, bandwidth and signal-to-noise. With reasonable care in reducing these errors, the up-link loss can be reduced to approximately 5 - 10 dB (depending on zenith angle), of which 2 - 5 dB can be attributed to atmospheric extinction.

* This work is sponsored by the Advanced Research Projects Agency.

SLC PRESENTATION

San Diego, CA

D.P. Greenwood

27 March 80

UP-LINK PROPAGATION AND ADAPTIVE OPTICS

PROBLEM STATEMENT

OBJECTIVE:

- To efficiently transfer power from a ground-based high power laser to a spaceborne target.

APPROACH:

- Estimate the aberrating effects of atmospheric turbulence and thermal blooming.
- For sufficiently large atmospheric aberrations with respect to jitter and device quality, consider the effectiveness of wavefront correction by adaptive optics, including fast tracking.

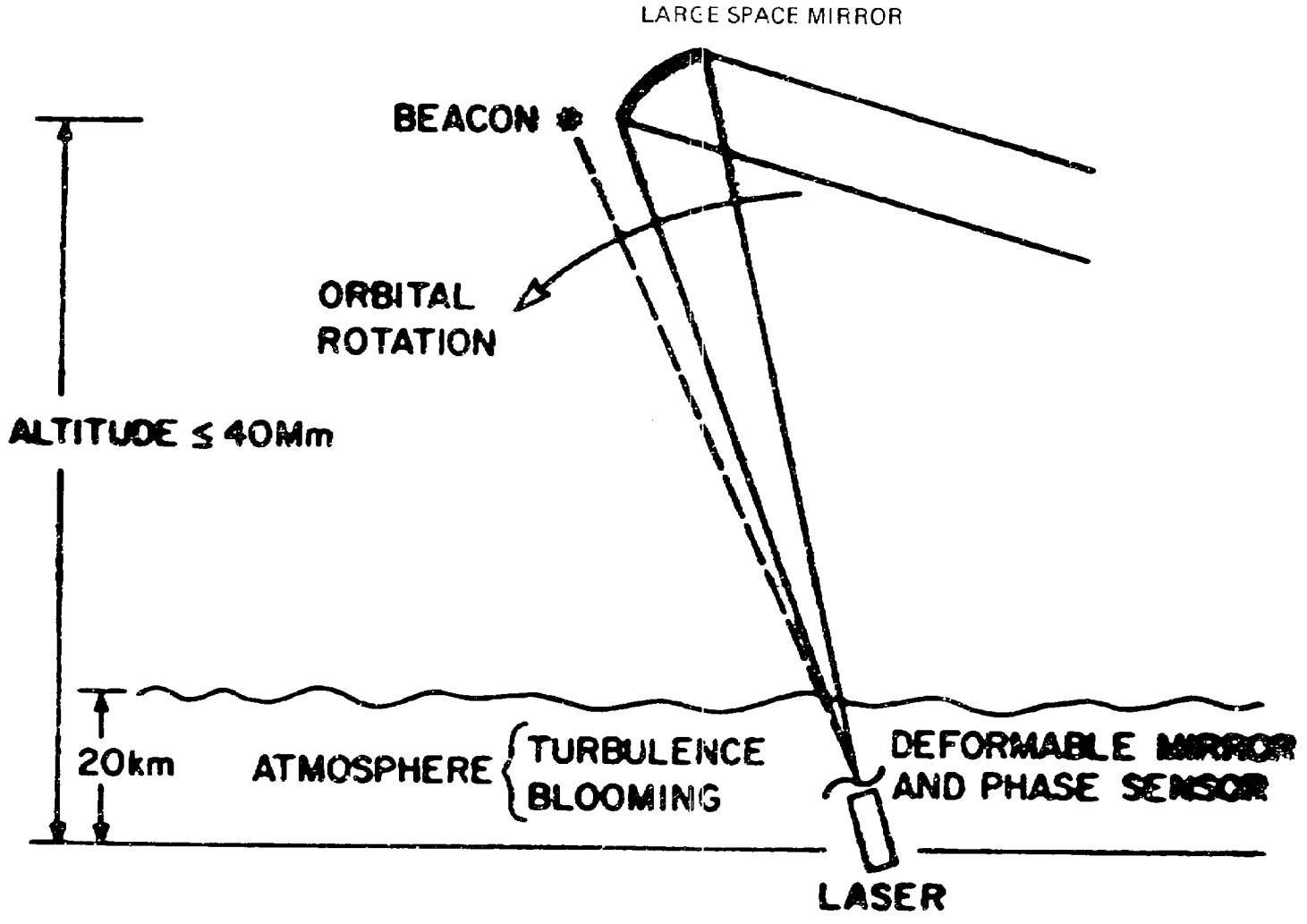

COMPENSATION FOR TURBULENCE AND BLOOMING ON AN UP-LINK

OUTLINE

1. Methodology

   Identifies sources of aberration causing beam spread

2. Discussion on extinction, beam quality, jitter

3. Turbulence

   - Uncorrected beam spread
   - Effectiveness of correction using adaptive optics

4. Thermal Blooming

   - Magnitude of error
   - Correction using adaptive optics

5. Combination of effects - computation of link loss

6. Summary

DEFINITION OF BEAM QUALITY

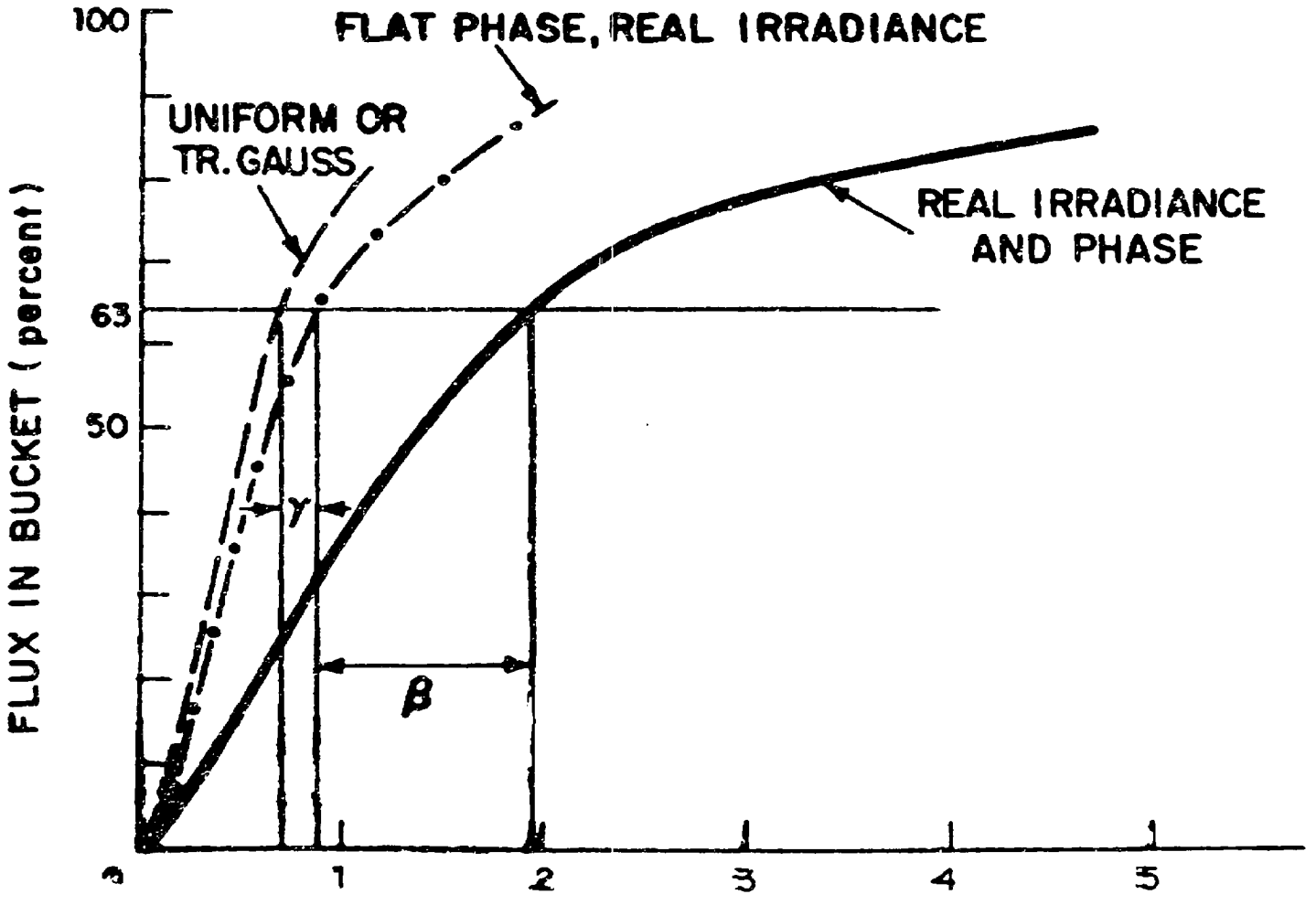

ATMOSPHERIC EXTINCTION (at 0.48 μm, Zenith, Sea Level to ∞)

Horizontal Visibility	N_e Aerosols	N_e Ozone[3]	N_e Rayleigh[4]	N_e Total	$\exp(-N_e)$
50 km f/w[1]	0.14	0.011	0.17	0.32	0.73*
s/s[2]	0.17			0.35	0.71
23 km f/w	0.40			0.58	0.56
s/s	0.44			0.62	0.54
10 km f/w	0.94			1.12	0.33
s/s	0.98			1.16	0.31**
5 km f/w	1.7			1.88	0.15
s/s	1.8			1.98	0.14
2 km f/w	4.3			4.5	0.11
s/s	4.3			4.5	0.11

*Sample system parameter

**Conservative value used

[1] f/w = fall/winter

[2] s/s = spring/summer

[3] For an equivalent column height of 0.35 cm (varies from 0.25 - 0.42 cm over US)

[4] Based on US Std. Atmosphere 1962

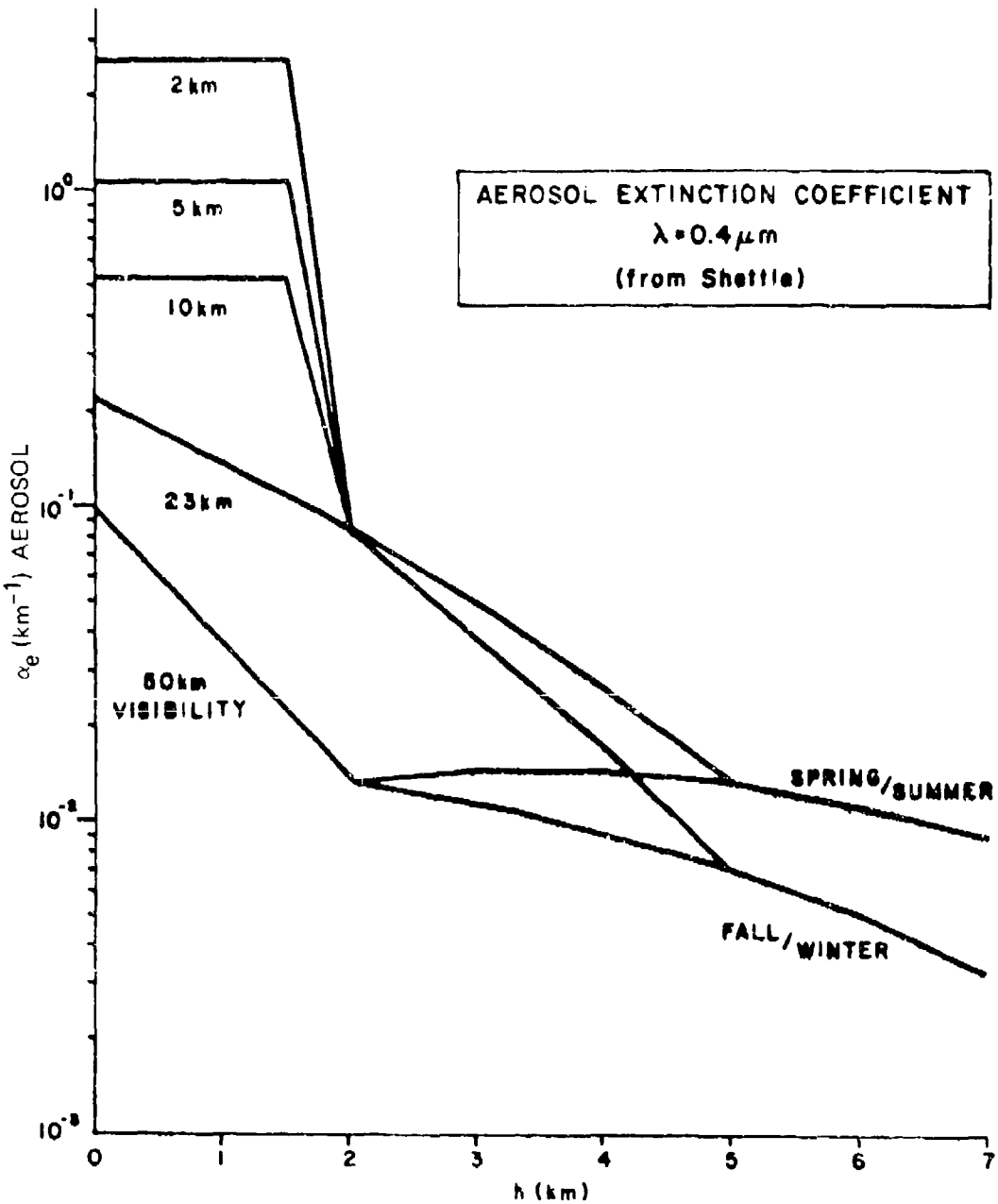
AEROSOL EXTINCTION COEFFICIENT
λ=0.4μm
(from Shettle)
2km
5km
10km
23km
50km
VISIBILITY
SPRING/SUMMER
FALL/WINTER
α_e (km^{-1}) AEROSOL
10^0
10^{-1}
10^{-2}
10^{-3}
0
1
2
3
4
5
6
7
h (km)

SPOT AREA AND IRRADIANCE

- AREA ON TARGET

$$A = A_{\infty}\left[\gamma^2\beta^2 + \frac{\Delta A_T}{A_{\infty}} + \frac{\Delta A_B}{A_{\infty}} + \frac{\Delta A_J}{A_{\infty}}\right]$$

WHERE

A_{∞} = DIFFRACTION LIMITED AREA

β, γ = DEFINE DEVICE QUALITY

ΔA_T = INCREASE IN AREA DUE TO TURBULENCE

ΔA_B = INCREASE IN AREA DUE TO THERMAL BLOOMING

ΔA_J = INCREASE IN AREA DUE TO JITTER $(=2\pi\sigma_J^2)$

- IRRADIANCE (Average)

$$I = 0.65\, PA^{-1} \exp(-N_e)$$

WHERE

P = LASER POWER

N_e = EXTINCTION NUMBER

ATMOSPHERIC TRANSMISSION TO ZENITH FROM SEA LEVEL,
BASED ON EXCELLENT VISIBILITY (50 miles)
(from ref. 2 or 4, same curve)

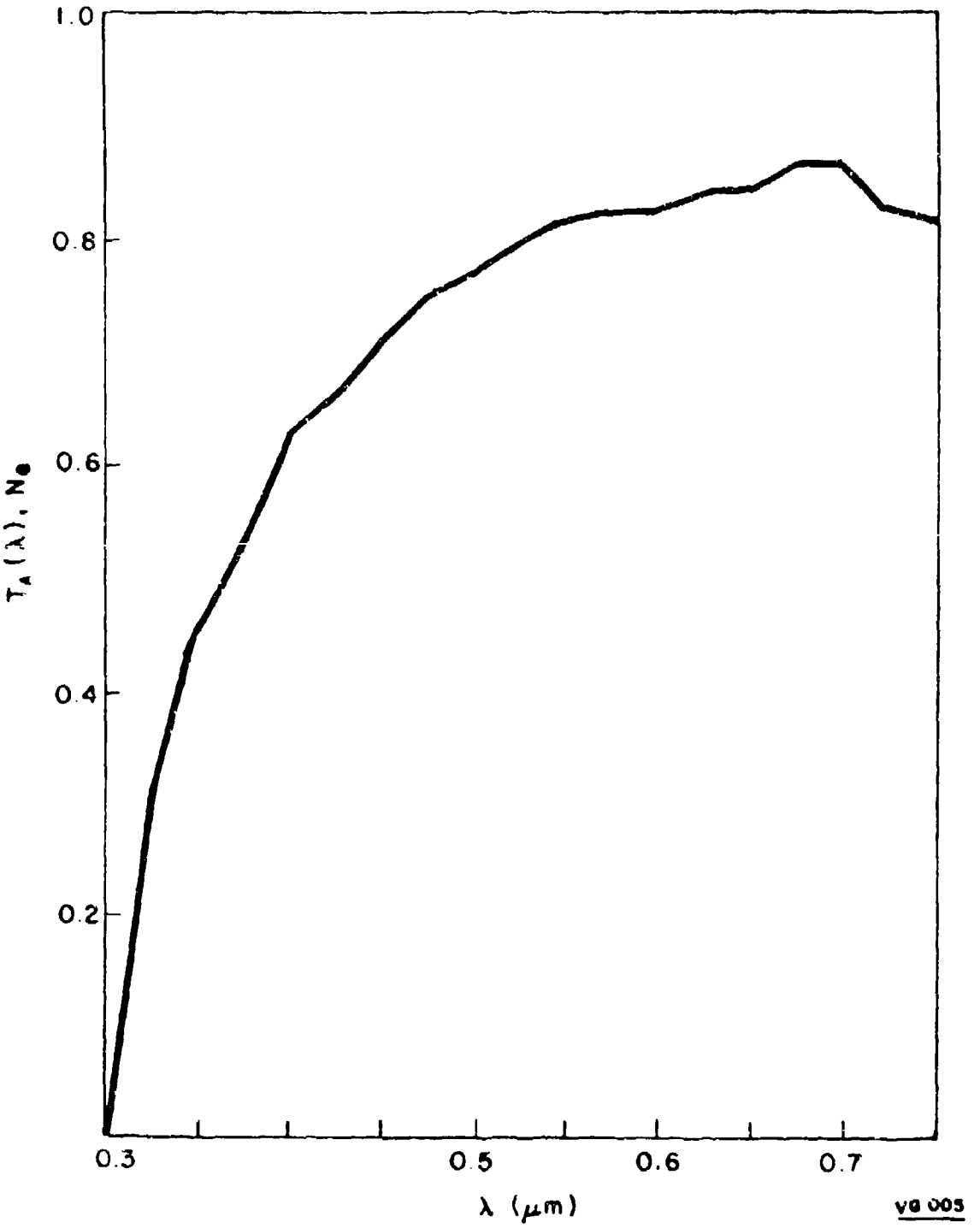

SAMPLE SYSTEM PARAMETERS USED IN COMPUTATIONS

Laser:

Power	P_{AV} = 120 kW or less*
Wavelength	λ = 0.48μm

System:

Ground-based	
Beam Quality	β = 1.2
Amplitude Factor	γ = 1.1
Output Aperture Diameter	D = 4m

Atmosphere: (Values at Zenith)

	Sample Sys	Conservative
Turbulence coherence length	r_0 = 10 cm	4 cm
Isoplanatic angle	θ_0 = 25 rad	15μrad
Log-amplitude mean square	σ_x^2 = 0.05 neper^2	0.1 neper^2

Satellite:

Synchronous	h_T = 40 Mm
Zenith angle	θ_z = 0-72^0
Aperture diameter	D_2 = 10m

*120 kW corresponds 4 kJ/pulse, 30 pps

DIFFRACTION AND DEVICE LIMITED AREA

$A_{00} = \pi(0.65\lambda L/D)^2$ Diffraction

$A_0 = \gamma^2\beta^2 A_{00}$ Device

Sample System:

$A_{00} = 30.6\ m^2$

$A_0 = 53.3\ m^2$

(Beam diameter 8.2 m)

JITTER CONTRIBUTION

$$\Delta A_J = 2\pi \sigma_J^2 L^2$$

Criterion: Have jitter contribution < device limited area

$$2\pi\sigma_J^2 L^2 < A_0$$

$$\sigma_J < 0.46\ \gamma^3 \lambda/D$$

Sample System: $\sigma_J < 70$ nrad

(Beyond current state of the art, but an even smaller jitter is desirable

UNCORRECTED TURBULENCE

$$\Delta A_T / A_{00} \approx (D/r_0)^2$$

where r_0 = atmospheric coherence length (Fried)

$$r_0^{-5/3} = 0.423\, k^2 \int_0^L C_n^2 (z)\, dz$$

$$r_0 \sim (\sec \theta_z)^{-3/5}$$

Sample System:

$$\left.\begin{aligned} \Delta A_T / A_{00} &= 1600 \\ \Delta A_T &= 4.9 \times 10^4 \text{ m}^2 \end{aligned}\right\} \text{ at } \theta_z = 0^0$$

$$\left.\begin{aligned} \Delta A_T / A_{00} &= 6.6 \times 10^3 \\ \Delta A_T &= 2.0 \times 10^5 \text{ m}^2 \end{aligned}\right\} \text{ at } \theta_z = 72^0$$

Clearly, turbulence must be corrected, and the correction must be very good, such that only $\leq 1\%$ remains.

TURBULENCE

MULTI-ELEMENT ADAPTIVE OPTICS CORRECTION

$$\frac{\Delta A_T}{A_{00}} \approx -1 + \exp\left[\sigma^2_{FIT} + \sigma^2_{AMPL} + \sigma^2_{ISO} + \sigma^2_{BW} + \sigma^2_{SN}\right]$$

where

FIT	~	Fitting Error
AMPL	~	Amplitude Error
ISO	~	Isoplanatic Error
BW	~	Bandwidth Error
SN	~	Signal-To-Noise Error

CAUTION: The above model is very simplistic and not rigorous. There are complex interactions between all terms listed.

FITTING ERROR

$$\sigma^2_{FIT} = 0.35\,(d/r_o)^{5/3} \qquad (rad^2)$$

where d = interactuator spacing

The number of actuators is

$$N_a = \pi(D/2d)^2$$

For a fitting error (minimum) of 1/10 wave:

$$\sigma^2_{FIT} = 0.395 \qquad (rad^2)$$

$$d/r_o = 1.1$$

Sample system:

$N_a = 1040$ $\qquad \theta_z = 0$

$N_a = 4260$ $\qquad \theta_z = 72^0$

Conservative system:

$N_a = 6500$ $\qquad \theta_z = 0^0$

$N_a = 26600$ $\qquad \theta_z = 72^0$

MATCHED FILTER ADAPTURE OPTIC SYSTEM

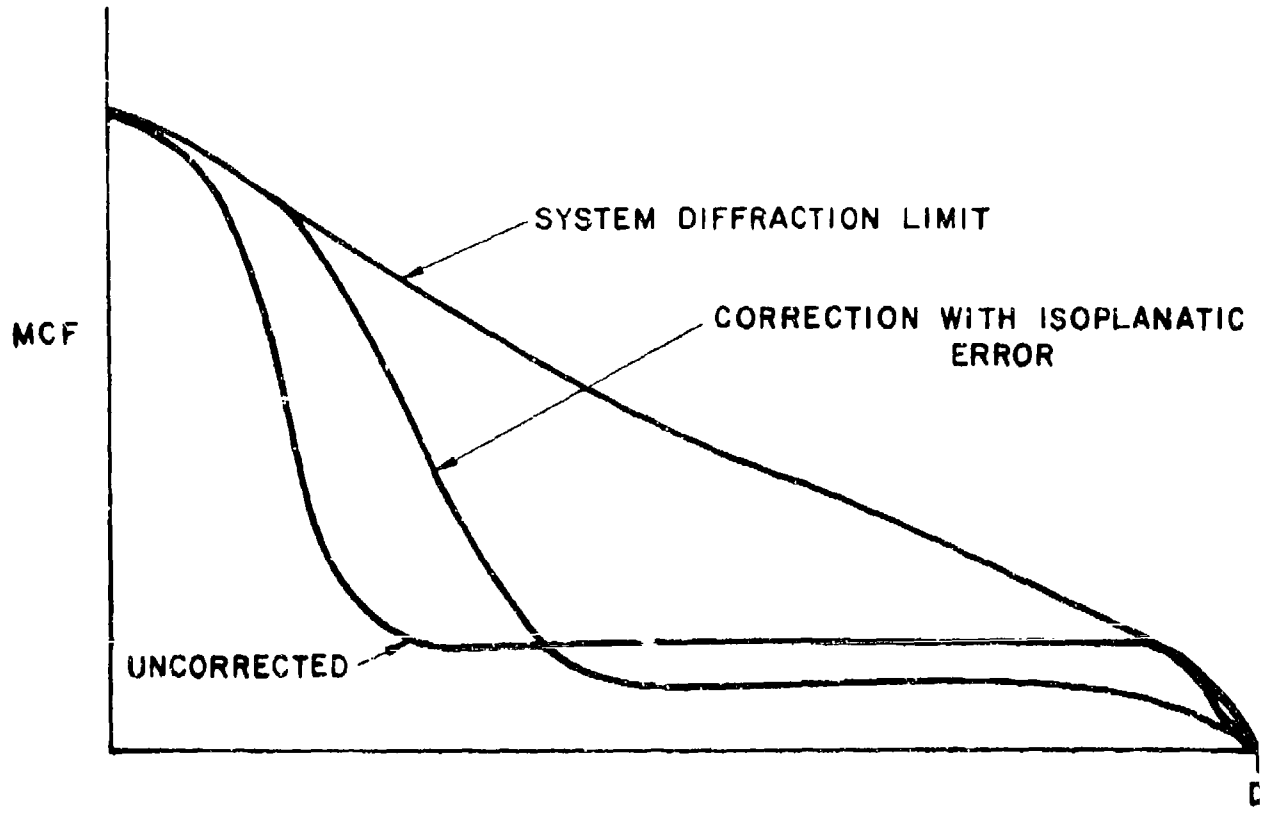

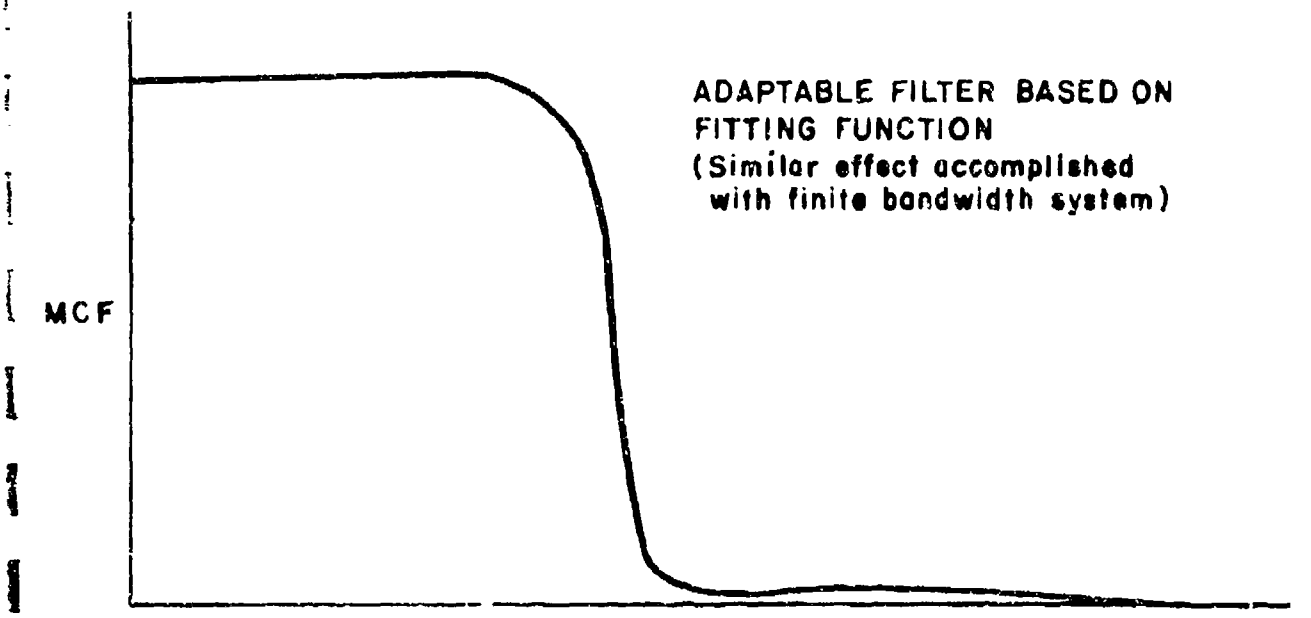

AMPLITUDE ERROR

$\sigma^2_{AMPL} = \sigma^2_x$, the log-amplitude mean-square value

J. J. Burke, J. Opt. Soc. Am., 60 , p. 1262-3.
has an average

$$\sigma^2_x = 0.05$$

Sample System:

$$\sigma^2_x = 0.05 \, (\sec \theta_z)^{11/6}$$

Conservative System:

$$\sigma^2_x = 0.1 \, (\sec \theta_z)^{11/6}$$

(Note σ^2_x saturates at about 0.5 hence second value too high at large θ_z)

ISOPLANATIC ERROR

(For synchronous altitude satellite)

$$\sigma^2_{ISO} \approx 6.88 \left(\delta\theta_e/\theta_0\right)^{5/3}$$

(Fried's Ist Definition)

where $\delta\theta_e$ = accuracy with which beacon is positioned relative to $2V_\perp/c$ point ahead angle

and θ_0 = isoplanatic angle

$$\theta_0^{-5/3} = 0.423\, k^2 \int_0^\infty C_n^2(z)\, z^{5/3}\, dz$$

Sample System:

$$\theta_0 = 25 \left(\sec \theta_z\right)^{-8/5} \qquad (\mu\text{rad})$$

Conservative System

$$\theta_0 = 15 \left(\sec \theta_z\right)^{-8/5}$$

ISOPLANATIC ERROR (cont.)

Set $\sigma^2_{ISO} = (2\pi/10)^2$ rad^2

Find $\delta\theta_e = 0.18\,\theta_0$

Sample System

$$\left.\begin{array}{l}\delta\theta_e = 4.5\,\mu\text{rad} \\ L\,\delta\theta_e = 180\text{m}\end{array}\right\} \theta_z = 0$$

$$\left.\begin{array}{l}\delta\theta_e = 0.69\,\mu\text{rad} \\ L\,\delta\theta_e = 28\text{ m}\end{array}\right\} \theta_z = 72^0$$

(relative to an offset of 760 m)

Conservative System

$\delta\theta_e = 2.7\ \mu$rad, $\theta_z = 0$

$\delta\theta_e = 0.41\,\mu$rad, $\theta_z = 72^0$

Note that for dynamic tracking, the offset will vary, as these numbers are a function of Zenith angle.

BANDWIDTH ERROR

$$\sigma_{BW}^2 = (2.69\, f_0/f_c)^{5/3}$$

(assumes a closed loop response equivalent to an RC filter)

$$f_0^{5/3} = 0.0196\, k^2 \int_0^L C_n^2(z)\, v^{5/3}(z)\, dz$$

f_0 = atmospheric frequency (depending on wind direction) $\sim \begin{cases} (\sec \theta_z)^{3/5} \\ (\sec \theta_z)^{-2/5} \end{cases}$

f_c = system cutoff frequency (3 dB point of RC filter)

AMOS Model $f_0 = 45$ Hz $(\theta_z = 0)$
(Conservative for ≈ 100 Hz)

Sample System:

Assume $\sigma_{BW}^2 = (2\pi/10)^2$ rad^2

$f_c = 211$ Hz

$\tau_c = 0.75$ sec

Conservative System: $f_c = 470$ Hz

SIGNAL-TO-NOISE ERROR

$$\sigma^2_{SN} = a/S_n^2 \quad \text{rad}^2$$

where a = constant on the order of unity, dependent on sensor wavelength and type. (Shearing interferometer at λ has a = 1.2)

and S_n = signal-to-noise ratio

For a desired $\sigma^2_{SN} = (2\pi/10)^2$ rad^2

$$S_n = 2$$

A beacon of 0.1 mWatt, diameter 0.1 m in visible gives $S_n = 2$, when interactuator spacing = 0.1 m

TURBULENCE SUMMARY

- Turbulence degradation is severe but in part correctable with adaptive o
- Adaptive optics residual errors to be considered are: isoplanatic, amplitude, bandwidth, fitting and signal-to-noise. All are important
- A more careful theoretical analysis is required to properly combine effects
- With a cooperative source, the beam spread can be restricted to probably no more than a few times device limited

THERMAL BLOOMING

Results from absorption of laser radiation in atmosphere, thus creating "thermal lens" due to temperature gradient across beam.

Methodology

$$\frac{\Delta A_B}{A'_0} = (N_D/N_{DC}) + 0.72\,(N_D/N_{DC})^2$$

where N_D = distortion number

N_{DC} = critical distortion number (depends on γ)

and $A'_0 = \gamma^2 A_{00}$

Wave Optics Code Runs:

$N_{DC} = 8$ truncated Gaussian

(Can be $N_{DC} \approx 3$-6 for real beams with irregular irradiance distribution)

INTEGRATED DISTORTION NUMBER

$$N_D = \frac{ckP}{\beta a} \int_0^{\infty} \frac{a(z) \exp\left(-\int_0^z a_e(z')\, dz'\right)}{v(z)}\, dz$$

where $c = 1.66 \times 10^{-9}\ m^3/J$

k = wave number $2\pi/\lambda$

a = beam radius = $D/(2\sqrt{2})$

P = laser power

$a(z)$ = absorption coefficient

$a_e(z)$ = extinction coefficient

$V(z)$ = wind velocity normal to path

and z = incremental position along path

SIMPLIFIED DISTORTION NUMBER

$$N_D \approx \frac{ckP}{\beta a} \exp(-N_e) \sum_{i=1}^{n} (N_a/V)_i$$

where $N_e = \int_0^\infty a_e(z)\, dz$, extinction number

and $\frac{N_a}{V} = \int_0^\infty \frac{a(z)}{V(z)}\, dz$

for each absorbing constituent

THERMAL BLOOMING FOR TRUNCATED GAUSSIAN BEAM

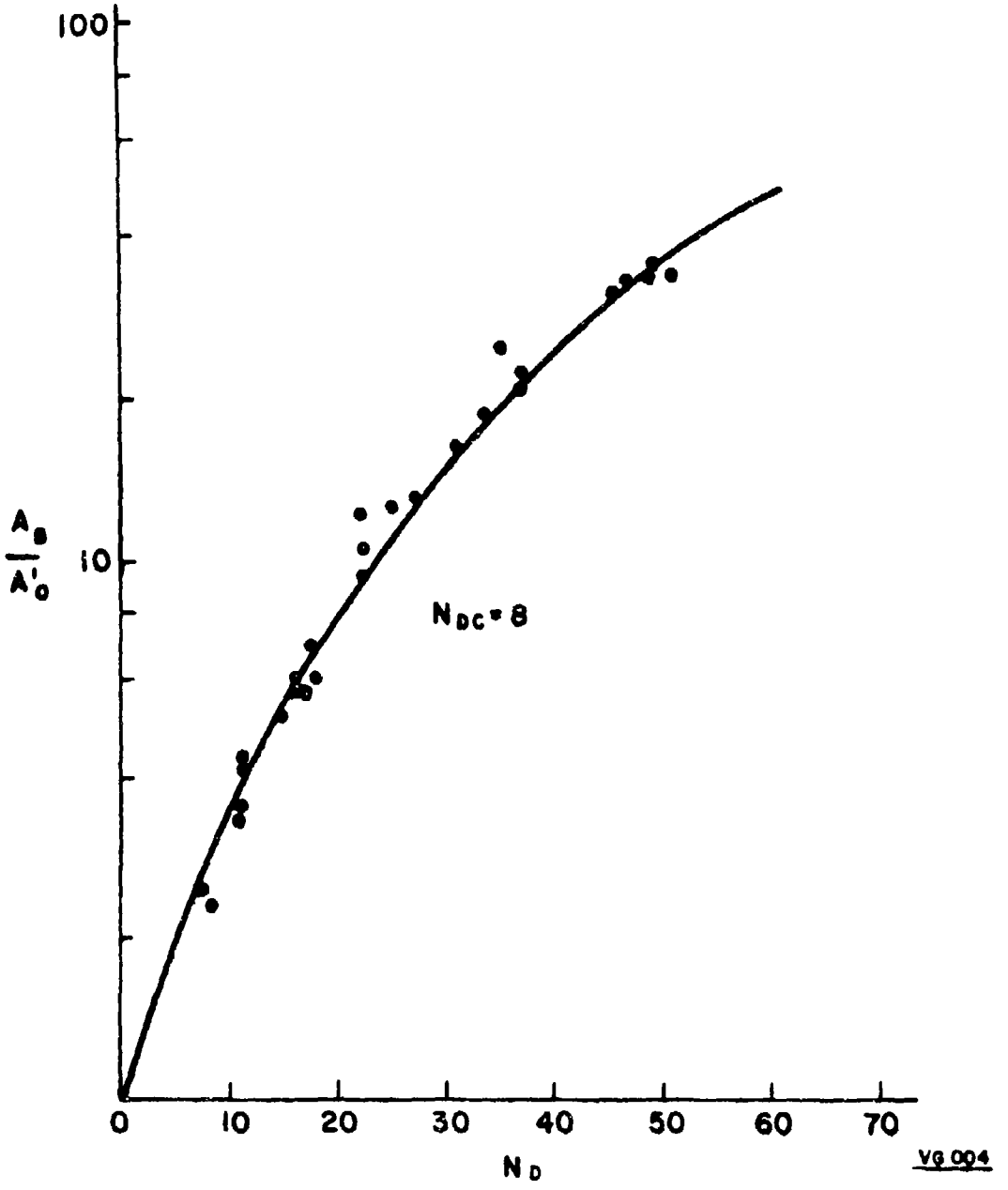

ABSORBING CONSTITUENTS

(at $\lambda = 0.48\ \mu m$)

Molecular - ozone

by photo dissociation

$$h\nu + O_3 \rightarrow O_2 + O + KE$$

approximately 1/3rd of energy goes into photodissociation, the rest into kinetic energy

$N_{a\,ozone} = \frac{2}{3}\ 0.0063 \sec \theta_z$ (for equivalent ozone column height of 0.35 cm)

(Conservative $N_a = \frac{2}{3}\ 0.0095 \sec \theta_z$)

Aerosol - carbonaceous, naturally occuring. Each particle absorbs as black body and reradiates to surrounding molecules.

ABSORBING CONSTITUENTS (cont.)

$N_{\alpha\,aerosol} = (\sec \theta_z) \cdot$

	Model:
7.79×10^{-3}	50 km vis. f/w[1]*
9.21×10^{-3}	s/s[2]
2.29×10^{-2}	23 km vis. f/w
2.47×10^{-2}	s/s
5.48×10^{-2}	10 km vis. f/w
5.66×10^{-2}	s/s**
0.103	5 km vis. f/w
0.105	s/s
0.256	2 km vis. f/w
0.258	s/s

[1]f/w = fall/winter,

[2]s/s = spring/summer

*Sample system number

**Conservative value used

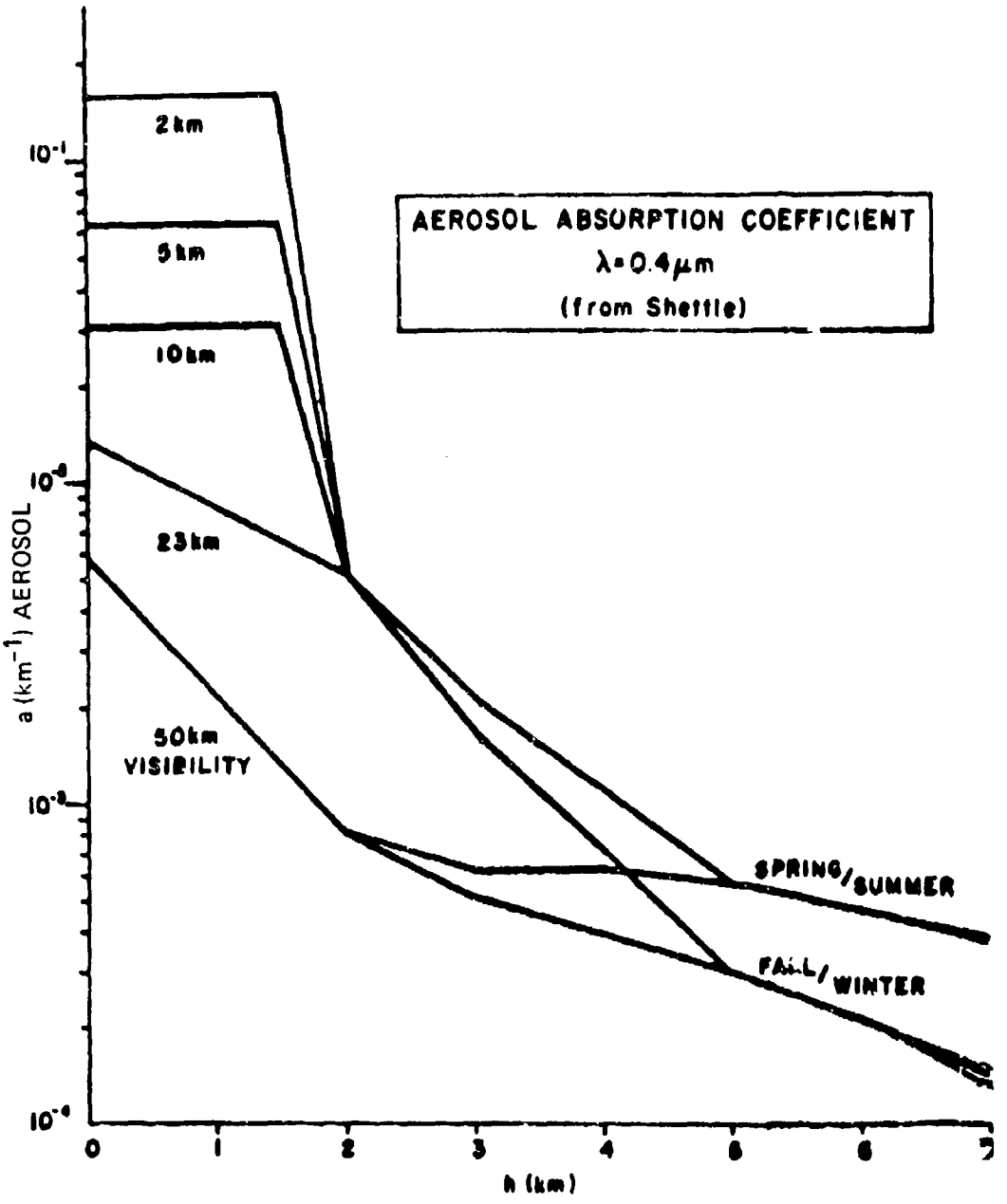
AEROSOL ABSORPTION COEFFICIENT
λ=0.4μm
(from Shettle)
2km
5km
10km
23km
50km
VISIBILITY
SPRING/SUMMER
FALL/WINTER
a (km⁻¹) AEROSOL
h (km)
10⁻¹
10⁻²
10⁻³
10⁻⁴
0
1
2
3
4
5
6
7

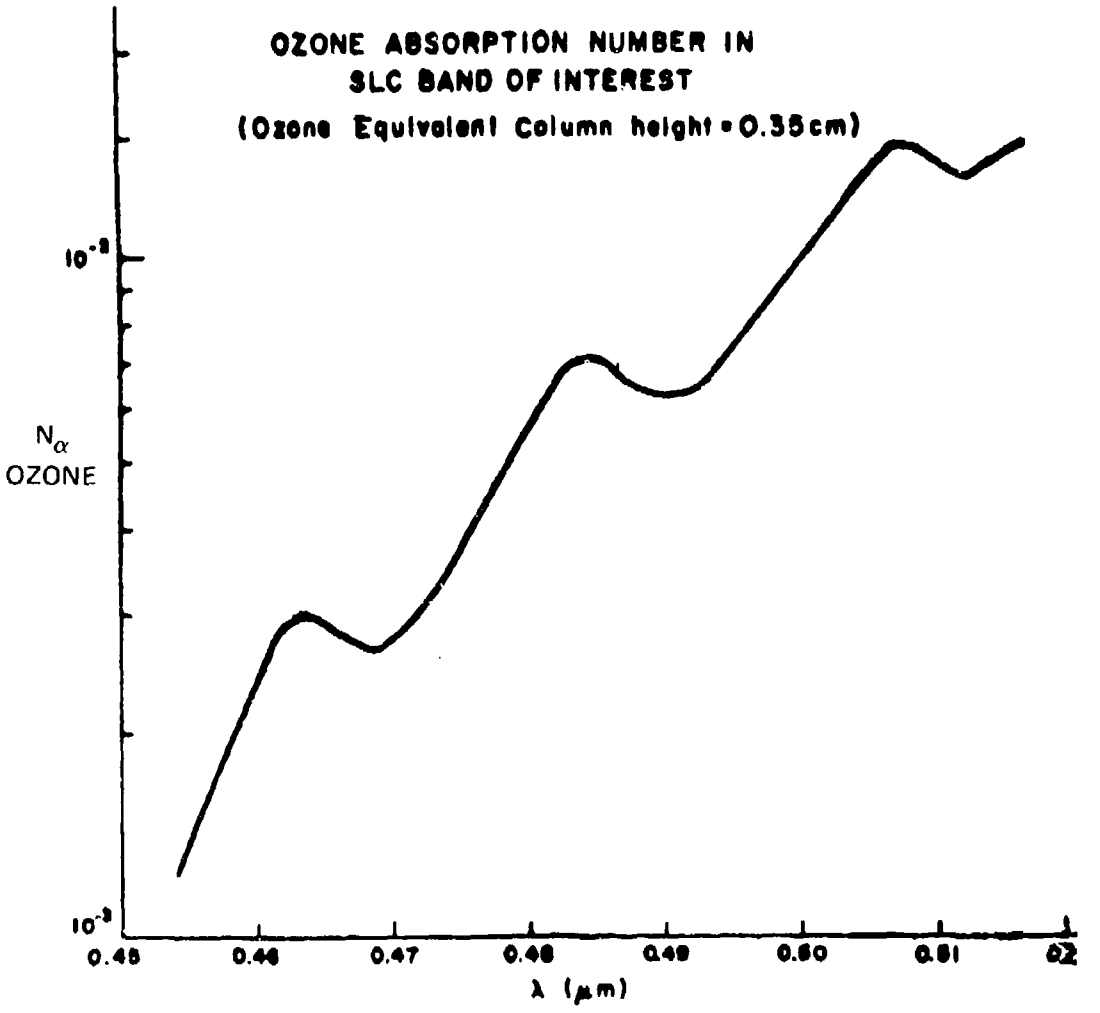
OZONE ABSORPTION NUMBER IN
SLC BAND OF INTEREST
(Ozone Equivalent Column height = 0.35cm)
N_α
OZONE
10^{-2}
10^{-3}
0.45
0.46
0.47
0.48
0.49
0.50
0.51
0.52
λ (μm)

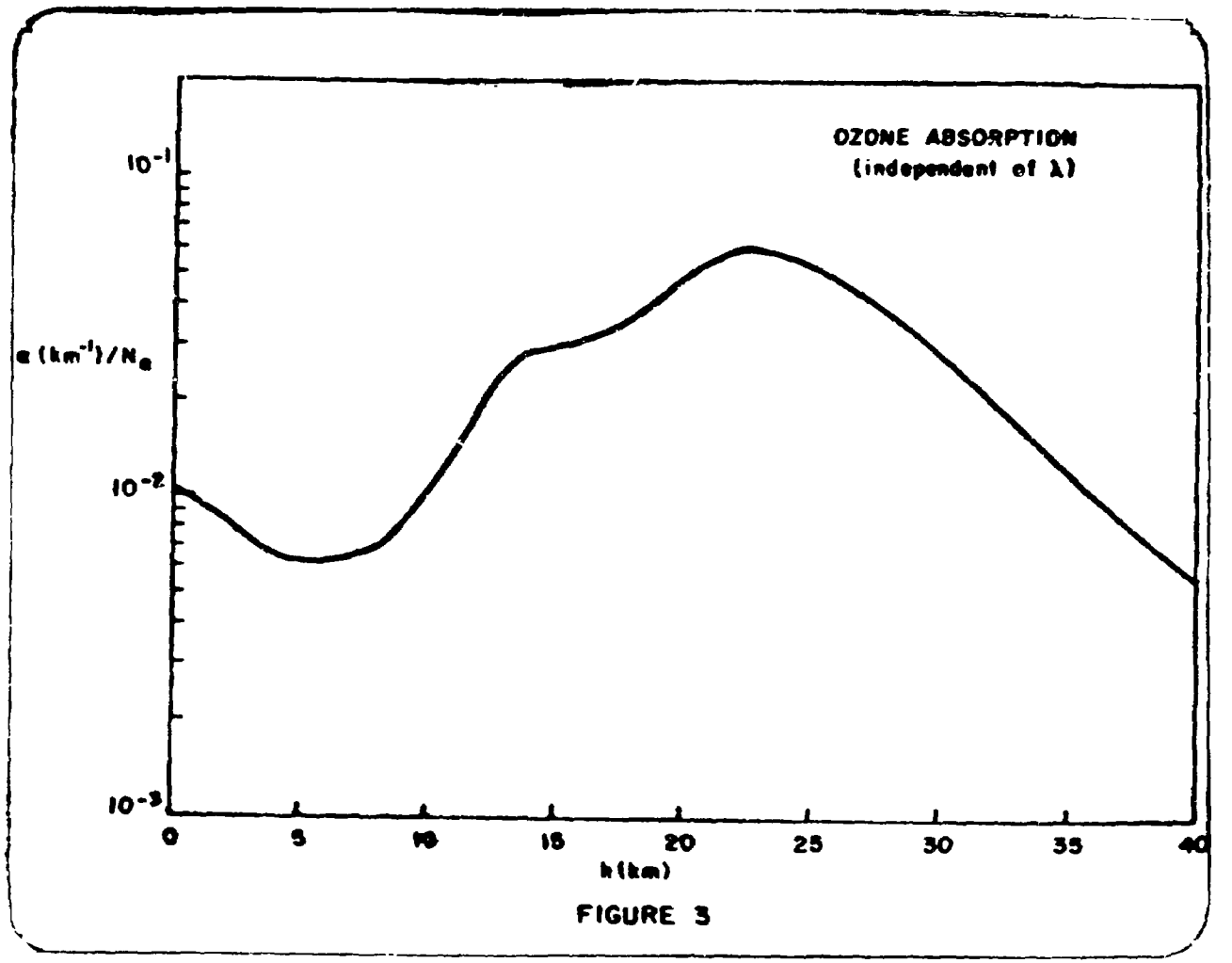
OZONE ABSORPTION
(independent of λ)
10^{-1}
$\alpha\,(km^{-1})/N_a$
10^{-2}
10^{-3}
0
5
10
15
20
25
30
35
40
h(km)

FIGURE 3

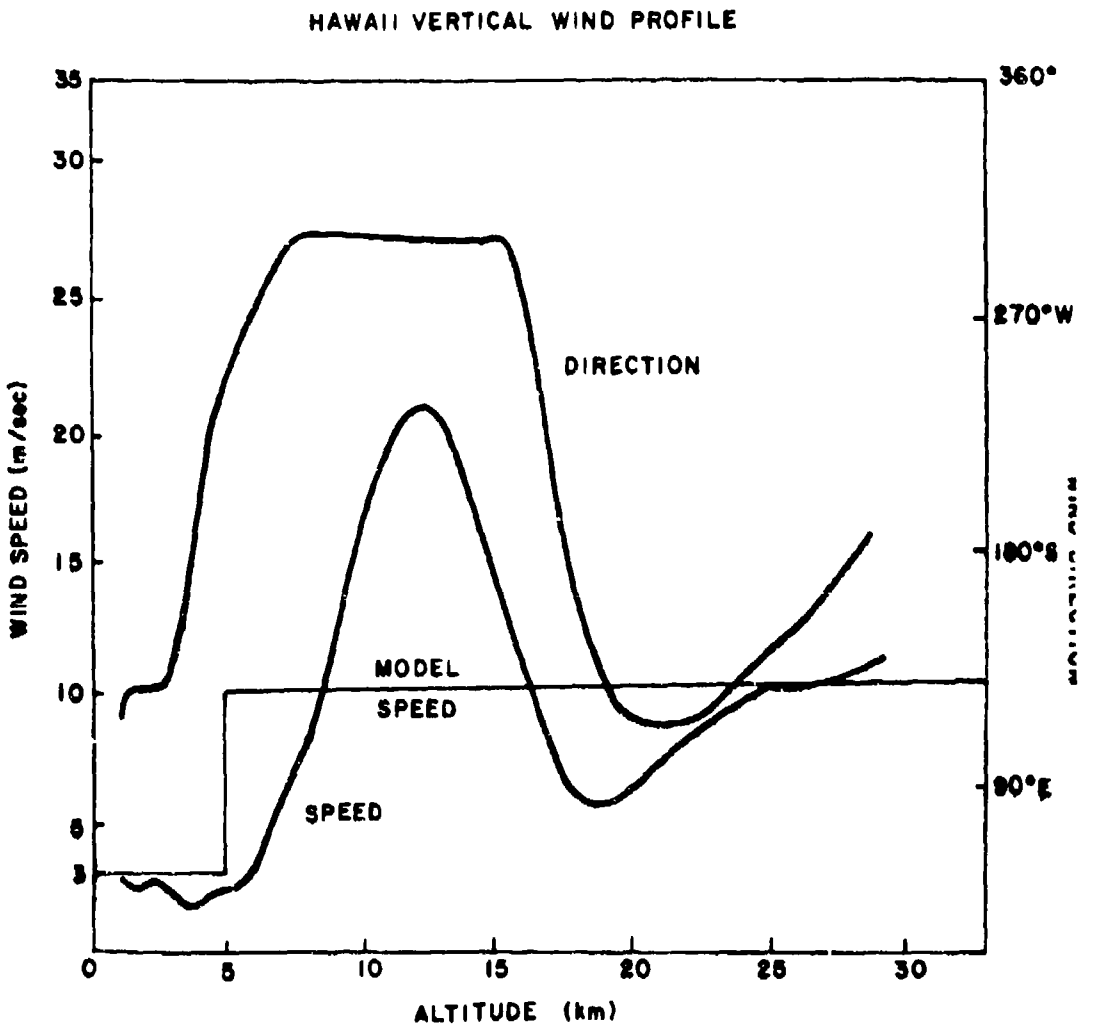
HAWAII VERTICAL WIND PROFILE
WIND SPEED (m/sec)
35
30
25
20
15
10
5
0
5
10
15
20
25
30
ALTITUDE (km)
360°
270°W
180°S
90°E
DIRECTION
MODEL
SPEED
SPEED

THERMAL BLOOMING CORRECTABILITY

- Absorbing constituents all in near field, hence thin lens correction possible

- Bandwidth, stroke and fitting* requirements for blooming are less stringent than turbulence requirements

- Thermal blooming correction modeled by adjusting N_{DC} in wave optics code

*Caution -- we assumed a fairly smooth irradiance profile and good beam quality. A higher γ will contribute to high spatial frequencies in blooming-induced phase error

UP-LINK LOSS COMPUTATIONS

Link Loss

$$\mathcal{L} = 10 \log_{10} \left[A^{-1} \pi (D_2/2)^2 \exp(-N_e)\right]$$

where A = far field beam spread

D_2 = receiving aperture diameter (in space)

N_e = extinction number

$$A = A_{00} \left[\gamma^2 \beta^2 + \frac{\Delta A_T}{A_{00}} + \frac{\Delta A_B}{A_{00}} + \frac{\Delta A_J}{A_{00}}\right]$$

UP-LINK LOSS COMPUTATIONS (cont.)

Sample System	$\theta_z = 0^0$	$\theta_z = 72^0$
System jitter	$\sigma_j = 70$ nrad	70 nrad
AO Cutoff frequency	$f_c = 211$ Hz	211 Hz
AO Number of actuators	$N_{act} = 1040$	4260
AO Signal-to-noise	$S_n = 2$	2
Beam position accuracy	$\delta\theta_e = 5$ μrad	0.7 μrad
Spot size	$A = 195$ m^2	254 m^2
Extinction Loss	1.4 dB	4.5 dB
UP LINK Loss	L = 5.3 dB	9.6 dB

UP-LINK COMPUTATIONS (cont.)

Conservative System	$\theta_z = 0^o$	$\theta_z = 72^o$
System jitter	σ_j = 70 nrad	70 nrad
AO Cutoff frequency	f_c = 470 Hz	470 Hz
AO Number of actuators	N_{act} = 6500	26600
AO Signal-to-noise	S_n = 2	2
Beacon Position Array	$\delta\theta_e$ = 2.7 μrad	0.4 μrad
Spot size	A = 222 m^2	258 m^2
Extinction loss	5 dB	16 dB
UP-LINK Loss	L = 9.6 dB	21.5 dB

SUMMARY

- Efficient transfer of a visible laser beam from ground to a space mirror seems possible, based on physics and extrapolated state of the art

- Adaptive optic correction for turbulence is required, and thermal blooming will be corrected as a subset of turbulence

- Critical areas where further work is required:

  - Large number of subapertures (preferably low voltage)
  - Accurate beacon positioning/pointing
  - Very precise jitter and boresight correction
  - Atmospheric measurements
  - Superb device quality (sufficient power assumed)

LABORATORY EXPERIMENTAL EFFORT

Approach:

Simulation, Involving Phase Screens For Turbulence And Absorption Cells For Thermal Blooming.

Simulates Full Atmosphere, And Includes Far Field Diagnostics

Schedule:

Closed Loop Circuitry, Diagnostics	Complete
Phase Sensor Delivery	May 1980
Integration	June-August 1980
Experimentation	September 1980 +

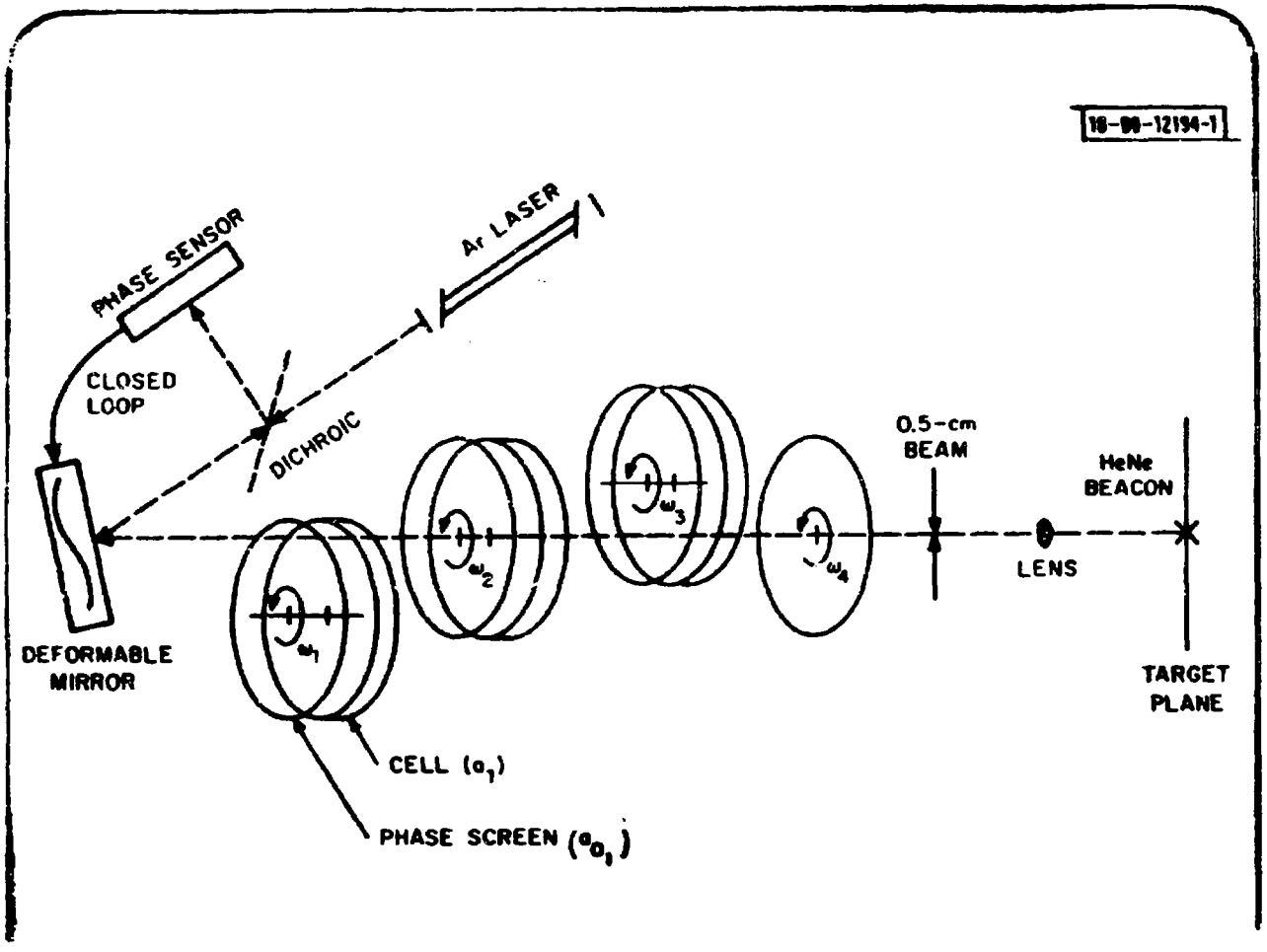
18-88-12194-1
PHASE SENSOR
Ar LASER
CLOSED LOOP
DICHROIC
0.5-cm BEAM
HeNe BEACON
LENS
DEFORMABLE MIRROR
TARGET PLANE
CELL (a_1)
PHASE SCREEN (a_{0_1})

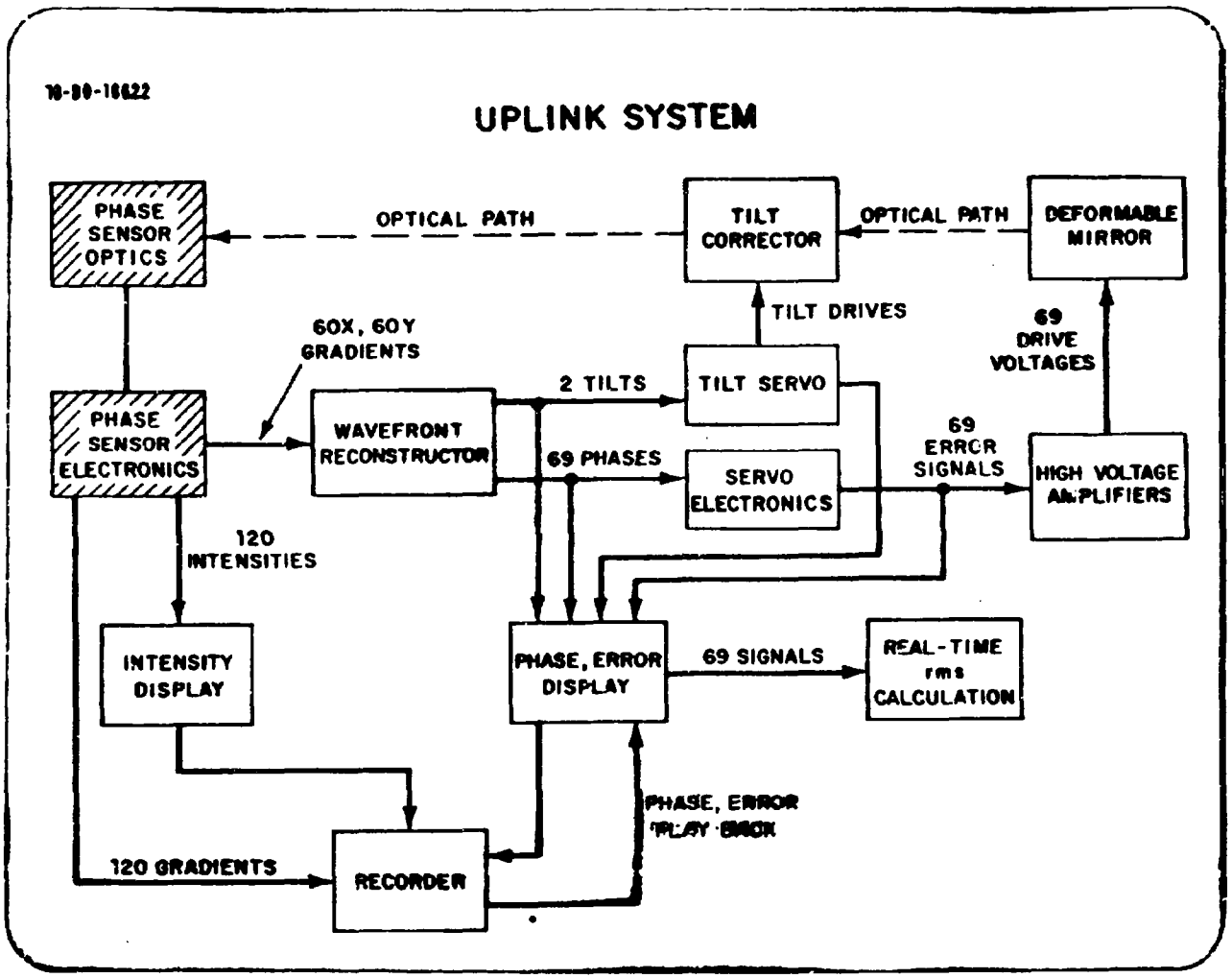
16-80-16822
UPLINK SYSTEM
PHASE SENSOR OPTICS
OPTICAL PATH
TILT CORRECTOR
OPTICAL PATH
DEFORMABLE MIRROR
TILT DRIVES
69 DRIVE VOLTAGES
60X, 60Y GRADIENTS
PHASE SENSOR ELECTRONICS
WAVEFRONT RECONSTRUCTOR
2 TILTS
TILT SERVO
69 PHASES
SERVO ELECTRONICS
69 ERROR SIGNALS
HIGH VOLTAGE AMPLIFIERS
120 INTENSITIES
INTENSITY DISPLAY
PHASE, ERROR DISPLAY
69 SIGNALS
REAL-TIME rms CALCULATION
PHASE, ERROR PLAY BACK
120 GRADIENTS
RECORDER

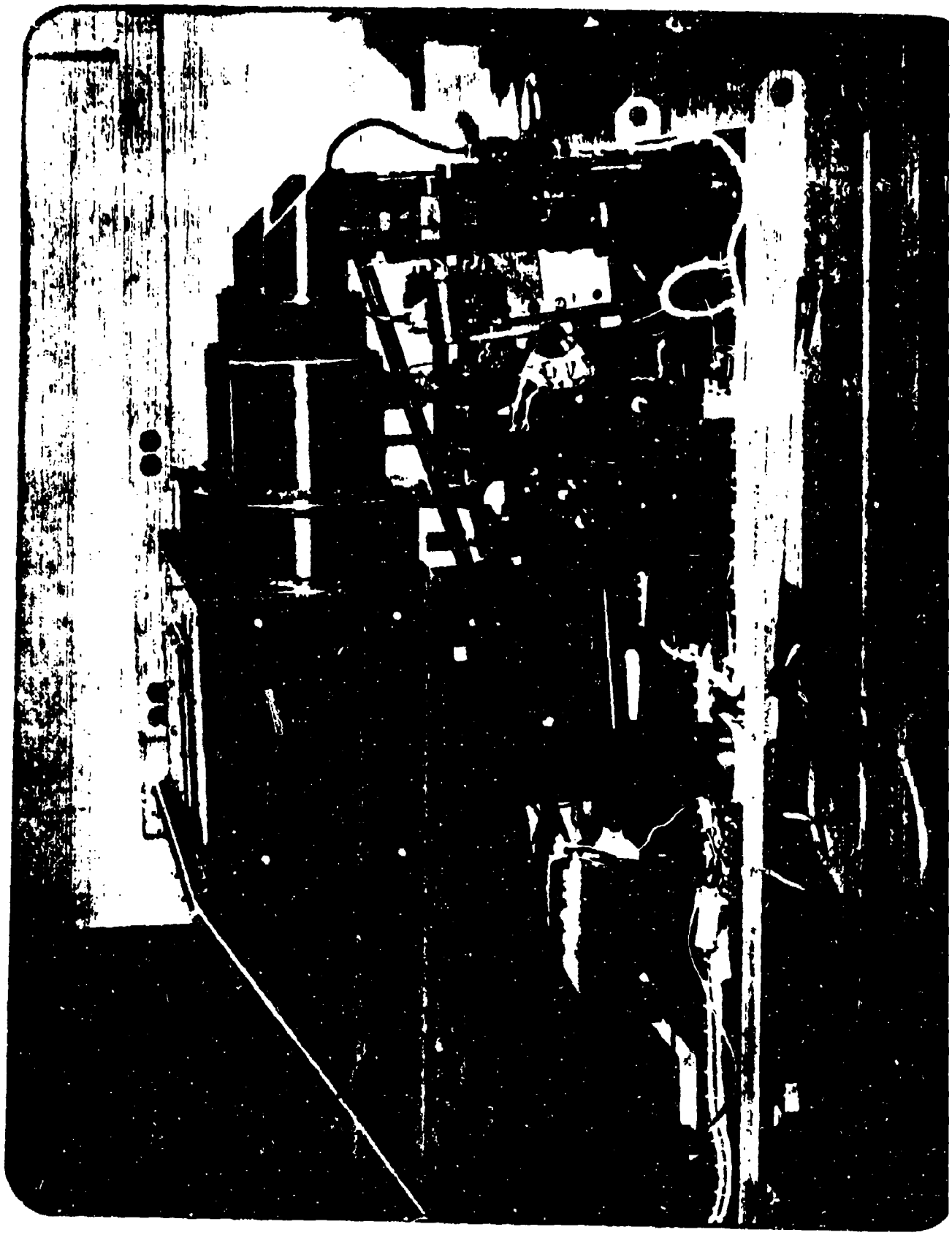

LABORATORY EXPERIMENTAL GOALS

- VERIFY INTEGRATED SYSTEM OPERATION
- INVESTIGATE PROPER CLOSED LOOP STABILITY IN THESE CONDITION
  - Relatively High/Low Turbulence and Blooming
  - Presence of 2π Ambiguities (Varying Shear)
  - Various Degrees of Anisoplanatism
  - High/Low S:N
  - Varying Wind Speed & Slew Rate
  - Overfilled/Underfilled Aperture
  - Presence of Central Obscuration
  - Tilt Control On/Off
  - Thermal Blooming Transients

Quadi-Inherent characteristics of the diffuse attenuation coefficient for irradiance

K. S. Baker and R. C. Smith

University of California, San Diego
Scripps Institution of Oceanography
Visibility Laboratory
San Diego, California 92152

Abstract

The diffuse attenuation coefficient for downwelling irradiance (K_d), the coefficient used to describe the attenuation of irradiance as a function of depth in natural waters, is an apparent optical property. As such, it is a function of the geometry of measurement and other factors which alter the radiance distribution as a function of depth. In spite of this, measurements of downwelling irradiance versus depth and sun zenith angle show that K_d is relatively insensitive to changes in sun angle, thus displaying "quasi-inherent" characteristics, except for very large sun zenith angles. Data will be shown to demonstrate this for a highly productive water type.

Introduction. The diffuse attenuation coefficient for downwelling irradiance is defined as .

$$K_d(Z) \equiv \frac{-1}{E_d(Z)} \left[\frac{dE_d(Z)}{dZ} \right], \tag{1}$$

or alternatively,

$$\frac{E_d(Z_2)}{E_d(Z_1)} = \exp\left[-K_d \cdot (Z_2 - Z_1) \right] \tag{2}$$

where K_d has units of reciprocal length, and Z is the depth at which the downwelling irradiance, $E_d(Z)$, is measured. Thus K_d is an optical property used for describing the attenuation with increasing depth of radiant energy in natural waters.

Preisendorfer[1] has defined inherent and apparent optical properties of the sea according to their invariance under changes in the radiance distribution about the point at which the property is measured. If the property is invariant with respect to changes in the radiance distribution, it is said to be an inherent optical property, otherwise it is an apparent optical property. The diffuse attenuation coefficient for downwelling irradiance (K_d) is an apparent optical property since it is derivable from the irradiance and radiance, both apparent optical properties.

Like other apparent optical properties irradiance K_d is so called because[1]: its behaviour with depth exhibits reproducible regularities in a wide range of natural water types; it is possible to formulate exact mathematical interrelationships that hold, for all practical cases, between K_d and the inherent optical properties; and the use of K_d permits practical solutions to a wide range of problems in ocean optics.

The concept of irradiance K_d is particularly useful in bio–optics[2,3]. It not only provides a measure of natural irradiance as a function of depth, *i.e.* from Eq. (2),

$$E_d(Z) = E_d(0^-)e^{-K_d \cdot Z} \tag{3}$$

but when $E_d(Z)$ is converted to quanta and hence photosynthetically available radiation, PAR(Z).

$$PAR(Z) = PAR(0^-)e^{-K_d \cdot Z}, \tag{4}$$

it can be used to optically classify ocean water types in terms of dissolved and suspended biogenous material[4]. Also, K_d is an important parameter for describing the remote sensing of ocean color[5], which in turn holds the possibility of synoptically determining ocean productivity.

Beyond the usefulness and regularities that have earned irradiance K_d the title of an apparent optical property, several workers have observed that K_d is relatively insensitive to changes in the solar zenith angle[6,7,8]. Hojerslev[7], in clear waters off Sardinia, and Aas[8], in more turbid Oslofjorden, measuring broad band irradiance or total quantum irradiance concluded that the "solar-elevation effect" in irradiance K_d was relatively small and limited to shallow depths. For some years Visibility Laboratory data has indicated the relative independence of K_d from solar zenith angle using a narrow band instrument[6].

In the following we present a recent and comprehensive suite of spectral irradiance data that demonstrates this relative invariance to solar-elevation of $K_d(\lambda)$ across the visible spectrum. We know of no previously published narrow bandwidth results that demonstrates this effect. To the extent that $K_d(\lambda)$ can be shown to be independent of the geometrical distribution of the sun's input, it may be viewed as a quasi-inherent (or at least as independent of the sun zenith angle θ) for a wide range of practical oceanographic problems.

The results presented here are derived from a set of data taken in July 1979 at San Vicente Reservoir, east of San Diego. The reservoir is representative of the most productive ocean waters having a chlorophyll concentration of approximately 7 $mg\ C/m^3$ and an attenuation length of 1/3 meter.

Data. To obtain a comprehensive suite of spectral irradiance data as a function of depth and solar elevation requires almost ideal environmental and experimental conditions. First, atmospheric conditions must remain uniform throughout the day. The data reported herein were obtained under clear skies through a dry "desert type" atmosphere. Second, the air-water interface must be relatively smooth. Waves increase the uncertainty in measuring depths accurately and require longer integration times to obtain average irradiance values at each depth. The latter is an important factor if complete spectral and depth data are to be obtained throughout the day as a function of θ since long integration times are inconsistent with the need to obtain depth profiles in a time short compared to a significant change of sun angle. Our San Vicente data were obtained when the water surface was flat calm and only slightly wind rippled. Third, the water column must be relatively uniform and remain so throughout the duration of the experiment. Figure 1, shows a plot of temperature and transmittance (λ=550 *nm*) vs depth. These data indicate that the water column was nearly uniform to a depth of about 6 meters. Subsequent similar measurements indicated that the optical properties of the water column remained relatively uniform throughout our experiment. Finally, for this type of study, favorable experimental conditions are required. Our data were obtained from a moored barge equipped with adequate rigging so that shadowing effects on our irradiance measurements were negligible (except at high noon). The barge provided a platform where rapid, efficient and continuous operation of several instruments could be carried out simultaneously from sunrise to sunset.

Spectral irradiance, $E_d(Z,\theta,\lambda)$ depth profiles were obtained throughout the day. Figure 2 shows the results of a single $E_d(Z,\theta,\lambda)$ depth profile obtained between 1136 and 1225. Eleven of these complete spectral irradiance depth profiles were obtained throughout the day. Between each $E_d(\lambda)$ profile a rapid monochromatic depth profile at 550 nm was obtained as an independent check on our analysis procedure for calculating $K_d(\lambda)$ values as a function of solar zenith angle. In addition, the calibration of the instrument was checked against an internal reference lamp several times during the day.

The spectral irradiance depth profile shown in Fig. 2 is composed of nine events where an event consists of a spectral scan at a fixed depth. Each of these events took approximately three to four minutes to complete. Data was taken every 5 nm from 350 to 750 nm. The beginning and ending time of each event was accurately recorded. As a consequence, each set of $E_d(Z,\lambda)$ data, *i.e.* each event, could be associated with a specific sun zenith angle (or more precisely a small range of angles associated with the specific three to four minute period). Thus it is possible to replot the $E_d(Z,\theta,\lambda)$ data, for a given wavelength, as a function of sun zenith angle with depth as a parameter.

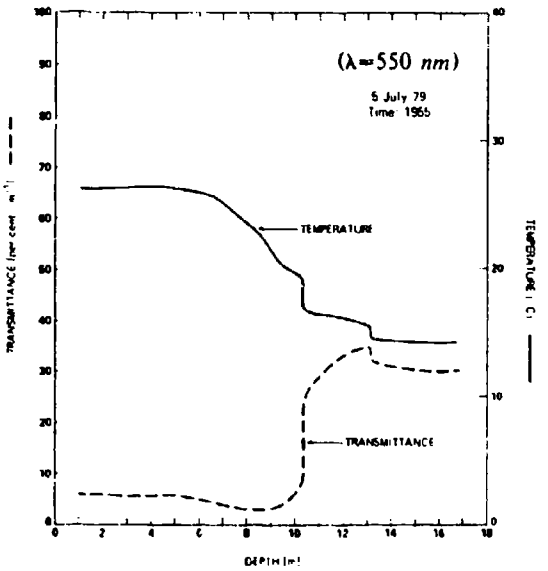

Figure 1. Temperature and transmittance vs depth for San Vicente Reservoir (32° 58'N, 116° 35'W) 5 July 1979.

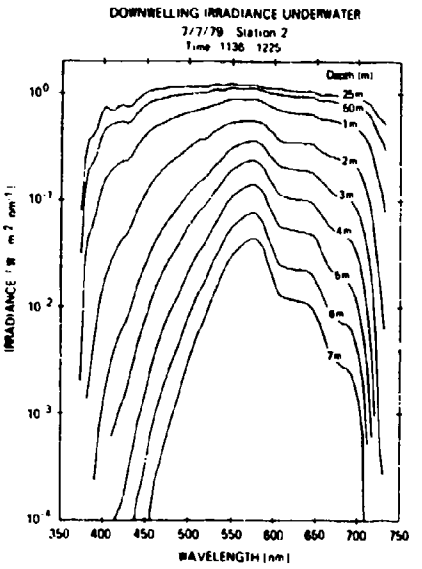

Figure 2. Downwelling spectral irradiance vs wavelength for several depths.

One half of such a plot is shown in Fig. 3. The data points, one from each event, are seen to progress with zenith angle (*i.e.* time) as a spectral depth profile is obtained. Our analysis procedure is, for each wavelength: to combine morning and afternoon data sets because they are virtually identical; to fit a best curve (by eye) through these E_d vs θ data points; and to then select from these curves for each λ the $E_d(Z)$ data at fixed θ values for use in determining $K_d(\theta,\lambda)$.

It should be noted that this analysis procedure corrects for sun elevation changes that occur during the measurement of a spectral irradiance depth profile. This correction is generally ignored or considered to be insignificant when E_d measurements are confined to small sun zenith angles. This correction is absolutely necessary in order to accurately describe solar elevation effects on irradiance K_d and its neglect may, in part, account for earlier misconceptions regarding the behaviour of K_d vs θ.

Analysis and Discussion. Figure 4 presents the results of this analysis, where we now show irradiance (at a fixed wavelength) vs depth for selected sun zenith angles. It can be noted immediately that these curves are almost parallel, indicating that derived K_d values will be relatively insensitive to changes in sun zenith angle.

For the present discussion we have chosen to ignore the variation of $K_d(\theta,\lambda)$ with depth; *i.e.* in determining $K_d(\theta,\lambda)$ values we have fit a straight line through the E_d vs Z data. This variation is currently being investigated and will be published elsewhere. For our current discussion it is important to recognize that, independent of how or at what optical depth K_d is determined, the slopes of the E_d vs Z curves behave in a "parallel", *i.e.* similar, manner for all sun angles. Thus our conclusions drawn for straight line K_d values are valid however we determine K_d.

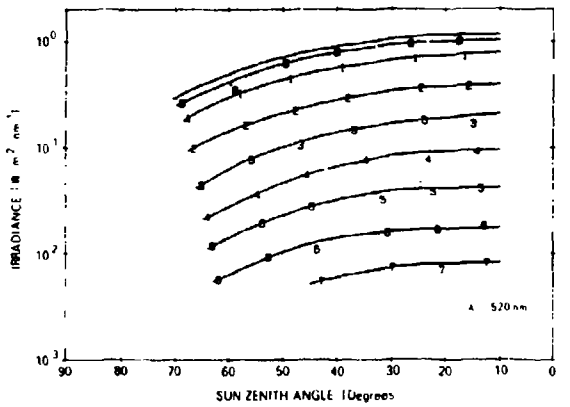

Figure 3. Downwelling irradiance, at 520 nm, versus sun zenith angle for several depths (0.25, 0.50, 1, 2, 3, 4, 5, 6 and 7 meters). Data points are indicated by the center of numerals specifying the depth in meters (except for the top two curves).

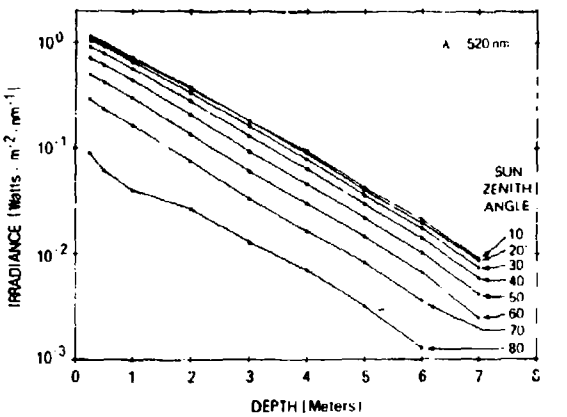

Figure 4. Downwelling irradiance, at 520 nm, vs depth for several sun zenith angles.

These data are replotted from the data shown in Fig. 3.

From data such as that shown in Fig. 4 the diffuse attenuation coefficient for downwelling irradiance, $K_d(\theta,\lambda)$, can be derived. Figure 5 presents $K_d(\theta)$ vs sun zenith angle for several selected wavelengths. Again, it can be seen that K_d is relatively insensitive to changes in sun zenith angle. Factors that may contribute to the insensitivity of K_d to sun angle include: first, that the full upper hemisphere is compressed by refraction to a half-angle 48° cone; second, that with increasing sun zenith angles the ratio of sky to total irradiance increases.

Variations of K_d with changes in sun zenith angle are shown quantitatively in Fig. 6. Here we have plotted the ratio of the diffuse attenuation coefficient at θ degrees to that at $\theta=10°$ ($K_d(\theta)/K_d(\theta=10°)$) versus sun zenith angle. A solar zenith angle of ten degrees was the highest sun elevation during these experiments. These data indicate that $K_d(\theta)/K_d(10°)$ varies less than five percent for sun zenith angles of less than 40° and the variability of K_d throughout the day ($\theta=10°$ to 80°) is less than twenty percent. This is true over the full spectral range of our data. Making a first order correction, using the cosine of the refracted sun zenith angle[7,8], does not significantly reduce the variability of K_d with θ.

These data indicate that the diffuse attenuation coefficient for downwelling irradiance, $K_d(\lambda)$, is relatively insensitive to changes in sun angle, thus displaying "quasi-inherent" characteristics. Thus, to within an estimateable accuracy, $K_d(\lambda)$ may be considered independent of sun elevation and is useful for a wide range of practical oceanographic problems. A complete theoretical analysis and description of these results is currently under study and will be presented elsewhere.

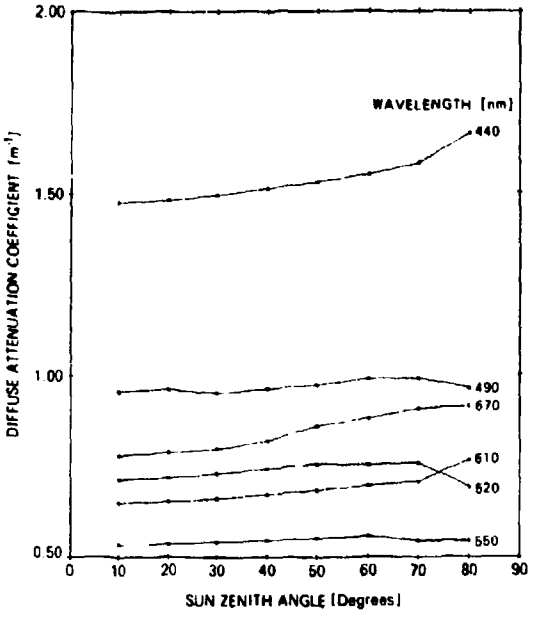

Figure 5. Diffuse attenuation coefficient for irradiance vs sun zenith angle for several wavelengths.

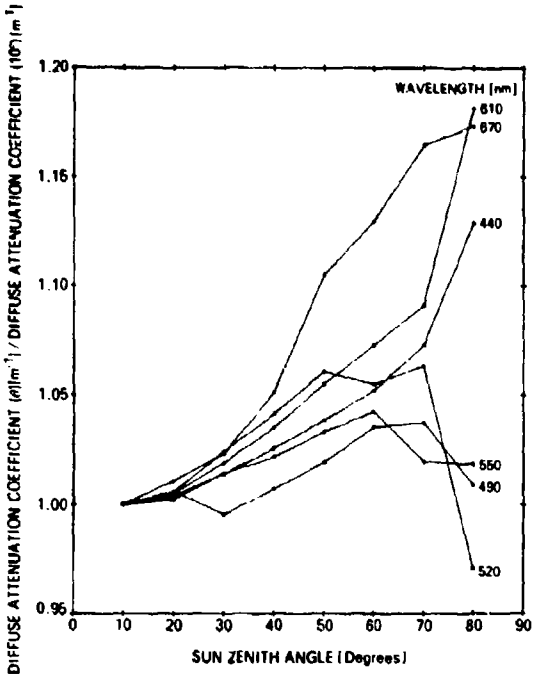

Figure 6. The ratio $K_d(\theta)/K_d(\theta = 10°)$ vs sun zenith angle for several wavelengths. These data were derived from the data presented in Fig. 5.

References

1. Preisendorfer, R. W. (1979) Hydrologic Optics

2. Morel, A. (1978) Available, useable, and stored radiant energy in relation to marine photosynthesis. Deep Sea Research **25**, 673-688.

3. Smith, R. C. (1979) Intro to Optical Oceanography. This volume.

4. Smith, R. C. and K. S. Baker (1978a) Optical Classification of natural waters. Limnol. Oceanogr. **23**, 260-267.

5. Smith, R. C. and K. S. Baker (1978b) The bio-optical state of ocean waters and remote sensing. Limnol. Oceanogr. **23**, 247-259.

6. Smith, R. C. (1970) Unpublished data

7. Hojerslev, N. K. (1974) Daylight measurements for photosynthetic studies in the western mediterranean. Univ. of Copenhagen, Report **26**, 38pp.

8. Nielsen, J. H. and E. Aas (1977) Relation between solar elevation and the vertical attenuation coefficient of irradiance in Oslofjorden. U. of Oslo, Report **31**, 42pp.

ASSESSMENT OF THE DIFFUSE ATTENUATION COEFFICIENT FROM REMOTE SENSED (CZCS) RADIANCE

R. W. Austin

Visibility Laboratory
of the
Scripps Institution of Oceanography
University of California, San Diego

Abstract: This program has as its goal, the accumulation and storage of ocean optical properties that can be used as a data base to assess the potential performance of optical communication systems. Available data from *in-situ* measurements are to be used where available but are totally inadequate in number for the large ocean areas required. A method utilizing the Coastal Zone Color Scanner (CZCS) is being tried which will permit the diffuse attenuation coefficient (K) of the surface waters to be determined synoptically over large areas. The characteristics of the CZCS are described. Examples of the spectral K's measured on surface validation cruises are shown and compared with the Jerlov, with pure sea water and with spectral K's generated using an algorithm developed by Smith and Baker.

A new algorithm for determining the K(490) and K(520) is presented which depends on the ratio of the upwelling water radiances at 443 and 520 nanometers---two of the spectral bands of the CZCS. A relationship between K(490) and plankton pigment concentration is given which may prove useful estimating K's in areas where chlorophyll concentrations have been made. The problem of the relationship between the K measured at the surface and that applying to the upper 100 meters is addressed and some examples shown. Four CZCS images where K's have been calculated over the entire scene are presented. A comparison is shown between the K's measured *in-situ* and calculated from the CZCS radiances for 4 stations.

OCEAN OPTICAL PROPERTIES

- REMOTE SENSING OF DIFFUSE ATTENUATION COEFFICIENT
  - K - algorithm Development
  - Surface Validation Cruises
  - NIMBUS 7/CZCS Data Acquisition
  - Digital Image Processing

- DEPTH DEPENDENCE OF K
  - Surface K vs K to 150 meters - emperical
  - Relationship between K(z) and STD profiles
  - Emperical Model Development

- AQUISITION OF ADDITIONAL DEEP WATER K's
  - R/V JORDON
  - R/V OCEANOGRAPHER

ORBIT PARAMETERS
USED FOR COVERAGE PLOTS

NOMINAL ORBIT PARAMETERS	
ALTITUDE	955 KM
INCLINATION	99.2^{0}
PERIOD	104.15 MINUTES
ORBITS PER DAY	13.82 (RESULTS IN DAILY ASCENDING NODE SEPARATION OF 4.55^{0})
ASCENDING NODE SEPARATION FOR ADJACENT ORBITS	26.04^{0} (WESTWARD MOTION)
LAUNCH PARAMETERS	
ASCENDING NODE TIME	11:52
DATE	Nov 25, 1978
RESULTING SUN ANGLE	8^{0}

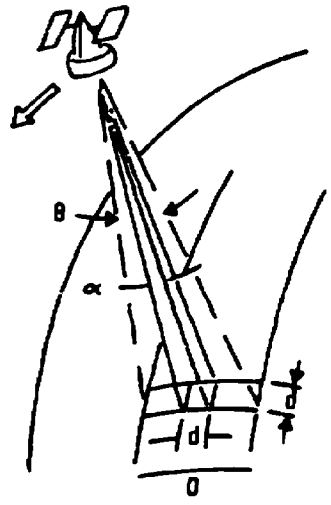

θ = 1.373 RADS (78.68°)
$\alpha = .865 \times 10^{-3}$ RADS (.0496°)
d = .825 km
orbital altitude = 955 km
D = 1659 km

Figure 2.4-1 CZCS Scanning Arrangement

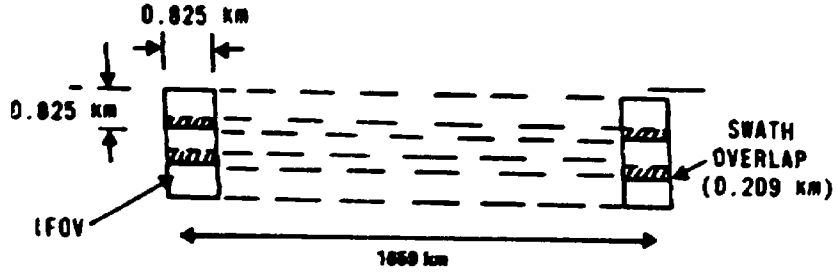

ACTIVE SCAN ANGLE = 78.68°

Figure 2.4-2 CZCS Earth Scan Pattern

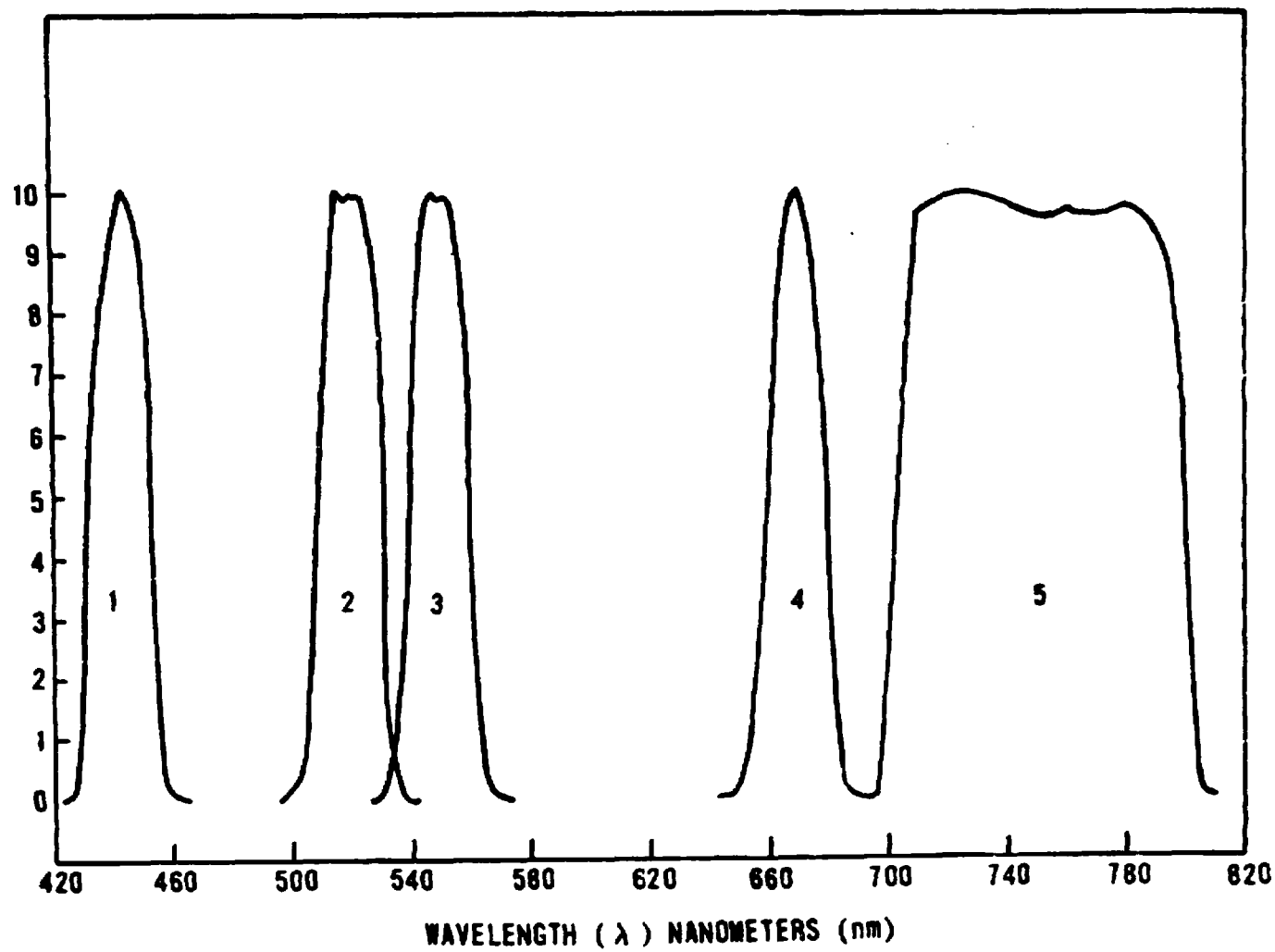

Figure 2-3. CZCS Spectral Response for Channels 1 through 5

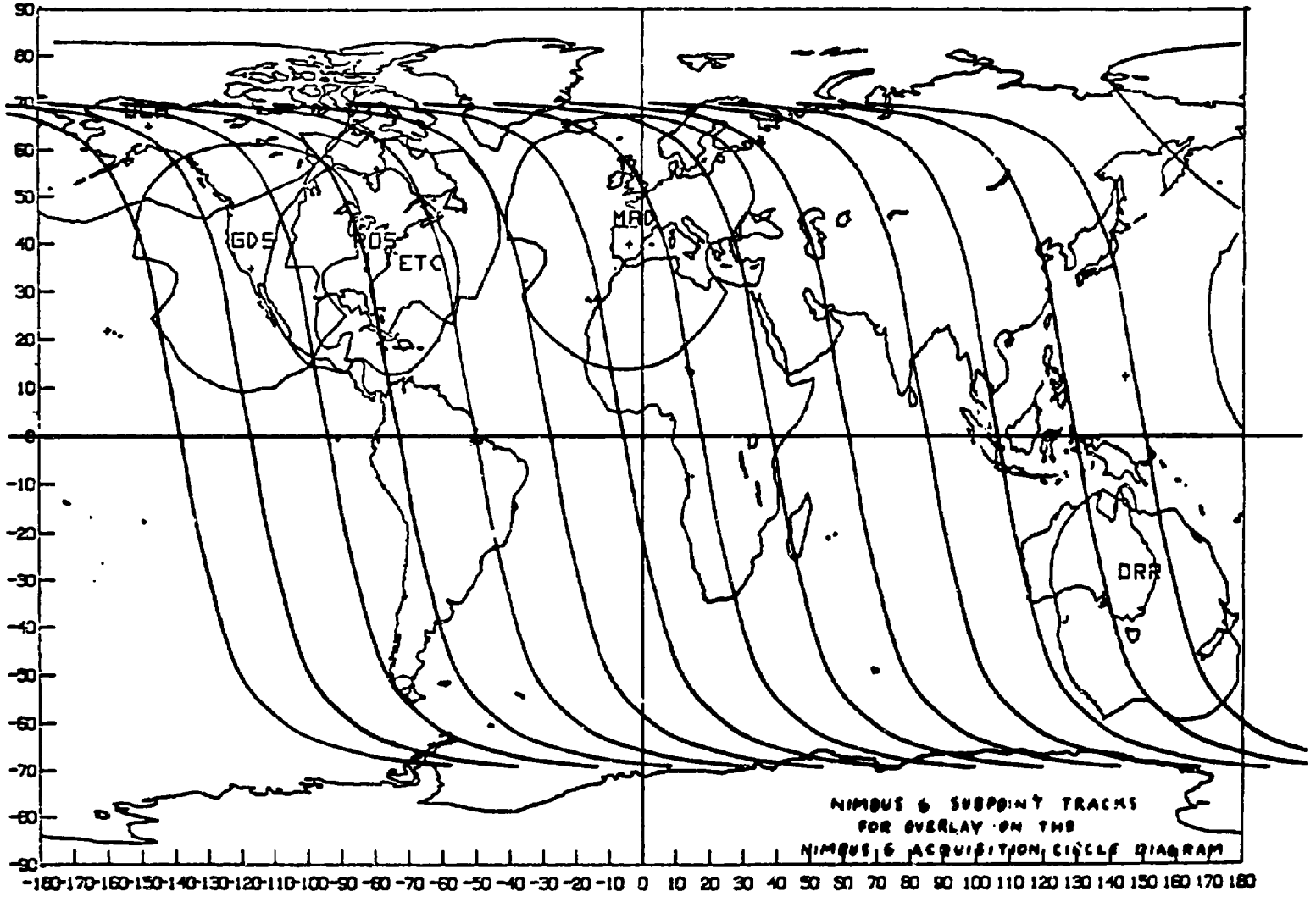
GDS
ROS
ETC
MAD
DRR
NIMBUS 6 SUBPOINT TRACKS
FOR OVERLAY ON THE
NIMBUS 6 ACQUISITION CIRCLE DIAGRAM

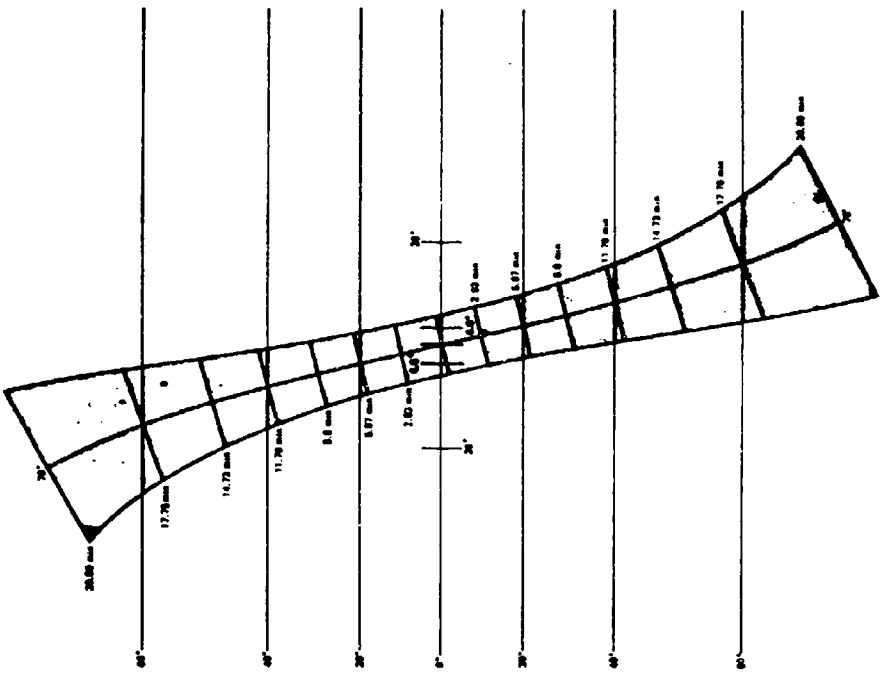

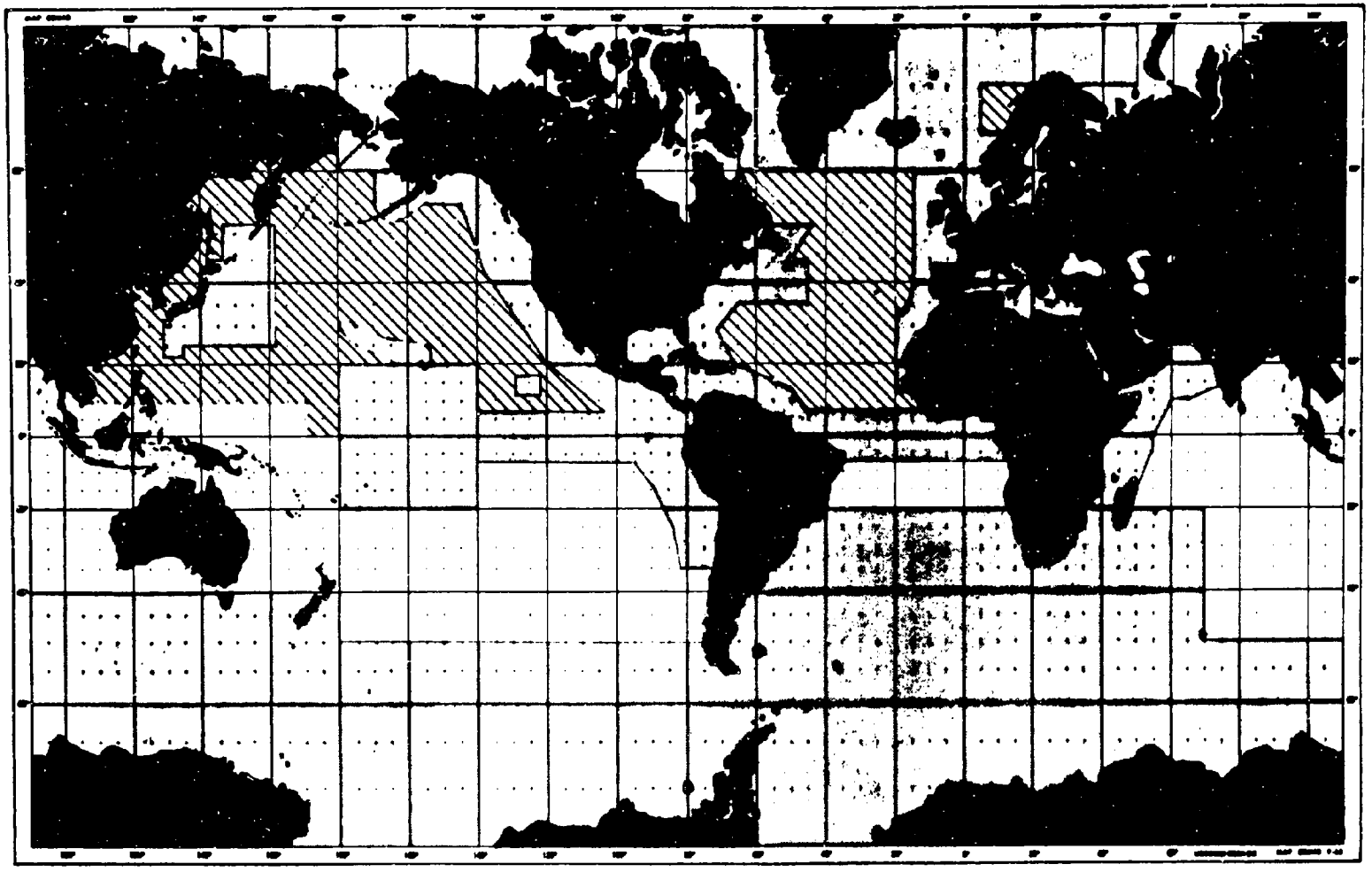

REQUESTED OCEAN COVERAGE COASTAL ZONE COLOR SCANNER

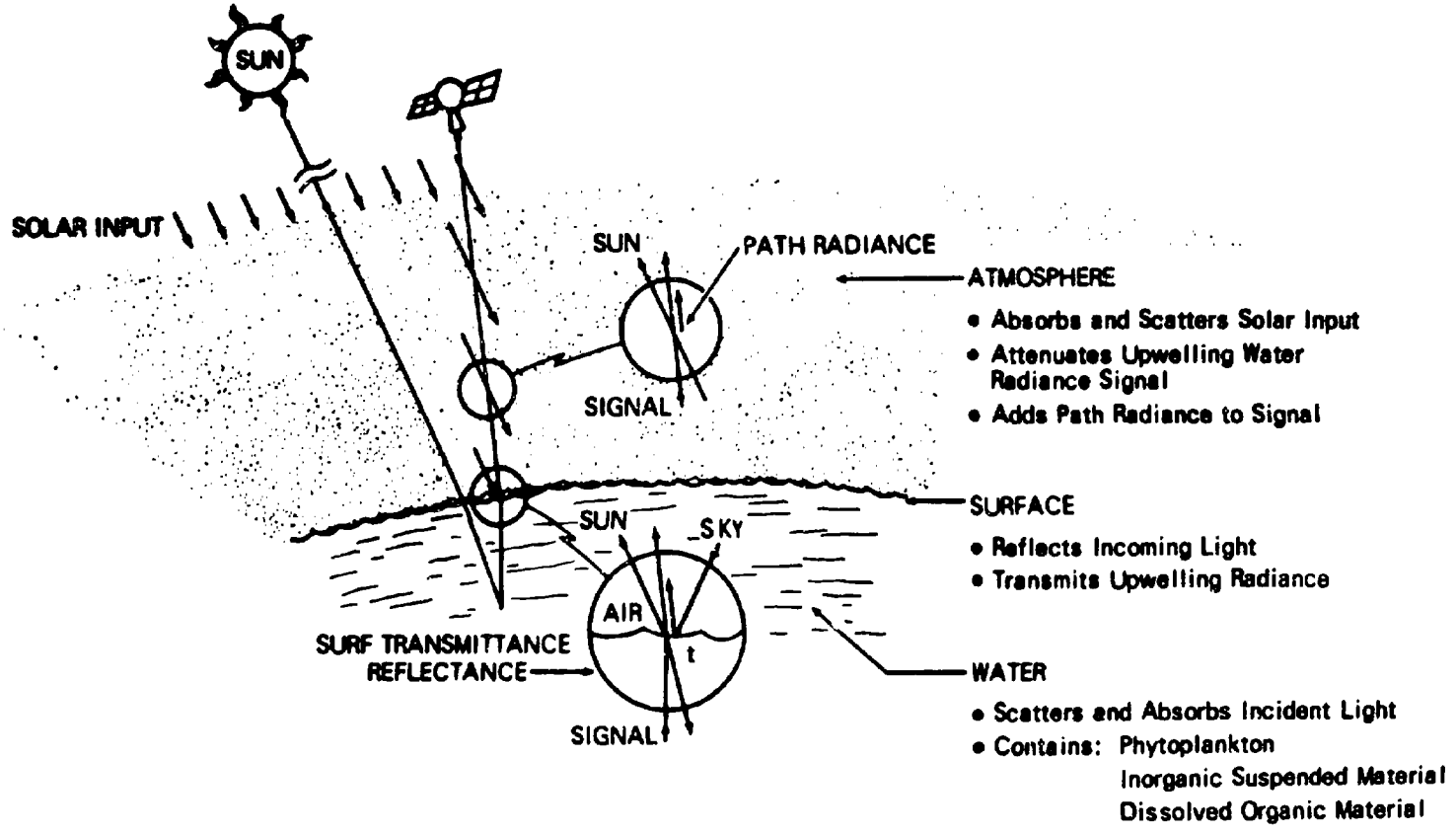
SUN
SOLAR INPUT
SUN
PATH RADIANCE
SIGNAL
ATMOSPHERE
• Absorbs and Scatters Solar Input
• Attenuates Upwelling Water Radiance Signal
• Adds Path Radiance to Signal
SURFACE
• Reflects Incoming Light
• Transmits Upwelling Radiance
SUN
SKY
AIR
t
SURF TRANSMITTANCE
REFLECTANCE
SIGNAL
WATER
• Scatters and Absorbs Incident Light
• Contains: Phytoplankton
Inorganic Suspended Material
Dissolved Organic Material

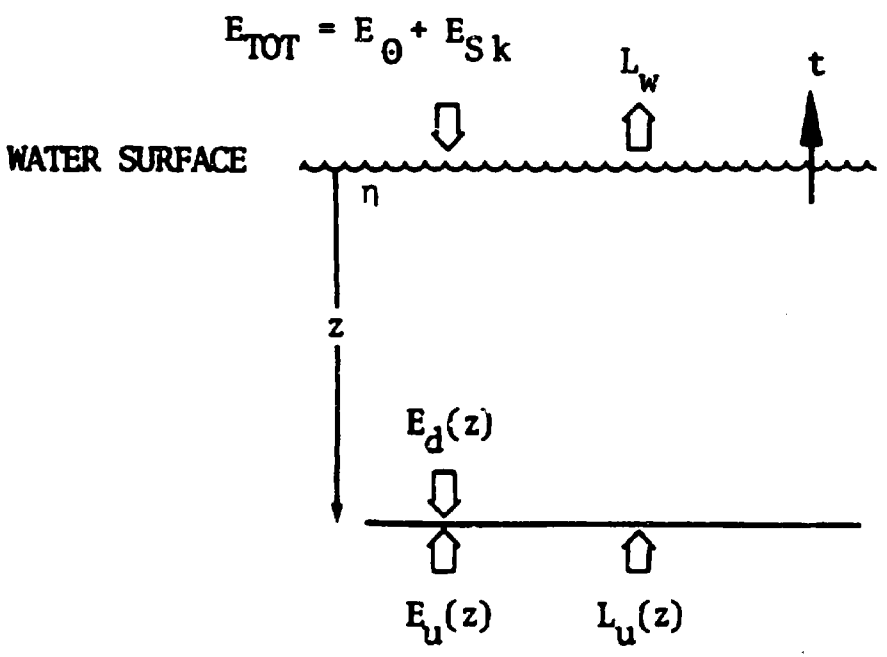

$$L_w = \frac{t}{\eta^2} \cdot e^{Kz} \cdot L_u(z)$$

$$\rho_E = \frac{E_u}{E_d}$$

$$\rho_L = \frac{L_u}{E_d}, \quad R_L = \frac{\pi L_u}{E_d}$$

$$K = -\frac{1}{z_2 - z_1} \ln \frac{E(z_2)}{E(z_1)}$$

$$Q = \frac{E_u}{L_u}$$

IN-WATER SPECTRO-RADIOMETRY

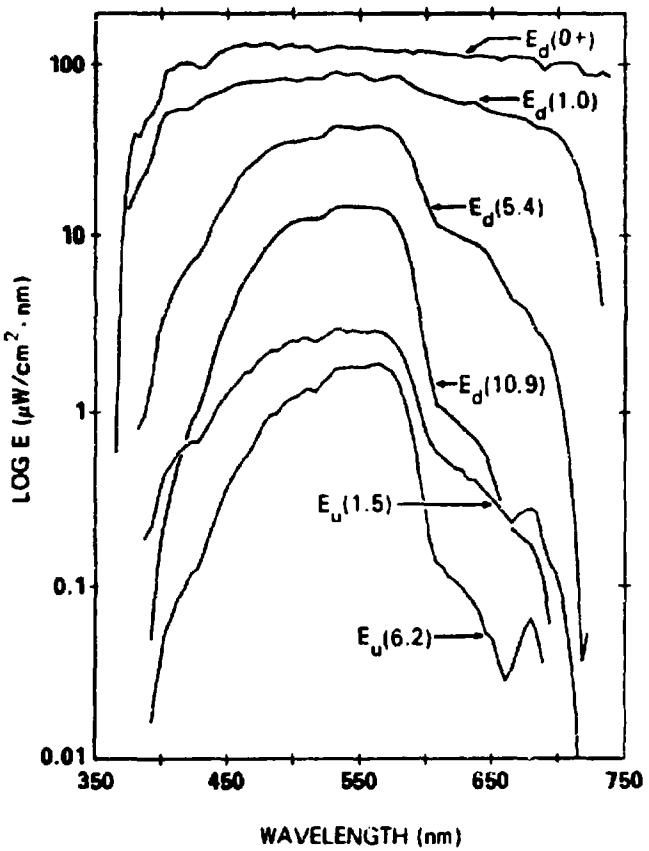
$E_d(0+)$
$E_d(1.0)$
$E_d(5.4)$
$E_d(10.9)$
$E_u(1.5)$
$E_u(6.2)$
100
10
1
0.1
0.01
350
450
550
650
750
LOG E ($\mu W/cm^2 \cdot nm$)
WAVELENGTH (nm)

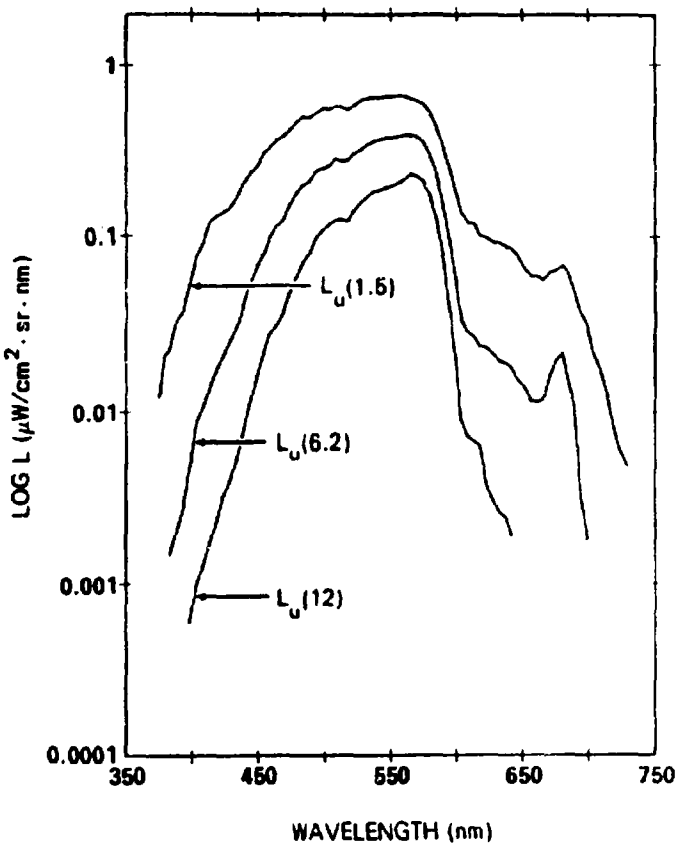
$L_u(1.6)$
$L_u(6.2)$
$L_u(12)$
1
0.1
0.01
0.001
0.0001
350
450
550
650
750
LOG L ($\mu W/cm^2 \cdot sr \cdot nm$)
WAVELENGTH (nm)

$K = (a^{*2} + 2a^{*}b_b^{*})^{1/2}$ DUNTLEY

$K \doteq a + \frac{b}{n}$ where n ~ 6 HONEY

$K_T = K_w + k_1 C_k + K_x$ SMITH & BAKER

$K_T - K_w = K_{DP}$

Let $K_w \doteq a_w + b_{bw}$

and since $\beta_w(\theta)$ is symmetric i.e.

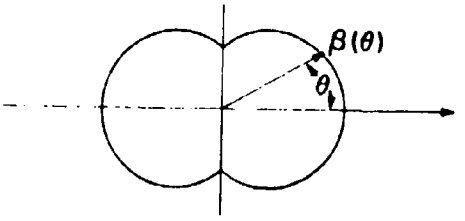

$b_{bw} = \frac{1}{2} b_w$,

Then

$K_w \doteq a_w + \frac{1}{2} b_w$

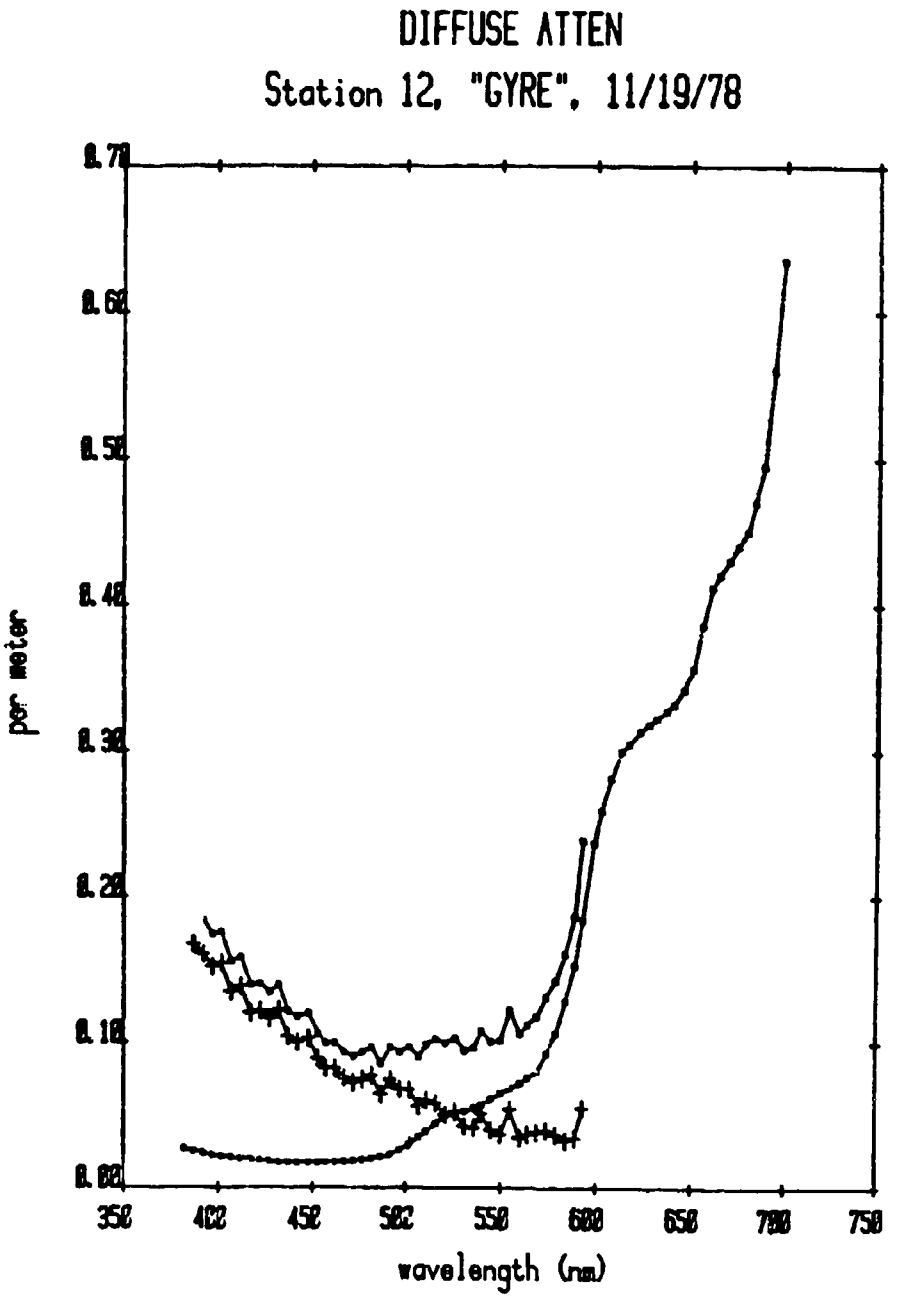
DIFFUSE ATTEN
Station 12, "GYRE", 11/19/78
per meter
wavelength (nm)

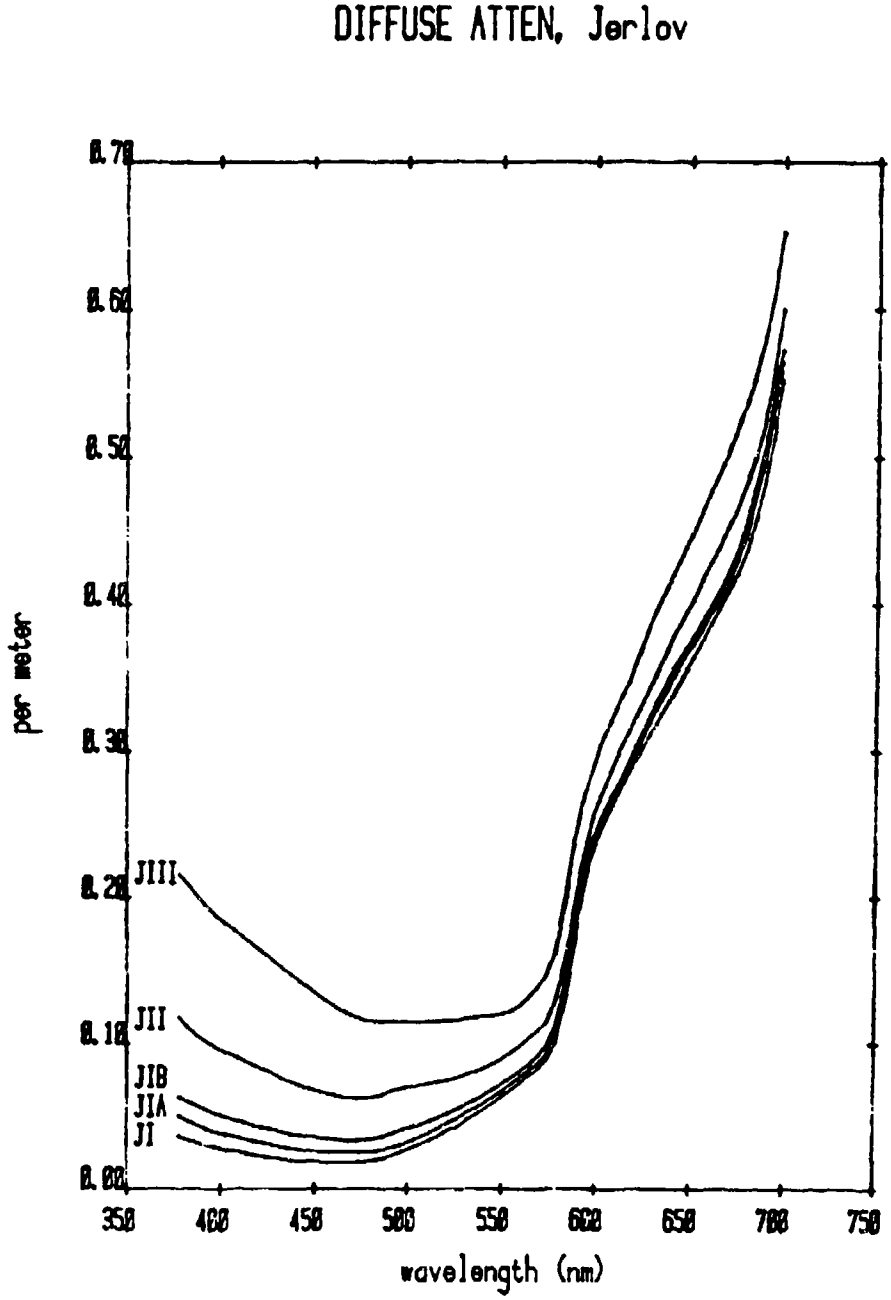
DIFFUSE ATTEN, Jerlov
per meter
JIII
JII
JIB
JIA
JI
350
400
450
500
550
600
650
700
750
wavelength (nm)

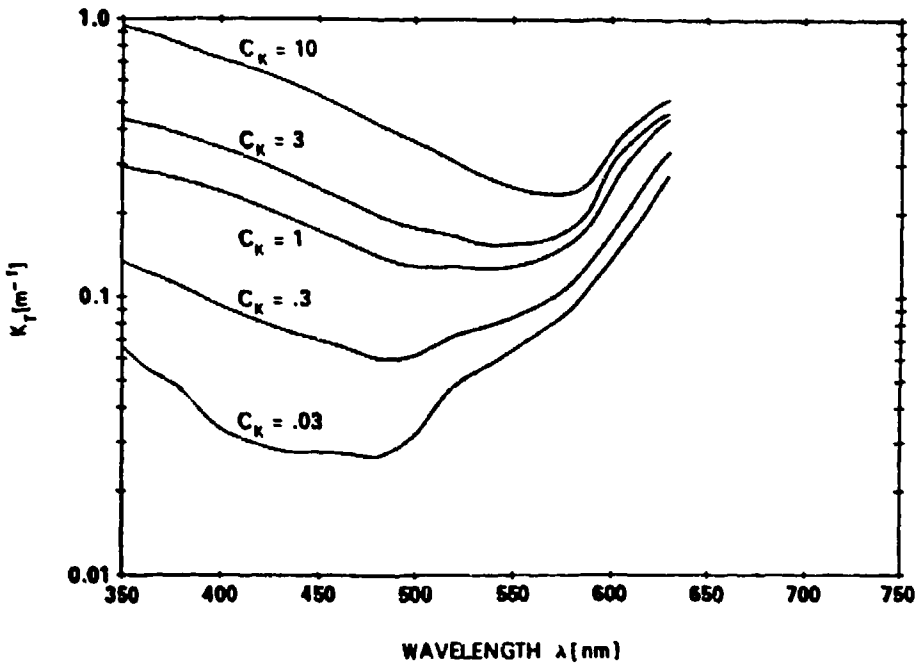

Fig. 4. Diffuse attenuation coefficient for irradiance $K_r[m^{-1}]$ as a function of wavelength for various values of chlorophyll-like pigment concentration C_K[(mg pigment · m^{-3})]. The curves were calculated using Eqs. 4 and Table 1.

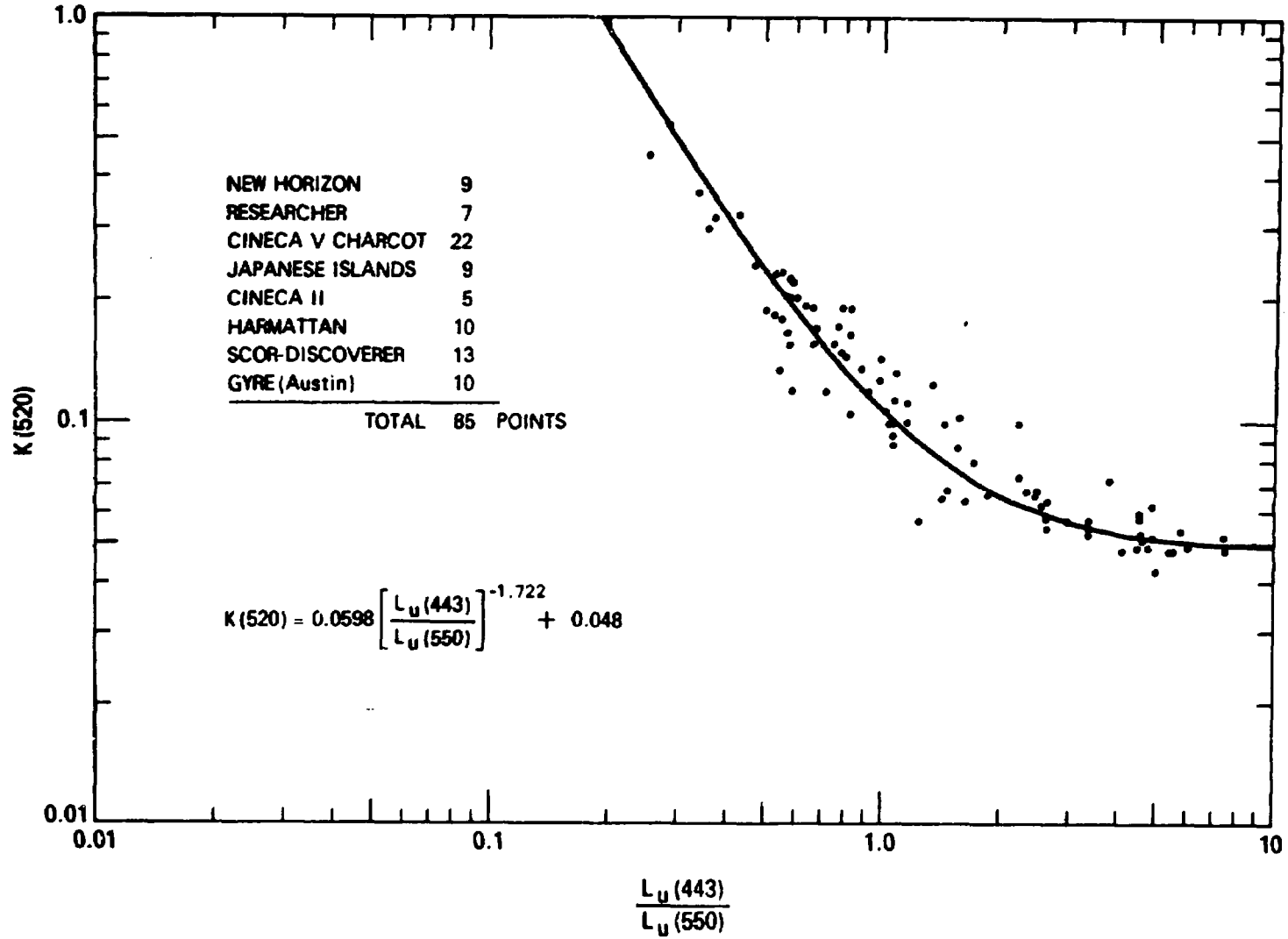
1.0
0.1
0.01
0.01
0.1
1.0
10
K(520)
$\frac{L_u(443)}{L_u(550)}$
NEW HORIZON 9
RESEARCHER 7
CINECA V CHARCOT 22
JAPANESE ISLANDS 9
CINECA II 5
HARMATTAN 10
SCOR-DISCOVERER 13
GYRE (Austin) 10
TOTAL 85 POINTS
$K(520) = 0.0598\left[\frac{L_u(443)}{L_u(550)}\right]^{-1.722} + 0.048$

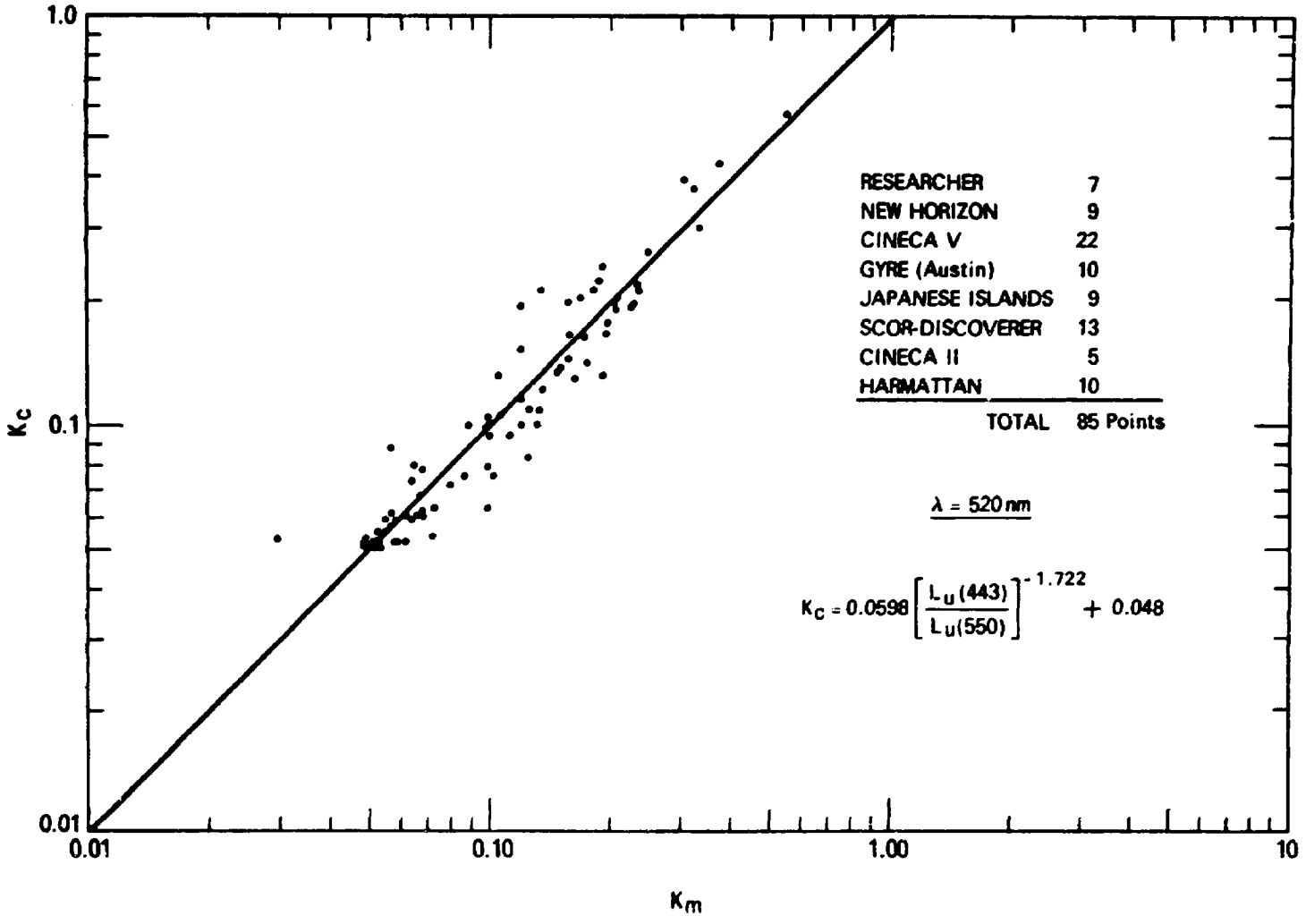
1.0
0.1
0.01
0.01
0.10
1.00
10
K_c
K_m
RESEARCHER 7
NEW HORIZON 9
CINECA V 22
GYRE (Austin) 10
JAPANESE ISLANDS 9
SCOR-DISCOVERER 13
CINECA II 5
HARMATTAN 10
TOTAL 85 Points
λ = 520 nm
$K_C = 0.0598 \left[\frac{L_u(443)}{L_u(550)}\right]^{-1.722} + 0.048$

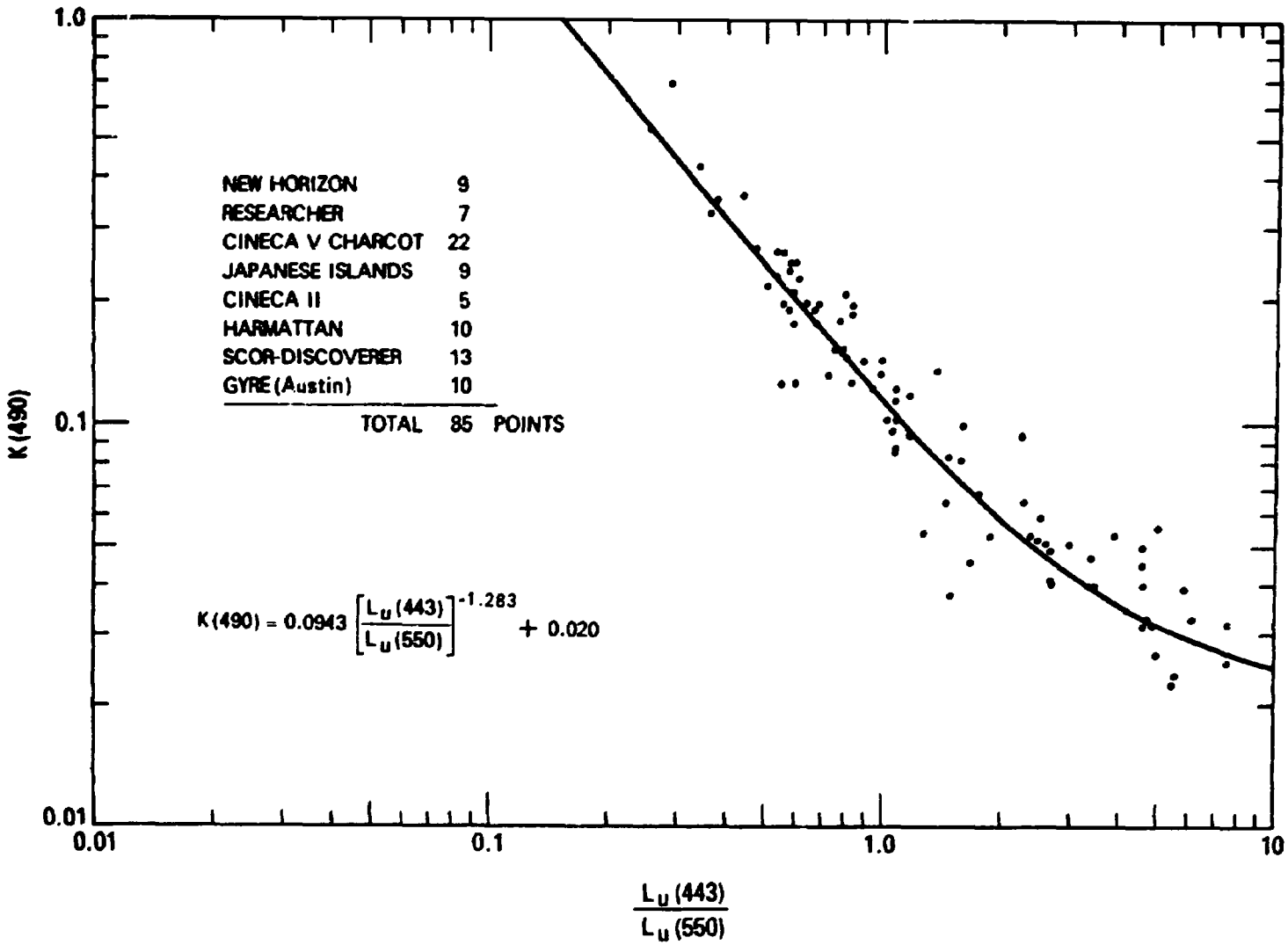
1.0
0.1
0.01
0.01
0.1
1.0
10
K(490)
$\frac{L_u(443)}{L_u(550)}$
NEW HORIZON 9
RESEARCHER 7
CINECA V CHARCOT 22
JAPANESE ISLANDS 9
CINECA II 5
HARMATTAN 10
SCOR-DISCOVERER 13
GYRE (Austin) 10
TOTAL 85 POINTS
$K(490) = 0.0943 \left[\frac{L_u(443)}{L_u(550)}\right]^{-1.283} + 0.020$

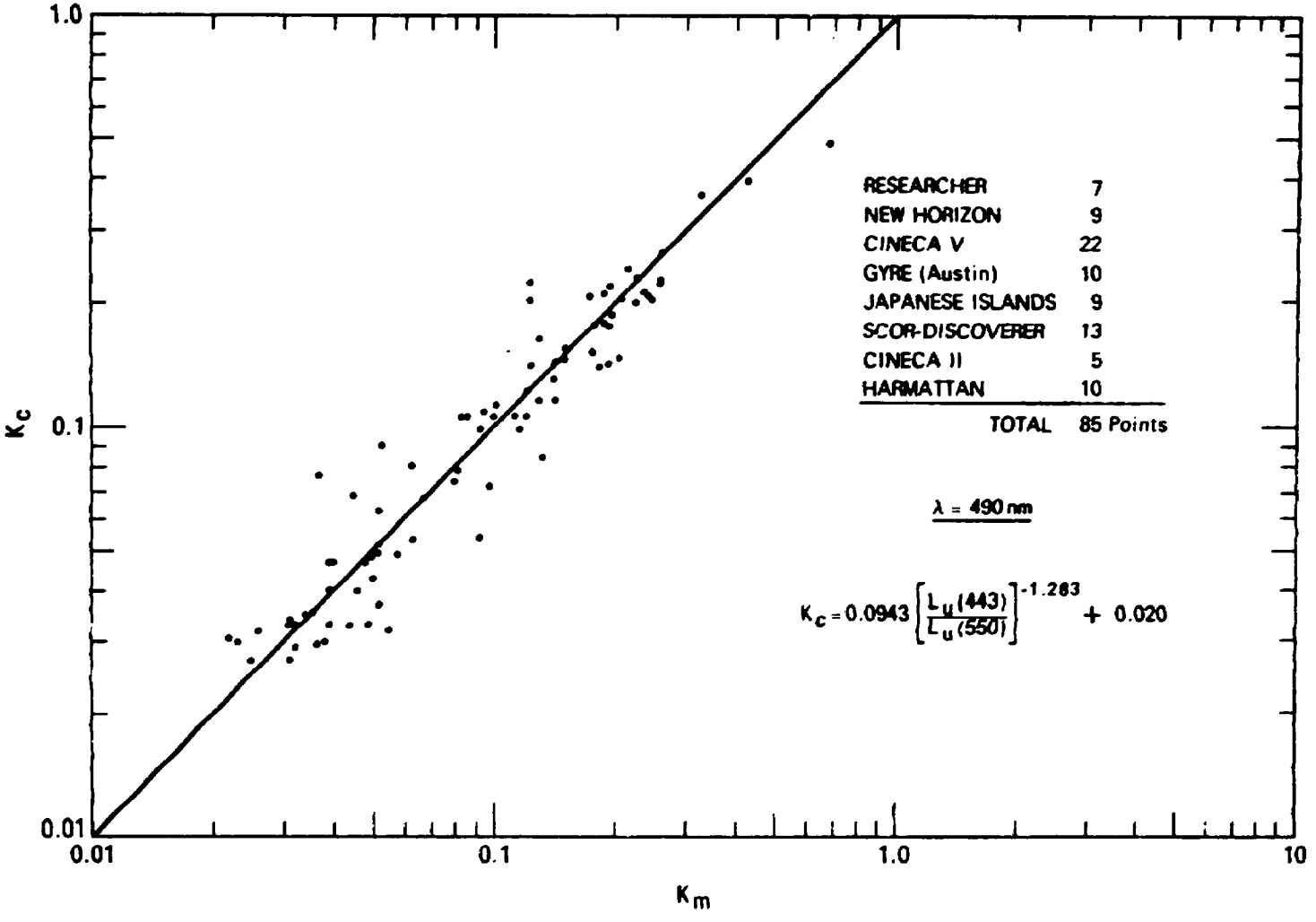
1.0
0.1
0.01
0.01
0.1
1.0
10
K_c
K_m
RESEARCHER 7
NEW HORIZON 9
CINECA V 22
GYRE (Austin) 10
JAPANESE ISLANDS 9
SCOR-DISCOVERER 13
CINECA II 5
HARMATTAN 10
TOTAL 85 Points
λ = 490 nm
$K_c = 0.0943 \left[\frac{L_u(443)}{L_u(550)}\right]^{-1.263} + 0.020$

$$K(490) = 0.0943 \left[\frac{L_u(550)}{L_u(443)} \right]^{1.283} + 0.02$$

85 STATIONS

		K_m / K_c	$K_m - K_c$
$K < 0.1$	$\bar{x}$ =	1.057	.002
	s =	0.275	.016
$K > 0.1$	$\bar{x}$ =	1.028	.007
	s =	0.185	.044

DIFFUSE ATTENUATION COEFFICIENT AND PLANT PIGMENT CONCENTRATION
vs BLUE-GREEN RADIANCE RATIO

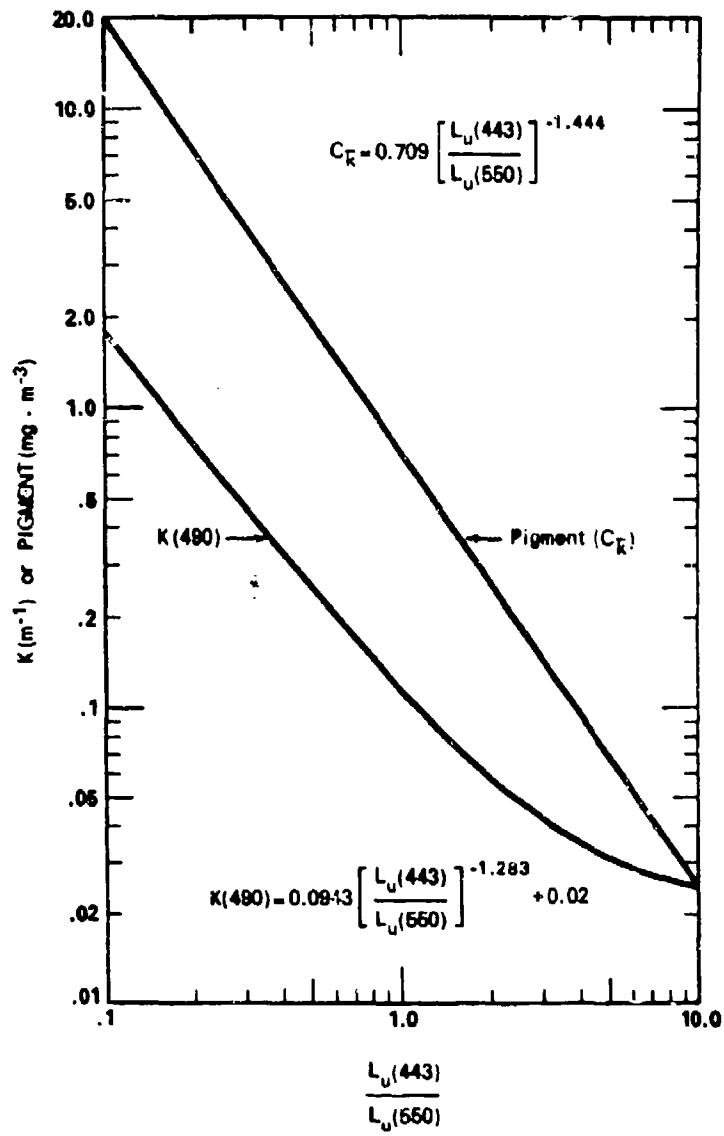

DIFFUSE ATTENUATION COEFFICIENT -K- vs CHLOROPHYLL
+ PHAEOPHYTIN PIGMENT CONCENTRATION

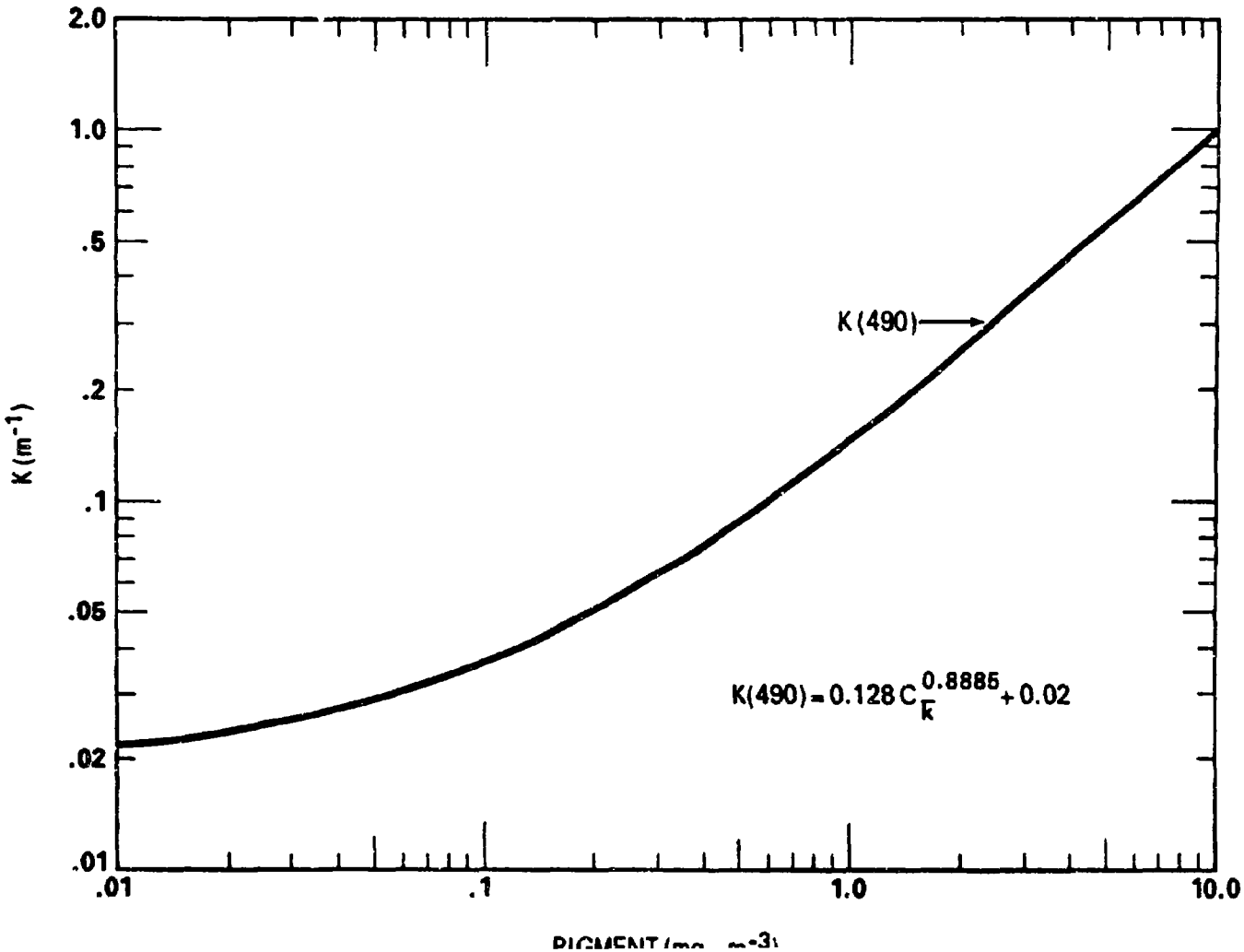

INDOPAC I MARCH–APRIL 1976

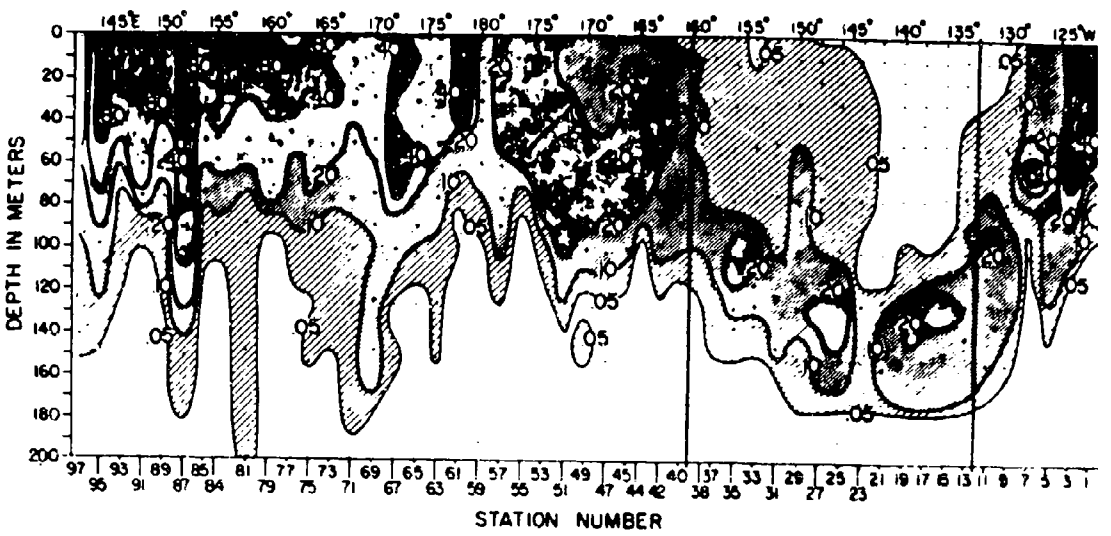

CHLOROPHYLL (mg/m³)

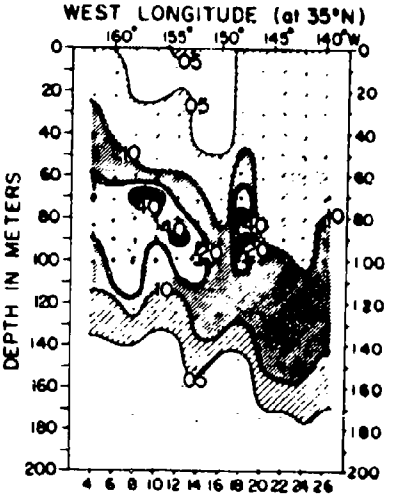

INDOPAC XVI JULY 1977

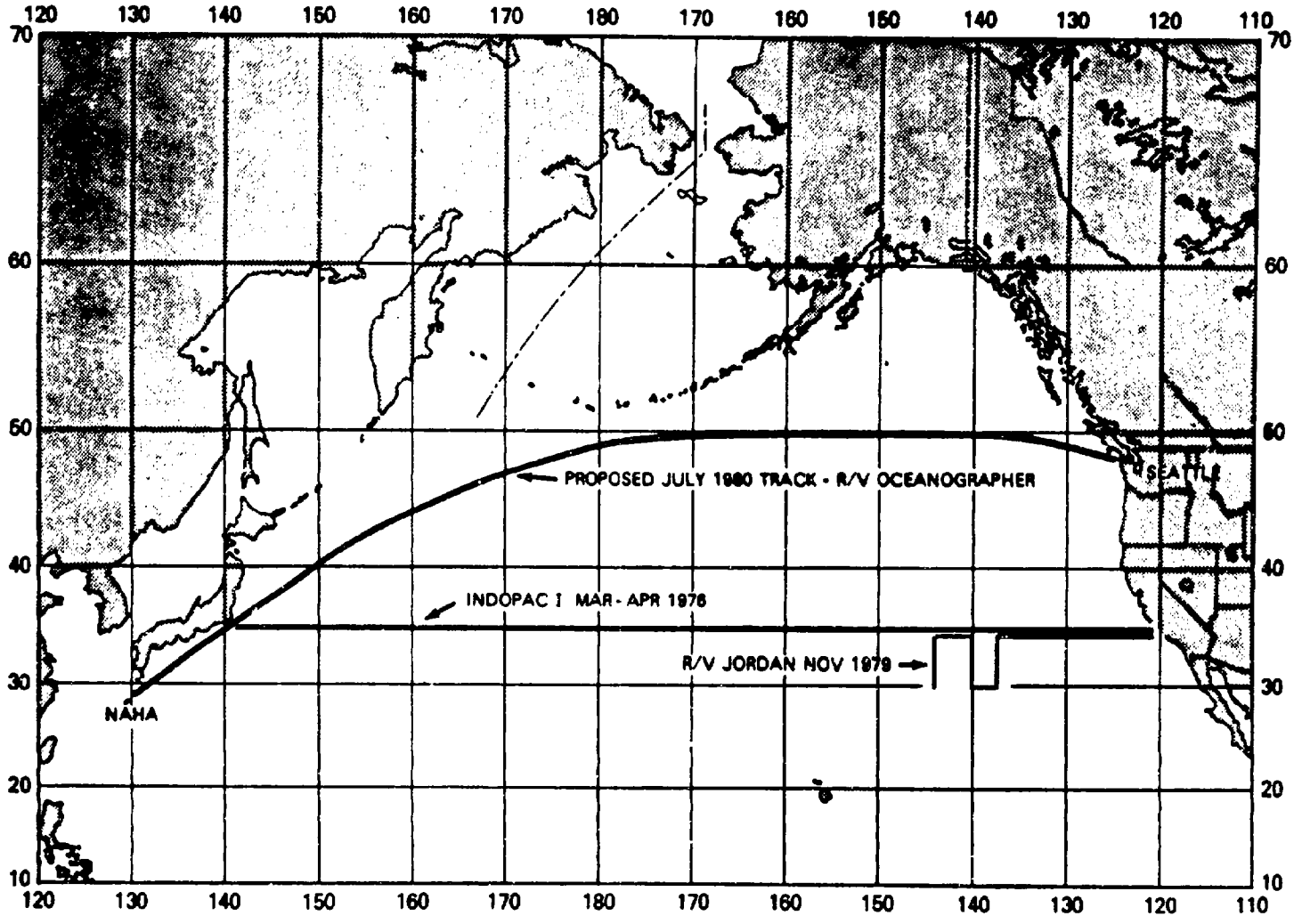
120 130 140 150 160 170 180 170 160 150 140 130 120 110
70
60
50
40
30
20
10
PROPOSED JULY 1980 TRACK - R/V OCEANOGRAPHER
INDOPAC I MAR - APR 1976
R/V JORDAN NOV 1979
NAHA
SEATTLE

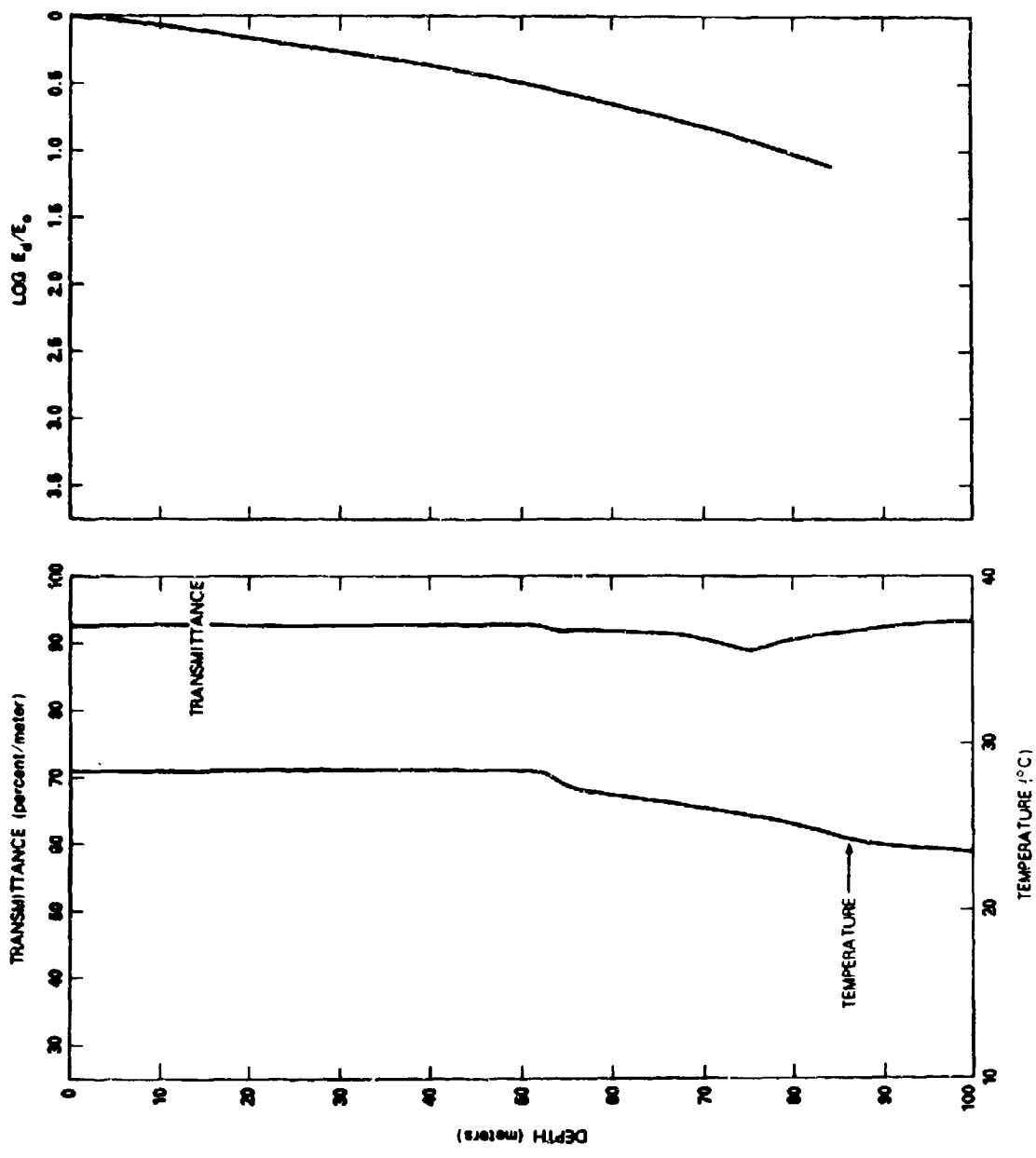
LOG E_d/E_o
0
0.5
1.0
1.5
2.0
2.5
3.0
3.5
TRANSMITTANCE (percent/meter)
TRANSMITTANCE
TEMPERATURE
DEPTH (meters)
TEMPERATURE (°C)
0
10
20
30
40
50
60
70
80
90
100
30
40
50
60
70
80
90
100
10
20
30
40

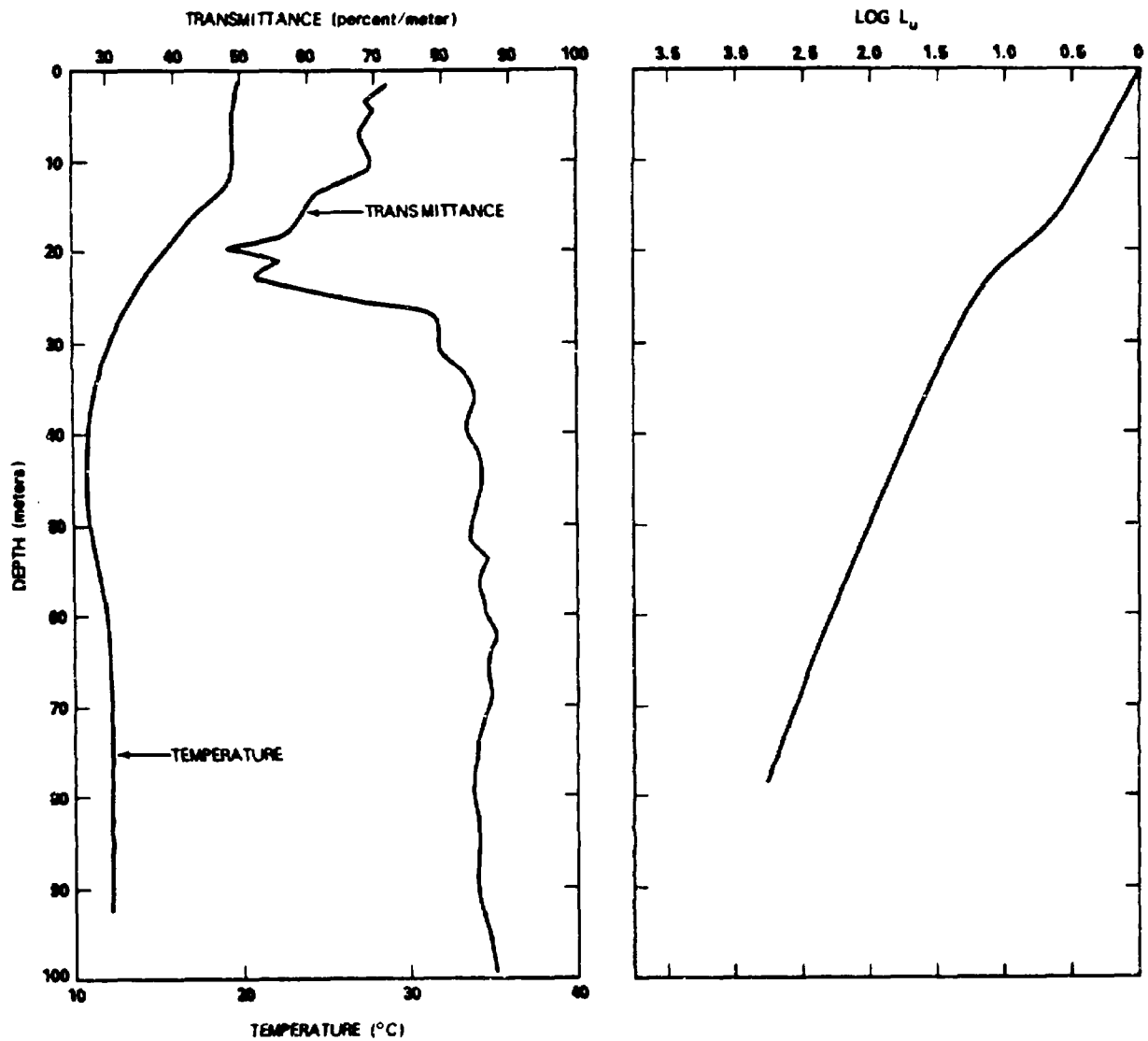

STATION OS-06 DATE 22 AUG 79 LAT. 40°36'N LONG. 67°28.8'W WATER DEPTH 93m
SPECTRAL FILTER NO. 2 λ 490.9 SURFACE TEMP. 19.1

K TO 100 METERS PLOTTED AGAINST K TO FIRST ATTENUATION DEPTH

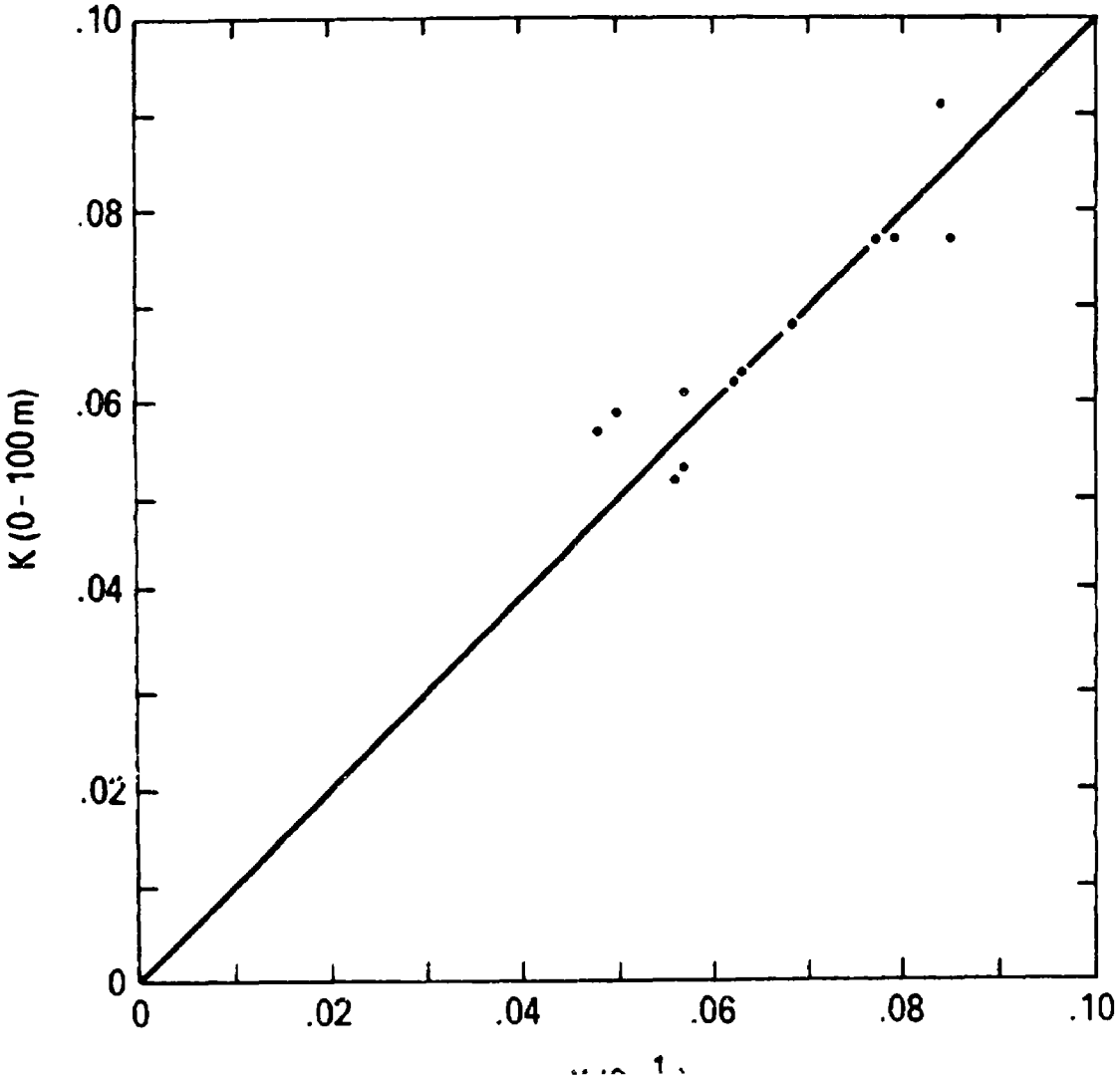

COINCIDENT WITH OVERPASS

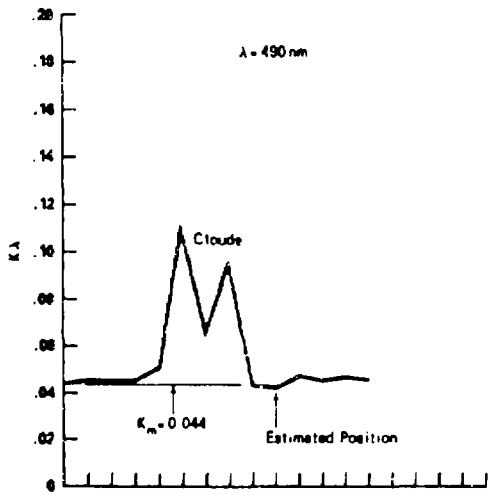

GYRE, Station 01;
9 Nov 1978 Orbit 227

NOT COINCIDENT WITH OVERPASS

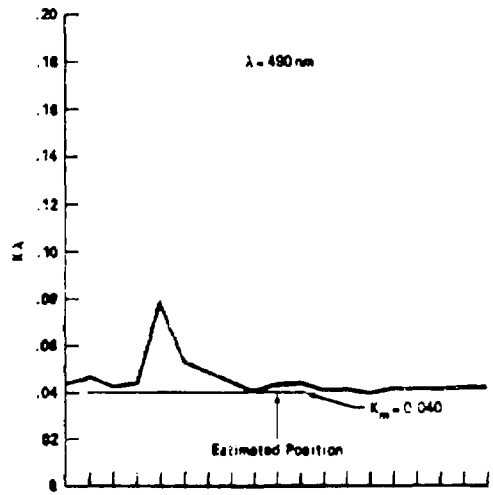

GYRE (Austin), Station 07;
18 Nov 1978 Orbit 227

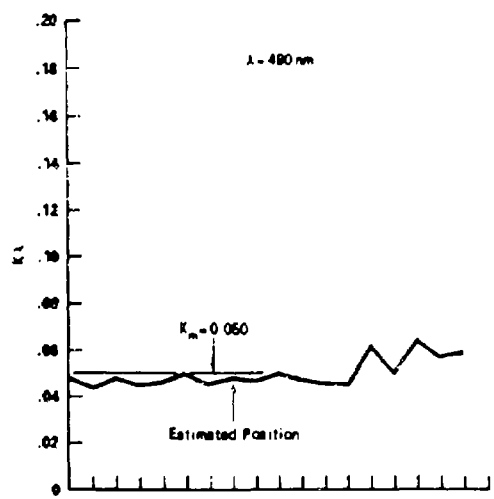

New Horizon Station 10
11 Mar 1980 Orbit 1915

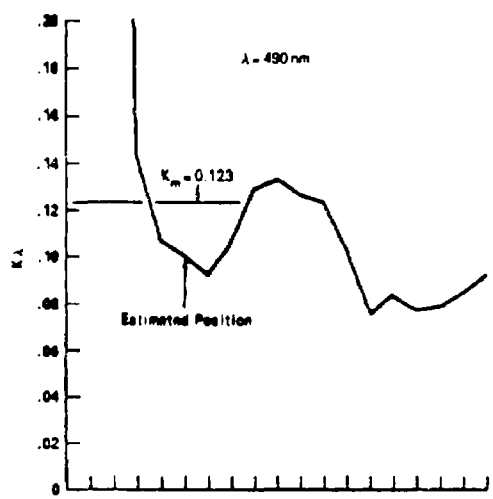

New Horizon Station 07
8 Mar 1979 Orbit 1818

AN ANALYTIC MODEL FOR CLOUD PROPAGATION

AP Ciervo

ABSTRACT

This paper presents an analytic model for the propagation of an optical pulse through a multiple scattering medium. Such a model is needed to investigate the effect of clouds on optical communications from satellite to submarine. Key results include simple expressions for the first two spatial and angular moments of the radiance distribution for a narrow delta-function source immersed in an infinite scattering medium. The moments support a diffusion approximation for the transport process in an infinite plane-parallel cloud. First the radiance is calculated at the cloud exit and on a plane an arbitrary distance below the cloud, then power collected by a finite receiver located on this plane is computed. The model is validated by comparing its results with computer simulation curve fits for optically thick clouds (i.e., $\tau > 15$). The model is capable of duplicating nearly all the simulation results but at significantly lower cost. Furthermore, finite receiver calculations that are impractical to simulate are readily computed.

Pacific Sierra Research
1456 Cloverfield Blvd
Santa Monica CA 90404

PSR

AN ANALYTIC MODEL FOR PROPAGATION THROUGH CLOUDS

- Advantages for Blue-Green Systems Analysis
  - efficient calculation of aperture and field of view effects on received pulse for optimization studies
  - provides physical insight into scattering process not apparent in Monte Carlo curve fits
  - may help resolve anomalies in experimental vs calculated results
  - confirms or suggests alternative modular expressions for current Navy single pulse blue-green downlink propagation model

PSR

PROPAGATION PATH

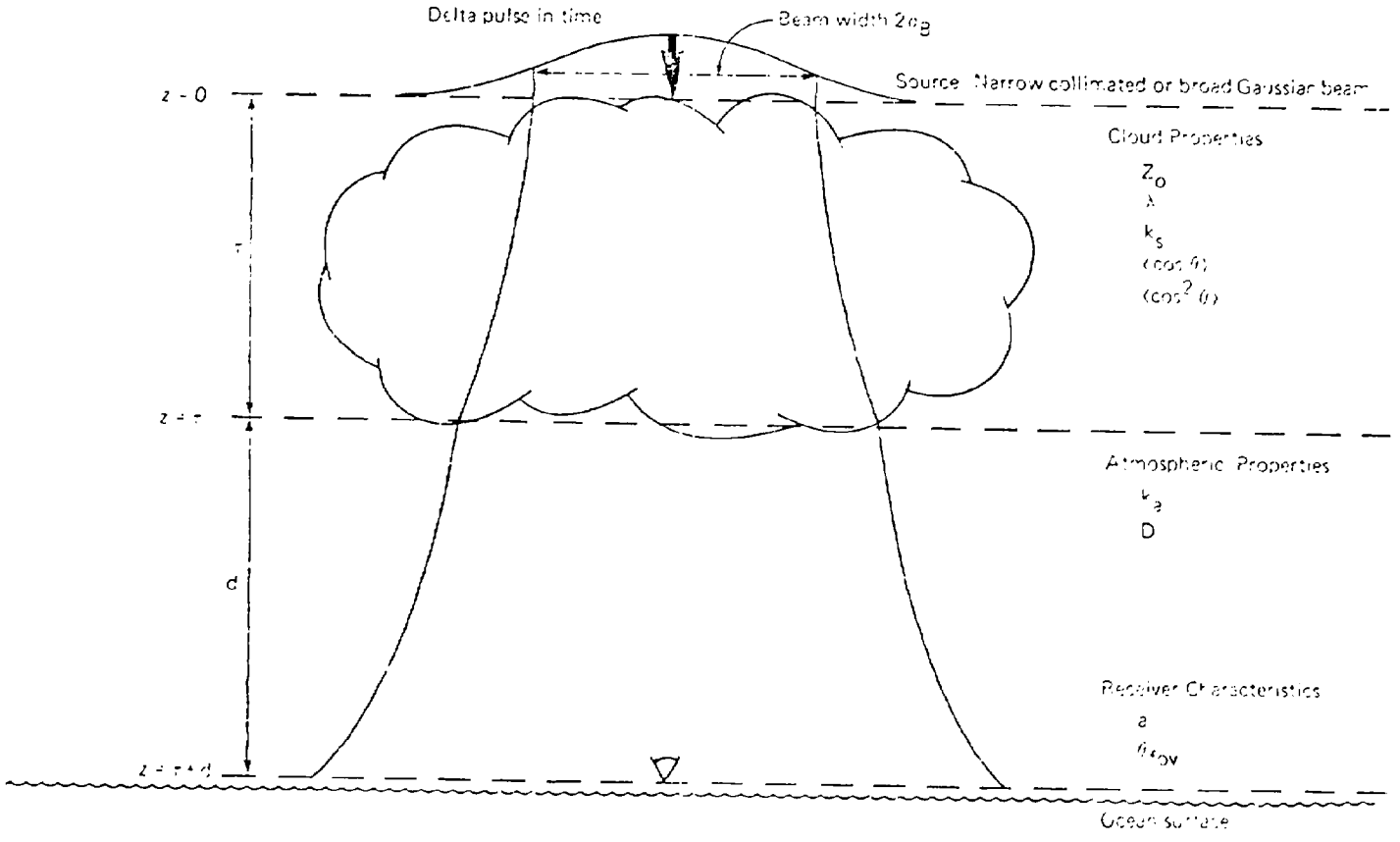

PSR

SCATTERING GEOMETRY

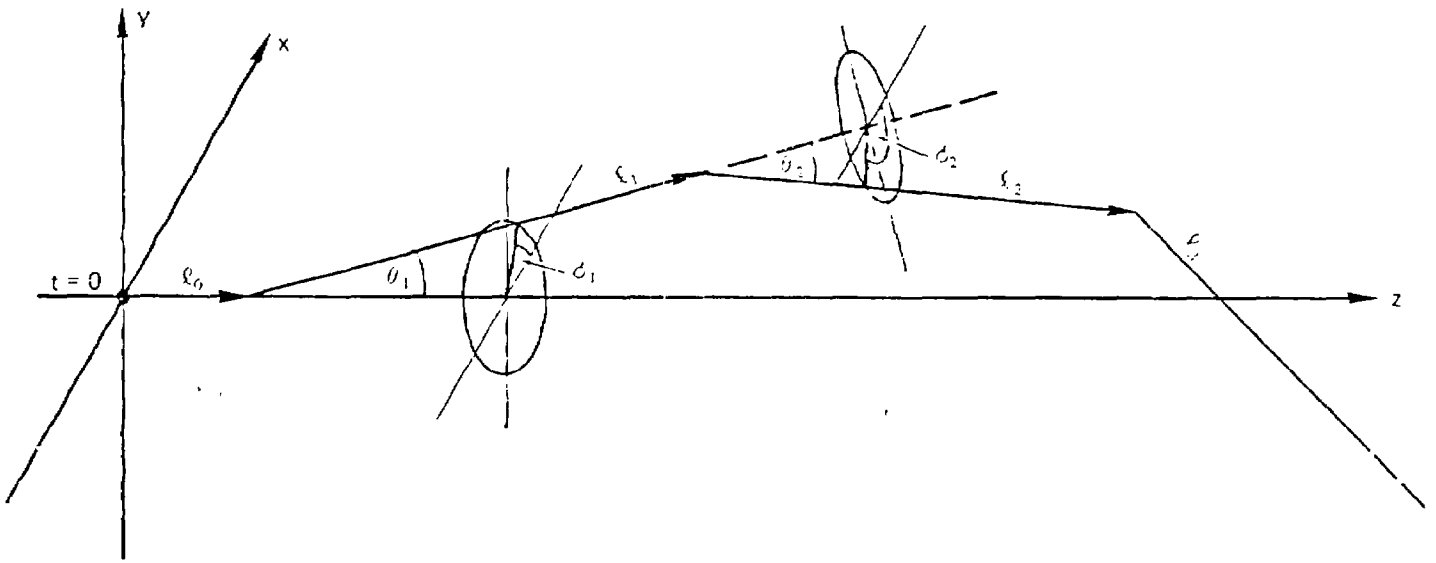

Notes: 1. Photon is at orgin directed along z-axis at t=0
2. Leg lengths ℓ_n exponentially distributed
3. Polar angles θ_n distributed according to scalar phase function
4. Azimuthal angles ϕ_n uniformly distributed

PSR

SPATIAL MOMENTS OF SCATTERED LIGHT

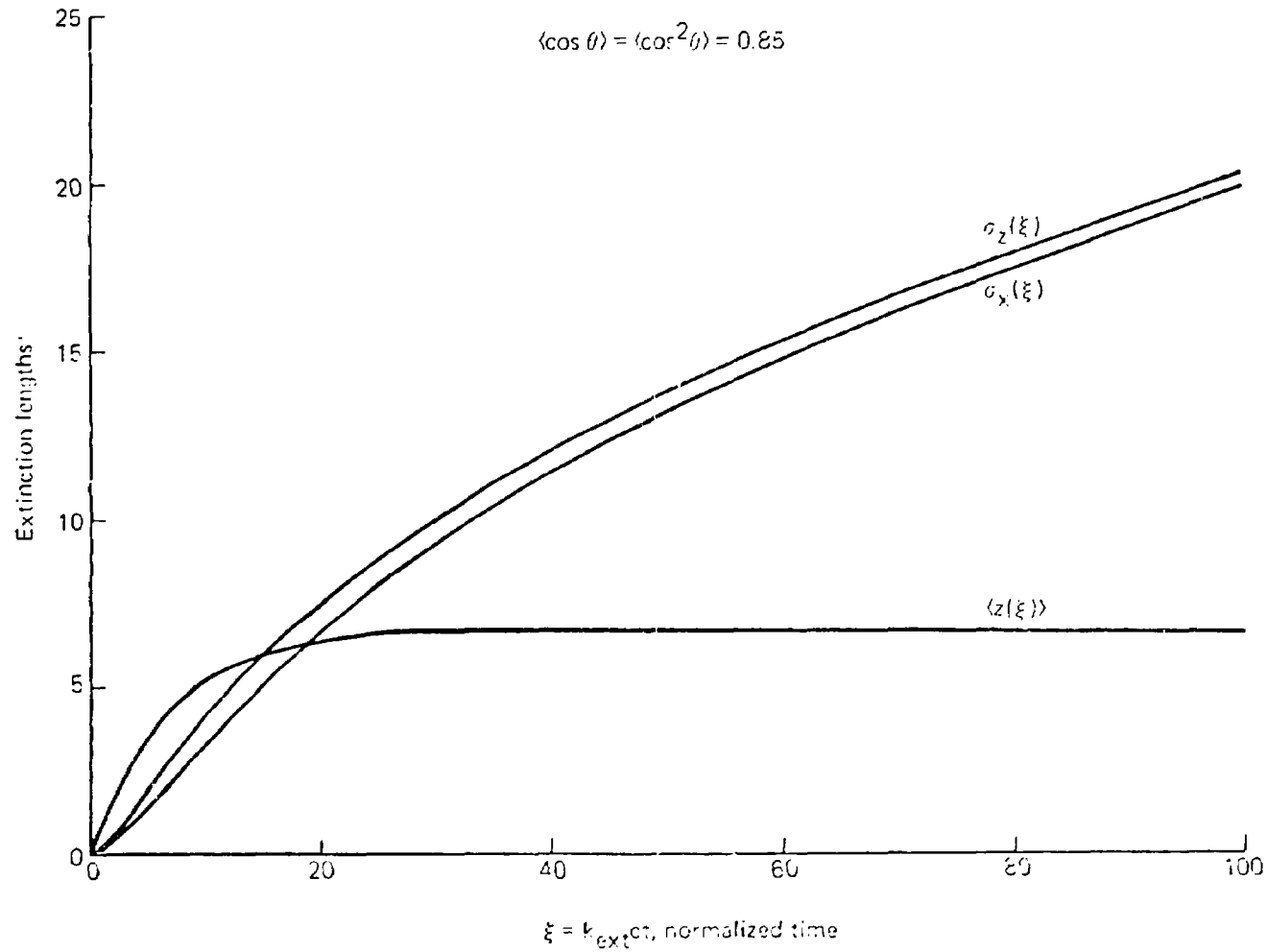

ANGULAR MOMENTS OF SCATTERED LIGHT

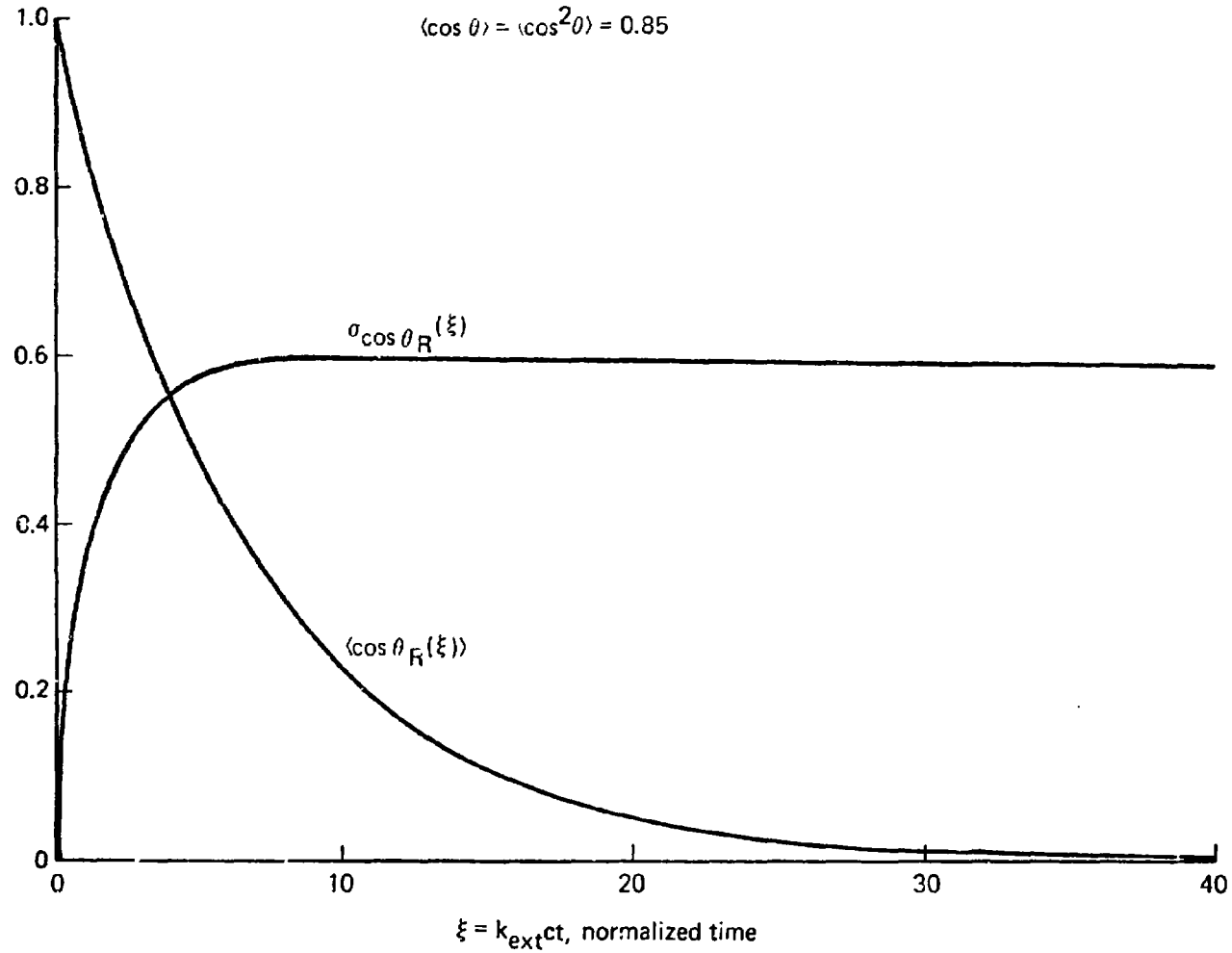

PSR

SPATIAL MOMENTS BY ORDER OF SCATTERING

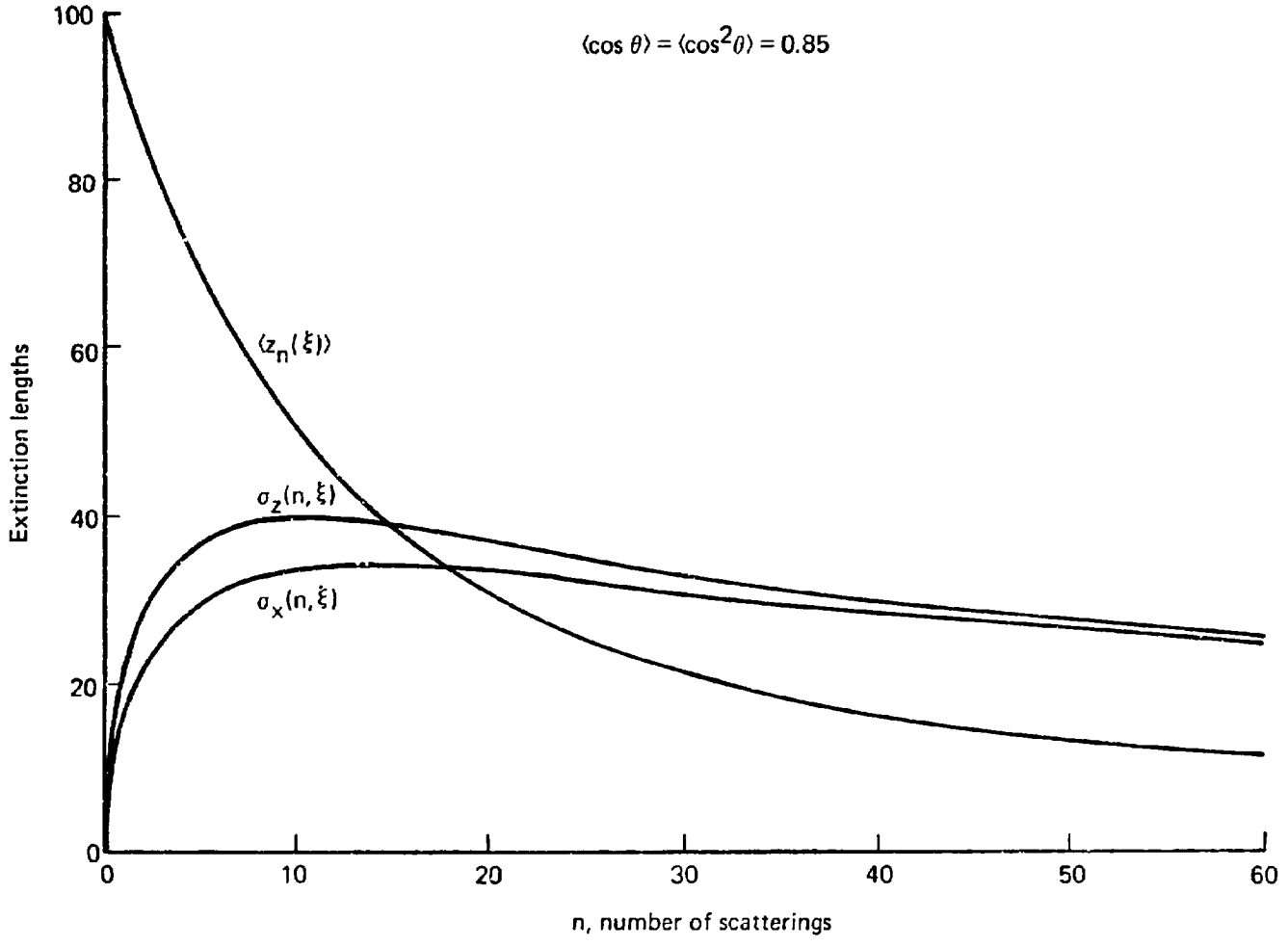

ANALYTIC VS SIMULATED PULSE SHAPES

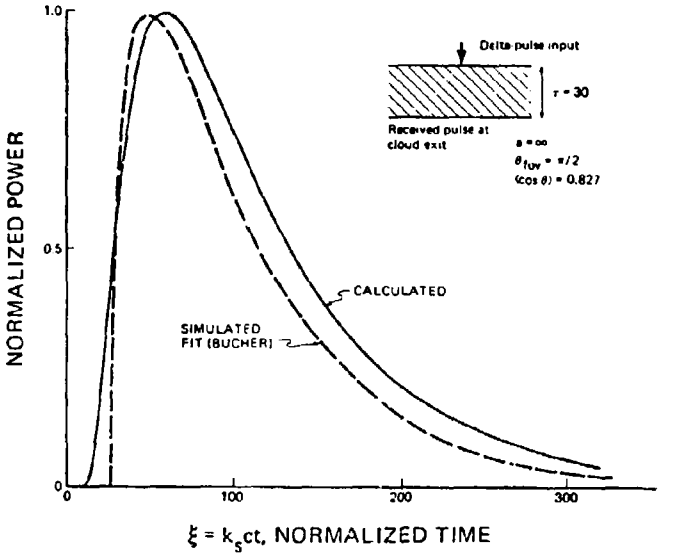

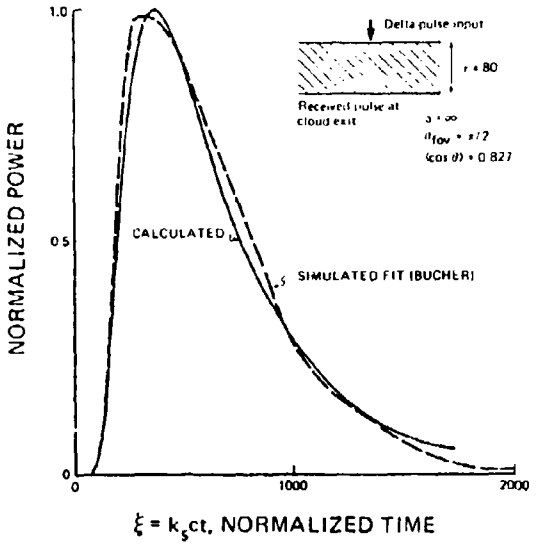

PSR

ENERGY TRANSMISSION VS OPTICAL THICKNESS

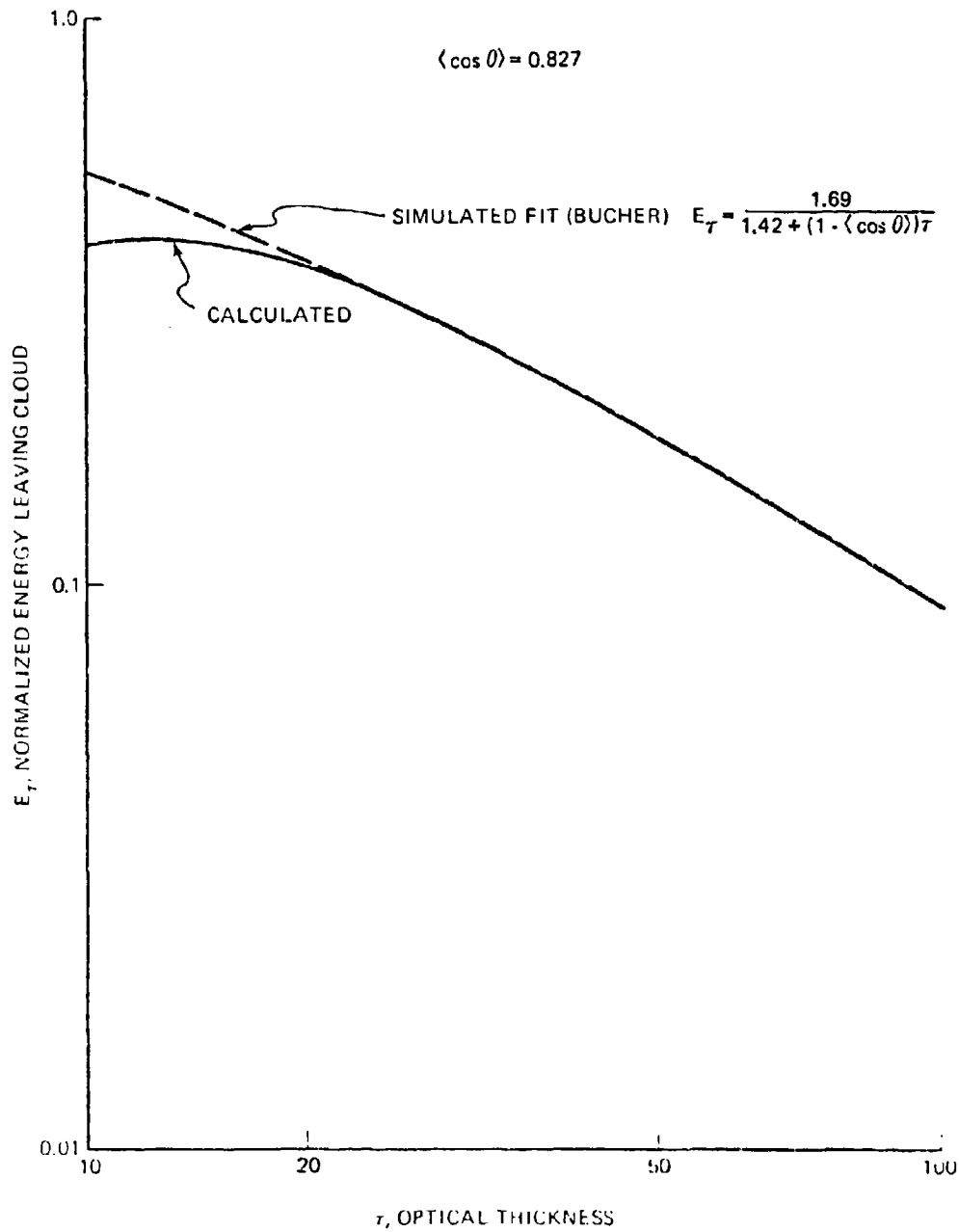

PSR

SPATIAL AND TEMPORAL PULSE SPREADING

$\langle \cos \theta \rangle = 0.827$

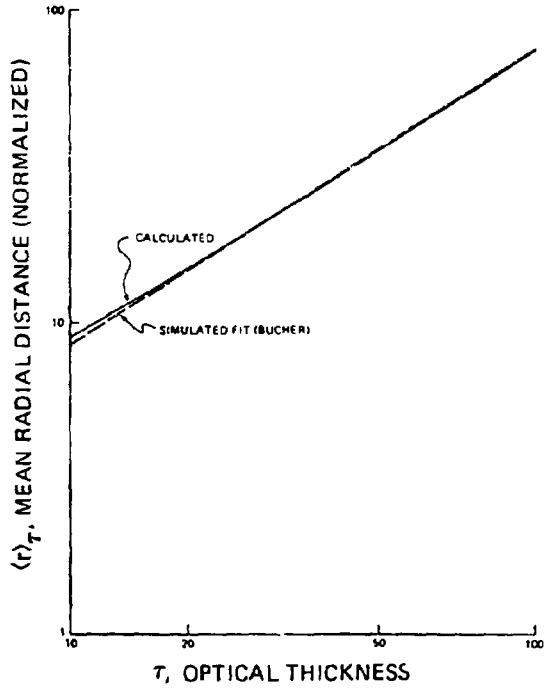

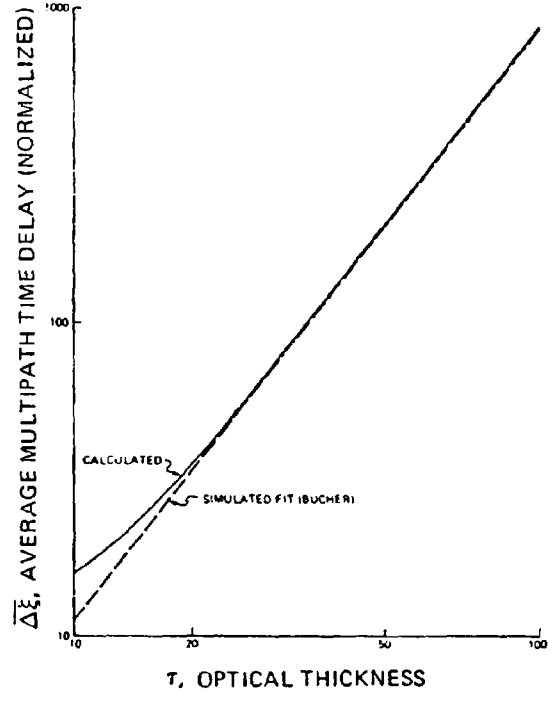

PSR

FOV EFFECTS ON RECEIVED ENERGY BELOW CLOUD

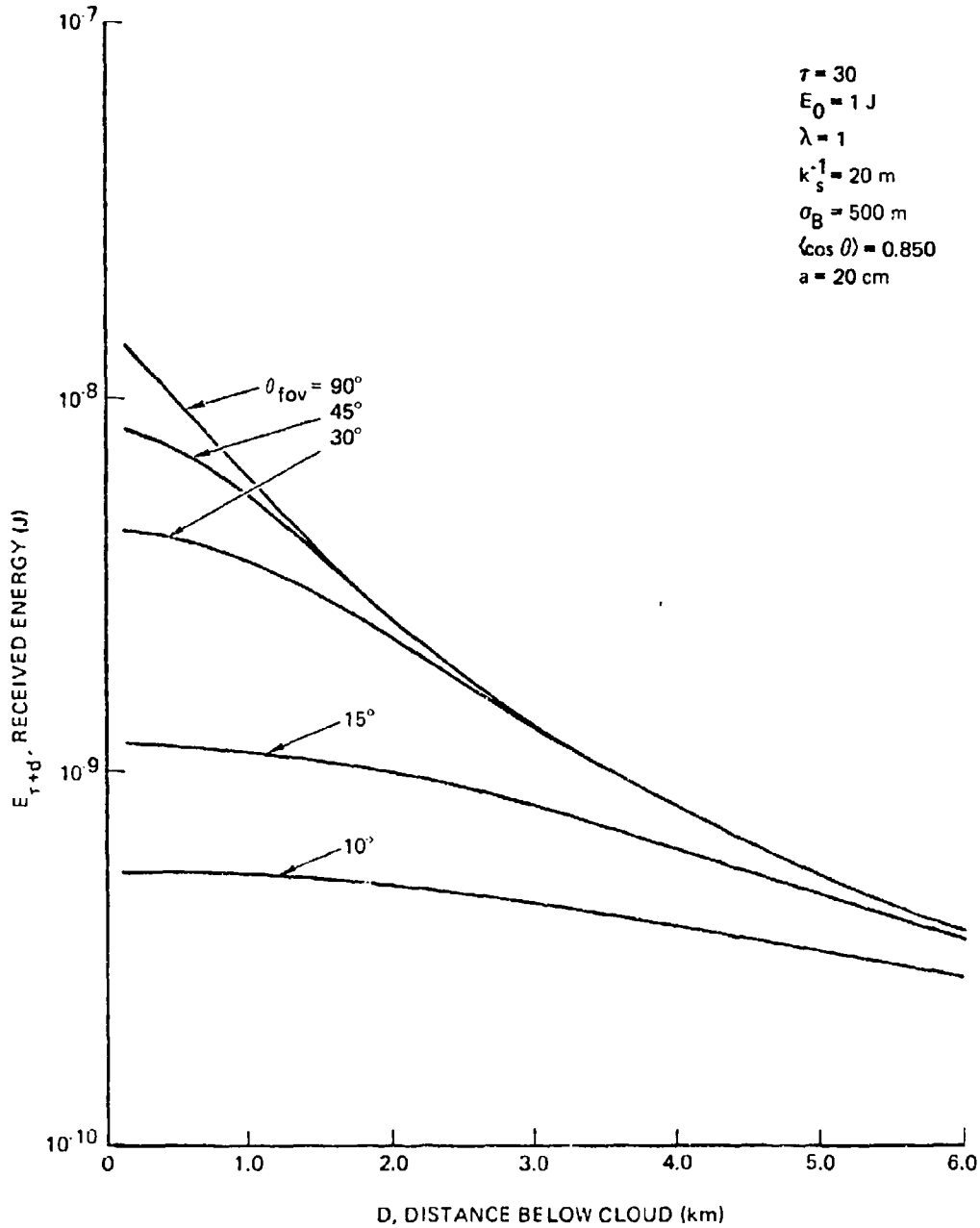

FOV EFFECTS ON MULTIPATH DELAY

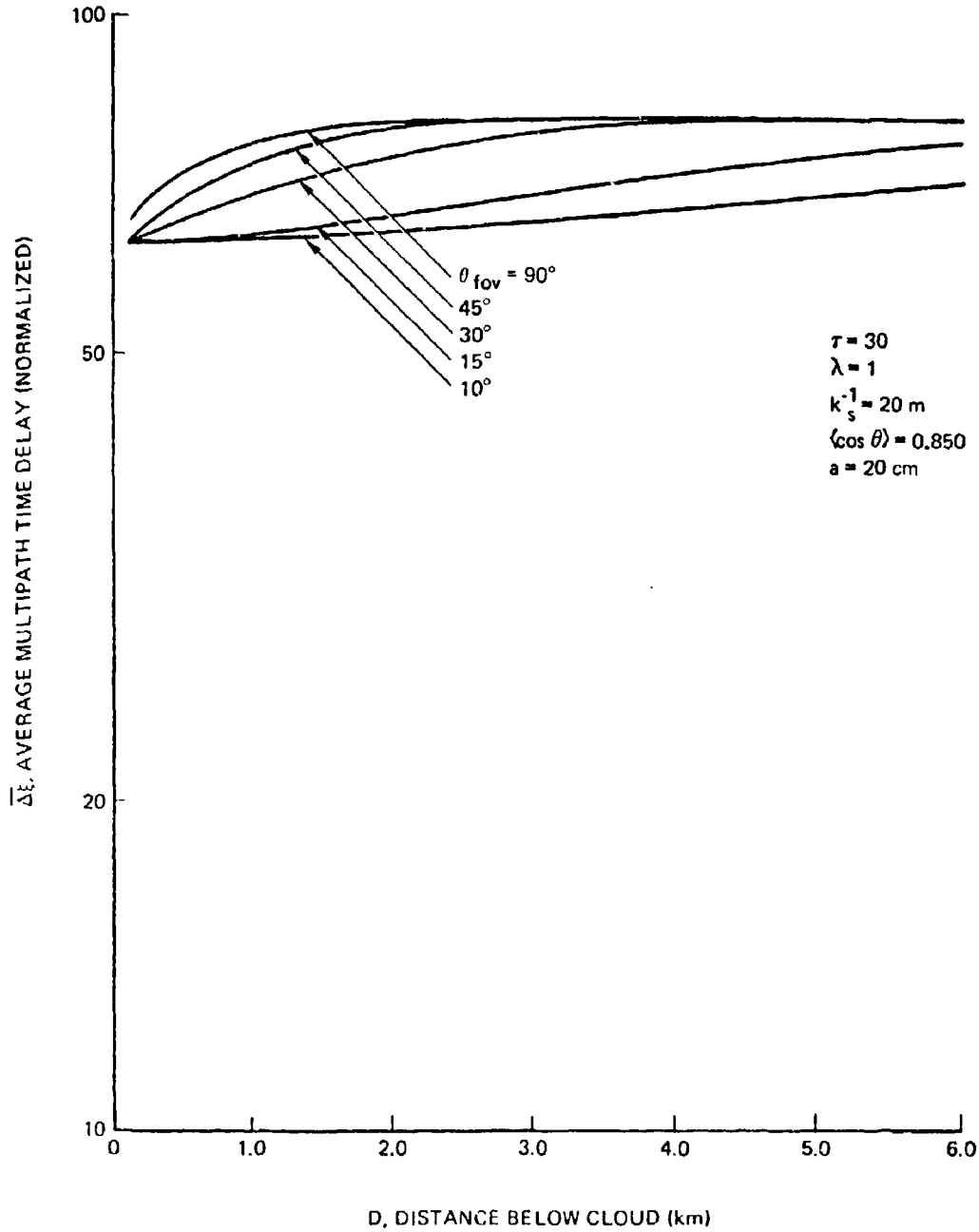

PSR

EFFECT OF CLOUD AND ATMOSPHERIC LAYER ON RECEIVED ENERGY

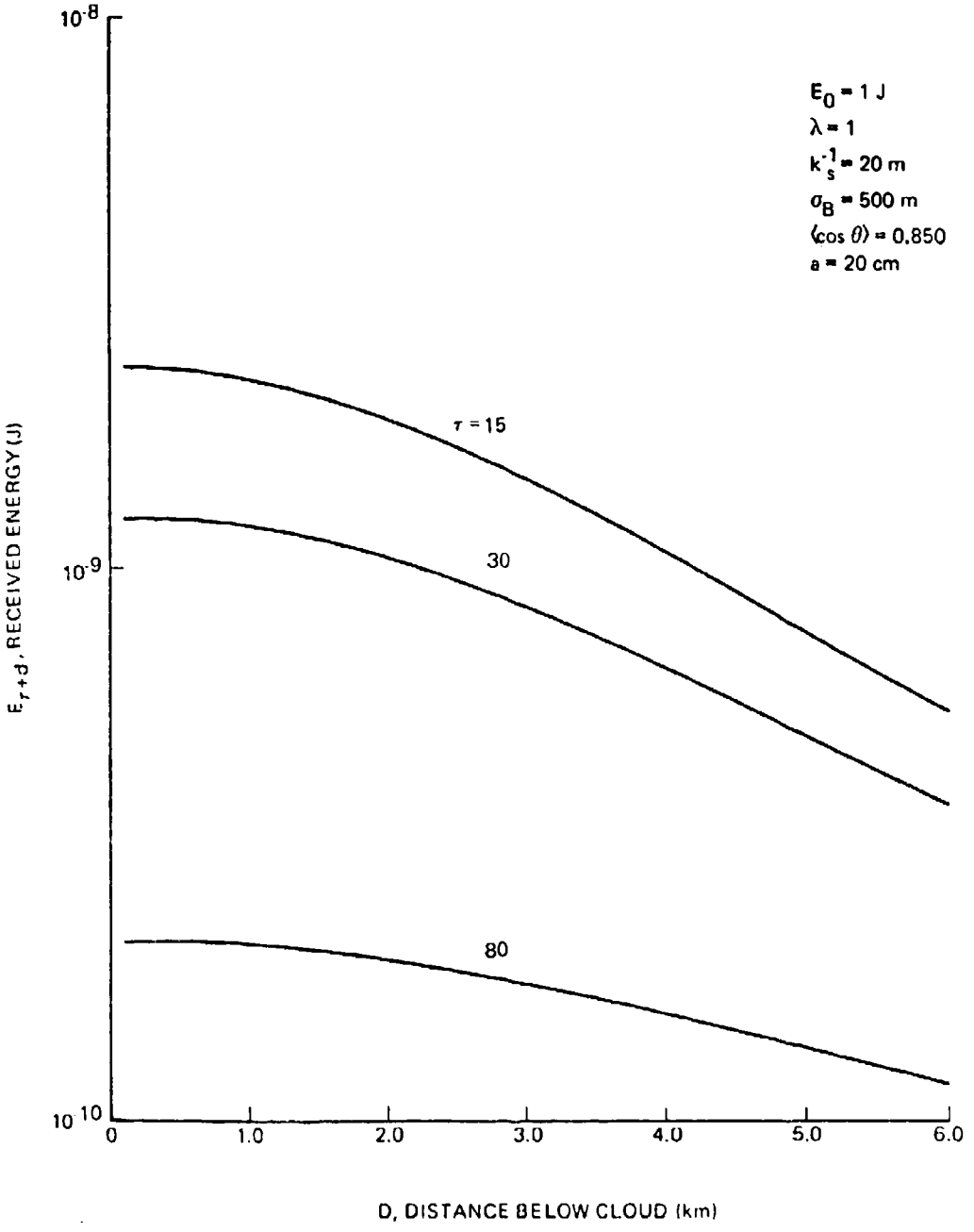

PSR

MODULAR EXPRESSIONS FOR CURRENT NAVY MODEL

PHYSICAL QUANTITY	NAVY MODEL EXPRESSION
Pulse shape	Confirmed
Pulse stretch due to clouds	Replace with Bucher expression
Energy transmission through cloud	Confirmed
Energy transmission, cloud to ocean	Compare with new expression
Angular spread of exiting photons	Replace with new expression